1997

ANNUAL TROPICAL CYCLONE REPORT

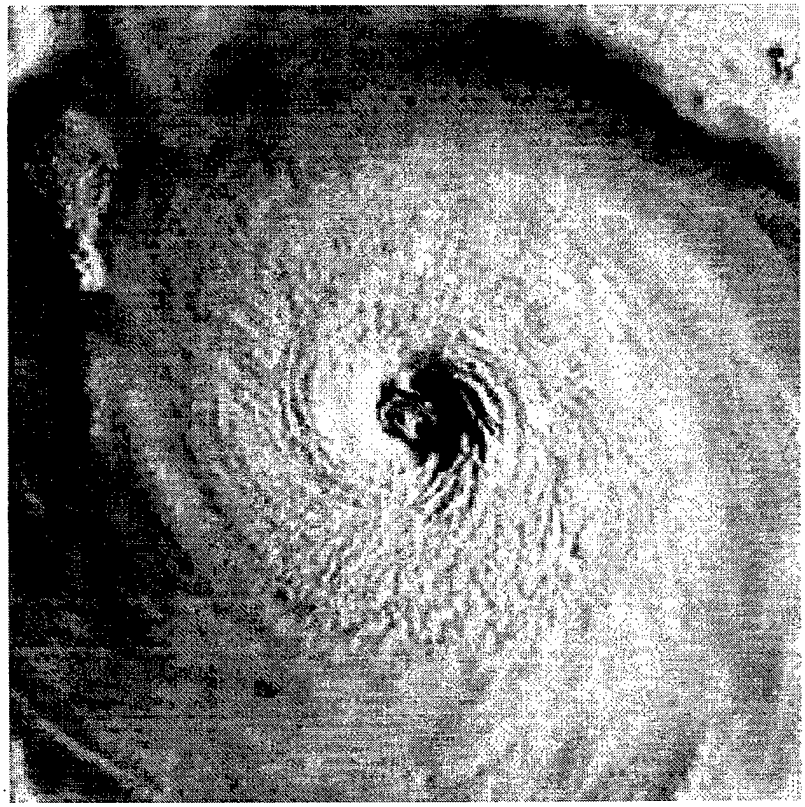

JOINT TYPHOON WARNING CENTER

COVER PHOTO: Super Typhoon Oliwa (02C), as seen by 2034Z visible GMS imagery on 9 September. The small comma shaped cloud on the inside of the eyewall is a possible manifestation of an eyewall mesovortex.

U.S. Naval Pacific Meteorology and Oceanography Center West
Joint Typhoon Warning Center

C. P. DILLON

Captain, United States Navy
Commanding Officer

MARK J. ANDREWS

Lieutenant Colonel, United States Air Force
Director, Joint Typhoon Warning Center

Work on this report was supported in part by
the Office of Naval Research Grant N00014-96-1-0744

STAFF

JOINT TYPHOON WARNING CENTER

LCOL	MARK ANDREWS	USAF	DIRECTOR
* LCDR	ERIC J. TREHUBENKO	USN	TDO, DEPUTY DIRECTOR
LCDR	KENNETH A. MALMQUIST	USN	TDO, DEPUTY DIRECTOR
MR	FRANK H. WELLS	CIV	TECHNICAL ADVISOR
**LCDR	STACY R. STEWART	USNR	TDO
LCDR	MARGARET A. SMITH	USN	TDO
*LT	MICHAEL S. KALAFSKY	USN	TDO
*CAPT	CARL A. MCELROY	USAF	TDO
***CAPT	CHRISTOPHER T. NICKLAS	USAF	TDO
LT	KIM F. BOYER	USN	TDO
CAPT	STEPHEN B. COCKS	USAF	TDO
*CAPT	GARY B. KUBAT	USAF	TDO
*CAPT	WILLIAM J. CARLE	USAF	TDO, STATISTICS OFFICER
LT	PAULA E. HILDEBRAND	USN	TDO
CAPT	TOM D. LUNSFORD	USAF	TDO
CAPT	CHRISTOPHER FINTA	USAF	TDO
MSGT	BRENT T. SULLINS	USAF	TDO
AG1	PAUL G. SANCHEZ	USN	LPO, SAT FORECASTER, TDA
A1C	JASON R. DOBBINS	USAF	TDA
AG2	KEYIA HALL	USN	TDA
AG2	BRYAN Y. HONG	USN	TDA
AG3	JOHN E. UROGI	USN	TDA
AG3	CAROL A. GILL	USN	TDA
SRA	SAMUEL R. PUGH	USAF	TDA
SRA	DIONNE M. TIRSCHEL	USAF	TDA
SRA	MATHEW A. BOYD	USAF	TDA
SRA	RYAN M. EIBLING	USAF	SAT FORECASTER,
PROGRAMMER			
SRA	CHRISTOPHER L. JONES	USAF	TDA
AGAR	STEPHEN R. BACON	USN	TDA

36 OSS/OSJ

MAJ	ROGER T. EDSON	USAF	TECHNIQUE DEVELOPMENT
*CAPT	RICHARD A. ANSTETT	USAF	TDO, OIC USPACOM SAT NETWORK
MSGT	RONALD L. HOOVER	USAF	SAT FORECASTER, NCOIC
*TSGT	SHIRLEY A. BROWN	USAF	CHIEF INFORMATION MANAGEMENT
TSGT	ROBERT P. MOTZ	USAF	CHIEF INFORMATION MANAGEMENT
*TSGT	DENNIS W. MILLER	USAF	SAT FORECASTER
TSGT	ROBERT J. PATTERSON	USAF	SAT FORECASTER
*SSGT	MERRYRUTH I. DEOCARIZA	USAF	SAT FORECASTER
*SSGT	LINDA R. HAM	USAF	SAT FORECASTER
SSGT	GARTH A. MCCULLUCH	USAF	SAT FORECASTER
SSGT	IRA L. JOHNSON	USAF	SAT FORECASTER
*SSGT	BRUCE W. WOFFORD	USAF	SAT FORECASTER
*SSGT	MELISSA E. HATFIELD	USAF	SAT FORECASTER
*SSGT	CRAIG S. BOUCHILLON	USAF	DATA DEVELOPMENT
*SRA	SEAN M. MCDUNN	USAF	DATA DEVELOPMENT

UNIVERSITY OF GUAM/JTWC RESEARCH LIAISON

DR	MARK A. LANDER	TROPICAL CYCLONE RESEARCH, TECHNICAL WRITING
MR	CHARLES P. GUARD	TROPICAL CYCLONE RESEARCH, TECHNICAL WRITING

* TRANSFERRED DURING 1997
** ACTIVE DUTY TRAINING
*** DECEASED

FOREWARD

The Annual Tropical Cyclone Report is prepared by the staff of the Joint Typhoon Warning Center (JTWC), a combined Air Force/Navy organization. In 1997, the period covered by this report, JTWC operated under the command of the Commanding Officer, U.S. Naval Pacific Meteorology and Oceanography Center West (NAVPACMETOCCEN WEST)/Joint Typhoon Warning Center, Guam. As this is being written, however, in January of 1999, JTWC has just completed transition from Guam to Pearl Harbor, Hawaii, as mandated by the 1995 Base Realignment And Closing Commission (BRAC). JTWC now operates under the command of the Commanding Officer, U.S. Naval Pacific Meteorology and Oceanography Center (NAVPACMETOCCEN)/Joint Typhoon Warning Center, Pearl Harbor, Hawaii. This move brings to an end the forty year history of JTWC on Guam, which began on 01 May 1959 when the U.S. Commander-in-Chief Pacific (USCINCPAC) forces directed that a single tropical cyclone warning center be established for the western North Pacific region. However, our customers can anticipate the same dedicated support they have come to expect from our new locations. The operations of JTWC are guided by USCINCPAC Instruction 3140.1W.

The mission of JTWC is multifaceted and includes:

1. Continuous monitoring of all tropical weather activity in the Northern and Southern Hemispheres, from 180 east longitude westward to the east coast of Africa, and the prompt issuance of appropriate advisories and alerts when tropical cyclone development is anticipated.
2. Issuance of warnings on all significant tropical cyclones in the above area of responsibility.
3. Determination of requirements for tropical cyclone reconnaissance and assignment of appropriate priorities.
4. Post-storm analysis of significant tropical cyclones occurring within the western North Pacific and North Indian Oceans.
5. Cooperation with the Naval Research Laboratory, Monterey, California on evaluation of tropical cyclone models and forecast aids, and the development of new techniques to support forecast requirements.

Special thanks to: the men and women of the Alternate Joint Typhoon Warning Center (AJTWC) for standing in for JTWC as needed (AJTWC will move to Yokosuka, Japan, as part of the BRAC relocation); Fleet Numerical Meteorology and Oceanography Center (FNMOC) for their operational support; the Naval Research Laboratory for its dedicated research; the Air Force Weather Agency (AFWA) and National Oceanic and Atmospheric Administration (NOAA) National Environmental Satellite, Data, and Information Service (NESDIS) for satellite support; the 36th Communications Squadron's Defense Meteorological Satellite Program (DMSP) Site 18 at Nimitz Hill, Guam (which will soon move to Andersen Air

Force Base as part of BRAC), and the Operations and Equipment Support departments of both NAVPACMETOCCEN WEST, Guam and NAVPACMETOCCEN Pearl Harbor, Hawaii, for their high quality support; all the men and women of the ships and facilities ashore throughout the JTWC area of responsibility (AOR), and especially on Guam, who took the observations that became the basis for our analyses, CDR (Ret) Lester E. Carr III and Dr. Russell L. Elsberry for their continuing efforts at the Naval Postgraduate School and their further work on the Systematic and Integrated Approach to Tropical Cyclone Track Forecasting; Dr. Robert F. Abbey Jr and the Office of Naval Research for their support to the University of Guam (UOG) for the Research Liaisons to JTWC; the UOG Research Liaisons for their contributions to this publication; Dr. Mark A. Lander for his training efforts, suggestions and valuable insights, and Mr. Charles P. Guard for his support and data collection efforts; Dr. Jeff D. Hawkins, Chris S. Veldon, Samuel Chang and Roger Weldon for their continuing efforts to exploit remote sensing technologies in new and innovative ways; Mr. Charles R. "Buck" Sampson, Sally A. Calvert (who sadly left the team in 1998 to pursue other opportunities-she will be missed), Rosemary Lande, Mike D. Frost, Mugur Georgescu, Daren H. Grant, and Ann J. Schrader for their support and continued development of the Automated Tropical Cyclone Forecasting (ATCF) system; SRA Ryan Eibling of the JTWC staff, who used his advanced knowledge of software development to solve tough automation problems; and, LCDR Kenneth Malmquist, LCDR Margret Smith, LT Kim Boyer, Frank H. Wells, Mark A. Lander, Charles P. Guard, AG2 Keyia Hall, and AG2 Bryan Hong for their editing, desktop publishing, web publishing, and computer graphics, without which this document would not have been possible.

EXECUTIVE SUMMARY

The Joint Typhoon Warning Center (JTWC), Guam worked very hard in 1997 to improve its data management processes. Our goal is to get the raw environmental data in-house, processed, and then displayed, in order to create finished products - warning, alert, advisory, prognostic reasoning - out (of house) to you, the user, faster, more efficiently, and with supporting, easily understood graphics. The use of the NPMOCW/JTWC Guam web site has revolutionized our ability to generate products that can be rapidly accessed. The growth of the JTWC home page has been nothing less than phenomenal -- as Super Typhoon Paka approached Guam, the web site received 107,000 "hits" in a 24-hour period. We realize this doesn't replace our primary distribution methods, but significantly augments our current capability.

We've been busy this year, but so have the tropical cyclones (TCs). In the Western North Pacific, thirty-three significant TCs occurred, two above the 37-year average of 31. Of these, 11 became super typhoons, which was a record - the 37-year average is four with seven being the previous maximum. Therefore, 1997 became the year of the super typhoon. Two of these super typhoons - Oliwa and Paka - were "borrowed" from the Central Pacific. In September, Oliwa passed through the northern Marianas and recurved over Japan, which was unusual for a Central Pacific cyclone. In December, Paka brushed by Kwajalein and Majuro before clobbering Guam.

Mean forecast track errors in 1997 continued to fall to lower values: 93 nm, 164 nm, and 247 nm at 24, 48, and 72 hours respectively - a new record. We are proud of these numbers, especially in light of continual manning shortages. However, these values are still a long way from the goals stated by COMNAVFOR JAPAN, Admiral McKay, at the 1984 Annual Tropical Cyclone Conference of 50, 100, and 150 nm. It is sobering to note a few of this year's recurving track forecasts still had individual forecast errors in excess of 1000 nm. The bottom line is that there's still a lot which needs to be accomplished, particularly in the areas of numerical guidance, remote sensing, basic research and tropical cyclone structure and structure change.

For the North Indian Ocean, four significant TCs occurred - one less than the 21-year average of five. The Southern Hemisphere TC-year (1 July 1996 - 30 June 1997) had a bumper crop of 38, which exceeds the record of 35 set in 1985, and is 11 more than the 15-year average of 27. Of interest, none of these TCs in the North Indian Ocean and Southern Hemisphere reached super typhoon intensity.

The total number of JTWC warnings provides a measure of our workload. During 1997 there were 950 in the Western North Pacific (15-year average 712), 56 in the North Indian Ocean (15-year average 58), and 566 Southern Hemisphere (15-year average 263). Adequate JTWC manning, resources, and communications are critical to surmounting the challenge presented by years with above average workload.

Looking ahead, we're trying to speed up the delivery of our post-analysis products to you by providing them in electronic form: HTML and PDF. This product will be available via the World Wide Web and compact diskette (CD). For instance, the document that follows was assembled in HTML for the Guam web site. It is the Tropical Cyclone Summary, which provides basic statistical data for the TC-year in

review. This document will be expanded with narratives, images, and climatology as they are developed, to become in final form Chapter 3 of the 1997 Annual Tropical Cyclone Report (ATCR). In this way, ATCR chapters can be built and made available on the Internet as they are finished, without the delays of having to wait for the final complete manuscript to be printed or "burned" into a CD. Our intent in providing a PDF version of the final document along with the HTML format is to allow you to locally produce a suitable printed version if desired. However, we realize that there will be a few users out there without the capability to do this, and we will be glad to print a copy for you on request.

I would be remiss if I didn't stop to thank the members of the JTWC "team", from the researchers providing us an ever increasing amount of precious weather data and new forecast techniques, to the 32 Air Force and Navy civilian and military personnel who have tirelessly worked overtime without complaint, and for the outstanding performance achieved this past year, even though we faced many difficult situations.

To the ultimate end user of our products, the operational units both ashore and afloat, we pledge to keep our eyes and ears open as to what types of products you want, when you want it, and how you want it delivered. We realize without your support we wouldn't have a reason for existence.

In closing, there will be plenty going on and more changes planned for 1998. However at JTWC we will never lose sight of the fact that, "the forecast is our only product."

LCOL Mark Andrews
Director, JTWC
Jan,1998

TABLE OF CONTENTS

North Indian Ocean Tropical Cyclones

1. OPERATIONAL PROCEDURES

1.1 GENERAL

The Joint Typhoon Warning Center (JTWC) provides a variety of routine products and services to the organizations within its area of responsibility (AOR) as prescribed by USCINCPACINST 3140.1W. JTWC issues the following products:

1.1.1 SIGNIFICANT TROPICAL WEATHER ADVISORY — Issued daily, or more frequently as needed, to describe all tropical disturbances and their potential for further development during the advisory period. Separate bulletins are issued for the Western Pacific and the Indian Ocean.

1.1.2 TROPICAL CYCLONE FORMATION ALERT — Defines a specific area when synoptic, satellite, or other germane data indicate development of a significant tropical cyclone (TC) is likely within 24 hours.

1.1.3 TROPICAL CYCLONE/TROPICAL DEPRESSION WARNING — Issued periodically throughout each day to provide forecasts of position, intensity, and wind distribution for TCs in JTWC's AOR. The tropical depression warning was dropped in 1998 as a separate product. Post-1997 tropical depressions in the western North Pacific receive regular tropical cyclone warnings.

1.1.4 PROGNOSTIC REASONING MESSAGE — Issued in conjunction with warnings for tropical cyclones, that have potential to reach tropical storm or typhoon strength in the western North Pacific. This discusses the rationale for the content of the specific JTWC warning.

1.1.5 PRODUCT CHANGES — The contents and availability of the above JTWC products are set forth in USCINCPACINST 3140.1W. Changes to USCINCPACINST 3140.1W as well as JTWC products and services are proposed and discussed at the annual U.S. Pacific Command (PACOM) Tropical Cyclone Conference.

1.2 DATA SOURCES

1.2.1. COMPUTER PRODUCTS

Numerical and statistical guidance are available from the USN Fleet Numerical Meteorology and Oceanography Center (FLENUMETOCCEN, or FNMOC) at Monterey, California. FNMOC supplies JTWC with analyses and prognoses from the Navy Operational Global Atmospheric Prediction System (NOGAPS) via the NIPRNET packet switched network (Internet gateway). NOGAPS products that are routinely disseminated to JTWC include: surface pressure and winds, upper-air winds, deep-layer-mean winds, geopotential height and height change, and sea-surface temperature. Also, additional various atmospheric components at all standard levels are available. These products are valid for the 00Z and 12Z synoptic times.

Along with selected products from the (U.S.) National Center for Environmental Prediction (NCEP), the European Centre for Medium-Range Weather Forecasts (ECMWF), and the Japanese Meteorological Agency (JMA) are received as electronic files via networked computers, and by computer modem connections on government and commercial telephone lines as a backup method for the network.

1.2.2 CONVENTIONAL DATA —

These data sets are comprised of land and shipboard surface observations, enroute meteorological observations from commercial and military aircraft (AIREPS) recorded within six hours of synoptic times, and cloud-motion winds derived from satellite data. This conventional data is computer plotted, and manually analyzed in the tropics for the surface/gradient and 200-mb levels. These analyses are prepared twice daily using 00Z and 12Z synoptic data.

1.2.3 SATELLITE RECONNAISSANCE—

Meteorological satellite imagery recorded at USAF/USN ground sites and U.S. Naval vessels supply day and night coverage in JTWC's AOR. Interpretation of these satellite data provides TC positions and estimates of current and forecast intensities (Dvorak 1984). The USAF tactical satellite sites and Air Force Weather Agency (AFWA) currently receive and analyze Special Sensor Microwave/Imager (SSM/I) data to provide TC locations and estimates of 35-kt (18-m/sec) wind radii when the low-level center is obscured by higher clouds

The Defense Meteorological Satellite Program (DMSP), National Oceanographic and Atmospheric Administration (NOAA), (Japanese) Geostationary Meteorological Satellite (GMS), and (European Geostationary) Meteorological Satellite (METEOSAT) provide the foundation for reconnaissance. Use of satellite reconnaissance is discussed further in the Section 2.3 Satellite Reconnaissance Summary.

In addition to imagery, scatterometry data from the European Remote Sensing (ERS)-2 satellite provide valuable insight as to the distribution of low-level winds around TCs. When remotely sensed data of this quality became available, JTWC immediately began using it to supplement other available data. Evolution of algorithms and subsequent display of scatterometer data has occurred rapidly over the past few years and JTWC has been fortunate to have access to this leading edge technology.

JTWC retrieves scatterometry data on a routine basis from web sites on the NIPRNET/Internet maintained by FNMOC, the Naval Oceanographic Office (NAVOCEANO), and the Oceanic Sciences Branch of NOAA. The scatterometry data available at these sites help to define TC position and low-level structure. Heavy-rain contamination near a TC's center limits the usefulness of intensity estimation to tropical storm strength and below. JTWC also uses scatterometry data to refine the twice daily manual analyses of the surface/gradient-level wind flow and atmospheric structure.

1.2.4 RADAR RECONNAISSANCE

Land-based radar observations are used to position TCs. Once a well-defined TC moves within range of land-based radar sites, radar reports are invaluable for determination of position, movement, and, in the case of Doppler radar, storm structure and wind information. JTWC's use of radar reports during 1997 is discussed in Section 2.4 Radar Reconnaissance Summary.

1.2.5. AIRCRAFT RECONNAISSANCE — Until the summer of 1987, dedicated aircraft reconnaissance was used routinely to locate and determine the wind structure of TCs. Now, aircraft fixes are only rarely available from transiting jet aircraft or from weather-reconnaissance aircraft involved in research missions. No aircraft fixes were available in 1997.

1.2.6. DRIFTING METEOROLOGICAL BUOYS — In 1989, the Commander, Naval Meteorology and Oceanography Command (COMNAVMETOCCOM) put the Integrated Drifting Buoy Plan into action to meet USCINCPACFLT requirements that included TC warning support. In 1997, 30 drifting buoys were deployed in the western North Pacific by a NAVOCEANO-contracted C-130 aircraft. Of the 30 buoys, 24 were Compact Meteorological and Oceanographic Drifters (CMOD) with temperature and pressure sensors and six were Wind Speed and Direction (WSD) with wind speed and direction, temperature and pressure. The buoys were evenly split by type over two deployments — the first in June, followed by the second in September. The purpose of the split deployment was to overlap the expected three-month lifespans of the CMOD buoys in order to provide continuous coverage during the peak of the western North Pacific TC season.

1.2.7. AUTOMATED METEOROLOGICAL OBSERVING STATIONS (AMOS) — Through a cooperative effort between COMNAVMETOCCOM, the Department of the Interior, and NOAA/NWS to increase data availability for tropical analysis and forecasting, a network of 20 AMOS stations is being installed in the Micronesian Islands (see Tables 1-1 and 1-2). Since September of 1991, in most of the sites, the capability to transmit data via Service ARGOS and NOAA polar-orbiting satellites has been available as a backup to regular data transmission to the Geostationary Operational Environmental Satellite (GOES) West and, more recently for sites to the west of Guam, to the GMS. Upgrades to existing sites are being accomplished as opportunities arise. JTWC receives data from the AMOS sites via the Automated Weather Network (AWN) under the KWBC bulletin headers SMPW01, SIPW01 and SNPW01 (SXMY10 for Tinian and Rota).

1.3. TELECOMMUNICATIONS

Telecommunications support for the Naval Pacific Meteorological and Oceanography Center West (NAVPACMETOCCEN WEST or NPMOCW)/Joint Typhoon Warning Center is provided by the Naval Computer And Telecommunications Station (NCTS), Guam, and their Base Communications Department. The telecommunications link to NCTS is a fiber-optic cable which incorporates several stand-by redundancy features. Connectivity includes "switched" secure and non-secure voice, facsimile, data services, and dedicated audio and digital circuits to NCTS. Telecommunications connectivity and the basic system configurations which are available to JTWC follow.

Table 1-1 Automated Meteorological Observing Stations Summary

Site	Location		Call Sign	ID#	System	Installed	Upgrade/Survey
Rota	14.2°N	145.2°E	15D16448	91221	ARC	1987	----
Enewetak	11.4°N	162.3°E	ENIP2	91251	C-MAN/ARGOS	1989	1998
Ujae*	08.9°N	165.7°E	UJAP2	91365	C-MAN	1989	1999
Pagan	18.1°N	145.8°E	PAGP2	91222	C-MAN/ARGOS	1990	1998
Kosrae	05.4°N	163.0°E	KOSP2	91355	C-MAN/ARGOS	1990	1998
Mili	06.1°N	172.1°E	MILP2	91377	C-MAN	1990	1999
Oroluk	07.6°N	155.2°E	ORKP2	91343	C-MAN	1991	----
Pingelap	06.2°N	160.7°E	PIGP2	91352	C-MAN/ARGOS	1991	1999
Ulul	08.4°N	149.4°E	NA	91328	C-MAN/ARGOS	1992	1999
Tinian	15.0°N	145.6°E	15D151D2	91231	ARC	1992	----
Satawan	06.1°N	153.8°E	SATP2	91338	C-MAN/ARGOS	1993	----
Ulithi	09.9°N	139.7°E	NA	91204	C-MAN/ARGOS	1995	1999
Ngulu	08.3°N	137.5°E	NA	91411	C-MAN/ARGOS	1995	----
Ebon	04.6°N	168.7°E	NA	91442	C-MAN/ARGOS	1996	----
Maloelap	08.7°N	171.2°E	NA	91374	C-MAN/ARGOS	1996	----

* Ujae site was destroyed on 18 November 1992 by Super Typhoon Gay; requires survey.

ARC = Automated Remote Collection system (via GOES West)
C-MAN = Coastal-Marine Automated Network (via GOES West or GMS)
ARGOS = Service ARGOS data collection (via NOAA's TIROS-N)

Table 1-2 Proposed Automated Meteorological Observing Stations

Site	Location	
Pulusuk	06.5°N	149.5°E
Faraulep	08.6°N	144.6°E
Eauripik	06.7°N	143.0°E
Utirik	11.2°N	169.7°E
Satawal	07.4°N	147.0°E
Sorol	08.1°N	140.4°E
Nukuoro	03.9°N	155.0°E
Alternate Sites	**Location**	
Sonsorol	05.3°N	132.2°E
Toangi	14.6°N	169.0°E
Wotho	10.2°N	166.0°E
Bikini	11.5°N	165.6°E

1.3.1 AUTOMATED DIGITAL NETWORK (AUTODIN)

— AUTODIN currently supports the message requirements for JTWC, with the process of converting to the new Defense Messaging System (DMS) in the near future. A personal computer (PC) system running the " Gateguard" software application provides transmit and receive message capabilities. Secure connectivity is provided by a dial-up Secure Telephone Unit-III path with NCTS. The Gateguard system is used to access the AUTODIN/DMS network for dissemination of warnings, alerts, related bulletins, and messages to Department of Defense (DoD) and U.S. Government installations. Message recipients can retransmit these messages for further dissemination using the Navy Fleet Broadcasts, Coast Guard continuous wave (CW) Morse code, and text-to-voice broadcasts. AUTODIN/DMS messages are also relayed via commercial telecommunications routes for delivery to non-DoD users. Inbound message traffic for JTWC is received via AUTODIN/DMS addressed to NAVPACMETOCCEN WEST GU// JTWC//.

1.3.2 AUTOMATED WEATHER NETWORK (AWN)

— The AWN provides weather data over the Pacific Meteorological Data System (PACMEDS). JTWC uses two PC systems which run the Windows based WINDS/AWNCOM software application package to interface with a dedicated 1.2 kb/sec (kilobits per second) PACMEDS circuit. These PC systems provide JTWC the PACMEDS transmit and receive capabilities needed to effectively store and manipulate large volumes of alphanumeric meteorological data available from reporting stations throughout JTWC's AOR. The AWN also allows JTWC access to data which are available on the Global Telecommunications System (GTS). JTWC's AWN station identifier is PGTW.

1.3.3 AUTOMATED WEATHER DISTRIBUTION SYSTEM (AWDS)

— The AWDS consists of two dual-monitor workstations which communicate with a UNIX based communications/data server via a private Local Area Network (LAN). The server's data connectivity is provided by two dedicated long-haul data circuits. The AWDS provides JTWC with additional transmit and receive access to alphanumeric AWN data at Tinker AFB using a dedicated 9.6 kb/sec circuit. Access to satellite imagery and computer graphics from Air Force Weather Agency (AFWA) is provided by another dedicated 9.6 kb/sec circuit.

The current configuration of AWDS was upgraded in 1996 to include improved workstation performance, and integration into NPMOCW's LAN backbone, this has access to the Defense Information Systems Network's (DISN), Non-secure Internet Protocol (IP) Router Network's (NIPRNET) Wide Area Network (WAN). The LAN and WAN connectivity allow JTWC to send and receive products among other AWDS.

1.3.4 DEFENSE SWITCHED NETWORK (DSN)

— DSN is a worldwide, general purpose, switched telecommunications network for the DoD. The network provides a voice and data link by which JTWC communicates

TC information with DoD installations and civilian agencies. JTWC utilizes DSN for all switched voice and data. The DSN and commercial telephone numbers for JTWC are 349-5240 or 349-4224. The commercial area code is 671 and the DSN Pacific area code is 315.

After January 1, 1999, JTWC will be operating from Pearl Harbor, Hawaii. The new telephone number will be 474-2320, with a commercial area code of 808.

1.3.5. NIPRNET—The TCP/IP based NIPRNET network has replaced the older MILNET computer communications network, providing a much needed boost in throughput speed for the transfer of large data and image files. NIPRNET has links or gateways to the non-DoD Internet, allowing data to be pulled and pushed from Internet based World Wide Web (WWW) and File Transfer Protocol (FTP) servers. This ability has enhanced JTWC's ability to exchange data with the Internet-based research community.

The JTWC's products are currently available to users of the DoD Secret IP Router Network (SIPRNET) using WWW browser software. The JTWC's unclassified NIPRNET/Internet web site address is http://www.npmocw.navy.mil. After 1 January 1999, this will change to http://www.npmoc.navy.mil.

1.3.6. TELEPHONE FACSIMILE — TELEFAX provides the capability to rapidly scan and transmit, or receive, documents over commercial telephone lines or DSN. TELEFAX is used to disseminate TC advisories and warnings to key agencies on Guam and, in special situations, to DoD, other U.S. Government agencies, and the other Micronesian Islands.

1.4. DATA DISPLAYS

1.4.1. AUTOMATED TROPICAL CYCLONE FORECAST (ATCF) SYSTEM — The ATCF is an advanced software program that assists the Typhoon Duty Officer (TDO) in the preparation, formatting, and dissemination of JTWC's products. It cuts message preparation time and reduces the number of corrections. The ATCF automatically displays the working and objective best tracks; forecasts of track, intensity, and wind distribution; information from computer generated forecast aids, and products from other agencies. It also computes the myriad of statistics calculated by JTWC.

1.4.2. AUTOMATED WEATHER DISTRIBUTION SYSTEM (AWDS) AWDS consists of two dual-monitor workstations which communicate with a UNIX based server. The server has connectivity to the alphanumeric AWN and through a dedicated 9.6 kb/sec circuit to imagery and graphics from the Air Force Weather Agency (AFWA).

1.4.3. NAVAL OCEANOGRAPHIC DATA DISTRIBUTION SYSTEM (NODDS) — NODDS is a PC-based system that uses a telephone modem to download, store and display both environmental and satellite products from FLENUMETOCCEN.

1.4.4. NAVAL SATELLITE DISPLAY

SYSTEM—GEOSTATIONARY
NSDS-G is NAVPACMETOCCEN WEST's primary geostationary imagery processing and display system is the NSDS-G. It can be used to process high resolution geostationary imagery for analysis of TC positions and intensity estimates for the Western Pacific Ocean. It also acts as a secondary system should the Meteorological Imagery, Data Display, and Analysis System (MIDDAS - see Chapter 2) and Mark IVB (see Chapter 2 also) fail.

1.4.5. Meteorology and Oceanography Integrated Data Display System (MIDDS)
MIDDS is a client-server based system designed to ingest, process, display and disseminate METOC data. This Web Information Service includes satellite imagery, digital and analog facsimile, alphanumeric, gridded fields, radar, lightning, and specialized applications.

1.4.6. SATELLITE WEATHER DATA IMAGING SYSTEM (SWDIS) — The SWDIS (also known as the M-1000) is a PC-based system that interfaces with the LAN to retrieve, store, and display various products, such as geostationary-satellite imagery from other sites at Rota (Spain), Pearl Harbor (Hawaii), or Norfolk (Virginia), scatterometer data from NAVOCEANO and NOAA, and composites of global geostationary-satellite imagery from the Internet. The SWDIS has proven instrumental in providing METEOSAT reduced-resolution coverage of TCs over the western Indian Ocean as well as long time-series animation of water-vapor imagery.

1.4.7 Joint METOC Viewer (JMV) — JMV is a powerful, fast, and easy-to-use tool that allows JTWC to retrieve, display, annotate and save meteorological and oceanographic data. The JMV uses World Wide Web browsers to access data from various meteorological centers worldwide.

1.5. ANALYSES

The JTWC TDO routinely performs manual streamline analyses of composite surface/gradient-level (3000 ft (914 m)) and upper-tropospheric (centered on the 200-mb level) data for 00Z and 12Z daily. Computer analyses of the surface, 925-, 850-, 700-, 500-, 400-, and 200-mb levels, deep-layer-mean winds, frontal boundary depiction, 1000-200 mb/400-200 mb/and 700-400-mb wind shear, 500-mb and 700-mb 24-hour height change, as well as a variety of other meteorological displays come from the 00Z and 12Z FLENUMETOCCEN data bases. Additional sectional charts at intermediate synoptic times and auxiliary charts, such as station-time plot diagrams, time-height cross-section charts and pressure-change charts, are analyzed during periods of significant TC activity.

1.6. FORECAST PROCEDURES

This section first introduces the Systematic and Integrated Approach to TC Track Forecasting by Carr and Elsberry (1994), referred to hereafter as the "Systematic Approach" and then provides JTWC's basic approach to track, intensity and wind radii forecasting.

1.6.1. THE SYSTEMATIC APPROACH — JTWC began applying the Systematic Approach (Figure 1.1) in 1994. The basic premise of this approach is that forecasters can improve upon dynamical track forecasts [guidance] generated by numerical models and other objective guidance if the forecasters are equipped with:

1) a meteorological knowledge base (Carr et al., 1997) of conceptual models that organizes a wide array of scenarios into a relatively few recurring, dynamically-related situations; and
2) a knowledge base of numerical model tropical cyclone- forecast traits and objective-aid traits within the different recurring situations that are organized around the meteorological knowledge base.

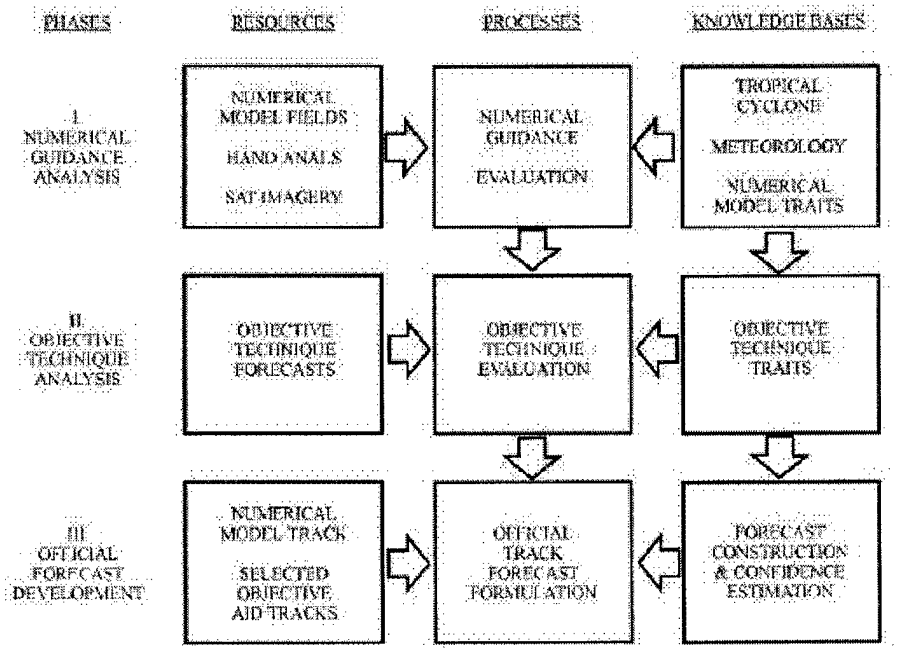

Figure 1-1 Systematic Approach Flowchart

1.6.1.1. General Concepts — Track, intensity, and size components of a TC forecast are dynamically interdependent.

1) TC motion affects intensity and how a TC intensifies can affect its motion.
2) TC size affects propagation relative to environmental steering. A large TC may significantly modify its environment. Thus, the present size of a TC and any subsequent changes in size can affect motion.
3) TC size may affect intensity indirectly through changes induced on TC motion.

1.6.1.2. Key Motion Concepts — TC motion results from a variety of causes.

1) **Environmental Steering** — To a first approximation, the TC vortex is advected by the winds of the large-scale environmental flow (i.e., the TC moves as a "cork in the stream").
2) **TC Propagation** — The motion of TCs usually departs in a minor, but not insignificant way from the large scale environmental steering vector.
3) **TC-Environment Interaction** — In certain situations, the circulation of the TC interacts with the environment in such a way as to significantly alter the structure of the environment, and thus modifies the steering vector that is the first-order effect on the motion of the TC.

1.6.1.3. Knowledge Base Framework

1.6.1.3.1. Environment Structure —Structure is classified in terms of a large-scale synoptic PATTERN and two or more synoptic REGIONS within the pattern that tend to produce characteristic directions and speeds of steering flow for a TC located therein. Five patterns with ten associated regions are recognized by the Systematic Approach. JTWC notes that not all TCs fit "neatly" into these patterns/regions at all times and that hybrids and transitions between patterns occur. These patterns/regions are briefly described below.

1.6.1.3.1.1. Patterns — There are five primary patterns:

STANDARD (S) (Figure 1.2)

1) Most frequently occurring pattern in the WNP; and
2) key feature is roughly zonally-oriented subtropical ridge (STR) anticyclones.

POLEWARD (P) (Figure 1.3)

1) Second highest frequency of occurrence in the WNP;
2) key feature is a ridge (anticyclone) that extends from the STR deep into the tropics and interrupts the tropical easterlies;
3) usually has SW-to-NE axis orientation; and,
4) usually produces strong poleward steering on its west and poleward side.

GYRE (G) (Figure 1.4)

1) Only occurs during June-November period;
2) key feature is a particularly large and deep monsoonal circulation (thus, "monsoon gyre"); and,
3) usually situated between a zonally-oriented STR anticyclone to the NW and a meridionally-oriented anticyclone on its eastern periphery.

MULTIPLE (M) (Figure 1.5)

1) Key feature is more than one TC with a large break in the STR in the vicinity of the two TCs;
2) the TCs are oriented approximately east-west (i.e., zonally-oriented TCs);
3) the TCs must be far enough apart to preclude significant mutual advection, but close enough to preclude the development of ridging

between them (typically greater than 10°, but less than about 25°);

4) the average latitude of the two TCs must be sufficiently close to the latitude of the STR axis (no more than about 10° equatorward or 5° poleward) so that regions of poleward/equatorward flow are established, which affect TC motion and intensification; and,
5) there are three subsets of the "M" pattern which describe varying degrees of interaction between the two cyclones.

HIGH AMPLITUDE (H) (Figure 1.6)

A newly identified pattern for the Southern Hemisphere (Carr et al., 1997). The key feature is a mid-latitude trough which penetrates very deeply into the tropics, almost to the equator. A combination of this trough and the subtropical ridge circulation to its east can produce long, southeastward oriented tracks. The ridge circulation to the west completes the pattern, by defining "Ridge Equatorward" and "Ridge Poleward" regions. A small area of "Equatorward Westerlies" is also defined.

1.6.1.3.1.2. Regions — There are ten primary regions associated with the four patterns:

EQUATORIAL WESTERLIES (EW) — The area of equatorial westerlies equatorward of the monsoon trough axis.

DOMINANT RIDGE (DR) — The area of tropical easterlies equatorward of the STR axis, except near any break in the STR.

WEAKENED RIDGE (WR) — The area of weaker southeasterly winds in the vicinity of a break in the STR.

MIDLATITUDE WESTERLIES (MW) — The area of eastward and poleward steering extending east from a break in the STR.

POLEWARD-ORIENTED (PO) -- The area of poleward steering west of the ridge feature in the "P" and "G" Patterns

POLEWARD FLOW (PF) — created in the vicinity of the eastern TC of a "M" Pattern as a result of the gradient between the western TC and the STR circulation to the east.

RIDGE POLEWARD (RP) — The poleward flow region of the HA pattern, where steering is provided by the western side of the anti-cyclone.

RIDGE EQUATORWARD (RE) — The equatorward flow region of the HA pattern, where steering is provided by the eastern side of the anti-cyclone.

TROUGH POLEWARD (TP) — The very long poleward flow region of the HA pattern, where steering is provided by the deeply penetrating mid-latitude trough.

EQUATORWARD FLOW (EF) — created in the region of the western TC of a "M" Pattern as a result of the gradient between the eastern TC and the STR circulation to the west.

1.6.1.3.1.3. Nomenclature — JTWC makes routine use of the aforementioned Patterns and Regions of the Systematic Approach. In order to quickly transcribe this information, a short-hand contraction standard has developed. By utilizing the one-letter contraction of a pattern and the two-letter contraction of an associated region (e.g., S/DR), an effective method of quickly and accurately describing Systematic Approach concepts in writing exists.

1.6.1.3.2. TC Structure — TC structure consists of an INTENSITY that is based on the maximum wind speed near the center of the TC, and a SIZE that is based on some measure of the extent of the cyclonic wind component in the lower atmosphere. TC intensity is related to steering level and TC size is related to propagation and environment modification.

1.6.1.3.3. Transitional Mechanisms — These mechanisms act to change the structure of the environment (pattern/region) and fall into two categories:

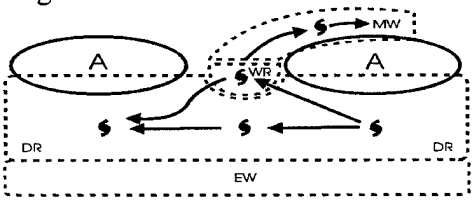

Figure 1-2 Standard Pattern

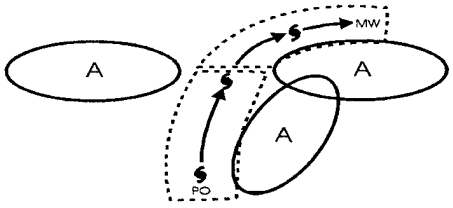

Figure 1-3 Poleward Pattern

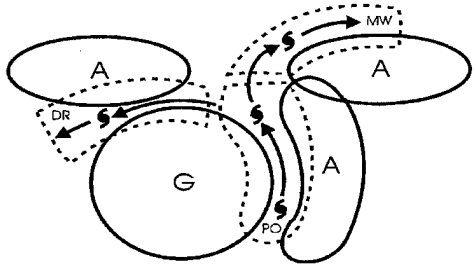

Figure 1-4 Gyre Pattern

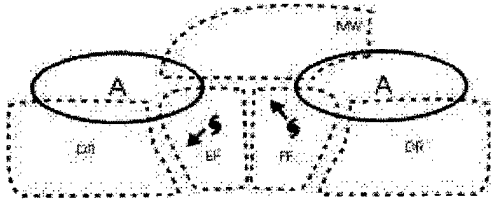

Figure 1-5 Multiple TC Pattern

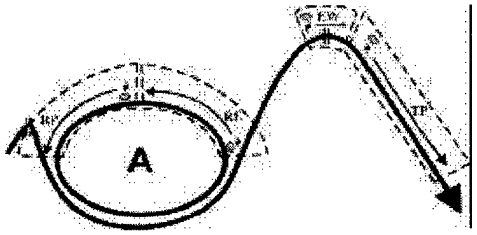

Figure 1-6 High Amplitude Pattern

LEGEND FOR FIGURES:

→ = CHARACTERISTIC TC TRACK	EF = EQUATORIAL
-- = REGIONAL BOUNDARY	PF = POLEWARD FLOW
DR = DOMINANT RIDGE	PO = POLEWARD ORIENTED
A = ANTICYCLONE	EW = EQUATORIAL WESTERLIES
MW = MIDLATITUDE WESTERLIES	
G = GYRE	
WR = WEAKENED RIDGE	

1)TC-Environment Transformations. The TC and the environment may interact, resulting in a change in environmental structure (pattern/region) and thus the direction/speed of the associated steering flow. In addition, TC-environment transformations may result in a change to TC structure. Listed below are recognized TC-environment transformations (refer to Carr and Elsberry (1994) for a more thorough treatment):

- Beta Effect Propagation

- Vertical Wind Shear
- Ridge Modification by TC
- Monsoon Gyre-TC Interaction
- TC Interaction (Direct (DTI), Semi-direct (STI), and Indirect (ITI)) (Figure 1.7)

2) Environmental Effects. These also result in changes to the structure of the environment (pattern/region) surrounding the TC, but do not depend on, are or largely independent of, the presence of the TC. Recognized environmental effects are listed below (refer to Carr and Elsberry (1994) for thorough treatment):

- Advection by Environment
- Monsoon Gyre Formation
- Monsoon Gyre Dissipation

Subtropical Ridge Modulation (by midlatitude troughs)

TC movement, intensification, and size evolution are closely linked, therefore, an "ideal TC forecast approach" may be defined as a fully integrated solution for the time evolution of the 3-dimensional three partial representations of the total TC circulation. TC track, intensity and size forecasts are then to be considered three partial representations of the total forecast solution.

1.6.2. BASIC APPROACH TO FORECASTING

1.6.2.1. Initial Positioning — The warning position is the best estimate of the center of the surface circulation at synoptic time. It is estimated from an analysis of all fix information received from one hour before to one and one-half hours after that synoptic time. The analysis is aided by a computer-generated objective best-track scheme that weights fix information based on its statistical accuracy. The TDO includes synoptic observations and other information to adjust the position, testing consistency with the past direction, speed of movement and the influence of the different scales of motions. If the fix data are not available due to reconnaissance-platform malfunction or communication problems, or are considered unrepresentative, synoptic data and/or extrapolation from previous fixes are used.

1.6.2.2. Track Forecasting — In preparing the JTWC official forecast, the TDO evaluates a wide variety of information and employs Systematic Approach methodology. JTWC uses a standardized, three-phase TC motion-forecasting process to improve forecast accuracy and forecast-to-forecast consistency. Figure 1.1 depicts the three phases and inputs to the Systematic Approach outlined below.

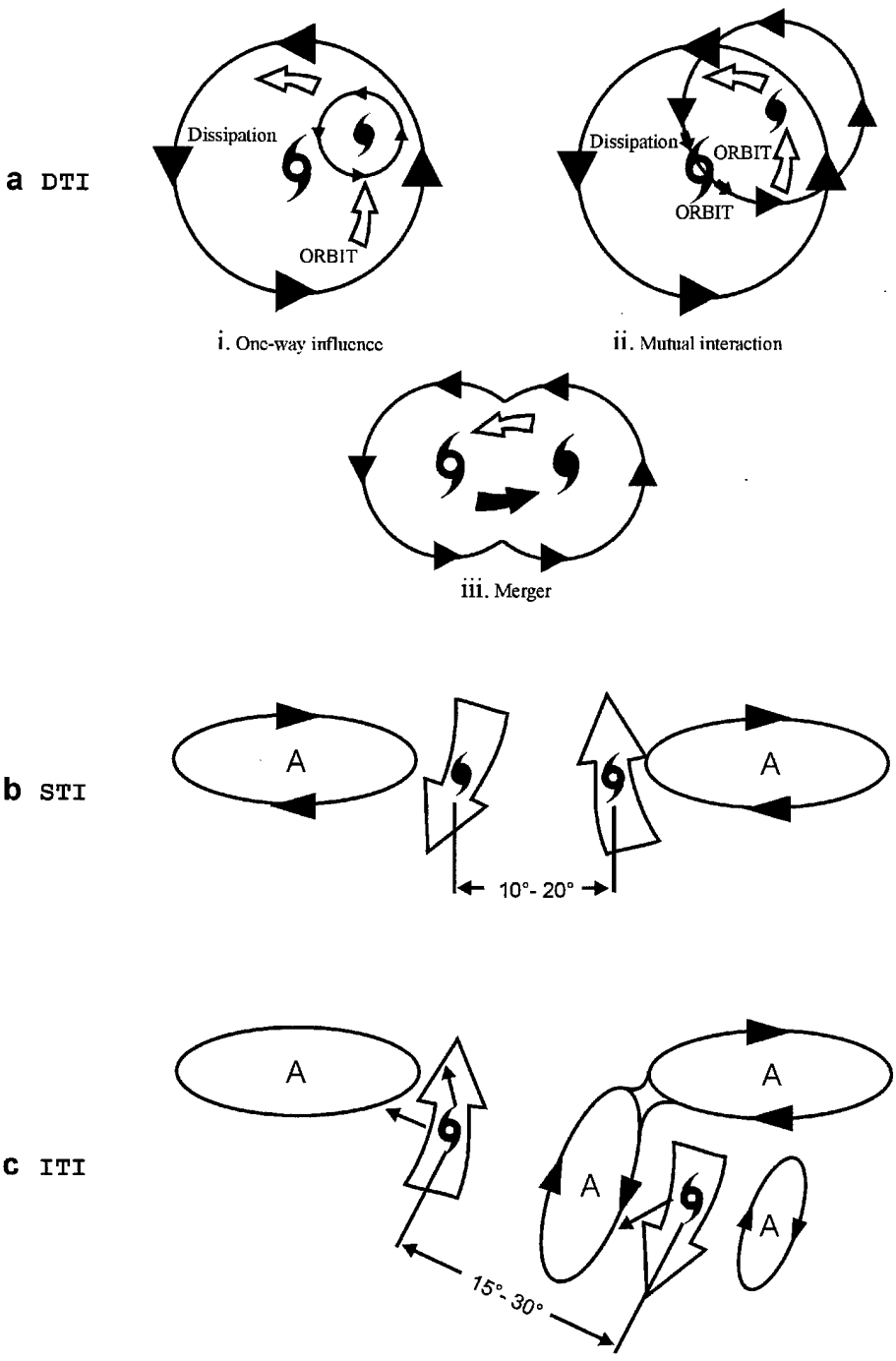

Figure 1-7 Tropical Cyclone Interaction: (a) Direct TC Interaction (DTI) is composed of three types — (i) one way influence, (ii) mutual interaction, and (iii) merger, (b) Semi-Direct TC Interaction (STI), and (c) Indirect TC Interaction (ITI).

1.6.2.2.1 Numerical Guidance Analysis Phase — NOGAPS analyses and prognoses at various levels are evaluated for position, development, and relevant synoptic features such as:

1) STR circulations;
2) midlatitude short/long-wave troughs and associated weaknesses in the STR monsoon surges;
3) influences of cyclonic cells in the tropical upper-tropospheric trough (TUTT);
4) other TCs;
5) the distribution of sea-surface temperature.

The TDO determines into which pattern/region the TC falls, and what environmental influences and transitional mechanisms are indicated in the model fields. The process outlined above permits the TDO to develop an initial impression of the environmental steering influences to which the TC is, and will be, subjected to as depicted by NOGAPS. The NOGAPS analyses are then compared to the manually-plotted and analyzed charts prepared by the Typhoon Duty Assistant (TDA) and TDO, and to the latest satellite imagery, in order to determine how well the NOGAPS-initialization process has conformed to the available synoptic data, and how well the resultant analysis fields agree with the synoptic situation inferred from the imagery. Finally, the TDO compares both the computer- and manually-analyzed charts to monthly climatology in order to make a preliminary determination of to what degree the TC is, and will continue to be, subject to a climatological or nonclimatological synoptic environment. Noting latitudinal and longitudinal displacements of STR and long-wave midlatitude features is of particular importance, and will partially determine the relative weights given to climatologically- or dynamically-based objective forecast guidance.

1.6.2.2.2 Objective Techniques Analysis Phase — By applying the systematic guidance with the NOGAPS model prognoses and real world conditions, performance characteristics for many of the objective techniques within the synoptic patterns/regions outlined in Section 1.6.1.3.1.1 have been determined. Estimating the likely biases of each of the objective-technique forecasts of TC track, intensity, and size given the current meteorological situation, the TDO eliminates those which are most likely inappropriate. The TDO also determines the degree to which the current situation is considered to be, and will continue to be, climatological by comparing the forecasts of the climatology-based objective techniques, dynamically-based techniques, and past motion of the present storm. Additionally, the spread of the set of objective forecasts, when plotted, is used to provide a measure of the predictability of subsequent motion, and the advisability of including a moderate-probability alternate forecast scenario in the prognostic reasoning message or warning (outside the western North Pacific). The directional spread of the plotted objective techniques is typically small well-before or well-after recurvature (providing high forecast confidence), and is typically large near the decision point of recurvature or non-recurvature, or during a quasi-stationary or erratic-movement phase. A large

spread increases the likelihood of alternate forecast scenarios.

1.6.2.2.3 Forecast Development Phase — The TDO then constructs the JTWC official forecast giving due consideration to:

1) Interpretation of the TC-environment scenario depicted by numerical model guidance;
2) known properties of individual objective techniques given the present synoptic situation or geographic location;
3) the extent to which the synoptic situation is, and is expected to remain, climatological; and,
4) past statistical performance of the various objective techniques on the current storm.

The following guidance for weighting the objective techniques is applied:

1) Weight persistence strongly in the first 12 to 24 hours of the forecast period;
2) use conceptual models of recurring, dynamically-related meteorological patterns with the traits of the numerical and objective-aid guidance associated with the specific synoptic situation; and
3) give significant weight to the last JTWC forecast at all forecast times, unless there is significant evidence to warrant departure (also consider the latest forecasts from regional warning centers, as applicable).

1.6.3. INTENSITY FORECASTING — The empirically derived Dvorak (1984) technique is used as a first guess for the intensity forecast. The TDO then adjusts the forecast after evaluating climatology and the synoptic situation. An interactive conditional-climatology scheme allows the TDO to define a situation similar to the system being forecast in terms of location, time of year, current intensity, and intensity trend. Synoptic influences such as the location of major troughs and ridges, and the position and intensity of the TUTT all play a large part in intensifying or weakening a TC. JTWC incorporates a checklist into the intensity-forecast procedure. Such criteria as upper-level outflow patterns, neutral points, sea-surface temperatures, enhanced monsoonal or cross-equatorial flow, and vertical wind shear are evaluated for their tendency to enhance or inhibit normal development, and are incorporated into the intensity-forecast process. In addition to climatology and synoptic influences, the first guess is modified for interactions with land, with other tropical cyclones, and with extratropical features. Climatological and statistical methods are also used to assess the potential for rapid intensification (Mundell, 1990).

1.6.4. WIND-RADII FORECASTING - Since the loss of dedicated aircraft reconnaissance in 1987, JTWC has turned to other data sources for determining the radii of winds around tropical cyclones. The determination of wind-radii forecasts is a three-step process:

1) Low-level satellite drift winds, scatterometer and microwave imager 35-kt (18 m/s) wind speed analysis (see Chapter 2), and synoptic data are used to derive the current wind distribution.

2) The first guess of the radii is then determined from statistically-derived empirical wind-radii models. The JTWC currently uses three models: the Tsui model, the Huntley model, and the Martin-Holland model. The latter model uses satellite-derived parameters to determine the size and shape of the wind profile associated with a particular tropical cyclone. The Martin-Holland model also incorporates latitude and speed of motion to produce an asymmetrical wind distribution. These models provide wind-distribution analyses and forecasts that are primarily influenced by the intensity forecasts. The analyses are then adjusted based on the actual analysis from step 1, and the forecasts are adjusted appropriately.
3) Synoptic considerations, such as the interaction of the cyclone with mid-latitude high pressure cells, are used to fine-tune the forecast wind radii.

1.6.5. EXTRATROPICAL

TRANSITION When a tropical cyclone moves into the mid-latitudes, it often enters an environment that is detrimental to the maintenance of the tropical cyclone's structure and energy-producing mechanisms. The effects of cooler sea-surface temperatures, cooler and dryer environmental air, and strong vertical wind shear all act to convert the tropical cyclone into an extratropical cyclone. JTWC indicates this conversion process is occurring by stating the tropical cyclone is "becoming extratropical." JTWC will indicate the conversion is expected to be complete by stating the system has "become extratropical." When a tropical cyclone is forecast to become extratropical, JTWC coordinates the transfer of warning responsibility to NAVPACMETOCCEN WEST.

1.6.6. TRANSFER OF WARNING RESPONSIBILITY JTWC coordinates the transfer of warning responsibility for tropical cyclones entering or exiting its AOR. For tropical cyclones crossing 180E longitude in the North Pacific Ocean, JTWC coordinates with the Central Pacific Hurricane Center (CPHC), Honolulu via NAVPACMETOCCEN, Pearl Harbor, Hawaii. For tropical cyclones crossing 180°E longitude in the South Pacific Ocean, JTWC coordinates with NAVPACMETOCCEN, which has responsibility for the eastern South Pacific. Whenever a tropical cyclone threatens Guam, files are electronically transferred from JTWC to Alternate Joint Typhoon Warning Center (AJTWC) collocated with NAVPACMETOCCEN. In the event that JTWC should become incapacitated, the AJTWC assumes JTWC's functions. Assistance in determining satellite reconnaissance requirements, and in obtaining the resultant data, is provided by the weather unit supporting the 15th Air Base Wing, Hickam AFB, Hawaii.

2. RECONNAISSANCE AND FIXES

2.1 GENERAL

JTWC depends primarily on two reconnaissance platforms, satellite and radar, to provide accurate and timely meteorological information in support of advisories, alerts and warnings. When available, synoptic and aircraft reconnaissance data are also used to supplement the above. As in past years, optimal use of all available reconnaissance resources to support JTWC's products remains a primary concern. Weighing the specific capabilities and limitations of each reconnaissance platform and the tropical cyclone's threat to life and property both afloat and ashore continues to be an important factor in careful product preparation.

2.2 RECONNAISSANCE AVAILABILITY

2.2.1 SATELLITE Interpretation of satellite imagery by analysts at Air Force/Navy tactical sites and on Navy ships yields tropical cyclone positions, estimates of the current intensity and 24-hour forecast intensity. Additional positioning and surface wind field estimation information are available for analysis from DMSP SSM/I data and the ERS-2 scatterometer.

2.2.2 RADAR Interpretation of land-based radar, which remotely senses and maps precipitation within tropical cyclones, provides positions in the proximity (usually within 175 nm (325 km)) of radar sites in Kwajalein, Guam, Japan, South Korea, China, Taiwan, Philippine Islands, Hong Kong, Thailand and Australia. Where Doppler radars are located, such as the Weather Surveillance Radar-1988 Doppler (WSR-88D) on Guam, Okinawa, and Korea, measurements of radial velocity are also available, and observations of the tropical cyclone's horizontal velocity field and vertical wind structure are possible.

2.2.3 AIRCRAFT No weather reconnaissance aircraft fixes were received at JTWC in 1997.

2.2.4 SYNOPTIC JTWC also determines tropical cyclone positions based on analysis of conventional surface/gradient-level synoptic data. These positions are an important supplement to fixes derived from remote sensing platforms, and become most valuable in situations where satellite, radar, and aircraft fixes are unavailable or are considered unrepresentative.

2.3 SATELLITE RECONNAISSANCE SUMMARY

Per USCINCPAC INSTRUCTION 3140.1W , the Pacific Air Force (PACAF) has primary responsibility for providing tropical cyclone reconnaissance for the U.S. Pacific Command (USPACOM). The JTWC tasks all reconnaissance requirements. Operational control of radar and satellite readout sites engaged in tropical cyclone reconnaissance remains in normal command channels. However, the Guam DMSP site is delegated the authority to manage the Pacific DMSP Tropical Cyclone Reconnaissance Network (hereafter referred to as Network) in support of JTWC. The Network control and the personnel of Satellite Operations

(SATOPS) are members of the 36 OSS/OSJ, and are collocated with JTWC at Nimitz Hill, Guam. The network sites are listed in Table 2-1.

TABLE 2-1 USPACOM SATELLITE RECONNAISSANCE NETWORK SITES

UNIT	ICAO
15 OSS/OSW, Hickam AFB, Hawaii	PHIK
18 OSS/OSW, Kadena AB, Japan	RODN
36 OSS/OSJ, Nimitz Hill, Guam	PGTW
607 COS/DOW, Yongsan Garrison Republic of Korea	RKSY
Air Force Weather Agency, KGWC Offutt AFB, Nebraska	
NPMOD DGAR, Diego Garcia	FJDG

Direct readout Network sites provide coverage of the tropical western North Pacific, South China Sea, and south central Indian Ocean using DMSP and NOAA TIROS polar orbiting satellites. PACAF Instruction 15-102 requires each network site to perform a minimum of two fixes per tropical cyclone per day if a tropical cyclone is within a site's coverage. Network direct readout site coverage is augmented by other sources of satellite-based reconnaissance. Air Force Weather Agency (AFWA) provides AOR-wide coverage to JTWC using recorded smooth DMSP and NOAA TIROS imagery. This imagery is recorded and stored on the satellites for later relay to a command readout site, which in turn passes the data via a communications satellite to AFWA. Civilian contract weather support for the Army at Kwajalein Atoll provides additional polar orbiting satellite-based tropical cyclone reconnaissance in the Marshall Islands and east of 180W as needed. The NOAA/NESDIS Satellite Applications Branch at Suitland, Maryland (ICAO identifier KWBC) also performs tropical cyclone fix and intensity analysis over the JTWC AOR using METEOSAT and GMS geostationary platforms.

The Network provides tropical cyclone positions and intensity estimates once JTWC issues either a TCFA or a warning. An example of the Dvorak code is shown in Figure 2-1. Each satellite-derived tropical cyclone position is assigned a Position Code Number (PCN) (Arnold and Olsen, 1974), which is a statistical estimate of fix position accuracy. The PCN is determined by: 1) the availablility of visible landmarks in the image that can be used as references for precise gridding, and 2) the degree of organization of the tropical cyclone's cloud system (Table 2-2)

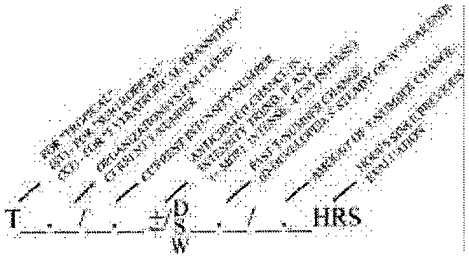

Example: T 3.5/4.5+/W1.5/24 HRS

Figure 2-1 Dvorak code for communicating estimates of current and forecast intensity derived from satellite data. In the example, the current "T-number" is 3.5, but the current intensity is 4.5. The cloud system has weakened by 1.5 "T-numbers" since the evaluation conducted 24 hours earlier. The plus (+) symbol indicates an expected reversal of the weakening of the tropical cyclone during the next 24-hour period.

TABLE 2-2 POSITION CODE NUMBER (PCN)

PCN	CENTER DETERMINATION/GRIDDING METHOD
1	EYE/GEOGRAPHY
2	EYE/EPHEMERIS
3	WELL DEFINED CIRCULATION CENTER/GEOGRAPHY
4	WELL DEFINED CIRCULATION CENTER/EPHEMERIS
5	POORLY DEFINED CIRCULATION CENTER/GEOGRAPHY
6	POORLY DEFINED CIRCULATION CENTER/EPHEMERIS

Once a tropical cyclone reaches an intensity of 50 kt (26 m/sec), AFWA and SATOPS analyze the 35-kt (18-m/sec) wind distribution surrounding the tropical cyclone based on microwave satellite imagery.

SATOPS provides three-hourly positions and six-hourly intensity estimates for all tropical cyclones in TCFA or warning status. Current intensity estimates are made using the Dvorak technique for both visible and enhanced infrared imagery. The standard relationship between tropical cyclone "T-number", maximum sustained surface wind speed, and minimum sea-level pressure (Atkinson and Holliday, 1977) for the Pacific is shown in Table 2-3. Subtropical cyclone intensity estimates are made using the Hebert and Poteat (1975) technique. Intensity estimates of tropical cyclones undergoing extratropical transition are made using the Miller and Lander (1997) technique.

Table 2-3 ESTIMATED MAXIMUM SUSTAINED WIND SPEED (KT) AS A FUNCTION OF DVORAK CURRENT AND FORECAST INTENSITY NUMBER AND MINIMUM SEA-LEVEL PRESSURE (MSLP)

T-NUMBER	ESTIMATED WIND SPEED-KT	(M/SEC)	MSLP(MB) (PACIFIC)
0.0	<25	<(13)	---
0.5	25	(13)	---
1.0	25	(13)	---
1.5	25	(13)	---
2.0	30	(13)	1000
2.5	35	(13)	997
3.0	45	(13)	991
3.5	55	(13)	984
4.0	65	(13)	976
4.5	77	(13)	966
5.0	90	(13)	954
5.5	102	(13)	941
6.0	115	(13)	927
6.5	127	(13)	914
7.0	140	(13)	898

SATOPS at Nimitz Hill uses hourly full disk GMS imagery to observe 70% of the JTWC Area Of Responsibility (AOR) from 80E to 180W (Figure 2-2). Images are remapped to a Mercator projection to enhance imagery limb coverage at 80E - 100E. Animated geostationary imagery is a valuable tool for determining the location and motion of tropical cyclones. Animated water vapor channel imagery is useful for observing environmental synoptic features that affect tropical cyclone development and movement.

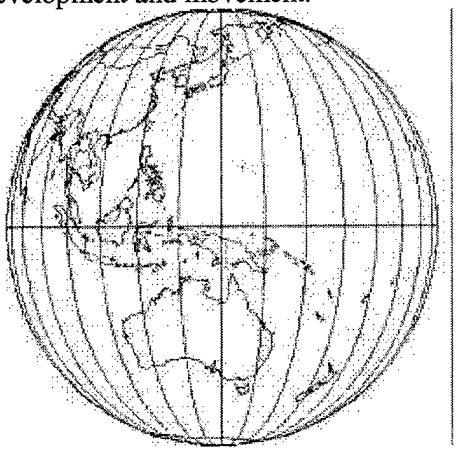

Figure 2-2 GMS full disk coverage

SATOPS has access to polar and geostationary data on both the Air Force Mark IVB workstation and the Meteorological Imagery, Data Display, and Analysis System (MIDDAS). The MIDDAS consists of a network of three DEC Vax 3400s running advanced graphics software, with two large screen workstations. The Mark IVB is the SATOPS backup satellite data analysis system with the ability to ingest and process both polar and geostationary satellite data, and display imagery on one large screen workstation. The Mark IVB also acts as a front end for the MIDDAS which has no independent receiver/antenna. Both the MIDDAS and the Mark IVB can display NOAA Advanced Very High Resolution Radiometer (AVHRR), DMSP Operational Linescan System (OLS) and Special Sensor Microwave/Imager

(SSM/I), and also geostationary visible, infrared and water vapor channel imagery. The MIDDAS can display NOAA TIROS Operational Vertical Sounder (TOVS) data, and the Mark IVB can display DMSP SSM/T1 and SSM/T2 sounder data.

NOAA TIROS AVHRR imagery provides five channels of imagery — visible, near and middle IR, and two in the far IR channels. DMSP OLS provides imagery in two channels — visible/near IR (commonly referred as broadband visible), and far IR. TOVS includes the High Resolution Infrared Radiation Sounder/2 (HIRS/2), the Microwave Sounding Unit (MSU), and the Stratospheric Sounding Unit (SSU).

2.3.1 SATELLITE PLATFORM SUMMARY Figure 2-3 shows the operational status of polar orbiting spacecraft. Imagery was received from five DMSP and two NOAA satellites during 1997. Both Operational Line Scan (OLS) and Special Sensor Microwave Imagery (SSM/I) was received from F13 and F14 (F14 began transmitting data in early summer). F12 produced only OLS imagery and F10 and F11 only SSM/I imagery. After transmitting four years beyond its normal life expectancy, F10 went into an uncontrollable spin in November and was unrecoverable. NOAA-12 and NOAA-14

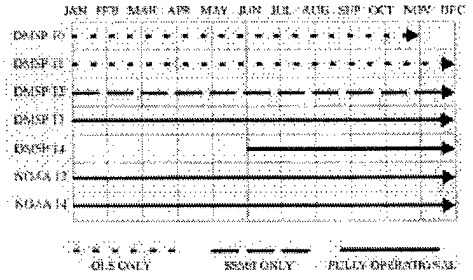

Figure 2-3 Polar orbiting spacecraft status for 1997.

were operational throughout the year, with fully functional AVHRR imagers.

2.3.2 STATISTICAL SUMMARY During 1997, over 91% of all fixes for input into JTWC's warnings were satellite based tropical cyclone positions and intensities. The PACOM satellite reconnaissance network and other agencies provided JTWC with 10,726 fixes: 6,114 western North Pacific, 313 northern Indian Ocean, 3,419 Southern Hemisphere, and 880 for circulations which did not develop into significant tropical cyclones. SATOPS provided 7,601, accounting for nearly 71% of all fixes. A comparison of total fixes from the network and western North Pacific over the past seven years is shown in Figure 2-4.

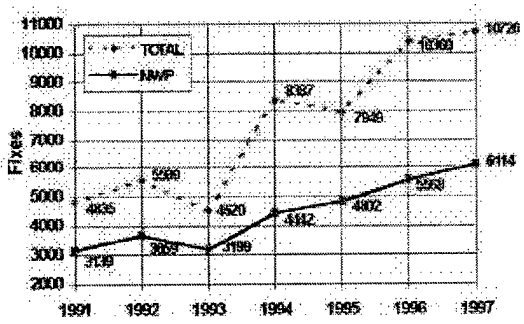

Figure 2-4 Comparison of fixes for the AOR (Total) and western North Pacific for the period 1991 - 1997.

2.3.3 APPLICATION OF NEW TECHNIQUES AND TECHNOLOGY

SATOPS continues to push advances in satellite meteorology to improve the support provided to JTWC. A new geostationary satellite, Feng Yun 2, owned by China/PRC, became operational for a short period during the year. Unfortunately, this satellite failed and became unusable within a few

Table 2-4 POSITION CODE NUMBER (PCN) CRITERIA AND FIX CODES FOR TC LOW-LEVEL CCs FROM SATELLITE

PCN Grid By Geog (note 2)	PCN Grid by Ephem (note2)	Definitions	Sensor /technique type and fix code					
			IR	Vis	Both	SSM/I only (note 3)	Vis/IR & SSM/I (note 3)	Anmtn (note 4)
1	2	Eye						
(EYE)	(EYE)	CDO type eye, geometric center (regular/round, any diameter) (note 6)	1	2	3	4	S	A
(EYE)	(EYE)	Small eye (irregular/ragged, diameter > 30 nm on long axis) (note 6)	5	6	7	8	S	A
3	4	Well defined CC						
(EYE)	(EYE)	Eye(ragged/irregular, diameter > 30 nm center > 1/2 enclosed by wall cloud) (note 6)	9	10	11	12	S	A
(EYE)	(EYE)	Tightly curved band/banding type eye (band curves at least 1/2 distance around center, diameter < 90 nm)	13	14	15	16	S	A
(LLCC)	(LLCC)	Exposed low-level CC	17	18	19	20	S	A
(CDO)	(CDO)	Small CDO (round with well Defined edges, positioned near Geometric center, diameter < 80 nm)		21	22	23	S	A
(EMB)	(EMB)	Small embedded center (diameter < 80 nm)	24		25	26	S	A
(CDO)	(CDO)	Large CDO (with clear Indications of shearing, low-level cloud lines, or overshooting tops that bias low-level center Position away from the geometric center, diameter > 80 nm)		27	28	29	S	A
(CDO)	(CDO)	Any CDO or Embedded Center with low-level CC clearly visible on co-registered SSM/I (note 7)	30	31	32	33	S	
5	6	Poorly Defined						
		Large eye (ragged/irregular, 30 nm diameter on long axis, 1/2 Enclosed by wall cloud)	34	35	36	37	S	A
		Spiral banding systems (convective curvature) not Classifiable as banding eye or Tightly curved band	38	39	40	41	S	A
		Large CDO		43	44	45	S	A
		Embedded center positioned with IR	46					A
		Partially exposed low-level Centers with the CC less than half Exposed	47	48	49	50	S	A
		Cloud minimum wedge/cold Comma	51	52	53	54	S	A
		Central cold cover	55	56	57	58	S	A
		Cirrus outflow - upper level Outflow provides the only Circulation parameters	59	60	61	62	S	A
		Poorly organized low-level center Evident only in high resolution Animation (Vis/IR or both)						
		All others						
		Monsoon depressions or multiple cloud clusters, positioned using any of the following methods:	Any combination of Vis , IR/EIR, and SSM/I					

Table 2-4 (Continued)

		Cirle method	68		
		Conservative feature	69		A
		Animation	70		
		Extrapolation	71		

Note 1: Use the following steps to determine the PCN and Fix Code:

a. Based on the analysis of the circulation parameters, determine a TC low-level CC position.

b. Go to Table 2-2, then to the definitions column. Choose a PCN based on the cloud pattern, discrete measurements, as necessary, and/or technique used to determine the position.

c. Move across to the Fix Code columns, and based on the sensor(s) used, select a fix code.

Note 2: Odd PCNs (1, 3, 5) are gridded with geography, the low-level CC being within 10 degrees (600 nm) of the geographic feature used for gridding. Even PCNs (2, 4, 6) are gridded with ephemeris, or the low-level CC is not within 10 degrees (600 nm) of the geographic feature used forgridding.

Note 3: SSM/I only fixes - Use PCN of 5 or 6, and fix code based on Note 1, para a & c.

Note 4: Append "S" to the numerical fix code entry to indicate Special Sensor Microwave Imager (SSM/I) and visible and/or infrared data was used in determining the low-level CC (i.e. 18S). Defense Meteorological Satellite Program (DMSP) fixes only. For the purposes of this fix code, SSM/I (S) and Animation (A) are mutually exclusive.

Note 5: Append "A" to the numerical fix code entry to indicate animation was used in determining the low-level CC (i.e. 11A). Geostationary fixes only. For the purposes of this fix code, SSM/I (S) and Animation (A) are mutually exclusive.

Note 6: For fix code entries 1-9, encode 01-09.

Note 7: In order to use SSM/I data to position low-level CCs, you must be able to correct the navigation/gridding and interrogate the SSM/I imagery directly for latitude/longitude (DMSP fixes only).

months. However, there were indications late in 1998 that some operational capability was being regained. When operational, this satellite has the potential of filling in the gap between METEOSAT and GMS-5 (Figure 2-5).

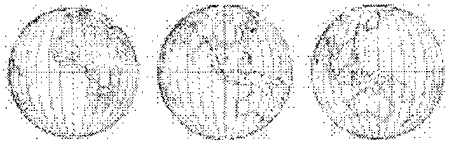

Meteosat **Feng-Yun 2** **GMS 5**

Figure 2-5 Geostationary spacecraft coverage of AOR. The PRC satellite Feng-Yun 2 was briefly available in late 1997 and early 1998 before being rendered useless by the failure of onboard instrumentation. There has been some success late in 1998 in restoring it to service.

SATOPS continued to make use of real-time SSM/I data on the Mark IVB to determine storm structure and better identify 35-kt (18 m/s) winds surrounding tropical cyclones. Several upgrades on the Mission Sensor Tactical Imaging Computer (MISTIC) helped us better interrogate time-late SSM/I data stored on DMSP spacecrafts and forwarded from FNMOC to provide full coverage of JTWC's AOR. The acquisition of DMSP F14 data in the early summer helped increase the area covered by microwave imagery.

Additionally, to give the TDO a better statistical value for each satellite derived fix, SATOPS used animated geostationary imagery and multispectral display capability to apply Position Code Numbers (PCN) (Table 2-4) and fix codes to a particular tropical cyclone pattern based on sensor type (See Statistical Summary and Figure 2-6).

The XT technique (Miller and Lander, 1997) was developed and used operationally to better estimate tropical cyclones undergoing extratropical transition.

Several Mark IVB Network sites received the new Build 8 software in late 1997. This upgrade made the system

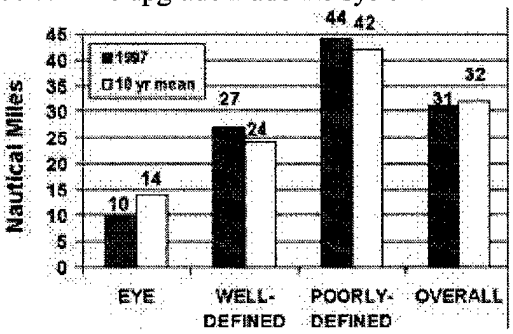

Figure 2-6 Western North Pacific Ocean satellite position errors (nm).

more user-friendly and much easier to interrogate several tropical cyclones at once--something previous software builds lacked.

2.3.4 FUTURE OF SATELLITE RECONNAISSANCE SATOPS will continue to strive to improve satellite reconnaissance to support JTWC in 1998. The 1995 Base Realignment and Closure (BRAC) directed JTWC to move from Guam to Hawaii by 1999. Preparing for this move, while continuing to provide uninterrupted support, will be a major challenge. Initiatives are currently being taken to move the Mark IVB to Andersen AFB,Guam by 1 April 1999.

2.4 RADAR RECONNAISSANCE SUMMARY

Of the 33 significant tropical cyclones in the western North Pacific during 1997, 13 passed within range of land-based radar with sufficient precipitation and organization to be fixed. A total of 466 land-based radar fixes were logged at JTWC. As defined by the World Meteorological Organization (WMO), the accuracy of these fixes falls within three categories: good [within 10 km (5 nm)], fair [within 10 - 30 km (5 - 16 nm)], and poor [within 30 - 50 km (16 - 27 nm)]. Of the 466 radar fixes encoded in this manner, 198 were good, 201 fair, and 182 poor. The radar network provided timely and accurate fixes which allowed JTWC to better track and forecast tropical cyclone movement. In addition to fixes, the Guam and Okinawa WSR-88D radars supplied meteorologists with a look into the vertical and horizontal structure of precipitation and winds in tropical cyclones passing nearby.

In the Southern Hemisphere, 40 radar reports were logged for tropical cyclones. No radar fixes were received for the North Indian Ocean.

2.5 TROPICAL CYCLONE FIX DATA

Table 2-5a delineates the number of fixes per platform for each individual tropical cyclone for the western North Pacific. Totals and percentages are also indicated. Similar information is provided for the North Indian Ocean in Table 2-5b, and for the South Pacific and South Indian Ocean in Table 2-5c.

Table 2-5a WESTERN NORTH PACIFIC OCEAN FIX PLATFORM SUMMARY FOR 1997

TROPICAL CYCLONE	SATELLITE	SCATTEROMETER	RADAR	SYNOPTIC	AIRCRAFT	TOTAL
01W HANNAH	117	1	0	0	0	118
02W ISA	362	7	32	0	0	401
03W JIMMY	114	5	0	0	0	119
04W KELLY	120	10	3	3	0	136
05W LEVI	116	3	9	0	0	128
06W MARIE	155	6	0	0	0	161
07W NESTOR	276	13	0	2	0	291
08W OPAL	173	7	34	11	0	225
09W PETER	156	14	37	23	0	230
10W ROSIE	221	1	45	8	0	275
11W SCOTT	173	3	0	0	0	176
12W TINA	300	4	96	4	0	404
13W VICTOR	75	0	17	0	0	92
14W WINNIE	385	2	71	7	0	465
15W YULE	157	3	0	1	0	161
16W -	49	2	0	0	0	51
17W ZITA	68	1	14	8	0	91
18W AMBER	238	4	18	9	0	269
19W BING	218	4	0	3	0	225
20W CASS	69	0	0	2	0	71
02C OLIWA	369	4	49	8	0	430
21W DAVID	197	5	0	3	0	205
22W FRITZ	95	1	0	3	0	99
23W ELLA	8	1	0	0	0	9
24W GINGER	156	4	0	0	0	160
25W HANK	50	2	0	0	0	52
26W -	82	0	0	0	0	82
27W IVAN	279	3	18	6	0	306
28W JOAN	269	3	23	2	0	297
29W KEITH	336	6	58	15	0	415
30W LINDA	196	3	0	5	0	204
31W MORT	162	3	0	8	0	173
05C PAKA	480	8	57	4	0	549
TOTALS	6221	133	581	135	0	7070
PERCENTAGE OF TOTAL	88%	2%	8%	2%	0%	100%

Table 2-5b NORTH INDIAN OCEAN FIX PLATFORM SUMMARY FOR 1997

TROPICAL CYCLONE	SATELLITE	SCATTEROMETER	RADAR	SYNOPTIC	AIRCRAFT	TOTAL
01B	137	5	0	0	0	142
02B	76	0	0	4	0	80
03A	23	2	0	1	0	26
04A	110	1	0	2	0	113
TOTALS	346	8	0	7	0	361
PERCENTAGE OF TOTAL	96%	2%	0%	2%	0%	100%

Table 2-5c SOUTH PACIFIC AND SOUTH INDIAN OCEAN FIX PLATFORM SUMMARY FOR 1997

TROPICAL CYCLONE	SATELLITE	SCATTEROMETER	RADAR	SYNOPTIC	AIRCRAFT	TOTAL
01S LINDSAY	41	1	0	0	0	42
02S -	91	2	0	0	0	93
03S -	78	1	0	0	0	79
04S ANTOINETTE	80	2	0	0	0	82
05S MELANIE/BELLAMI	242	4	0	0	0	246
06P CYRIL	106	2	0	1	0	109
07S CHANTELLE	121	2	0	0	0	123
08S DANIELLA	67	4	0	5	0	76
09S ELVINA	130	0	0	8	0	138
10P NICHOLAS	60	3	0	5	0	68
11S OPHELIA	147	0	0	0	0	147
12P PHIL	247	1	1	1	0	250
13P FERGUS	123	1	0	4	0	128
14S FABRIOLA	42	1	0	7	0	50
15S RACHEL	128	3	16	14	0	161
16P DRENA	130	2	0	7	0	139
17P EVAN	49	2	0	1	0	52
18S -	80	1	0	0	0	81
19S PANCHO-HELINDA	378	4	0	0	0	382
20S GRETELLE	76	3	0	4	0	83
21S ILETTA	76	2	0	0	0	78
22P FREDA	133	1	0	1	0	135
23S JOSIE	93	2	0	1	0	96
24P GILLIAN	47	1	0	1	0	49
25S KARLETTE	135	2	0	0	0	137
26P HAROLD	102	1	0	1	0	104
27S -	107	2	0	0	0	109
28P ITA	13	0	0	0	0	13
29P -	12	0	0	3	0	15
30S LIZETTE	19	2	0	0	0	21
31P GAVIN	151	4	4	1	0	160
32P JUSTIN	343	8	18	3	0	372
33P HINA	72	1	0	0	0	73
34P IAN	53	7	0	3	0	63
35P JUNE	135	10	0	2	0	147
36S RHONDA	178	9	0	0	0	187
37P -	54	0	0	0	0	54
38P KELI	113	4	0	0	0	117
TOTALS	4252	95	39	73	0	4459
PERCENTAGE OF TOTAL	95%	2%	1%	2%	0%	100%

3. Summary of Western North Pacific and North Indian Ocean Tropical Cyclones

3.1 Western North Pacific Ocean Tropical Cyclones

The year of 1997 was an El Niño year, and by some measures (e.g., the magnitude of the warming of the Sea Surface Temperature (SST) in the eastern equatorial Pacific), the El Niño episode of 1997 was one of the strongest in recorded history (Climate Prediction Center (CPC) 1997). El Niño had a large influence on the distribution of western North Pacific (WNP) TCs during 1997. The signature characteristics of the distribution, character and behavior of the tropical cyclones (TCs) of the WNP during 1997 (some known to be related to El Niño) include:

(1) a very high number of super typhoons;

(2) an early start of WNP TC activity with a higher than average number during the early season (01 January to 15 July);

(3) a tendency -- especially during the first half of the year -- for the TC tracks to be north oriented;

(4) a substantial eastward displacement of the mean genesis location for all TCs and for many of the individual TCs;

(5) the formation, east of the international dateline, of two TCs which moved into the WNP and became super typhoons -- Oliwa (02C) and Paka (05C) (these are Hawaiian names given to them by the Central Pacific Hurricane Center (CPHC));

(6) the landfall of only one TC in the Philippines;

(7) the formation in the monsoon trough of all but one of the TCs -- (Scott (07W) formed in direct association with a cyclonic circulation (cell) in the tropical upper tropospheric trough (TUTT)); and,

(8) the simultaneous existence in the Philippine Sea of 2 super typhoons -- Ivan (28W) and Joan (29W) -- each possessing an extreme intensity of 160 kt (82 m/sec).

Some of these unusual characteristics of the distribution and behavior of the TCs in the western North Pacific during 1997 are likely related to the large-scale atmospheric and oceanic circulation anomalies associated with 1997's strong El Niño/Southern Oscillation (ENSO) event. Of the items in this list, (2), (4) and (7) are typical features of El Niño years.

The annual number of significant TCs in the WNP during 1997 (Table 3-1) was almost normal: 33 versus the climatological average of 32 (Table 3-2). The year of 1997 included 11 super typhoons, 12 lesser typhoons, 8 tropical storms and 2 tropical depressions. The calendar-year total of 31 TCs (of at least tropical storm intensity) was one higher than the climatological average (Figure 3-1). The calendar-year total of 23 typhoons was five above the long-term average, and is the highest annual number of typhoons recorded in the WNP basin since 1971 when there were 24. The 11 super typhoons is an unprecedented value. Since 1970, as best-track wind and intensities became ever more constrained to conform to standardized TC wind-pressure relationships (e.g., Atkinson and Holiday 1977), the highest annual number of super typhoons is 7. (Figure 3-2). The high number of super typhoons in the WNP was one of the most significant highlights of 1997. The annual number of super typhoons may be weakly related to El Niño: the El Niño years of 1972, 76, 82, 87, 91, 93 and 94 had 2, 5, 5, 7, 7, 3, and 6 super typhoons respectively (for an average of 5.0); and, the La Niña years of 1973, 83, 88, 89, 95, and 96 had 3, 4, 3, 7, 5 and 6 super typhoons respectively (for an average of 4.7). A suggested physical mechanism for the increase in super typhoons during El Niño years is the longer over-water, low-latitude trajectories of the TCs which, because of El Niño, form well to the east of normal. The

annual number of super typhoons during 1997 is unprecedented, and its association with one of the strongest recorded El Niño events may be more than just a coincidence.

During the Boreal Spring of 1997, El Niño (i.e., very warm SST in the central and eastern equatorial Pacific) developed rapidly, coupled with a drop in the magnitude of the Southern Oscillation Index (Figure 3-3). Unusually persistent low-level westerly wind flow became established at low latitutudes in the WNP. This westerly wind flow was also displaced eastward from its normal domain (Figure 3-4). The set-up of low-level, low-latitude westerly wind flow early in the year led to the establishment of a near-equatorial trough across Micronesia from the western Caroline Islands eastward into the Marshall Islands. This trough supported the development of several TCs early season. According to Lander (1994), the only statistic of numbers of TCs in the WNP which is significantly correlated with any ENSO index is an increase in the number of cyclones from 01 January to 15 July.

Table 3-1 WESTERN NORTH PACIFIC SIGNIFICANT TROPICAL CYCLONES FOR 1997

TROPICAL CYCLONE	PERIOD OF WARNING	NUMBER WARNING ISSUED	ESTIMATED MAXIMUM INTENSITY KT (M/SEC)	ESTIMATED MSLP (MB)
01W TS HANNAH	19 JAN - 24 JAN	17	50 (26)	987
02W STY ISA	11 APR - 23 APR	47	145 (75)	892
03W TS JIMMY	22 APR - 25 APR	15	55 (28)	984
04W TS KELLY	07 MAY - 10 MAY	14	45 (23)	991
05W TS LEVI	25 MAY - 30 MAY	19	45 (23)	991
06W TY MARIE	26 MAY - 02 JUN	27	90 (46)	954
07W STY NESTOR	06 JUN - 15 JUN	37	140 (72)	898
08W TY OPAL	15 JUN - 21 JUN	26	90 (46)	954
09W TY PETER	23 JUN - 29 JUN	24	65 (33)	976
10W STY ROSIE	18 JUL - 28 JUL	38	140 (72)	898
11W TS SCOTT*	24-25 JUL/27-02 AUG	30	55 (28)	984
12W TY TINA	29 JUL - 09 AUG	44	90 (46)	954
13W TY VICTOR	30 JUL - 03 AUG	15	65 (33)	976
14W STY WINNIE	08 AUG - 19 AUG	44	140 (72)	898
15W TY YULE	16 AUG - 23 AUG	27	65 (33)	976
16W TD	18 AUG - 19 AUG	5	30 (15)	1000
17W TY ZITA	21 AUG - 23 AUG	10	75 (39)	967
18W TY AMBER	21 AUG - 30 AUG	36	110 (57)	933
19W STY BING	27 AUG - 05 SEP	36	135 (69)	904
20W TS CASS	28 AUG - 30 AUG	11	45 (23)	991
02C STY OLIWA#	02 SEP - 17 SEP	53(6)	140 (72)	898
21W TY DAVID	11 SEP - 20 SEP	35	95 (49)	949
22W TY FRITZ	20 SEP - 25 SEP	21	75 (39)	968
23W TS ELLA	21 SEP - 25 SEP	14	40 (21)	994
24W STY GINGER	22 SEP - 30 SEP	31	145 (75)	892
25W TS HANK	03 OCT - 04 OCT	7	40 (21)	994
26W TD	04 OCT - 07 OCT	10	30 (15)	1000
27W STY IVAN	13 OCT - 24 OCT	46	160 (82)	872
28W STY JOAN	13 OCT - 24 OCT	44	160 (82)	872
29W STY KEITH	27 OCT - 08 NOV	48	155 (80)	878
30W TY LINDA	31 OCT - 09 NOV	35	65 (33)	976
31W TY MORT	10 NOV - 16 NOV	23	65 (33)	976
05C STY PAKA#	02 DEC - 21 DEC	61(17)	160 (82)	901**
	JTWC TOTAL	950		
	#NPMOC TOTAL	(23)		
	GRAND TOTAL	973		

* REGENERATED
** ATLANTIC INTENSITY - MSLP RELATIONSHIP USED
\# WARNINGS ISSUED BY NPMOC

Table 3-2 DISTRIBUTION OF WESTERN NORTH PACIFIC TROPICAL CYCLONES FOR 1959 - 1997

YEAR	JAN	FEB	MAR	APR	MAY	JUN	JUL	AUG	SEP	OCT	NOV	DEC	TOTALS
1959	0	1	1	1	0	1	3	8	9	3	2	2	31
	000	010	010	100	000	001	111	512	423	210	200	200	17 7 7
1960	1	0	1	1	1	3	3	9	5	4	1	1	30
	001	000	001	100	010	210	210	810	041	400	100	100	19 8 3
1961	1	1	1	1	4	6	5	7	6	7	2	1	42
	010	010	100	010	211	114	320	313	510	322	101	100	20 11 11
1962	0	1	0	1	3	0	8	8	7	5	4	2	39
	000	010	000	100	201	000	512	701	313	311	301	020	24 6 9
1963	0	0	1	1	0	4	5	4	4	6	0	3	28
	000	000	001	100	000	310	311	301	220	510	000	210	19 6 3
1964	0	0	0	0	3	2	8	8	8	7	6	2	44
	000	000	000	000	201	200	611	350	521	331	420	101	26 13 5
1965	2	2	1	1	2	4	6	7	9	3	2	1	40
	110	020	010	100	101	310	411	322	531	201	110	010	21 13 6
1966	0	0	0	1	2	1	4	9	10	4	5	2	38
	000	000	000	100	200	100	310	531	532	112	122	101	20 10 8
1967	1	0	2	1	1	1	8	10	8	4	4	1	41
	010	000	110	100	010	100	332	343	530	211	400	010	20 15 6
1968	0	1	0	1	0	4	3	8	4	6	4	0	31
	000	001	000	100	000	202	120	341	400	510	400	000	20 7 4
1969	1	0	1	1	0	0	3	3	6	5	2	1	23
	100	000	010	100	000	000	210	210	204	410	110	010	13 6 4
1970	0	1	0	0	0	2	3	7	4	6	4	0	27
	000	100	000	000	000	110	021	421	220	321	130	000	12 12 3
1971	1	0	1	2	5	2	8	5	7	4	2	0	37
	010	000	010	200	230	200	620	311	511	310	110	000	24 11 2
1972	1	0	1	0	0	4	5	5	6	5	2	3	32
	100	000	001	000	000	220	410	320	411	410	200	210	22 8 2
1973	0	0	0	0	0	0	7	6	3	4	3	0	23
	000	000	000	000	000	000	430	231	201	400	030	000	12 9 2
1974	1	0	1	1	1	4	5	7	5	4	4	2	35
	010	000	010	010	100	121	230	232	320	400	220	020	15 17 3
1975	1	0	0	1	0	0	1	6	5	6	3	2	25
	100	000	000	001	000	000	010	411	410	321	210	002	14 6 5
1976	1	1	0	2	2	2	4	4	5	0	2	2	25
	100	010	000	110	200	200	220	130	410	000	110	020	14 11 0
1977	0	0	1	0	1	1	4	2	5	4	2	1	21
	000	000	010	000	001	010	301	020	230	310	200	100	11 8 2
1978	1	0	0	1	0	3	4	8	4	7	4	0	32
	010	000	000	100	000	030	310	341	310	412	121	000	15 13 4
1979	1	0	1	1	2	0	5	4	6	3	2	3	28
	100	000	100	100	011	000	221	202	330	210	110	111	14 9 5
1980	0	0	1	1	4	1	5	3	7	4	1	1	28
	000	000	001	010	220	010	311	201	511	220	100	010	15 9 4
1981	0	0	1	1	1	2	5	8	4	2	3	2	29
	000	000	100	010	010	200	230	251	400	110	210	200	16 12 1
1982	0	0	3	0	1	3	4	5	6	4	1	1	28
	000	000	210	000	100	120	220	500	321	301	100	100	19 7 2
1983	0	0	0	0	0	1	3	6	3	5	5	2	25
	000	000	000	000	000	010	300	231	111	320	320	020	12 11 2
1984	0	0	0	0	0	2	5	7	4	8	3	1	30
	000	000	000	000	000	020	410	232	130	521	300	100	16 11 3
1985	2	0	0	0	1	3	1	7	5	5	1	2	27
	020	000	000	000	100	201	100	520	320	410	010	110	17 9 1
1986	0	1	0	1	2	2	2	5	2	5	4	3	27
	000	100	000	100	110	110	200	410	200	320	220	210	19 8 0
1987	1	0	0	1	0	2	4	4	7	2	3	1	25
	100	000	000	010	000	110	400	310	511	200	120	100	18 6 1
1988	1	0	0	0	1	3	2	5	8	4	2	1	27
	100	000	000	000	100	111	110	230	260	400	200	010	14 12 1
1989	1	0	0	1	2	2	6	8	4	6	3	2	35
	010	000	000	100	200	110	231	332	220	600	300	101	21 10 4
1990	1	0	0	1	2	4	4	5	5	5	4	1	31
	100	000	000	010	110	211	220	500	410	230	310	100	21 9 1
1991	0	0	2	1	1	1	4	8	6	3	6	0	32
	000	000	110	010	100	100	400	332	420	300	330	000	20 10 2

(TABLE CONTINUED ON TOP OF NEXT PAGE)

Table 3-2 (CONTINUED FROM PREVIOUS PAGE)

YEAR	JAN	FEB	MAR	APR	MAY	JUN	JUL	AUG	SEP	OCT	NOV	DEC	TOTALS
1992	1	1	0	0	0	3	4	8	5	6	5	0	33
	100	010	000	000	000	210	220	440	410	510	311	000	21 11 1
1993	0	0	2	2	1	2	5	8	5	6	4	3	38
	000	000	011	002	010	101	320	611	410	321	112	300	21 9 8
1994	1	0	1	0	2	2	9	9	8	7	0	2	41
	001	000	100	000	101	020	342	630	440	511	000	110	21 15 5
1995	1	0	0	0	1	2	3	7	7	8	2	3	34
	001	000	000	000	010	020	210	421	412	512	020	012	15 11 8
1996	0	1	0	2	2	0	7	10	7	5	6	3	43
	000	001	000	011	110	000	610	433	610	212	132	111	21 12 10
1997	1	0	0	2	3	3	4	8	4	6	1	1	33
	010	000	000	110	120	300	310	611	310	411	100	100	23 8 2
(1959-1996)													
MEAN	0.6	0.3	0.6	0.8	1.3	2.1	4.6	6.5	5.8	4.8	3.0	1.5	31.9
CASES	22	11	23	29	48	79	175	248	219	182	113	57	1206

The criteria used in TABLE 3-2 are as follows:

1) If a tropical cyclone was first warned on during the last two days of a particular month and continued into the next month for longer than two days, then that system was attributed to the second month.

2) If a tropical cyclone was warned on prior to the last two days of a month, it was attributed to the first month, regardless of how long the system lasted.

3) If a tropical cyclone began on the last day of the month and ended on the first day of the next month, that system was attributed to the first month. However, if a tropical cyclone began on the last day of the month and continued into the next month for only two days, then it was attributed to the second month.

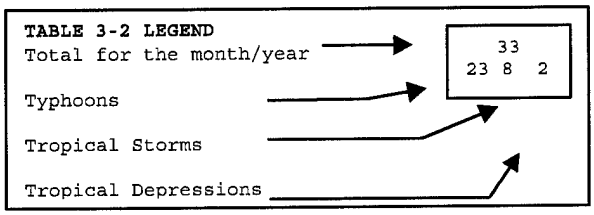

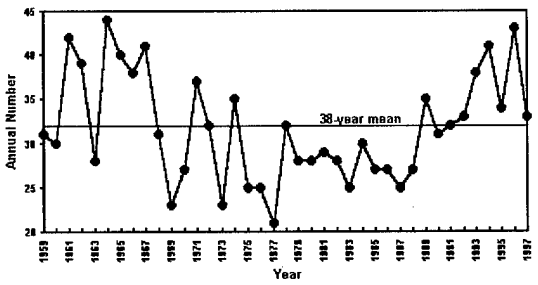

Figure 3-1 Tropical cyclones of tropical storm or greater intensity in the western North Pacific (1960-1997).

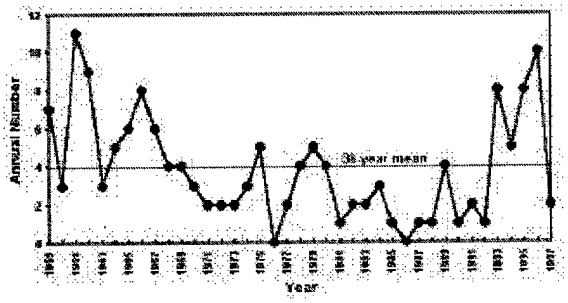

Figure 3-2 Number of western North Pacific super typhoons (1960-1997).

The annual mean genesis location of TCs which form in the WNP is related to the status of ENSO: it tends to be east of normal during El Niño years and west of normal during those years characterized by large-scale climatic anomalies opposite to those of El Niño, years known as La Niña or ENSO cold phase. Consistent with the TC distribution typically associated with El Niño (or an ENSO warm phase), the annual mean genesis location for all TCs during 1997 was substantially east of normal (Figure 3-5a). This was a pronounced change from the TC distributions during 1995 and 1996 (both weak La Niña years) when this statistic was west of normal. A breakdown of the genesis locations of the individual WNP TCs of 1997 (Figure 3-5b) shows that most formed east of 140E. Eleven formed east of 160E, while only two -- two below normal -- formed in the South China Sea. Through the period of 1960 to 1991, the five years with the highest annual average of the Southern Oscillation Index (SOI) (i.e., 1988, 1975, 1974, 1973,

and 1971) had an average of 2.4 TCs east of 160E, and the five years with the lowest annual average SOI (i.e., 1991, 1987, 1982, 1977, and 1972) had an average of 7.4 TCs east of 160E. (Note: all El Niño years have below normal values of the SOI.) During 1996, only one TC formed within the region designated as the "El Niño" box on Figure 3-5b, while 10 TCs formed there during 1997 (including those TCs that originated east of the International Date Line).

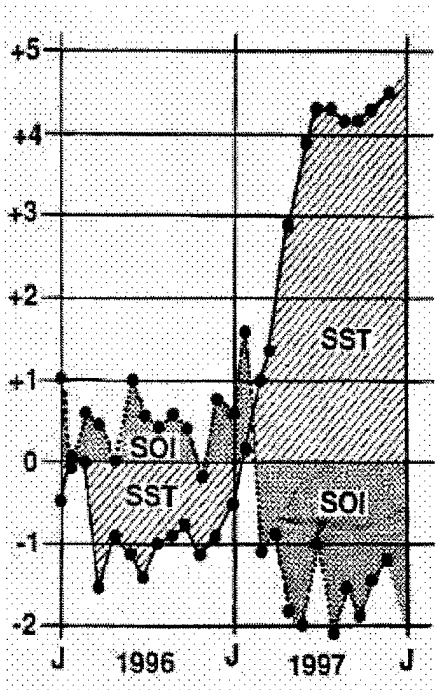

Figure 3-3 Anomalies from the monthly mean for eastern equatorial Pacific Ocean sea-surface temperature (hatched) in degrees Celsius and the Southern Oscillation Index (SOI) (shaded) for the period 1996 through 1997. (Adapted from Climate Prediction Center, 1997).

The annual number of TCs which form in this "El Niño" box has been shown by Lander (1994) to be dramatically affected by El Niño: far more TCs form within it during EL Niño years than during normal and La Niña years. Only one TC during 1997 -- Scott (07W) -- formed north of 20N in direct association with a TUTT cell. All other TCs of 1997 formed at low latitudes in the monsoon trough. There was a tendency during 1997 for low-level monsoon winds to persist at low latitudes and for the axis of the monsoon trough to remain near 10N across Micronesia (Figure 3-6).

Low-level westerly wind anomalies persisted throughout Micronesia with the largest westerly wind anomalies located at low latitudes near and to the east of the international dateline. Corresponding anomalies in the upper troposphere consisted of easterly wind anomalies over most of the low latitudes of the WNP. These large-scale atmospheric flow-pattern anomalies of 1997 were nearly everywhere the reverse of those that persisted for most of 1995 and 1996. The atmospheric flow anomalies of 1997 over the WNP are typical of those expected during an El Niño year.

Monsoon westerlies and the axis of the monsoon trough frequently stretched across all of Micronesia as far as the international dateline (and occasionally beyond) during most of 1997. Despite the nearly continuous presence of the monsoon trough and abundant deep convection, the number of TCs (of at least tropical storm intensity) was near normal; and, compared with 1995 and 1996, the number of TCs which failed to mature and remained only at tropical depression intensity was much reduced. The TCs of 1997 tended to emerge one-by-one from the eastern portion of the basin and then recurve or move north; each subsequent development at low latitude tended to occur after the prior TC had exited the tropics; and, the TCs emerging from the eastern end of the monsoon trough tended to be large, very intense and slow-moving. There were few cases of multiple TCs (i.e., the simultaneous occurrence of two or more) in the WNP during 1997. The most noteworthy case of multiple TCs was the simultaneous formation and development in October of Ivan (28W) and Joan (29W).

These two TCs formed simultaneously along a segment of the monsoon trough axis, which stretched across the Marshall Islands and eastward beyond the international dateline. Moving west-northwestward, these two TCs intensified and, while in the Philippine Sea, they simultaneously attained an extreme intensity of 160 kt (82 m/sec) -- the first time in the JTWC archives that two TCs of such extreme intensity co-existed in the WNP. The westernmost of these TCs, Ivan (28W), was the first and only TC of 1997 to make landfall in the Philippine archipelago. It grazed the northern tip of Luzon before recurving behind Joan (29W). The low number of landfalling TCs in the Philippines and along the coast of Asia (excluding Japan) may be partly related to El Niño (e.g., Dong 1988). Despite the low number of TCs to make landfall in eastern Asia, two that did, Winnie (10W) and Linda (31W), were significant natural disasters which caused much loss of life and great destruction at their respective landfall sites in China andVietnam. Mainland Japan, the Ryukyu Islands, the Bonin Islands, and the Mariana Islands were each affected by several typhoons. The last TC of 1997 in the WNP, Paka (05C), affected the Marshall Islands and the island of Guam and Rota.

The tracks of the TCs, which formed in the WNP during 1997, indicate a below-normal number of TCs in the South China Sea, and a below-normal number of straight-moving tracks. By contrast, there were a large number of TCs that moved northward, either on north-oriented tracks or conventional recurving tracks. Of the 33 significant TCs in the WNP during 1997, 8 (24%) were straight moving, 15 (46%) were recurvers, 6 (18%) moved on north-oriented tracks, and 4 (12%) were designated as "other".

In summary, a chronology of all the TC activity in the JTWC AOR during 1997 is provided in Figure 3-7. Composite best tracks for the WNP TCs are provided for the periods: 01 January to 02 August (Figure 3-8a), 21 July to 22 September (Figure 3-8b), and 17 September to 22 December (Figure 3-8c). Table 3-3 includes: a climatology of typhoons, and tropical storms/typhoons for the WNP for the period 1945-1997.

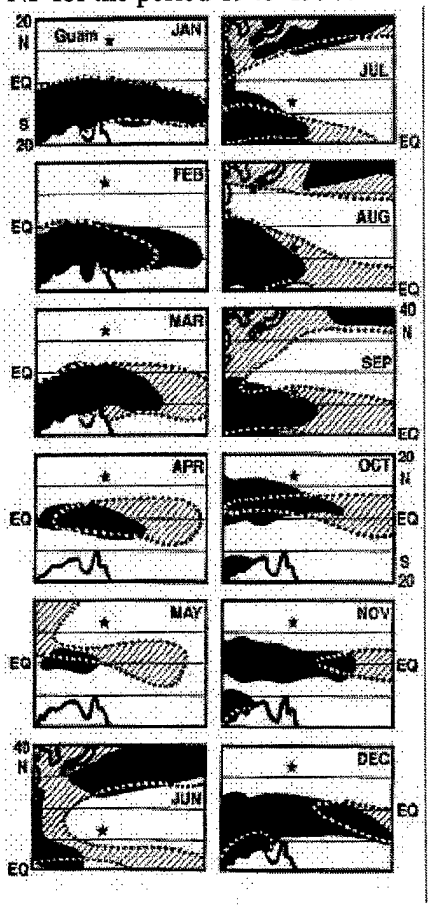

Figure 3-4 Comparison between climatological (black) and analyzed (shaded) mean monthly winds with a westerly component for the WNP in 1997. For June, July, and August the area of coverage is shifted northward to include the subtropics. For reference, the star indicates Guam's location. The outline of Australia appears in the lower left of each panel except for June, July and August where the Korean peninsula and Japan appear in the upper left. The climatology is adapted from Sadler et al. (1987). The 1997 monthly mean winds were adapted from the CPC (1997).

3.1.1 Monthly Activity Summary

JANUARY

Beginning during November of 1996, episodes of strong low-level monsoon westerlies began to occur in the low latitudes of the WNP. Most of the WNP TCs of November and December 1996 were associated with these episodes of enhanced low-level westerly wind flow. The simultaneous occurrence of TCs in the Southern Hemisphere -- some of them twins to the WNP TCs -- was a signature characteristic of the TC distribution as 1996 came to a close. Although the monsoon trough of the southern hemisphere became the dominant site of TC development by January of 1997, there were some episodes of enhanced westerly wind flow along the equator associated with a concurrent establishment of a near-equatorial trough in the WNP.

During just such time of enhanced westerly flow along the equator, the tropical disturbance which became **Hannah (01W)** formed in the near-equatorial trough south of the Marshall Islands. Moving on a long westward track for over two weeks, it reached a peak intensity of 50 kt (26m/s), and then dissipated in the Philippine Sea. Many of TCs of 1997 (including Hannah) shared the unusual characteristic of forming well to the east of normal: a typical behavior of TC's during an El Niño year. Although Tropical Storm Hannah was in most aspects relatively unremarkable, it was, in retrospect, an early manifestation of an unusual large-scale tropical circulation pattern which would see many of the TC's of 1997 form well east of normal in the Marshall Islands. We now know that the weather events over the low latitudes of the western Pacific during the late 1996 and early 1997 may be looked upon as the antecedent (or onset) conditions leading to the development of strong El Niño conditions by April of 1997. An eastward displacement of the mean genesis location of TCs in the WNP is a hallmark signature of El Niño.

FEBRUARY

In keeping with February's climatology as the month of lowest TC frequency in the WNP, there were no significant TCs in the WNP basin during February.

MARCH

There were no significant tropical cyclones in the WNP basin during March.

APRIL

During most of April, a monsoon trough stretched across Micronesia and westerly low-level winds persisted at low latitudes. During the final week of the month, sea-level pressure fell across the eastern Caroline Islands, abundant deep convection increased, and a monsoon depression developed. This monsoon depression moved westward and became **Super Typhoon Isa (02W)** -- the first of 11 super typhoons, the most ever in a single year -- to occur in 1997. Passing to the south of Guam on 16 April, Isa produced up to 10 inches (250 mm) of rain and wind gusts to near 60 kt (31 m/sec). Moving into the Philippine Sea late in the month, the typhoon turned to the north, intensified to a super typhoon, and then recurved over water to the southeast of Japan.

As Isa was recurving, monsoon westerlies persisted in low levels of Micronesia, and extended to the international dateline. **Tropical Storm Jimmy (03W)** formed a low latitude in a near-equatorial trough which extended across the southern Marshall Islands. This small TC moved northwest and intensified, reaching a peak of 55 kt (28 m/sec) as it made a turn to the northeast. It then encountered a shear line and dissipated over water during the final week of April.

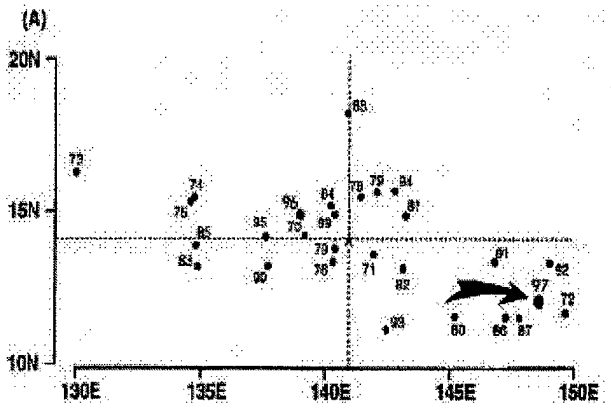

Figure 3-5a Mean annual genesis locations for the period 1970-1997. 1997's location is indicated by the arrow. The star lies at the intersection of the 28-year average latitude and longitude of genesis for statistical purposes, genesis is defined as the first 25 kt (13 m/sec) intensity on the best track.

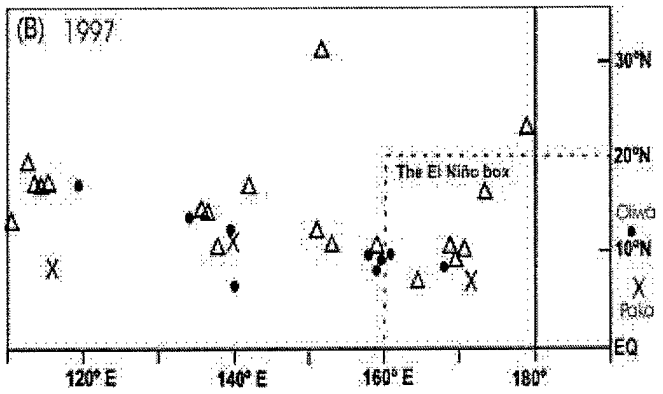

Figure 3-5b Point of formation of significant tropical cyclones in 1997 as indicated by the initial intensity of 25 kt (13 m/sec) on the best track. The symbols indicate: solid dots = 16 July to 15 October; and, X = 16 October to 31 December.

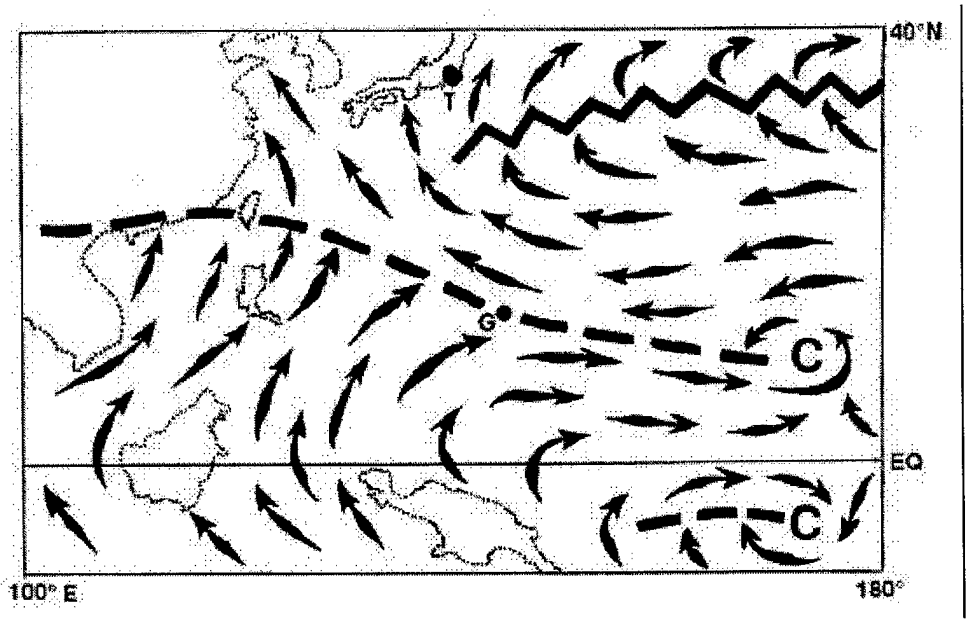

Figure 3-6 Schematic illustration of the low-level circulation pattern which dominated the WNP during August. Arrows indicate wind direction, dashed line indicates the axis of the monsoon trough, C indicates LLCCs, A= anticyclone center, G=Guam, and T=Tokyo.

Table 2-5a WESTERN NORTH PACIFIC OCEAN FIX PLATFORM SUMMARY FOR 1997

TROPICAL CYCLONE	SATELLITE	SCATTEROMETER	RADAR	SYNOPTIC	AIRCRAFT	TOTAL
01W HANNAH	117	1	0	0	0	118
02W ISA	362	7	32	0	0	401
03W JIMMY	114	5	0	0	0	119
04W KELLY	120	10	3	3	0	136
05W LEVI	116	3	9	0	0	128
06W MARIE	155	6	0	0	0	161
07W NESTOR	276	13	0	2	0	291
08W OPAL	173	7	34	11	0	225
09W PETER	156	14	37	23	0	230
10W ROSIE	221	1	45	8	0	275
11W SCOTT	173	3	0	0	0	176
12W TINA	300	4	96	4	0	404
13W VICTOR	75	0	17	0	0	92
14W WINNIE	385	2	71	7	0	465
15W YULE	157	3	0	1	0	161
16W -	49	2	0	0	0	51
17W ZITA	68	1	14	8	0	91
18W AMBER	238	4	18	9	0	269
19W BING	218	4	0	3	0	225
20W CASS	69	0	0	2	0	71
02C OLIWA	369	4	49	8	0	430
21W DAVID	197	5	0	3	0	205
22W FRITZ	95	1	0	3	0	99
23W ELLA	8	1	0	0	0	9
24W GINGER	156	4	0	0	0	160
25W HANK	50	2	0	0	0	52
26W -	82	0	0	0	0	82
27W IVAN	279	3	18	6	0	306
28W JOAN	269	3	23	2	0	297
29W KEITH	336	6	58	15	0	415
30W LINDA	196	3	0	5	0	204
31W MORT	162	3	0	8	0	173
05C PAKA	480	8	57	4	0	549
TOTALS	6221	133	581	135	0	7070
PERCENTAGE OF TOTAL	88%	2%	8%	2%	0%	100%

Table 2-5b NORTH INDIAN OCEAN FIX PLATFORM SUMMARY FOR 1997

TROPICAL CYCLONE	SATELLITE	SCATTEROMETER	RADAR	SYNOPTIC	AIRCRAFT	TOTAL
01B	137	5	0	0	0	142
02B	76	0	0	4	0	80
03A	23	2	0	1	0	26
04A	110	1	0	2	0	113
TOTALS	346	8	0	7	0	361
PERCENTAGE OF TOTAL	96%	2%	0%	2%	0%	100%

Table 2-5c SOUTH PACIFIC AND SOUTH INDIAN OCEAN FIX PLATFORM SUMMARY FOR 1997

TROPICAL CYCLONE	SATELLITE	SCATTEROMETER	RADAR	SYNOPTIC	AIRCRAFT	TOTAL
01S LINDSAY	41	1	0	0	0	42
02S -	91	2	0	0	0	93
03S -	78	1	0	0	0	79
04S ANTOINETTE	80	2	0	0	0	82
05S MELANIE/BELLAMI	242	4	0	0	0	246
06P CYRIL	106	2	0	1	0	109
07S CHANTELLE	121	2	0	0	0	123
08S DANIELLA	67	4	0	5	0	76
09S ELVINA	130	0	0	8	0	138
10P NICHOLAS	60	3	0	5	0	68
11S OPHELIA	147	0	0	0	0	147
12P PHIL	247	1	1	1	0	250
13P FERGUS	123	1	0	4	0	128
14S FABRIOLA	42	1	0	7	0	50
15S RACHEL	128	3	16	14	0	161
16P DRENA	130	2	0	7	0	139
17P EVAN	49	2	0	1	0	52
18S -	80	1	0	0	0	81
19S PANCHO-HELINDA	378	4	0	0	0	382
20S GRETELLE	76	3	0	4	0	83
21S ILETTA	76	2	0	0	0	78
22P FREDA	133	1	0	1	0	135
23S JOSIE	93	2	0	1	0	96
24P GILLIAN	47	1	0	1	0	49
25S KARLETTE	135	2	0	0	0	137
26P HAROLD	102	1	0	1	0	104
27S -	107	2	0	0	0	109
28P ITA	13	0	0	0	0	13
29P -	12	0	0	3	0	15
30S LIZETTE	19	2	0	0	0	21
31P GAVIN	151	4	4	1	0	160
32P JUSTIN	343	8	18	3	0	372
33P HINA	72	1	0	0	0	73
34P IAN	53	7	0	3	0	63
35P JUNE	135	10	0	2	0	147
36S RHONDA	178	9	0	0	0	187
37P -	54	0	0	0	0	54
38P KELI	113	4	0	0	0	117
TOTALS	4252	95	39	73	0	4459
PERCENTAGE OF TOTAL	95%	2%	1%	2%	0%	100%

3. Summary of Western North Pacific and North Indian Ocean Tropical Cyclones

3.1 Western North Pacific Ocean Tropical Cyclones

The year of 1997 was an El Niño year, and by some measures (e.g., the magnitude of the warming of the Sea Surface Temperature (SST) in the eastern equatorial Pacific), the El Niño episode of 1997 was one of the strongest in recorded history (Climate Prediction Center (CPC) 1997). El Niño had a large influence on the distribution of western North Pacific (WNP) TCs during 1997. The signature characteristics of the distribution, character and behavior of the tropical cyclones (TCs) of the WNP during 1997 (some known to be related to El Niño) include:

(1) a very high number of super typhoons;

(2) an early start of WNP TC activity with a higher than average number during the early season (01 January to 15 July);

(3) a tendency -- especially during the first half of the year -- for the TC tracks to be north oriented;

(4) a substantial eastward displacement of the mean genesis location for all TCs and for many of the individual TCs;

(5) the formation, east of the international dateline, of two TCs which moved into the WNP and became super typhoons -- Oliwa (02C) and Paka (05C) (these are Hawaiian names given to them by the Central Pacific Hurricane Center (CPHC));

(6) the landfall of only one TC in the Philippines;

(7) the formation in the monsoon trough of all but one of the TCs -- (Scott (07W) formed in direct association with a cyclonic circulation (cell) in the tropical upper tropospheric trough (TUTT)); and,

(8) the simultaneous existence in the Philippine Sea of 2 super typhoons -- Ivan (28W) and Joan (29W) -- each possessing an extreme intensity of 160 kt (82 m/sec).

Some of these unusual characteristics of the distribution and behavior of the TCs in the western North Pacific during 1997 are likely related to the large-scale atmospheric and oceanic circulation anomalies associated with 1997's strong El Niño/Southern Oscillation (ENSO) event. Of the items in this list, (2), (4) and (7) are typical features of El Niño years.

The annual number of significant TCs in the WNP during 1997 (Table 3-1) was almost normal: 33 versus the climatological average of 32 (Table 3-2). The year of 1997 included 11 super typhoons, 12 lesser typhoons, 8 tropical storms and 2 tropical depressions. The calendar-year total of 31 TCs (of at least tropical storm intensity) was one higher than the climatological average (Figure 3-1). The calendar-year total of 23 typhoons was five above the long-term average, and is the highest annual number of typhoons recorded in the WNP basin since 1971 when there were 24. The 11 super typhoons is an unprecedented value. Since 1970, as best-track wind and intensities became ever more constrained to conform to standardized TC wind-pressure relationships (e.g., Atkinson and Holiday 1977), the highest annual number of super typhoons is 7. (Figure 3-2). The high number of super typhoons in the WNP was one of the most significant highlights of 1997. The annual number of super typhoons may be weakly related to El Niño: the El Niño years of 1972, 76, 82, 87, 91, 93 and 94 had 2, 5, 5, 7, 7, 3, and 6 super typhoons respectively (for an average of 5.0); and, the La Niña years of 1973, 83, 88, 89, 95, and 96 had 3, 4, 3, 7, 5 and 6 super typhoons respectively (for an average of 4.7). A suggested physical mechanism for the increase in super typhoons during El Niño years is the longer over-water, low-latitude trajectories of the TCs which, because of El Niño, form well to the east of normal. The

annual number of super typhoons during 1997 is unprecedented, and its association with one of the strongest recorded El Niño events may be more than just a coincidence.

During the Boreal Spring of 1997, El Niño (i.e., very warm SST in the central and eastern equatorial Pacific) developed rapidly, coupled with a drop in the magnitude of the Southern Oscillation Index (Figure 3-3). Unusually persistent low-level westerly wind flow became established at low latitutudes in the WNP. This westerly wind flow was also displaced eastward from its normal domain (Figure 3-4). The set-up of low-level, low-latitude westerly wind flow early in the year led to the establishment of a near-equatorial trough across Micronesia from the western Caroline Islands eastward into the Marshall Islands. This trough supported the development of several TCs early season. According to Lander (1994), the only statistic of numbers of TCs in the WNP which is significantly correlated with any ENSO index is an increase in the number of cyclones from 01 January to 15 July.

Table 3-1 WESTERN NORTH PACIFIC SIGNIFICANT TROPICAL CYCLONES FOR 1997

TROPICAL CYCLONE	PERIOD OF WARNING	NUMBER WARNING ISSUED	ESTIMATED MAXIMUM INTENSITY KT (M/SEC)	ESTIMATED MSLP (MB)
01W TS HANNAH	19 JAN - 24 JAN	17	50 (26)	987
02W STY ISA	11 APR - 23 APR	47	145 (75)	892
03W TS JIMMY	22 APR - 25 APR	15	55 (28)	984
04W TS KELLY	07 MAY - 10 MAY	14	45 (23)	991
05W TS LEVI	25 MAY - 30 MAY	19	45 (23)	991
06W TY MARIE	26 MAY - 02 JUN	27	90 (46)	954
07W STY NESTOR	06 JUN - 15 JUN	37	140 (72)	898
08W TY OPAL	15 JUN - 21 JUN	26	90 (46)	954
09W TY PETER	23 JUN - 29 JUN	24	65 (33)	976
10W STY ROSIE	18 JUL - 28 JUL	38	140 (72)	898
11W TS SCOTT*	24-25 JUL/27-02 AUG	30	55 (28)	984
12W TY TINA	29 JUL - 09 AUG	44	90 (46)	954
13W TY VICTOR	30 JUL - 03 AUG	15	65 (33)	976
14W STY WINNIE	08 AUG - 19 AUG	44	140 (72)	898
15W TY YULE	16 AUG - 23 AUG	27	65 (33)	976
16W TD	18 AUG - 19 AUG	5	30 (15)	1000
17W TY ZITA	21 AUG - 23 AUG	10	75 (39)	967
18W TY AMBER	21 AUG - 30 AUG	36	110 (57)	933
19W STY BING	27 AUG - 05 SEP	36	135 (69)	904
20W TS CASS	28 AUG - 30 AUG	11	45 (23)	991
02C STY OLIWA#	02 SEP - 17 SEP	53(6)	140 (72)	898
21W TY DAVID	11 SEP - 20 SEP	35	95 (49)	949
22W TY FRITZ	20 SEP - 25 SEP	21	75 (39)	968
23W TS ELLA	21 SEP - 25 SEP	14	40 (21)	994
24W STY GINGER	22 SEP - 30 SEP	31	145 (75)	892
25W TS HANK	03 OCT - 04 OCT	7	40 (21)	994
26W TD	04 OCT - 07 OCT	10	30 (15)	1000
27W STY IVAN	13 OCT - 24 OCT	46	160 (82)	872
28W STY JOAN	13 OCT - 24 OCT	44	160 (82)	872
29W STY KEITH	27 OCT - 08 NOV	48	155 (80)	878
30W TY LINDA	31 OCT - 09 NOV	35	65 (33)	976
31W TY MORT	10 NOV - 16 NOV	23	65 (33)	976
05C STY PAKA#	02 DEC - 21 DEC	61(17)	160 (82)	901**
	JTWC TOTAL	950		
	#NPMOC TOTAL	(23)		
	GRAND TOTAL	973		

* REGENERATED
** ATLANTIC INTENSITY - MSLP RELATIONSHIP USED
\# WARNINGS ISSUED BY NPMOC

Table 3-2 DISTRIBUTION OF WESTERN NORTH PACIFIC TROPICAL CYCLONES FOR 1959 - 1997

YEAR	JAN	FEB	MAR	APR	MAY	JUN	JUL	AUG	SEP	OCT	NOV	DEC	TOTALS
1959	0	1	1	1	0	1	3	8	9	3	2	2	31
	000	010	010	100	000	001	111	512	423	210	200	200	17 7 7
1960	1	0	1	1	1	3	3	9	5	4	1	1	30
	001	000	001	100	010	210	210	810	041	400	100	100	19 8 3
1961	1	1	1	1	4	6	5	7	6	7	2	1	42
	010	010	100	010	211	114	320	313	510	322	101	100	20 11 11
1962	0	1	0	1	3	0	8	8	7	5	4	2	39
	000	010	000	100	201	000	512	701	313	311	301	020	24 6 9
1963	0	0	1	1	0	4	5	4	4	6	0	3	28
	000	000	001	100	000	310	311	301	220	510	000	210	19 6 3
1964	0	0	0	0	3	2	8	8	8	7	6	2	44
	000	000	000	000	201	200	611	350	521	331	420	101	26 13 5
1965	2	2	1	1	2	4	6	7	9	3	2	1	40
	110	020	010	100	101	310	411	322	531	201	110	010	21 13 6
1966	0	0	0	1	2	1	4	9	10	4	5	2	38
	000	000	000	100	200	100	310	531	532	112	122	101	20 10 8
1967	1	0	2	1	1	1	8	10	8	4	4	1	41
	010	000	110	100	010	100	332	343	530	211	400	010	20 15 6
1968	0	1	0	1	0	4	3	8	4	6	4	0	31
	000	001	000	100	000	202	120	341	400	510	400	000	20 7 4
1969	1	0	1	1	0	0	3	3	6	5	2	1	23
	100	000	010	100	000	000	210	210	204	410	110	010	13 6 4
1970	0	1	0	0	0	2	3	7	4	6	4	0	27
	000	100	000	000	000	110	021	421	220	321	130	000	12 12 3
1971	1	0	1	2	5	2	8	5	7	4	2	0	37
	010	000	010	200	230	200	620	311	511	310	110	000	24 11 2
1972	1	0	1	0	0	4	5	5	6	5	2	3	32
	100	000	001	000	000	220	410	320	411	410	200	210	22 8 2
1973	0	0	0	0	0	0	7	6	3	4	3	0	23
	000	000	000	000	000	000	430	231	201	400	030	000	12 9 2
1974	1	0	1	1	1	4	5	7	5	4	4	2	35
	010	000	010	010	100	121	230	232	320	400	220	020	15 17 3
1975	1	0	0	1	0	0	1	6	5	6	3	2	25
	100	000	000	001	000	000	010	411	410	321	210	002	14 6 5
1976	1	1	0	2	2	2	4	4	5	0	2	2	25
	100	010	000	110	200	200	220	130	410	000	110	020	14 11 0
1977	0	0	1	0	1	1	4	2	5	4	2	1	21
	000	000	010	000	001	010	301	020	230	310	200	100	11 8 2
1978	1	0	0	1	0	3	4	8	4	7	4	0	32
	010	000	000	100	000	030	310	341	310	412	121	000	15 13 4
1979	1	0	1	1	2	0	5	4	6	3	2	3	28
	100	000	100	100	011	000	221	202	330	210	110	111	14 9 5
1980	0	0	1	1	4	1	5	3	7	4	1	1	28
	000	000	001	010	220	010	311	201	511	220	100	010	15 9 4
1981	0	0	1	1	1	2	5	8	4	2	3	2	29
	000	000	100	010	010	200	230	251	400	110	210	200	16 12 1
1982	0	0	3	0	1	3	4	5	6	4	1	1	28
	000	000	210	000	100	120	220	500	321	301	100	100	19 7 2
1983	0	0	0	0	0	1	3	6	3	5	5	2	25
	000	000	000	000	000	010	300	231	111	320	320	020	12 11 2
1984	0	0	0	0	0	2	5	7	4	8	3	1	30
	000	000	000	000	000	020	410	232	130	521	300	100	16 11 3
1985	2	0	0	0	1	3	1	7	5	5	1	2	27
	020	000	000	000	100	201	100	520	320	410	010	110	17 9 1
1986	0	1	0	1	2	2	2	5	2	5	4	3	27
	000	100	000	100	110	110	200	410	200	320	220	210	19 8 0
1987	1	0	0	1	0	2	4	4	7	2	3	1	25
	100	000	000	010	000	110	400	310	511	200	120	100	18 6 1
1988	1	0	0	0	1	3	2	5	8	4	2	1	27
	100	000	000	000	100	111	110	230	260	400	200	010	14 12 1
1989	1	0	0	1	2	2	6	8	4	6	3	2	35
	010	000	000	100	200	110	231	332	220	600	300	101	21 10 4
1990	1	0	0	1	2	4	4	5	5	5	4	1	31
	100	000	000	010	110	211	220	500	410	230	310	100	21 9 1
1991	0	0	2	1	1	1	4	8	6	3	6	0	32
	000	000	110	010	100	100	400	332	420	300	330	000	20 10 2

(TABLE CONTINUED ON TOP OF NEXT PAGE)

Table 3-2 (CONTINUED FROM PREVIOUS PAGE)

YEAR	JAN	FEB	MAR	APR	MAY	JUN	JUL	AUG	SEP	OCT	NOV	DEC	TOTALS
1992	1	1	0	0	0	3	4	8	5	6	5	0	33
	100	010	000	000	000	210	220	440	410	510	311	000	21 11 1
1993	0	0	2	2	1	2	5	8	5	6	4	3	38
	000	000	011	002	010	101	320	611	410	321	112	300	21 9 8
1994	1	0	1	0	2	2	9	9	8	7	0	2	41
	001	000	100	000	101	020	342	630	440	511	000	110	21 15 5
1995	1	0	0	0	1	2	3	7	7	8	2	3	34
	001	000	000	000	010	020	210	421	412	512	020	012	15 11 8
1996	0	1	0	2	2	0	7	10	7	5	6	3	43
	000	001	000	011	110	000	610	433	610	212	132	111	21 12 10
1997	1	0	0	2	3	3	4	8	4	6	1	1	33
	010	000	000	110	120	300	310	611	310	411	100	100	23 8 2
(1959-1996)													
MEAN	0.6	0.3	0.6	0.8	1.3	2.1	4.6	6.5	5.8	4.8	3.0	1.5	31.9
CASES	22	11	23	29	48	79	175	248	219	182	113	57	1206

The criteria used in TABLE 3-2 are as follows:

1) If a tropical cyclone was first warned on during the last two days of a particular month and continued into the next month for longer than two days, then that system was attributed to the second month.

2) If a tropical cyclone was warned on prior to the last two days of a month, it was attributed to the first month, regardless of how long the system lasted.

3) If a tropical cyclone began on the last day of the month and ended on the first day of the next month, that system was attributed to the first month. However, if a tropical cyclone began on the last day of the month and continued into the next month for only two days, then it was attributed to the second month.

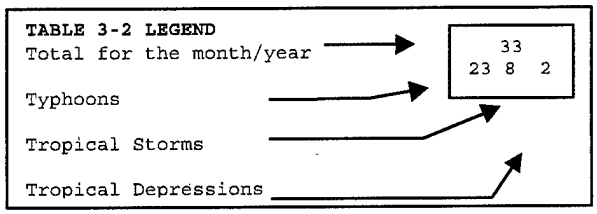

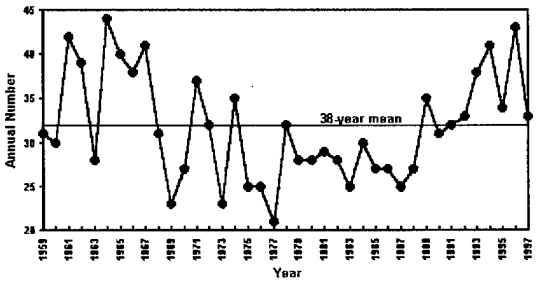

Figure 3-1 Tropical cyclones of tropical storm or greater intensity in the western North Pacific (1960-1997).

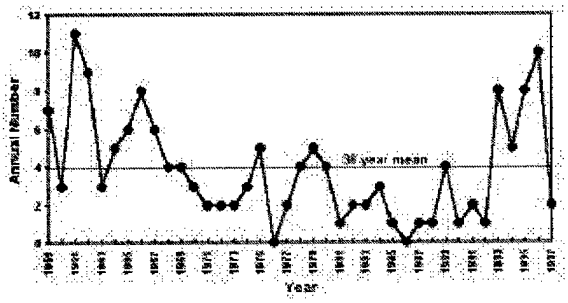

Figure 3-2 Number of western North Pacific super typhoons (1960-1997).

The annual mean genesis location of TCs which form in the WNP is related to the status of ENSO: it tends to be east of normal during El Niño years and west of normal during those years characterized by large-scale climatic anomalies opposite to those of El Niño, years known as La Niña or ENSO cold phase. Consistent with the TC distribution typically associated with El Niño (or an ENSO warm phase), the annual mean genesis location for all TCs during 1997 was substantially east of normal (Figure 3-5a). This was a pronounced change from the TC distributions during 1995 and 1996 (both weak La Niña years) when this statistic was west of normal. A breakdown of the genesis locations of the individual WNP TCs of 1997 (Figure 3-5b) shows that most formed east of 140E. Eleven formed east of 160E, while only two -- two below normal -- formed in the South China Sea. Through the period of 1960 to 1991, the five years with the highest annual average of the Southern Oscillation Index (SOI) (i.e., 1988, 1975, 1974, 1973,

and 1971) had an average of 2.4 TCs east of 160E, and the five years with the lowest annual average SOI (i.e., 1991, 1987, 1982, 1977, and 1972) had an average of 7.4 TCs east of 160E. (Note: all El Niño years have below normal values of the SOI.) During 1996, only one TC formed within the region designated as the "El Niño" box on Figure 3-5b, while 10 TCs formed there during 1997 (including those TCs that originated east of the International Date Line).

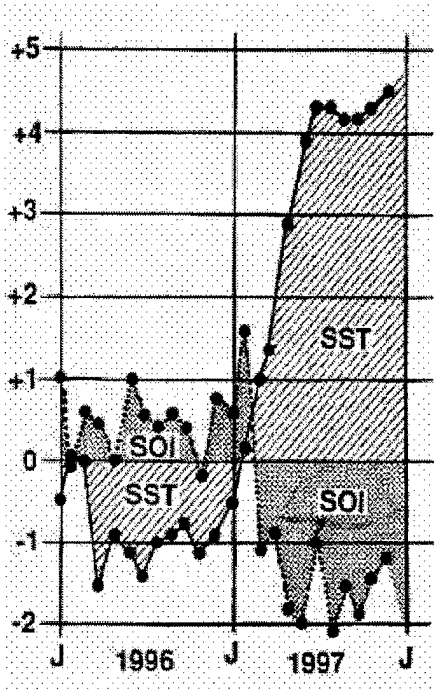

Figure 3-3 Anomalies from the monthly mean for eastern equatorial Pacific Ocean sea-surface temperature (hatched) in degrees Celsius and the Southern Oscillation Index (SOI) (shaded) for the period 1996 through 1997. (Adapted from Climate Prediction Center, 1997).

The annual number of TCs which form in this "El Niño" box has been shown by Lander (1994) to be dramatically affected by El Niño: far more TCs form within it during EL Niño years than during normal and La Niña years. Only one TC during 1997 -- Scott (07W) -- formed north of 20N in direct association with a TUTT cell. All other TCs of 1997 formed at low latitudes in the monsoon trough. There was a tendency during 1997 for low-level monsoon winds to persist at low latitudes and for the axis of the monsoon trough to remain near 10N across Micronesia (Figure 3-6).

Low-level westerly wind anomalies persisted throughout Micronesia with the largest westerly wind anomalies located at low latitudes near and to the east of the international dateline. Corresponding anomalies in the upper troposphere consisted of easterly wind anomalies over most of the low latitudes of the WNP. These large-scale atmospheric flow-pattern anomalies of 1997 were nearly everywhere the reverse of those that persisted for most of 1995 and 1996. The atmospheric flow anomalies of 1997 over the WNP are typical of those expected during an El Niño year.

Monsoon westerlies and the axis of the monsoon trough frequently stretched across all of Micronesia as far as the international dateline (and occasionally beyond) during most of 1997. Despite the nearly continuous presence of the monsoon trough and abundant deep convection, the number of TCs (of at least tropical storm intensity) was near normal; and, compared with 1995 and 1996, the number of TCs which failed to mature and remained only at tropical depression intensity was much reduced. The TCs of 1997 tended to emerge one-by-one from the eastern portion of the basin and then recurve or move north; each subsequent development at low latitude tended to occur after the prior TC had exited the tropics; and, the TCs emerging from the eastern end of the monsoon trough tended to be large, very intense and slow-moving. There were few cases of multiple TCs (i.e., the simultaneous occurrence of two or more) in the WNP during 1997. The most noteworthy case of multiple TCs was the simultaneous formation and development in October of Ivan (28W) and Joan (29W).

These two TCs formed simultaneously along a segment of the monsoon trough axis, which stretched across the Marshall Islands and eastward beyond the international dateline. Moving west-northwestward, these two TCs intensified and, while in the Philippine Sea, they simultaneously attained an extreme intensity of 160 kt (82 m/sec) -- the first time in the JTWC archives that two TCs of such extreme intensity co-existed in the WNP. The westernmost of these TCs, Ivan (28W), was the first and only TC of 1997 to make landfall in the Philippine archipelago. It grazed the northern tip of Luzon before recurving behind Joan (29W). The low number of landfalling TCs in the Philippines and along the coast of Asia (excluding Japan) may be partly related to El Niño (e.g., Dong 1988). Despite the low number of TCs to make landfall in eastern Asia, two that did, Winnie (10W) and Linda (31W), were significant natural disasters which caused much loss of life and great destruction at their respective landfall sites in China andVietnam. Mainland Japan, the Ryukyu Islands, the Bonin Islands, and the Mariana Islands were each affected by several typhoons. The last TC of 1997 in the WNP, Paka (05C), affected the Marshall Islands and the island of Guam and Rota.

The tracks of the TCs, which formed in the WNP during 1997, indicate a below-normal number of TCs in the South China Sea, and a below-normal number of straight-moving tracks. By contrast, there were a large number of TCs that moved northward, either on north-oriented tracks or conventional recurving tracks. Of the 33 significant TCs in the WNP during 1997, 8 (24%) were straight moving, 15 (46%) were recurvers, 6 (18%) moved on north-oriented tracks, and 4 (12%) were designated as "other".

In summary, a chronology of all the TC activity in the JTWC AOR during 1997 is provided in Figure 3-7. Composite best tracks for the WNP TCs are provided for the periods: 01 January to 02 August (Figure 3-8a), 21 July to 22 September (Figure 3-8b), and 17 September to 22 December (Figure 3-8c). Table 3-3 includes: a climatology of typhoons, and tropical storms/typhoons for the WNP for the period 1945-1997.

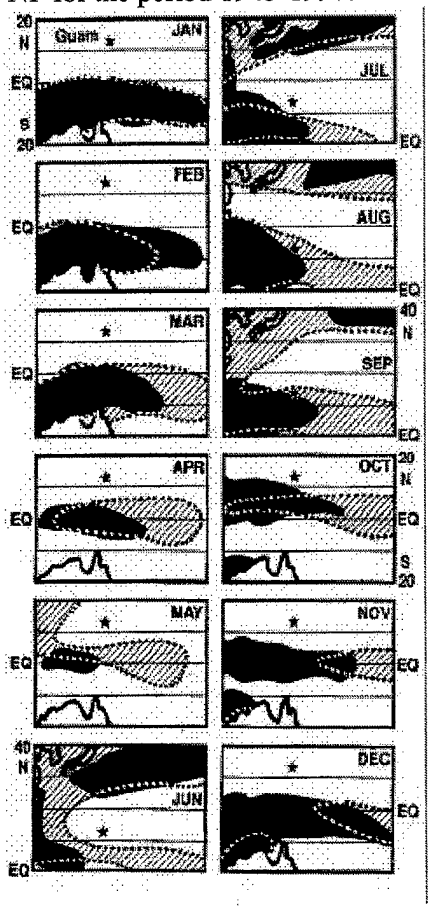

Figure 3-4 Comparison between climatological (black) and analyzed (shaded) mean monthly winds with a westerly component for the WNP in 1997. For June, July, and August the area of coverage is shifted northward to include the subtropics. For reference, the star indicates Guam's location. The outline of Australia appears in the lower left of each panel except for June, July and August where the Korean peninsula and Japan appear in the upper left. The climatology is adapted from Sadler et al. (1987). The 1997 monthly mean winds were adapted from the CPC (1997).

3.1.1 Monthly Activity Summary

JANUARY

Beginning during November of 1996, episodes of strong low-level monsoon westerlies began to occur in the low latitudes of the WNP. Most of the WNP TCs of November and December 1996 were associated with these episodes of enhanced low-level westerly wind flow. The simultaneous occurrence of TCs in the Southern Hemisphere -- some of them twins to the WNP TCs -- was a signature characteristic of the TC distribution as 1996 came to a close. Although the monsoon trough of the southern hemisphere became the dominant site of TC development by January of 1997, there were some episodes of enhanced westerly wind flow along the equator associated with a concurrent establishment of a near-equatorial trough in the WNP.

During just such time of enhanced westerly flow along the equator, the tropical disturbance which became **Hannah (01W)** formed in the near-equatorial trough south of the Marshall Islands. Moving on a long westward track for over two weeks, it reached a peak intensity of 50 kt (26m/s), and then dissipated in the Philippine Sea. Many of TCs of 1997 (including Hannah) shared the unusual characteristic of forming well to the east of normal: a typical behavior of TC's during an El Niño year. Although Tropical Storm Hannah was in most aspects relatively unremarkable, it was, in retrospect, an early manifestation of an unusual large-scale tropical circulation pattern which would see many of the TC's of 1997 form well east of normal in the Marshall Islands. We now know that the weather events over the low latitudes of the western Pacific during the late 1996 and early 1997 may be looked upon as the antecedent (or onset) conditions leading to the development of strong El Niño conditions by April of 1997. An eastward displacement of the mean genesis location of TCs in the WNP is a hallmark signature of El Niño.

FEBRUARY

In keeping with February's climatology as the month of lowest TC frequency in the WNP, there were no significant TCs in the WNP basin during February.

MARCH

There were no significant tropical cyclones in the WNP basin during March.

APRIL

During most of April, a monsoon trough stretched across Micronesia and westerly low-level winds persisted at low latitudes. During the final week of the month, sea-level pressure fell across the eastern Caroline Islands, abundant deep convection increased, and a monsoon depression developed. This monsoon depression moved westward and became **Super Typhoon Isa (02W)** -- the first of 11 super typhoons, the most ever in a single year -- to occur in 1997. Passing to the south of Guam on 16 April, Isa produced up to 10 inches (250 mm) of rain and wind gusts to near 60 kt (31 m/sec). Moving into the Philippine Sea late in the month, the typhoon turned to the north, intensified to a super typhoon, and then recurved over water to the southeast of Japan.

As Isa was recurving, monsoon westerlies persisted in low levels of Micronesia, and extended to the international dateline. **Tropical Storm Jimmy (03W)** formed a low latitude in a near-equatorial trough which extended across the southern Marshall Islands. This small TC moved northwest and intensified, reaching a peak of 55 kt (28 m/sec) as it made a turn to the northeast. It then encountered a shear line and dissipated over water during the final week of April.

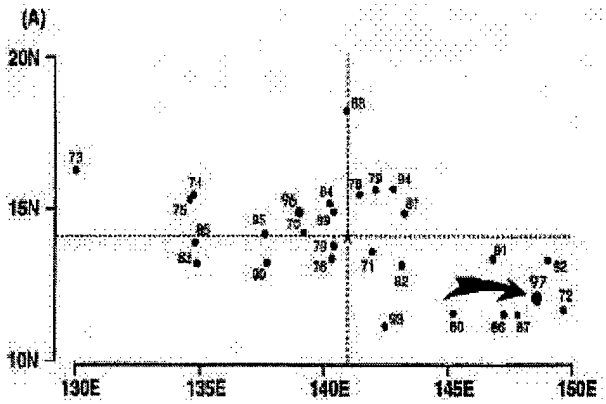

Figure 3-5a Mean annual genesis locations for the period 1970-1997. 1997's location is indicated by the arrow. The star lies at the intersection of the 28-year average latitude and longitude of genesis for statistical purposes, genesis is defined as the first 25 kt (13 m/sec) intensity on the best track.

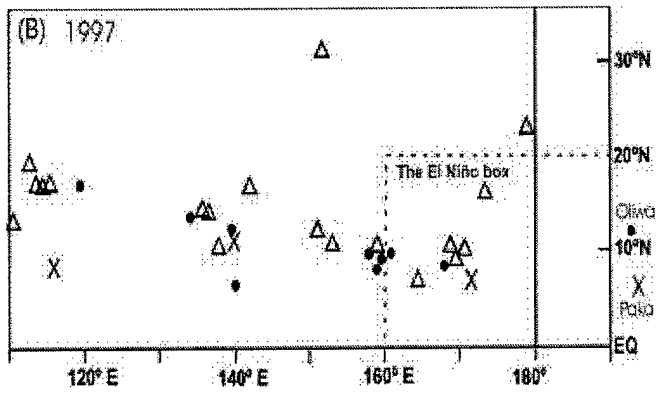

Figure 3-5b Point of formation of significant tropical cyclones in 1997 as indicated by the initial intensity of 25 kt (13 m/sec) on the best track. The symbols indicate: solid dots = 16 July to 15 October; and, X = 16 October to 31 December.

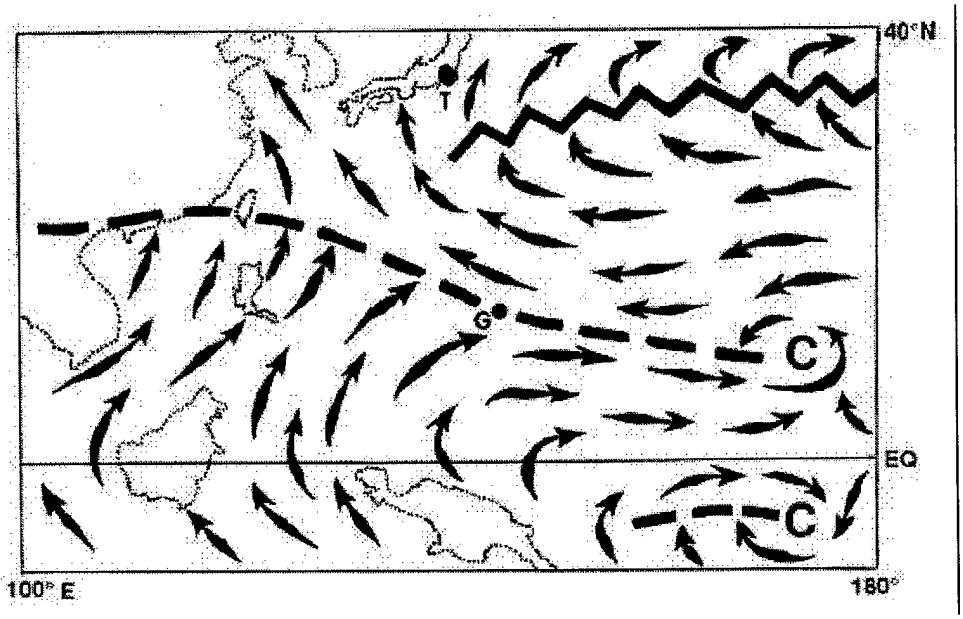

Figure 3-6 Schematic illustration of the low-level circulation pattern which dominated the WNP during August. Arrows indicate wind direction, dashed line indicates the axis of the monsoon trough, C indicates LLCCs, A= anticyclone center, G=Guam, and T=Tokyo.

MAY

As the month of May began, monsoon westerlies persisted across the low latitudes of the eastern half of Micronesia. **Tropical Storm Kelly (04W)**, like Jimmy (03W) two weeks earlier, formed at low latitude in the southern Marshall Islands. It was a relatively weak TC, which moved slowly to the northwest, then after heeling over to a faster westward track, it dissipated over water. During mid-May, the tropics of the WNP became inactive.

The next episode of TC development commenced during the final week of May when two TCs -- **Tropical Storm Levi (05W) and Typhoon Marie (06W) --** formed at opposite ends of the basin: Levi in the South China Sea and Marie at low latitude near 160E. While still a depression, Levi moved eastward across Luzon where it caused severe flooding in Metro-Manila. Ivan (27W) was the only mature system to hit the Philippines. After entering the Philippine Sea, it turned to the north, reached its maximum intensity of 45 kt (23 m/sec), and eventually recurved on 28 May, merging with the Mei-Yu front south of Japan. Marie initially moved westward, then turned to the north and maintained a northward track for several days. While intensification was initially slow, Marie eventually reached a maximum intensity of 90 kt (47 m/sec). Shortly thereafter, Marie recurved and eventually became extratropical.

JUNE

Levi and Marie were still active in early June as they accelerated into midlatitudes, became extratropical, and crossed the international dateline to become mid- latitude lows northwest of Hawaii. Low-latitude monsoon westerlies continued to persist across Micronesia during June, and three TCs -- Nestor (07W), Opal (08W) and Peter (09W) -- formed in the monsoon trough.

Super Typhoon Nestor (07W) began as a monsoon depression in the Marshall Islands. It moved toward the west-northwest and slowly intensified. After becoming a tropical storm, it jogged to the north-northwest passing to the east and over the top of the Mariana Island chain. It became the second super typhoon of the season when located about 200 nm (370 km) northeast of Saipan (WMO 91232). Undergoing another synoptic-scale meander, it swung back to a northwesterly track before undergoing recurvature to the east of Japan.

As Nestor (07W) recurved, another monsoon depression -- originating in the eastern Caroline Islands -- consolidated and became **Typhoon Opal (08W)**. Opal moved on a north oriented track and began to rapidly intensify, but ran into westerly shear as it reached its maximum intensity of 90 kt (47 m/sec). It then turned to the northeast and became the first TC of the season to hit Japan, making landfall in southern Honshu. Opal then accelerated north of Tokyo, entered the Pacific Ocean, and became extratropical.

After Opal (08W) recurved, another monsoon depression, originating again in the eastern Caroline Islands, consolidated and became **Typhoon Peter (09W)**. During the last week of June, Peter approached Luzon, but then turned north and became a minimal typhoon of 65 kt (34 m/sec) as it neared the Ryukyu Island Chain. After Peter reached 30N, it turned to the northeast, made landfall in Kyushu, and traversed nearly the entire length of Honshu. Exiting Honshu and moving over water, the TC reintensified to become a typhoon once again as it passed to the south of the Kamchatka peninsula.

JULY

During the first few days of July, Typhoon Peter (09W) moved eastward at high latitude and slowly weakened. It crossed the international dateline and became a weak

extratropical low on 04 July. During the first half of July there was a break in TC activity.

There wasn't another named TC in the WNP basin until 19 July when **Super Typhoon Rosie (10W)** was upgraded from a tropical depression to a tropical storm. Rosie formed as a monsoon depression at low latitudes to the south of Guam. It moved on a north-oriented track and became the year's third super typhoon while it was moving toward the north approximately 600 nm (1110 km) east-northeast of Luzon. During the last week of July, Rosie made landfall on the south coast of Shikoku, and then passed across Honshu into the Sea of Japan where it stalled and weakened. The remnants of Rosie, drifted southeastward back across Honshu and dissipated over water southwest of Tokyo.

While most of the tropical cyclones had developed in the monsoon trough in the eastern and western parts of the basin, the birth of **Tropical Storm Scott (11W)** occurred north of 20N in direct association with a cyclonic circulation in the Tropical Upper Tropospheric Trough. As TD 11W, the system interacted with the outflow of Super Typhoon Rosie (10W), and was steered to the southeast for a few days. It eventually turned to the northwest for 24 hours, then recurved and reached its maximum intensity of 55 kt (29 m/sec). Scott spent its entire life over water.

Like so many other 1997 tropical cyclones, the disturbance that became **Typhoon Tina (12W)** developed in the El Niño-induced monsoon trough in the eastern Caroline Islands. Organization was very slow for over a week as the disturbance moved to the northwest. On 29 July, the system became TD 12W and on 05 August it reached its 90 kt (47 m/sec) maximum intensity. Tina then turned to the north, passed between Taiwan and Okinawa, made landfall in southern Korea, and dissipated in the Sea of Japan on 10 August.

As Tina was developing in the eastern part of the basin, the cloud system that became **Typhoon Victor (13W)** was consolidating together west of Luzon in the South China Sea. The system moved on a northward track and intensified slowly against northerly upper-level shear. It finally reached minimal typhoon intensity just prior to making landfall near Waglin Island, Hong Kong on 02 August.

AUGUST

August was an extremely busy with a total of ten TCs spending some part of their life in the month. As Tina (12W) and Victor (13W) were maturing in the western portion of the WNP basin, yet another monsoon depression was developing in association with El Nino-induced westerlies in the Marshall Islands. The new monsoon depression soon reached tropical storm intensity, and then intensified into **Super Typhoon Winnie (14W)**, the fourth of the eleven super typhoons. Winnie was unique in that as it moved toward Okinawa, a large rain band completely encircled the eye wall cloud, producing an outer eye wall cloud with a diameter of nearly 200 nm (370 km), one of the largest ever observed. Doppler radar at Kadena AB (Okinawa) clocked winds of 100 kt (52 m/sec) in the outer eye wall cloud. Winnie later made landfall south of Shanghai, China and dissipated rapidly. Torrential rains associated with Winnie caused considerable death and destruction in China.

As Winnie was forming its unusual concentric eye wall clouds, **Typhoon Yule (15W) and Tropical Depression 16 (TD 16W)** were organizing in the prolific monsoon trough that extended from east of the international dateline westward to the Caroline Islands. The disturbance that became Yule began at the extremely low latitude of 03N, while the system that became 16W started east of the Date Line. The two systems engaged in a direct interaction, with

Yule moving to the north-northeast and TD16W moving to the west. The two systems eventually merged with Yule becoming the dominant circulation. Yule briefly attained typhoon intensity, and after a long north-oriented track, it became an intense tropical-extratropical hybrid system with typhoon-force winds. The weakened system finally recurved at almost 50N.

Typhoon Zita (17W) was one of the three TCs to reach typhoon intensity in the South China Sea, and one of four TCs to develop in the monsoon trough in a 8-day period. It developed in the monsoon trough about 300 nm (560 km) to the west of Luzon and moved in a northward direction. The system rapidly moved into easterly steering flow and turned to the west. Despite its proximity to the China mainland, it intensified significantly, reaching a maximum intensity of 75 kt (39 m/sec) over the Luichow Peninsula. Zita maintained this strength across the Gulf of Tonkin, and made landfall in Vietnam on the morning of 23 August.

The pre-**Typhoon Amber (18W)** disturbance developed southwest of Guam and took a slow westward, then northwestward track toward Taiwan. Amber intensified slightly faster than the normal Dvorak one T-number per day, and had reached 100 kt (52 m/sec) on the morning of 25 August. At this time, **Tropical Storm Cass (20W)** began to form southwest of Amber in the South China Sea, about 160 nm (296 km) south of Hong Kong. Shear from the outflow from Typhoon Amber inhibited Cass' intensification. On 28 August, the two TCs underwent a binary interaction, which accelerated Amber toward Taiwan and caused Cass to move slowly to the east. After some vacillation in intensity, Amber reached its peak of 110 kt (57 m/sec) just prior to hitting Taiwan on 29 August. Amber weakened over the mountainous island, and later made landfall on mainland China. Tropical Storm Cass (20W) was very short-lived, spending only 2.5 days in warning. Once Amber move over Taiwan, Cass moved to the north and intensified to its peak of 45 kt (23 m/sec). Cass made landfall in mainland China, 150 nm (278 km) west of Taiwan, and later dissipated over the mountains of southern China.

While Amber (18W) was developing southwest of Guam, the disturbance destined to become **Super Typhoon Bing (19W)** was developing near the eastern extent of the monsoon trough in the Marshall Islands. The system was upgraded to TD 19W on 27 August and tracked westward at 13-15 kt (24-28 km/hr) toward the Mariana Islands. On the afternoon of 29 August, Tropical Storm Bing passed through the channel that separates Guam and Rota with 40-kt (21-m/sec) sustained winds. After passing Guam, Bing began to rapidly intensify, and 54 hours later, it reached its peak intensity of 135 kt (70 m/sec), becoming the fifth super typhoon of the season. Near 143E, Bing slowed its forward motion and turned to the north. Shortly thereafter, it accelerated to a speed of 11-13 kt (20-24 km/hr), maintaining northward motion for three days, until it recurved to the northeast about 300 nm (555 km) south of eastern Japan. Bing's forward speed accelerated to 30 kt (56 km/hr) as it transitioned into a 55-kt (29 m/sec) extratropical cyclone on 05 September.

SEPTEMBER

September was also a busy month with five TCs. At the end of August, a tropical disturbance formed to the southwest of Hawaii in the monsoon trough displaced far to the east as a result of the intense El Niño event. The disturbance would eventually become **Super Typhoon Oliwa (02C)** (a Hawaiian name -- pronounced "Oh'-lee-vah") after it crossed the international dateline. Oliwa reached tropical storm intensity in the Central North Pacific and proceeded on a westward track, crossing the dateline on 04

September. In the WNP, Oliwa intensified slowly to typhoon intensity, then explosively deepened, with its winds increasing from 75 kt (39 m/sec) to its peak of 140 kt (72 m/sec) in only 24 hours. Super Typhoon Oliwa (02C) continued it's west-northwest motion, slowly weakening. At mid-month, it recurved northeast of the Ryukyu Islands and made landfall in southern Kyushu with an intensity of 70 kt (36 m/sec), causing some deaths and considerable destruction. Oliwa dissipated in the Sea of Japan.

The disturbance that became **Typhoon David (21W)**, initially developed east of the dateline in the active monsoon trough. TD 21W moved to the northwest, intensifying at a normal one T-number/day rate. The system was large, and the northward component was attributed to the "Beta effect" of its large size. David attained its maximum intensity of 95 kt (49 m/sec) on the morning of 15 September. Typhoon David recurved, passed south of Japan, and became extratropical on 21 September en route to the Gulf of Alaska.

While David (21W) was recurving southeast of Japan, the disturbance that became **Super Typhoon Ginger (24W)**, was consolidating near the international dateline as one of 10 TCs which formed east of 160E and south of 20N -- within the El Niño box (See Figure 3-3a). Ginger moved on a north-oriented track in the eastern portion of the WNP basin. Ginger underwent a 24-hour period of explosive deepening, and as it neared its peak intensity of 145 kt (75 m/sec), the typhoon possessed an extensive system of primary and peripheral rain bands. When Ginger reached 30N, it accelerated within the mid-latitude westerlies where it transitioned into a vigorous extratropical low.

Typhoon Fritz (22W) was first seen as an area of enhanced convection in the South China Sea. As the system moved away from the coast of Vietnam, it slowly intensified. After a few days of eastward movement, Fritz turned back to the west toward Vietnam and continued to intensify. It reached its peak intensity of 75 kt (39 m/sec), which it maintained until it made landfall in Vietnam on 25 September. The system dissipated over land, but torrential rains triggered landslides that took the lives of many gold prospectors.

Tropical Storm Ella (23W) developed as a very small circulation east of the dateline. By 21 September, convection had become well-organized, abeit small (30 nm (56 km), over the system center. Ella sped to the west-northwest at 18-25 kt (33-46 km/hr), reached its maximum intensity of 40 kt (21 m/sec) on 22 September, recurved and dissipated on 24 September near 40N 170E.

OCTOBER

Tropical Storm Hank (25W) was the shortest-lived tropical cyclone of the season, with warnings issued for only 36 hours. The disturbance that became Hank, was first observed on 27 September in the South China Sea, but the first warning was not issued until 03 September. The system moved erratically, and upper-level wind shear prevented it from intensifying beyond 40 kt (21 m/sec). Hank made landfall in northern Vietnam on 05 September and dissipated soon thereafter.

As Hank was developing in the South China Sea, **Tropical Depression 26W (TD 26W)** formed southeast of Guam. The disturbance initially moved northward, then healed over to the west and passed north of Guam on 03 October, where it attained its maximum intensity of 30 kt (16 m/sec). TD 26W maintained this intensity for three more days, but strong westerly upper level shear never allowed it to intensify. As an exposed low level circulation, TD 26W merged with a frontal boundary over the Philippine Sea.

Super Typhoon Ivan (27W) and Super Typhoon Joan (28W) were two of three TCs in the WNP during 1997 to attain an extreme intensity of 160 kt (82 m/sec), and were the 8th and 9th of 1997's unprecedented number of 11 super typhoons. An equatorial westerly

wind burst associated with the El Niño preceeded the formation of Ivan, Joan and a Southern Hemisphere twin -- Tropical Cyclone Lusi (02P). After developing, Ivan moved to the west-northwest and eventually passed 55 nm (102 km) south of Guam. From 150600Z to 171800Z, Ivan intensified from 65 kt (34 m/sec) to 160 kt (83 m/sec). The typhoon continued its westward movement, becoming the first and only named TC in 1997 to hit the Philippines. Ivan recurved in the Luzon Strait, and after weakening, became extratropical south of Japan. Joan developed just east of Ivan, and took a similar track to the west, but passed 155 nm (287 km) north of Guam. Joan explosively deepened, intensifying from 70 kt (36 m/sec) to 160 kt (83 m/sec) in 36 hours -- a deepening rate of 2.8 mb per hour. Joan remained at or above the super typhoon threshold (130 kt, 68 m/sec) for 4.5 days -- a record. Joan and Ivan were the two most intense TCs ever seen to exist simultaneously. Joan slowly weakened, finally recurved, and while traveling eastward along 30N, became an intense extratropical cyclone.

As Ivan and Joan began to recurve, yet another disturbance was developing in the El Niño-induced monsoon trough in the eastern Caroline and Marshall Islands. This disturbance would become the tenth of eleven 1997 super typhoons -- **Super Typhoon Keith (29W)**. After several days of westward movement and difficulty in organizing, the system finally consolidated and began to intensify at a normal rate of one Dvorak "T-number" per day. Once it reached 105 kt (55 m/sec), the typhoon began to rapidly intensify, peaking at 155 kt (81 m/sec) in just 24 hours. The small eye and narrow wall cloud of Keith passed between the islands of Saipan and Rota in the Mariana Islands, and no island endured the full force of the typhoon. Keith remained a super typhoon for 3.5 days as it moved to the northwest at the end of the month. On 04 November, **Super Typhoon Keith's (29W)** forward motion slowed, and the typhoon began to weaken and recurve. A few days later, a weakened Keith was speeding at 45 kt (83 km/hr) to the east-northeast and becoming extratropical.

NOVEMBER

The disturbance that became **Typhoon Linda (30W)**, developed near the end of October near 10N about 200 nm (370 km) east of the Philippines. The system moved westward and reached tropical storm intensity within 24 hours of moving into the South China Sea. The system continued to intensify as it approached the Ca Mau province of Vietnam on 02 November, and reached typhoon intensity in the Gulf of Thailand. The typhoon weakened while crossing the Malay Peninsula, but reintensified in the Bay of Bengal. Linda was the first TC since Typhoon Forrest (30W) in 1992 to successfully make this low latitude trek. After attaining typhoon intensity in the Bay of Bengal on 06 November, Linda ran into progressively more severe wind shear, and four days later, it dissipated over the Bay. Linda caused considerable damage and loss of life in Vietnam.

Typhoon Mort (31W) was the last TC of November and the last 1997 TC to form west of the international dateline. Mort began in a weak monsoon trough south of Guam. The system moved to the west and reached it maximum intensity of 65 kt (34 m/sec) in the Philippine Sea on 12 November. Mort peaked at 55 kt (29 m/sec), before it again ran into strong shear, which pushed the convection to the south at the low-level circulation center. On 16 November, Mort made landfall on the east coast of Luzon as a tropical depression.

DECEMBER

No TCs originated in the WNP during December 1997, and were it not for the entry of **Super Typhoon Paka (05C)** into the basin from the central North Pacific, it is probable

that there would have been no TCs in the WNP during December.

Trade winds dominated the tropics of the WNP for most of December. Anomalous easterly wind flow became established at low latitudes, except at eastern longitudes near the international dateline where El Niño-related low-level westerly wind flow persisted. The majority of monsoon-related deep convection had moved to the east of the international dateline, and twin near equatorial troughs extended along 8N and 5S from near 160E to the south of Hawaii at about 160W. A tropical storm -- Paka (05C) -- which had formed south of Hawaii during late November, moved steadily westward during December. It crossed the International Date Line on 07 December, and became a typhoon in the Marshall Islands. Continuing on a west-northwestward track, it intensified into a super typhoon and passed over Guam on 16 December, where the 600 million dollar level of destruction resulted in a Presidential declaration of Guam as a disaster area. Reliable measurements of wind gusts on Guam were as high as 149 kt (77 m/sec) and storm total rainfall amounts in excess of 15 inches (635 mm) occurred. Paka continued to move west-northwestward into the Philippine Sea where it eventually dissipated over water after reaching an extreme estimated intensity of 160 kt (82 m/sec).

With the dissipation of Paka, the "year of the super typhoon" in the western North Pacific came to a close. At the end of December, high pressure, persistent easterly winds, and reduced amounts of deep convection prevailed in the tropics of the basin. ENSO-related drought conditions worsened to record proportions in Micronesia, and TC activity shifted into the Southern Hemisphere with a classical El Niño shift to the east.

During 1997 for the western North Pacific, JTWC issued 950 warnings. Super Typhoons Paka (05C) and Oliwa (02C) were the longest lived TCs of the year, requiring 78 and 59 warnings respectively, even after moving from their genesis regions in the central North Pacific across the international dateline into the JTWC area of responsibility.

Table 3-3 WESTERN NORTH PACIFIC TROPICAL CYCLONES

TYPHOONS (1945-1959)

	JAN	FEB	MAR	APR	MAY	JUN	JUL	AUG	SEP	OCT	NOV	DEC	TOTALS
MEAN	0.3	0.1	0.3	0.4	0.7	1	2.9	3.1	3.3	2.4	2	0.9	16.4
CASES	5	1	4	6	10	15	29	46	49	36	30	14	245

TYPHOONS (1960-1997)

	JAN	FEB	MAR	APR	MAY	JUN	JUL	AUG	SEP	OCT	NOV	DEC	TOTALS
MEAN	0.3	0.1	0.2	0.4	0.7	1.1	2.8	3.5	3.4	3.3	1.7	0.7	18
CASES	10	2	8	16	27	41	107	132	129	124	63	26	685

TROPICAL STORMS AND TYPHOONS (1945-1959)

	JAN	FEB	MAR	APR	MAY	JUN	JUL	AUG	SEP	OCT	NOV	DEC	TOTALS
MEAN	0.4	0.1	0.5	0.5	0.8	1.6	2.9	4	4.2	3.3	2.7	1.2	22.2
CASES	6	2	7	8	11	22	44	60	64	49	41	18	332

TROPICAL STORMS AND TYPHOONS (1960-1997)

	JAN	FEB	MAR	APR	MAY	JUN	JUL	AUG	SEP	OCT	NOV	DEC	TOTALS
MEAN	0.5	0.2	0.4	0.7	1.2	1.8	4.3	5.7	5.1	4.3	2.7	1.2	28.1
CASES	20	9	17	25	44	70	163	215	193	164	101	47	1068

TABLE 3-4 TROPICAL CYCLONE FORMATION ALERTS FOR THE WESTERN NORTH PACIFIC OCEAN FOR 1976-1997

YEAR	INITIAL TCFAS	TROPICAL CYCLONES WITH TCFAS	TOTAL TROPICAL CYCLONES	PROBABILITY OF TCFA WITHOUT WARNING*	PROBABILITY OF TCFA BEFORE WARNING
1976	34	25	25	26%	100%
1977	26	20	21	23%	95%
1978	32	27	32	16%	84%
1979	27	23	28	15%	82%
1980	37	28	28	24%	100%
1981	29	28	29	3%	96%
1982	36	26	28	28%	93%
1983	31	25	25	19%	100%
1984	37	30	30	19%	100%
1985	39	26	27	33%	96%
1986	38	27	27	29%	100%
1987	31	24	25	23%	96%
1988	33	26	27	21%	96%
1989	51	32	35	37%	91%
1990	33	30	31	9%	97%
1991	37	29	31	22%	94%
1992	36	32	32	20%	100%
1993	50	35	38	30%	92%
1994	50	40	40	20%	100%
1995	54	33	35	39%	94%
1996	41	39	43	5%	91%
1997	36	30	33	17%	91%
(1976-1997) MEAN:	37	29	30	22%	97%
TOTALS:	818	635	670		

* Percentage of initial TCFA's not followed by warnings.

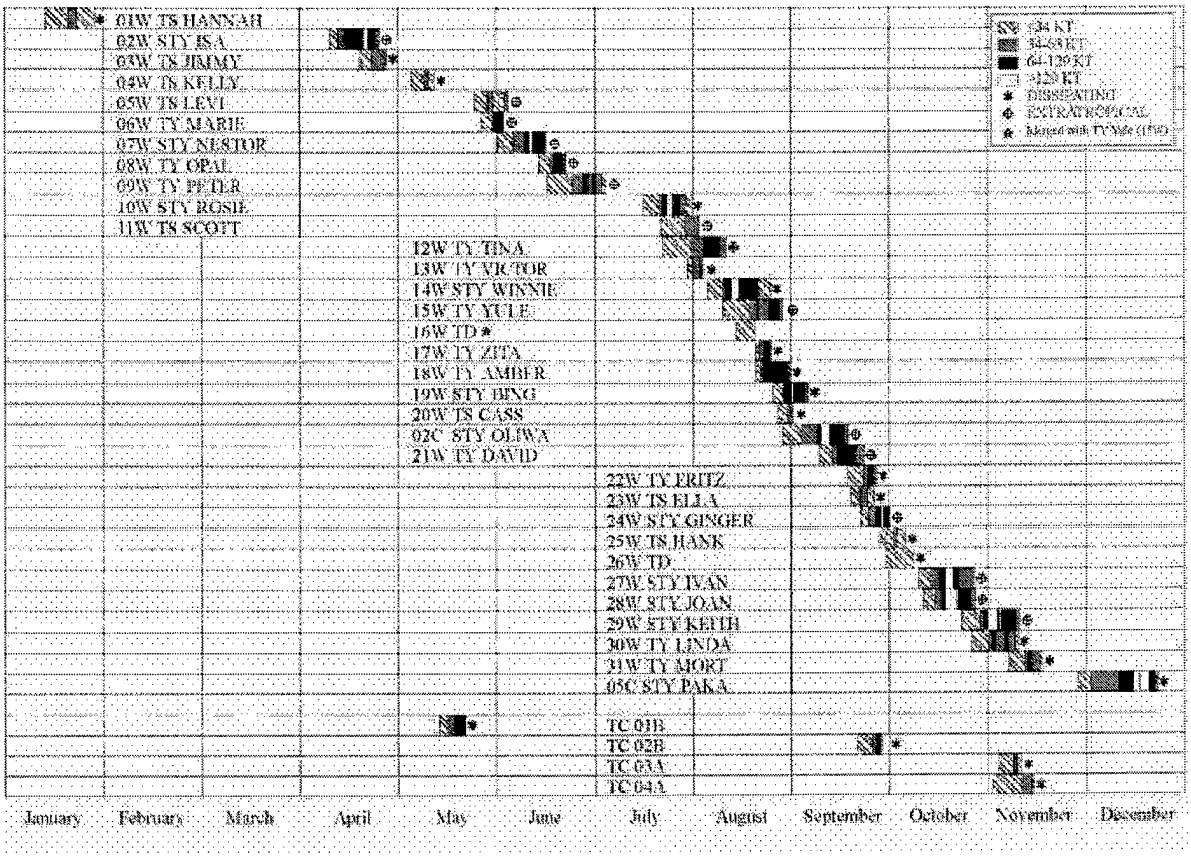

Figure 3-7 Chronology of western North Pacific and North Indian Ocean tropical cyclones for 1997 .

TABLE 3-5 NORTH INDIAN OCEAN SIGNIFICANT TROPICAL CYCLONES FOR 1997

TROPICAL CYCLONE	PERIOD OF WARNING	NUMBERS OF WARNINGS ISSUED	ESTIMATED MAX INTENSITY KT (M/SEC)	EST MSLP (MB)
01B	14 MAY - 20 MAY	22	115 (59)	927
02B	24 SEP - 27 SEP	10	65 (33)	976
03A	08 NOV - 09 NOV	7	35 (18)	997
04A	10 NOV - 14 NOV	17	55 (28)	984
TOTAL		56		

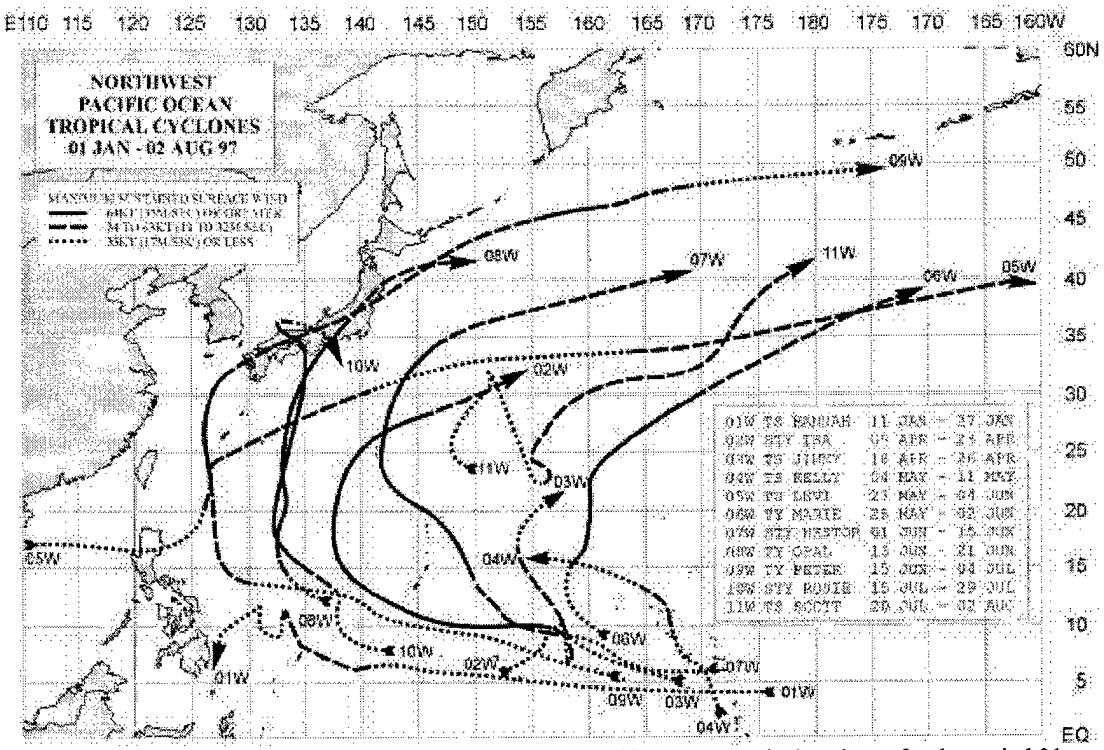

Figure 3-8a Composite best tracks for the western North Pacific Ocean tropical cyclones for the period 01 January to 02 August 1997

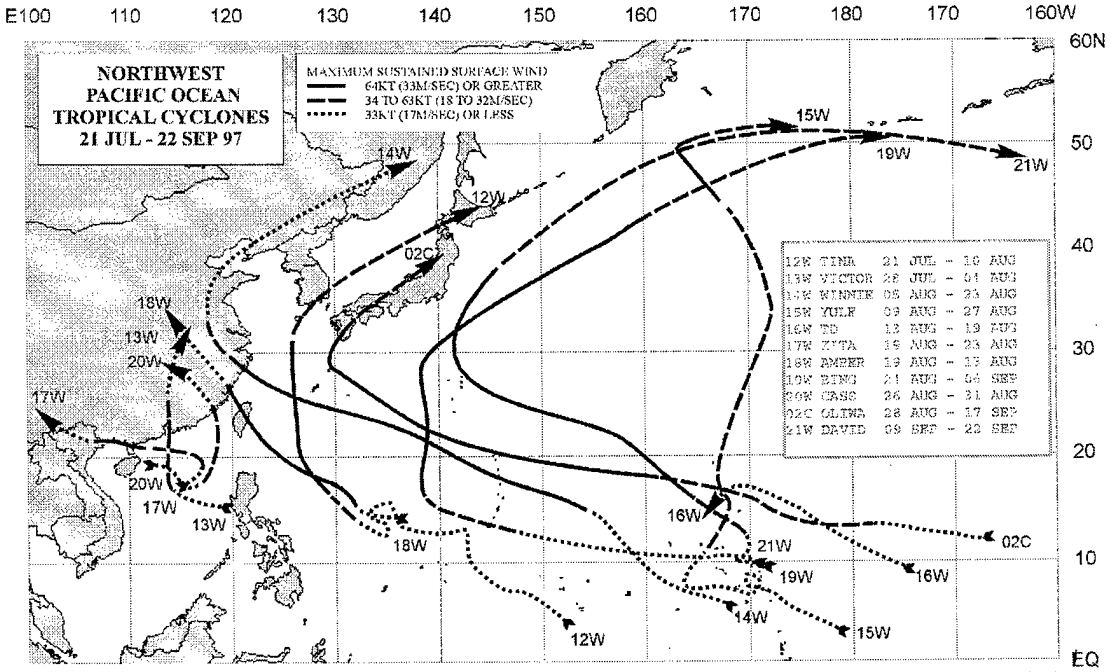

Figure 3-8b Composite best tracks for the western North Pacific Ocean tropical cyclones for the period 21 July to 22 September 1997

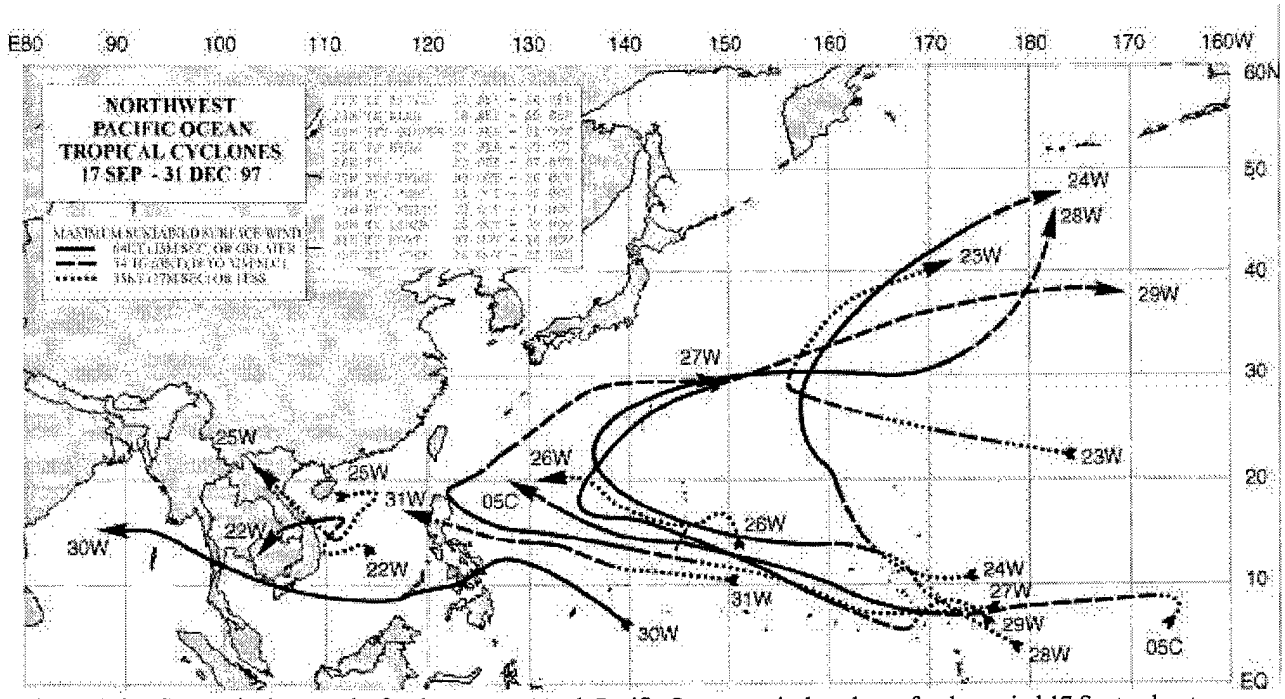

Figure 3-8c Composite best tracks for the western North Pacific Ocean tropical cyclones for the period 17 September to 22 December 1997

TROPICAL STORM HANNAH (01W)

I. HIGHLIGHTS

The first named tropical cyclone of 1997, Hannah, developed from a tropical disturbance in a near-equatorial trough south of the Marshall Islands. Moving on a long westward track for over two weeks, it reached a peak intensity of 50 kt (26 m/sec), and then dissipated in the Philippine Sea. Many of the tropical cyclones of 1997 (including Hannah) shared the unusual characteristic of forming well to the east of normal; a typical behavior of tropical cyclones during an El Niño year.

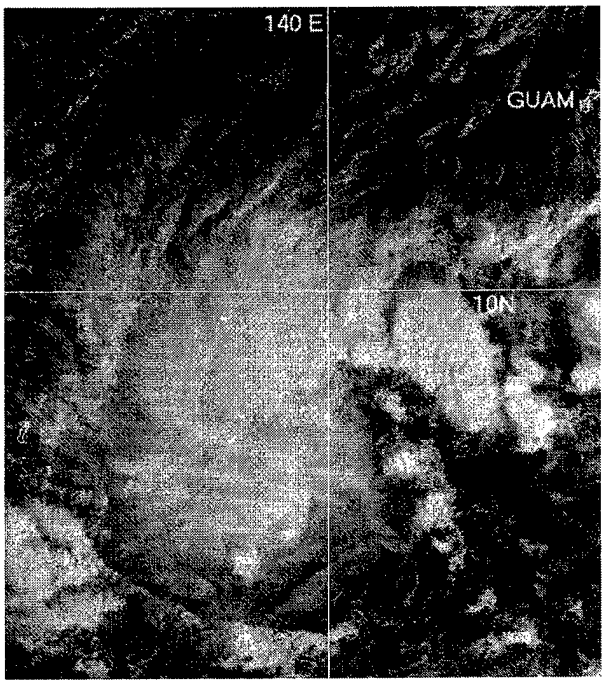

Figure 3-01-1 The deep convection associated with the pre-Hannah tropical disturbance becomes better organized, and JTWC responds by issuing a Tropical Cyclone Formation Alert. Note the large extent of low-level westerly winds along the equator and at low latitudes in both hemispheres implied by the distribution and pattern of the deep convection (182333Z January infrared GMS imagery).

II. TRACK AND INTENSITY

The tropical disturbance which became Hannah was first described on the 11 January significant tropical weather advisory as an area of persistent deep convection located at very low latitude (4°N) and just to the west of the International Date Line (IDL). The disturbance remained poorly organized for several days as it moved steadily westward along 4°N. After a westward journey covering over 2000 nm (3700 km) in a period of one week, it began to show signs of development. On 19 January, when the system was south-southwest of Guam, an increase in the amount of deep convection and the presence of a low-level circulation center were detected by multi-spectral satellite imagery (Figure 3-01-1) and synoptic data. This prompted JTWC to issue a Tropical Cyclone Formation Alert valid at 00Z on 19 January. The first warning on Tropical Depression (TD) 01W was issued valid at 0600Z on the nineteenth based on a blend of synoptic data, scatterometer data, and satellite intensity estimates, which indicated that the winds in the system had increased to at least 25 kt (13 m/sec). Twelve hours later, at 191800Z, TD 01W was upgraded to Tropical Storm Hannah. This was based, once again, on a blend of synoptic data, scatterometer data, and satellite intensity estimates which indicated intensification to 35 kt (18 m/sec). Hannah reached peak intensity of 50 kt (26m/sec) at 0600Z on 20 January based on conventional satellite intensity estimates, and special sensor microwave imagery (SSM/I). These sources all indicated

that the deep convection and the low-level cloud lines had become organized into well-defined cyclonic bands. After 0600Z the cyclone approached a region of low-level northeasterly flow overlaid by upper level southeasterly winds. Weakening ensued as vertical wind shear forced the dwindling amounts of deep convection to the northern quadrant. Hannah's motion became erratic on 21 January as the system began to interact with a shear line that trailed into the tropics from a large and vigorous extratropical low moving eastward off the coast of Japan. Trapped at the end of the shear line, the areal extent of Hannah's deep convection began to rapidly diminish, and the final warning was issued valid at 1800Z on the 24th when the intensity had fallen to 25 kt (13 m/sec) and further weakening was expected. Post analysis revealed that the remains of Hannah maintained an intensity of about 25 kt (13m/sec) for the next three days as it moved slowly toward Mindanao.

III. DISCUSSION

Although Tropical Storm Hannah was in most respects unremarkable, in retrospect it's development can be seen as part of the unusual large-scale tropical circulation pattern associated with El Niño, which would cause many of the tropical cyclones of 1997 to form well east of normal. We now know that the weather events over the Pacific warm pool during late 1996 and early 1997 may be looked upon as the antecedent (or onset) conditions leading to the development of strong El Niño conditions by April of 1997. An eastward displacement of the mean genesis location of tropical cyclones in the western North Pacific is a signature of El Niño.

IV. IMPACT

No reports of significant damage or injuries were received at JTWC.

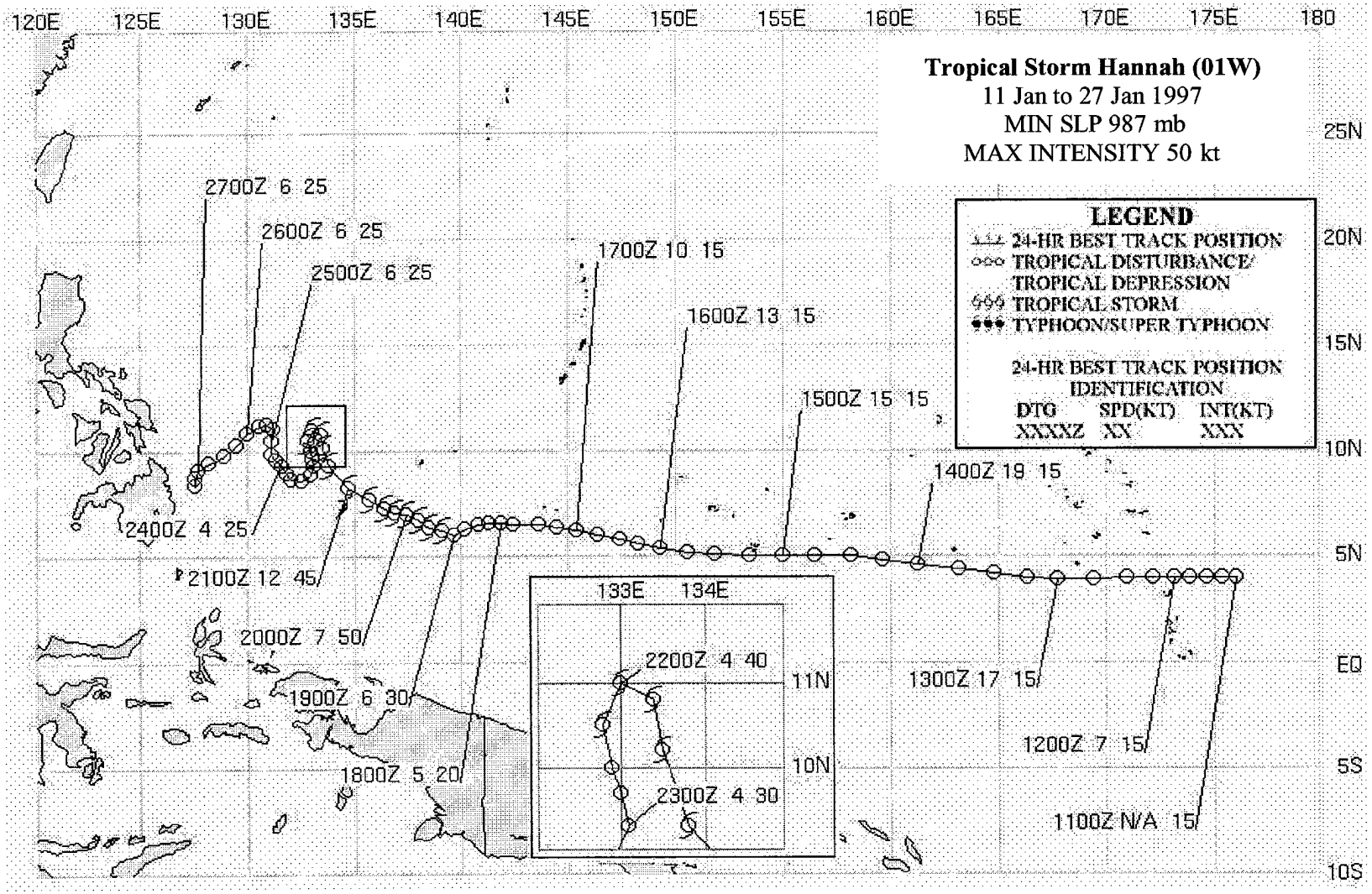
Tropical Storm Hannah (01W)
11 Jan to 27 Jan 1997
MIN SLP 987 mb
MAX INTENSITY 50 kt
LEGEND
24-HR BEST TRACK POSITION
TROPICAL DISTURBANCE/
TROPICAL DEPRESSION
TROPICAL STORM
TYPHOON/SUPER TYPHOON
24-HR BEST TRACK POSITION
IDENTIFICATION
DTG SPD(KT) INT(KT)
XXXXZ XX XXX
120E
125E
130E
135E
140E
145E
150E
155E
160E
165E
170E
175E
180
25N
20N
15N
10N
5N
EQ
5S
10S
2700Z 6 25
2600Z 6 25
2500Z 6 25
2400Z 4 25
2100Z 12 45
2000Z 7 50
1900Z 6 30
1800Z 5 20
1700Z 10 15
1600Z 13 15
1500Z 15 15
1400Z 19 15
1300Z 17 15
1200Z 7 15
1100Z N/A 15
133E
134E
11N
10N
2200Z 4 40
2300Z 4 30

SUPER TYPHOON ISA (02W)

I. HIGHLIGHTS

The first of eleven super typhoons to occur in the western North Pacific during 1997, Isa formed at a low latitude in the Caroline Islands along the axis of the near equatorial trough. On the night of 16 April, Isa passed 140 nm (260 km) to the south of Guam. There was no significant damage reported (the peak wind gust on island was 61 kt (31 m/sec)), though peripheral rainbands of the typhoon produced rainfall of 6 to 10 inches (15 to 25 cm) across the island. Most of the objective track guidance available to JTWC turned Isa to the north well before it happened; a common model bias that is identified and explained in the model-traits knowledge base of the "Systematic Approach".

II. TRACK AND INTENSITY

The tropical disturbance that became Isa developed in a near-equatorial trough that had become established across Micronesia. On 09 April, a large cloud cluster with the characteristics of a monsoon depression formed in the Caroline Islands, and was subsequently described in the 09 April 0600Z Significant Tropical Weather Advisory (ABPW). Synoptic data and animated satellite imagery indicated that a large, weak, low-level cyclonic circulation accompanied this cloud cluster. After several cycles of mesoscale cloud cluster growth, dissipation and regeneration, the system acquired a persistent and well-organized area of deep convection on 11 April, prompting JTWC to issue a Tropical Cyclone Formation Alert (TCFA), valid at 0000Z. The first warning on Tropical Depression (TD) 02W was issued valid at 1800Z on 11 April, based on satellite intensity estimates of 30 kt (15 m/sec), cooling cloud tops, and increased organization of the outflow aloft.

TD 02W was a large tropical cyclone that intensified slowly. The strong, deep monsoonal westerlies to its south prevented much movement from 0000Z on 10 April to 0000Z on 12 April. Based on satellite intensity estimates of 35 kt (18 m/sec), 02W was upgraded to Tropical Storm Isa (02W) on the warning valid at 0600Z on 12 April. After becoming a tropical storm, intensification occurred more rapidly, and the system began to move toward the west-northwest. Isa was upgraded to a typhoon on the 13 April 1800Z warning. At this point, the motion of the system became more westward, and the rate of intensification slowed. During the six-day period from 0000Z on the 14th to 0000Z on the 20th, the intensity of the typhoon steadily increased from 65 kt (33 m/sec) to its peak of 145 kt (75 m/sec) (Figure 3-02-1). This rate of intensification (approximately one-half a T-number per day) is defined by Dvorak (1975, 1984) as slow. Approximately 36 hours prior to reaching peak intensity, Isa turned to the north, a major track change indicated by most of the numerical guidance for several days (although the models made the turn far too early). Moving slowly north along 137E during the 24-hour period from 20 April 0000Z to 21 April 0000Z, Isa began to weaken. At 0000Z, on 21 April, the typhoon turned to the north-northeast and doubled its forward speed to approximately 12 kt (22 km/hr) while continuing to weaken. At 0000Z on the 22nd, the typhoon, having weakened to 80 kt (41 m/sec), began to accelerate in the midlatitude flow and the speed of translation increased from 12 kt (22

km/hr) to 17 kt (32 km/hr) at 0000Z on the 23rd, and to 24 kt (44 km/hr) at 1200Z on the 23rd. The final warning on Isa was issued valid at 0600Z on the 23rd, as the system accelerated to the northeast and its cloud system became sheared. The remnants of Isa later merged with the cloud band on the northeast side of a vigorous extratropical low that had developed and moved eastward into the Pacific from northern Japan.

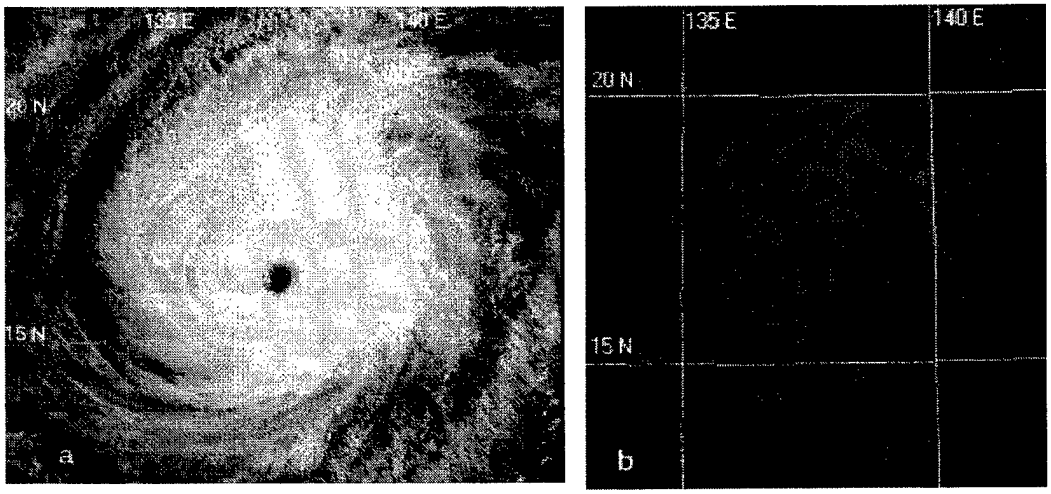

Figure 3-02-1 Isa near the time of its peak intensity. (a) Visible imagery within three hours of its best track peak (192131Z April visible GMS imagery) and (b) microwave imagery within two hours of the peak (200146Z April 85 GHz horizontally polarized microwave DMSP imagery).

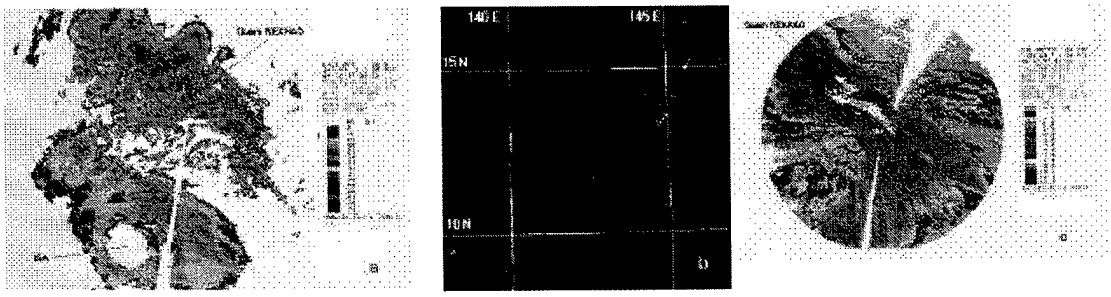

Figure 3-02-2 A peripheral rainband on the northeast side of Isa remained in a fixed position over Guam for over 12 hours resulting in rainfall totals of up to 10 inches. (a) As Isa's eye moved westward away from Guam, heavy showers and thunderstorms embedded in an outer rainband were directed over the island for an extended period (162029Z April NEXRAD base reflectivity). (b) The rainband as it appeared in microwave imagery (170805Z April 85 GHz horizontally polarized microwave DMSP imagery). (c) The narrowness of the ribbon of high amounts of rainfall is apparent on NEXRAD integrations of precipitation (NEXRAD storm-total precipitation ending at 172154Z April).

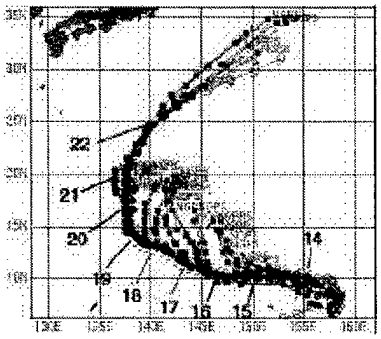

Figure 3-02-3 Most of the objective guidance available at the JTWC had a persistent and strong northward bias for much of Isa's track. (NOGAPS forecasts out to 72 hours are superimposed over Isa's best track.

III. DISCUSSION

a. A Next-generation Radar (NEXRAD) view of Isa as it passed Guam

Isa passed closest to Guam during the early morning of 17 April. Most of the rainfall and the highest winds associated with the typhoon, however, occurred after Isa began moving away from the island, and was associated with a peripheral rainband (see the NEXRAD display of Figure 3-02-2a and the microwave imagery of Figure 3-02-2b). Twenty-four hour rainfall measurements on Guam approached 10 inches in some places. The NEXRAD storm-total precipitation product (Figure 3-02-2c) shows the narrow ribbon of very high rainfall produced over Guam (and adjacent ocean) by the nearly stationary typhoon rainband. Although the rainband was stationary, the convective elements within the band were moving rapidly northwestward in deep-layer southeasterly flow of 45-50 kt (23-26 m/sec).

b. Model biases

Numerical track prediction biases (predominantly those of the NOGAPS model), as described in the "Systematic and Integrated Approach" to tropical cyclone forecasting (Carr and Elsberry 1994), were observed in Typhoon Isa, particularly the NOGAPS tendency to prematurely turn a westward moving tropical cyclone to the north. Although JTWC forecasters were aware of the model bias and delayed forecasting the turn, the actual delay was longer than anticipated. JTWC forecast Isa's northward turn to occur near its actual closest point of approach to Guam, leading to over-forecasting of wind on the island. While the "Systematic Approach" deserves credit for alerting the forecaster's to the model's bias, and for correctly identifying that the northward turn would eventually occur, the turn was delayed for a very long time relative to other examples of this type, as illustrated in Carr and Elsberry (1994) and in training materials devised for the JTWC forecasters. Recent work by Carr (personal communication) on the problem of premature recurvature in model guidance (e.g., NOGAPS and GFDN) has led to new findings. In the early formulations of the "Systematic Approach", there were only two scenarios in which the numerical guidance tended to turn a westward moving tropical cyclone towards the north too early: 1) During cases of Indirect Tropical Cyclone Interaction, and 2) during cases of westward motion equatorward of a Dominant Subtropical Ridge when the model analysis of the tropical cyclone was too large. An additional scenario has recently been identified, and applies to Isa: Premature recurvature forecasts also occur in the transition seasons (spring; and late fall through early winter) when the subtropical ridge is meridionally thin, particularly if the tropical cyclone is intense. Presumably the intense tropical cyclone in the model is too large and drives through a weakness in the thin ridge sooner than its real-world counterpart (as was the case with Isa) or indicates a false recurvature in the case of a straight runner (as was the case with 05C, Paka).

IV. IMPACT

No reports of significant damage or injuries were received at JTWC. Welcome dry-season rainfall of up to 10 inches (25 cm) was recorded on Guam as Isa passed near.

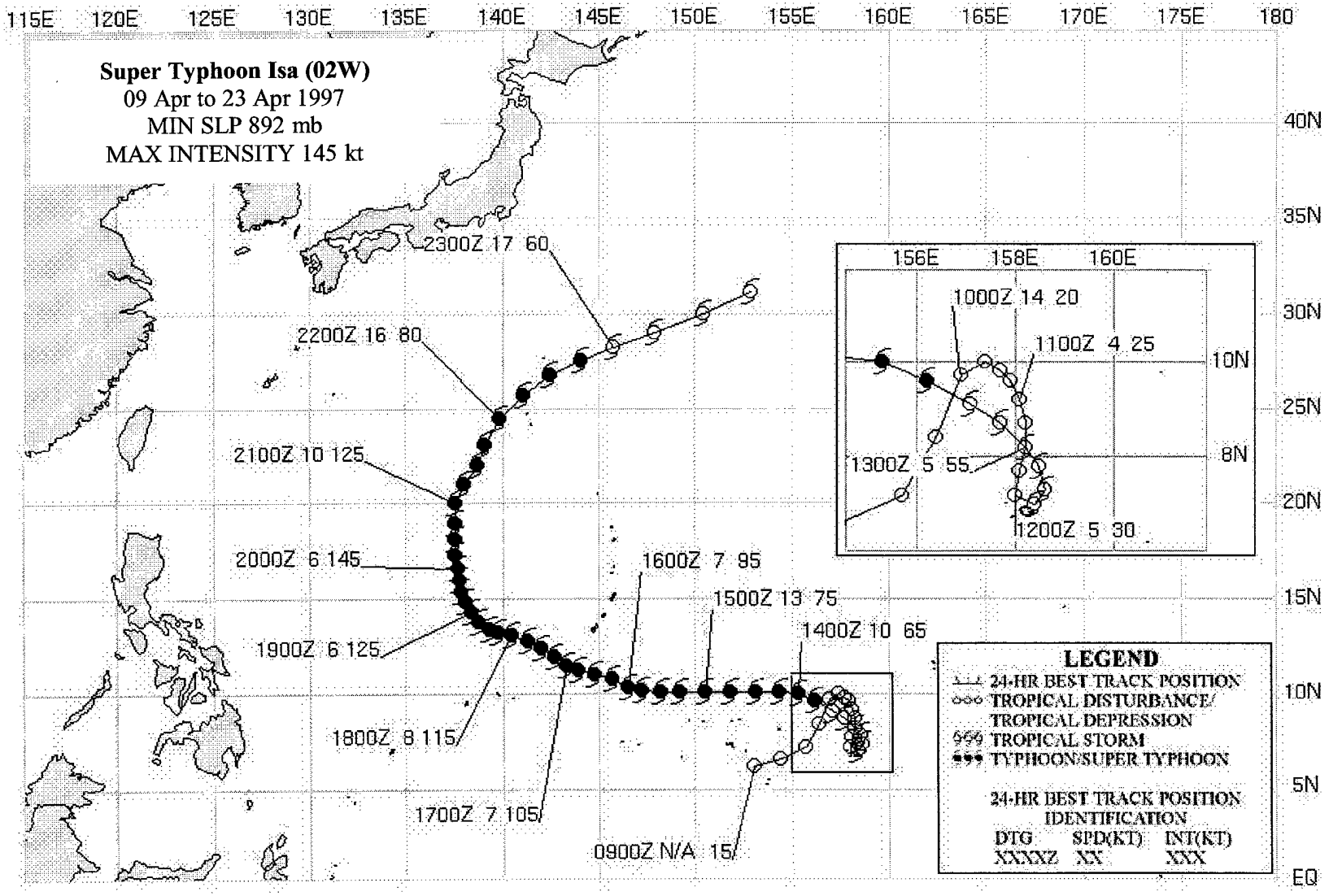
Super Typhoon Isa (02W)
09 Apr to 23 Apr 1997
MIN SLP 892 mb
MAX INTENSITY 145 kt
115E
120E
125E
130E
135E
140E
145E
150E
155E
160E
165E
170E
175E
180
40N
35N
30N
25N
20N
15N
10N
5N
EQ
2300Z 17 60
2200Z 16 80
2100Z 10 125
2000Z 6 145
1900Z 6 125
1800Z 8 115
1700Z 7 105
0900Z N/A 15
1600Z 7 95
1500Z 13 75
1400Z 10 65
156E
158E
160E
1000Z 14 20
1100Z 4 25
1300Z 5 55
1200Z 5 30
10N
8N
LEGEND
24-HR BEST TRACK POSITION
TROPICAL DISTURBANCE/
TROPICAL DEPRESSION
TROPICAL STORM
TYPHOON/SUPER TYPHOON
24-HR BEST TRACK POSITION
IDENTIFICATION
DTG SPD(KT) INT(KT)
XXXXZ XX XXX

TROPICAL STORM JIMMY (03W)

The tropical disturbance that was to become Tropical Storm Jimmy (03W) formed in mid-April from the same low-level equatorial westerly wind system that produced Super Typhoon Isa (02W) and Tropical Cyclone 34P (Ian) a week earlier. First mention of the pre-Jimmy disturbance appeared on the 0600Z Significant Tropical Weather Advisory (ABPW) on 18 April. After three days of tracking slowly to the west-northwest, the pre-Jimmy disturbance separated from the low-latitude maximum cloud zone and began its intensification. JTWC issued a Tropical Cyclone Formation Alert (TCFA) at 0400Z on 22 April. The system developed very rapidly and the first warning, valid at 0600Z on 22 April, was for Tropical Storm Jimmy (03W). By this time, Isa had already broken through the subtropical ridge, leaving the ridge weakened to non-existent west of 150E. Water vapor wind data showed southerly and southwesterly winds aloft over the Philippine Sea, preventing movement west of 150E. Jimmy tracked around the western periphery of the maritime subtropical ridge reaching 153E before recurving. Jimmy peaked just after its recurvature at 55 kt (28 m/sec) in the low-shear environment near the subtropical ridge axis. After moving north of the subtropical ridge, Jimmy quickly weakened due to increased southwesterly winds aloft. JTWC issued the final warning, valid at 1800Z, on 25 April, as the low-level circulation center became completely exposed and it was clear that the remnants of Jimmy would soon merge with an approaching frontal boundary.

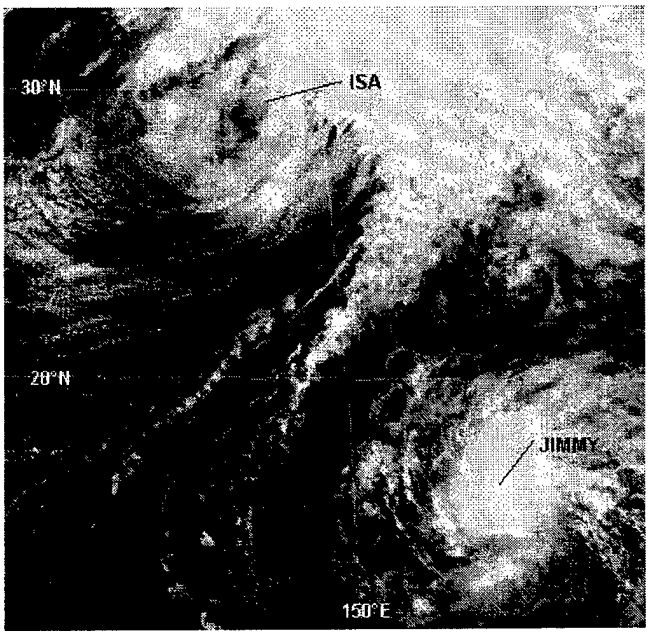

Figure 3-03-1 Tropical Storm Jimmy intensifies as it follows the remnants of Isa (02W) through the weakened subtropical ridge (230531Z April visible GMS imagery).

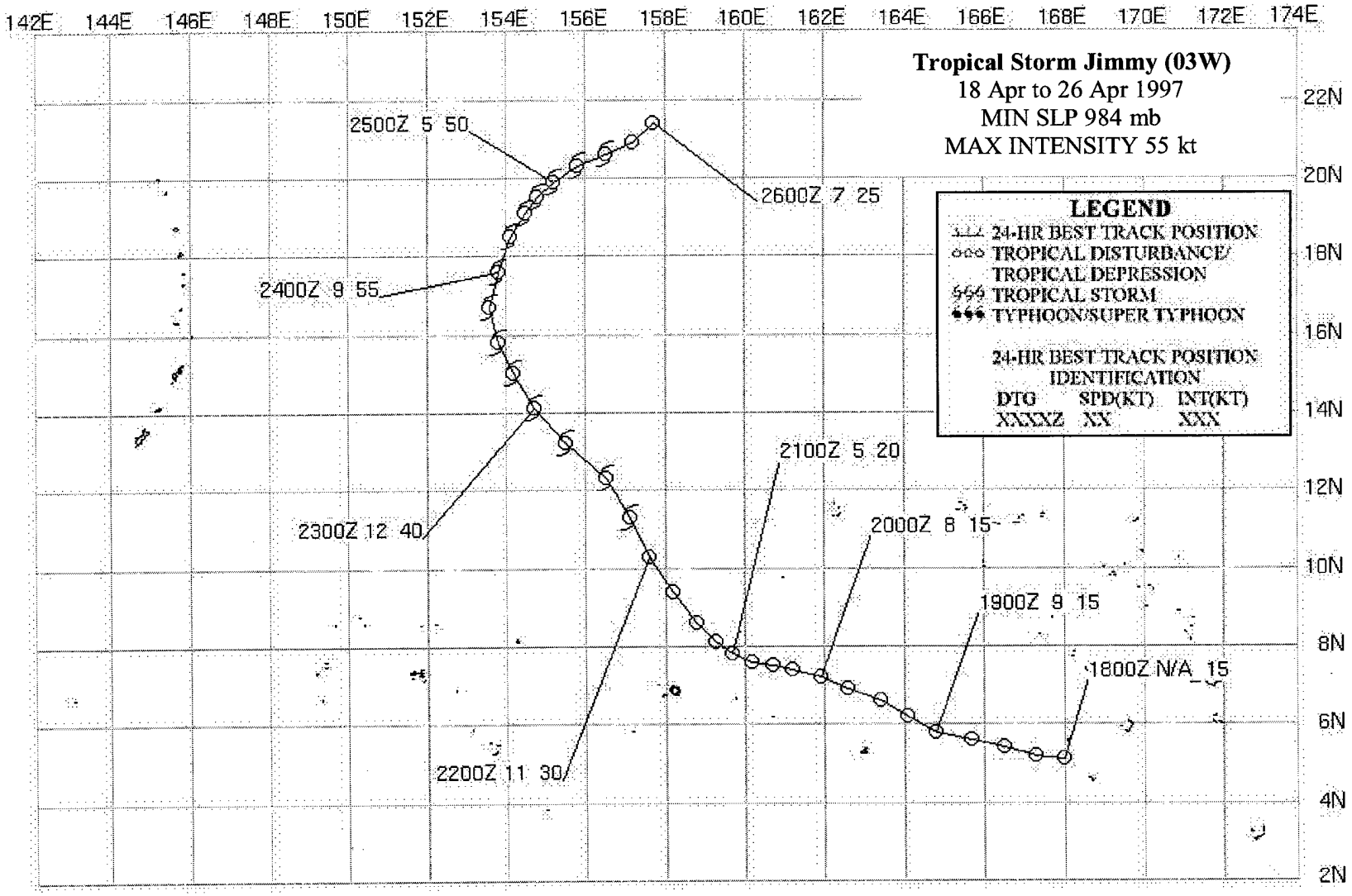
Tropical Storm Jimmy (03W)
18 Apr to 26 Apr 1997
MIN SLP 984 mb
MAX INTENSITY 55 kt
LEGEND
24-HR BEST TRACK POSITION
TROPICAL DISTURBANCE/ TROPICAL DEPRESSION
TROPICAL STORM
TYPHOON/SUPER TYPHOON
24-HR BEST TRACK POSITION IDENTIFICATION
DTG SPD(KT) INT(KT)
XXXXZ XX XXX
2500Z 5 50
2600Z 7 25
2400Z 9 55
2300Z 12 40
2200Z 11 30
2100Z 5 20
2000Z 8 15
1900Z 9 15
1800Z N/A 15
142E 144E 146E 148E 150E 152E 154E 156E 158E 160E 162E 164E 166E 168E 170E 172E 174E
22N 20N 18N 16N 14N 12N 10N 8N 6N 4N 2N

TROPICAL STORM KELLY (04W)

On 4 May, as Tropical Cyclone 35P (June) moved southeastward across Fiji, a band of convection flared up (Figure 3-04-1) north of the equator. The Significant Tropical Weather Advisory (ABPW) was reissued at 0200Z on the 5th to mention that this convection was associated with a low-level circulation in the near-equatorial trough. The convection persisted, prompting JTWC to issue a Tropical Cyclone Formation Alert (TCFA) at 2300Z on the 6th, and, as convection organization continued to improve, a warning for Tropical Depression (TD) 04W, valid at 0000Z on the 7th. TD 04W continued to intensify, developing a small, central dense overcast feature (CDO) that contributed to a 35 kt (18 m/sec) satellite intensity estimate at 0000Z on the 8th. The system peaked at 45 kt (23 m/sec) on 08 May at 1200Z. On 9 May, increased vertical wind shear began displacing Kelly's persistent deep central convection to the east of the low-level circulation center (LLCC). As the circulation weakened, the exposed LLCC separated from the convection and tracked to the west-northwest in the low-level flow. Kelly continued to weaken and JTWC issued the final warning, valid at 1800Z on 10 May. No reports of damage or injuries were received. During Kelly's passage through the southern Marshall Islands, Majuro received nearly 8 inches (20 cm) of rain in 24 hours from an outer rainband.

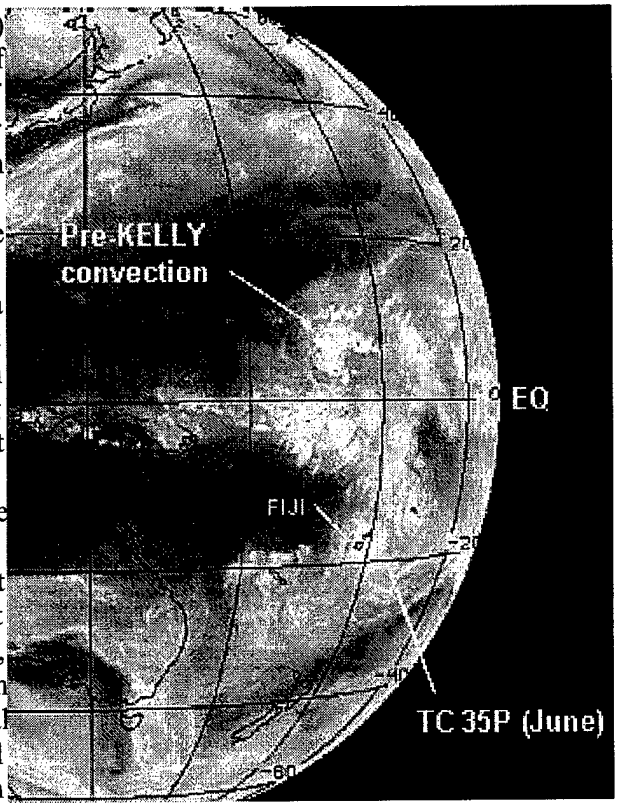

Figure 3-04-1 Cloudiness associated with the pre-Kelly tropical disturbance appears north of the equator as Tropical Cyclone 35P (June) tracks southeastward across Fiji (042233Z May visual GMS imagery).

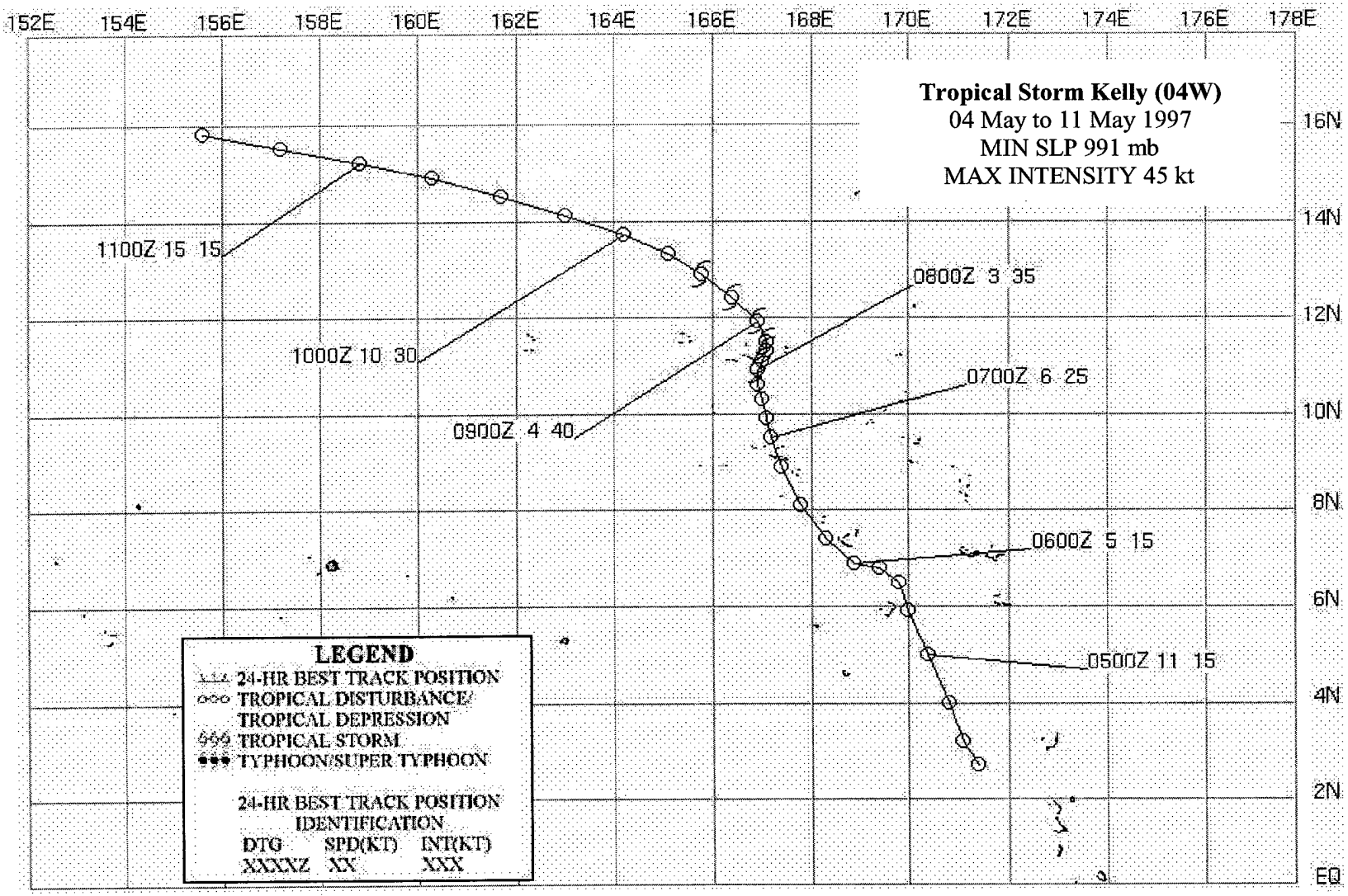
152E
154E
156E
158E
160E
162E
164E
166E
168E
170E
172E
174E
176E
178E
16N
14N
12N
10N
8N
6N
4N
2N
EQ
Tropical Storm Kelly (04W)
04 May to 11 May 1997
MIN SLP 991 mb
MAX INTENSITY 45 kt
1100Z 15 15
1000Z 10 30
0900Z 4 40
0800Z 3 35
0700Z 6 25
0600Z 5 15
0500Z 11 15
LEGEND
24-HR BEST TRACK POSITION
TROPICAL DISTURBANCE/
TROPICAL DEPRESSION
TROPICAL STORM
TYPHOON/SUPER TYPHOON
24-HR BEST TRACK POSITION
IDENTIFICATION
DTG SPD(KT) INT(KT)
XXXXZ XX XXX

TROPICAL STORM LEVI (05W)

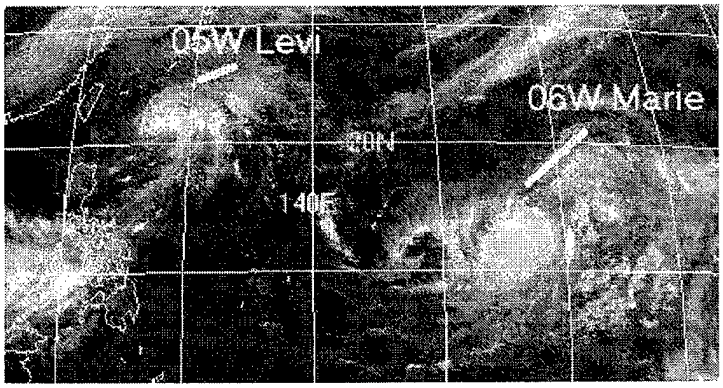

Figure 3-05-1. 281233Z May 1997 infrared imagery of Tropical Storm Levi (05W) as it moves on a northward track at its 45-kt (23-m/s) maximum intensity.

Tropical Storm Levi (05W), one of three tropical cyclones to develop in May, formed in the monsoon trough in the center of the South China Sea, between central Vietnam and Luzon. A low-level circulation center (LLCC) was first analyzed at 0000Z on 23 May. It was mentioned on the Significant Tropical Weather Advisory (ABPW) 6 hours later. The system assumed the form of a monsoon depression, having deep convection on the eastern and southern peripheries, with little consolidation near the center. On 24 May, convection began to organize near the LLCC, and a Tropical Cyclone Formation Alert (TCFA) was issued at 0600Z on the 25th. Twelve hours later, the first warning was released on Tropical Depression (TD) 05W. The depression moved eastward and crossed central Luzon on 26 May, producing copious amounts of rainfall which caused severe flooding. This forced the closure of government offices, schools, and the Philippine stock market in Manila. The main generator at the Ninoy Aquino International Airport in Manila was totally submerged by floodwater, shutting down the airport for several hours. A total of 33 peole lost their lives in the Philippines, primarily from flooding and mudslides.

After emerging into the Philippine Sea late on 26 May, TD 05W began to move to the northeast and was soon upgraded to Tropical Storm Levi (05W). On 28 May, the tropical storm reached its maximum intensity of 45 kt (23 m/sec). At this point, the system began to move on a northward track, steered by the monsoonal mid-tropospheric flow which connected the southwest monsoon with the Mei-yu front south of the Ryukyu Islands. Levi maintained its 45-kt (23 m/sec) winds during recurvature until 29 May at 1800Z when upper level westerly shear began to weaken the cyclone. The final warning on Tropical Storm Levi (05W), valid at 0600Z on the 30th, was issued as the system raced off to the northeast.

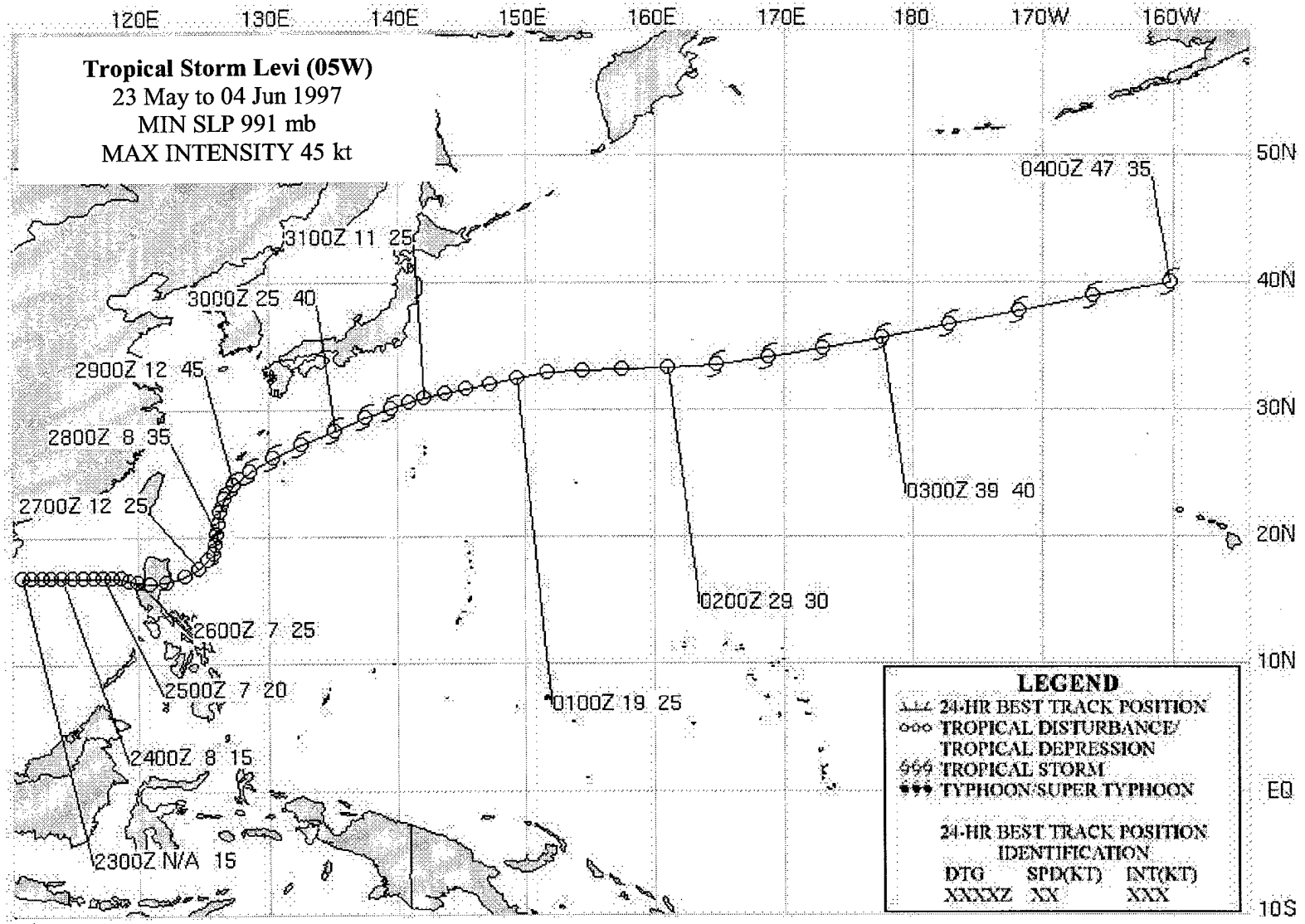
Tropical Storm Levi (05W)
23 May to 04 Jun 1997
MIN SLP 991 mb
MAX INTENSITY 45 kt
120E
130E
140E
150E
160E
170E
180
170W
160W
50N
40N
30N
20N
10N
EQ
10S
0400Z 47 35
3100Z 11 25
3000Z 25 40
2900Z 12 45
2800Z 8 35
2700Z 12 25
0300Z 39 40
0200Z 29 30
2600Z 7 25
2500Z 7 20
0100Z 19 25
2400Z 8 15
2300Z N/A 15
LEGEND
24-HR BEST TRACK POSITION
TROPICAL DISTURBANCE/
TROPICAL DEPRESSION
TROPICAL STORM
TYPHOON/SUPER TYPHOON
24-HR BEST TRACK POSITION
IDENTIFICATION
DTG SPD(KT) INT(KT)
XXXXZ XX XXX

TYPHOON MARIE (06W)

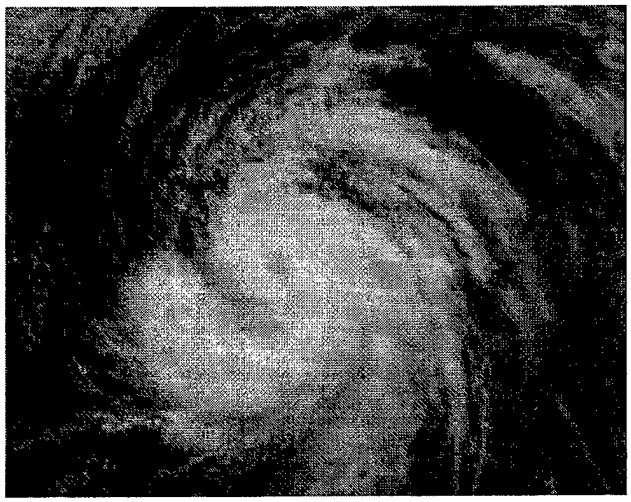

Figure 3-06-1. 302132Z May 97 GMS visible imagery of Typhoon Marie near its 90 kt (47 m/s) peak intensity. At this time, Marie was moving northward at 12 kt (22 km/hr).

Typhoon Marie (06W) was the only of the three May tropical cyclones to develop into a typhoon. The disturbance that eventually became Marie developed much farther east than normal for a May tropical cyclone. An active monsoon trough extended to the Marshall Islands in response to strong low level equatorial westerly winds associated with the developing 1997 El Niño. The disturbance was first mentioned on the 26 May Significant Tropical Weather Advisory (ABPW) and was located about 250 nm (463 km) east of Kwajalien Atoll (WMO 91366). A Tropical Cyclone Formation Alert (TCFA) was issued at 1630Z on 26 May, and the first warning was produced soon thereafter at 1800Z. For the next two days, Tropical Depression 06W intensified slowly as it moved northward through the subtropical ridge, which had been bisected by the passage of a short wave trough. The system reached tropical storm strength at 1800Z on the 28th and then intensified for the next 24 hours, while moving to the north-northeast at 5-9 kt (9-17 km/hr). At 1200Z on 29 May, Marie achieved typhoon intensity. While moving on a nearly northward track, Typhoon Marie continued to intensify, reaching its maximum intensity of 90 kt (46 m/s) at 0000Z on 31 May. Afterwards, the typhoon moved towards the northeast and began to slowly weaken. By 1800Z on 1 June, Marie's intensity had fallen below typhoon intensity, and the system was undergoing extratropical transition. The final warning was issued at 0600Z on the 2nd as the system accelerated to over 40 kt (74 km/hr), and its transition was nearly complete. Marie spent its entire life over water, and there were no reports of significant impact received by JTWC.

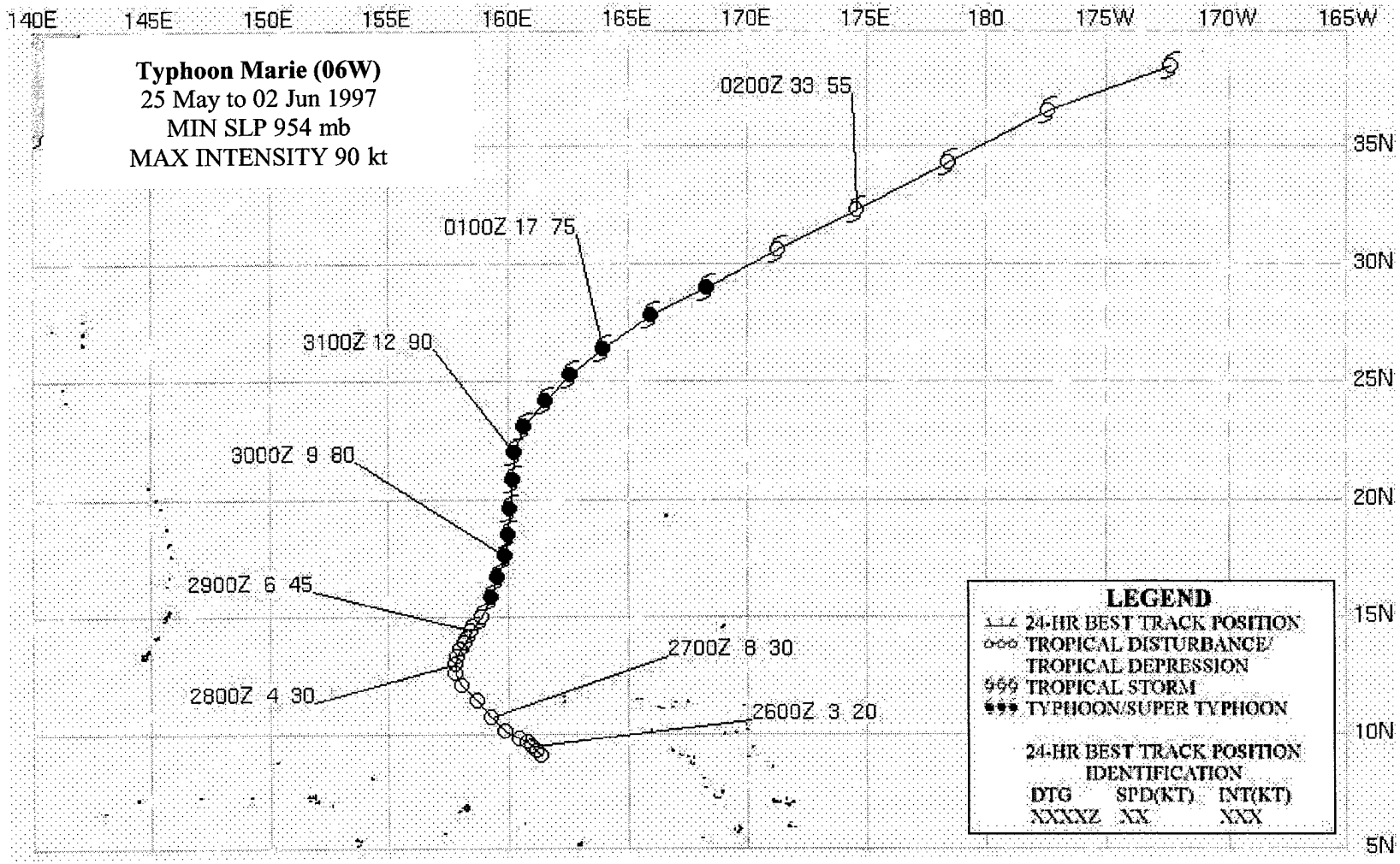
Typhoon Marie (06W)
25 May to 02 Jun 1997
MIN SLP 954 mb
MAX INTENSITY 90 kt
140E
145E
150E
155E
160E
165E
170E
175E
180
175W
170W
165W
35N
30N
25N
20N
15N
10N
5N
0200Z 33 55
0100Z 17 75
3100Z 12 90
3000Z 9 80
2900Z 6 45
2800Z 4 30
2700Z 8 30
2600Z 3 20
LEGEND
24-HR BEST TRACK POSITION
TROPICAL DISTURBANCE/
TROPICAL DEPRESSION
TROPICAL STORM
TYPHOON/SUPER TYPHOON
24-HR BEST TRACK POSITION
IDENTIFICATION
DTG SPD(KT) INT(KT)
XXXXZ XX XXX

SUPER TYPHOON NESTOR (07W)

I. HIGHLIGHTS

Super Typhoon Nestor (07W) was the strongest of three typhoons to develop in June, and was the second of 11 super typhoons to occur in 1997. It was a spin-off of strong equatorial westerly winds associated with the developing 1997 El Niño. Nestor's development in the southern Marshall Islands is the farthest east a June typhoon has developed since records have been kept.

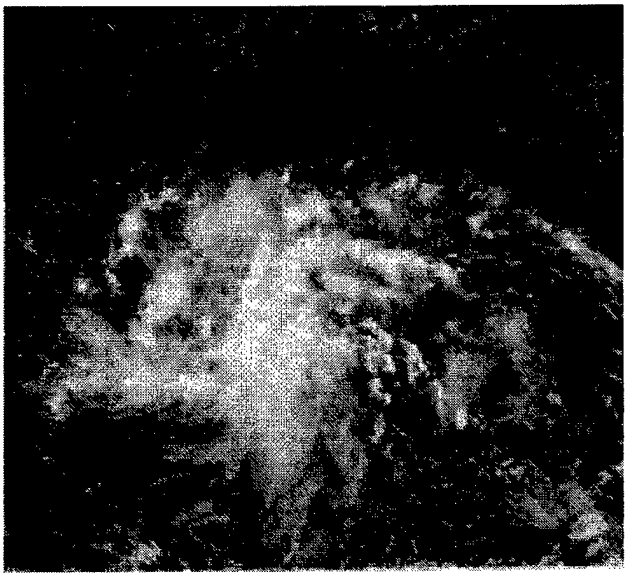

Figure 3-07-1 040232Z June 1997 GMS visual imagery of the tropical disturbance that would eventually become Super Typhoon Nestor (07W).

II. TRACK AND INTENSITY

In early June, strong equatorial low level westerly winds extended to the International Date Line (IDL) in association with the development of the 1997 El Niño. As Typhoon Marie (06W) was nearing the end of its tropical life, the disturbance that would become Super Typhoon Nestor (07W) was beginning its 2-week tropical existence. It was first identified on the Significant Tropical Weather Advisory (ABPW) at 0600Z on 1 June as a persistent area of convection about 70 nm (130 km) south-southwest of Majuro. For the next two days, the disturbance moved to the west-southwest at 5-7 kt (9-13 km/hr), with no noticeable intensification. On the evening of 03 June, near 165E, the system turned to the northwest, but it continued to have difficulty organizing (Fig. 3-07-1). A Tropical Cyclone Formation Alert (TCFA) was isssued at 0830Z on the 4th. A second TCFA was issued 24 hours later. Beginning at 1800Z on the 5th, the system quickly pulled itself together and reached tropical storm intensity by the time the first warning was issued at 0000Z on the 6th. Nestor assumed a heading toward the Mariana Islands. Statistical and statistical-dynamic prediction models indicated west-northwestward movement for several days, initially taking the storm south of Guam. However, these models soon started walking the track up over Saipan. On the morning of 08 June, Tropical Storm Nestor (07W) veered away from the Mariana Islands to a north-northwestward track and continued intensifying for four days, reaching peak intensity of 140 kt (72 m/s) at 1200Z on the 10th, approximately 200 nm (370 km) northeast of Saipan. Figure 3-7-2 compares the Dvorak enhancement image (a) with the microwave image (b) just before Nestor attained its maximum intensity. The system temporarily heeled over to the northwest before turning to the north and recurving about 20 nm (37 km) east of Iwo Jima (WMO 47981). Iwo Jima recorded wind gusts to 102 kt (51 m/s) at 1500Z on the 12th when the typhoon passed about 20 nm (37 km) to the

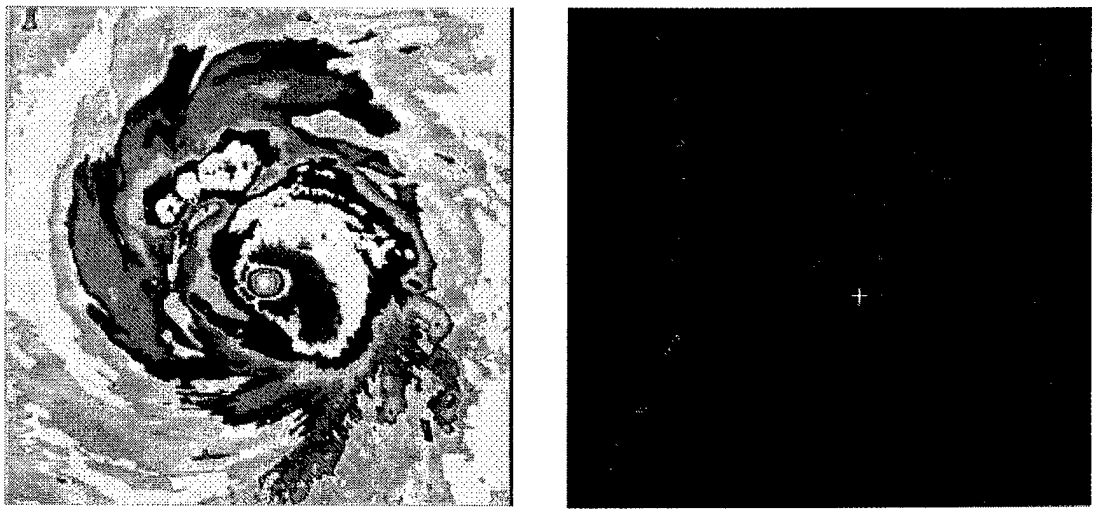

Figure 3-07-2 (a) 091547Z June 1997 enhanced infrared imagery using the BD enhancement curve and (b) 092013Z June 1997 DMSP microwave imagery (SSM/I) of Super Typhoon Nestor (07W) at an estimated intensity of 125-130 kt (65-68 m/s). The system is approximately 190 nm (352 km) east-northeast of Saipan.

Figure 3-07-3 120332Z June 1997 GMS visual imagery of the eye of Nestor just prior to recurvature. The intensity at this time was estimated to be 115 kt (60 m/s).

east. At 0200Z on the 13th, the typhoon passed about 30 nm (56 km) west of Chichijima (WMO 47971), which reported wind gusts to 96 kt (50 m/s). Nestor took a parabolic track to the northeast and east, eventually doubling its forward speed to over 30 kt (56 km/hr). The final warning by JTWC was issued at 0000Z on the 15th. Twelve hours later, the system had become a 50-kt (26-m/s) extratropical cyclone.

III. DISCUSSION

Statistical and statistical-dynamic models from 04 June to 08 June predicted west-northward motion for Nestor's circulation. These models consistently targeted an area 100 nm (185 km) to either side of Guam. When the first dynamic models became available, they predicted a northward turn as early as 06 June. This was first indicated by an abrupt turn to the north by NOGAPS, followed by northwestward motion. The Geophysical Fluid Dynamics Navy model (GFDN) and the British Meteorological Office model (EGRR) mimicked the motion of NOGAPS, but were slower to accelerate the system to the northwest. The short term predictions turned too abruptly (nearly perpendicular to the actual track), but the longer term predictions of NOGAPS were relatively accurate. This occurrence of premature and abrupt track changes has been discussed by Carr and Elsberry (1997), who attribute it to a tendancy towards early pattern/region transition from the Standard/Dominant Ridge to Poleward/Poleward Oriented, especially for early (12 to 24 hrs) forecast points. They point out the characteristic good accuracy of the 72-hour forecasts and recommend using the 72-hour dynamic model prediction guidance and merging it into the shorter term statistical predictions to derive an overall forecast. The daily changes in the NOGAPS predictions are superimposed upon Nestor's best track to illustrate the premature turning of the short term predictions.

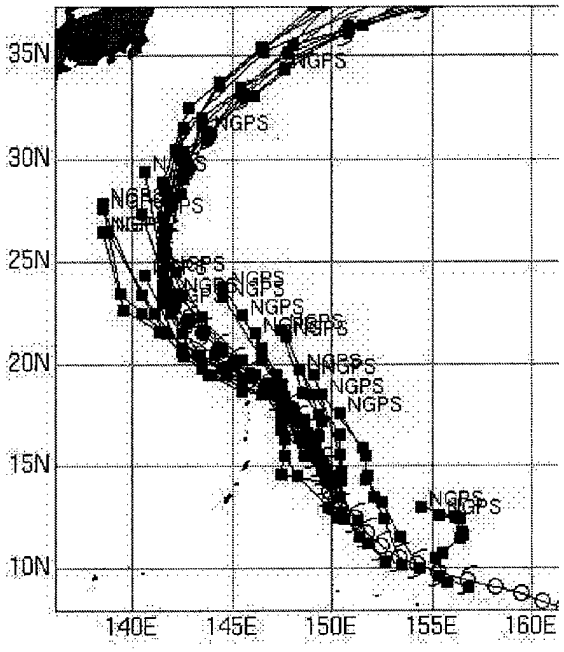

Figure 3-07-4 A history of NOGAPS track forecasts illustrating the models tendency toward premature short term turning.

IV. IMPACTS

Aside from passing through the Volcano Islands and the Bonin Islands of Japan, Nestor remained over water. Nestor did produce some high waves on Saipan. No reports of significant damage were received at JTWC.

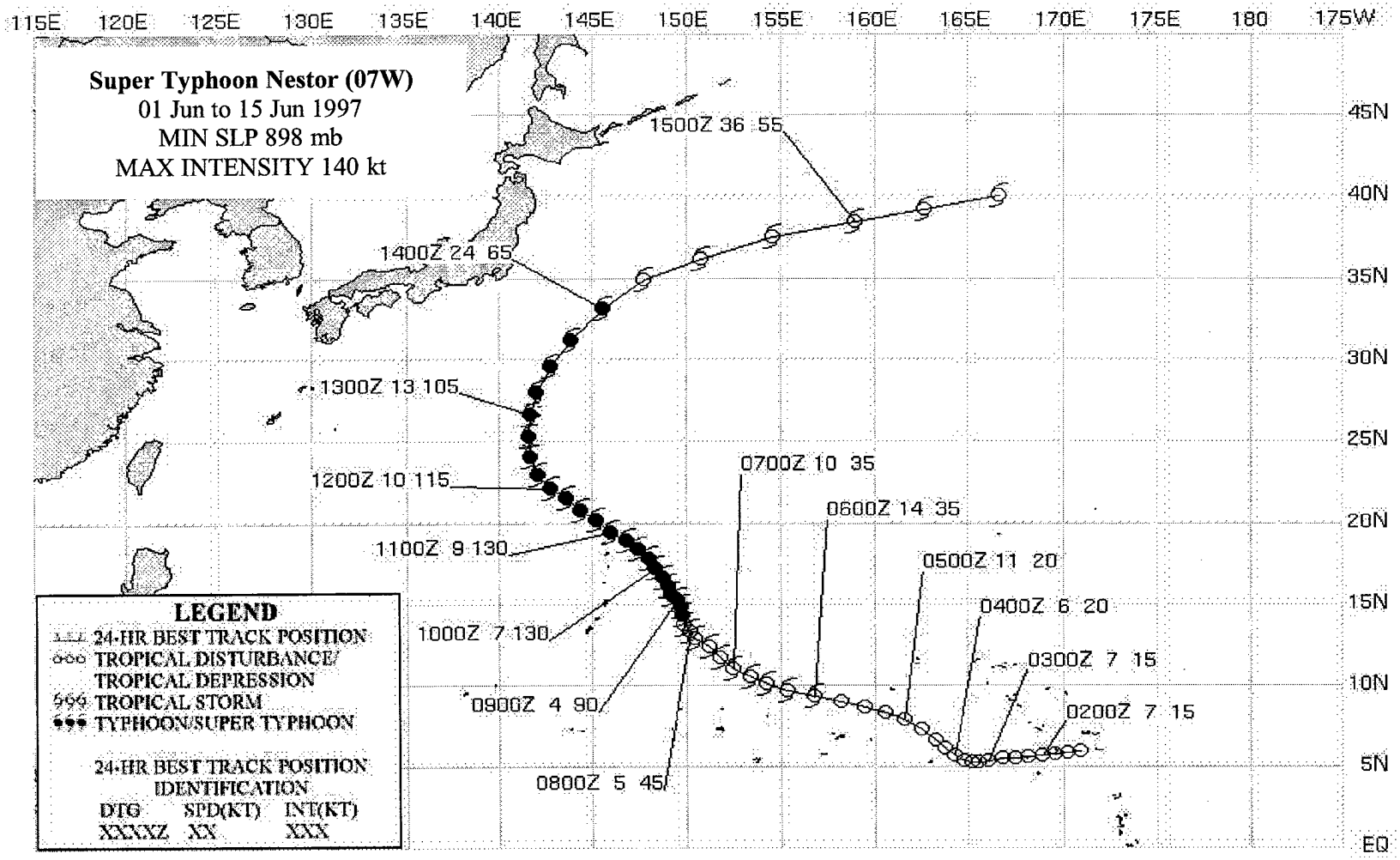
Super Typhoon Nestor (07W)
01 Jun to 15 Jun 1997
MIN SLP 898 mb
MAX INTENSITY 140 kt
115E
120E
125E
130E
135E
140E
145E
150E
155E
160E
165E
170E
175E
180
175W
45N
40N
35N
30N
25N
20N
15N
10N
5N
EQ
1500Z 36 55
1400Z 24 65
1300Z 13 105
1200Z 10 115
1100Z 9 130
1000Z 7 130
0900Z 4 90
0800Z 5 45
0700Z 10 35
0600Z 14 35
0500Z 11 20
0400Z 6 20
0300Z 7 15
0200Z 7 15
LEGEND
24-HR BEST TRACK POSITION
TROPICAL DISTURBANCE/
TROPICAL DEPRESSION
TROPICAL STORM
TYPHOON/SUPER TYPHOON
24-HR BEST TRACK POSITION
IDENTIFICATION
DTG SPD(KT) INT(KT)
XXXXZ XX XXX

TYPHOON OPAL (08W)

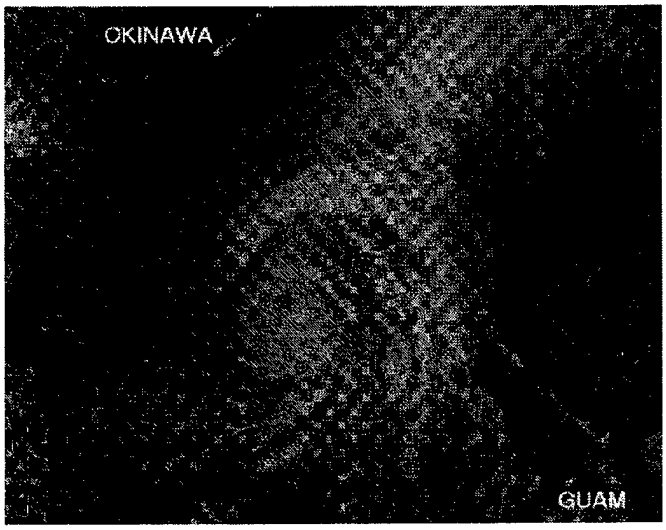

Figure 3-08-1. Opal reaches its peak of 90 kt (47 m/s) while moving on a north-oriented track (171059Z June low-light visible DMSP imagery).

The disturbance that was to become Typhoon Opal (08W) was first mentioned on the Significant Tropical Weather Advisory (ABPW) on 12 June as an area of persistent convection about 150 nm (278 km) southwest of Guam. The disturbance was slow to develop as it moved to the west-northwest at 6-8 kt (11-15 km/hr). However, by 14 June at 2030Z, the system had organized sufficiently to warrant the issuance of a Tropical Cyclone Formation Alert (TCFA). The first warning on Tropical Depression 08W was valid at 0000Z on the 15th. One day later, the depression attained tropical storm strength (35 kt or 18 m/sec), and began to track toward the north. By 0000Z on 17 June, it had reached an intensity of 65 kt (34 m/sec). Twelve hours later, Typhoon Opal was at its maximum intensity of 90 kt (47 m/sec), which it maintained for 36 hours (Figure 3-08-1). As Opal approached 20N latitude, it accelerated to speeds ranging from 14-17 kt (26-31 km/hr). By 0000Z on 18 June, westerlies from a trough to the northwest began to impinge upon Opal's outflow. This can be seen in Figure 3-08-1. As Opal neared 30N latitude, it began to turn to the northeast, subsequently accelerating and weakening. Opal made landfall near Shionomisaki, Japan (WMO 47778) at 2200Z on 19 June with an intensity near 65 kt (33 m/sec). A minimum pressure of 980.3 mb was observed during the passage. Six hours after making landfall, Tropical Storm Opal (08W) passed about 50 nm (93 km) northwest of Tokyo, and at 1500Z on 20 June, Opal exited Honshu on an east-northeast track with 55 kt (29 m/sec) winds. The final warning was issued at 0600Z on the 21st as the system became extratropical near 42N 167E while maintaining 40 kt (21 m/sec) winds.

Opal was one of three typhoons to develop in June. This level of activity has not been seen in the western North Pacific in June since 1965. It was the first tropical cyclone of 1997 to strike Japan.

As Opal approached south central Japan, a fisherman drowned while tying his boat to a pier. Opal caused only minor damage in Yokohama and Tokyo. Transportation was disrupted throughout eastern Japan, and 70 domestic flights were canceled.

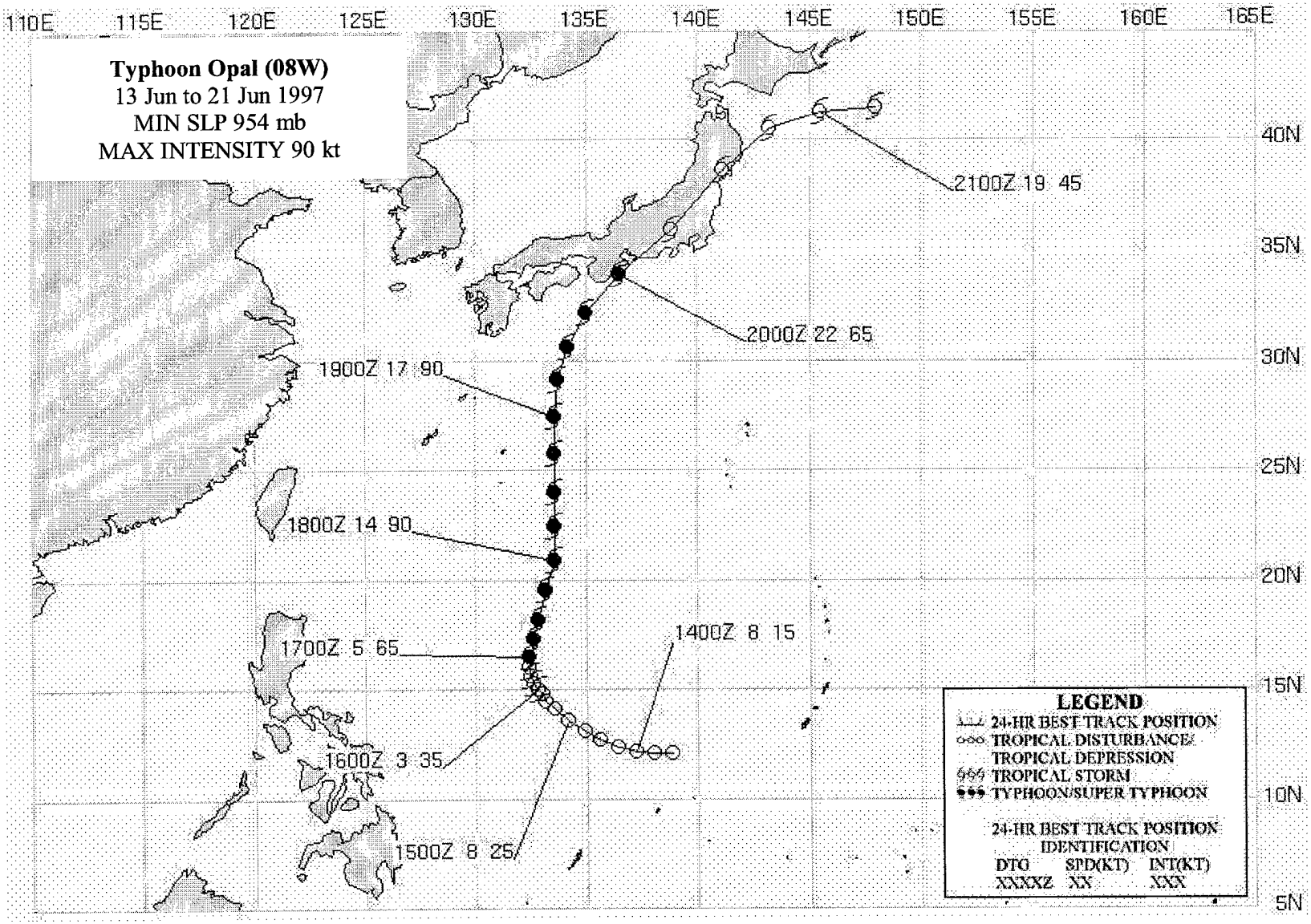
Typhoon Opal (08W)
13 Jun to 21 Jun 1997
MIN SLP 954 mb
MAX INTENSITY 90 kt
110E
115E
120E
125E
130E
135E
140E
145E
150E
155E
160E
165E
40N
35N
30N
25N
20N
15N
10N
5N
2100Z 19 45
2000Z 22 65
1900Z 17 90
1800Z 14 90
1700Z 5 65
1600Z 3 35
1500Z 8 25
1400Z 8 15
LEGEND
24-HR BEST TRACK POSITION
TROPICAL DISTURBANCE/
TROPICAL DEPRESSION
TROPICAL STORM
TYPHOON/SUPER TYPHOON
24-HR BEST TRACK POSITION
IDENTIFICATION
DTG SPD(KT) INT(KT)
XXXXZ XX XXX

TYPHOON PETER (09W)

I. HIGHLIGHTS

One of three typhoons to develop in June, Typhoon Peter (09W) achieved only minimal typhoon intensity. The cyclone moved on a northward track nearly 900 nm (1665 km) before recurving. It made landfall near Sasebo, Japan, paralleled the mountainous spine of Honshu, and eventually became one of the most intense extratropical cyclones of the year.

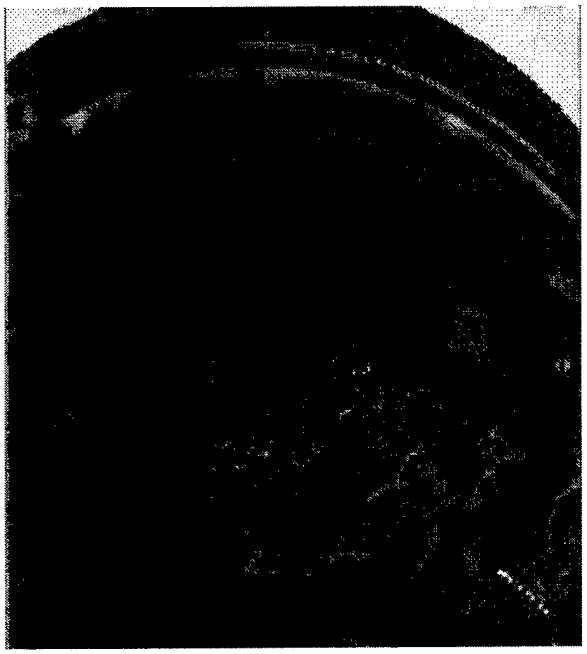

Figure 3-09-1. 251023Z June 1997 microwave image of Tropical Storm Peter (09W).

II. MOVEMENT AND INTENSITY

Typhoon Peter (09W) developed from a disturbance that was first detected early on the morning of 19 June as an area of persistent convection at the eastern edge of the monsoon trough, about 300 nm (560 km) southeast of Guam. This area, mentioned on the Significant Tropical Weather Advisory (ABPW) on 20 June, had characteristics of a monsoon depression with most convection on the south and east peripheries. After two days of slow development, deep convection began to consolidate near the center. As a result, the first Tropical Cyclone Formation Alert (TCFA) was issued at 0400Z on 22 June and a second TCFA was issued 24 hours later. However, when ERS-2 and NSCAT scatterometer-derived winds became available a short time later, the first warning was issued on Tropical Depression 09W at 0600Z on the 23rd. Scatterometer data played a critical role in ascertaining the cyclone's location and intensity throughout its life (see the discussion section). The developing cyclone spent its first four days on a west-northwest track, except for a temporary stair-step to the northwest on 20 June. Scatterometer wind data was again valuable as it indicated that the depression reached tropical storm intensity at 1200Z on the 23rd. By 24 June, a mid-tropospheric ridge had built to the southeast of Peter. This ridge imposed southerly steering, causing the tropical cyclone (TC) to take a sharp northward turn. Peter maintained this track for three days, covering about 900 nm (1665 km). On 25 June, conventional satellite imagery indicated that Peter was moving to the northeast, but microwave imagery data (SSM/I) revealed that the low level circulation center (LLCC) was maintaining a northward motion (Fig. 3-09-1). On 260600Z, Peter was upgraded to typhoon. It maintained a 65 knot (33 m/s) intensity for 36 hours, but developed no further. While tracking northward, Peter accelerated from an average speed of 10 kt (19 m/s) to 20 kt (38 m/s). Late on 27 June, Typhoon Peter began to weaken and turn northeastward. At 1800Z,on the 27th, Peter passed over

Nagasaki, Japan (WMO 47817) with 55-kt (29-m/s) 1-minute average sustained winds. Peter traveled to the northeast along the mountainous spine of Honshu and, less than one day after landfall, had nearly traversed the entire country from the southwest to the northeast. At 1900Z on the 28th, the weakened tropical storm entered the Pacific Ocean near Sendai (WMO 47590). On 29 June, Peter merged with a frontal system and completed its extratropical transition. As an extratropical system, the remnants of Peter became more intense than the system had been as a tropical system, reaching an intensity of 70 kt (36 m/s) on 30 June. It eventually weakened, and could no longer be found by 04 July.

III. DISCUSSION

Microwave and scatterometer data was used extensively to track and to ascertain the intensity and wind distribution of Peter. Figure 3-09-2 shows the scatterometer derived winds used to justify the issuance of the first warning on Tropical Depression 09W and then, later, to upgrade it. Scatterometer data was gathered from both the European Research Satellite (ERS-2) and the joint US-Japan Adobe satellite (N-Scat). The ERS provided a single swath of data, while the N-Scat provided dual swaths. Unfortunately, the N-Scat instrument ceased operation late in 1997. Figure 3-09-1 illustrates the value of microwave imager data in locating the center of a TC where the center is obscured by clouds. Both visual and infrared imagery from 1800Z on the 24th through 1800Z on the 25th suggested that Peter was moving to the northeast. However, microwave data allowed the analysts to confidently position the LLCC well to the west of the location indicated by conventional satellite imagery. Another data source became available when Peter moved within view of the Japanese weather radar network in the Ryukyu Islands, Kyushu, Shikoku, and Honshu.

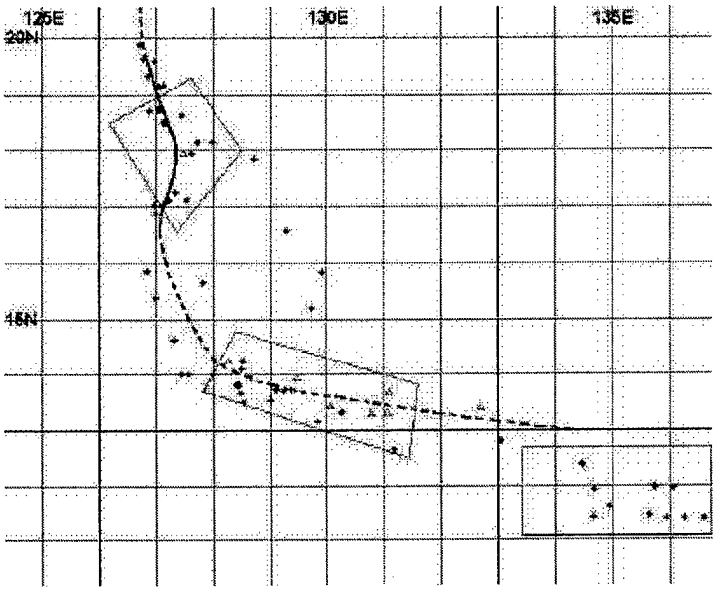

Figure 3-09-2. Conventional satellite fixes (+), scatterometer fixes (Δ), and microwave imager fixes (•) superimposed along the best track of Peter. The significance of the three boxes is explained in the text in the Discussion Section.

IV. IMPACT

Two American servicemen from Iwakuni Marine Corps Air Station were washed away in the high surf produced by Peter. At the Sasebo Naval Facility, damage was reported to be light. In port at Sasebo, the USS BELLEAU WOOD reported gusts to 54 kt (28 m/s), and the USS DUBUQUE measured gusts to 45 kt (23 m/s).

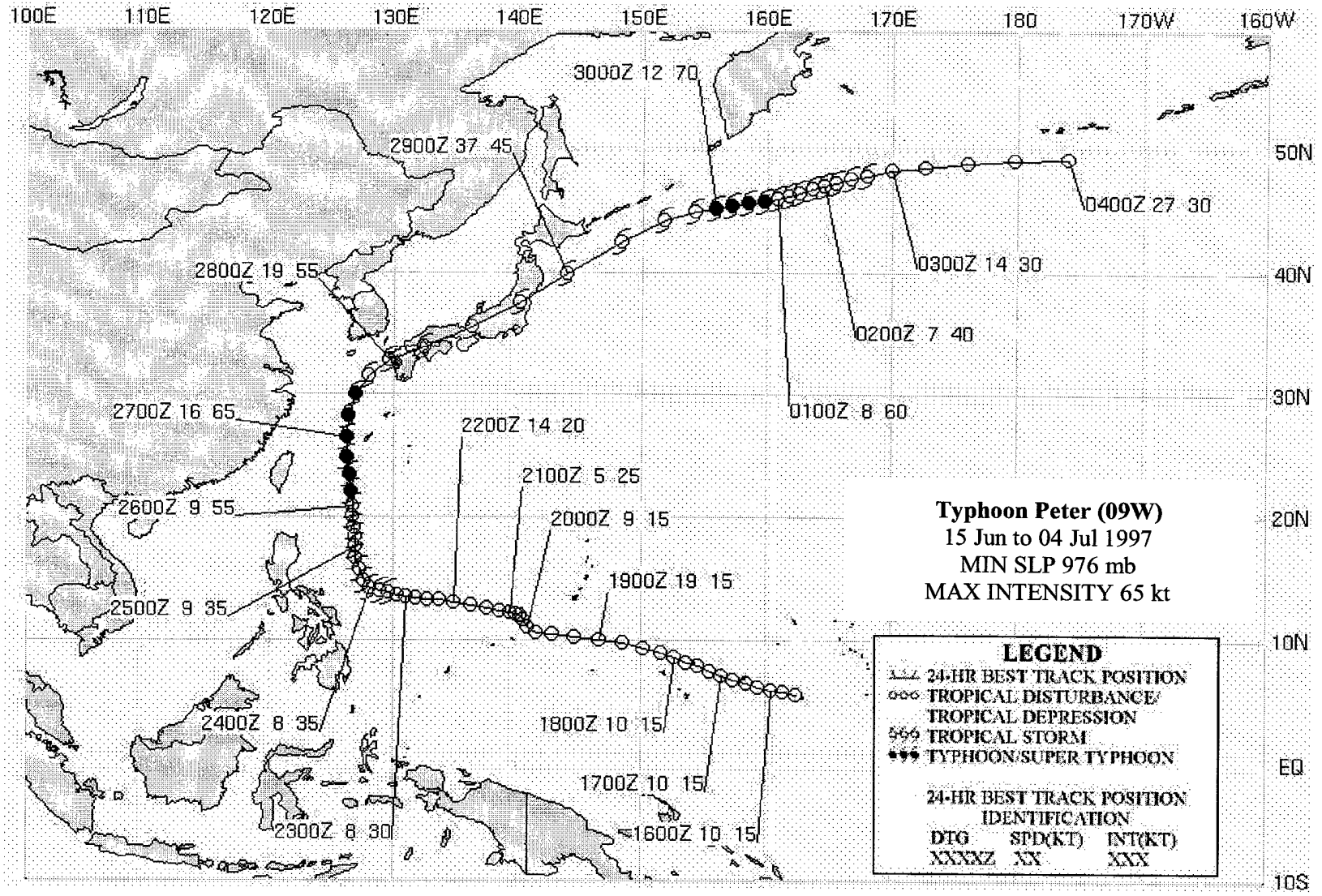
100E
110E
120E
130E
140E
150E
160E
170E
180
170W
160W
50N
40N
30N
20N
10N
EQ
10S
3000Z 12 70
2900Z 37 45
0400Z 27 30
2800Z 19 55
0300Z 14 30
0200Z 7 40
0100Z 8 60
2700Z 16 65
2200Z 14 20
2100Z 5 25
2600Z 9 55
2000Z 9 15
1900Z 19 15
2500Z 9 35
2400Z 8 35
1800Z 10 15
1700Z 10 15
2300Z 8 30
1600Z 10 15
Typhoon Peter (09W)
15 Jun to 04 Jul 1997
MIN SLP 976 mb
MAX INTENSITY 65 kt
LEGEND
24-HR BEST TRACK POSITION
TROPICAL DISTURBANCE/
TROPICAL DEPRESSION
TROPICAL STORM
TYPHOON/SUPER TYPHOON
24-HR BEST TRACK POSITION
IDENTIFICATION
DTG SPD(KT) INT(KT)
XXXXZ XX XXX

SUPER TYPHOON ROSIE (10W)

Super Typhoon (STY) Rosie (10W) originated as a tropical disturbance in the western Caroline Islands along the monsoon trough. The disturbance was first noted on the 15 July Significant Tropical Weather Advisory (ABPW) as an area of persistent convection. The pre-Rosie disturbance slowly tracked west-northwestward over the next few days; and on 18 July at 1400Z, a Tropical Cyclone Formation Alert (TCFA) was issued by JTWC. The first warning on Tropical Depression (TD) 10W was issued only four hours later. The now northwestward moving TC intensified to a typhoon by 0000Z on 21 July and reached its peak intensity of 140 kt (72 m/s) on the 22nd at 1200Z. Twelve hours later, Rosie began to weaken and slowly accelerate toward the north-northeast. The system made landfall near Okayama on the Japanese island of Shikoku around 0800Z on 26 July as a minimal typhoon with 65 kt (33 m/s) winds. Crossing over land, Rosie rapidly weakened as the main convection sheared away from the low-level circulation. It continued to weaken in the Sea of Japan as the exposed low-level and its remnants were tracked back over Japan and into the Philippine Sea where it dissipated. Rosie left two dead in Japan; and its passage resulted in power failures, landslides and widespread damage to buildings in the southern and central parts of the country.

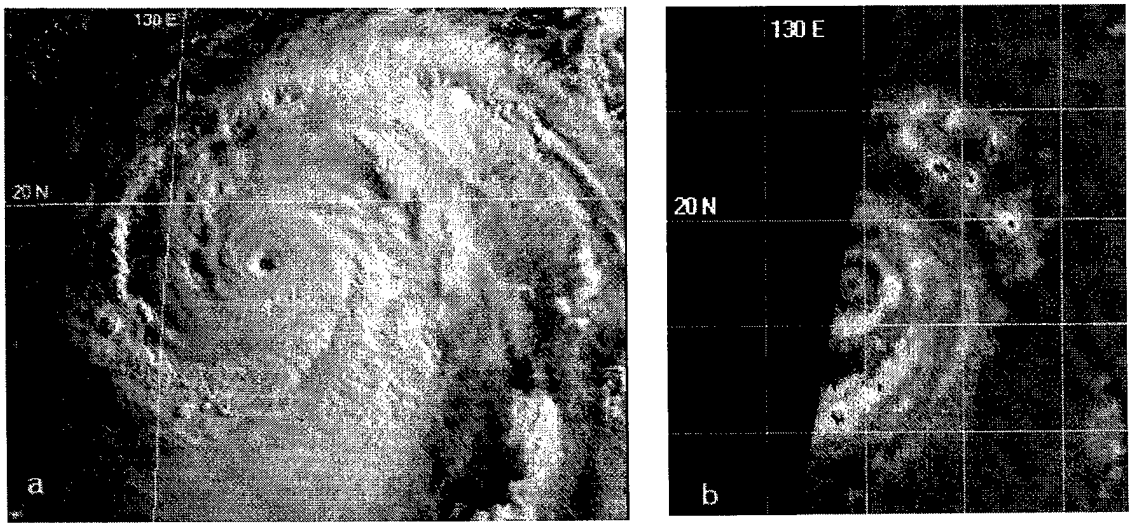

Figure 3-10-1 Rosie near peak intensity. (a) 222131Z July visible GMS imagery and (b) 222147Z July 85 GHz horizontally polarized DMSP imagery.

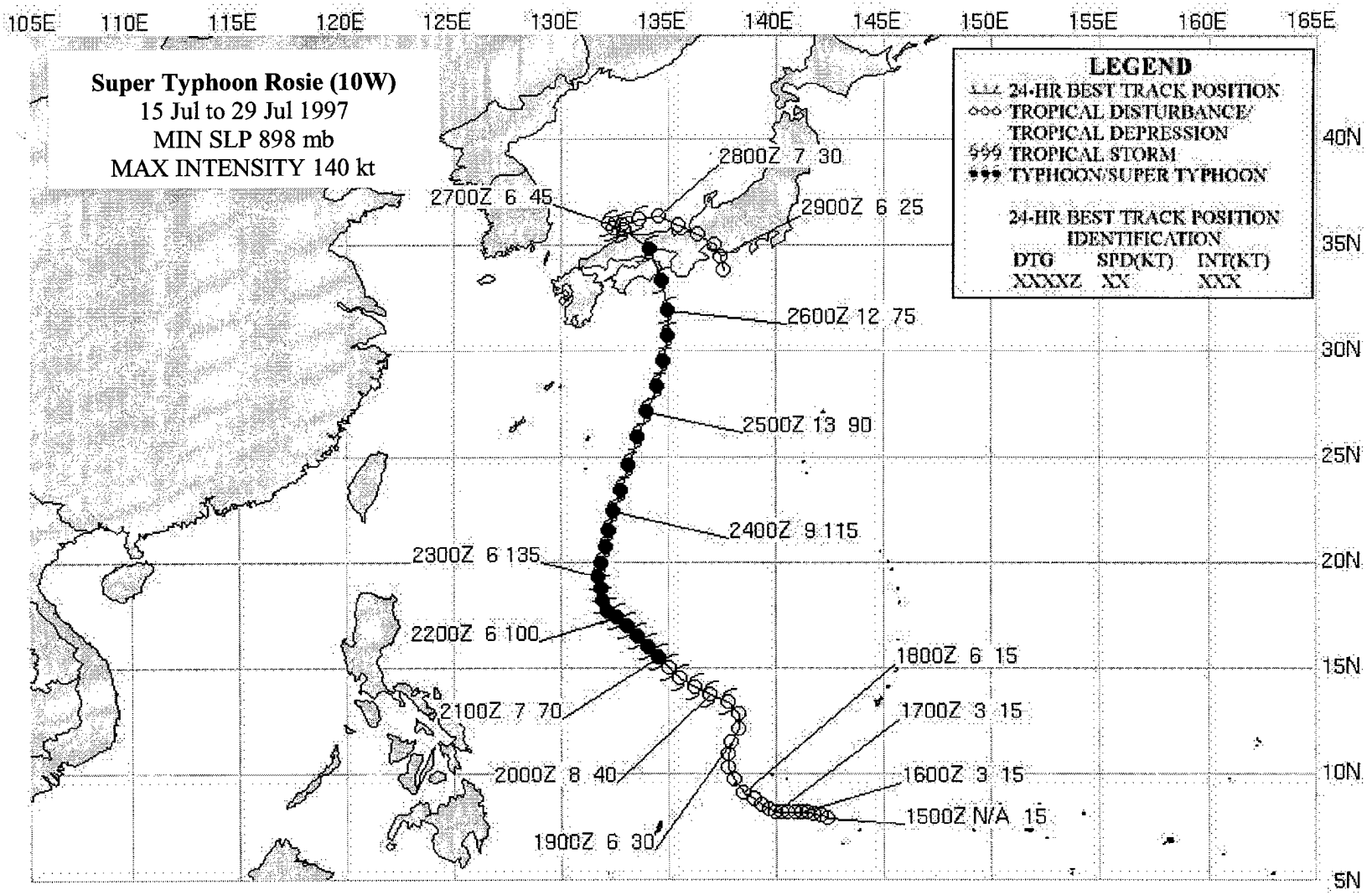
105E
110E
115E
120E
125E
130E
135E
140E
145E
150E
155E
160E
165E
40N
35N
30N
25N
20N
15N
10N
5N
Super Typhoon Rosie (10W)
15 Jul to 29 Jul 1997
MIN SLP 898 mb
MAX INTENSITY 140 kt
LEGEND
24-HR BEST TRACK POSITION
TROPICAL DISTURBANCE/
TROPICAL DEPRESSION
TROPICAL STORM
TYPHOON/SUPER TYPHOON
24-HR BEST TRACK POSITION
IDENTIFICATION
DTG SPD(KT) INT(KT)
XXXXZ XX XXX
2800Z 7 30
2700Z 6 45
2900Z 6 25
2600Z 12 75
2500Z 13 90
2400Z 9 115
2300Z 6 135
2200Z 6 100
1800Z 6 15
2100Z 7 70
1700Z 3 15
2000Z 8 40
1600Z 3 15
1500Z N/A 15
1900Z 6 30

TROPICAL STORM SCOTT (11W)

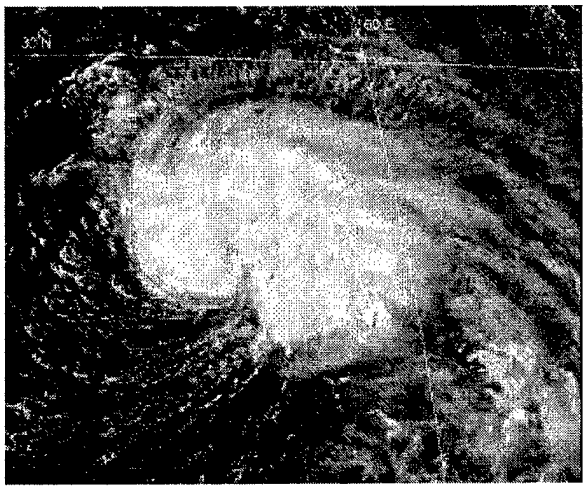

Figure 3-11-1 Tropical Storm Scott at peak intensity of 55 kt (28 m/s) on 29 July at 0633Z

Tropical Storm Scott formed in mid-July near 24N 150E from a Tropical Upper Tropospheric Trough (TUTT)-induced mid level disturbance. It was first noted on the 20 July Significant Tropical Weather Advisory (ABPW) as a closed low-level circulation with associated scattered convection. Initial development of the pre-Scott disturbance was inhibited by outflow from Super Typhoon (STY) Rosie (10W). However by 0000Z on 24 July system organization improved significantly, leading to issuance of a Tropical Cyclone Formation Alert (TCFA). The first warning on Tropical Depression (TD) 11W was issued just 6 hours later, at which time Rosie was located approximately 20 degrees west of TD 11W and moving north-northeastward with a large trailing anti-cyclone. The influence of this anti-cyclone caused TD 11W's northward track to shift to the southeast. TD 11W took a southeastward track instead of the more usual southwestward track attributed to the Indirect Tropical Cyclone Interaction (ITI) pattern because of the northwest-southeast orientation of the trailing anticyclone. After Rosie (10W) made landfall in Japan, this anticyclone became less significant as a steering influence on TD 11W. By 26 July, TD 11W appeared to be dissipating and JTWC issued what was thought to be the final warning. Soon afterward, development recommenced, resulting in a second TCFA issued at 1730Z on the 26th. Scott reached tropical storm intensity at 0600Z on the 27th and began its second major track change as it turned first toward the northwest for 24 hours and then finally to the northeast. The system reached its peak intensity of 55 kt (28 m/s), at 0600Z on the 29th and held it through 1800Z the same day. Scott began to slowly weaken, continuing northeastward, until it merged with a frontal system on 2 August. JTWC issued a final warning at 1200Z on this day. Tropical Storm Scott remained over water for its entire existence and JTWC received no reports of damage.

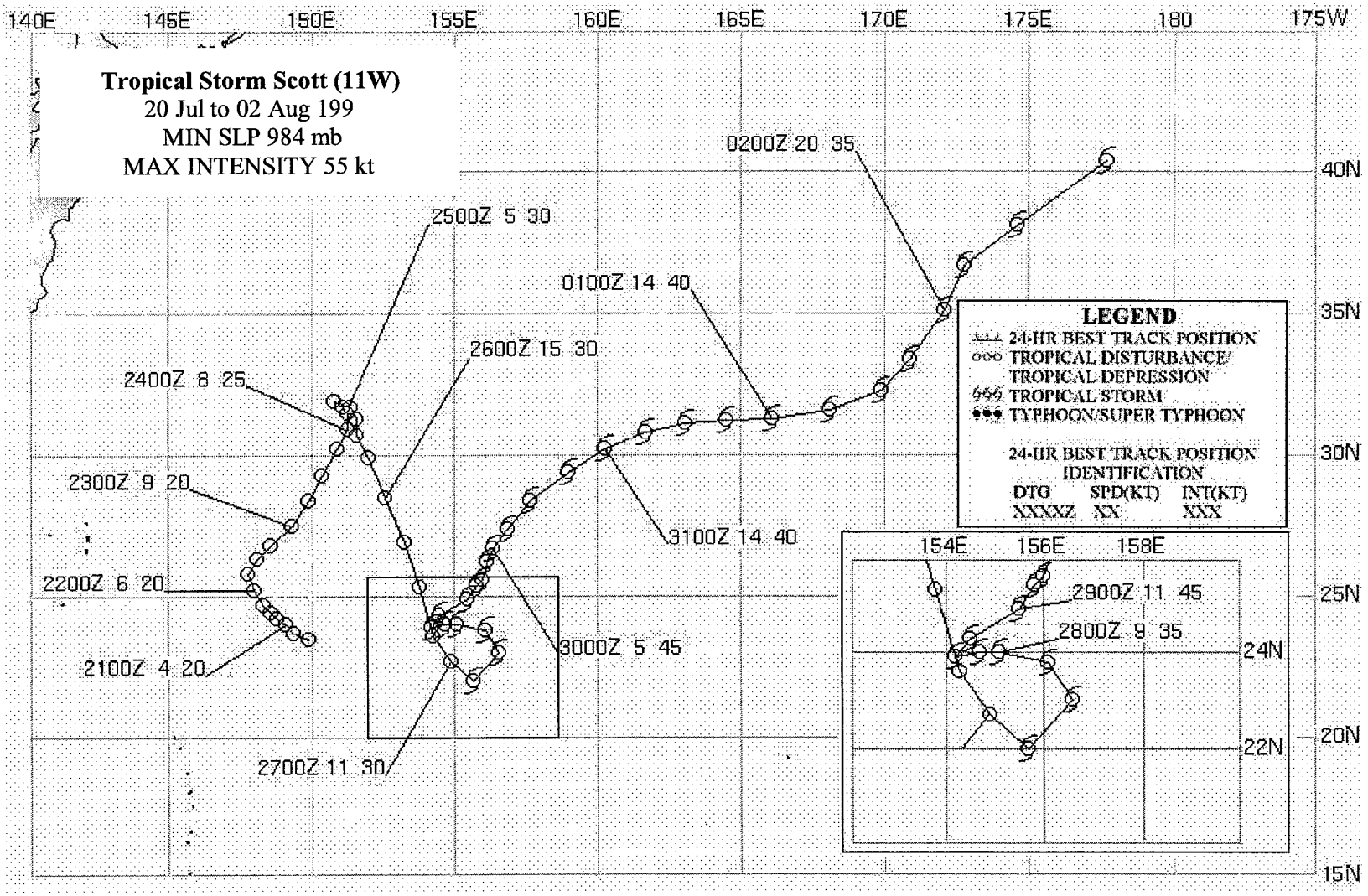
Tropical Storm Scott (11W)
20 Jul to 02 Aug 199
MIN SLP 984 mb
MAX INTENSITY 55 kt
140E
145E
150E
155E
160E
165E
170E
175E
180
175W
40N
35N
30N
25N
20N
15N
0200Z 20 35
2500Z 5 30
0100Z 14 40
2600Z 15 30
2400Z 8 25
2300Z 9 20
3100Z 14 40
2200Z 6 20
3000Z 5 45
2100Z 4 20
2700Z 11 30
LEGEND
24-HR BEST TRACK POSITION
TROPICAL DISTURBANCE/
TROPICAL DEPRESSION
TROPICAL STORM
TYPHOON/SUPER TYPHOON
24-HR BEST TRACK POSITION
IDENTIFICATION
DTG SPD(KT) INT(KT)
XXXXZ XX XXX
154E
156E
158E
24N
22N
2900Z 11 45
2800Z 9 35

TYPHOON TINA (12W)

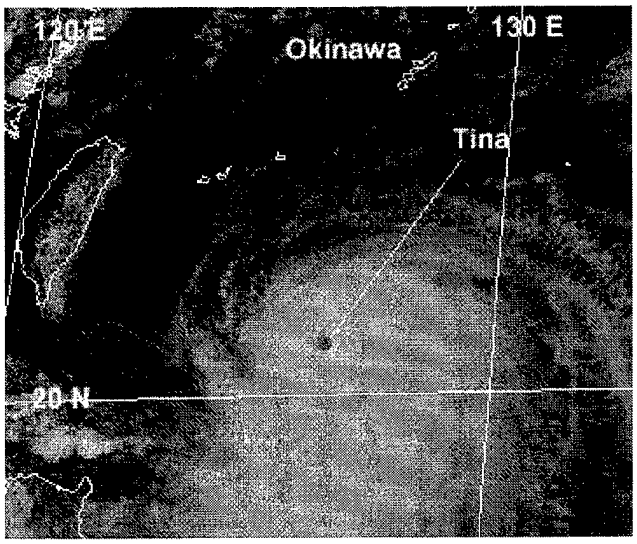

Figure 3-12-1 Typhoon Tina (12W) at 0730 on 5 Aug, near peak intensity of 90 kt (GMS 5 visible imagery).

The tropical disturbance that became Typhoon Tina (12W) initially formed as an area of convection in the eastern Caroline Islands and was first noted on the Significant Tropical Weather Advisory (ABPW) at 0600Z on 21 July. The first Tropical Cyclone Formation Alert (TCFA) was issued at 1000Z on 23 July. However, upper level wind shear caused the system to lose much of its deep convection and the TCFA was cancelled. As the disturbance continued to track northwestward, vertical wind shear gradually relaxed and the system began to reorganize. A second TCFA was issued at 0830Z on the 29th. The system's organization continued to improve and the first warning on Tropical Depression (TD) 12W was issued at 1800Z the same day. TD 12W continued to track northwestward under the steering influence of the subtropical ridge, and was upgraded to Tropical Storm Tina (12W) with the 30 July 1800Z warning. The system reached typhoon strength by 1200Z on 3 August, with continued movement to the northwest. Interaction between the cyclone and the subtropical ridge resulted in a Poleward/Poleward Oriented pattern/region (see chapter 1), causing a gradual track change from northwestward to northward. Typhoon Tina (12W) reached its peak intensity of 90 kt (46 m/s), on 5 August at 0600Z. Naha airport in Okinawa reported 50 kt (26 m/s), sustained winds on the evening of 6 August as Tina passed west of the island. The system began to weaken as it moved toward the Korean Peninsula and encountered vertical wind shear. Tina made landfall along the South Korean coast at approximately 2200Z on 8 August. JTWC issued the final warning on the system at 1200Z, 9 August. Tina passed close to Pohang, Korea, early on the 9th, which recorded wind of 25 kt (13 m/s) sustained with gusts to 48 kt (25 m/s), and a minimum pressure of 995.3 mb. The system continued to track northeastward and dissipated over the Sea of Japan.

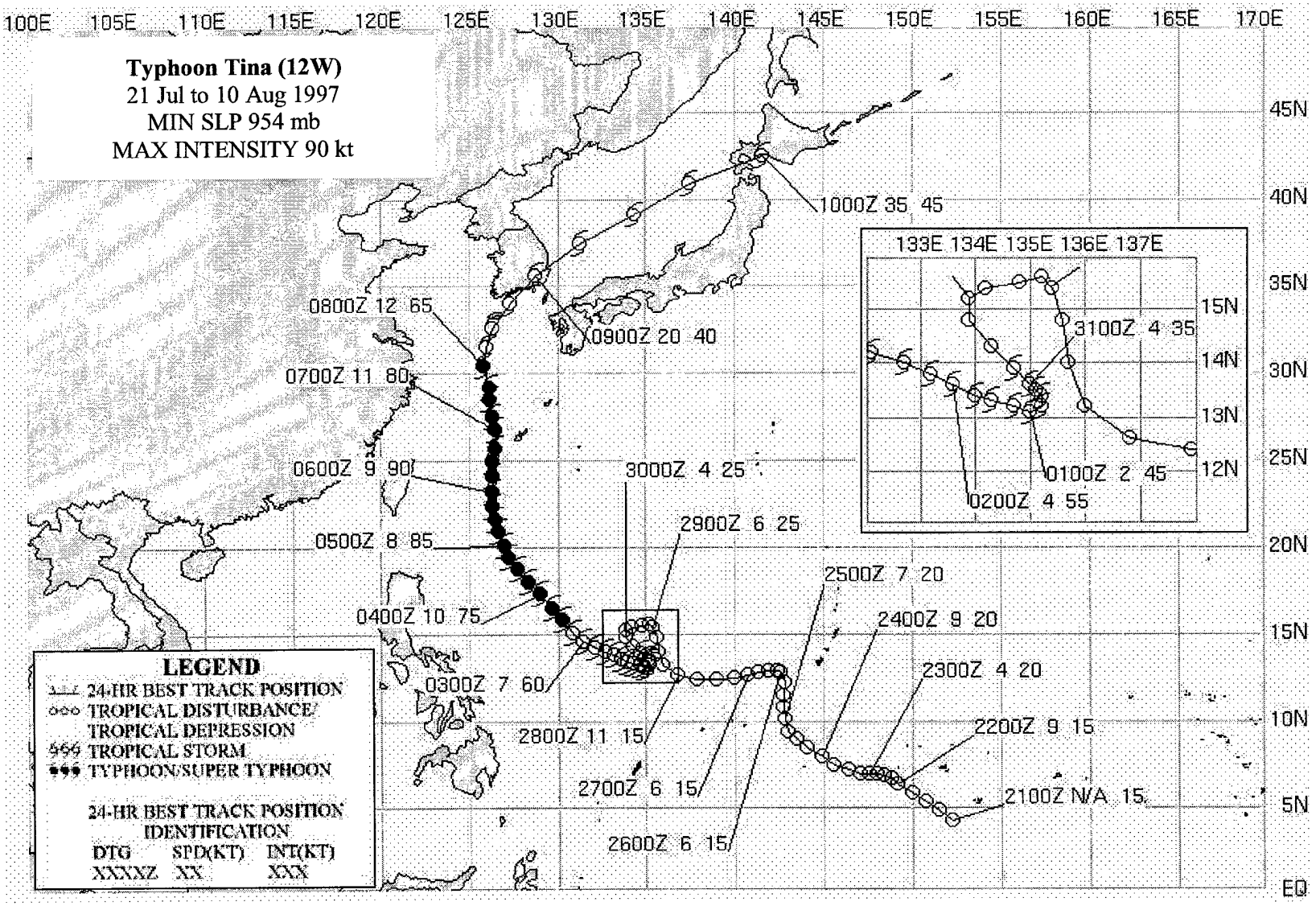
Typhoon Tina (12W)
21 Jul to 10 Aug 1997
MIN SLP 954 mb
MAX INTENSITY 90 kt
100E 105E 110E 115E 120E 125E 130E 135E 140E 145E 150E 155E 160E 165E 170E
45N 40N 35N 30N 25N 20N 15N 10N 5N EQ
1000Z 35 45
0800Z 12 65
0900Z 20 40
0700Z 11 80
0600Z 9 90
3000Z 4 25
2900Z 6 25
0500Z 8 85
2500Z 7 20
0400Z 10 75
2400Z 9 20
2300Z 4 20
0300Z 7 60
2800Z 11 15
2200Z 9 15
2700Z 6 15
2100Z N/A 15
2600Z 6 15
133E 134E 135E 136E 137E
15N 14N 13N 12N
3100Z 4 35
0100Z 2 45
0200Z 4 55
LEGEND
24-HR BEST TRACK POSITION
TROPICAL DISTURBANCE/ TROPICAL DEPRESSION
TROPICAL STORM
TYPHOON/SUPER TYPHOON
24-HR BEST TRACK POSITION IDENTIFICATION
DTG SPD(KT) INT(KT)
XXXXZ XX XXX

TYPHOON VICTOR (13W)

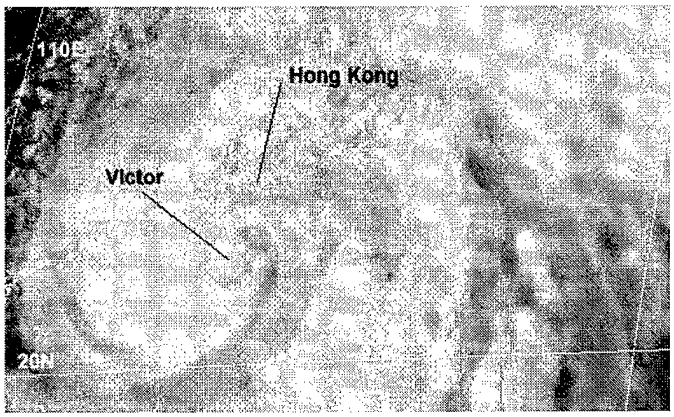

Figure 3-13-1 Typhoon Victor (13W) at 020634Z August, just prior to landfall (GMS 5 visible imagery).

The topical disturbance that became Typhoon Victor (13W) initially formed around 28 July, developing from an area of convection moving west-northwestward within the monsoon trough, just west of Luzon. Initially, moderate upper-level wind shear kept the deep convection to the south of the low-level circulation center. The disturbance was first noted on the Significant Tropical Weather Advisory (ABPW) at 0600Z on 30 July. The first warning on Tropical Depression 13W was issued at 1800Z the same day (A TCFA was not issued). TD 13W was initially steered by a mid-level ridge located to its southeast, resulting in a northward track. At 1200Z on 31 July, the system was upgraded to a tropical storm. Victor continued tracking northward, intensifying slowly under moderate vertical wind shear. By 0600Z on 2 August the deep convection consolidated over the low-level circulation center and intensification became more rapid. Victor reached its peak intensity of 65 knots just prior to making landfall at 1200Z on 2 August near Hong Kong (Figure 3-13-1). The cyclone weakened over land as it accelerated and tracked northward over southern China. By 4 August, the remnants of Victor merged with a frontal boundary west of Shanghai.

Although originally classified as a tropical storm, Victor was upgraded to a minimal strength typhoon in post analysis, based on synoptic data recorded as it made landfall. Published press reports attributed one death and over 30 injuries in Hong Kong to Victor. In Guangzhou Province, China, heavy flooding left 49 dead and 12,000 homes destroyed.

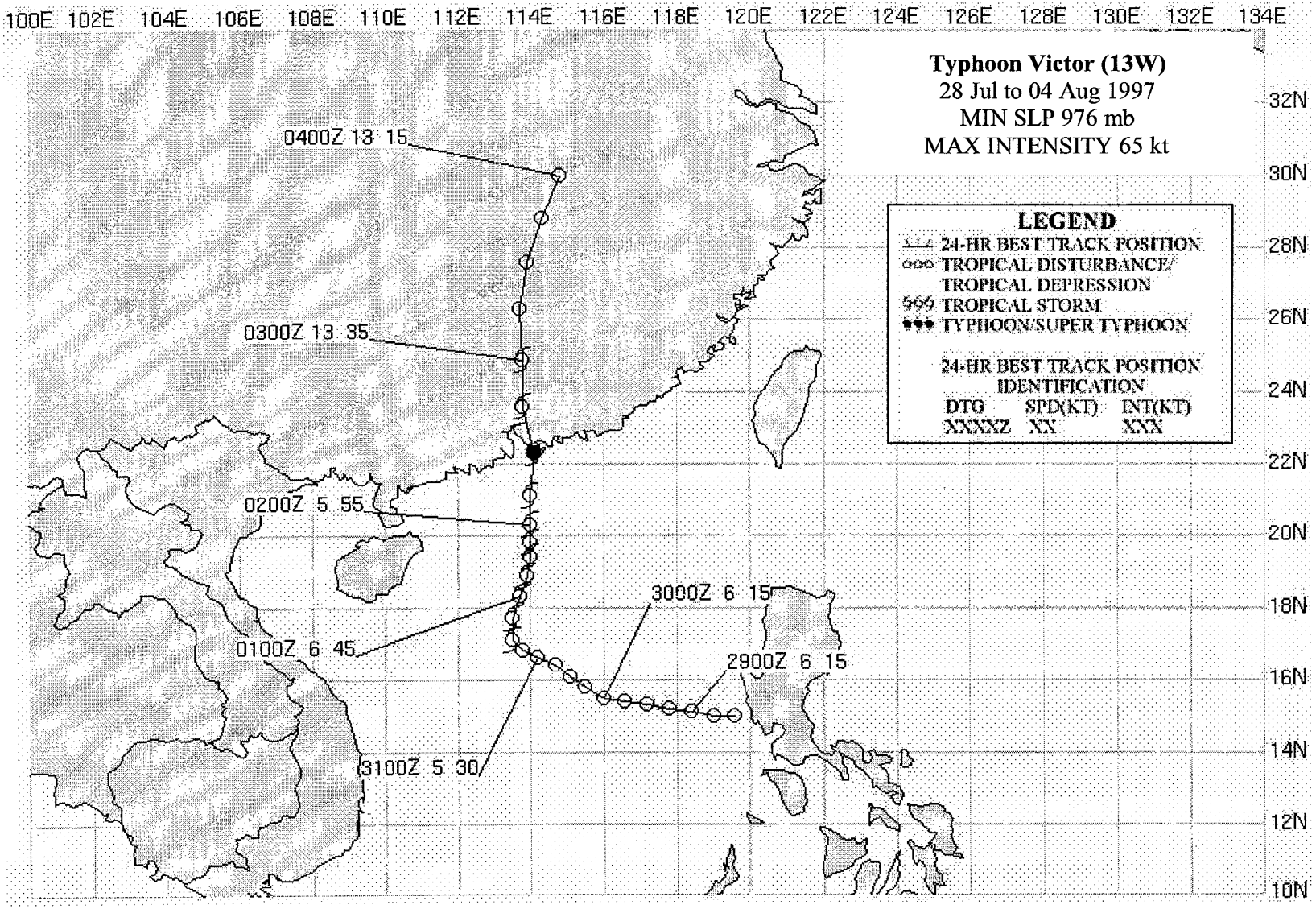
100E 102E 104E 106E 108E 110E 112E 114E 116E 118E 120E 122E 124E 126E 128E 130E 132E 134E
32N
30N
28N
26N
24N
22N
20N
18N
16N
14N
12N
10N
Typhoon Victor (13W)
28 Jul to 04 Aug 1997
MIN SLP 976 mb
MAX INTENSITY 65 kt
LEGEND
24-HR BEST TRACK POSITION
TROPICAL DISTURBANCE/ TROPICAL DEPRESSION
TROPICAL STORM
TYPHOON/SUPER TYPHOON
24-HR BEST TRACK POSITION IDENTIFICATION
DTG SPD(KT) INT(KT)
XXXXZ XX XXX
0400Z 13 15
0300Z 13 35
0200Z 5 55
0100Z 6 45
3100Z 5 30
3000Z 6 15
2900Z 6 15

SUPER TYPHOON WINNIE (14W)

I. HIGHLIGHTS

Winnie formed at low latitudes in the Marshall Islands and was the fourth of eleven tropical cyclones (TCs) to attain super typhoon intensity in the western North Pacific during 1997. It was one of ten TCs that formed east of 160E and south of 20N; the "El Niño" box in Figure 3-3a. Winnie was a straight running TC that passed over Okinawa, and later made landfall on the eastern coast of China, where it was responsible for loss of life and considerable damage. When it was near Okinawa, the typhoon formed concentric eyewall clouds. The 200 nm (370 km) diameter of the outer eyewall cloud, observed by satellite and radar, was one of the largest ever recorded.

II. TRACK AND INTENSITY

During the first week of August, two TCs, Tina (12W), and Victor (13W), moved northward in the western portion of the West North Pacific (WNP) basin. Concurrent with the evolution of these TCs, an area of deep convection associated with the El Niño related low latitude westerly wind flow east of 160E persisted near the Marshall Islands. The disturbance was added to the 5 August Significant Tropical Weather Advisory (ABPW) after satellite imagery and synoptic data indicated a low-level cyclonic circulation with sea-level pressure in the region approximately 2 mb below normal.

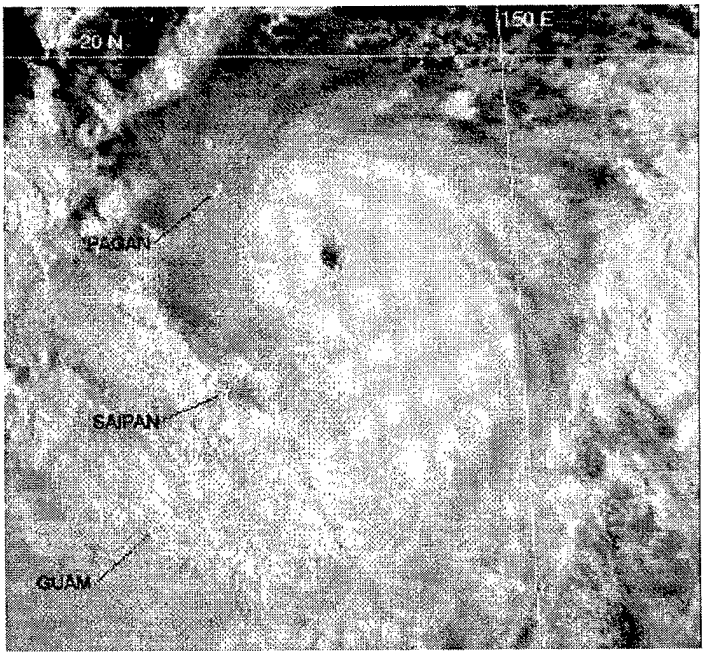

Figure 3-14-1 Winnie nears its peak intensity of 140 kt (72 m/sec) as it approaches the Northern Mariana Islands (112133Z August visible GMS imagery).

The monsoon depression gradually became better organized as it moved steadily toward the west-northwest. The deep convection became more consolidated and cirrus outflow became organized in a well-defined anticyclonic pattern, while the sea-level pressure slowly fell. Based on increased organization of the deep convection, sea-level pressures estimated at 1006 mb, and divergent outflow aloft (as indicated by animated water-vapor imagery) a Tropical Cyclone Formation Alert (TCFA) was issued at 0230Z on the 8th. The first warning on Tropical Depression (TD) 14W soon followed, valid at 0600Z the same day, based on a satellite intensity estimate of 30 kt (15 m/sec). This large TC intensified and was upgraded to Tropical Storm

Winnie (14W) with the 0600Z warning on 9 August. Winnie intensified quickly and became a typhoon by 0000Z on the 10th, and peaked at an intensity of 140 kt (72 m/sec) at 0000Z on the 12th (Figure 3-14-1). While still east of the Mariana Island chain. At 0600Z on the 12th, the system passed between the islands of Alamagan and Pagan. Winnie continued on its west-northwestward course and maintained an intensity of 140 kt (72 m/sec) for 24 hours, then began to slowly weaken as it approached the Ryukyu Islands. By 14 August, Winnie showed signs of developing concentric wall clouds which became more distinct on 15 and 16 August. As the typhoon passed through the Ryukyu Islands on 17 August, the inner wall cloud began to dissipate as the large-diameter outer wall cloud became well defined (see discussion below). Winnie moved across the East China Sea and made landfall on the eastern coast of China approximately 140 nm (260 km) south of Shanghai shortly before 1200Z on 18 August. The system passed across Manchuria and quickly dissipated as it moved into the mountainous terrain north of Vladivostok. The final warning was issued valid at 0000Z on the 19th. The remnants of Winnie were eventually observed to have recurved to the northeast.

III. DISCUSSION

a. Winnie's large-diameter outer eye wall cloud.

The well-defined eye of a mature TC is probably one of nature's most remarkable and awe-inspiring phenomena. In the Dvorak (1975, 1984) classification scheme, the intensity of a TC is estimated from several characteristics of satellite imagery. These include the distance of the low-level circulation center to the deep convection; the size of the central dense overcast; the cloud-top temperatures, the horizontal width of the eye wall cloud; and the width and extent of peripheral banding features. The basic TC pattern types identified by Dvorak are: (1) the "shear" pattern; (2) the "curved band" pattern; (3) the "central dense overcast" pattern; and, (4) the "eye" pattern. Of these pattern types, the "eye" pattern is probably the best known to the laymen.

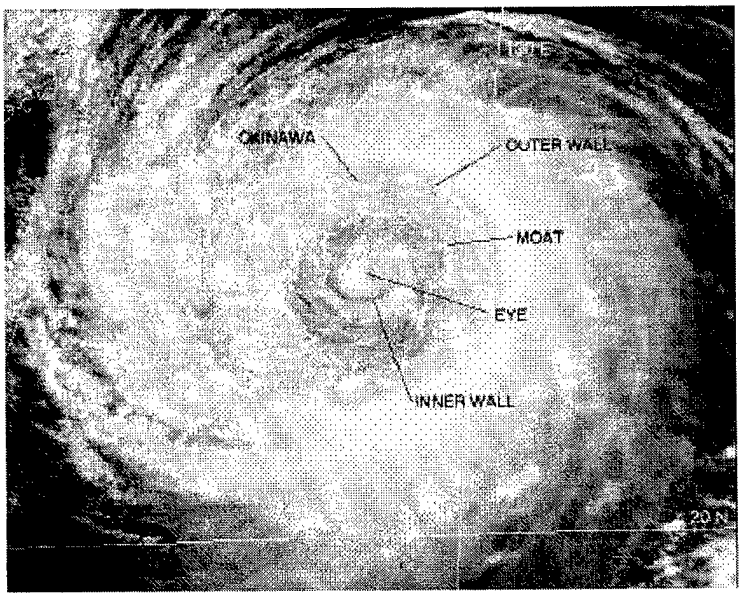

Figure 3-14-2 Winnie's outer wall cloud passes over Okinawa bringing typhoon-force winds as the small eye and inner wall cloud (within a relatively cloud-free moat) pass to the south. (170133Z August visible GMS imagery.) The black dot indicates the Kadena NEXRAD location.

The TC eye can be ragged or well-defined. In general, the more sharply defined the eye becomes on satellite imagery, the more intense the TC is likely to be. The average satellite-observed TC

eye diameter is between 30 and 45 nm (55 - 85 km) (Weatherford 1984). Eyes with diameters less than 30 nm (55 km) are considered to be small, while those with diameters greater than 45 nm (85 km) are considered to be large. In the Dvorak scheme, the intensity of a TC with a large well-defined eye is capped at 115 kt (59 m /sec), and the intensity of a TC with a large ragged eye is capped at 90 kt (46 m/sec), regardless of other characteristics observed on the satellite imagery. Some extremes of eye sizes include the small, 8-nm (15-km) diameter eye of Super Typhoon Tip (JTWC 1979 - observed by aircraft), and the radar-observed, large, 200-nm (370-km) diameter eye of Typhoon Carmen (JTWC 1960).

Some TCs, especially the intense ones, develop concentric wall clouds separated by a relatively cloud-free moat. In such cases, the outer wall cloud may contract while the inner one collapses in a process known as eyewall replacement. This has been discussed at length by Willoughby et al. (1982) and Willoughby (1990). These authors also note that TC eyes almost invariably contract during intensification so that smaller eyes and extreme intensity tend to be correlated. The Dvorak scheme has no special rules for concentric eyewall clouds. This is most likely because a cirrus overcast normally obscures the outer wall cloud in satellite imagery.

As Winnie moved toward Okinawa on August 16, a large outer rain band began to encircle the wall cloud that defined the eye. By the time the typhoon passed over Okinawa, the rainband had become a complete, 200 nm (370 km) diameter, concentric outer wall cloud (Figures 3-14-2 and 3-14-3).

The largest eye diameter ever reported by JTWC was that of Typhoon Carmen (JTWC 1960) as it passed over Okinawa. By coincidence, Winnie also passed over Okinawa. Carmen's eye diameter, as measured by the weather radar at Kadena Air Force Base was 200 nm (370 km), approximately the same diameter as Winnie's outer eyewall cloud. The 1960 Annual Typhoon Report commented: "Another feature quite unusual about this typhoon was the diameter of its eye. Reconnaissance aircraft frequently reported eye diameters of 100 [nm] [185 km], using as the basis of measurement, surface winds and pressure gradient. However, with respect to wall clouds surrounding the eye, radar photographs taken from the CPS-9 at Kadena AB show quite clearly that on 20 August, the eye had a diameter of approximately

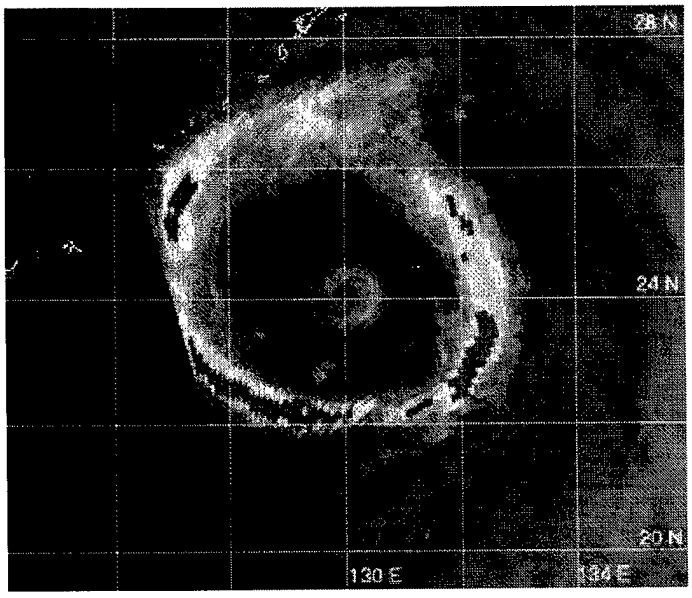

Figure 3-14-3 Winnie's outer wall cloud is nicely highlighted by microwave imagery. This is sensitive to regions containing precipitation-sized hydrometeors (especially large ice-phase particles). The eye and inner wall cloud are present but less distinct. (161311Z August horizontally polarized 85 GHz microwave DMSP imagery.)

200 [nm] [370 km]. The eye diameter of Carmen was probably one of the largest ever reported . . ." Winnie, like Carmen, was also viewed by radar at Kadena AB, a NEXRAD WSR 88D (Figure 3-14-4a,b).

As the outer wall cloud passed over Okinawa on 16 August, wind gusts of 82 kt (42 m/sec) were recorded (Figure 3-14-5) and the sea level pressure (SLP) fell to 964 mb (Figure 3-14-6). The center of the eye passed approximately 80 nm (150 km) south of the island. Doppler radar indicated 100-kt (51-m/sec) winds in the large outer eye wall in a layer from 3,000 ft (914 m) to 6,000 ft (1829 m). The NEXRAD base velocity product (Figure 3-14-4b) shows inbound wind speeds between 50 kt and 80 kt (26 m/sec and 41 m/sec) at an altitude of 8,000 ft (2438 m) above sea level on the eastern side of the inner wall cloud.

Although concentric wall clouds are not rare, especially for intense TCs, the extreme diameter of Winnie's outer eyewall cloud is an infrequent occurance. Such large diameters are restricted primarily to the western North Pacific basin. In the Atlantic, TCs with large-diameter outer eye wall clouds have been observed, but not as large as these WNP examples. Such Atlantic storms include Allen (1980), Diana (1984), Gilbert (1988), and Luis (1995). These had outer eyewall clouds with diameters greater than 135 nm (250 km) and very small inner eyewall clouds with diameters less than 15 nm (28 km).

Sometimes typhoons which form in the monsoon trough of the western North Pacific generate very large circulations and eyes. The 370 km diameter of Winnie's outer eye wall cloud during passage over Okinawa is one of the largest ever observed in a TC. These cases are important because they define the most extreme possibilities of TC dynamics.

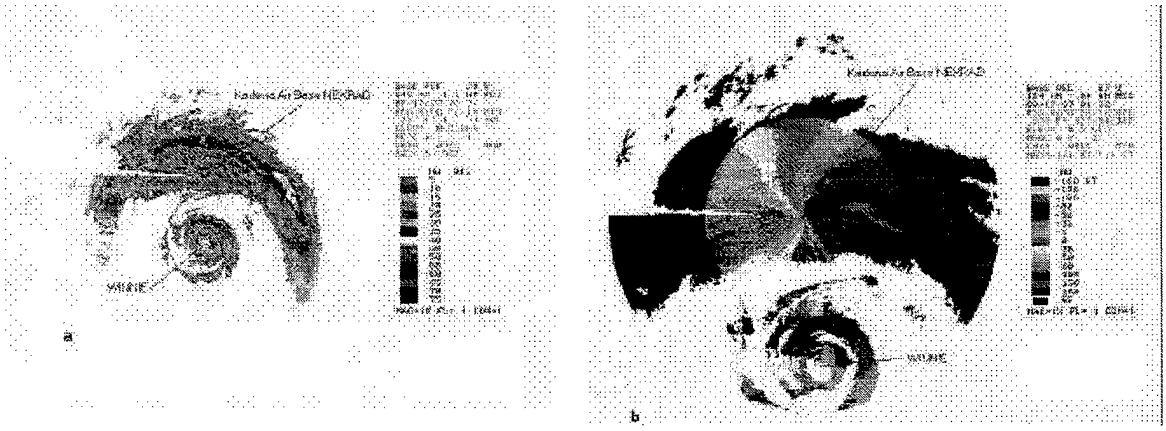

Figure 3-14-4 Winnie's outer wall cloud, and smaller inner wall cloud and eye, as depicted by the NEXRAD WSR 88D located near Kadena AB on Okinawa. (a) The base reflectivity at 170226Z August, and (b) the 170122Z August base velocity product. The NEXRAD is able to compute Doppler velocities within 125 nm (230 km) of the radar. The black dot (with arrow) shows the location of the NEXRAD in both panels.

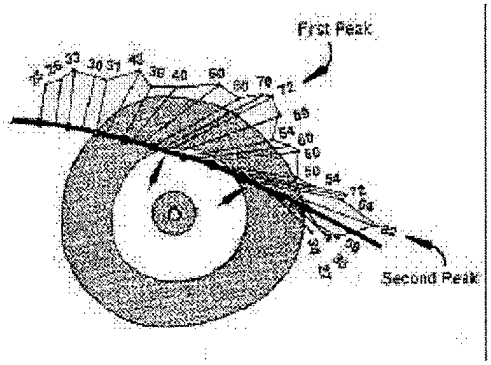

Figure 3-14-5 Wind reports from Kadena AB received at JTWC are plotted with respect to Winnie's cloud system (shaded regions). Winds are peak gusts in kt. Note that the peak gusts (indicated by arrows) at Kadena occur on the inward edge of the outer wall cloud in agreement with Jorgensen's (1984) synthesis of aircraft observations of the wind distribution in the large outer wall cloud of Hurricane Allen (1980). The small black dots along the indicated track are at 5-hour intervals from 160100Z to 172200Z August.

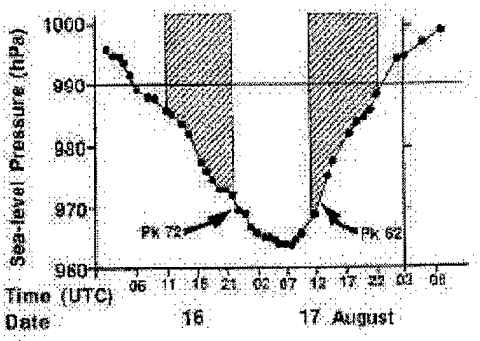

Figure 3-14-6 A time series of the sea-level pressure (SLP) recorded at Kadena AB as Winnie's outer wall cloud (hatched region) passed. Again, note the peak gusts occurring near the inner edge of the satellite observed outer wall cloud.

b. Winnie's Digital Dvorak (DD) time series

The magnitude of Winnie's Digital Dvorak (DD) numbers increased more rapidly than the warning intensity as the TC intensified on 11 and 12 August (a frequent occurance). Winnie's series did not exhibit any obvious diurnal variations. Some typhoons exhibit a strong diurnal variation, while others (like Winnie) show little or none. Although not shown below, DD numbers were calculated for Winnie on 16 and 17 August when it possessed a very large diameter outer eye wall cloud by adapting the DD algorithm to use cloud-top temperature of the outer eye wall cloud to arrive at an intensity estimate. These DD numbers were observed to fluctuate between about 4.5 and 5.0. The corresponding intensity range of 77-90 kt

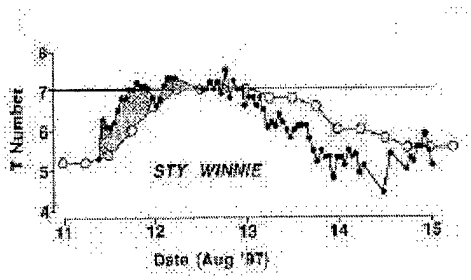

Figure 3-14-7 A time series of Winnie's hourly DD numbers (small black dots) compared with the warning intensity (open circles). As the TC was intensifying on 11 and 12 August, the DD numbers increase faster than the warning intensity (shaded region) -- a common behavior of the DD numbers. Note that the warning intensity is higher than the DD numbers as the TC begins to weaken, which is consistent with Dvorak's rule to delay the current intensity behind the decreasing data T-numbers.

(40-46 m/sec) fits well with synoptic reports from Okinawa (e.g., the 82 kt (42 m/sec) peak gust at Kadena, and the NEXRAD indications of 100 kt (51 m/sec) winds within the outer eyewall layer between 3,000 ft (914 m) and 6000 ft (1829 m)).

IV. IMPACT

As Winnie passed through the northern Mariana Islands, the populated islands of Guam, Rota, Tinian, and Saipan (well to the south of Winnie's track, but within its gale area) reported damage to crops and vegetation from winds and sea-salt spray. In Taiwan, 27 people were reported killed when an apartment building collapsed. Another 12 people were reported killed from mudslides, flooding and high wind. In mainland China, torrential rains and winds caused at least 25 deaths. Damage from wind and flooding was extensive.

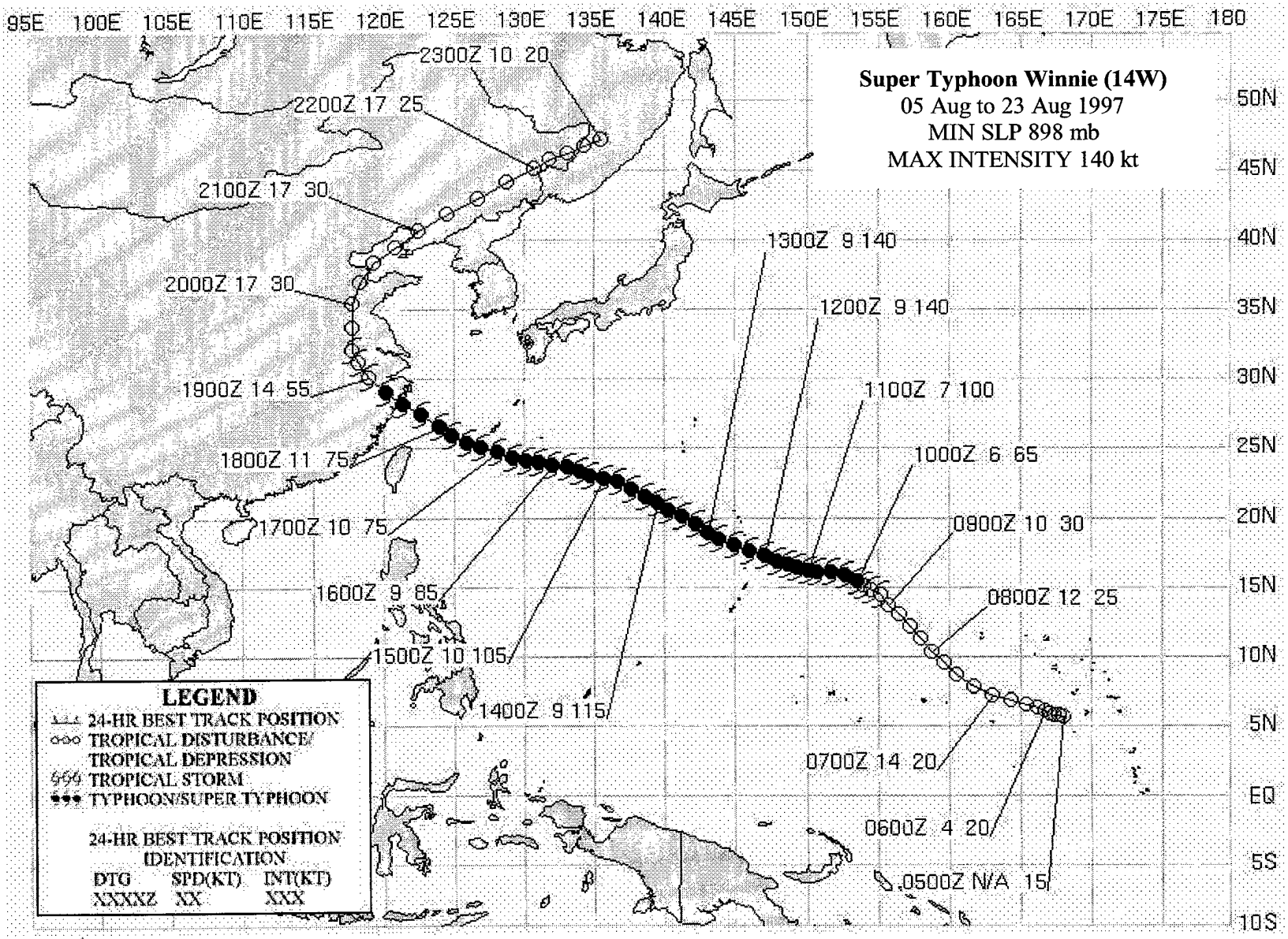
95E 100E 105E 110E 115E 120E 125E 130E 135E 140E 145E 150E 155E 160E 165E 170E 175E 180
50N
45N
40N
35N
30N
25N
20N
15N
10N
5N
EQ
5S
10S
Super Typhoon Winnie (14W)
05 Aug to 23 Aug 1997
MIN SLP 898 mb
MAX INTENSITY 140 kt
2300Z 10 20
2200Z 17 25
2100Z 17 30
2000Z 17 30
1900Z 14 55
1800Z 11 75
1700Z 10 75
1600Z 9 85
1500Z 10 105
1400Z 9 115
1300Z 9 140
1200Z 9 140
1100Z 7 100
1000Z 6 65
0900Z 10 30
0800Z 12 25
0700Z 14 20
0600Z 4 20
0500Z N/A 15
LEGEND
24-HR BEST TRACK POSITION
TROPICAL DISTURBANCE/
TROPICAL DEPRESSION
TROPICAL STORM
TYPHOON/SUPER TYPHOON
24-HR BEST TRACK POSITION
IDENTIFICATION
DTG SPD(KT) INT(KT)
XXXXZ XX XXX

TYPHOON YULE (15W) AND TROPICAL DEPRESSION 16W

I. HIGHLIGHTS

Yule and Tropical Depression (TD) 16W were two of ten tropical cyclones (TCs) during 1997 which formed east of 160E and south of 20N — within the "El Niño box" in Figure 3-5b. These two TCs existed simultaneously, and underwent a binary interaction resulting in their merger. After merger, the single resultant TC (retaining the name Yule) moved on a north-oriented track and passed close to Wake Island. When it reached the mid-latitudes, the system became a vigorous hybrid system possessing typhoon-force winds.

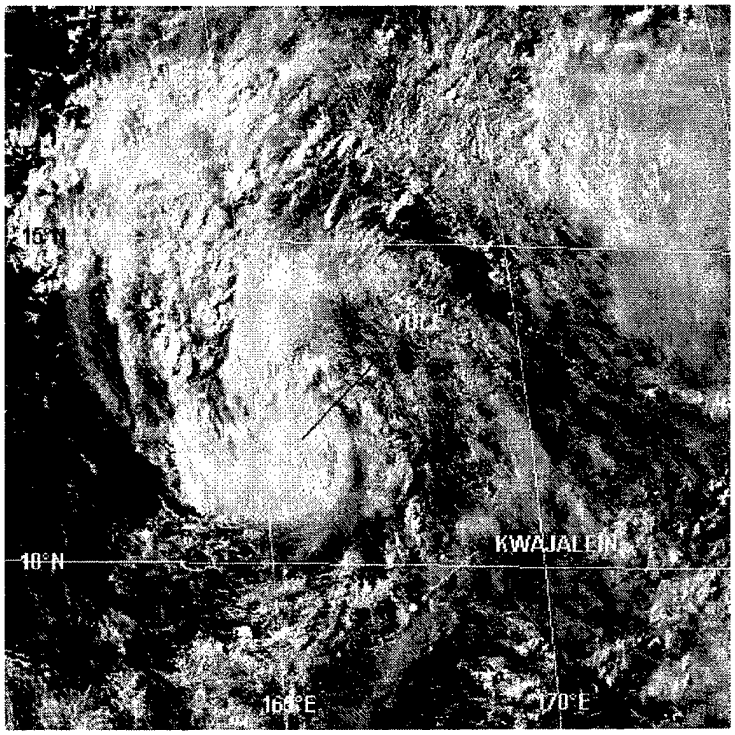

Figure 3-15/16-1 Yule becomes a tropical storm when located about 180 nm (330 km) northwest of Kwajalein (170533Z August visible GMS imagery). Properties of the centroid-relative motion help to reveal the nature of the interaction (which is not always apparent in the actual earth-relative tracks).

II. TRACK AND INTENSITY

During the middle of August, as the large-sized Winnie (14W) approached Okinawa and the east coast of China, low-level westerly winds persisted at low latitude from the Philippines eastward across Micronesia as far as the international date line (IDL). A monsoon cloud band (with some well-defined tropical upper tropospheric trough (TUTT) cells to its north) stretched from Winnie to the eastern end of the monsoon trough. Yule and TD 16W originated from tropical disturbances located at low latitude: Yule from a tropical disturbance west of the IDL in the Marshall Islands, and TD 16W from a tropical disturbance east of the IDL at low latitudes to the southwest of Hawaii.

a. Yule (15W)

Yule (the westernmost of the Yule-TD 16W pair) originated from a very poorly organized tropical disturbance in the monsoon trough which stretched at low latitude across the eastern Caroline and Marshall Island groups. It was first mentioned on the 090600Z August Significant Tropical Weather Advisory (ABPW) when satellite imagery indicated that a possible low-level circulation center was associated with an area of deep convection at very low latitude (3N) and

just to the west of the IDL. For nearly a week, this tropical disturbance remained poorly organized and difficult to follow. Then, on 15 August, satellite imagery indicated deep convection had increased and the organization of this deep convection (and other cloud lines) had improved. The first Tropical Cyclone Formation Alert (TCFA) — of two — was issued at 150730Z August. Because of unusual north-northeastward motion of the low-level circulation center, a second TCFA was issued at 160030Z to reposition the alert box. The influence of monsoonal westerlies to its south, and the onset of a binary interaction with the pre-TD 16W tropical disturbance may have been responsible for this north-northeastward motion.

When satellite intensity estimates reached 30 kt (15 m/sec), the first warning, valid at 161800Z, was issued on TD 15W. The warning indicated TD 15W would move northwest and intensify. Although the TD did intensify, it continued tracking to the north-northeast. On the second warning, valid at 170000Z, the warning acknowledged the north-northeast motion and forecast it to become northwest during the forecast period. Based on satellite intensity estimates of 35 kt (18 m/sec), TD 15W was upgraded to Tropical Storm Yule at 170600Z (Figure 3-15/16-1). Once again, the system, though moving north-northeast, was expected to turn to the northwest after 24 hours. By 180000Z, it was recognized that Yule was interacting with the newly formed TD 16W. The official forecast given on the warning valid at 180000Z was for Yule to move northeast for 24 hours and then turn toward the west and follow TD 16W. The alternate scenario of merger with TD 16W was mentioned on the Prognostic Reasoning message accompanying this warning.

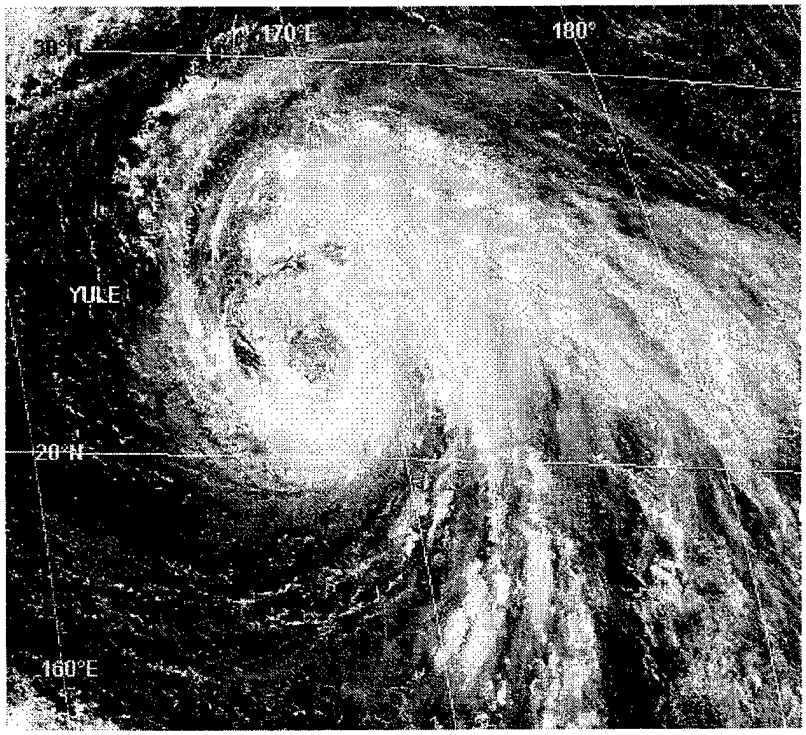

Figure 3-15/16-2 Possessing a large ragged eye, Yule briefly attains typhoon intensity (210333Z August visible GMS imagery).

At 190000Z, Yule and TD 16W merged (for more details on this merger, see the Discussion Section). The merger was asymmetric in that the low-level circulation center of TD 16W was horizontally sheared and swept into the intact circulation of Yule. Based on this analysis, JTWC decided the merged system would retain the name Yule. The system continued to move north-northeast on a long north-oriented track following the merger. The system also intensified, and briefly became a typhoon with a large ragged eye at 210600Z (Figure 3-15/16-2).

On 22 August, Yule approached a cloud band which was located to the east of an upper-level midlatitude trough and to the west of a blocking high. Entering this baroclinic cloud zone on 23 August, Yule was steered back toward the northwest. Acquiring extratropical characteristics, the final warning on Yule was issued valid at 230600Z. Instead of weakening, Yule intensified after it transitioned to an extratropical low. This was anticipated and was mentioned on the final warning. As a vigorous extratropical low (with some tropical characteristics) (see the Discussion Section) the system possessed typhoon-force winds of 65 kt (33 m/sec) during the period 231200Z to 251800Z. At nearly 50°N, the system finally entered weak westerly steering. It turned to the east after 241800Z. The system dropped below typhoon intensity after 251800Z as it drifted slowly eastward and weakened.

b. Tropical Depression 16W

Tropical Depression 16W (the easternmost of the Yule-TD 16W pair) originated from a poorly organized tropical disturbance which was first detected when it was east of the IDL. This tropical disturbance was first mentioned on the 130600Z August Significant Tropical Weather Advisory when synoptic data indicated a low-level cyclonic circulation was associated with a persistent but disorganized area of deep convection, and water vapor imagery indicated good upper-level outflow. The system was still east of the IDL at this time, but was heading westward. Moving slowly westward, the disturbance remained poorly organized for several days. It crossed the IDL and moved into JTWC's AOR on 15 August. On 17 August, the deep convection associated with this disturbance became better organized and a TCFA was issued at 172030Z. Located less than 450 nm (830 km) to the northeast of Tropical Storm Yule, the tropical disturbance which became TD 16W was already locked in a binary interaction with Yule (Figure 3-15/16-3). The first warning on TD 16W was issued valid at 180000Z based upon satellite intensity estimates of 25 kt (13 m/sec). Its binary interaction with Yule was entered as a comment on the warning message. Two scenarios of the outcome of the binary interaction of TD 16W with Yule were mentioned on the prognostic reasoning message for the first warning: the primary scenario was for TD 16W to slow as it moved westward, lose latitude, and increase its separation distance from Yule; an alternate scenario called for TD 16W to merge with Yule. The latter scenario is what occurred. The final warning was issued on TD 16W, valid at 190000Z, when it was apparent that the two systems were merging (Figure 3-15/16-4), and the sheared remains of TD 16W were being swept into the dominant circulation of Yule.

III. DISCUSSION

a. Tropical cyclone merger

In order to study the interaction between two TCs, it is best to produce a diagram illustrating the motion of each TC with respect to their centroid.

In the case of Yule and TD 16W, the centroid-relative motion (Figure 3-15/16-5) indicates little interaction at first, then a period of rapid approach followed by merger at 190000Z. The common features of TC interaction noted by Lander and Holland (1993) of mutual approach followed by a period of cyclonic orbit ending in merger are present, albeit somewhat distorted from their ideal model: the centroid relative motion of Yule and TD 16W is dominated by a rapid, zonally-

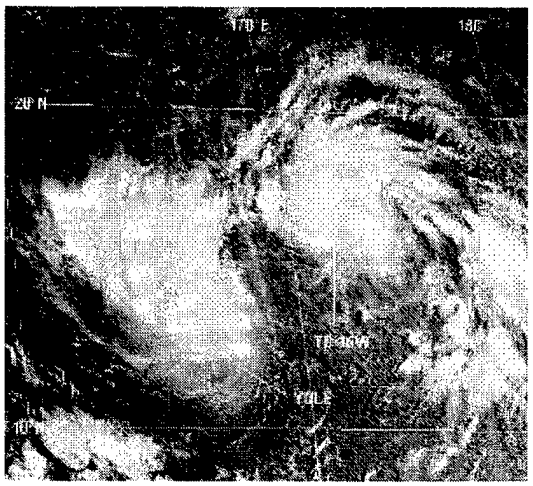

Figure 3-15/16-3 Yule and TD 16W are locked in a binary interaction that will end in merger (172133Z August visible GMS imagery).

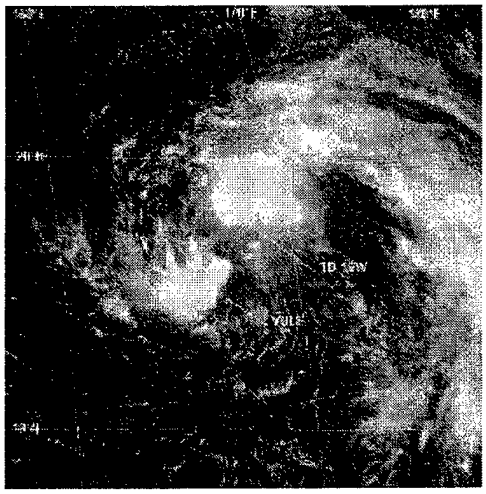

Figure 3-15/16-4 The merger of Yule and TD 16W is nearly complete (190133Z August visible GMS imagery).

oriented approach, with a curved cyclonic orbit noted only within 24 hours of merger. The location of these two TCs in a large-scale sheared flow (i.e., the monsoon trough with westerlies to its south and easterlies to its north) might lead one to expect such a departure from the idealized binary interaction of Lander and Holland. Such an effect is described by Dong and Neuman (1983).

In summary, Yule and TD 16W underwent a binary interaction ending in merger. Although satellite imagery was somewhat ambiguous, scatterometer data (Figure 3-15/16-6) clearly indicated that Yule was the dominant system during the merger and that TD 16W became horizontally sheared apart as the merger occurred.

b. The fate of a TC as it enters the midlatitudes

Establishing the defining characteristics of a TC is not a trivial exercise. For purposes of public warning, the nature of a TC has been simplified to a stratification based upon its intensity. Dvorak (1975, 1984) developed techniques for estimating the intensity of TCs from satellite imagery. The basic TC pattern types identified by Dvorak are: (1) the "shear" pattern; (2) the "curved band" pattern; the "central dense overcast" (CDO) pattern; and the "eye" pattern. These are the set of basic, or conventional, TC pattern types. At the highest taxonomic level, there are two categories of atmospheric storms of synoptic scale that possess a region of low pressure accompanied by a cyclonic wind circulation: the extratropical (ET) cyclone and the TC. Besides the basic differences of latitude of formation, the ET cyclone and the conventional TC differ in their primary source of energy and in their thermal structure. The ET cyclone derives the larger portion of its energy from potential energy present along the polar front of midlatitudes. The TC derives the bulk of its energy from the latent heat released by deep convection. The thermal structure of the ET cyclone is commonly said to be cold core, while that of the TC is said to be warm core. The term "cold core low", however, is actually an oxymoron, since lowered sea-level

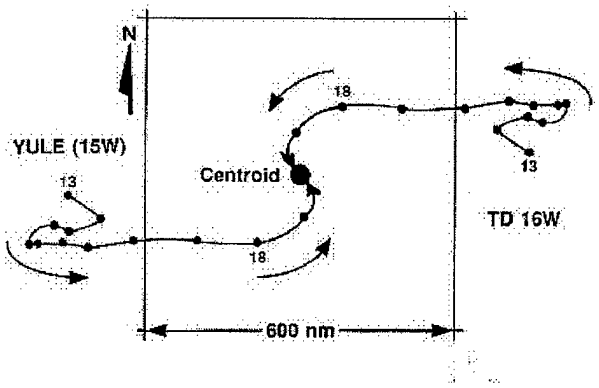

Figure 3-15/16-5 The centroid-relative motion of Yule and TD 16W. Black dots indicate positions at 12-hour intervals beginning on 130000Z August and ending at the merger location (large black dot) at 190000Z August. The square provides a length scale (as indicated) and the orientation of the cardinal directions.

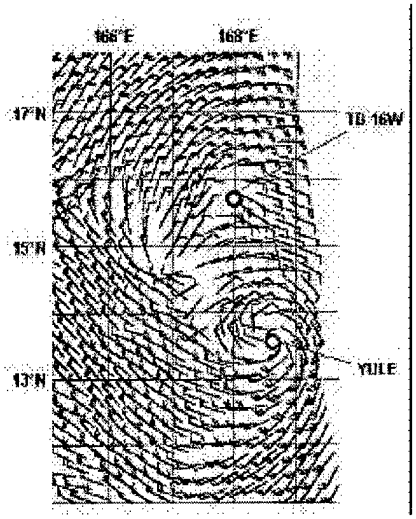

Figure 3-15/16-6 Scatterometer-derived marine surface wind speed and direction in a swath over both Yule and TD 16W (locations indicated). This scatterometer pass over these two TCs occurred approximately 12 hours prior to their merger. One can clearly see that the circulation of TD 16W is being sheared into the circulation of Yule (181131Z August ERS-2 scatterometer-derived marine surface wind vector).

pressure must, by hydrostatic considerations, be the result of an integrated density deficit in the atmospheric column above the area of lowered sea-level pressure. This density deficit is primarily the result of a warm anomaly somewhere in the atmospheric column. Therefore both the ET cyclone and the TC must possess warm cores; the true difference is in the location of the warm anomaly that results in the lowered sea-level pressure. In the mature ET cyclone, although much of the troposphere is generally colder than in the surrounding regions (hence its cold core designation), the tropopause is greatly lowered, and the stratosphere above the system is much warmer than in the surrounding regions. The lowered tropopause accompanied with the stratospheric warmth accounts for the lowered sea-level pressure in the mature ET cyclone. In the TC, the column density deficit due to higher core temperature occurs in the troposphere. In addition to tropospheric warmth above the TC low-pressure center, the TC differs from the typical ET cyclone in horizontal structure as well. The maximum winds in a mature TC are usually found very close to the center. The radius of maximum winds of even very intense TCs may be on the order of 10 km. The winds beyond the radius of maximum wind may fall off quickly. The maximum winds in an ET cyclone are usually displaced farther from the center than they are in the TC, and the highest winds are spread out across a larger area.

So far, it seems as if the differences between the ET cyclone and the conventional TC are so

great that their differential diagnosis should be simple. This, however, is not the case. There exists, in nature, types of cyclones that possess characteristics of both ET cyclones and conventional TCs. For example, the subtropical cyclone (Hebert and Poteat 1975), the arctic hurricane (Businger and Baik 1991), the monsoon depression (Ramage 1971, and JTWC 1993), and the monsoon gyre (Lander 1994, Carr and Elsberry 1994). These types of cyclones have caused confusion and forecast problems for decades. Further complicating things is the fact that transitions among the types are possible. For example, at what point does a TC entering the midlatitudes become extratropical?

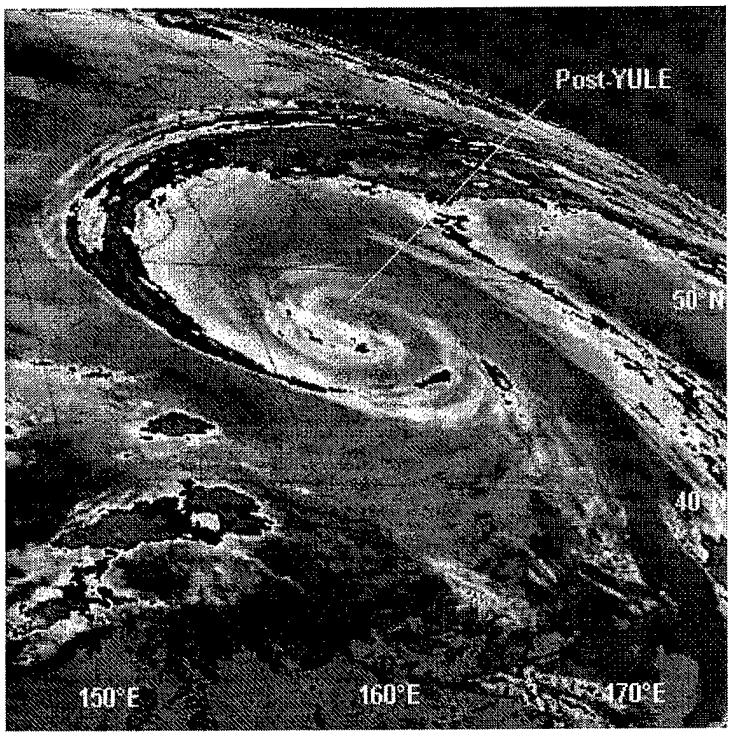

Figure 3-15/16-7 After Yule entered a baroclinic cloud band, it transformed into a vigorous extratropical low. In this enhanced infrared image, the transformed Yule is moving northwest toward the Kamchatka peninsula with maximum winds of typhoon intensity (282333Z August enhanced infrared GMS imagery). Enhancement curve is "BD" (Basic Dvorak).

In the case of Yule, it transformed into a vigorous extratropical low (Figure 3-15/16-7) after it moved into the cloud band associated with the baroclinic zone located between a midlatitude upper-level trough and a blocking high. Yule, as a transforming — or transformed — low, intensified. Maximum wind speeds increased to typhoon intensity as the system moved northwest from 45°N to 50°N. Few TCs intensify as they become extratropical, nor is the extratropical low into which they transform generally more intense than the transforming system. Some TCs dissipate when they enter the midlatitudes. According to Harr (personal communication 1997) the fate of a TC which enters the midlatitudes may be governed primarily by what type of mid-latitude flow pattern is in place when the TC arrives there. Certainly the extratropical transition of TCs is a topic requiring much study.

IV IMPACT

Prior to becoming a typhoon, and as it moved to the north-northeast, Yule passed to the east of Wake Island. Peak winds on Wake (WMO 91245) reached 45 kt (23m/sec) sustained with a gust to 58 kt (30 m/sec) from the north at 201000Z August. Damage on Wake was light with one power pole down. A few palm and ironwood trees were also downed. No buildings were damaged. High surf pushed rocks onto the road going around the east end of the main runway, forcing the road's closure.

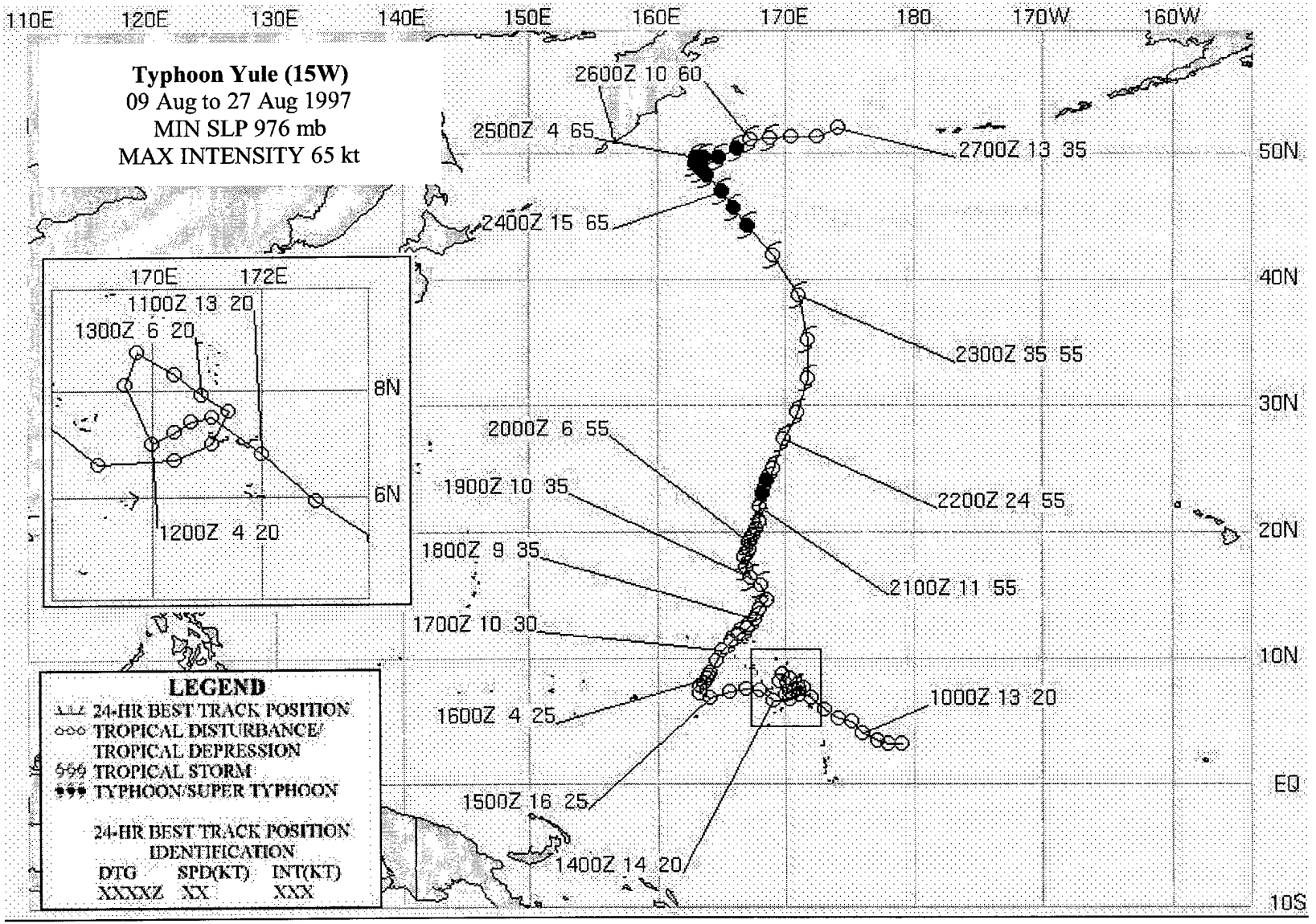
Typhoon Yule (15W)
09 Aug to 27 Aug 1997
MIN SLP 976 mb
MAX INTENSITY 65 kt
110E
120E
130E
140E
150E
160E
170E
180
170W
160W
50N
40N
30N
20N
10N
EQ
10S
2600Z 10 60
2500Z 4 65
2700Z 13 35
2400Z 15 65
2300Z 35 55
2000Z 6 55
2200Z 24 55
1900Z 10 35
1800Z 9 35
2100Z 11 55
1700Z 10 30
1000Z 13 20
1600Z 4 25
1500Z 16 25
1400Z 14 20
170E
172E
1100Z 13 20
1300Z 6 20
8N
6N
1200Z 4 20
LEGEND
24-HR BEST TRACK POSITION
TROPICAL DISTURBANCE/
TROPICAL DEPRESSION
TROPICAL STORM
TYPHOON/SUPER TYPHOON
24-HR BEST TRACK POSITION
IDENTIFICATION
DTG SPD(KT) INT(KT)
XXXXZ XX XXX

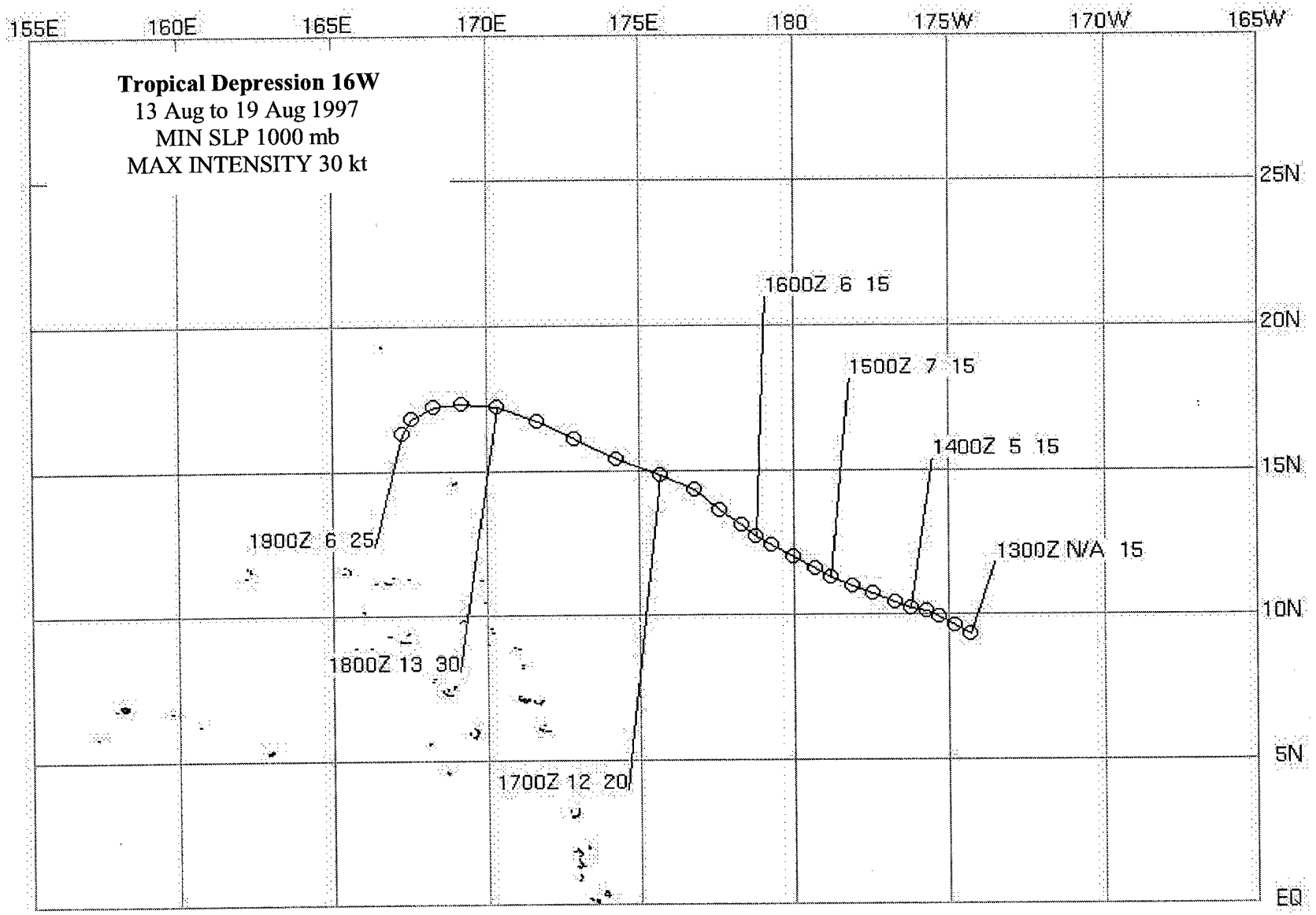
155E
160E
165E
170E
175E
180
175W
170W
165W
25N
20N
15N
10N
5N
EQ
Tropical Depression 16W
13 Aug to 19 Aug 1997
MIN SLP 1000 mb
MAX INTENSITY 30 kt
1900Z 6 25
1800Z 13 30
1700Z 12 20
1600Z 6 15
1500Z 7 15
1400Z 5 15
1300Z N/A 15

TYPHOON ZITA (17W)

Typhoon Zita (TY) (17W) was the second of four tropical cyclones, TY Victor (13W), TY Zita (17W), TY Fritz (22W), and TY Linda (30W) to develop and reach typhoon intensity in the South China Sea during 1997. Although short-lived, the system reached a peak intensity of 75 kt (39 m/sec) as it entered the Gulf of Tonkin and maintained that intensity until landfall was made over Vietnam.

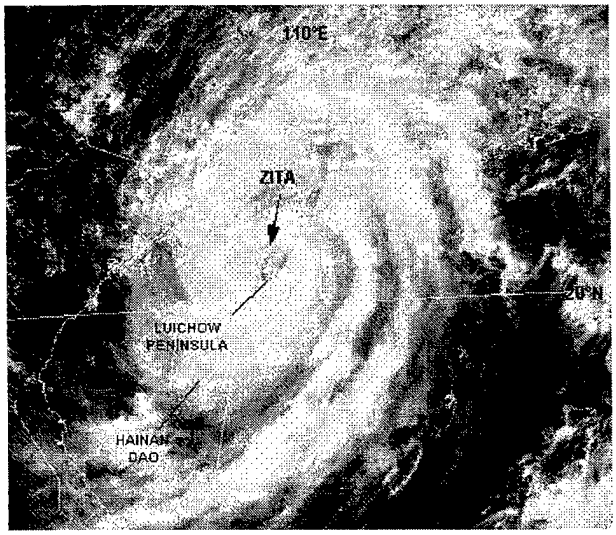

Figure 3-17-1 Zita develops a ragged eye over the Luichow Peninsula, just north of Hainan Dao At peak intensity, (220427Z August visible GMS imagery).

On 19 August, a tropical disturbance formed in the South China Sea approximately 300 nm (560 km) to the west of the Philippine island of Luzon. This disturbance was first mentioned on the 20 August Significant Tropical Weather Advisory (ABPW) after an area of deep convection had persisted for 12 hours in association with a weak low-level cyclonic circulation. As the system moved into an area of easterly environmental steering flow, convective organization improved and became more centrally located. This prompted JTWC to issue a Tropical Cyclone Formation Alert (TCFA), valid at 2030Z on 20 August. Shortly thereafter, banding features developed and JTWC issued its first warning on Tropical Storm Zita (17W) valid at 0000Z on the 21st. Zita continued tracking towards the west under the influence of easterly steering flow, equatorward of the subtropical ridge. Outflow aloft was good in all quadrants with little to no vertical wind sheer. Despite the proximity to China's southern coastline, the system reached typhoon intensity at 0000Z on the 22nd, approximately 180 nm (330 km) southwest of Hong Kong. Zita reached its peak intensity of 75 kt (39 m/sec) at 0600Z the same day over the Luichow Peninsula, just north of Hainan Dao (Figure 3-17-1). Zita maintained this intensity for 18 hours as it tracked westward through the Gulf of Tonkin. The cyclone made landfall over Vietnam on 2100Z on the 22nd and dissipated as it moved into the mountainous terrain. The final JTWC warning was issued at 0600Z on the 23rd. No reports of damage or injuries were received.

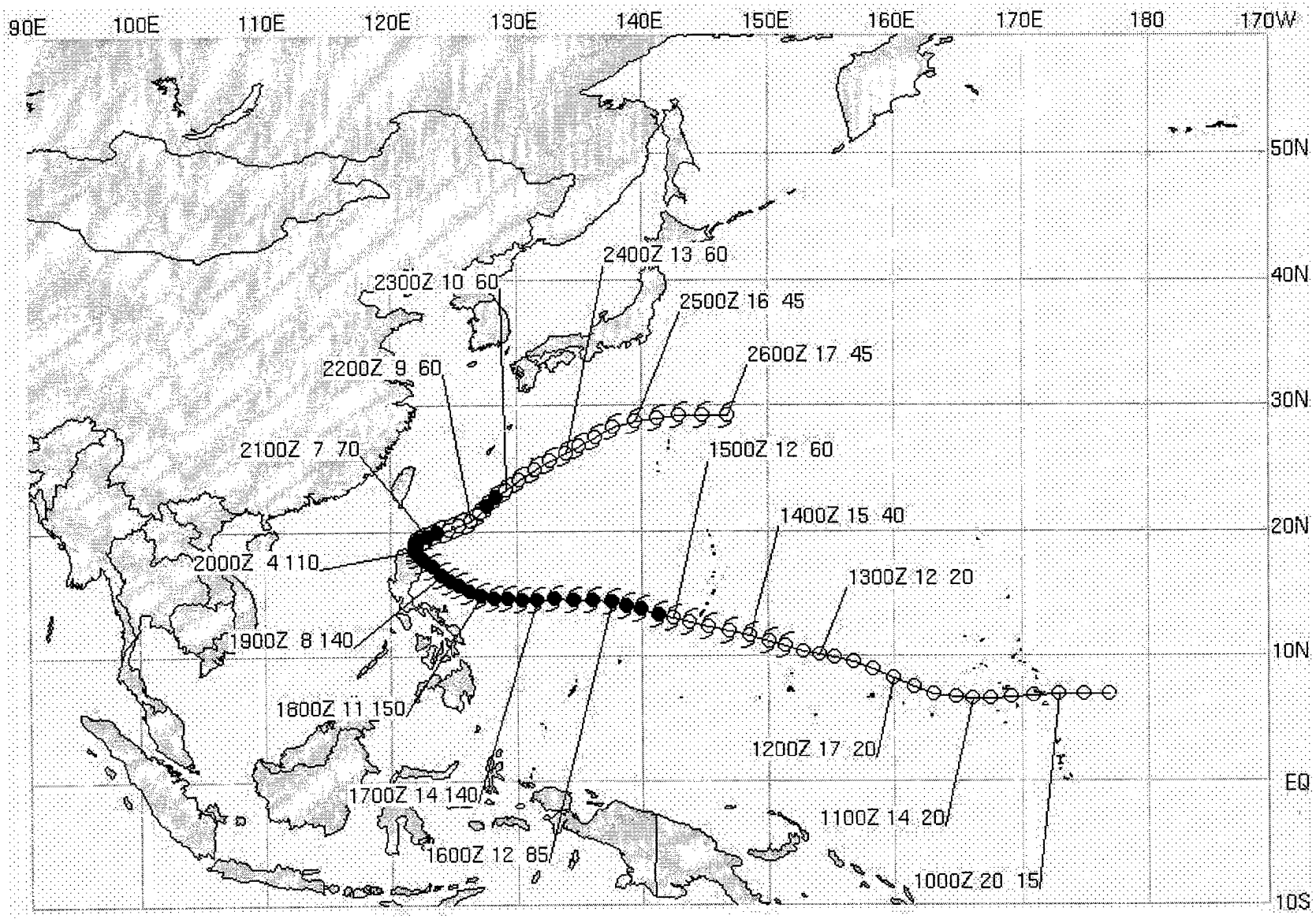
90E
100E
110E
120E
130E
140E
150E
160E
170E
180
170W
50N
40N
30N
20N
10N
EQ
10S
2400Z 13 60
2300Z 10 60
2500Z 16 45
2600Z 17 45
2200Z 9 60
2100Z 7 70
1500Z 12 60
1400Z 15 40
2000Z 4 110
1300Z 12 20
1900Z 8 140
1800Z 11 150
1200Z 17 20
1700Z 14 140
1100Z 14 20
1600Z 12 85
1000Z 20 15

TYPHOON AMBER 18W

I. HIGHLIGHTS

Typhoon Amber (18W) was the second of four tropical cyclones which would develop within the monsoon trough during an eight day period. The system would later interact with Tropical Storm (TS) Cass (20W) then move across the island of Taiwan and the Formosa Strait and into China.

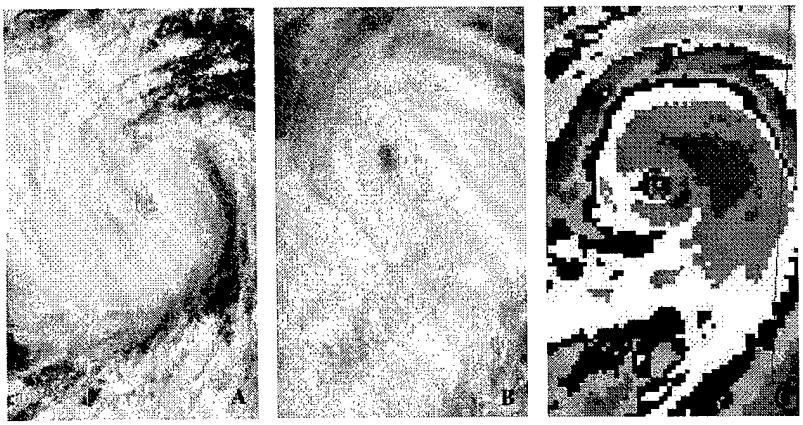

Figure 3-18-1 Typhoon Amber as seen by visible and infrared satellite imagery over a 36 hour period beginning 26 August at 0633Z. The valid times of the images are: far left 260633Z; middle and far right 242224Z. Note the banding type eye feature in the image at far left has developed into a more circular eye feature (better defined in the infrared imagery).

II. TRACK AND INTENSITY

By the 20th of August, the monsoon trough extended from southeastern Asia into the South China Sea, eastward through the Luzon strait, across the southern Mariana Islands and east-northeastward to Wake Island (where Typhoon Yule was approaching from the south-southwest). The monsoon trough was very active. Four different tropical cyclones would form during the next eight days: Typhoon Zita (17W) and TS Cass (20W), which formed in the South China Sea; Super Typhoon Bing (19W) which developed east of the Mariana Islands; and finally Typhoon Amber (18W) which began in the Philippine Sea. The pre-Amber (18W) disturbance developed in a region of upper-level divergence overlying the surface trough. It was first mentioned on the Significant Tropical Weather Advisory (ABPW) on 20

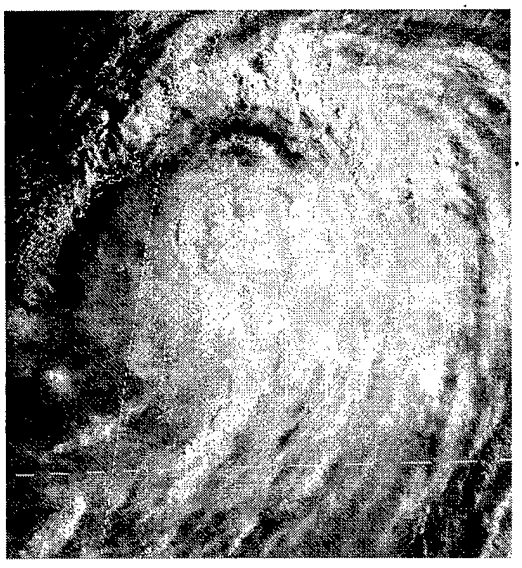

Figure 3-18-2 Visible imagery valid at 282227Z.

August. A scatterometer pass at 1340Z indicated at least 20 to 25 kt (10 to 13 m/s) of sustained wind. A Tropical Cyclone Formation Alert (TCFA) was issued at 0300Z on 21 August followed by a warning at 0600Z, prompted by a ship report of 40 kt (20 m/s).

Amber remained in deep monsoonal flow with the subtropical ridge to the north and ridging associated with Typhoon Zita (17W) to the west-southwest. This ridging allowed only a slow west-northwest motion ranging from 3 to 5 kt (6 to 9 km/hr), lower than what is normally associated with a tropical cyclone south of the sub-tropical ridge. This motion continued until 26 August when Tropical Storm Cass (20W) formed west-southwest of Typhoon Amber, close enough for direct interaction to occur. By 28 August, the effect of Tropical Storm Cass' circulation was to cause Amber's forward speed to increase to near 8 to 10 kt (15 - 19 km/hr) with a more northwestward motion. This motion continued as Amber moved across Taiwan and then China on 29 August.

Typhoon Amber (18W) intensified at a slightly faster than the climatological (one Dvorak 'T' number per day) rate. On 23 August at 0633Z, the intensity was estimated at 70 kt (35 m/s), based on visible satellite imagery which showed the development of a banding type eye. This eye became better defined in visible and infrared imagery on 24 August at 2246Z, when the intensity was 100 kt (50 m/s) (see figure 1). The system subsequently weakened to 85 kt (43 m/s) for a short time, but re-intensified to 110 kt (55 m/s) by the morning of 28 August as it began to approach Taiwan. Reports from the island indicated northeast winds of 75 kt (38 m/s) and a surface pressure of 992 mb at 0300Z 28 August; 6 hours later the pressure had dropped to 984 mb with north winds of 45 kt (23 m/s). By the morning of 29 August, Typhoon Amber began to move across Taiwan with an intensity of 95 kt (figure 3-18-2) maintaining typhoon intensity as it crossed the island's central mountains, some of which range from 8500 to 13000 feet (2600 to 4000 m). Land interaction weakened Typhoon Amber as it crossed into the Formosa Strait with an intensity of 80 kt (40 m/s). The system subsequently made landfall in China with an intensity of 65 kt (33 m/s).

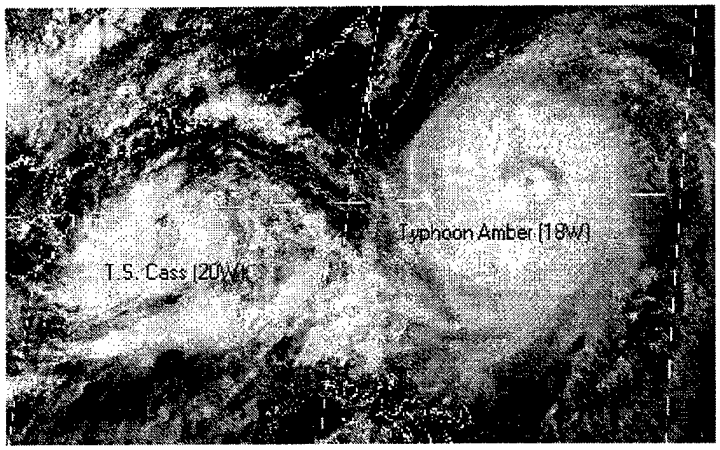

Figure 3-18-3 Visible satellite image (valid time, 27 August 0733Z) of Tropical Storm Cass and Typhoon Amber over the South China and Philippine Seas.

III. DISCUSSION

a) The formation of concentric eyes during intensification

Satellite imagery over a 48-hour period beginning from 25 through 27 August indicated that Typhoon Amber developed concentric eyes, a feature typically found only in intense tropical cyclones. The process starts when banding begins to wrap around the established central convective feature. An outer eye wall begins to form and dominates the inflow of moisture flowing towards the center, while

the inner eye wall begins to contract and may eventually dissipate. Refer to Figure 3-18-4. The image at top left shows a solid area of convection surrounding a cloud filled eye with a banding feature stretching from west to south of the center. The image at top right, which was taken about a day later. shows an area free of convection (known as the "moat" region) developing between the eyewall and the outer banding feature. The banding feature is closer to the eyewall and is wrapping around the center. The image at bottom left is 19 hours later and clearly shows a banding type structure. Microwave imagery 10 hours earlier indicated the presence of an eye; therefore cloud cover is probably obscuring it in this image. The image at bottom right shows fully developed concentric eyes with a moat in between. About 9 hours after the last image, Typhoon Amber reached a peak intensity of 110 kt (55 m/s). The concentric eye feature became less apparent in subsequent satellite imagery as Amber approached Taiwan.

b) Interaction With TS Cass, and Numerical Model Track Performance

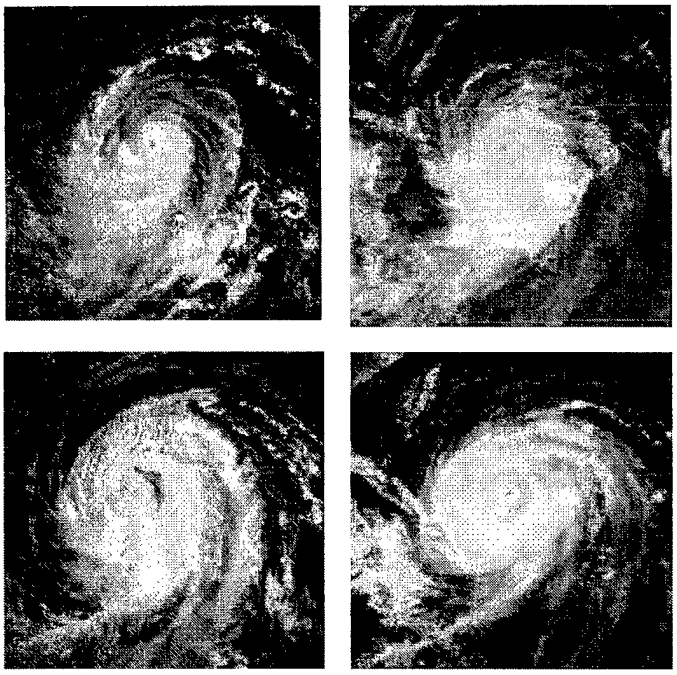

Figure 3-18-4 Development of concentric eye walls in Typhoon Amber during a 53 hour period beginning 242226Z August, as seen in visible satellite imagery. Valid times of satellite images are: top left, 242226Z; top right, 260334Z; bottom left, 262226Z; bottom right 270334Z. Peak intensity occurred shortly after concentric eye wall formation.

While Typhoon Amber was transiting the Philippine Sea, TS Cass formed in the South China Sea approximately 700 nm (1300 km) to the west-southwest. The distance between these tropical cyclone, as shown in Figure 3-18-3, was close enough for direct interaction to occur (Carr and Elsberry, 1994). However, due to the smaller size and lesser organization of TS Cass, Typhoon Amber's track was only slightly more northwestward and faster than would otherwise be expected. The direct interaction was primarily one way as Typhoon Amber significantly altered the motion track of TS Cass. Although TS Cass had only a small effect on the actual motion of Typhoon Amber, it did complicate the forecasting process, because the models tended to exaggerate the extent of interaction Figures 3-18-5, 3-18-6 and 3-18-7 show the track reconstruction of Typhoon Amber along with the forecasted tracks from the NOGAPS, GFDN and FBAM models. Each model showed a poleward bias (as they normally do) early on, then switched to an equatorward bias as Typhoon Amber was just northeast of the island of Luzon.

IV. IMPACT

No reports were received by the JTWC on damage, injuries or fatalities due to Typhoon Amber.

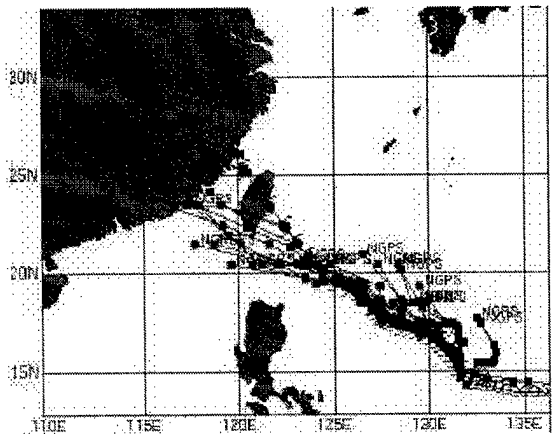

Figure 3-18-5 The best track and the NGPS forecast tracks for Amber (18W).

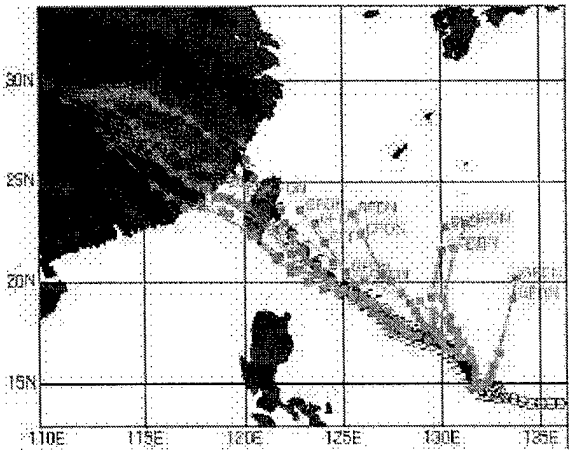

Figure 3-18-6 The best track and the GFDN forecast tracks for Amber (18W).

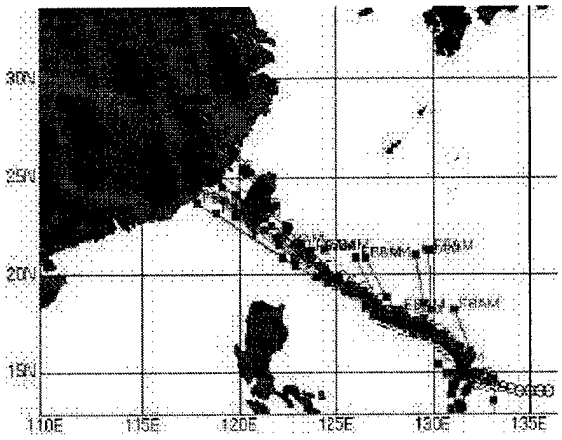

Figure 3-18-7 The best track and the FBAM forecast tracks for Amber (18W).

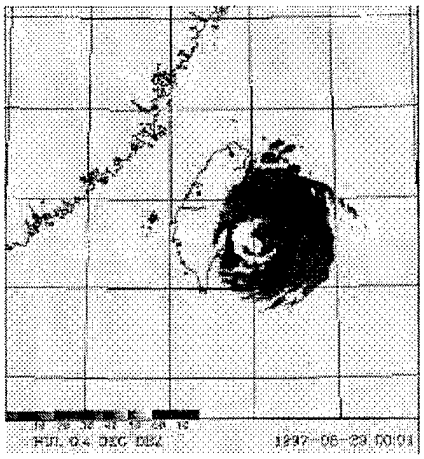

Figure 3-18-8 Radar image of Typhoon Amber as it is approaching Taiwan. Valid time is 290001Z

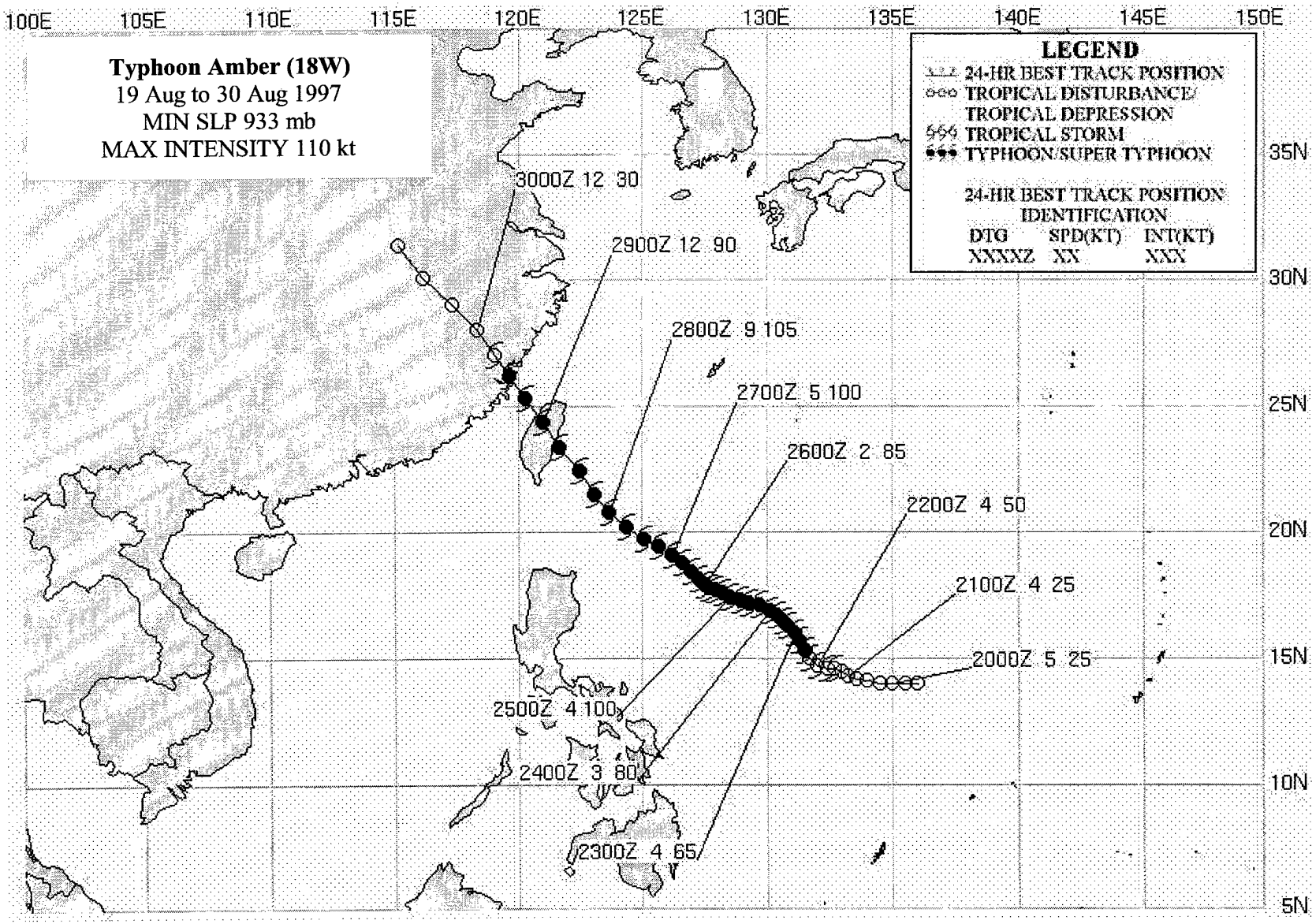
Typhoon Amber (18W)
19 Aug to 30 Aug 1997
MIN SLP 933 mb
MAX INTENSITY 110 kt
LEGEND
24-HR BEST TRACK POSITION
TROPICAL DISTURBANCE/ TROPICAL DEPRESSION
TROPICAL STORM
TYPHOON/SUPER TYPHOON
24-HR BEST TRACK POSITION IDENTIFICATION
DTG SPD(KT) INT(KT)
XXXXZ XX XXX
100E
105E
110E
115E
120E
125E
130E
135E
140E
145E
150E
35N
30N
25N
20N
15N
10N
5N
3000Z 12 30
2900Z 12 90
2800Z 9 105
2700Z 5 100
2600Z 2 85
2200Z 4 50
2100Z 4 25
2000Z 5 25
2500Z 4 100
2400Z 3 80
2300Z 4 65

SUPER TYPHOON BING (19W)

I. HIGHLIGHTS

Super Typhoon Bing (STY) (19W) was the third of four tropical cyclones that would form within the monsoon trough during a period of eight days. It produced heavy rainfall while tracking near Guam as a tropical storm on 29 August. Rapid intensification began as Bing moved west of Guam, and two days later it became the fifth super typhoon of the 1997 season.

II. TRACK AND INTENSITY

By 26 August, the monsoon trough extended from the South China Sea to north of the Philippine Islands, through the central Mariana and Marshall Islands to the dateline. Low level westerly winds were observed all the way to 177E. During a normal year, the monsoon trough usually does not extend past 160E. The observed eastward extension was most likely an effect of El Niño.

The disturbance that became STY Bing (19W) started in the eastward extension of the monsoon trough near the Marshall Islands. The disturbance formed to the south-southeast of a large scale upper level anticyclone. Vigorous convection associated with the disturbance was enhanced by strongly divergent upper level wind flow. At 2330Z on 25 August, the Significant Tropical Weather Advisory (ABPW) was re-issued to add the disturbance as a suspect area. However, the convection (see Figure 3-19-1) quickly organized and a Tropical Cyclone Formation Alert (TCFA) was issued only eight hours later. At 0600Z on the 24th, the disturbance was upgraded to a Tropical Depression (TD).

The newly formed TD 19W tracked westward at speeds of 13 to 15 kt (24 to 28 km/hr). This was due to strong low to mid-level easterly steering flow south of the subtropical ridge. This westward track continued as it passed near Guam and Rota on 29 August. Fortunately for the islands, only slow intensification took place as it approached. At 1800Z on the 28th, Bing was upgraded to tropical storm intensity, but had an intensity of only 40 kt (21 m/sec) during its passage through the Marianas (Figure 3-19-2). Shortly after passing the Marianas, the system underwent a period of rapid intensification, beginning about 1200Z on 30 August and ending 54 hours later with a peak intensity of 135 kt (69 m/sec). Figure 3-19-3 shows visual satellite imagery which illustrates how quickly the central cloud structure changed in little more than a day. The satellite image at left shows Bing as a 80 kt (41 m/sec) typhoon with a developing eye, while the image at right, when Bing's intensity was near 130 kt (67 m/sec), shows a smooth eyewall with a very well defined eye. This represented a change of approximately two Dvorak "T" numbers. During the intensification process, mid-level ridging began to build to the east-southeast of the tropical cyclone causing the steering flow to gradually shift from an easterly to south-southeasterly. At approximately the same time, mid-latitude disturbances moving down the east side of a large mid-level ridge over eastern Asia were acting to weaken the mid level subtropical ridge structure north of the tropical cyclone. Both factors were significant in causing Bing's forward motion to slow as a turn to the north developed on 30 August. On 31 August, the

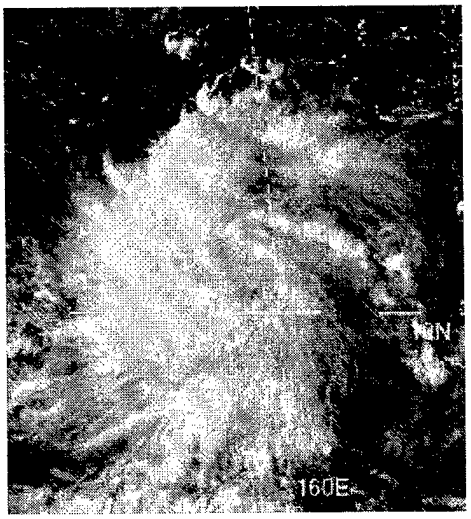

Figure 3-19-1 Visible satellite imagery of the tropical disturbance that became Bing. Valid time of imagery is 260533Z.

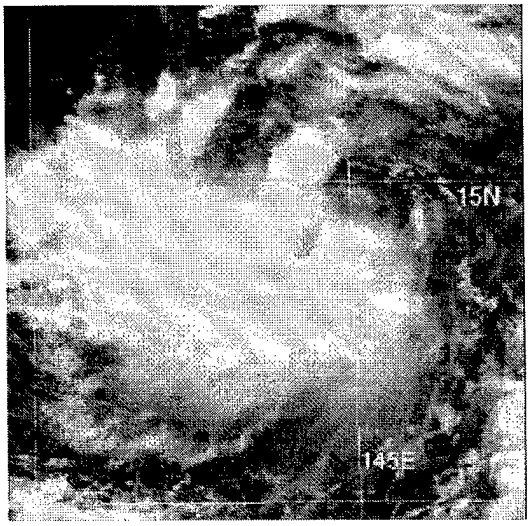

Figure 3-19-2 Visible satellite imagery of Tropical Storm Bing (19W) as it passed through the Rota Channel on 290333Z August.

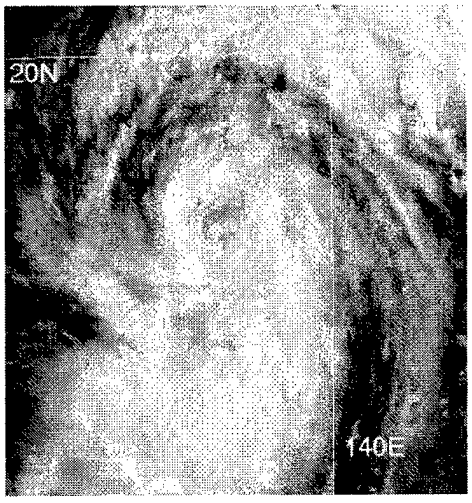

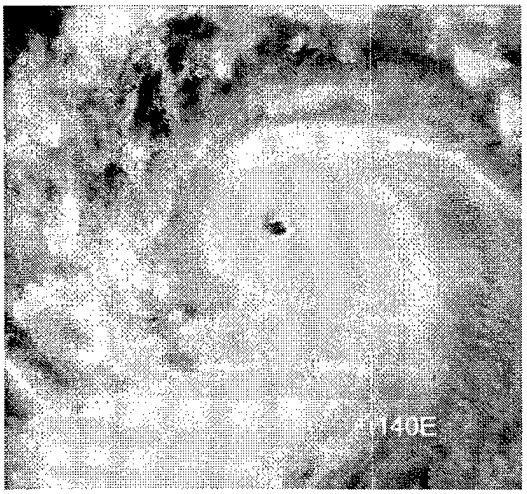

Figure 3-19-3 Visual Satellite imagery of Super Typhoon Bing (19W) during rapid intensification. The valid time of the left image is 302330Z August and the intensity was 80 kt (41 m/sec). The valid time of the right image is 010334Z September and the intensity was near 130 kt (67 m/sec).

cyclone began following a northward oriented track with speeds between 11 and 13 kt (20 to 24 km/hr), thus completing the transition from a Standard (S) to a Poleward Oriented (PO) synoptic pattern as described by the systematic and integrated approach of Carr and Elsberry (1994). As the cyclone continued north, it passed west of the islands of Iwo Jima and Chi Chi Jima on 01 and 02 September, respectively. During the closest point of approach, each island reported sustained winds of 30 kt (15 m/sec) with peak gusts ranging from 52 kt (26 m/sec), at Iwo Jima, to 40 kt (21 m/sec), at Chi Chi Jima. By 02 September, STY Bing was located south of the Japanese island of Honshu. Although the system was beginning to weaken, it remained a threat to Honshu. However, a shift in the sub-tropical ridge over Honshu enabled a band of relatively strong westerly winds to develop across the Japanese islands, causing the steering flow to become more westerly. Bing's track shifted to the northeast, and Honshu was spared.

By 03 September, Bing had moved far enough northward that it began to merge with a strong mid- and upper-level westerly wind flow. Accordingly, Bing turned towards the east-northeast and accelerated to speeds above 30 kt (15 m/sec) by 04 September. By 1000Z on the 4th, Special Sensor Microwave/Imager (SSM/I) indicated that upper-level westerly winds had sheared the system's convection and left the low-level circulation center exposed. Figure 3-19-4 shows Bing on 05 September. Although there was no longer central convection, it remained a potent extratropical cyclone with maximum sustained winds estimated to be 55 kt (28 m/sec).

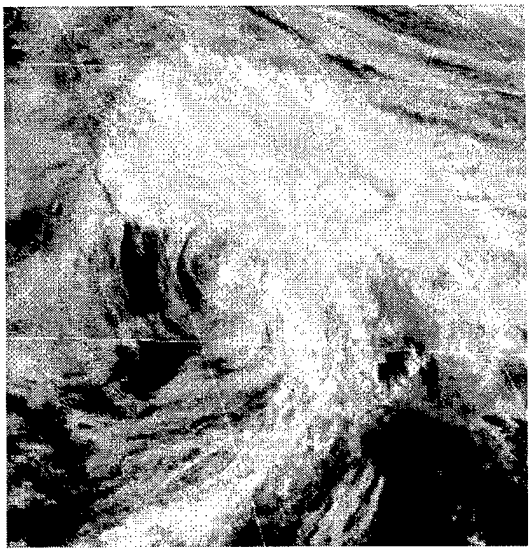

Figure 3-19-4 Visible satellite imagery of Super Typhoon Bing (19W) as a potent extratropical system with maximum sustained winds estimated to be 55 kt (28 m/sec). Valid time of image is 042227Z September.

III. DISCUSSION

a) Heavy Rainfall over Guam

Although STY Bing (19W) was a minimal tropical storm as it passed through the Rota channel, just north of Guam, it did bring a lot of rain. The National Weather Service Office at Tiyan reported 5.19 inches (13.2 cm) as Bing passed on 29 August. Andersen Air Force Base reported 6.17 inches (15.7 cm) of rain during a 36 hour period beginning at 0900Z on 28 August. The soil on the island was already saturated from repeated rainfall during the month, and the additional rain resulted in flooding of low-lying areas and around small streams. The excessive rainfall triggered a landslide in the village of Santa Rita on 30 August that caused extensive local damage. August 1997 turned out to be the wettest month in Guam's history as the final rainfall total reached 39.5 inches (100 cm). This was partially due to the monsoon trough being positioned over the southern and central Mariana Islands, allowing numerous tropical disturbances to track close to the island.

b) The Formation of Concentric Eye Walls

After Bing reached its peak intensity of 135 kt (69 m/sec), satellite and microwave imagery indicated the development of concentric eyewalls. Figure 3-19-5 shows the development over a 48 hour period. The image at the left shows Bing at peak intensity with a very small eye and intense convection in the eyewall. The middle image is about 24 hours later, when the cyclone had an intensity of 110 kt (56 m/sec). The central convection has diminished although a small eye feature is still discernable. However, convection in the outer bands has started to increase and wrap around the center. The image at right shows a newly formed, very large outer eye measuring approximately 90 nm (167 km) in diameter. The inner eye has almost disappeared with only a very small area of central convection remaining. At this point, the intensity has weakened to 85 kt (44 m/sec). This eyewall cycling process was very similar to that which occurred in STY Winnie (14W), TY Amber (18W) and STY Paka (05C) during the 1997 Western Pacific season.

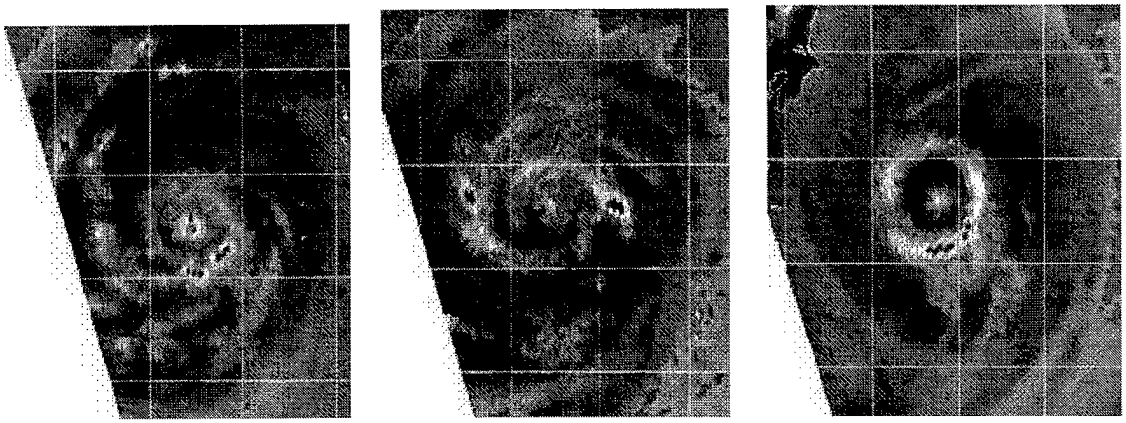

Figure 3-19-5 The development of concentric eye walls in Super Typhoon Bing (19W) as seen by SSM/I. From left to right, the valid times are 001011Z, 021205Z, and 030946Z September.

c) A comparison between two objective aids in forecasting Super Typhoon Bing's (19W) motion track

Many objective aids (forecast models) are used by the Typhoon Duty Officer (TDO) in determining the track forecast of a tropical cyclone. In order to produce the best forecast product possible, TDOs are thoroughly trained in the weaknesses and strengths of the various objective aids under certain synoptic conditions. Some examples of these strengths and weaknesses can be seen in an analysis of Bing's track. An example is the Colorado State University Model (CSUM), which is a statistical-dynamical model based on the work of Matsumoto (1984). The model is further discussed in Chapter 5, section 2.3.2. Because CSUM uses statistically developed regression equations, it has a problem predicting future changes in the synoptic environment which could alter the tropical cyclone's motion. This is illustrated in Figure 3-19-6. Although a distinct poleward bias can be seen, CSUM does a reasonable job of predicting the future track as long as the system remains south of the subtropical ridge. For example, during a 24-hour period beginning at 0000Z on the 28th, CSUM's 72-hour forecast errors averaged about

1.5 times lower than the Naval Oceanographic Global Atmospheric Prediction System (NOGAPS), a purely dynamical model. However, one to two days prior to the development of a poleward/poleward oriented pattern, CSUM continues to indicate westward motion. Westward forecasts continue until the model determines that the tropical cyclone is on the subtropical ridge axis, which is itself triggered by a northward (330 to 029 degrees) motion vector. Once the northward motion has been detected, CSUM begins to forecast northward motion. Bing's track was predominately northward by 1800Z on 30 August.

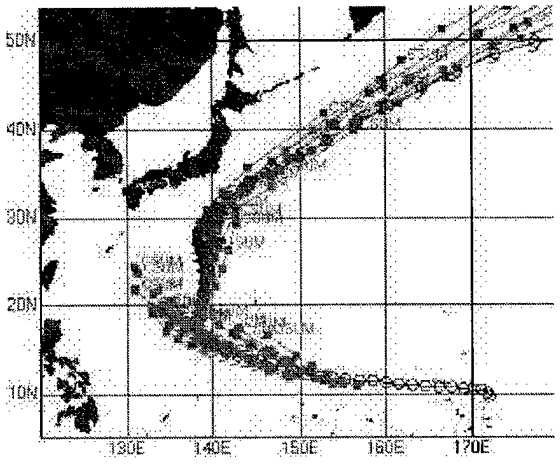

Figure 3-19-6 Forecast tracks given by CSUM for Super Typhoon Bing (19W).

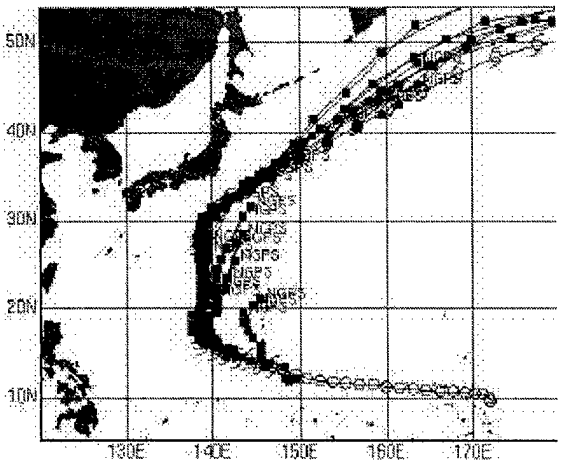

Figure 3-19-7: Forecast tracks given by NOGAPS for Super Typhoon Bing (19W).

On the other hand, NOGAPS is known to do fairly well when compared to other models in transitioning from a Standard/Dominant Ridge (S/DR) to a Poleward/Poleward Oriented (P/PO) environment. One documented bias of NOGAPS is to indicate northward motion for a TC a few days before it actually occurs. In the case of Super Typhoon Bing (19W), this is illustrated by Figure 3-19-7. Both NOGAPS and CSUM had a tendency to be right of the forecast track during the northward motion portion of the track. However, during the 54-hour period beginning at 0000Z on 31 August during which northward motion was prevalent, NOGAPS errors were about 2.3 times lower than CSUM. The tendency of NOGAPS to surpass CSUM in this synoptic regime has also been documented. These and other model tendencies are known by the TDOs, greatly enhancing their ability to choose among a plethora of aids during forecast development.

IV. IMPACT

The main impact on the island of Guam was heavy rainfall and associated flooding. The previously mentioned landslide in Santa Rita caused extensive damage to the Namo Falls Tourist Park, as well as some broken sewage pipes, which allowed open sewage to flow into the Namo River. However, there were no reports of injuries. There were no reports of injuries or damage from the islands of Iwo and Chi Chi Jima.

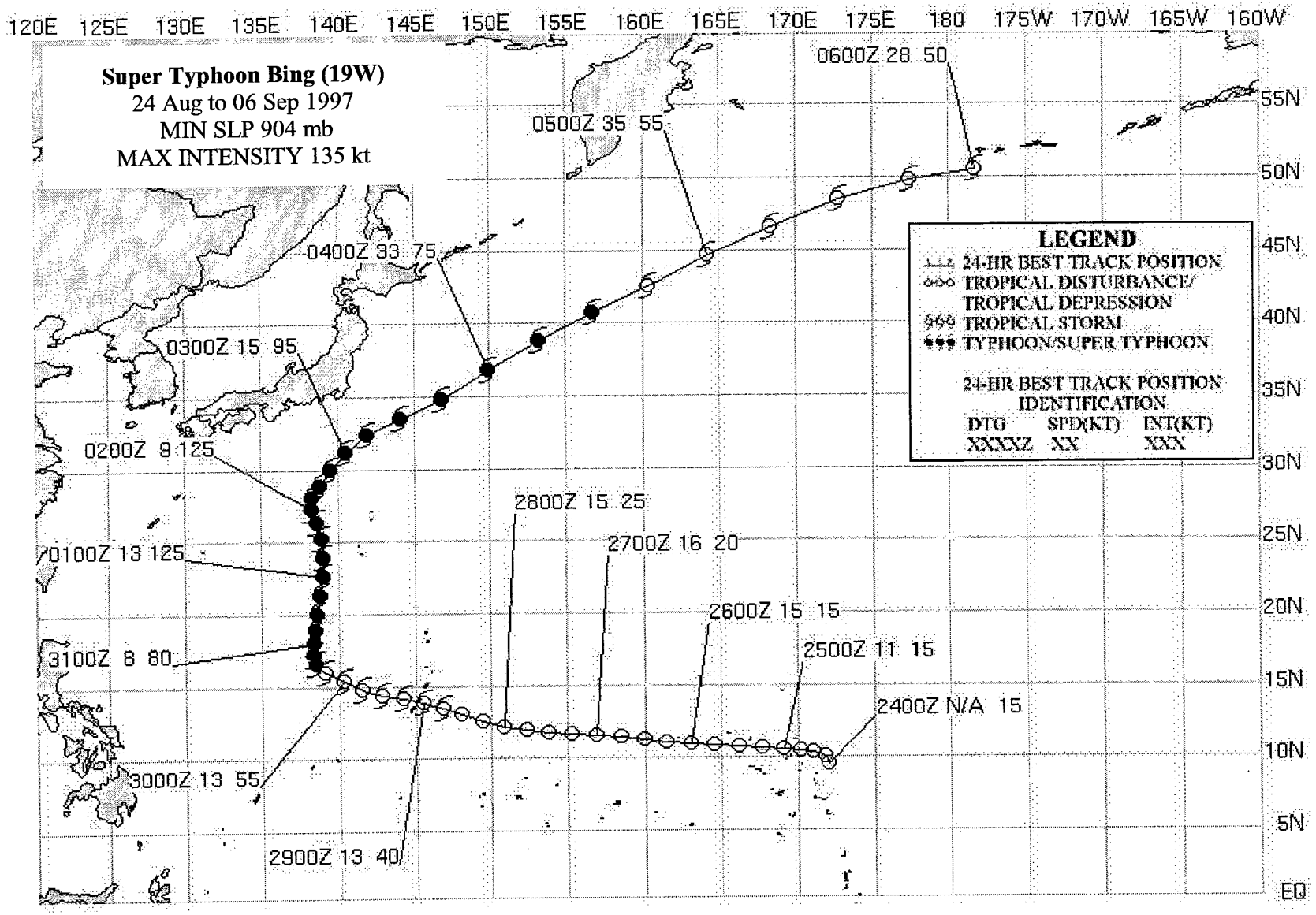
Super Typhoon Bing (19W)
24 Aug to 06 Sep 1997
MIN SLP 904 mb
MAX INTENSITY 135 kt
120E 125E 130E 135E 140E 145E 150E 155E 160E 165E 170E 175E 180 175W 170W 165W 160W
55N 50N 45N 40N 35N 30N 25N 20N 15N 10N 5N EQ
0600Z 28 50
0500Z 35 55
0400Z 33 75
0300Z 15 95
0200Z 9 125
0100Z 13 125
3100Z 8 80
3000Z 13 55
2900Z 13 40
2800Z 15 25
2700Z 16 20
2600Z 15 15
2500Z 11 15
2400Z N/A 15
LEGEND
24-HR BEST TRACK POSITION
TROPICAL DISTURBANCE/ TROPICAL DEPRESSION
TROPICAL STORM
TYPHOON/SUPER TYPHOON
24-HR BEST TRACK POSITION IDENTIFICATION
DTG SPD(KT) INT(KT)
XXXXZ XX XXX

TROPICAL STORM CASS (20W)

On 26 August, an area of convection developed approximately 160 nm (297 km) to the south of Hong Kong, due east of Hainan Dao, in the South China Sea. Over a 24-hour period, this area became considerably more organized and at 1830Z on the 27th, a Tropical Cyclone Formation Alert (TCFA) was issued. An exposed low-level circulation was evident with convection developing near the center. However, development was inhibited by outflow from Typhoon Amber (18W), which was approximately 600 nm (1100 km) to the east. At 0000Z on the 28th, a warning was issued for Tropical Depression (TD) 20W with an intensity of 30 kt (16 m/sec). The system tracked very slowly towards the east as it continued to intensify, primarily due to a direct interaction with the steering flow from Amber. The cyclone became Tropical Storm Cass (20W) at 0000Z on 29 August as inhibiting effects from Amber lessened. At this point, Cass turned toward the northeast and increased its forward speed slightly. On 29 August, Cass turned northward, as effects from Amber diminished and the steering flow became south-southwesterly. Outflow from Amber continued to inhibit full development of Cass, which peaked at 45 kt (23 m/sec) on 29 August at 1200Z. Cass maintained this intensity for 12 hours. On 30 August, Cass made landfall near Xinglin, China. The 0600Z synoptic reports from surrounding areas indicated winds of 35 kt (18 m/sec) in the immediate coastal area. At 1200Z the same day, the final tropical cyclone warning was issued by JTWC as the system tracked north-northwestward and dissipated in the mountains of southeastern China.

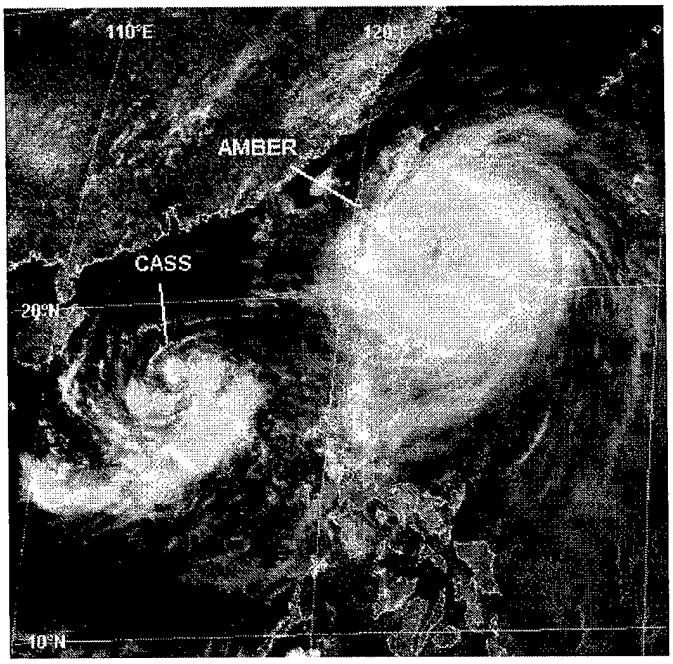

Figure 3-20-1 Tropical Storm Cass (20W) during its TD stage as it interacts with Typhoon Amber (18W) (280333Z August visible GMS imagery).

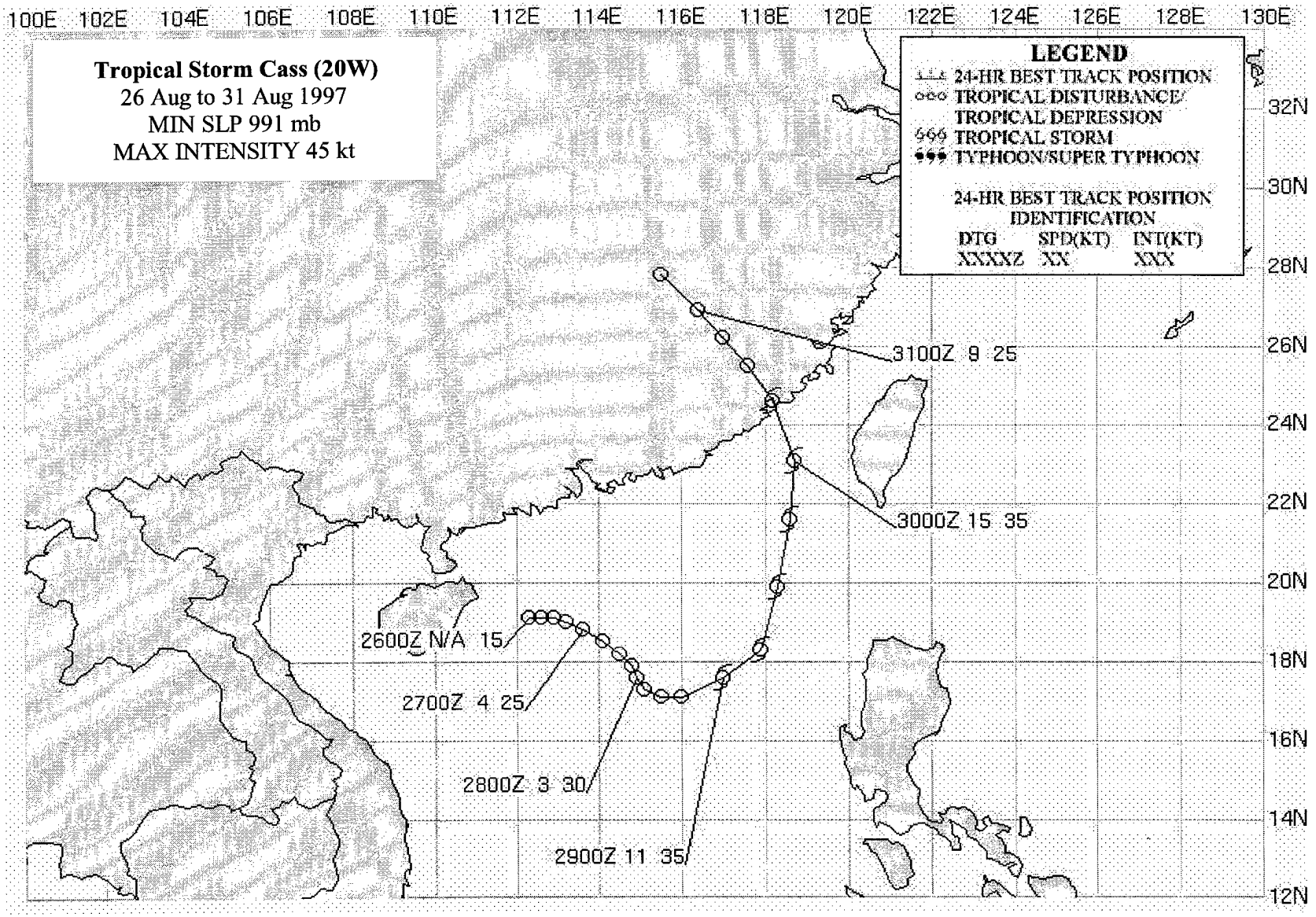
Tropical Storm Cass (20W)
26 Aug to 31 Aug 1997
MIN SLP 991 mb
MAX INTENSITY 45 kt
LEGEND
24-HR BEST TRACK POSITION
TROPICAL DISTURBANCE/
TROPICAL DEPRESSION
TROPICAL STORM
TYPHOON/SUPER TYPHOON
24-HR BEST TRACK POSITION
IDENTIFICATION
DTG SPD(KT) INT(KT)
XXXXZ XX XXX
3100Z 9 25
3000Z 15 35
2600Z N/A 15
2700Z 4 25
2800Z 3 30
2900Z 11 35
100E
102E
104E
106E
108E
110E
112E
114E
116E
118E
120E
122E
124E
126E
128E
130E
32N
30N
28N
26N
24N
22N
20N
18N
16N
14N
12N

SUPER TYPHOON OLIWA (02C)

I. HIGHLIGHTS

The sixth of eleven tropical cyclones (TCs) to attain super typhoon intensity in the western North Pacific (WPN) during 1997, Oliwa formed east of the international dateline (IDL) and to the southwest of the Hawaiian Islands. After becoming a tropical storm in the Central Pacific Hurricane Center (CPHC) area of responsibility (AOR), this TC was named Oliwa. Oliwa moved on a long straight running track which brought it across the IDL into the WPN, and eventually to landfall in southwestern Japan. As it moved westward from its region of formation in an eastward displaced monsoon trough and into the WNP basin (which was unusually cloud free for the time of year), the intensity forecasts for Oliwa were nearly all too low. Early in its life, Oliwa was accompanied by a weak, unnamed Southern Hemisphere twin. While near its peak intensity, a possible eye-wall meso vortex was revealed by visible satellite imagery. After its peak, well-defined concentric eye wall clouds were observed, which were especially distinct in microwave imagery.

II. TRACK AND INTENSITY

During late August, low-level monsoon westerlies extended across the IDL and stretched eastward at low latitudes to the southwest of Hawaii. At the end of August, a tropical disturbance formed southwest of Hawaii at the eastern end of the monsoon trough associated with these eastward-displaced low-latitude westerlies. This disturbance moved slowly westward and intensified. On 02 September, while it was still east of the IDL, the CPHC (located in Honolulu, Hawaii) upgraded it to Tropical Depression (TD) 02C. After becoming a tropical storm in CPHC's AOR at 030000Z September, TD 02C was named Oliwa (Hawaiian for "Oliver", the letter "w" in Oliwa is pronounced as a "v" in this case). On 04 September, Oliwa crossed the IDL and entered the JTWC AOR. The first warning issued by JTWC was valid at 040600Z September.

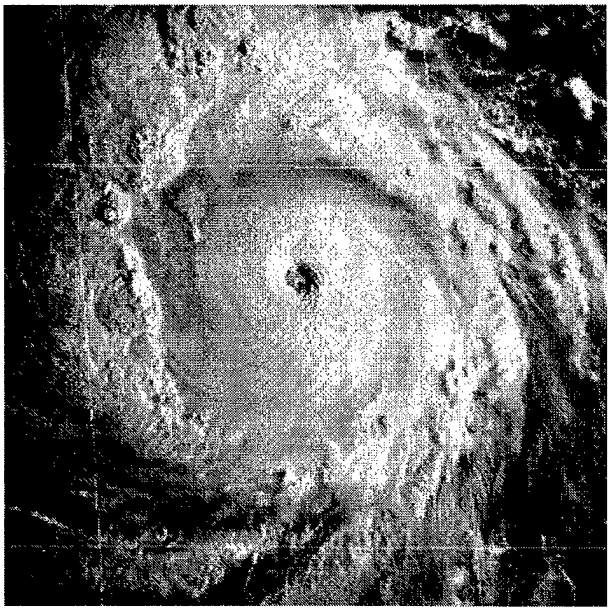

3-02C-1 The low-angle morning sun nicely highlights the features of the cloud tops of Oliwa's eye wall cloud and peripheral rainbands as the typhoon reached its peak of 140 kt (72 m/sec) (092034Z September visible GMS imagery).

After crossing the IDL into the WNP basin, Oliwa moved on a steady west-northwestward track and intensified. At first, the rate of intensification was slow; during the 72-hr period from 0600Z on 04 September to 0600Z on 07 September, Oliwa's intensity increased from 35 kt (18 m/sec) to only 50 kt (26 m/sec). After another 30 hours (by 1200Z on the 8th), its intensity had slowly climbed to that of a minimum typhoon (65 kt or 33 m/sec). Between 1800Z on the 08th and 1800Z on the 09th, Oliwa explosively deepened as its intensity climbed from 75kt (39 m/sec) to its peak of 140 kt (72 m/sec), as shown in Figure 3-02C-1. The 24- hour pressure drop associated with this wind-speed increase was 69 mb (see the discussion below for more details on Oliwa's explosive deepening).

For five days after reaching peak intensity, Oliwa continued its steady motion toward the west-northwest and slowly weakened. On 14 September, the typhoon passed to the northeast of Okinawa where it slowed, and on 15 September, it reached its point of recurvature and turned northeastward toward Kyushu. Early on the morning of 16 September, Oliwa made landfall on the coast of southern Kyushu, where despite having weakened considerably (down to 70 kt - 36 m/sec), it was responsible for loss of life and considerable damage (see the Impacts Section). After landfall, the typhoon moved across Japan and weakened. By the morning of 17 September, it had moved to the Sea of Japan where it dissipated. The final JTWC warning was issued at 170600Z.

III. DISCUSSION

a. Oliwa's Digital Dvorak (DD) time series: a case of explosive deepening

Oliwa was one of several typhoons during 1997 for which a time series of its hourly DD numbers (Figure 3-02C-2) was calculated. Oliwa's DD numbers are in overall agreement with the best-track intensity. The rate of intensification (a drop in the sea level pressure of 69 mb in 24 hours for an average of 2.9 mb/hr), as indicated by both the DD time series and the best-track intensities during the 24-hour period from 1800Z on 08 September to 1800Z on 09 September, qualifies as a case of explosive deepening (a drop of minimum sea level pressure of 2.5 mb/hr for at least 12 hours (Dunnavan 1981)). Many typhoons which reach high peak intensities (i.e., more than 100 kt (51 m/sec)) undergo a period of rapid or explosive deepening which tends to commence when the TC reaches minimal typhoon intensity.

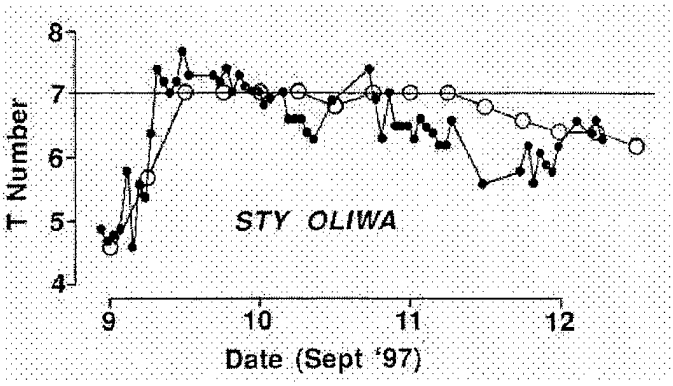

Figure 3-02C-2 A time series of Oliwa's hourly DD numbers (small black dots) compared with the warning intensity (open circles). On 09 September, the TC underwent a period of explosive deepening as indicated by both the DD numbers and the best-track intensities. After reaching its peak intensity, the typhoon's intensity changed very little for nearly two days.

Oliwa's explosive deepening was unforeseen. Neither the official forecasts, nor numerical guidance indicated that this event would take place. The official forecasts prior to Oliwa's peak intensity were up to 40, 60, 65 and 90 kt too low for the 12-, 24-, 48- and 72-hour forecast periods respectively. While much progress has been made toward reducing the errors of track

forecasts, and real skill as measured against such benchmarks as CLIPER has been achieved, errors of intensity forecasts remain large, and there is much room for improvements.

b. A possible eye wall mesovortex

Eyewall mesocyclonic vortices (EMs) were first detected and documented in airborne Doppler radar data by Marks and Houze (1984) and also with aircraft inertial navigation equipment as noted by Black and Marks (1991). Stewart and Lyons (1996) identified EMs with the Guam NEXRAD in association with the passage of Ed (1993) over Guam. Until the implementation of the NEXRAD radar network in the United States during the early 1990s, only chance encounters with EMs have occurred during reconnaissance aircraft penetrations. However, now that Doppler velocity data are available, strong mesocyclones associated with TC outer convective bands and eyewall convection are frequently detected. Stewart et al. (1997) used NEXRAD data to show that mesocyclonic vortices in the wall clouds of TC eyes may be a mechanism for TC intensification and for extreme wind bursts in TCs, as noted with Hurricane Andrew damage (Wakimoto and Black 1993). In three cases, a TC underwent a period of rapid intensification during which time several vertically deep EMs formed prior to the occurrence of rapid intensification and persisted for several hours while rapid deepening was occurring.

In the case of Oliwa, a possible EM was observed in its eye on visible satellite imagery (Figure 3-02C-3) in the early daylight hours of 10 September. Possible EMs were evident on only two image frames: at 092030Z and 092130Z September. Unlike the cases investigated by Stewart et al. (1997), the EMs observed in Oliwa's eye wall cloud occurred after the TC had reached its peak intensity.

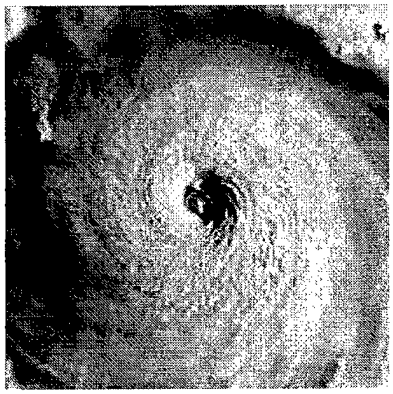

Figure 3-02C-3 A small comma shaped cloud along the inner edge of Oliwa's eye wall cloud is a possible manifestation of an eyewall mesovortex. This image is a zoom of the eye and eye wall cloud which appears in Figure 3-02C-1 (092034Z September visible GMS imagery).

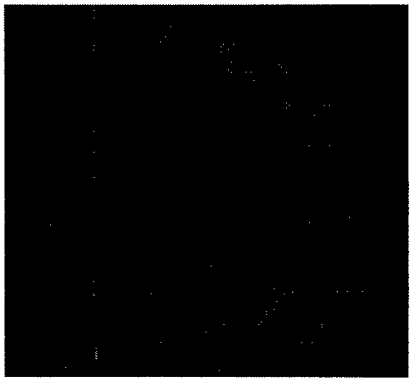

Figure 3-02C-4 Microwave imagery is especially suited to view concentric wall clouds in a TC. Oliwa developed well-defined concentric wall clouds as it began to weaken (120104Z September 85 GHz horizontally polarized microwave DMSP imagery).

c. Concentric wall clouds

Oliwa was yet another example of an intense WNP typhoon acquiring concentric eye wall clouds which were easily seen on conventional visible and infrared imagery, and especially well-defined on microwave imagery (Figure 3-02C-4). Microwave imagery is particularly well-suited to observe and document the evolution of concentric eye wall clouds (e.g., Paka's (05C) eye-wall replacement cycle was exceptionally well documented on microwave imagery) There is a tendency for high-end typhoons (i.e., those with peak intensity greater than 100 kt (51 m/sec)) to develop concentric eye wall clouds.

IV. IMPACT

Oliwa made landfall in southwestern Japan where it was responsible for widespread damage and for loss of life. On Japan's southern island of Kyushu, seven people were reported killed. One thousand homes were flooded and dozens of homes were destroyed. Along Korea's southern coast, twenty-eight ships sank or were wrecked in strong winds and high waves. A crabbing ship with 10 crewmen aboard was reported missing. Earlier in its life, Oliwa passed close to the island of Agrihan in the Marianas, which reported winds of about 85 mph (74 kt). No reports of damage or injuries were received at JTWC.

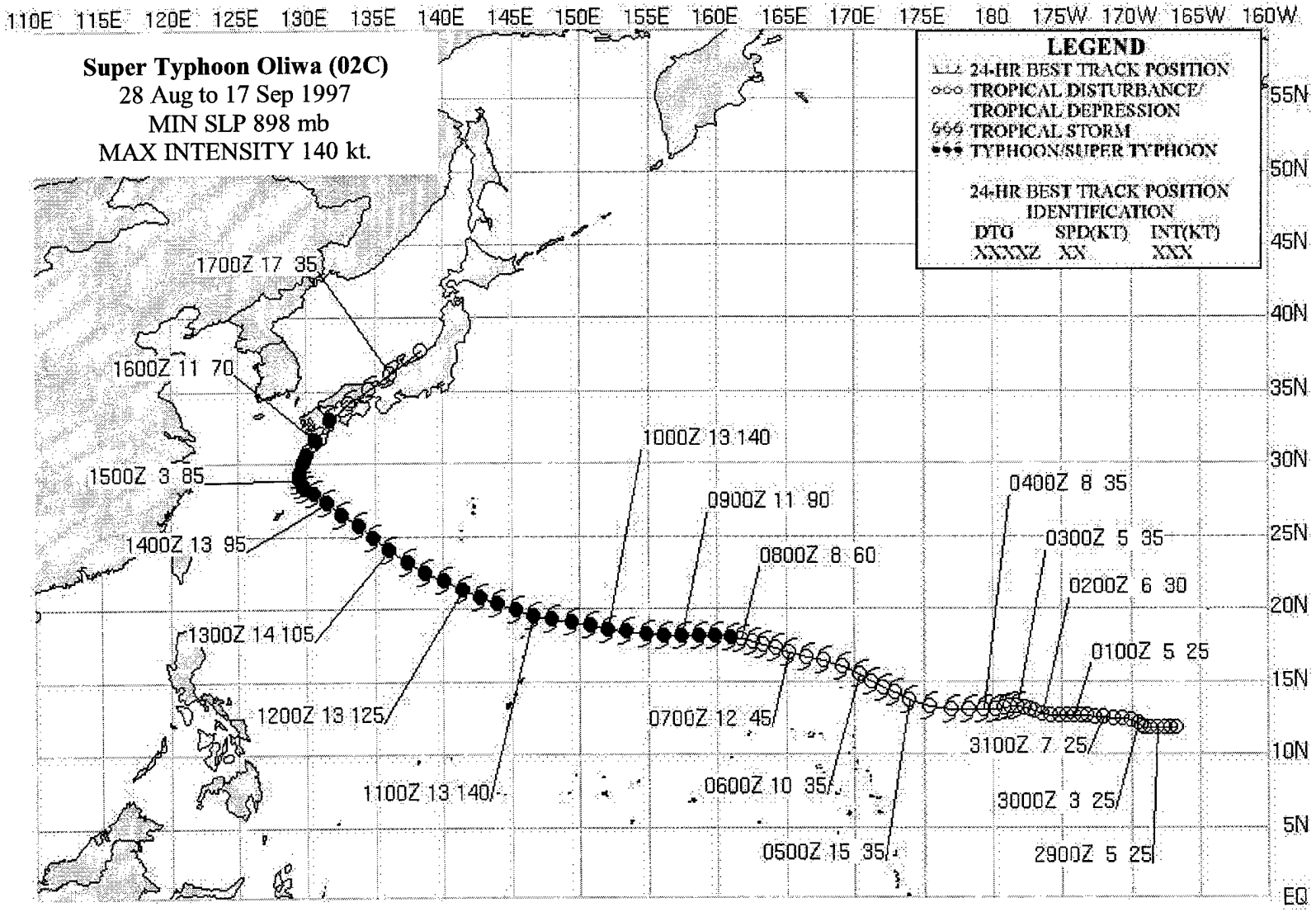
Super Typhoon Oliwa (02C)
28 Aug to 17 Sep 1997
MIN SLP 898 mb
MAX INTENSITY 140 kt.
LEGEND
24-HR BEST TRACK POSITION
TROPICAL DISTURBANCE/
TROPICAL DEPRESSION
TROPICAL STORM
TYPHOON/SUPER TYPHOON
24-HR BEST TRACK POSITION
IDENTIFICATION
DTG SPD(KT) INT(KT)
XXXXZ XX XXX
110E 115E 120E 125E 130E 135E 140E 145E 150E 155E 160E 165E 170E 175E 180 175W 170W 165W 160W
55N
50N
45N
40N
35N
30N
25N
20N
15N
10N
5N
EQ
1700Z 17 35
1600Z 11 70
1500Z 3 85
1400Z 13 95
1300Z 14 105
1200Z 13 125
1100Z 13 140
1000Z 13 140
0900Z 11 90
0800Z 8 60
0700Z 12 45
0600Z 10 35
0500Z 15 35
0400Z 8 35
0300Z 5 35
0200Z 6 30
0100Z 5 25
3100Z 7 25
3000Z 3 25
2900Z 5 25

TYPHOON DAVID (21W)

The disturbance which would become Typhoon David (21W) was first noted in the monsoon trough northeast of Kwajalein on 09 September. Visible satellite imagery on 10 September showed Super Typhoon Oliwa (02C), moving northwestward south of the subtropical ridge axis. Southeast of Oliwa, the monsoon trough extended from 155E to 175W along the 10N latitude line in conjunction with a weaker near-equatorial trough in the southern hemisphere that extended from 160E to 173E near 5S to 8S. The twin troughs were indicative of a large area of westerly winds straddling the equator between 10N and 8S. The system was initially mentioned on the Significant Tropical Weather Advisory (ABPW) at 0600 on 10 September; six hours later a Tropical Cyclone Formation Alert (TCFA) was issued. By 12 September at 0034Z, visible satellite imagery indicated that the developing depression had a very large associated low-level circulation, with westerly winds feeding into the vortex from as far west as 150E. On the eastern side, flow into the vortex extended well past the dateline. At 1800Z that day, JTWC issued the first warning on the system. Post-analysis would later indicate that the system had actually reached tropical depression intensity (25 kt(13 m/sec)) two days earlier on 10 September. The system continued to organize as it tracked northwestward at approximately 10 kt (19 km/hr).

David intensified at a climatological rate, becoming a typhoon by 1800Z on 13 September. The cyclone tracked steadily in a northwestward direction equatorward of the sub-tropical ridge (Standard Dominant Ridge pattern/region of the Systematic and Integrated Approach – see Chapter 1). David's large size contributed to the strong northwestward component of its motion due to the "Beta Effect". This is the mechanism by which large tropical cyclones tend to self-propagate northward due to their disturbance of the earth's vorticity field.

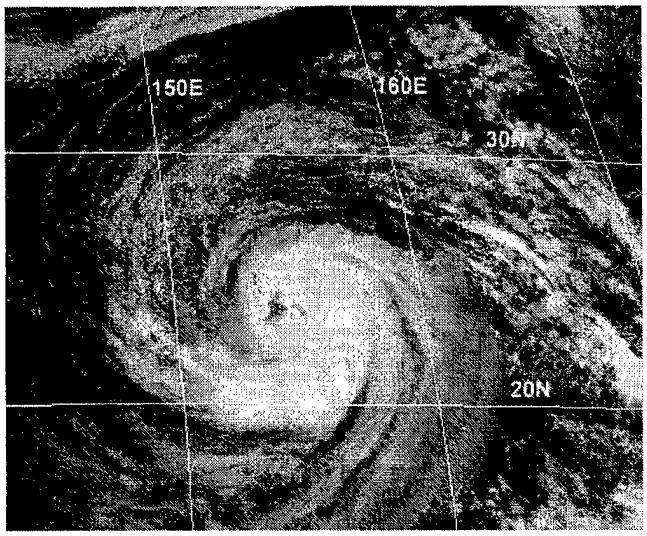

Figure 3-21-1 Typhoon David (21W) at 2230Z on 15 September 1997.

By 1800Z on 14 September, David had reached its peak of 95 kt (49 m/sec), remaining at this intensity for 36 hours. It continued traveling in a generally northwestward direction at speeds ranging from 12 - 15 kt (22 - 28 km/hr). By 16 September, strong mid-level ridging (related to the large Beta Effect) had developed east of the system. This was indicative of the formation of a Poleward/Poleward Oriented pattern/region (Systematic and Integrated Approach, see Chapter 1). Transition to the poleward pattern, along with a passing mid-latitude trough, caused David to recurve.

David passed near the island of Minami Tori Shima (WMO 479910) on the 16th, where sustained winds of 65 kt (33 m/sec) and a minimum sea level pressure of 968mb were recorded. Deep convection started to decrease near the system center as the cyclone began to weaken. However, the convection around the periphery began to increase and visible satellite imagery indicated a large cloud free area around the tropical cyclone's center.

At 0000Z on the 18th, David made its closest approach to the island of Chi Chi Jima (WMO 47971), where sustained wind speeds of 40 kt (21 m/sec) and a minimum sea level pressure of 967mb were reported. The intensity had dropped to 65 kt (33 m/sec), but the system remained a threat to the islands of Japan. Fortunately, David continued to turn toward the northeast, making its closest approach to Honshu on 19 September. Yokosuka reported 30 kt (15 m/sec) sustained winds at 0300Z.

JTWC issued its final warning at 0600Z on 20 September as the system transitioned to an extratropical low. The remnants of Typhoon David (21W) continued moving into the Gulf Of Alaska. There were no reports of damage or injuries as a result of David.

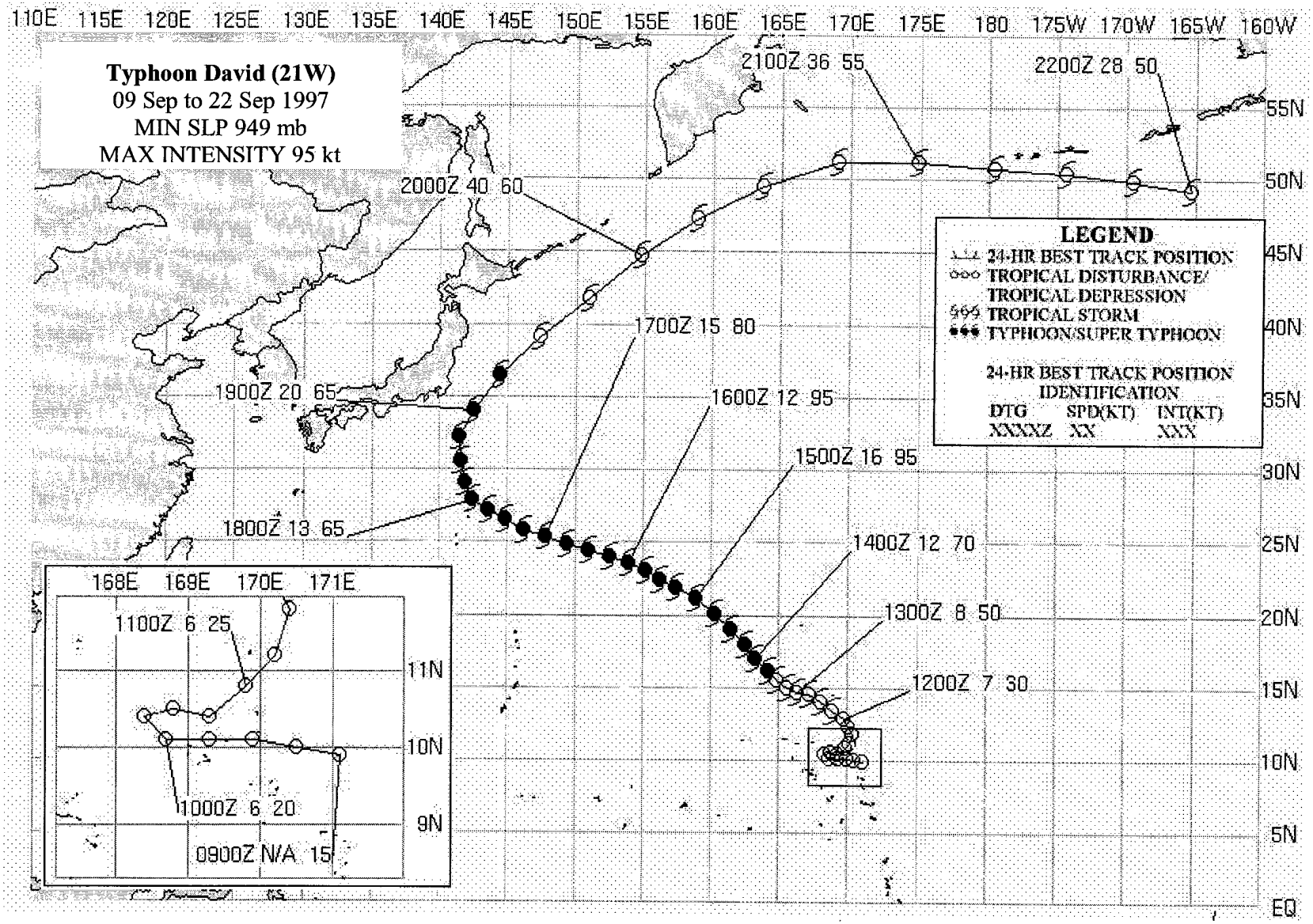
Typhoon David (21W)
09 Sep to 22 Sep 1997
MIN SLP 949 mb
MAX INTENSITY 95 kt
110E 115E 120E 125E 130E 135E 140E 145E 150E 155E 160E 165E 170E 175E 180 175W 170W 165W 160W
55N
50N
45N
40N
35N
30N
25N
20N
15N
10N
5N
EQ
2100Z 36 55
2200Z 28 50
2000Z 40 60
1700Z 15 80
1900Z 20 65
1600Z 12 95
1500Z 16 95
1800Z 13 65
1400Z 12 70
1300Z 8 50
1200Z 7 30
LEGEND
24-HR BEST TRACK POSITION
TROPICAL DISTURBANCE/ TROPICAL DEPRESSION
TROPICAL STORM
TYPHOON/SUPER TYPHOON
24-HR BEST TRACK POSITION IDENTIFICATION
DTG SPD(KT) INT(KT)
XXXXZ XX XXX
168E 169E 170E 171E
11N
10N
9N
1100Z 6 25
1000Z 6 20
0900Z N/A 15

TYPHOON FRITZ (22W)

The tropical disturbance that became Typhoon Fritz (22W) originated in the South China Sea (near the Philippine archipelago) within a long east-west cloud band associated with the monsoon trough. When first mentioned on the 19 September Significant Tropical Weather Advisory (ABPW), the deep convection associated with this disturbance had formed a distinct cloud cluster embedded in an otherwise unbroken monsoonal cloud band that stretched eastward along 10N from Southeast Asia to 170E. On 20 September, JTWC went directly to the first warning on Tropical Depression (TD) 22W. At 1800Z that day, satellite data indicated that the winds in the system had increased to 25 kt (13 m/sec). The cyclone was expected to intensify after it moved into open water away from the coast of Vietnam. As expected, TD 22W turned sharply to the right and began a slow track toward the north-northeast. The system failed to intensify until 22 September when it slowed southeast of Hainan Island, and organization of the deep convection began to improve. TD 22W was upgraded to Tropical Storm Fritz (22W) on the warning valid at 0000Z on the 23rd, based on satellite intensity estimates of 45 kt (23 m/sec). After becoming a tropical storm, Fritz turned toward the west and began to track toward the coast of Vietnam while continuing to intensify. Fritz reached typhoon intensity at 0000Z on the 24th (Figure 3-22-1). The intensity peaked at 75 kt (39 m/sec) at 0600Z on 24 September and held steady until the 25th when Fritz made landfall. Fritz steadily weakened after landfall, and the final warning was issued valid at 1800Z on 25 September, when it was expected that the system would dissipate over land within 24 hours. In Vietnam, at least 25 people were reported killed and dozens were missing. Most of the victims were gold prospectors buried in landslides triggered by flash flooding.

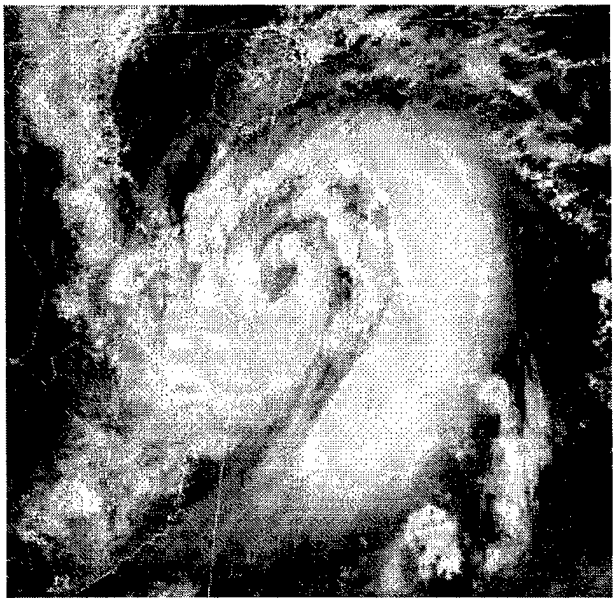

Figure 3-22-1 Tightly wrapped coils of deep convection surrounding a ragged ragged eye indicate that Fritz has become a typhoon (240133Z September visible GMS imagery).

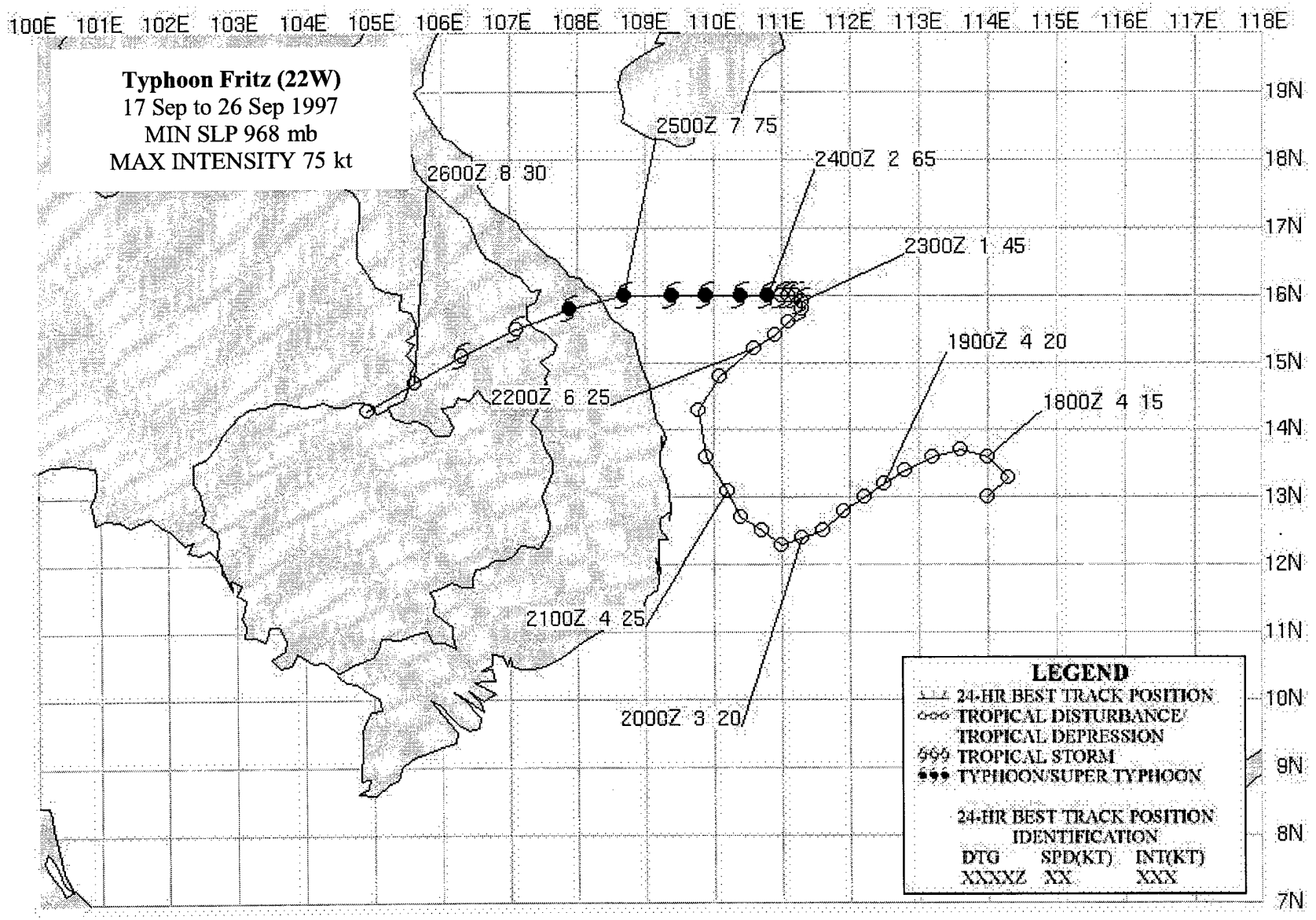
Typhoon Fritz (22W)
17 Sep to 26 Sep 1997
MIN SLP 968 mb
MAX INTENSITY 75 kt
100E 101E 102E 103E 104E 105E 106E 107E 108E 109E 110E 111E 112E 113E 114E 115E 116E 117E 118E
19N
18N
17N
16N
15N
14N
13N
12N
11N
10N
9N
8N
7N
2500Z 7 75
2400Z 2 65
2600Z 8 30
2300Z 1 45
1900Z 4 20
2200Z 6 25
1800Z 4 15
2100Z 4 25
2000Z 3 20
LEGEND
24-HR BEST TRACK POSITION
TROPICAL DISTURBANCE/
TROPICAL DEPRESSION
TROPICAL STORM
TYPHOON/SUPER TYPHOON
24-HR BEST TRACK POSITION
IDENTIFICATION
DTG SPD(KT) INT(KT)
XXXXZ XX XXX

TROPICAL STORM ELLA (23W)

The disturbance that became Tropical Storm Ella (23W) began as a small circulation east of the dateline, with scattered convection emerging from a larger area of convection on 19 September. By 21 September, visible imagery indicated that the convection had become well developed over the system's center. Now a tropical storm, Ella moved rapidly to the west-northwest at 18 to 25 kt (33 to 46 km/hr) under the influence of easterly steering flow south of the subtropical ridge. However, by 22 September, the system began to slow as it approached a break in the ridge, and on 23 September Tropical Storm Ella (23W) moved through the break and recurved to the northeast.

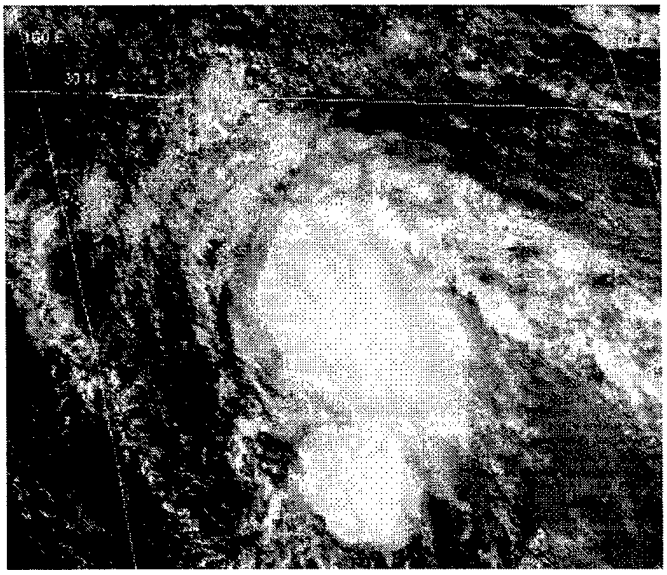

Figure 3-23-1 Tropcial Storm Ella (23W) showing a partially exposed low-level circulation (212132Z September visible GMS imagery).

Tropical Storm Ella (23W) was an unusually small system. The central convection associated with the low-level circulation on 20 September was only about 30 nm (56 km) in diameter. The cyclone's small size in conjunction with moderate vertical wind shear kept Tropical Storm Ella (23W) from intensifying beyond a minimal tropical storm (peak intensity was 40 kt (20m/s) on 22 September). Tropical Storm Ella (23W) dissipated on 24 September near 40N 170E in the vicinity of a frontal zone.

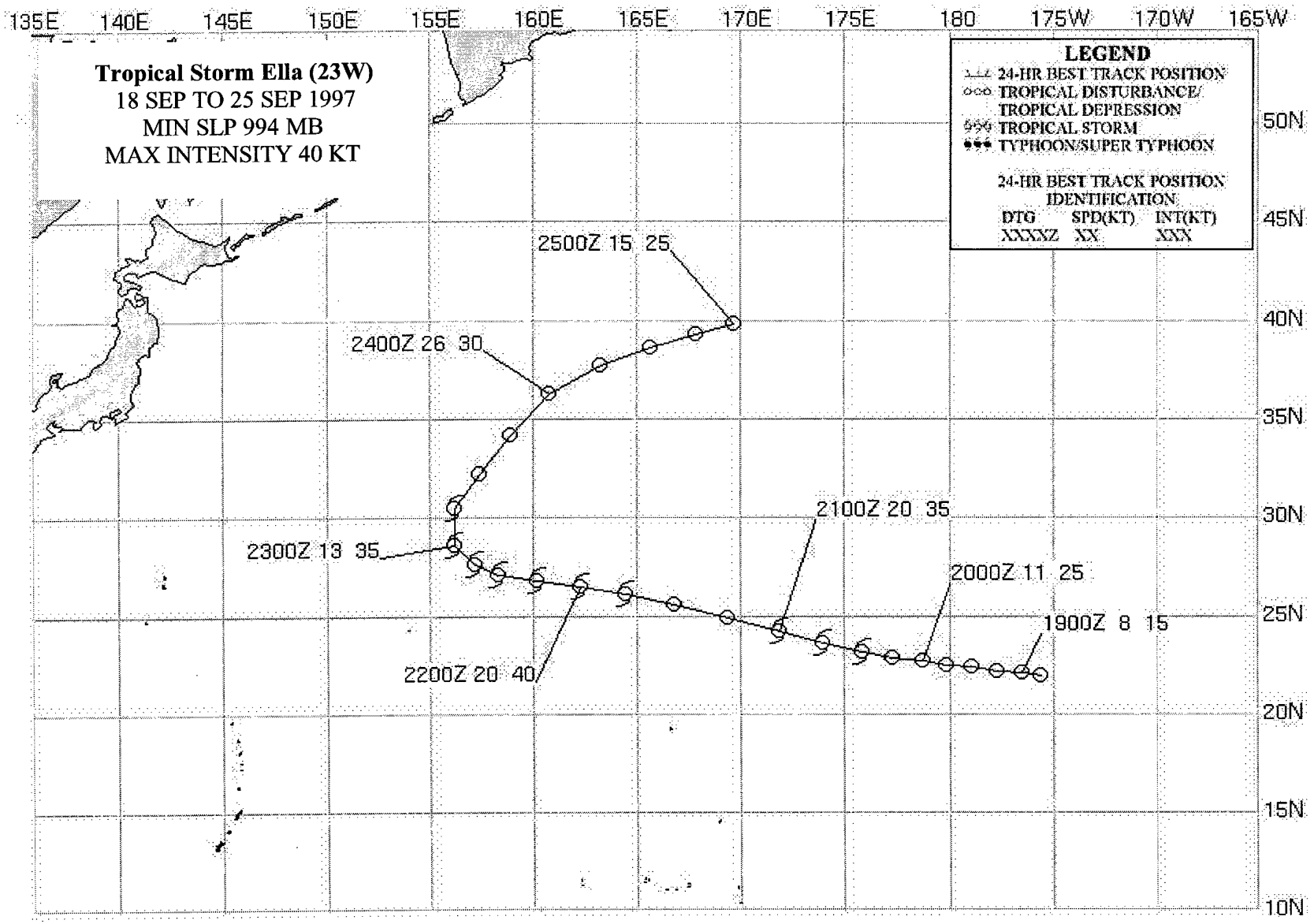
Tropical Storm Ella (23W)
18 SEP TO 25 SEP 1997
MIN SLP 994 MB
MAX INTENSITY 40 KT
LEGEND
24-HR BEST TRACK POSITION
TROPICAL DISTURBANCE/
TROPICAL DEPRESSION
TROPICAL STORM
TYPHOON/SUPER TYPHOON
24-HR BEST TRACK POSITION
IDENTIFICATION
DTG SPD(KT) INT(KT)
XXXXZ XX XXX
135E
140E
145E
150E
155E
160E
165E
170E
175E
180
175W
170W
165W
50N
45N
40N
35N
30N
25N
20N
15N
10N
2500Z 15 25
2400Z 26 30
2300Z 13 35
2200Z 20 40
2100Z 20 35
2000Z 11 25
1900Z 8 15

SUPER TYPHOON GINGER (24W)

I. HIGHLIGHTS

The seventh of eleven Tropical Cyclones (TCs) to attain super typhoon intensity in the western North Pacific (WNP) during 1997, Ginger formed at low latitudes in the Marshall Islands. It was one of ten TCs that formed east of 160E and south of 20N; within the "El Niño" box in Figure 3-3a. Ginger moved on a north-oriented track through the eastern portion of the western North Pacific basin. As it neared its peak intensity, the typhoon possessed an extensive system of primary and peripheral rainbands. When it reached 30N, it accelerated within the mid-latitude westerlies where it transitioned into a vigorous extratropical low. Ginger was one of the many 1997 TCs that formed at the eastern end of the monsoon trough near the international dateline (IDL) and evolved into a large solitary TC's (i.e., much of the WNP basin, with the exception of the single typhoon, was unusually free of deep convection).

II. TRACK AND INTENSITY

During the first two weeks of September 1997, two TCs, STY Oliwa (02C) and TY David (21W), formed near the IDL, moved across the basin as large solitary typhoons, and recurved near Japan. On 21 September, as David was recurving east of Japan, the tropical disturbance that was to become Ginger had consolidated at low latitude near the IDL. On 22 September, this tropical disturbance became better organized, as evidenced by a low-level cyclonic circulation that was well-defined by synoptic data. Deep convection associated with the low-level circulation became organized into curved bands; and animated water vapor imagery indicated the presence of anticyclonic flow at upper levels over the low-level center. This disturbance was first mentioned on the Significant Tropical Weather Advisory (ABPW) valid at 0000Z on 22 September. A Tropical Cyclone Formation Alert (TCFA) was issued at 0530Z on the 22nd, when satellite data indicated continued improvement in the system's organization and the presence of factors deemed favorable for TC formation (e.g., the water vapor derived winds showed strong upper-level divergence over the system). Based on satellite derived intensity estimates of 25 kt (13 m/sec), the first warning on Tropical Depression

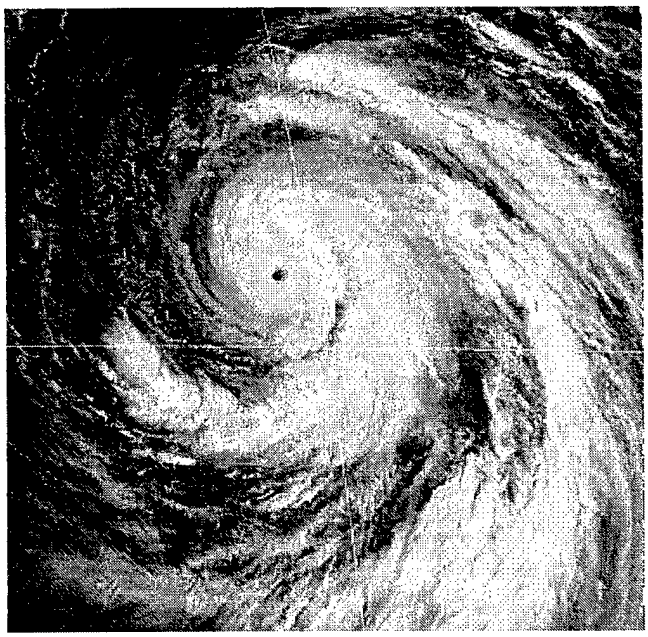

Figure 3-24-1 Ginger nears its peak intensity of 145 kt (75 m/sec). Extensive banding features accompanied this TC (262132Z September visible GMS imagery).

(TD) 24W was issued valid at 1800Z on 22 September. For 36 hours, TD 24W moved northwest and slowly intensified. Based on satellite intensity estimates, it was upgraded to Tropical Storm Ginger (24W) on the warning valid at 0600Z on 24 September. Ginger began to track in a more northerly direction. Intensifying at a normal climatological rate, it became a typhoon at 1200Z on the 25th. At this point Ginger began a period of explosive deepening (see Discussion Section) and in the 24-hour period from the 26th at 0000Z to the 27th at 0000Z, the intensity jumped from 75 kt (39 m/sec) to 145 kt (75 m/sec).

As it neared its peak intensity, Ginger's structure provided spectacular views via visible satellite imagery (e.g., Figure 3-24-1). It had a small well-defined eye embedded in a smooth symmetrical Central Dense Overcast (CDO), which in turn was surrounded by an extensive pattern of primary and peripheral cloud bands. The unusually cloud free structure of the large-scale environment served to highlight Ginger in the imagery (Figure 3-24-2).

After Ginger peaked on 27 September, it moved slowly north-northwestward and arrived at its point of recurvature 36 hours later at 1200Z on 28 September with an intensity of 110 kt (57 m/sec). Typically, weak typhoons peak at or near their point of recurvature, while more intense typhoons, like Ginger, experience a delay between reaching peak intensity and arriving at their point of recurvature (JTWC 1994).

After recurving, Ginger began a slow acceleration into the midlatitudes. Finally, the intensity fell below typhoon force at 1800Z on the 30th, and the system made a smooth transition into a vigorous extratropical low. The final warning was issued, valid at 0600Z on 30 September, when a complete extratropical transition was expected within six hours.

III. DISCUSSION

a. Ginger's Digital Dvorak (DD) time series

Ginger was one of several typhoons during 1997 for which a time series of hourly DD-numbers (Figure 3-24-3) was recorded. Ginger's DD-numbers are in overall agreement with the best-track intensity; although there are two notable exceptions. First, the drop of the DD-numbers below the values of the best track intensities as Ginger was weakening, is an intrinsic feature of Dvorak analysis for a TC weakening over water. The decrease of the Current Intensity (CI) is delayed, by about one day behind a falling computed Data T (DT) number. In general this results in the CI remaining one T-number higher than the DT for steadily weakening systems. The second discrepancy is harder to explain, and carries both operational and research implications with it. The best-track intensity values are all lower than their corresponding DD-numbers as Ginger intensified. The rate of intensification during the 24-hr period from 0000Z on 26 September to 0000Z on September, as shown by Digital Dvorak (50 mb for an average of 2.1 mb/hr), is quite different from that computed from the best track (74 mb for an average of 3.1 mb/hr). The former rate of intensification qualifies as a case of explosive deepening (defined as meeting or exceeding a drop of minimum sea-level pressure of at least 2.5 mb/hr for 12 hours (Dunnavan 1981)). The latter rate of deepening is not so extreme, but qualifies as a case of rapid deepening (defined as a drop of minimum sea-level pressure of at least 1.75 mb/hr, or 42 mb/24 hrs (Holliday and Thompson 1979).

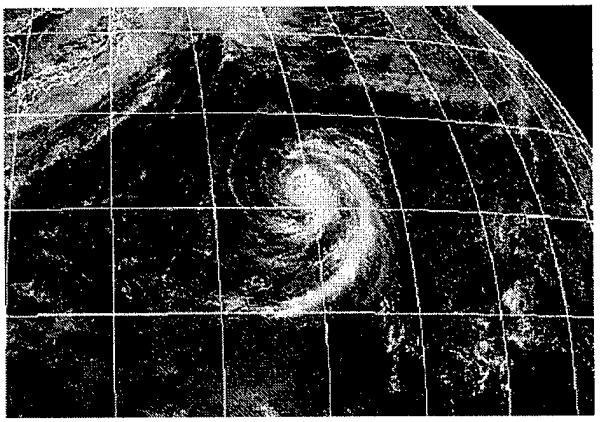

Figure 3-24-2 Ginger and its extensive pattern of primary and peripheral cloud bands are isolated in an otherwise relatively cloud free tropics (270033Z September visible GMS imagery).

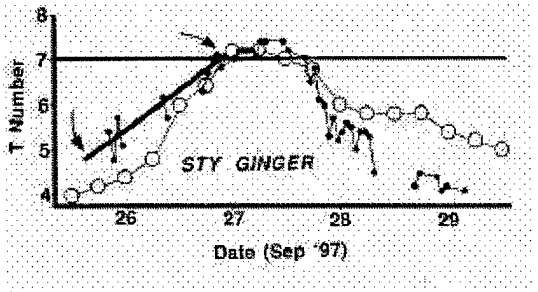

Figure 3-24-3 A time series of Ginger's hourly DD-numbers (small black dots) compared with the best-track intensity (open circles). Note that as Ginger was intensifying the best-track intensity rises faster than the value of the DD-numbers (indicated by the thick black line).

The discrepancy between the DD-numbers and best track intensities during intensification is not uncommon. However, in the case of Ginger, one can see that the resulting rate of deepening is quite different depending on whether the best-track or the DD-numbers are used to compute it. The results of research into TC intensification processes may be very different depending upon which method is used. DD-numbers are still experimental, and methods for incorporating them into operational practice are being explored. Reasons for the disagreement between the DD-numbers and the best-track intensities must be determined before any modifications are made to the current methods of estimating TC intensity utilizing satellite imagery.

b. Large and solitary

Ginger was one of many TCs of the 1997 season that formed at the eastern end of the monsoon trough near the IDL and became large solitary typhoons (Figure 3-24-2 and Figure 3-24-4). The persistent reduction of deep convection throughout much of Micronesia and within the low latitudes of the WNP basin became more pronounced during the latter half of 1997. The low-level monsoon westerlies and their associated deep convection moved eastward to the IDL (and beyond) in association with large-scale climatic anomalies related to El Niño. Other large and solitary typhoons during 1997 included TY David (21W), STY Oliwa (02C), STY Ivan (27W), STY Joan (28W), STY Keith (29W), and STY Paka (05C).

c. Concentric eye wall clouds

Ginger was yet another example of an intense WNP typhoon acquiring concentric eye wall clouds that are easily seen on conventional visible and infrared imagery, and are especially well-defined on microwave imagery (Figure 3-24-5). Microwave imagery is particularly well-suited to observe concentric eye wall clouds, and to document their evolution. (Paka's eye-wall replacement cycle was exceptionally well documented on microwave imagery; see the Paka

(05C) summary). The rapid fall of Ginger's DD-numbers (Figure 3-24-3) within 24 hours of its peak was a manifestation of its acquisition of concentric wall clouds. There is a tendency for the most intense typhoons (e.g., STY Dale (36W), in 1996, and STY Paka (05C)) to develop concentric eye wall clouds within 24 hours of their first or only peak.

IV. IMPACT

Ginger remained at sea for its entire life, and no reports of damage or injury were received at JTWC.

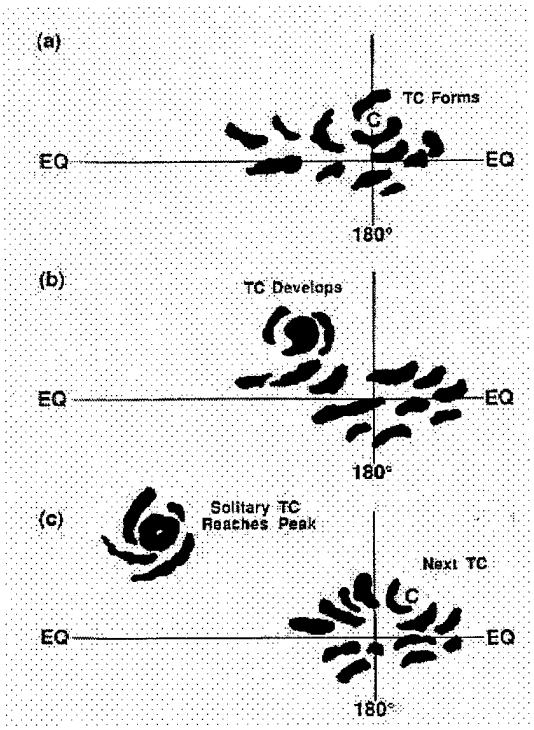

Figure 3-24-4 A graphic illustration of the process whereby a large solitary TC forms in an eastward displaced monsoon system, and then tracks northwestward, intensifies, and becomes isolated in a relatively cloud-free environment. This process was typical of most of the very intense TCs that occurred during the latter half of 1997

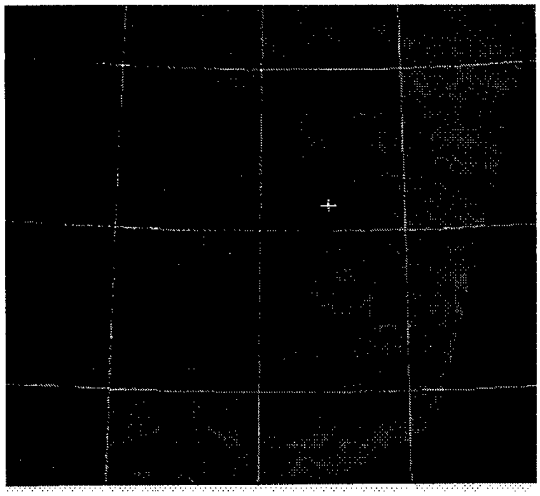

Figure 3-24-5 Microwave imagery clearly reveals the acquisition of concentric eye wall clouds by Ginger within 24 hours of reaching its peak intensity (272132Z September horizontally polarized 85 GHz microwave DMSP imagery).

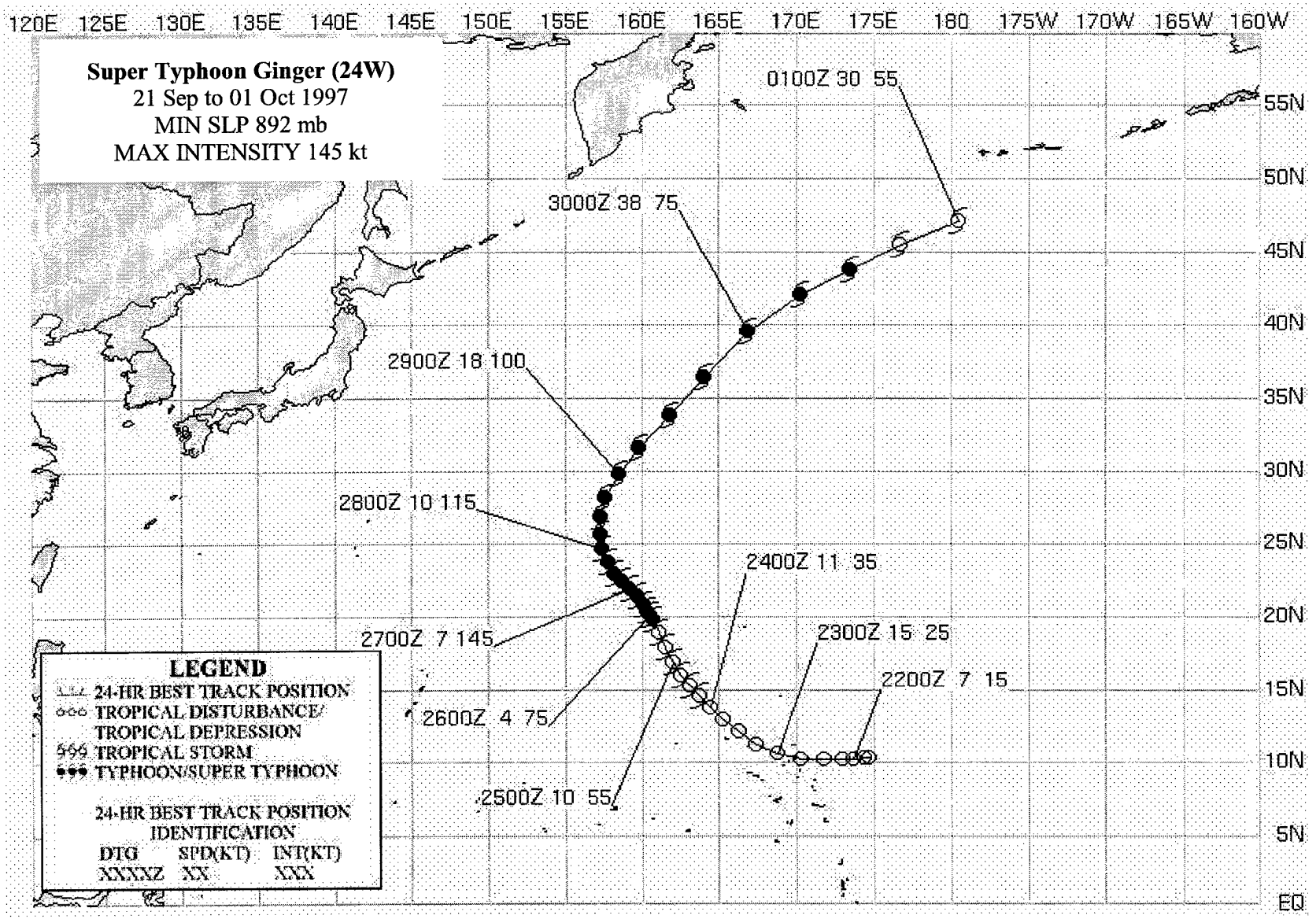
Super Typhoon Ginger (24W)
21 Sep to 01 Oct 1997
MIN SLP 892 mb
MAX INTENSITY 145 kt
120E 125E 130E 135E 140E 145E 150E 155E 160E 165E 170E 175E 180 175W 170W 165W 160W
55N 50N 45N 40N 35N 30N 25N 20N 15N 10N 5N EQ
0100Z 30 55
3000Z 38 75
2900Z 18 100
2800Z 10 115
2400Z 11 35
2300Z 15 25
2200Z 7 15
2700Z 7 145
2600Z 4 75
2500Z 10 55
LEGEND
24-HR BEST TRACK POSITION
TROPICAL DISTURBANCE/ TROPICAL DEPRESSION
TROPICAL STORM
TYPHOON/SUPER TYPHOON
24-HR BEST TRACK POSITION IDENTIFICATION
DTG SPD(KT) INT(KT)
XXXXZ XX XXX

TROPICAL STORM HANK (25W)

Tropical Storm (TS) Hank (25W) originated as a surface circulation in the South China Sea on the 27th of September. For several days, synoptic data suggested the presence of this circulation, but with light winds and minimal convection. It first appeared as a suspect area on the 30 September Significant Tropical Weather Advisory (ABPW). The system's convective signature experienced fluctuation over the next few days. No Tropical Cyclone Formation Alert (TCFA) was issued on this system; JTWC issued a warning at 0000Z on 3 October with a 35 kt (70 m/s) intensity based on synoptic data and cloud signature. Hank peaked at 40 kt (80 m/s) during the next 6 to 12 hours, before being subjected to strong vertical wind shear. During its early existence, the disturbance drifted in the South China Sea, eventually moving equatorward. At about the time JTWC began issuing warnings, it began tracking northward along the Vietnam coast. Although infrared imagery indicated very convincing convective cloud masses over land as early as 2032Z on October 3, the circulation center was actually further east and landfall was not made until about 0000Z on the 5th. Landfall occurred near 18°N (figure 3-25-1). No reports of damage were received by JTWC.

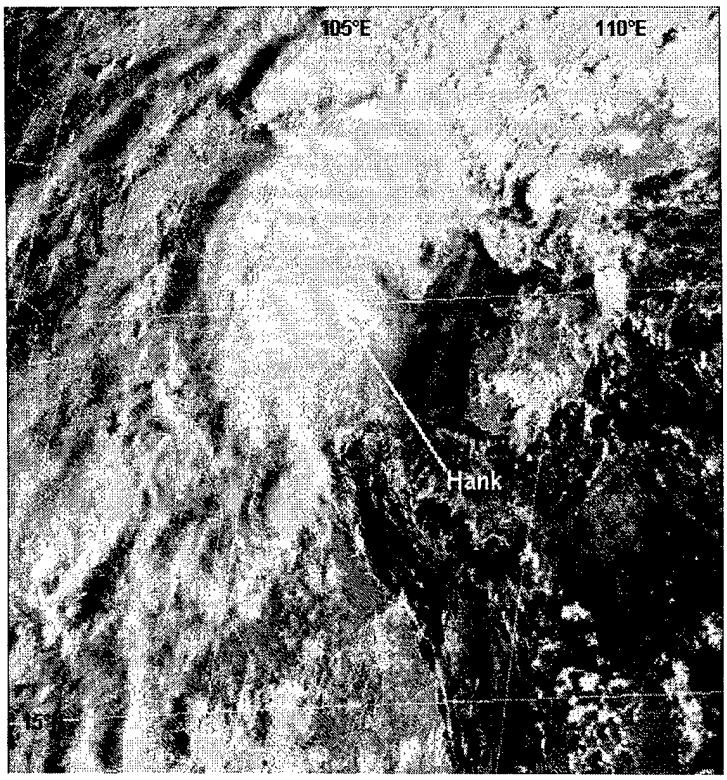

Figure 3-25-1 Hank makes landfall (042333Z October visible GMS imagery).

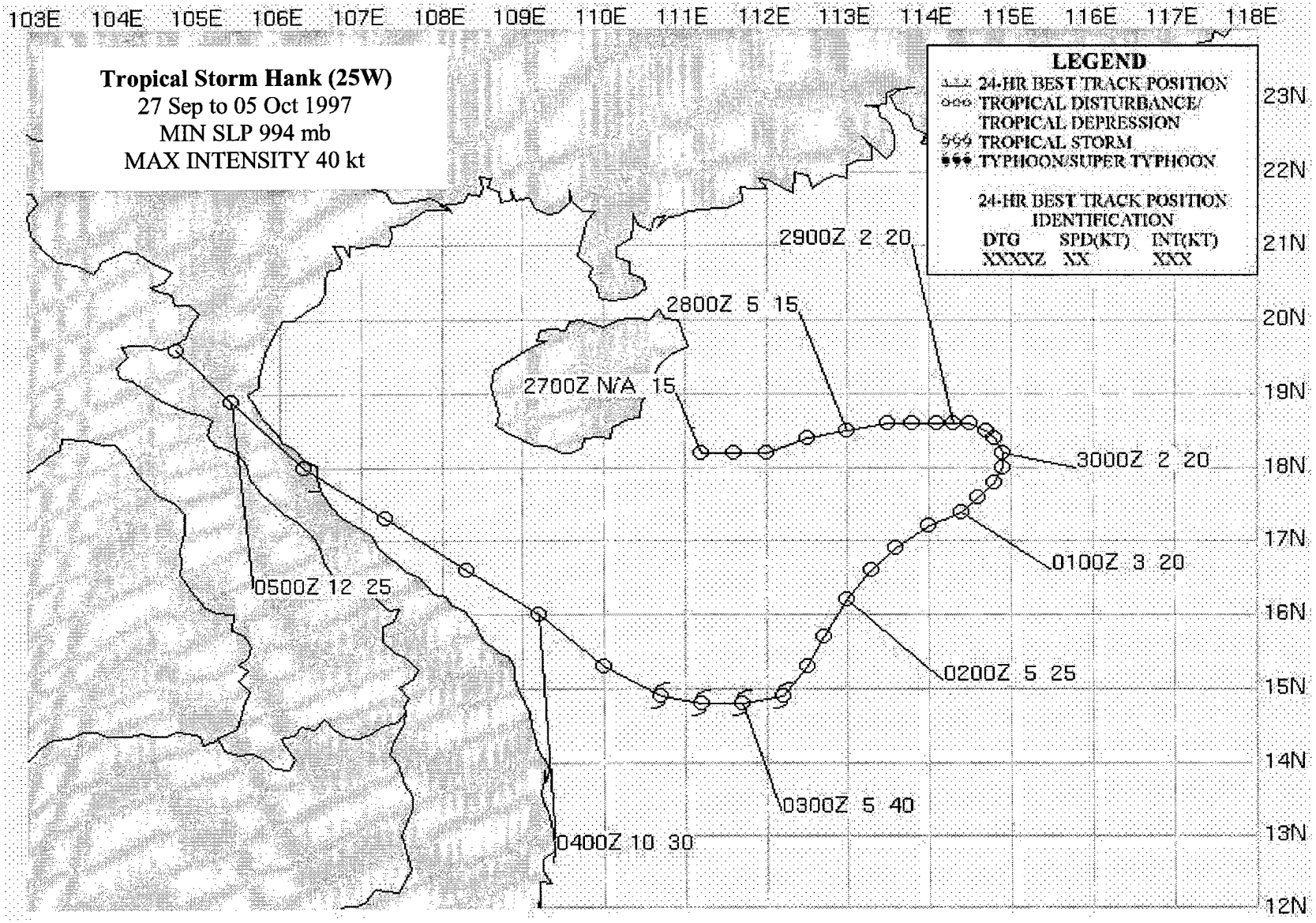
Tropical Storm Hank (25W)
27 Sep to 05 Oct 1997
MIN SLP 994 mb
MAX INTENSITY 40 kt
LEGEND
24-HR BEST TRACK POSITION
TROPICAL DISTURBANCE/
TROPICAL DEPRESSION
TROPICAL STORM
TYPHOON/SUPER TYPHOON
24-HR BEST TRACK POSITION
IDENTIFICATION
DTG SPD(KT) INT(KT)
XXXXZ XX XXX
103E 104E 105E 106E 107E 108E 109E 110E 111E 112E 113E 114E 115E 116E 117E 118E
23N 22N 21N 20N 19N 18N 17N 16N 15N 14N 13N 12N
2900Z 2 20
2800Z 5 15
2700Z N/A 15
3000Z 2 20
0100Z 3 20
0200Z 5 25
0300Z 5 40
0400Z 10 30
0500Z 12 25

TROPICAL DEPRESSION 26W

Tropical Depression 26W initially formed as a disturbance southeast of the Marianas on 29 September. After an initial slow track to the north, the disturbance turned briskly westward at about 14 kts (26 km/hr) as the subtropical ridge built to its north. The disturbance tracked just north of Guam bringing the island showers and thunderstorms early on 02 October. The disturbance became Tropical Depression 26W northwest of Guam late on 02 October. On 03 October at 00Z, a 30 kt (60 m/s) sustained ship observation was reported within 1 degree of the system center. Satellite imagery at this time indicated a low-level circulation with only scattered convection near the center. The convection became more widespread during the next 24 hours as the Tropical Depression 26W's forward motion slowed in the weak steering region associated with a break in the mid-level subtropical ridge. Tropical Depression 26W did not intensify further. Satellite imagery from 4 October and 5 October showed it to be affected by increasing vertical wind shear. By 5 October, Tropical Depression 26W had increased its westward speed as the subtropical ridge redeveloped to its north. Tropical Depression 26W continued to experience vertical wind shear, as evident by 00Z 6 October visible imagery indicating that the main area of convection was distinctly separated from its low-level circulation center. The system remained a tropical depression as indicated by 30 kt (60m/s) wind ship observations near its center. Tropical Depression 26W dissipated over the Philippine Sea on 7 October as it merged with a frontal boundary.

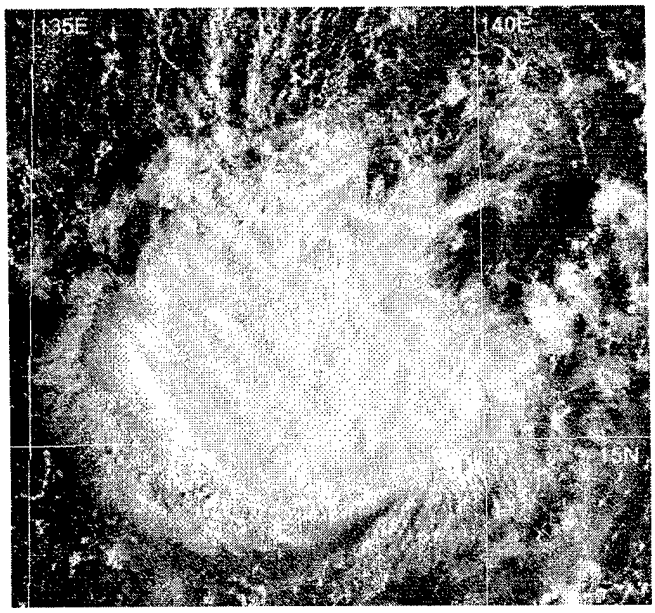

Figure 3-26-1 Tropical Depression 26W increasing in convection (032132Z October visible GMS imagery).

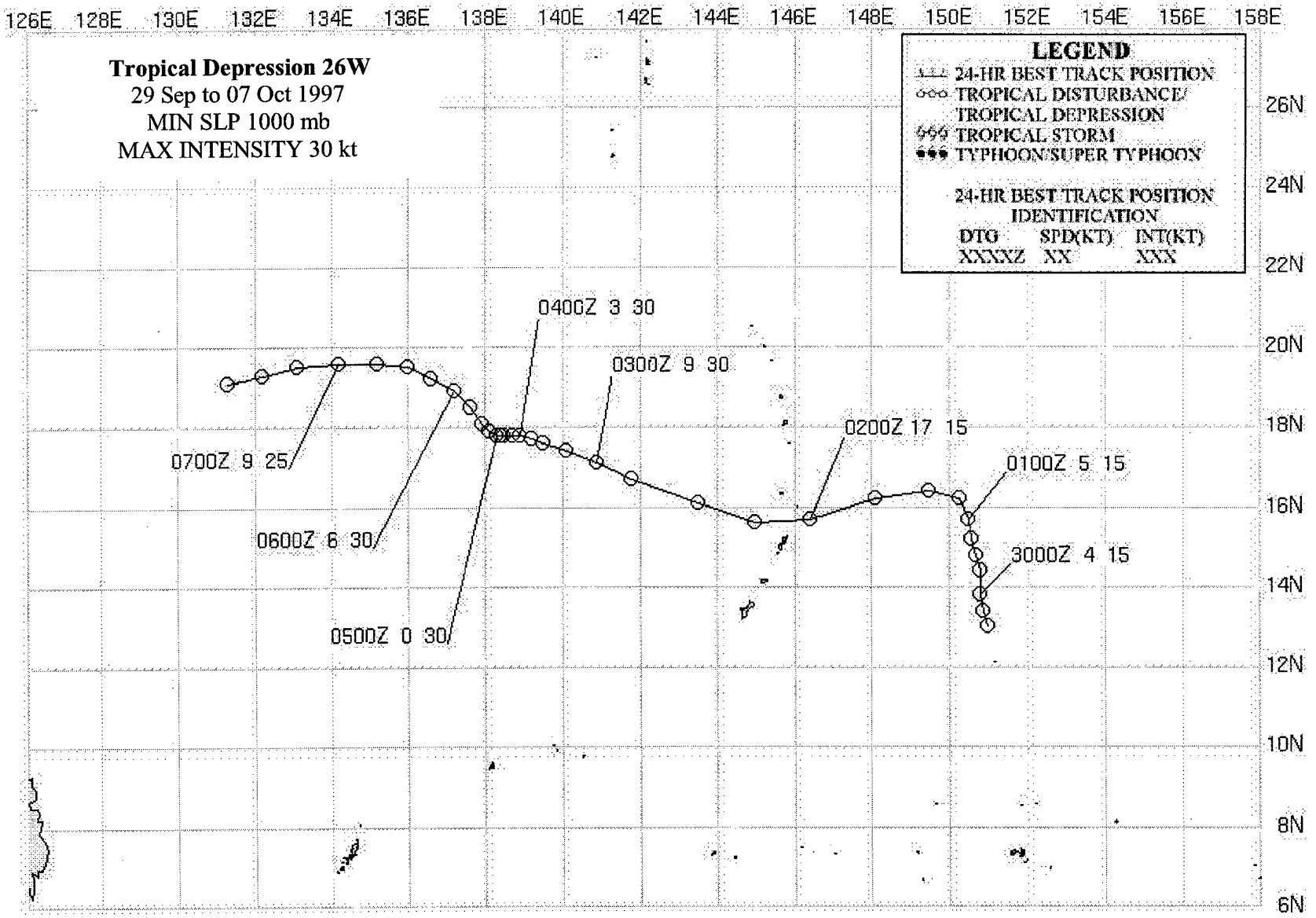
126E 128E 130E 132E 134E 136E 138E 140E 142E 144E 146E 148E 150E 152E 154E 156E 158E
26N
24N
22N
20N
18N
16N
14N
12N
10N
8N
6N
Tropical Depression 26W
29 Sep to 07 Oct 1997
MIN SLP 1000 mb
MAX INTENSITY 30 kt
LEGEND
24-HR BEST TRACK POSITION
TROPICAL DISTURBANCE/
TROPICAL DEPRESSION
TROPICAL STORM
TYPHOON/SUPER TYPHOON
24-HR BEST TRACK POSITION
IDENTIFICATION
DTG SPD(KT) INT(KT)
XXXXZ XX XXX
0400Z 3 30
0300Z 9 30
0200Z 17 15
0100Z 5 15
0700Z 9 25
0600Z 6 30
3000Z 4 15
0500Z 0 30

SUPER TYPHOONS IVAN (27W) AND JOAN (28W)

I. HIGHLIGHTS

Super Typhoon Ivan (27W) and Super Typhoon Joan (28W) were two of three tropical cyclones (TCs) in the western North Pacific (WNP) during 1997 to attain an extreme intensity of 160 kt (82 m/sec), and were the 8th and 9th super typhoons of 1997's unprecedented annual total of eleven. They reached their peak intensities at nearly the same time: Ivan at 171800Z October and Joan at 170600Z October. At 171200Z, Ivan was at 155 kt (80 m/sec) while Joan was still at 160 kt (82 m/sec); the first observation of two TCs of such extreme intensity existing simultaneously in the WNP. Both Ivan and Joan affected the Mariana Islands, and Ivan was the first and only TC during 1997 of at least tropical storm intensity to make landfall on Luzon. An equatorial westerly wind burst (bounded by twin near-equatorial troughs) preceded the formation of Ivan, Joan and a Southern Hemisphere twin, TC 02P (Lusi).

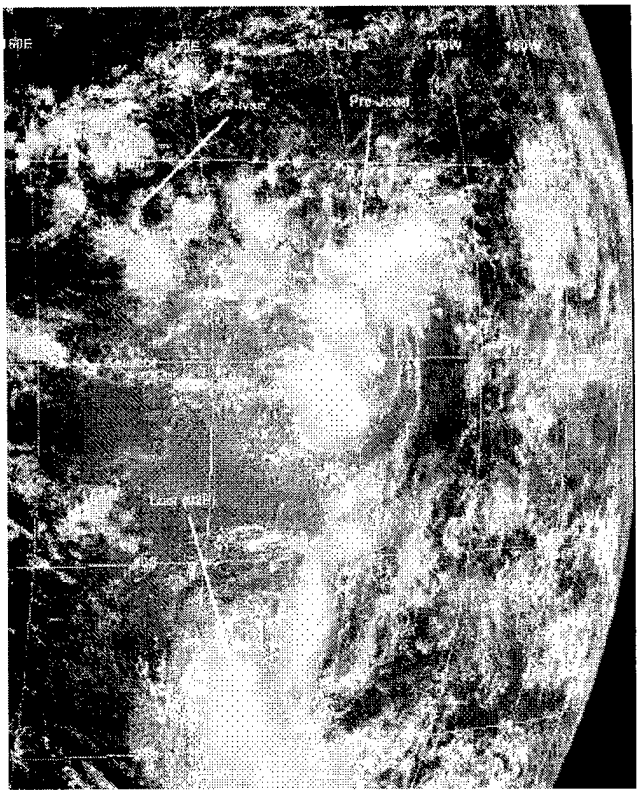

Figure 3-27/28-1 The pre-Ivan and pre-Joan tropical disturbances are poorly organized at low latitude in the eastern portion of the WNP basin. A Southern Hemisphere twin, Lusi, is passing southward between Fiji and the islands of Vanuatu (102132Z October visible GMS imagery).

II. TRACK AND INTENSITY

During the first week of October, low-latitude, low-level, westerly winds blew along the equator from approximately 150E eastward, across the international dateline (IDL), to near 170W. Twin near-equatorial troughs (one in the Northern Hemisphere, the other in the Southern Hemisphere) bounded these westerly winds and a region of deep convection. As the deep convection along the equator diminished, three TCs emerged from this synoptic flow pattern. The first -- Lusi -- formed in the Southern Hemisphere on 08 October and moved southward between Fiji and Vanuatu. On 13 October, Ivan and Joan formed in the Northern Hemisphere in the eastern half of Micronesia and began to track toward the west-northwest. As they were initially poorly organized (Figure 3-27/28-1) and isolated in an environment relatively free of deep convection (Figure 3-27/28-2), neither numerical guidance nor human forecaster anticipated the extreme intensity which these two TCs would attain. Also lacking during the lifetimes of the two TCs was any significant monsoon flow to their south and west.

a. STY Ivan (27W)

Ivan (the westernmost of the pair) originated from a very poorly organized tropical disturbance in the near-equatorial trough that stretched across the eastern Caroline and Marshall Island groups (see Figure 3-27/28-1). It was first mentioned on the 110600Z October Significant Tropical Weather Advisory (ABPW), when animated satellite imagery and synoptic data indicated the presence of a low-level circulation in association with an area of deep convection near 6N 165E. The pre-Joan tropical disturbance, located further to the east, was also first noted on this advisory.

With an increase in the organization and coverage of deep convection, a Tropical Cyclone Formation Alert (TCFA) was issued valid at 120800Z October as the pre-Ivan tropical disturbance (TD) moved rapidly (18 kt / 33 km/hr) west- northwest on a track which, if extrapolated, would pass just to the south of Guam. Based upon intensity estimates from satellite, the first warning on TD 27W was issued valid at 130600Z. There was still no expectation of any significant intensification, and remarks on the first warning indicated that the system was expected to intensify at a less than climatological rate. See the Discussion Section for further comments on Ivan (and Joan's) intensification. With increased banding of the deep convection, TD 27W was upgraded to Tropical Storm Ivan (27W) at 131800Z. Visible imagery on the morning of 14 October (Figure 3-27/28-3) gave clear indication of Ivan's location to the east-southeast of Guam. Passing 55 nm (102 km) to the south of Guam on the night of 14 October, Ivan's circulation center was well-defined on Guam's NEXRAD. A velocity cross section through Ivan's "eye" at 141120Z showed, at azimuth and range of 139 degrees and 75 nm (139 km) respectively, a maximum inbound velocity of 47 kt (24 m/sec) at 7,000 ft (210 m) (the lowest observable altitude); and, at azimuth 148 degrees and 79 nm (146 km) respectively, a

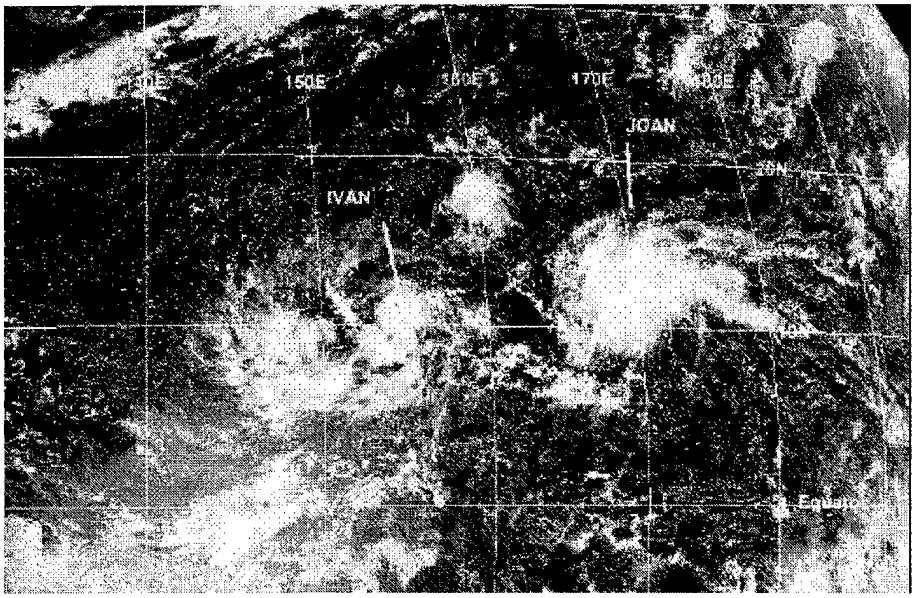

Figure 3-27/28-2. A high-contrast visible image shows the relative isolation of Ivan and Joan as they emerged from the near equatorial trough and moved west-northwestward across the relatively cloud-free basin (130132Z October visible GMS imagery).

maximum outbound velocity of 42 kt (22 m/sec), also at 7,000 ft (210 m). After passing Guam, Ivan became a typhoon at 150600Z, and then began to intensify at a fast rate (1.5 T numbers per day) (Figure 3-27/28-4). During the 48-hour period from 150600Z to 170600Z Ivan intensified from 65 kt (33 m/sec) to 145 kt (75 m/sec) approximately 3 T-numbers. The peak intensity of 160 kt (82 m/sec) was reached at 171800Z. On 16 October, Ivan slowed and began to track toward Luzon. Numerical guidance and the synoptic flow pattern suggested that the TC would recurve before reaching the Philippines. The anticipated northward turn did commence on 18 October, but it was too late to spare the Philippines. At approximately 191800Z October, the

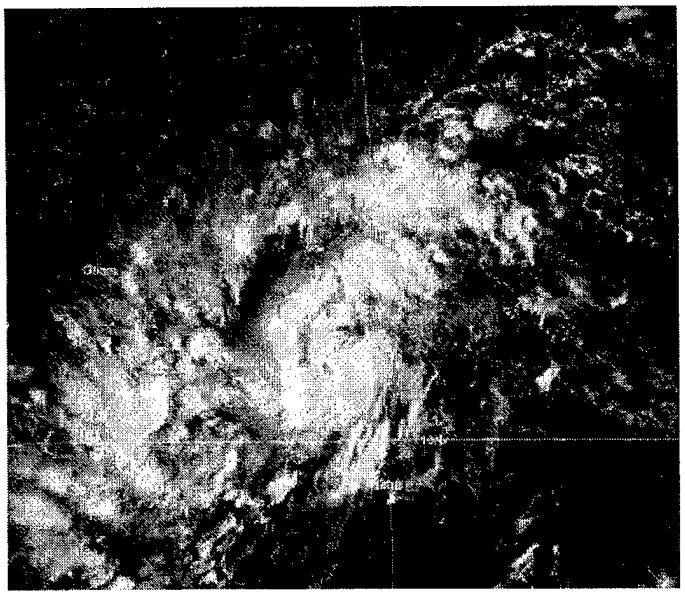

Figure 3-27/28-3 Ivan approaches Guam after becoming a tropical storm (132132Z October visible GMS imagery).

center of Ivan made landfall on the extreme northeastern tip of Luzon with an intensity of 120 kt (62 m/sec). On 20 October, the typhoon moved into the Luzon Strait and recurved. After recurving, it dropped below typhoon intensity on 21 October, then briefly reintensified to typhoon intensity on 22 October as it moved northeastward south of Okinawa. A steady weakening trend then set in, and the final warning was issued, valid at 241200Z, as the system became extratropical.

b. Joan (28W)

Joan (the easternmost of the Ivan-Joan pair) originated from a very poorly organized tropical disturbance in a near-equatorial trough that stretched across the eastern Caroline and Marshall Island groups (see Figure 3-27/28-1). The system was first mentioned on the 110600Z October ABPW. Animated satellite imagery and synoptic data indicated the possible presence of a low-level circulation in association with an area of deep convection at a low latitude near 4N 176E. Synoptic data indicated that equatorial westerlies were present to the south of this disturbance. The pre-Ivan tropical disturbance -- located further to the west -- was also first noted on this advisory. The pre-Joan tropical disturbance moved northwestward, and was north of 10N by 13

October. With an increase in the areal coverage and organization of deep convection, a TCFA was issued valid at 130400Z October.

The system now made a turn to the left and began to track to the west and slowly intensify. The first warning on TD 28W was issued, valid at 130600Z, based on satellite intensity estimates of 25 kt (13 m/sec). The system was expected to intensify at a climatological rate. Based upon satellite intensity estimates of 35 kt (18 m/sec), TD 28W was upgraded to Tropical Storm Joan (28W) on the warning valid at 140600Z. The system now tracked just north of due west, approached the Mariana Islands, and intensified. After becoming a typhoon, between 151200Z and 151800Z, Joan began to intensify very rapidly, increasing from 70 kt (36 m/sec) at 151800Z to its peak of 160 kt (82 m/sec) 36 hours later (Figure 3-27/28-5a,b). The equivalent pressure fall of 100 mb over this 36-hour period, for an average of 2.8 mb per hour, qualifies as a case of explosive deepening (Dunnavan 1981). As it approached the Mariana Islands, Joan made turned to the northwest. Weakening slightly, it passed between the Islands of Saipan and Anatahan on the morning of 18 October (see the Impact Section for details on the effects of Joan on the Marianas). Its well-defined eye was tracked by Guam's NEXRAD as it passed to the north. However, at a range of 155 nm (287 km) from the site, it was beyond Doppler radial velocity range. Joan remained at or above the super typhoon threshold (130 kt, 67 m/sec) for 4.5 days (170000Z to 211200Z) -- a record. Moving slowly, but making a sharp recurve during the 48-hour period 200000Z to 220000Z , Joan weakened steadily from 140 kt (72 m/sec) to 115 kt (59 m/sec). On 23 October, Joan moved eastward along 30N and continued to weaken. On 24 October, the system turned toward the northeast and accelerated. The final warning was issued, valid at 240000Z, when it appeared that Joan was transitioning into an intense extratropical low. In postanalysis, Joan remained at typhoon intensity until 241800Z, and its transition into an extratropical low was completed at 251800Z.

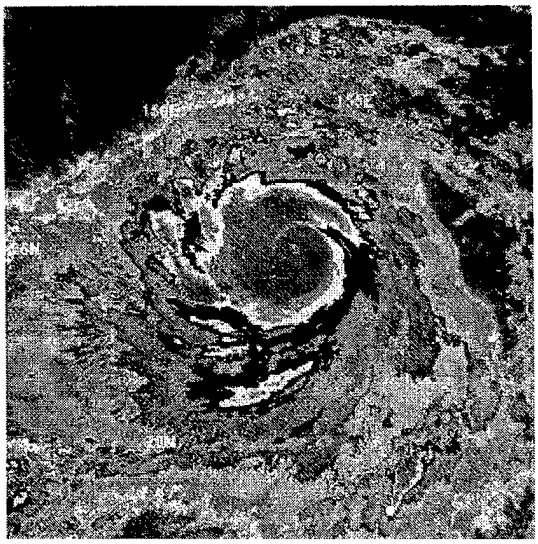

Figure 3-27/28-4 Ivan becomes the year's eighth super typhoon (161913Z October enhanced IR DMSP imagery). Enhancement curve is "BD".

III. DISCUSSION

a. On the extreme intensities reached by Ivan and Joan

Ivan and Joan both emerged from a near equatorial trough in the Marshall Islands. As the two TCs moved west-northwestward in tandem, they both intensified to an extreme value of 160 kt (82 m/sec) -- two of three WNP TCs to do so during 1997 (the other was STY Paka (05C)). At 171200Z, Ivan was at 155 kt (80 m/sec) while Joan was still at 160 kt (82 m/sec); the first time noted that two TCs of such extreme intensity existed simultaneously in the WNP basin (Figure 3-27/28-6a,b). On the enhanced infrared image of Figure 3-27/28-5b, Joan's cold dark-gray eye

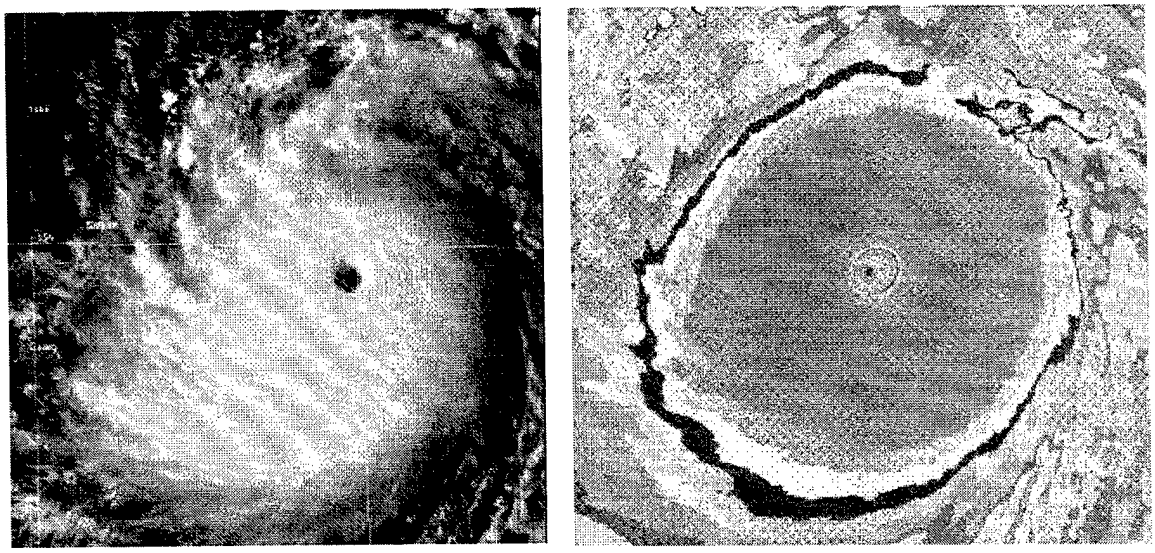

Figure 3-27/28-5 Joan reaches its peak intensity of 160 kt (82 m/sec). (a) The low sun-angle of late afternoon helps highlight features on the tops of Joan's eye wall cloud (170632Z October visible GMS imagery). (b) The cold dard gray ring surrounding Joan's eye-indicative of temperatures of -81C or colder-puts Joan off the scale of Dvorak's intensity estimation techniques using enhanced IR imagery (170803Z October enhanced IR DMSP imagery). Enhancement curve is "BD"

wall cloud (indicating cloud-top temperatures of -81 degrees C or colder), is off of Dvorak's scale for subjectively determining TC intensity from infrared imagery (Dvorak 1984). The Digital Dvorak (DD) algorithm, however, has no intrinsic upper bound (although there may be actual physical upper limits), and the DD numbers for both Ivan and Joan (Figure 3-27/28-7a,b) reached T8.0 (hypothetically equivalent to 170 kt (87 m/sec) intensity). Since 1995, the highest DD number computed for a typhoon by the DD algorithm on the satellite image processing equipment at JTWC was T8.3 for Super Typhoon Angela (29W) (1995), as it approached the Philippines. No other TC since then has reached a DD number of 8.0 or higher. Why these two TCs became so intense is unknown. Early in their lives, neither objective guidance nor human forecaster anticipated the extreme intensities that Ivan and Joan would reach. The initial disturbances from which they developed were very poorly organized and were isolated in an environment that was unusually free of deep convection. The monsoon trough across the WNP was relatively weak and sea-level pressures were near or above normal. For Ivan, nearly every intensity forecast leading up to its peak was low by as much as 40 kt (21 m/sec) for the 12-hour forecast, and 45, 50, 45, and 50 kt for the 24-, 36-, 48-, and 72-hour forecasts respectively. For Joan, the intensity forecasts were even lower: nearly all forecasts for the entire life of the TC were too low. Leading up to its peak, the intensity forecasts for Joan were low by as much as 30, 55, 65, 65, and 65 kt for the 12-, 24-, 36-, 48-, and 72-hour forecasts respectively. Despite the passage of these two TCs across much of the WNP basin, the monthly average wind for October (Figure 3-3) was more easterly than normal everywhere except in the low-latitudes east of 150E (an El Niño-related anomaly).

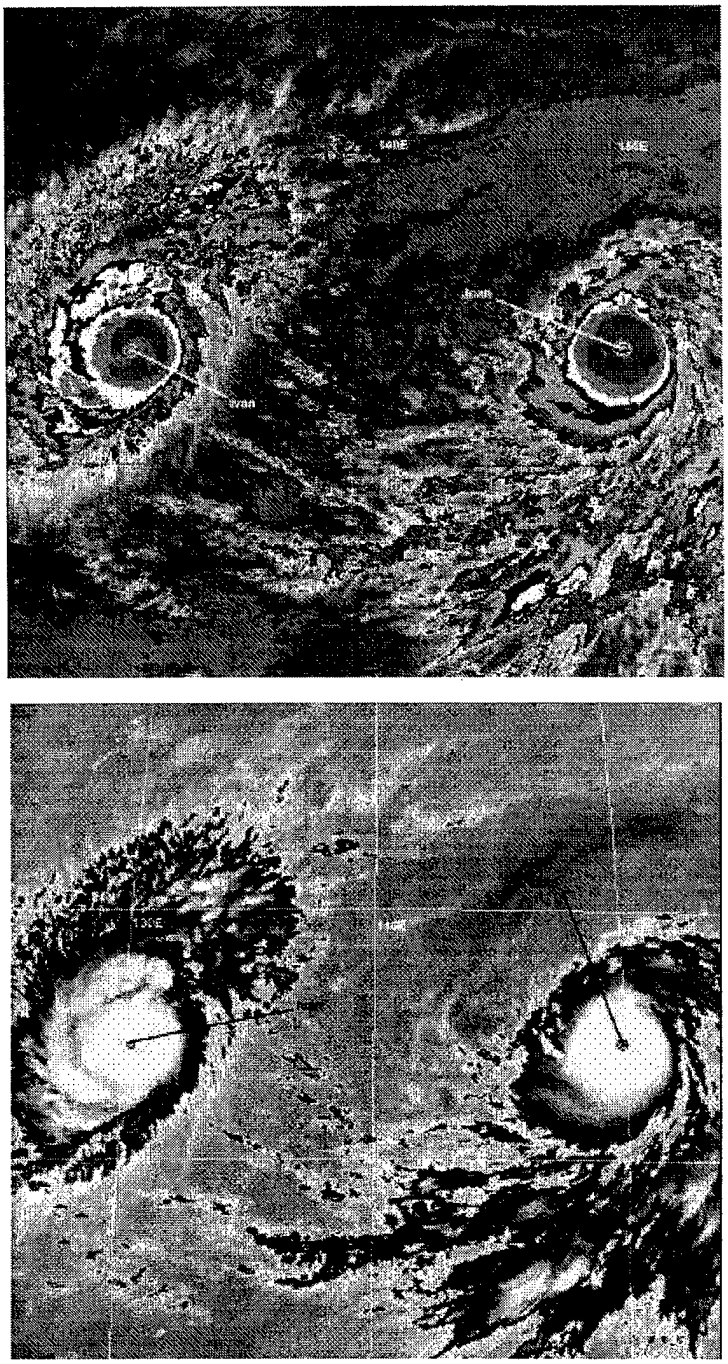

Figure 3-27/28-6 For the first time observed, two spatially proximate super typhoons coexisted in the WNP with near-record intensities. At the time of these images, Ivan is at 145 kt (75 m/sec) intensity and Joan is at 160 kt (82 m/sec) intensity. (170632Z October enhanced IR GMS imagery.) Enhancement curve in (a) is "BD", and enhancement curve in (b) is "MB".

b. TC-TC interactions?

In the Systematic and Integrated Approach to Tropical Cyclone Forecasting (Elsberry 1994) there are three basic modes of interactions between two spatially proximate TCs: 1) direct TC interaction (whereby each TC is advected by the flow of the other); 2) semi-direct TC interaction (whereby each TC is advected by the altered flow between the other TC and the high pressure system on the opposite side); and, 3) indirect TC interaction (whereby the TC to the west induces a ridge between the two TCs which, in turn, imposes an equatorward component to the steering flow on the eastern TC). In order to study the interaction between two TCs, it is best to produce a diagram illustrating the motion of each TC with respect to their centroid. Properties of the centroid-relative motion help to reveal the nature of the interaction (which is not always apparent in the actual earth-relative tracks). In the case of Ivan and Joan, the centroid-relative motion (Figure 3-27/28-8) does not seem to indicate that any form of TC interaction took place.

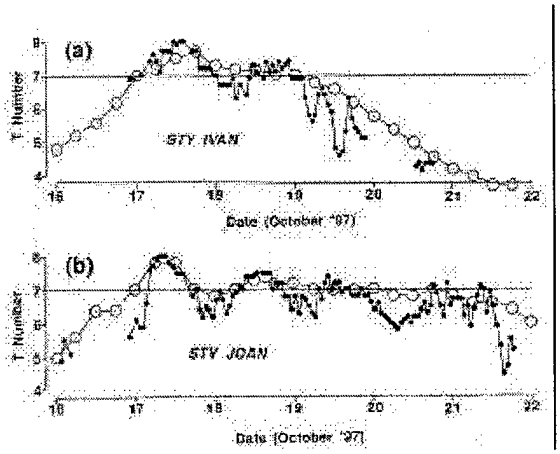

Figure 3-27/28-7 A time series of (a) Ivan's, and (b) Joan's hourly DD numbers (small black dots) compared with the best-track intensity (open circles). Both Joan and Ivan reached an extreme DD magnitude of 8.0 (equivalent to an intensity of 170 kt (87 m/sec)). There is a slight diurnal cycle apparent in these time series with a tendency for higher DD numbers just prior to sunrise (1800Z).

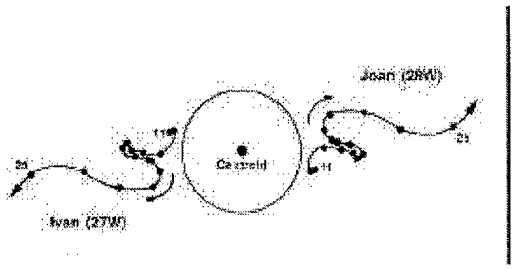

Figure 3-27/28-8 The centroid-relative motion of Ivan and Joan. Black dots indicate positions at 0000Z at 24-hour intervals beginning on 11 October and ending on 25 October. The inscribed circle has a diameter of 600 nm (1100 km).

Although initially within the 780-nm (1446 km) threshold noted by Brand (1970) for mutual cyclonic rotation about the centroid to dominate, very little centroid-relative cyclonic orbit is noted for the period. The common features of TC interaction noted by Lander and Holland (1993) of mutual approach followed by a period of stable cyclonic orbit are also missing. Only the rapid increase of separation distance as the two TCs recurved is a typical feature of binary interaction noted by Lander and Holland. This so-called "escape" phase indicates that the binary interaction has ceased. In summary, Ivan and Joan appear to have undergone no form of TC interaction. They simply moved along similarly shaped adjacent recurving tracks and, recurving

at approximately the same time, the centroid relative motion became one of rapid increase in separation distance as Joan recurved east of Ivan and accelerated faster into the midlatitudes

IV. IMPACT

Both Ivan and Joan affected the Mariana Islands. On the night of 14 October, Ivan passed 55 nm (100 km) to the south of Guam where a peak wind gust of 41 kt (21 m/sec) was recorded at Andersen Air Force Base; the heaviest 24-hr rainfall of 5.85 inches was also recorded at Andersen. Ivan also affected the Philippines. At least one person was reported drowned and another missing on the northeastern tip of Luzon. Ivan damaged thousands of houses and destroyed large amounts of rice and corn in this region. More than $US 500,000 worth of fish stocks in ponds and cages were also destroyed. Joan largely spared the Mariana Islands any significant damage when it passed between the Islands of Saipan and Anatahan on 18 October. Peak wind gusts of 85 kt (44 m/sec) were experienced on Saipan when Joan passed approximately 45 nm (80 km) to the north. A Red Cross initial assessment indicated that Joan destroyed four houses, caused major damage to 15 other tin and wood structures and caused minor damage to 17 homes on Saipan. On Guam, winds gusted to only 33 kt (17 m/sec) at the commercial port on the west side of the island.

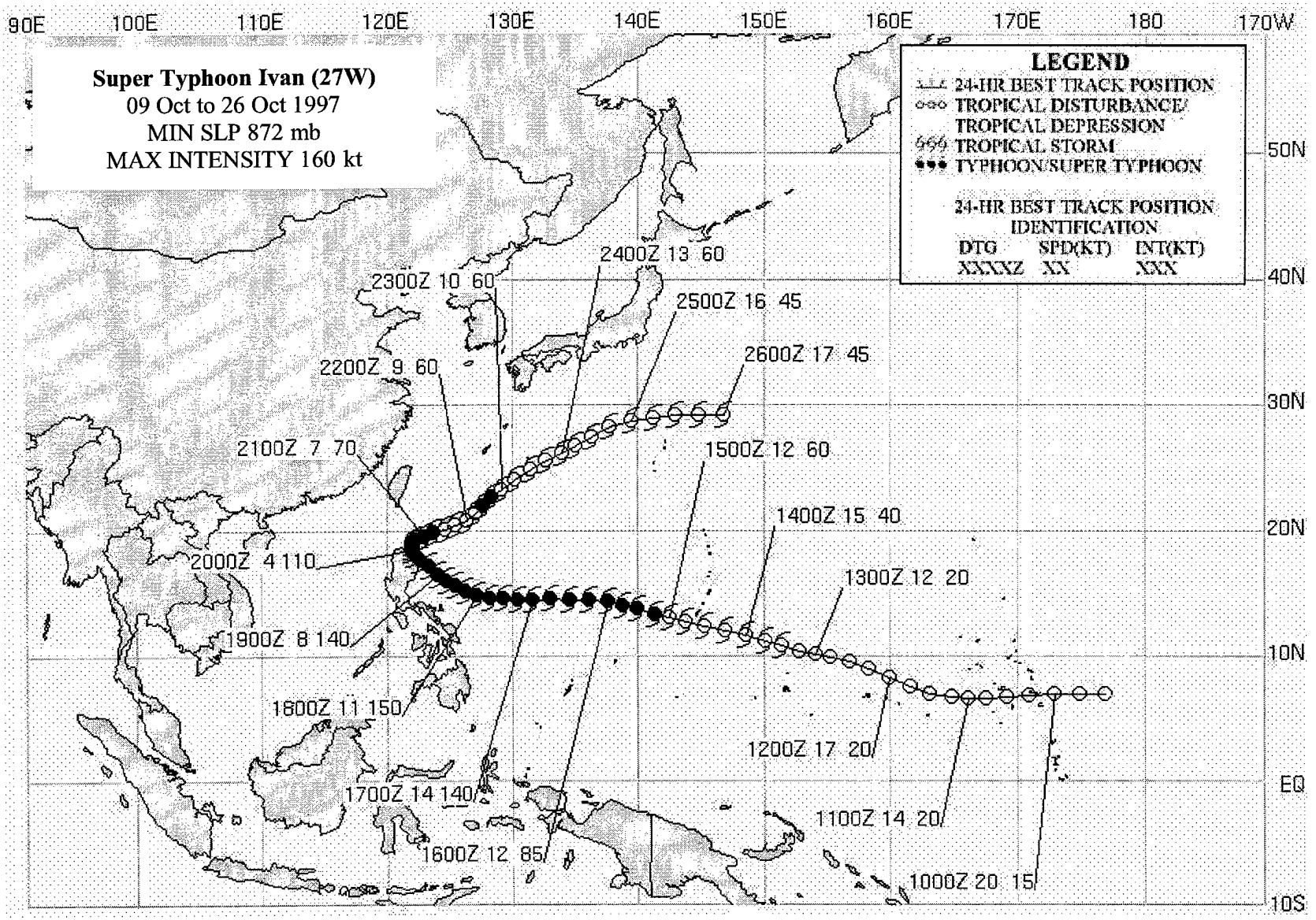
Super Typhoon Ivan (27W)
09 Oct to 26 Oct 1997
MIN SLP 872 mb
MAX INTENSITY 160 kt
LEGEND
24-HR BEST TRACK POSITION
TROPICAL DISTURBANCE/
TROPICAL DEPRESSION
TROPICAL STORM
TYPHOON/SUPER TYPHOON
24-HR BEST TRACK POSITION
IDENTIFICATION
DTG SPD(KT) INT(KT)
XXXXZ XX XXX
90E
100E
110E
120E
130E
140E
150E
160E
170E
180
170W
50N
40N
30N
20N
10N
EQ
10S
2400Z 13 60
2300Z 10 60
2500Z 16 45
2600Z 17 45
2200Z 9 60
2100Z 7 70
1500Z 12 60
1400Z 15 40
2000Z 4 110
1300Z 12 20
1900Z 8 140
1600Z 11 150
1200Z 17 20
1700Z 14 140
1100Z 14 20
1600Z 12 85
1000Z 20 15

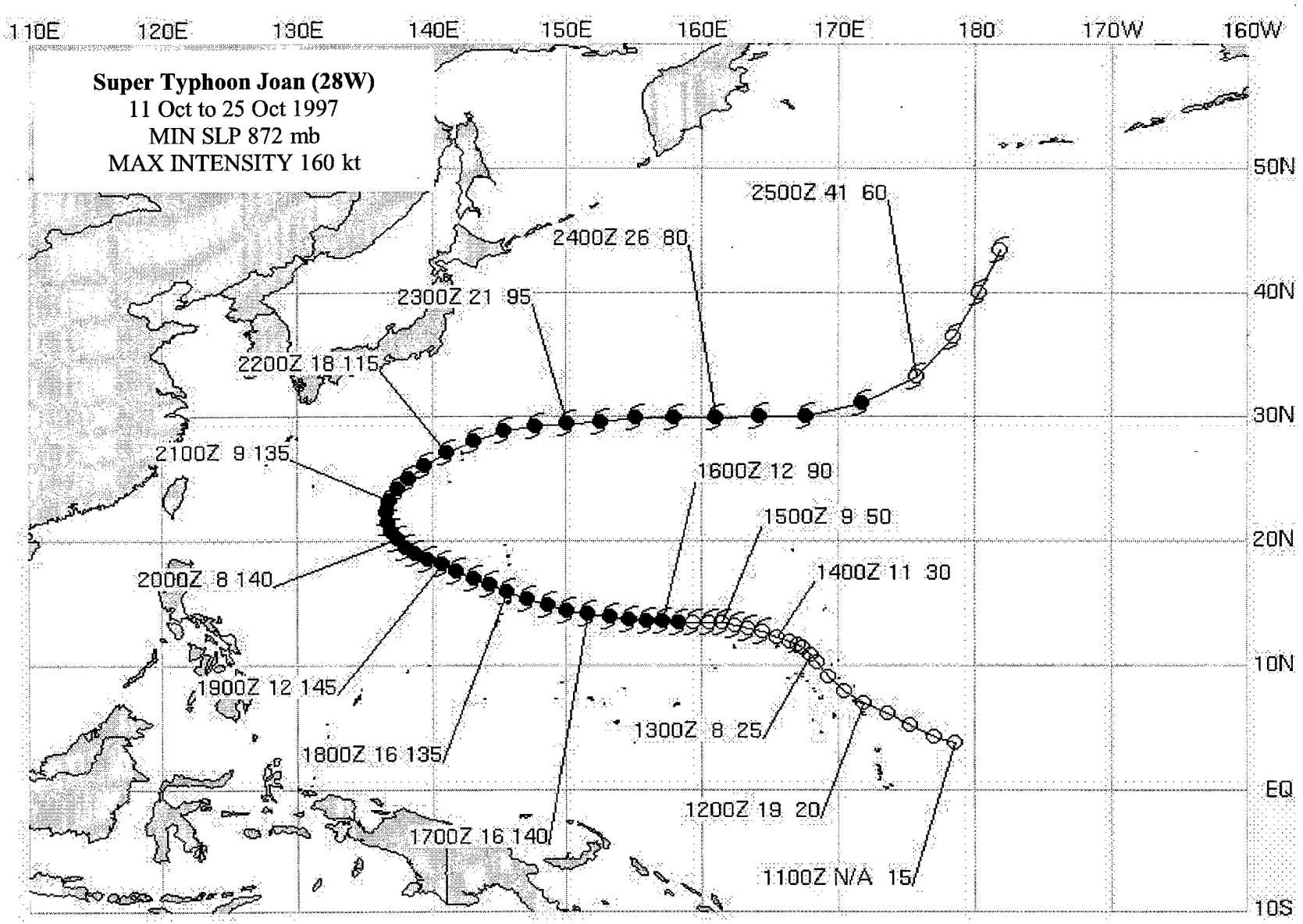
Super Typhoon Joan (28W)
11 Oct to 25 Oct 1997
MIN SLP 872 mb
MAX INTENSITY 160 kt
110E
120E
130E
140E
150E
160E
170E
180
170W
160W
50N
40N
30N
20N
10N
EQ
10S
2500Z 41 60
2400Z 26 80
2300Z 21 95
2200Z 18 115
2100Z 9 135
1600Z 12 90
1500Z 9 50
1400Z 11 30
2000Z 8 140
1900Z 12 145
1300Z 8 25
1800Z 16 135
1200Z 19 20
1700Z 16 140
1100Z N/A 15

SUPER TYPHOON KEITH (29W)

I. HIGHLIGHTS

The tenth of eleven tropical cyclones (TCs) to attain super typhoon intensity in the western North Pacific during 1997, Keith formed at low latitudes in the Marshall Islands. It was one of ten TCs which formed east of 160E and south of 20N — within the "El Niño" box in Figure 3-3a. Keith was a recurving TC which passed between the Islands of Rota and Tinian (only 50 nm (93 km) apart) on the west-bound leg of its recurving track. NEXRAD imagery from Guam indicated the eye wall cloud of Keith never touched land as it threaded the narrow channel between these two islands. As such, the Mariana Islands were spared the full force of Keith (see the Impacts Section). Keith's compact wind and cloud structure were revealed by Guam's NEXRAD (see the Discussion Section). Equatorial westerly winds bounded by twin near-equatorial troughs preceded the formation of Keith and a Southern Hemisphere twin, TC 03P 98.

II. TRACK AND INTENSITY

During most of October, low-latitude, low-level, westerly winds blew along the equator from approximately 150E and eastward across the international dateline to near 170W. Twin near-equatorial troughs (one in the Northern Hemisphere, another in the Southern Hemisphere) bounded these westerly winds and most of the region's deep convection. During the first week of October, deep convection increased between the twin troughs in association with an equatorial westerly wind burst; and then, during the second week of October, it decreased as three TCs emerged from the twin near-equatorial trough synoptic flow pattern: Ivan (27W) and Joan (28W) in the Northern Hemisphere, and a twin, Lusi (02P98), in the Southern Hemisphere.

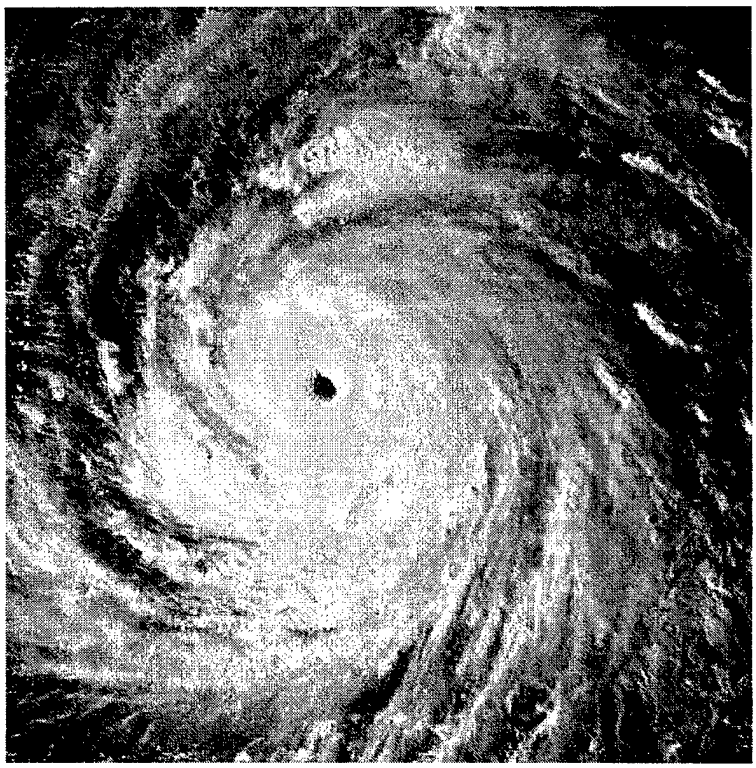

Figure 3-29-1 A low evening sun angle brings out the relief in Keith's clouds. From the satellite perspective, it is hard to imagine that the eye wall cloud, and the extreme winds remained over water between the relatively closely spaced islands of the Marianas (020632Z November visible GMS imagery).

When Ivan (27W) and Joan (28W) began to recurve, deep convection once again increased in the aforementioned region, and two more TCs emerged from the twin near-equatorial trough flow pattern: Keith developed in the Marshall Islands, and a Southern Hemisphere twin, TC 03P98, moved south between Fiji and the Islands of Vanuatu. An area of deep convection located in the Marshall Islands was, for several days (beginning at 181730Z October), mentioned on the Significant Tropical Weather Advisory (ABPW). Deep convection (in varying amounts) persisted in the Marshalls, and in postanalysis, the area of deep convection that could be unambiguously linked to the low-level circulation center which became Keith was mentioned on the 230600Z ABPW. This area of deep convection moved slowly westward and remained poorly organized for three days. On 26 October, the organization of the deep convection improved. Water-vapor derived winds showed anticyclonic outflow had become more symmetrical over the system, and synoptic data from Kwajalein and Majuro indicated falling sea-level pressure within a persistent low-level circulation. These factors prompted JTWC to issue a Tropical Cyclone Formation Alert (TCFA) at 260500Z October. During the valid period of this TCFA, the system failed to develop into a significant TC. Since conditions still appeared to be favorable for the formation of a significant TC, a second TCFA was issued at 270500Z. During the night of 27 October, the deep convection became better organized, and based on satellite intensity estimates of 25 kt (13 m/sec), the disturbance was upgraded to Tropical Depression (TD) 29W on the warning valid at 271800Z. On the morning of 28 October, satellite intensity estimates increased to 35 kt (18 m/sec) and TD 29W was upgraded to Tropical Storm Keith at 280000Z. At this time, Keith was anticipated to develop at a normal rate of one T-number per day, and move toward the west-northwest.

For two days, beginning on 280000Z, Keith intensified slowly, increasing by only one T-number (i.e., from 35 kt (18 m/sec) at 280000Z to 55 kt (28 m/sec) at 300000Z). Then, like Ivan (27W) and Joan (28W) before it, Keith underwent a period of rapid intensification which was unforeseen. By 310000Z, Keith had intensified to 105 kt (54 m/sec). The equivalent pressure drop of 43 mb in 24 hours (for an average of 1.79 mb/hr) qualifies as a case of rapid deepening (Holliday and Thompson 1979). Keith continued to intensify rapidly until 011200Z November when it reached its peak of 155 kt (80 m/sec).

When it reached its peak intensity, Keith was moving west-northwest and was just over a day away from passing through the Mariana Island chain. During the 6 hour period 020600Z-021200Z November, Keith passed between the Islands of Rota and Tinian. Though weakened slightly from its peak, it was still a powerful 140 kt (72 m/sec) super typhoon (Figure 3-29-1) as it made its closest approach to these islands. Fortunately, as Guam's NEXRAD showed, the eye wall cloud of Keith remained over water, and no island experienced the full force of Keith, although some damage was reported (see the Discussion and the Impact Sections).

Keith remained at or above super typhoon intensity for three-and-one-half days (311800Z October to 030600Z November), dropped to 125 kt (64 m/sec) for two warning times at 031200Z and 031800Z, and became a super typhoon briefly again for two warning times at 040000Z and 040600Z. Then, late on 04 November, Keith slowed, weakened, and began to recurve. For two days (05-06 November), Keith moved slowly northeastward and continued to weaken. On 07

November, Keith turned more eastward, weakened further, and began its acceleration in the westerly flow to the north of the subtropical ridge. The final warning was issued, valid at 0812200Z, as Keith raced east-northeastward with a translation speed of 45 kt (23 m/sec) and became extratropical.

III. DISCUSSION

a. Keith's structure as revealed by Guam's NEXRAD

As Keith moved between the islands of Rota and Tinian on 02 November, it passed well within the range of Guam's NEXRAD. The most striking aspect of the NEXRAD data was the compact structure of the TC core. A 5-nm-wide (9-km-wide) eye wall cloud surrounded a 20-nm-wide (37-km-wide) eye at beam altitude of approximately 7,000 ft (2134 m) (Figure 3-29-2a). The base velocity product (Figure 3-29-2b) showed that winds in excess of 100 kt were occurring in the eye wall cloud. Peak NEXRAD-observed winds of 135-140 kt (69-72 m/sec) were found in the eye wall cloud; and, as a velocity cross section (Figure 3-29-2c) revealed, these highest wind speeds were found at the lowest altitudes of the cross section.

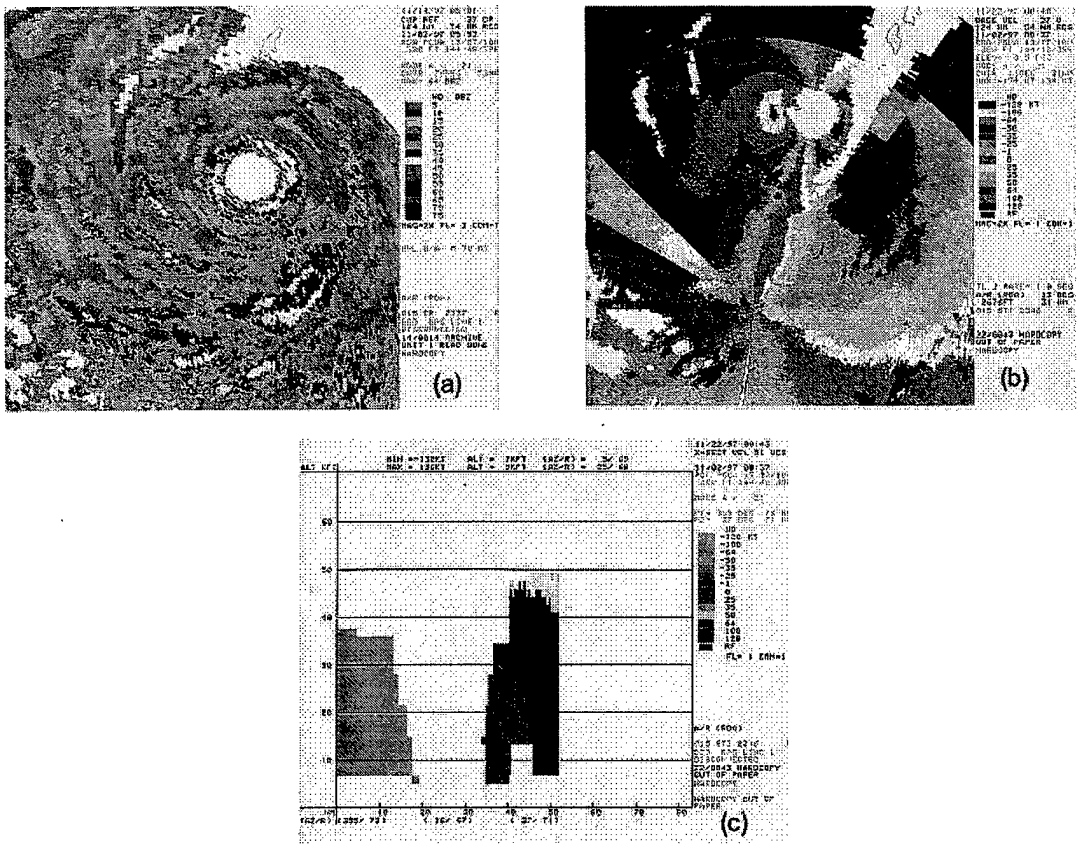

Figure 3-29-2 (a) Keith's eye and eye wall cloud pass between the islands of Rota and Tinian (020553Z November NEXRAD Composite Reflectivity product). (b) A dramatic couplet of high inbound wind and high outbound winds within Keith's eye wall cloud is revealed by the NEXRAD (020837Z November NEXRAD Base Velocity product). Note the narrow width of the region of inbound and outbound winds of 128 kt (66 m/sec) or

greater. (c) Typical of the structure of warm-core vortices, the peak azimuthal flow is at the lowest levels of the vortex and decreases with height (020837Z November NEXRAD velocity cross section in an east-west slice through Keith's eye).

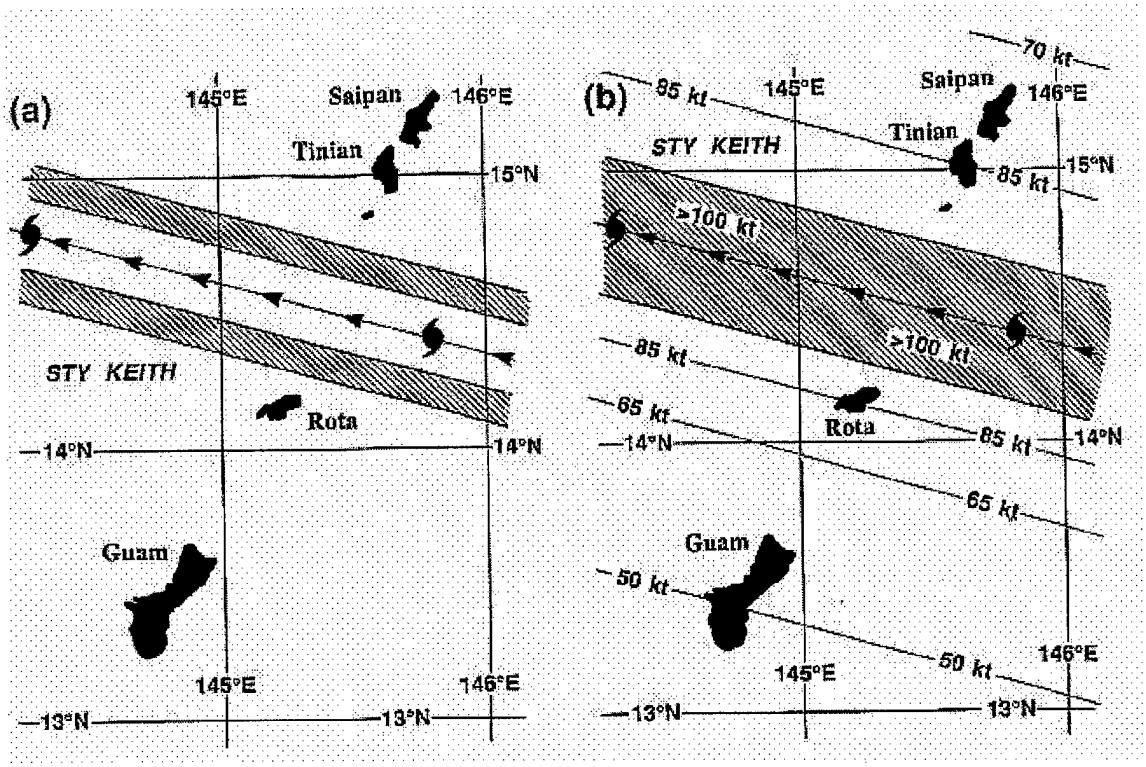

Figure 3-29-3 (a) The path of Keith's eye through the Marianas as depicted by Guam's NEXRAD. The typhoon symbols indicate the position of Keith at 020600Z and 021200Z November. The path of the 5-nm-wide (9-km-wide) eye wall cloud is indicated by the hatched swaths. (b) The wind distribution of Keith as it passed through the Marianas based upon the NEXRAD Base Velocity product, and from synoptic data from Guam and Saipan. Winds of 100 kt (51 m/sec) or greater occurred in Keith's eye wall cloud. An asymmetry in the wind field has been introduced by considering Keith's 15-kt (28-km/hr) speed of translation.

The NEXRAD data showed that the eye-wall cloud of Keith did not touch any land as it passed between islands only 50 nm (93 km) apart (Figure 3-29-3a). Also, the base velocity measurements (coupled with synoptic reports from the islands) indicated that sustained winds in excess of 100 kt (51 m/sec) most likely did not occur on any of the islands (Figure 3-29-3b), but passed between them in the same 30-nm-wide (56-km-wide) swath as traversed by the eye wall cloud. The super typhoon pictured in Figure 3-29-1 passed through the Marianas and left the islands relatively untouched. On a clear day, free of salt haze, each of the Mariana Islands can be viewed from the shores of its immediate neighbors. It is hard to imagine, viewing the neighbor islands from the shore, that the eye, eye wall cloud, and the destructive winds of a super typhoon can all fit over the waters of the channel and largely spare the islands. In Paka's (05C) summary, this is borne out even more dramatically. As Paka passed over the northern half of the island of Guam, wind gusts of approximately 150 kt (77 m/sec) and major damage to vegetation and structures were experienced on the parts of the island where the eye wall cloud passed, while

only 10 nm (20 km) to the south, outside of the eye wall cloud, gusts reached only to minimal typhoon intensity and little damage to structures or vegetation was noted.

b. Keith's Digital Dvorak (DD) time series

Keith was one of several typhoons during 1997 for which a time series of its hourly DD-numbers (Figure 3-29-4) was calculated. Keith's DD-numbers are unusually well-behaved. During the two-day period 010000Z-030000Z November, the DD-numbers fluctuated only a few tenths above and below T 7.0. The eye was obscured by cirrus on 03 November (possibly as a manifestation of an eyewall replacement cycle), but then reappeared and became well-defined on 04 November as Keith neared its point of recurvature. Keith's DD time series shows little or no diurnal variation, which for some typhoons is quite prominent. Why some typhoons show a strong diurnal signal in the DD-numbers and why others do not is an unsolved mystery.

c. Asymmetries in pressure fluctuations on microbarographic recordings

In the microbarograph trace of the pressure recorded at JTWC as Keith passed to the north of the station (Figure 3-29-5), an asymmetry is observed in the small fluctuations of pressure which are superimposed on the general longer period trends: the fall of pressure as the typhoon approaches is smoother than the rise of pressure after the TC is moving away from the station. This feature is presented here, because it also occurs in pressure traces from two different locations recorded as Super Typhoon Paka (05C) passed over Guam. While only a curiosity with perhaps a simple explanation, its repeated occurrence in two different typhoons, and at two separate locations during the same typhoon, raises the level of interest.

IV. IMPACT

Despite its track between the islands, Keith caused damage on Rota, Tinian, and Saipan in the Marianas. Red Cross officials reported that at least 790 houses were destroyed or damaged on these islands. About 15 power poles were reported downed on Saipan, and 20 on Tinian. Wind gusts of 95 kt (49 m/sec) were reported at Saipan's International Airport. Sea-level pressures fell to 964 mb on Rota and to 977 mb on Saipan. On Guam, little damage occurred, but power was knocked out to the entire island for nearly a day. Wind gusts reached 67 kt (35 m/sec) and nearly 6 inches of rain fell on parts of the island. Very large surf from the east deposited rubble on the coastal road on the southeast side of the island, forcing officials to close the road.

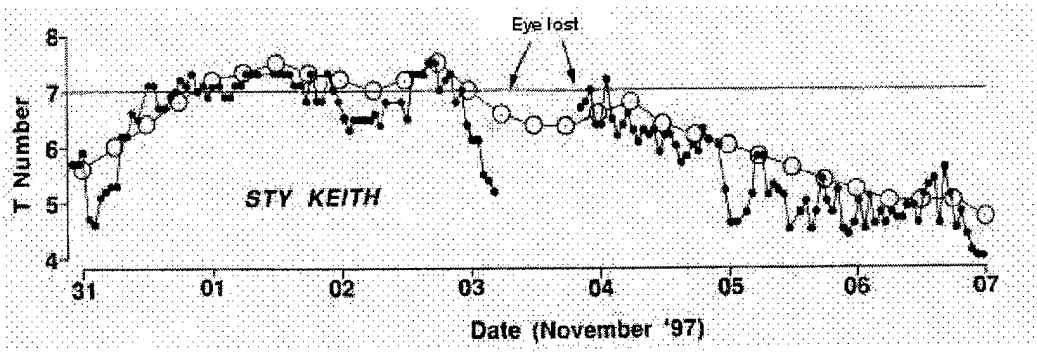

Figure **3-29-4** A time series of Keith's hourly DD numbers (small black dots) compared with the best-track intensity (open circles).

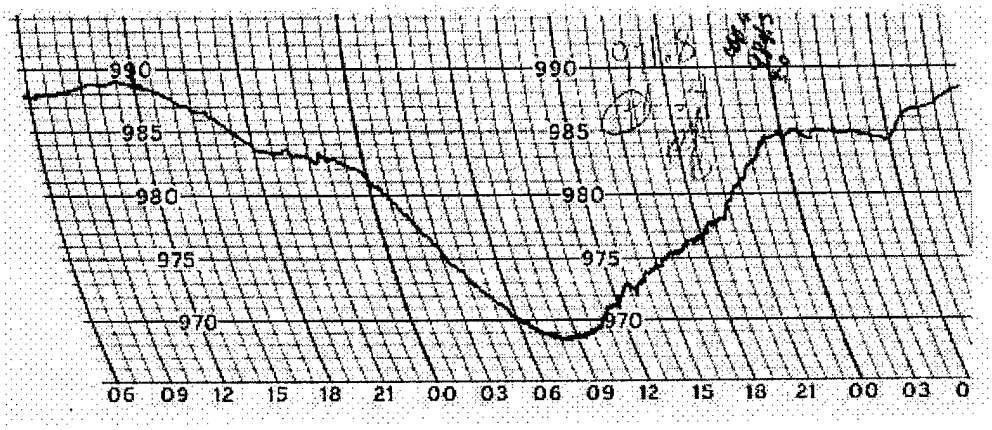

Figure 3-29-5 Microbarograph trace of the station pressure (in millibars) at the JTWC as Keith passed to the north of the island. At the 600-ft (183-m) elevation of the station approximately 18.5 mb must be added to obtain an estimate of the SLP. Note the smooth fall of pressure followed by and increase in small fluctuations as the pressure begins to rise.

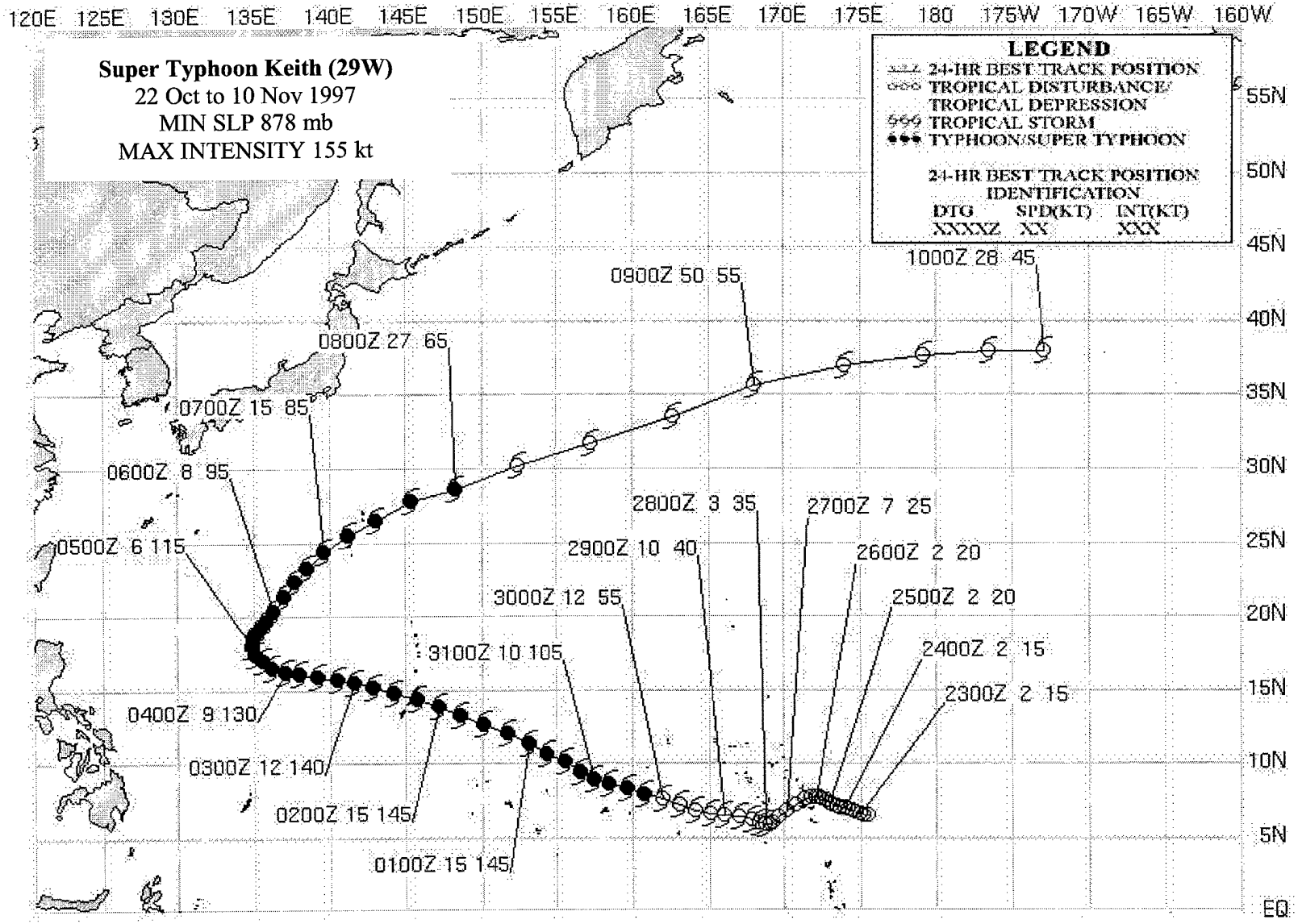
120E 125E 130E 135E 140E 145E 150E 155E 160E 165E 170E 175E 180 175W 170W 165W 160W
55N 50N 45N 40N 35N 30N 25N 20N 15N 10N 5N EQ
Super Typhoon Keith (29W)
22 Oct to 10 Nov 1997
MIN SLP 878 mb
MAX INTENSITY 155 kt
LEGEND
24-HR BEST TRACK POSITION
TROPICAL DISTURBANCE/ TROPICAL DEPRESSION
TROPICAL STORM
TYPHOON/SUPER TYPHOON
24-HR BEST TRACK POSITION IDENTIFICATION
DTG SPD(KT) INT(KT)
XXXXZ XX XXX
1000Z 28 45
0900Z 50 55
0800Z 27 65
0700Z 15 85
0600Z 8 95
0500Z 6 115
2800Z 3 35
2700Z 7 25
2900Z 10 40
2600Z 2 20
3000Z 12 55
2500Z 2 20
3100Z 10 105
2400Z 2 15
2300Z 2 15
0400Z 9 130
0300Z 12 140
0200Z 15 145
0100Z 15 145

TYPHOON LINDA (30W)

The tropical disturbance that would become Typhoon Linda (30W) formed within an area of convection east of the Philippine Islands near 10N 130E on 26 October. The disturbance was mentioned in the Significant Tropical Weather Advisory (ABPW) as it tracked westward over the next several days under the subtropical ridge to the north. Convection began to increase over the disturbance as it entered the Sulu Sea on 30 October. At 0730Z on the 31st, a Tropical Cyclone Formation Alert (TCFA) was issued as deep convection continued to organize about the disturbance's center. The first warning on Tropical Depression (TD) 30W was issued approximately 12 hours later.

The newly formed tropical cyclone reached tropical storm intensity within 24 hours as it tracked over the South China Sea. At this point, Tropical Storm Linda (30W) accelerated westward toward the southern tip of Vietnam. It tracked over the Vietnamese province of Ca Mau at 0900Z on 02 November with an intensity of 55 kt (28 m/sec).

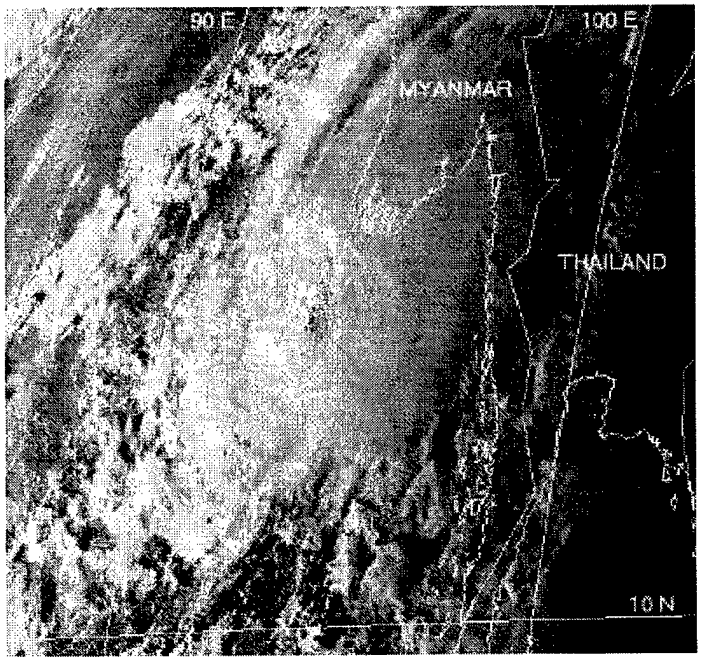

Figure 3-30-1 Typhoon Linda (30W) re-intensifying over the Andaman Sea after crossing the Malay Peninsula (051025Z November visible GMS imagery).

Linda reached typhoon intensity shortly after entering the Gulf of Thailand. The cyclone turned northwestward following steering from the subtropical ridge. The system weakened slightly to 55 kt (28 m/sec) prior to striking the Malay Peninsula at 1600Z on 03 November. Crossing the Malay Peninsula, Linda further weakened as it encountered the region's 3000 ft (914 m) to 5000 ft (1524 m) mountains. However, once over the warm waters of the Andaman Sea, the system began to reconsolidate. This was the first tropical cyclone since Typhoon Forrest (30W) in 1992 to cross from the Western North Pacific to the North Indian Ocean.

Soon after moving into the Andaman Sea, a weakness in the subtropical ridge began to develop to the north, causing Linda's forward speed to slow. Over open water once again, Linda reintensified and became a typhoon once again at 0000Z on the 6th. This was short-lived, however, as interaction with a mid-latitude trough began to introduce vertical wind shear. Linda stalled in the Bay of Bengal within an area of weak steering located between the subtropical

ridge axis at 500 mb and sub-tropical ridge axis at 200 mb. Upper level vertical wind shear continued across the system center, allowing slow weakening of the system for several days. By 10 November, Linda had dissipated.

Linda produced considerable damage and loss of life in Vietnam and Thailand. Vietnam's Ca Mau province, located to the northern side of Linda's passage, reported significant damage. Newspaper reports as late as 08 November indicated that at least 330 people were killed in Vietnam and Thailand with approximately 2250 people still missing. Many of the missing were Vietnamese fisherman or sailors caught at sea in the path of the tropical cyclone.

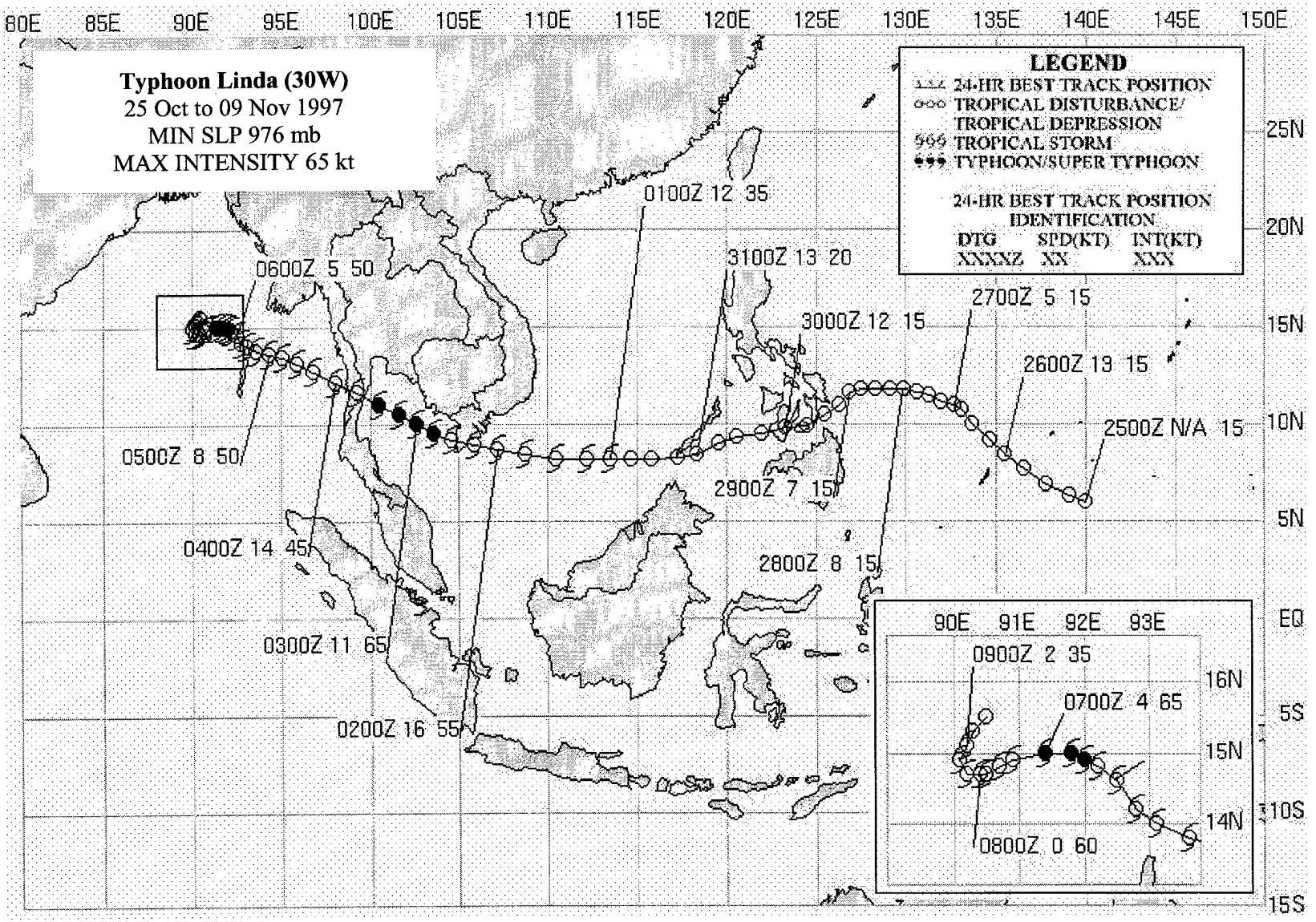
80E 85E 90E 95E 100E 105E 110E 115E 120E 125E 130E 135E 140E 145E 150E
25N
20N
15N
10N
5N
EQ
5S
10S
15S
Typhoon Linda (30W)
25 Oct to 09 Nov 1997
MIN SLP 976 mb
MAX INTENSITY 65 kt
LEGEND
24-HR BEST TRACK POSITION
TROPICAL DISTURBANCE/ TROPICAL DEPRESSION
TROPICAL STORM
TYPHOON/SUPER TYPHOON
24-HR BEST TRACK POSITION IDENTIFICATION
DTG SPD(KT) INT(KT)
XXXXZ XX XXX
0100Z 12 35
3100Z 13 20
0600Z 5 50
2700Z 5 15
3000Z 12 15
2600Z 19 15
2500Z N/A 15
0500Z 8 50
2900Z 7 15
0400Z 14 45
2800Z 8 15
0300Z 11 65
0200Z 16 55
90E 91E 92E 93E
16N
15N
14N
0900Z 2 35
0700Z 4 65
0800Z 0 60

TYPHOON MORT (31W)

I. HIGHLIGHTS

Typhoon Mort (31W) was the last tropical cyclone to form west of the international dateline (IDL) for the western North Pacific season. It tracked over the open waters of the Philippine Sea but vertical shear weakened it to a tropical depression by the time it made landfall over the island of Luzon.

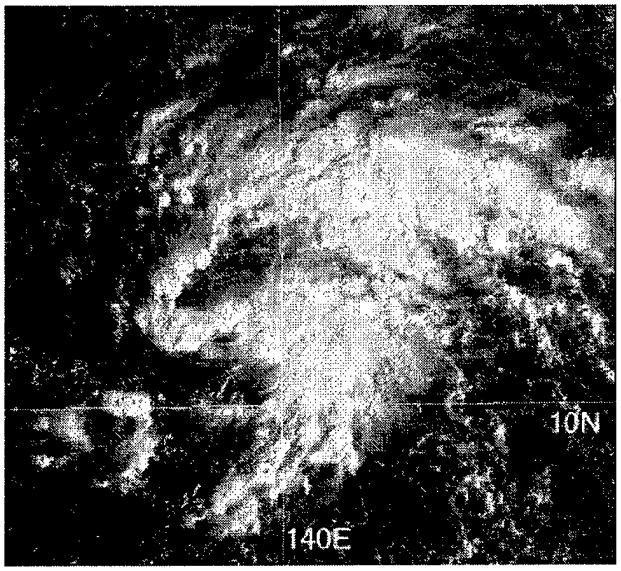

Figure 3-31-1 Visible satellite imagery of TD 31W; valid time is 102225Z November

II. TRACK AND INTENSITY

The disturbance that would become Typhoon Mort (31W) was first noted on the Significant Tropical Weather Advisory (ABPW) as an area of convection south of Guam on 08 November at 0600Z. The convection was located within a weak monsoon trough that stretched from the southern Philippine Sea to just south of Guam. An area of divergence overlaid the disturbance, which was located equatorward of mid-level ridging. By 09 November, the disturbance had become better organized with satellite imagery indicating a developing banding feature. Animation of satellite imagery also indicated some cyclonic motion within the convection. As development continued to progress, a Tropical Cyclone Formation Alert (TCFA) was issued at 1900Z on 09 November. The disturbance was upgraded to tropical depression (TD) status with a 101800Z warning. Figure 3-31-1 shows the TD just four and a half hours after this warning, and is an example of how a typical 25 - 30 kt (13 - 15 m/sec) system appears in visible satellite imagery.

The system tracked in a westerly direction at speeds of 7 to 9 kt (13 to 17-km/hr) due to easterly steering flow in the lower to mid-levels south of the subtropical ridge. This motion would continue for the remainder of the tropical cyclone's lifecycle. Figure 3-31-2 indicates the progression in development as seen by visible satellite imagery during a 66- hour period beginning at 0425Z on 11 November. The image at top left is Mort near the time it was upgraded to a tropical storm. Eighteen hours later (top right image), Mort is a strong tropical storm with winds estimated to be 55 kt (28m/sec). The system has a cold dense overcast over the center, with a good banding feature. Twenty-four hours later (bottom left image), the overall convective cloud structure is becoming disorganized, probably due to increased vertical wind shear relative to the moving system. At this time, Mort was at its peak intensity of 65 kt (33 m/sec), and would develop no further. Between 0600Z and 2100Z on the 13th, vertical wind shear caused the low-

level circulation to separate from the deep convection. The convection was sheared off to the east-southeast of the low-level circulation, which continued to track westward toward the Philippine Islands. The low-level circulation, and the associated convection can be seen in the image at bottom right. Due to the presence of an exposed low level circulation, the system was downgraded to tropical storm intensity (35 kt/ 18 m/sec) on the 14th at 0000Z. However, vertical wind shear lessened over the next day and a convective banding feature soon re-developed. This was only short-lived as vertical wind shear once again increased late on the 15th, eventually causing convection to shear to the south of the center. Mort proceeded to weaken to TD strength by 0600Z on the 16th and shortly thereafter made landfall on the island of Luzon. The system subsequently dissipated over the mountains within the island's interior.

III. DISCUSION

Unexpected Vertical Wind Shear

The shearing of Mort's convection on the 14th was unexpected and surprised JTWC forecasters. Strong vertical wind shear was not indicated by NOGAPS prognostic charts. Although animated satellite imagery indicated the system's development had arrested on the 13th, it didn't appear to indicate the presence of strong vertical wind shear. Some calculations were made using upper-level water vapor wind derived data (supplied by the University of Wisconsin) and the storm's motion. The upper-level wind data was used to find an average wind vector across the system center, and the storm's motion vector was used as a proxy for the lower-level wind vector. The difference between the two vectors gave the shear across the system center. Values were calculated for the 13th and 14th at 0000Z. The shear vector value more than doubled over the 24-hour period, changing from a west-southwest direction at 12 kt (22 km/hr), to west-southwest at 26 kt (48 km/hr). In a statistical study, Zehr (1992) found a shear value of 20 kt generally inhibits tropical cyclone development. This illustrates one of the ways in which water vapor wind derived wind data can help forecasters in evaluating tropical cyclones.

IV. IMPACT:

No reports of damage or injuries associated with Typhoon Mort (31W) were received by JTWC.

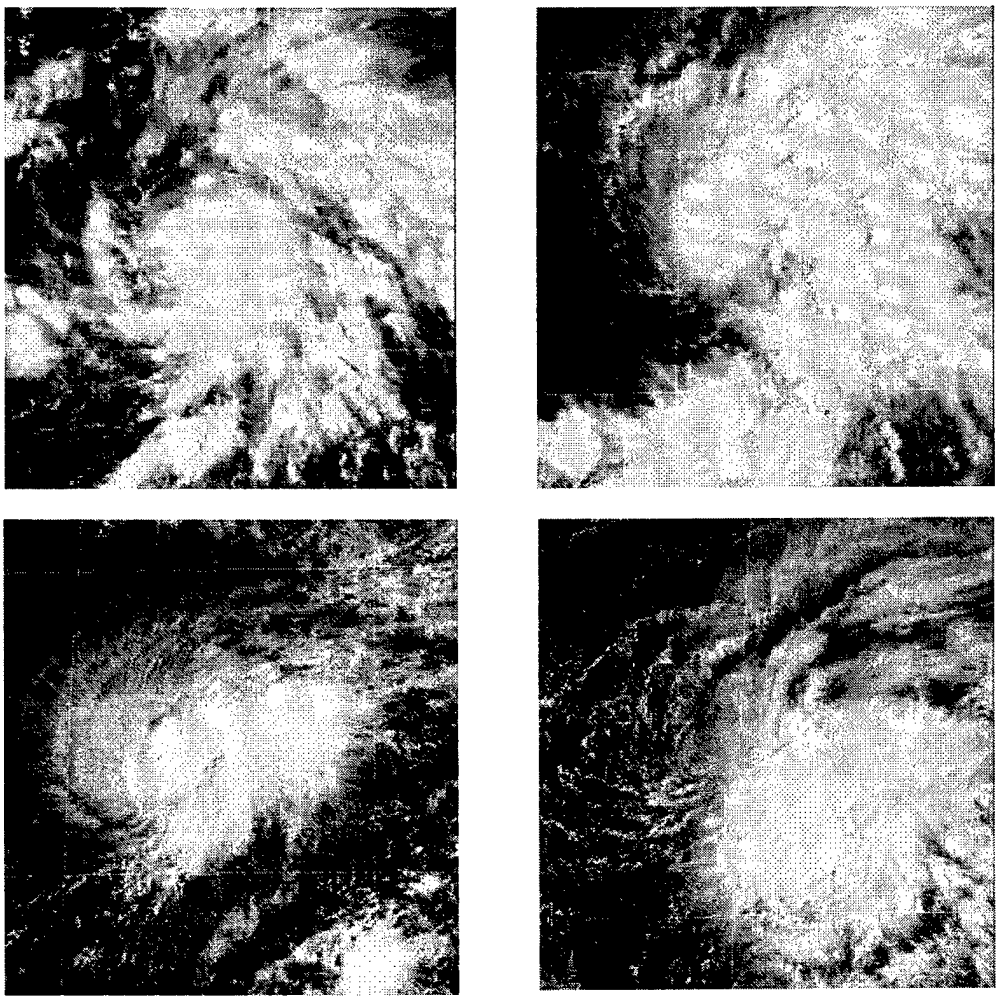

Figure 3-31-2 The different developmental stages of Typhoon Mort as seen by visible satellite imagery over a 66-hour period. Tropical cyclone best track intensities and valid times of imagery are: top left, 35 kt (18 m/sec) at 110425Z; top right, 55 kt (28 m/sec) at 112225Z; bottom left, 65 kt (33 m/sec) at 122225Z; bottom right, 35 kt (18 m/sec) at 132225Z. Note the exposed low level circulation center northwest of the convection at 132225Z.

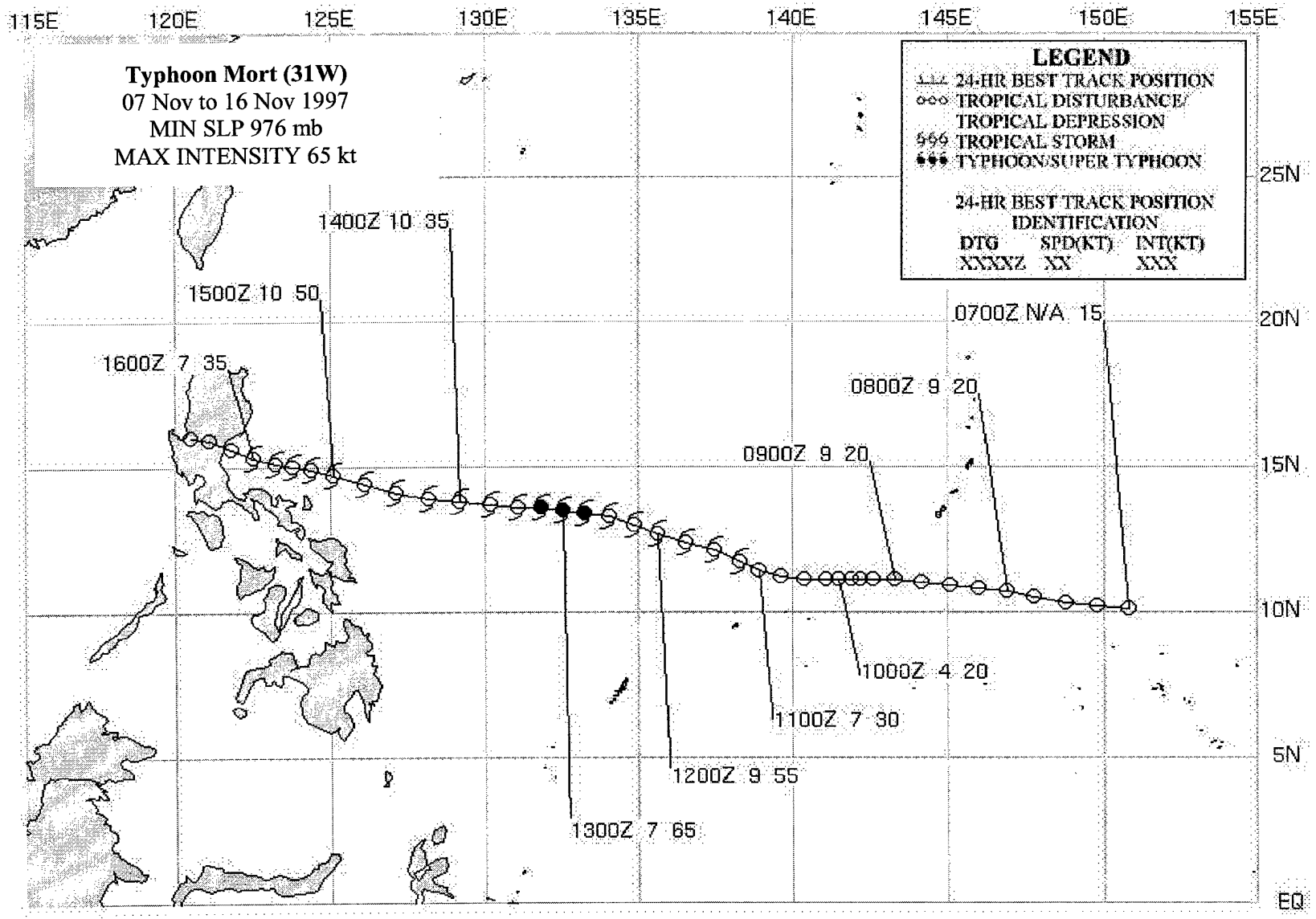
115E
120E
125E
130E
135E
140E
145E
150E
155E
25N
20N
15N
10N
5N
EQ
Typhoon Mort (31W)
07 Nov to 16 Nov 1997
MIN SLP 976 mb
MAX INTENSITY 65 kt
LEGEND
24-HR BEST TRACK POSITION
TROPICAL DISTURBANCE/
TROPICAL DEPRESSION
TROPICAL STORM
TYPHOON/SUPER TYPHOON
24-HR BEST TRACK POSITION
IDENTIFICATION
DTG SPD(KT) INT(KT)
XXXXZ XX XXX
1400Z 10 35
1500Z 10 50
1600Z 7 35
0700Z N/A 15
0800Z 9 20
0900Z 9 20
1000Z 4 20
1100Z 7 30
1200Z 9 55
1300Z 7 65

SUPER TYPHOON PAKA (05C)

I. HIGHLIGHTS

Paka formed in the Central Pacific southwest of Hawaii on 28 November 1997. Paka tracked steadily westward for two and one half weeks before slamming into the islands of Guam and Rota. As Paka's eye passed over northern Guam, destructive winds caused extensive damage to private and commercial buildings, infrastructure, crops, and vegetation. More intense than Typhoons Pamela (May 1976) and Omar (August 1992), Paka, with estimated maximum sustained surface winds of 130 kt (67 m/sec) gusting to 160 kt (82 m/sec) approached, but did not exceed, the intensity of Karen (estimated 135 kt (69 m/sec) gusting to 165 kt (85 m/sec)) in November 1962. No life was lost as a direct result of Paka's passage. Preliminary estimates of total losses run in the hundreds of millions of dollars.

II. TRACK AND INTENSITY

During the last week of November convection associated with an equatorial westerly wind burst flared up 1080 nm (2000 km) southwest of Hawaii. This led to the formation of twin tropical cyclones - Paka (05C), in the Northern Hemisphere, and Pam (07P) in the Southern. Pam (07P), in the summer hemisphere, became a hurricane and began recurving southeastward (Figure 3-05C-1). After issuing the first 17 advisories on Paka, the Central Pacific Hurricane Center transferred warning responsibility to the Joint Typhoon Warning Center as the system approached the international dateline (IDL). The first JTWC warning was number 18, valid at 1800Z on 06 December. After reaching 60 kt (31 m/sec) on 08 December, Paka began to weaken again. JTWC forecasters believed this weakening trend would continue, because upper level analysis and prognostic charts indicated that the cyclone would remain in a region of significant vertical shear. At 1800Z on 09 December, JTWC analyzed the cyclone as a 45 kt (23 m/sec) system and forecast this to remain constant for 36 hours, followed by a weakening trend. However, by 0600Z on 10 December, this thinking had begun to change, as upper level analysis showed that vertical shear was lessening. JTWC now depicted a 55 kt (28 m/sec) system which would peak as a minimal strength typhoon within 24 hours. Eighteen hours later, it became apparent that Paka was continuing to develop, and the 00Z warning on 11 December predicted it would peak at over 100 kt (50 m/sec). Majuro

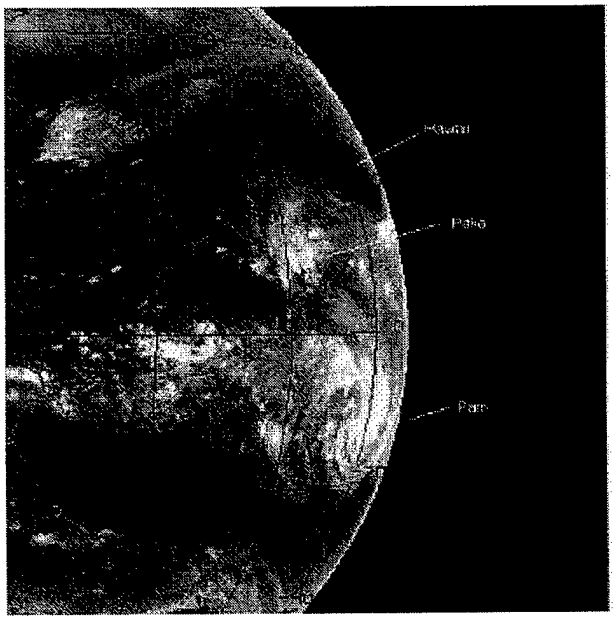

Figure 3-05C-1 Paka (05C) and Southern Hemisphere twin Pam (07P) early on 6 December, 1997

and Kwajalein atolls both received peak wind gusts of over 40 kt (20 m/sec) as Paka passed near on the 10th and the 11th, respectively.

After reaching an intensity of 115 kt (59 m/sec) on 12 December, Paka briefly weakened as along-track acceleration commenced. Despite forward speeds of 16 and 17 kt (30 and 31 km/hr), the typhoon started to intensify once again, peaking at 140 kt (72 m/sec) (160 mph) on 15 December. Paka was now a very serious threat to the southern Marianas. For Guam and Rota, the question rapidly changed from "if it arrives" to "when will it arrive?"

A day away from Guam, Paka began slowing, as anticipated, and there were signs of weakening. Now within NEXRAD Doppler radar range, the inner structure of Paka was revealed. There were concentric wall clouds - a primary approximately 40 nm (74 km) in diameter and a secondary fragmented inner wall cloud 10 nm (19 km) in diameter (Figure 3-05C-2). At 0600Z on 16 December, the center of Paka's eye was located 25 nm (46 km) south of the eastern point of Rota. The along-track speed was down to nine kt (17 km/hr), and the estimated intensity at 125 kt (64 m/sec) gusting to 150 kt (77 m/sec). At 161200Z, Paka had slowed to 6 kt (11 km/hr), and was at its closest point of approach (CPA) 15 nm (28 km) north of Agana, Guam. However, intensification was, once again, underway reaching an estimated maximum of 130 kt (67 m/sec) gusting to 160 (82 m/sec).

After seriously damaging the islands of Guam and Rota, Paka continued to intensify and reached a peak of 160 kt (82 m/sec) briefly on 18 December. Then, rapid weakening began and persisted until the cloud system completely dissipated four days later on 22 December. See Chapter 6 for a listing of the 6-hourly best track position, intensity, track direction and speed.

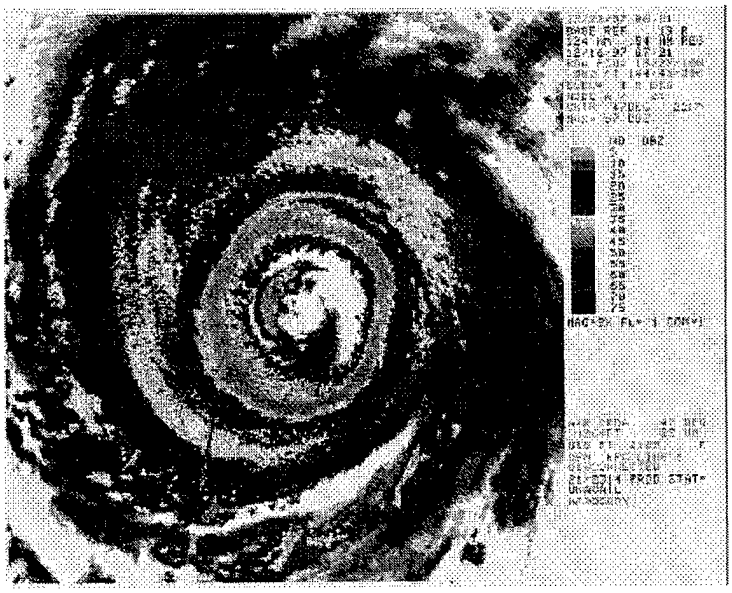

Figure 3-05C-2 NEXRAD imagery of Paka early on 16 December, 1997.

III DISCUSSION

a. Data Collection Difficulties

Considering the strength and duration of Paka's surface winds, it is not surprising that the wind records for areas that experienced passage of the primary wall cloud were fragmentary. The approach taken with these incomplete and noisy raw data records was to work sustained wind observations against the peak wind gusts, using a standard gust factor of 1.20 to 1.25 over water (Atkinson, 1974) and 1.60 overland. For example, gusts to 120 kt (62 m/sec) over water would be associated with a sustained surface wind of 100 kt (51 m/sec); overland gusts to 120 kt

(62 m/sec) would relate to 75 kt (39 m/sec) sustained wind. This technique identifies the representative data, for example: Commercial Port NWS HANDAR at Apra Harbor reported sustained/peak gust of 100/149 kt (51/77 m/sec) which is plausible; the Andersen AFB anemometer recorded 96/205 kt (49/105 m/sec) which is not considered representative. The Commercial Port sensor failed after recording four hours of 135 to 149 kt (69 to 77 m/sec) gusts in the wall cloud, Andersen AFB sensor lost power during passage of the western wall cloud. Additionally, the NWS sensor at Tiyan lost power during the onset of the primary wall cloud, the NPMOCW/JTWC anemometer at Nimitz Hill failed at 103 kt (53 m/sec) before the wall cloud arrived, the wind bird at the Apra Harbor tide guage failed in the wall cloud, and the NWS HANDAR at the University of Guam, Mangilao weathered the storm to report a peak gust to 123 kt (63 m/sec). In the final analysis the HANDAR instrument at Apra Harbor becomes the benchmark. It faithfully recorded peak gusts up to 149 kt (77 m/sec) until the winds began backing to the southwest, at which point it failed. This implies that the later southwesterly flow or second wind was stronger than the initial northwest to west wind (or first wind). This is borne out by the reports from other records at the Rota HANDAR and airport, DanDan and Merizo (Figure 3-05C-3). The only complete wind trace that records the peak winds in the wall cloud and the relative calm within the eye was from the Kuentos Communications, Inc. in Maite (Figure 3-05C-4). Relative to the lowest pressure which occurred at the CPA of Paka, the strength and duration of the highest winds on either side were compared. The wind from the southwest after the eye passage was more intense and of a longer duration. If this increase of 10 kt (5 m/sec) at Maite is applied to the Apra Harbor benchmark, a peak gust of 160 kt (82 m/sec) can be inferred.

b. Pressure Assessment

Microbarographs fortunately are less exposed than wind sensors which accounts for their survival, hence the pressure records were complete for Guam. The minimum sea-level pressure (MSLP) values (see Figure 3-05C-3) dropped from a high at DanDan (983 mb) and Merizo (980 mb) to Mangilao (953 mb), Apra Harbor (953 mb) and Tiyan (951 mb) to the lowest at Andersen AFB of 948 mb (Figure 3-05C-5). Using the MSLPs, which occurred at CPA, the passage of the center of Paka to the north of Guam can be followed across the checkerboard (Figure 3-05C-3). In addition, there is an empirical relationship (Dvorak, 1984) that can be used to relate the intensity (maximum sustained 1-minute mean surface winds over water) with the MSLP. The relationship has two scales: one for the Pacific and one for the Atlantic (Figure 3-05C-6). The reason for this is that the ambient pressure for the Pacific is in the mean lower than the Atlantic Ocean. Applying Dvorak's scale to Paka's 130 kt (67 m/sec) estimated intensity yields a 914 mb MSLP on the Pacific scale, which is much too low in relation to the values observed on Guam. However, a value for the Atlantic is 935 mb which is closer to what was observed. In summary, the basic reason for the difference between Pacific and Atlantic scales is that most tropical cyclones in the western North Pacific occur during the summer monsoon season when the ambient pressures are lower because of the presence of the monsoon trough. The Pacific scale doesn't address seasonal differences, therefore a bias exists. If a tropical cyclone, such as Paka, occurs in the winter, it follows that the scale will yield too low a MSLP. Therefore, a MSLP of 935 mb for Paka's 130-kt intensity appears reasonable.

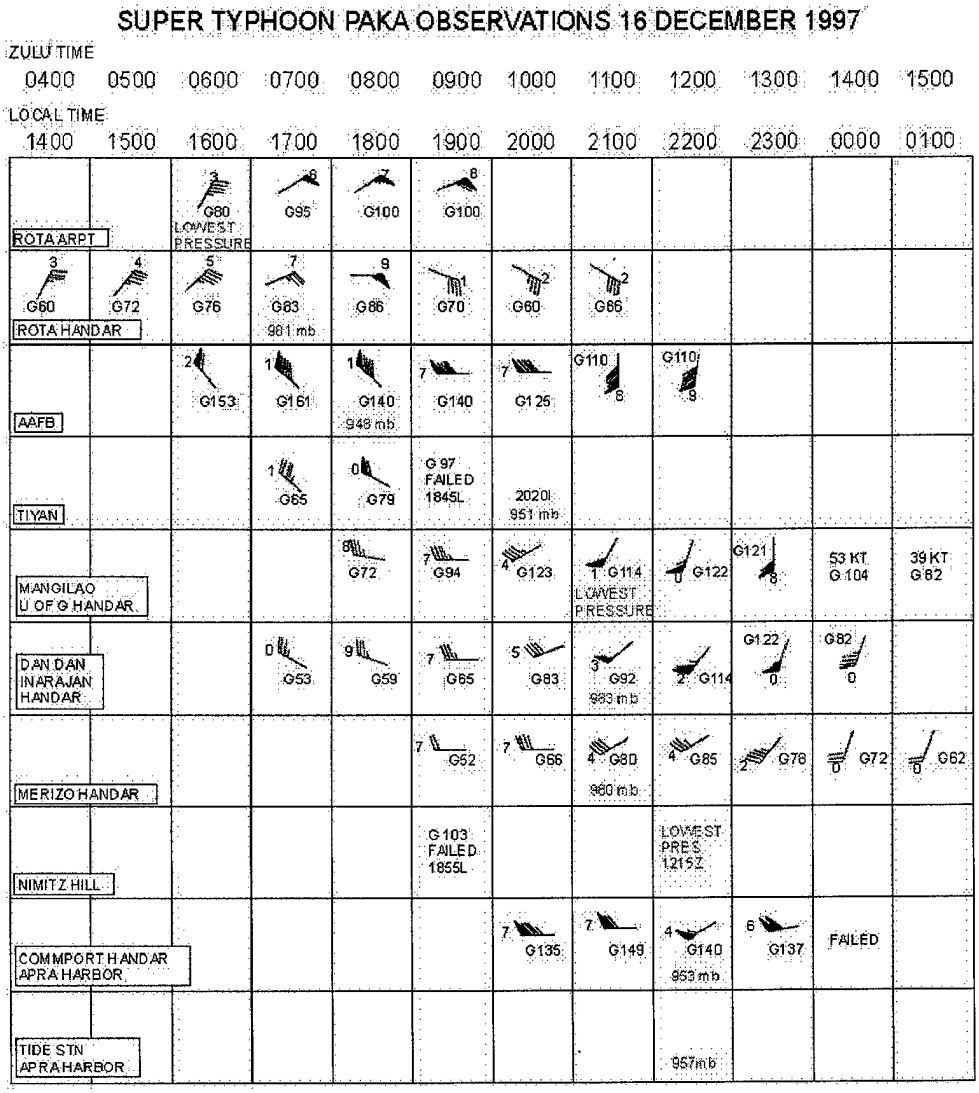

Figure 3-05C-3 Wind and pressure reports during the passage of Paka (05C) near Guam.

c. Radar Assessment

1) The NEXRAD Doppler radar, which is located at Mangilao and is maintained by Andersen AFB proved to be an invaluable tool for locating the center of Paka's eye and observing its convective structure. The last reflectivity product (Figure 3-05C-2) shows Pati Point, at the extreme northeastern end of Guam, just entering the relatively convection-free portion of the eye. The fragmented inner wall cloud is located over the Rota Channel to the northeast. The comparison radial velocity product (Figure 3-05C-7) indicates 144 kt (75 m/sec) inbound at the radar at 2000 feet (610 m) and 124 kt (64 m/sec) outbound. The 1-hour precipitation product (Figure 3-05C-8) indicates 1.50 to 2.00 inches (3.8 to 5 cm) in the wall cloud. Note: the absence of return over Rota to the northeast of the radar is due to lowest elevation beams being blocked by Mount Barrigada. No products were received after these because the NEXRAD radar went into standby mode and could not be remotely reset from the Unit Control Position at Andersen AFB. (The radar site weathered the storm without major damage.)

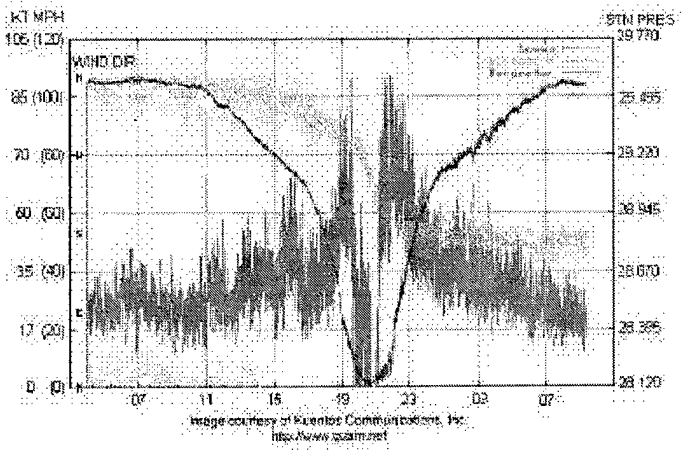

Figure 3-05C-4 This wind instrument, owned by Kuentos Communications, Inc, was the only one on Guam to recort the entire system passage.

2) The conventional FAA (Center-Radar Approach Control) CERAP radar located at Mount Santa Rosa proved invaluable for fixing Paka after the NEXRAD went into standby mode at 160721Z December. This support continued until the FAA radar failed at 161119Z.

IV IMPACT

Based on aerial and surface surveys, the following can be stated:

1) On Guam, as indicated by vegetation and crop blow downs and debris trails, the first wind (northwest through west) was less damaging than the second from the southwest through south . On Rota, the first wind (northeast through east) was less severe than the later second from the southeast. These observations support the fact that Paka was becoming more intense as it passed westward through the Rota Channel.

2) Moderate damage with pockets of heavy damage to private and commercial structures occurred on the northern half of Guam, which experienced outer wall cloud passage (Figure 3-05C-9). The slow passage (six hours) of the outer wall cloud across the center portion of the island allowed more time for high winds and rain to weaken structures.

3) In general, concrete roofs survived in areas where all structures with corrugated sheet iron lost their roofs. Steel framed buildings withstood the winds' onslaught and, although many lost sheet iron paneling and roofs, the structural integrity was maintained.

4) Minor distortion occurred to two smaller fuel storage tanks at Commercial Port, and one large, empty storage tank lost its fixed roof and collapsed. Damage to the power infrastructure was similar to that caused by Typhoon Omar in 1992.

5) Steel reinforced hollow concrete power poles failed under wind loading when they were not guyed, planted in shallow holes, or set in concrete without guys. These poles when guyed were observed to also fail when adjacent poles snapped, bringing the whole series down together.

In general, the damage assessment of northern Guam indicated a mixture of tropical cyclone scale categories 3 and 4 (Saffir-Simpson Hurricane Scale as modified by Guard and Lander, 1995) depending upon the exposure sites. This provides a wide range of maximum sustained wind speeds from 96-115 kt (49-59 m/sec) for category 3 to 116-135 kt (59-69 m/sec) for category 4.

Considering the magnitude and size of the debris trails, and the private structure and power infrastructure failures which occurred, it is indeed a tribute to preparation and common sense displayed by the combined population (160,000) of Guam and Rota that not a single life was lost as a direct result of Paka's passage.

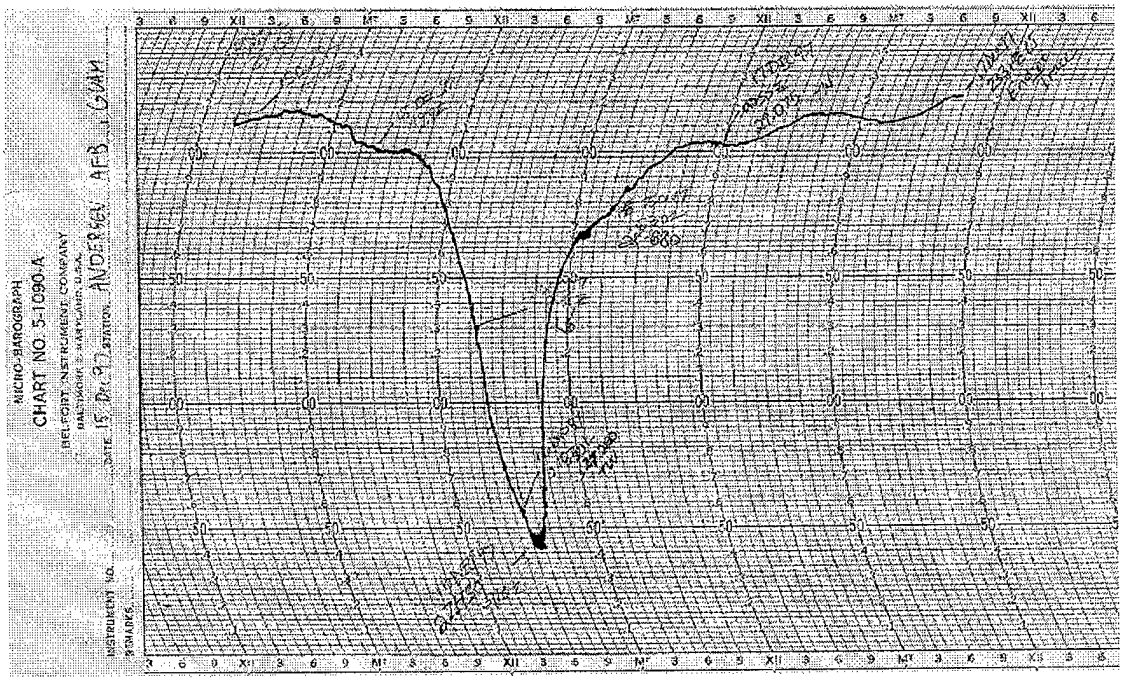

Figure 3-05C-5 Andersen AFB micro-barograph trace of Paka's (05C) passage.

C.I. NUMBER	MAXIMUM WIND SPEED	T-NUMBER	MINIMUM SEA-LEVEL PRESSURE (Atlantic)	(NW Pacific)
0	<25 kt			
0.5	25			
1	25	1		
1.5	25	1.5		
2	30	2	1009mb	1000mb
2.5	35	2.5	1005	997
3	45	3	1000	991
3.5	55	3.5	994	984
4	65	4	987	976
4.5	77	4.5	979	966
5	90	5	970	954
5.5	102	5.5	960	941
6	115	6	948	927
6.5	127	6.5	935	914
7	140	7	921	898
7.5	155	7.5	906	879
8	170	8	890	858

Figure 3-05C-6 Wind, pressure, and Dvorak relationship for both the Atlantic and Pacific.

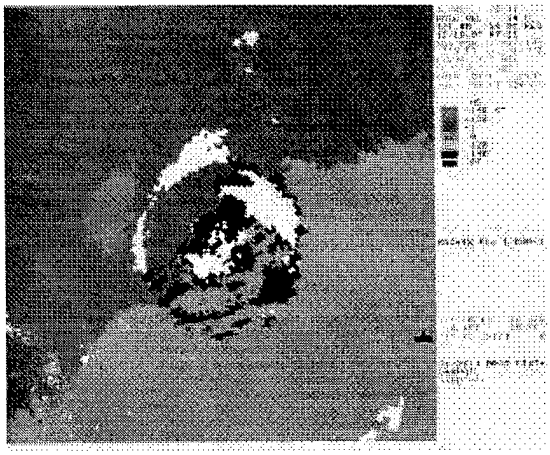

Figure 3-05C-7 NEXRAD radial velocity product for 0721Z on 16 December 97.

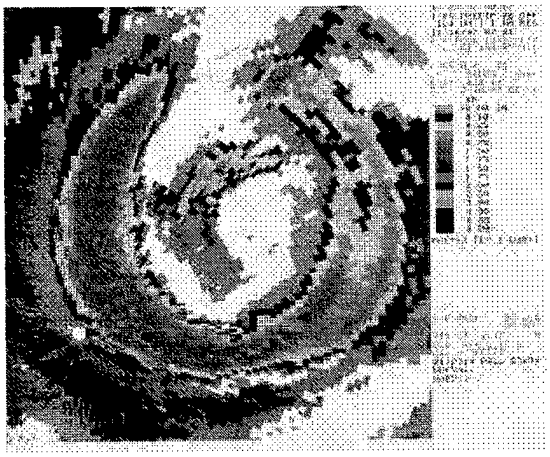

Figure 3-05C-8 NEXRAD one hour precipitation product for 0721Z on 16 December 97.

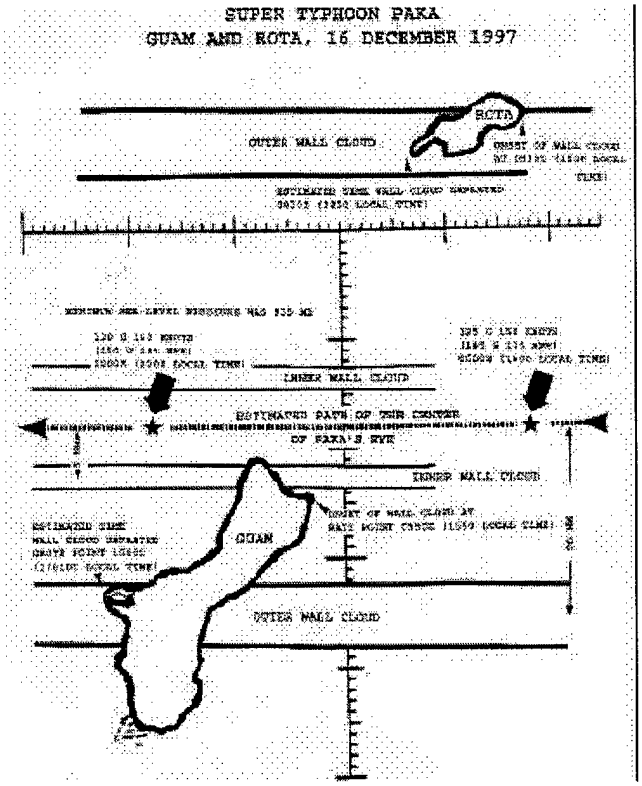

Figure 3-05C-9 Paka's (05C) track across Guam.

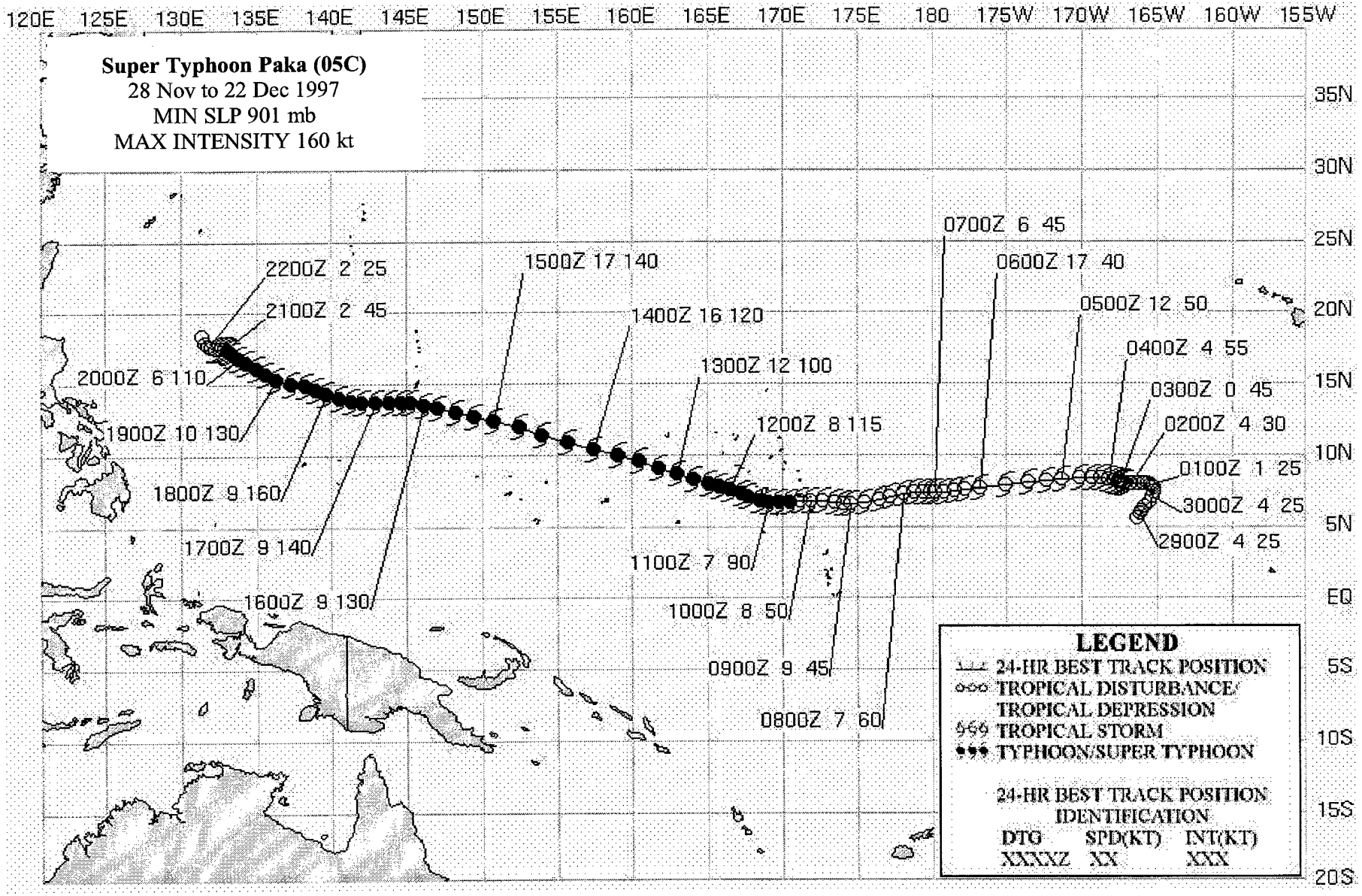
120E 125E 130E 135E 140E 145E 150E 155E 160E 165E 170E 175E 180 175W 170W 165W 160W 155W
35N
30N
25N
20N
15N
10N
5N
EQ
5S
10S
15S
20S
Super Typhoon Paka (05C)
28 Nov to 22 Dec 1997
MIN SLP 901 mb
MAX INTENSITY 160 kt
2200Z 2 25
2100Z 2 45
2000Z 6 110
1900Z 10 130
1800Z 9 160
1700Z 9 140
1600Z 9 130
1500Z 17 140
1400Z 16 120
1300Z 12 100
1200Z 8 115
1100Z 7 90
1000Z 8 50
0900Z 9 45
0800Z 7 60
0700Z 6 45
0600Z 17 40
0500Z 12 50
0400Z 4 55
0300Z 0 45
0200Z 4 30
0100Z 1 25
3000Z 4 25
2900Z 4 25
LEGEND
24-HR BEST TRACK POSITION
TROPICAL DISTURBANCE/
TROPICAL DEPRESSION
TROPICAL STORM
TYPHOON/SUPER TYPHOON
24-HR BEST TRACK POSITION
IDENTIFICATION
DTG SPD(KT) INT(KT)
XXXXZ XX XXX

TROPICAL CYCLONE 01B

Tropical Cyclone (TC) 01B emerged from a poorly organized area of convection embedded within the near-equatorial trough. It was first noted on the Significant Tropical Weather Advisory (ABIO) bulletin for the Indian Ocean valid 13 May. The system slowly developed as it drifted in a generally northward direction within the Bay of Bengal. The first warning was issued at 1800Z on 14 May based on a satellite derived intensity estimate of 25 kt (13 m/sec) and indications that the system was developing. The presence of equatorial westerlies and good upper level outflow meant that the cyclone should continue to intensify. Intensity estimates ranging from 35 to 40 kt (18-21 m/sec) were received less than six hours later. Beginning at 1200Z on the 15th, TC 01B slowed and veered toward the east, remaining at a constant intensity of 50 kt (26 m/sec) for approximately 24 hours. Afterwards the cyclone picked up speed and again tracked generally northward while further intensifying. By 0000Z on the 17th, TC 01B had reached 65 kt (33 m/sec). By 1800Z on the 18th the system developed an eye. Twelve hours later it peaked at 115 kt (59 m/sec). This intensity was maintained until landfall occurred in Bangladesh shortly after 1200Z on 19 May. Once over land, the system continued its north-northeastward track, increased its speed significantly north of the subtropical ridge axis, and dissipated due to land interaction as it neared China. TC 01B caused significant damage and several hundred casualties in Bangladesh.

Figure 3-01B-1 Visible imagery of TC 01B from 180034Z May.

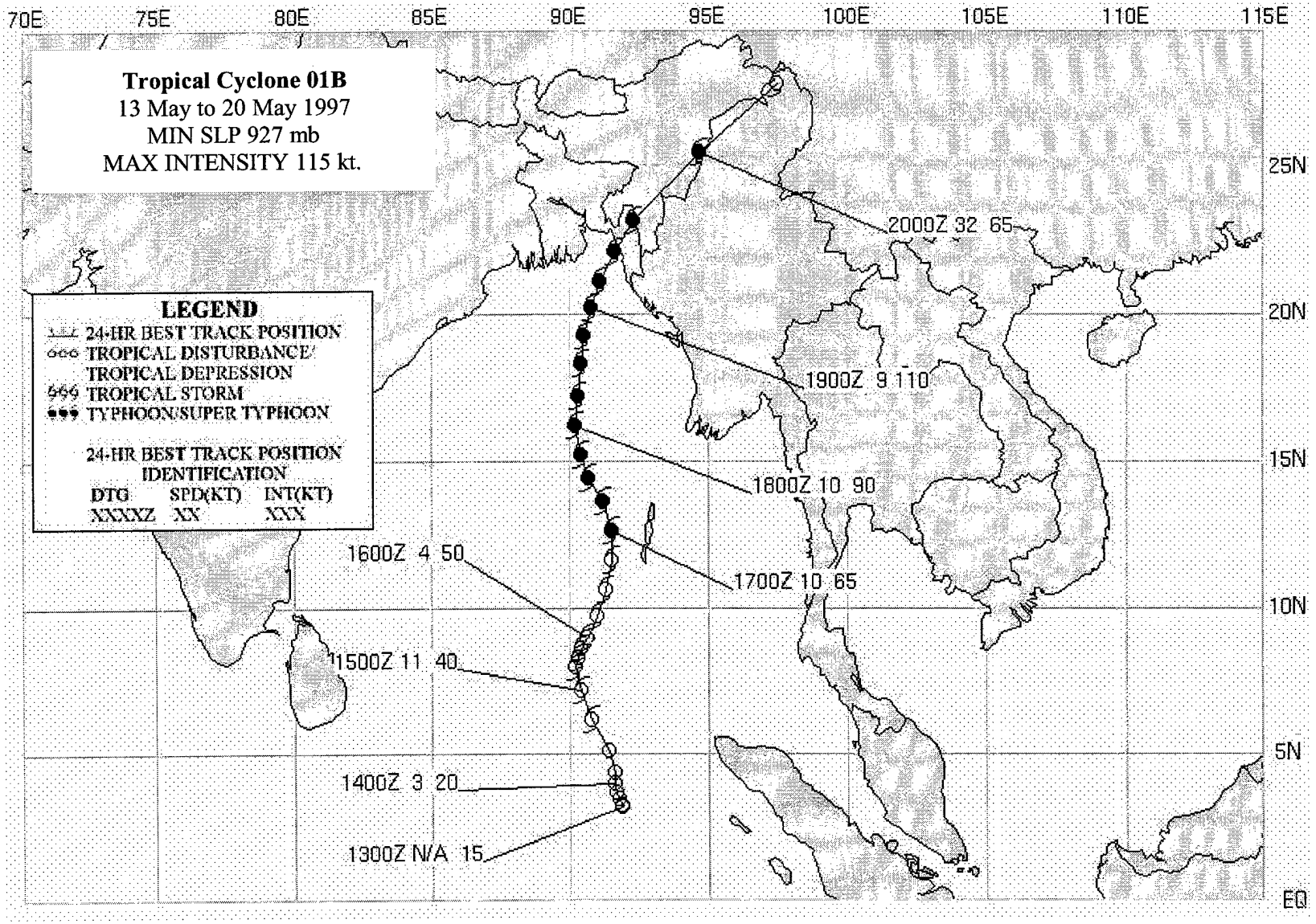
70E
75E
80E
85E
90E
95E
100E
105E
110E
115E
25N
20N
15N
10N
5N
EQ
Tropical Cyclone 01B
13 May to 20 May 1997
MIN SLP 927 mb
MAX INTENSITY 115 kt.
LEGEND
24-HR BEST TRACK POSITION
TROPICAL DISTURBANCE/ TROPICAL DEPRESSION
TROPICAL STORM
TYPHOON/SUPER TYPHOON
24-HR BEST TRACK POSITION IDENTIFICATION
DTG SPD(KT) INT(KT)
XXXXZ XX XXX
2000Z 32 65
1900Z 9 110
1800Z 10 90
1700Z 10 65
1600Z 4 50
1500Z 11 40
1400Z 3 20
1300Z N/A 15

TROPICAL CYCLONE 02B

Tropical Cyclone 02B began as an area of disturbed weather in the western Bay of Bengal and was first mentioned on the 19 September Significant Tropical Weather Advisory (ABIO). The disturbance continued to improve in organization through 21 September remaining quasi-stationary in the monsoon trough. After 21 September, the system began to move slowly northwestward until 24 September. On 24 September, the first warning was issued. At about this time, a developing mid-latitude trough northwest of the cyclone shifted the steering flow to southwesterly and by 26 September, the forward motion had increased from 6 kt (11 km/hr) to 14 kt (26 km/hr). Tropical Cyclone 02B increased in intensity as it tracked along the eastern coast of India. The system reached a peak intensity of 65 kt (33 m/s) approximately 12 hours before making landfall in Bangladesh on 27 September. Forty-seven people were reported killed and more than 1000 injured as heavy surf, rain and wind gusts of 80 kt (40 m/s) swept the coastline. Tropical Cyclone 02B moved further inland where it eventually dissipated.

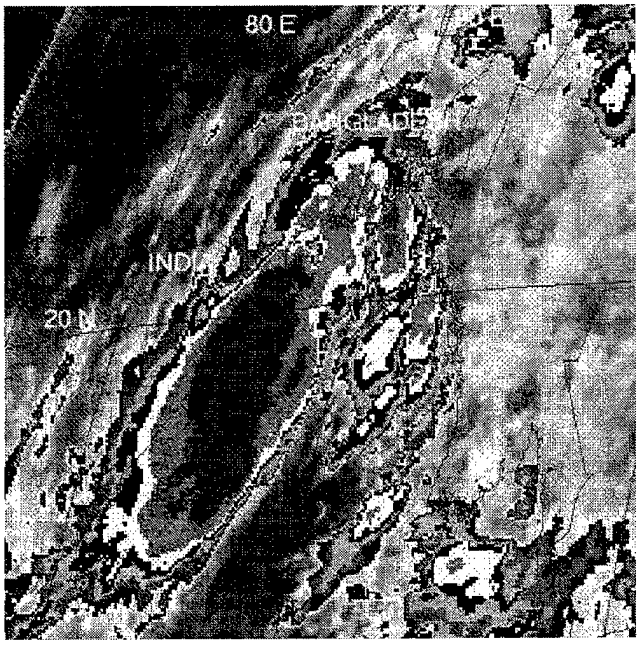

Figure 3-02B-1 Tropical Cyclone 02B as it skirts the eastern coast of India (242225Z September enhanced infrared GMS imagery).

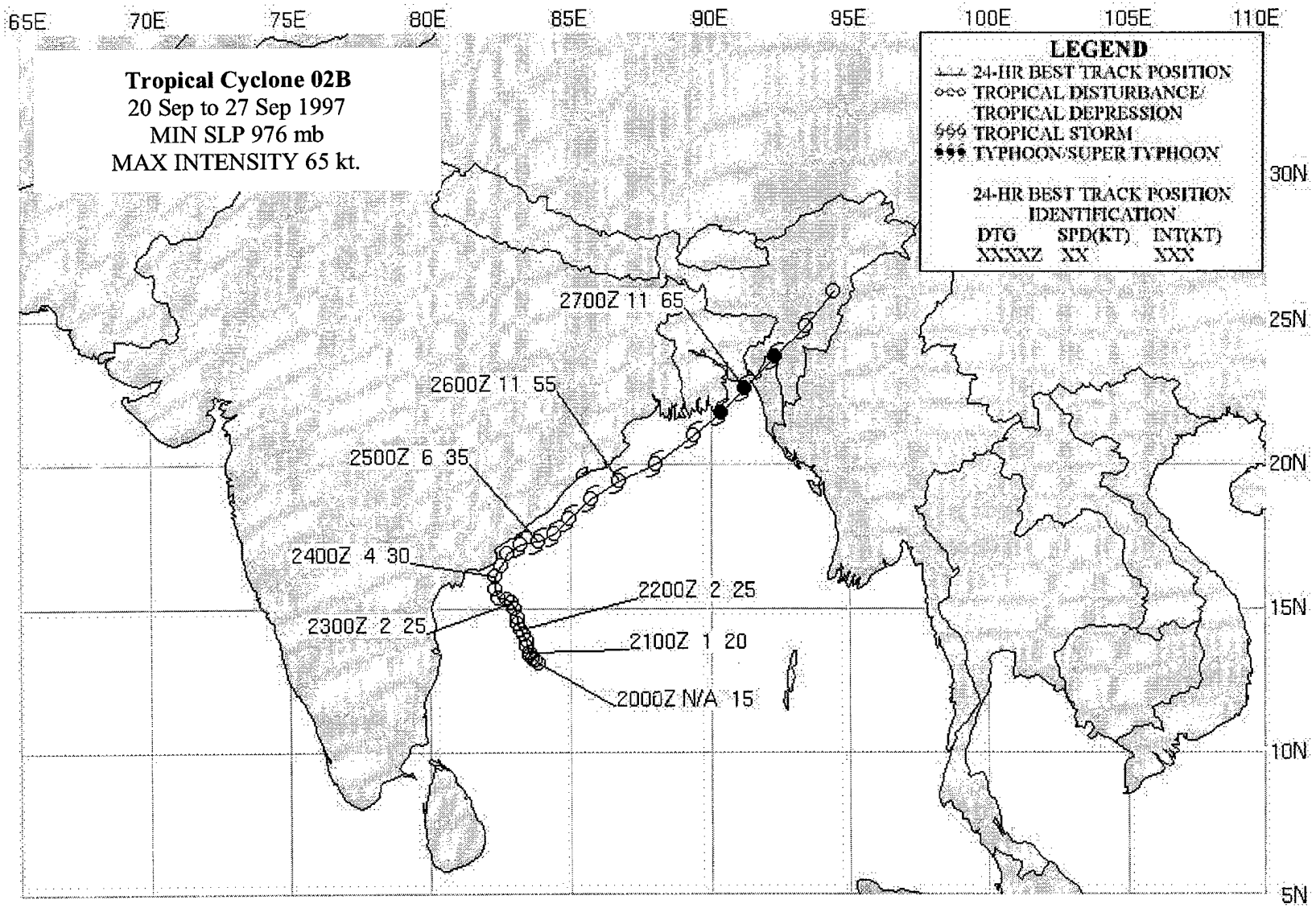
65E
70E
75E
80E
85E
90E
95E
100E
105E
110E
30N
25N
20N
15N
10N
5N
Tropical Cyclone 02B
20 Sep to 27 Sep 1997
MIN SLP 976 mb
MAX INTENSITY 65 kt.
LEGEND
24-HR BEST TRACK POSITION
TROPICAL DISTURBANCE/
TROPICAL DEPRESSION
TROPICAL STORM
TYPHOON/SUPER TYPHOON
24-HR BEST TRACK POSITION
IDENTIFICATION
DTG SPD(KT) INT(KT)
XXXXZ XX XXX
2700Z 11 65
2600Z 11 55
2500Z 6 35
2400Z 4 30
2300Z 2 25
2200Z 2 25
2100Z 1 20
2000Z N/A 15

TROPICAL CYCLONE 03A

The disturbance which became Tropical Cyclone (TC) 03A was first noted on the 07 November Significant Tropical Weather Advisory (ABIO) at 9N 54E. It was embedded within a widespread area of convection associated with broad troughing. The first warning was issued at 0600Z on 08 November. The system initially tracked northwestward at 6 kt (11 km/hr) towards the coast of Somalia with an intensity of 35 kt (18 m/sec), It maintained a 35 kt (18 m/sec) intensity over the next 18 hours despite the presence of moderate vertical wind shear as it approached the coast. By 0000Z on 09 November, TC 03A had made landfall over the northeast tip of Somalia. The partially exposed low-level center dissipated completely over land within the next 06 to 18 hours. No reports of damage were received by JTWC.

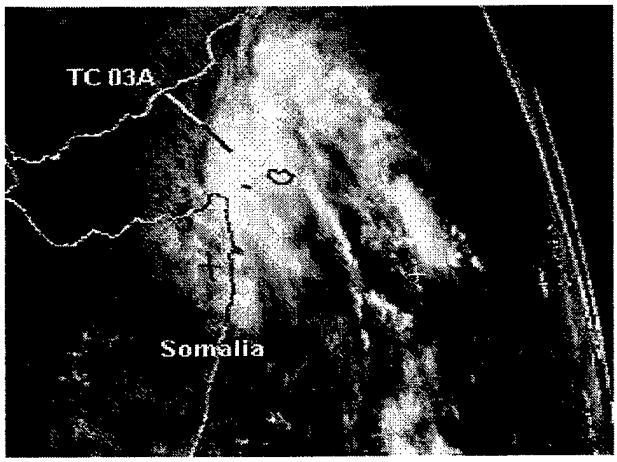

Figure 3-3A-1 TC 03A after reaching landfall (080830Z November visible Meteosat imagery).

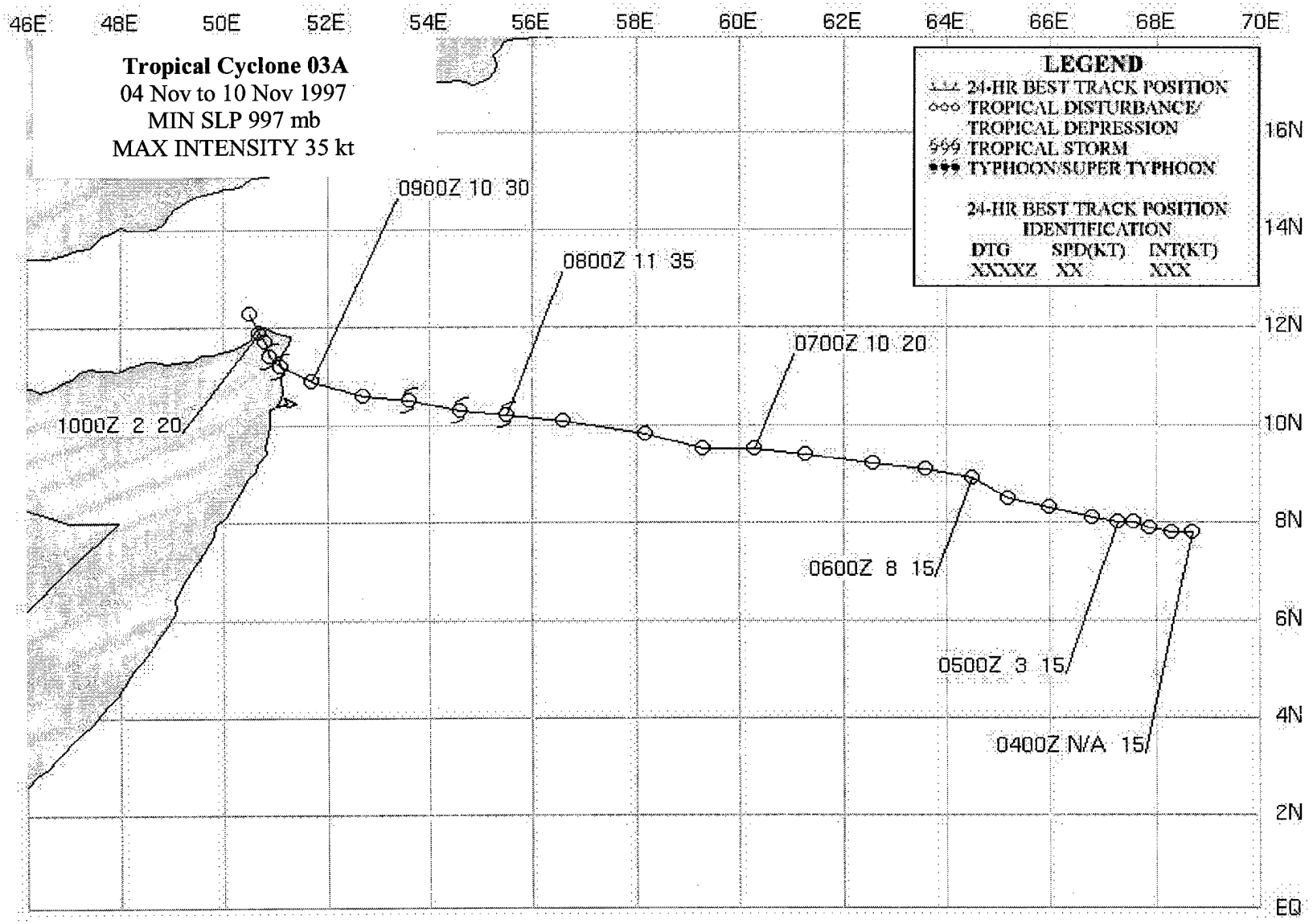
Tropical Cyclone 03A
04 Nov to 10 Nov 1997
MIN SLP 997 mb
MAX INTENSITY 35 kt
LEGEND
24-HR BEST TRACK POSITION
TROPICAL DISTURBANCE/
TROPICAL DEPRESSION
TROPICAL STORM
TYPHOON/SUPER TYPHOON
24-HR BEST TRACK POSITION
IDENTIFICATION
DTG SPD(KT) INT(KT)
XXXXZ XX XXX
0900Z 10 30
0800Z 11 35
0700Z 10 20
1000Z 2 20
0600Z 8 15
0500Z 3 15
0400Z N/A 15
46E
48E
50E
52E
54E
56E
58E
60E
62E
64E
66E
68E
70E
16N
14N
12N
10N
8N
6N
4N
2N
EQ

TROPICAL CYCLONE 04A

Tropical Cyclone 04A started as a disturbance over Sri Lanka. It was first mentioned on the Indian Ocean Significant Tropical Weather Advisory (ABIO) at 1800Z on 6 November. Near 1200Z on the 7th, the circulation began moving to the north and then to the west over the lower tip of India. A Tropical Cyclone Formation Alert (TCFA) was issued at 1900Z on 9 November. The first warning was issued valid at 0000Z on 10 November. At 110600Z TC 04A reached its peak intensity of 55 kt (28 m/sec) while moving northwestward. It held this intensity for just over 24 hours, then began weakening under vertical wind shear. The remaining low-level circulation weakened, lost latitude, and dissipated over water. JTWC issued its final warning at 0000Z on the 14th. No reports of damage were received at JTWC.

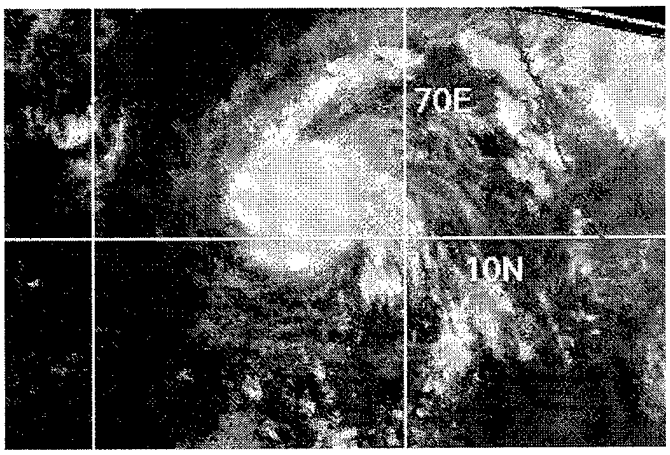

Figure 3-04A-1 Infrared imagery from 101200Z.

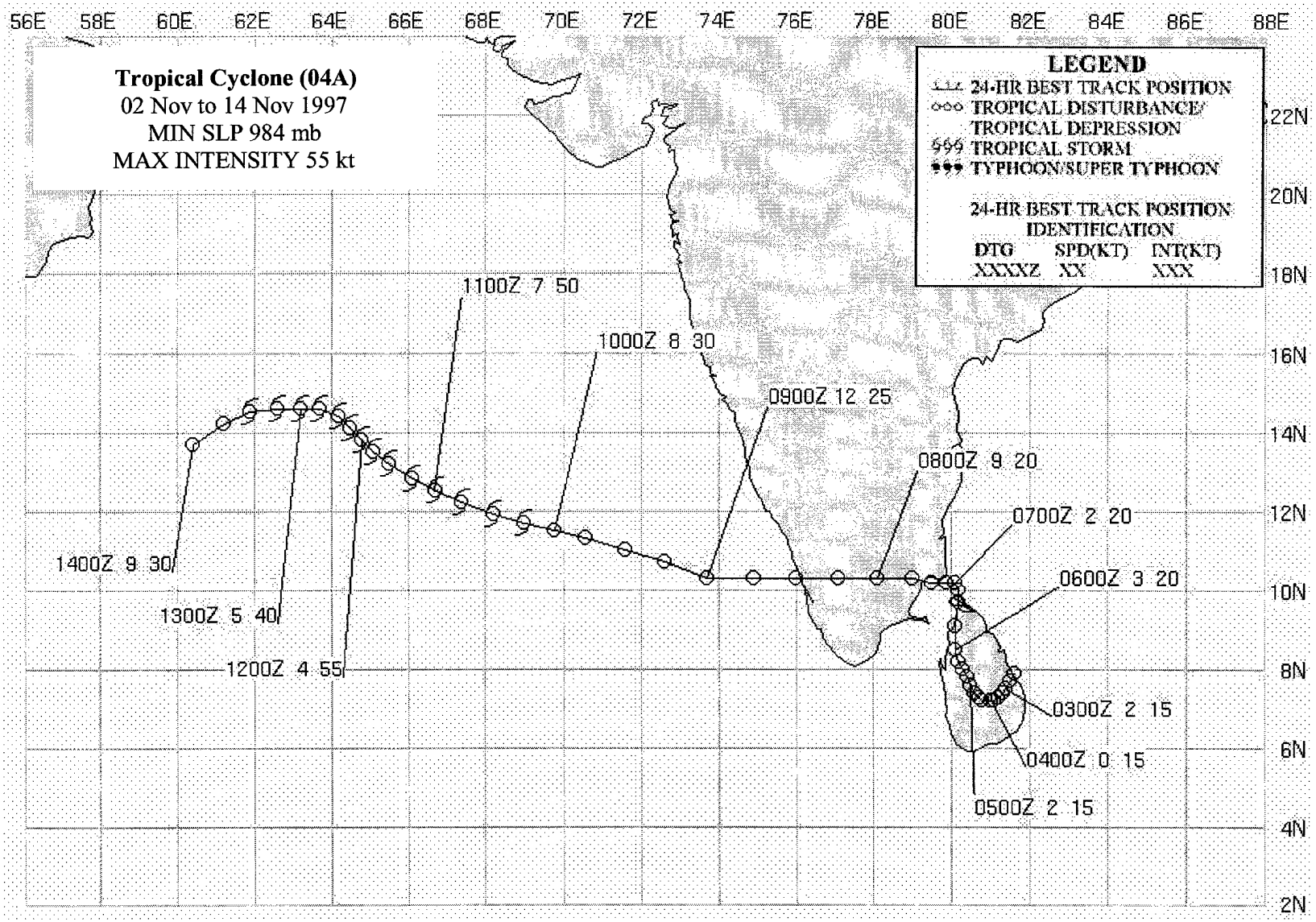
Tropical Cyclone (04A)
02 Nov to 14 Nov 1997
MIN SLP 984 mb
MAX INTENSITY 55 kt
LEGEND
24-HR BEST TRACK POSITION
TROPICAL DISTURBANCE/ TROPICAL DEPRESSION
TROPICAL STORM
TYPHOON/SUPER TYPHOON
24-HR BEST TRACK POSITION IDENTIFICATION
DTG SPD(KT) INT(KT)
XXXXZ XX XXX
1400Z 9 30
1300Z 5 40
1200Z 4 55
1100Z 7 50
1000Z 8 30
0900Z 12 25
0800Z 9 20
0700Z 2 20
0600Z 3 20
0300Z 2 15
0400Z 0 15
0500Z 2 15
56E
58E
60E
62E
64E
66E
68E
70E
72E
74E
76E
78E
80E
82E
84E
86E
88E
22N
20N
18N
16N
14N
12N
10N
8N
6N
4N
2N

4. SUMMARY OF SOUTH PACIFIC AND SOUTH INDIAN OCEAN TROPICAL CYCLONES

4.1 GENERAL

On 1 October 1980, JTWC's area of responsibility (AOR) was expanded to include the Southern Hemisphere from 180° longitude, westward to the coast of Africa. Details on Southern Hemisphere tropical cyclones and JTWC warnings from July 1980 through June 1982 are contained in Diercks et al. (1982), and from July 1982 through June 1984 in Wirfel and Sandgathe (1986). Information on Southern Hemisphere tropical cyclones after June 1984 can be found in the applicable Annual Tropical Cyclone Report.

The NAVPACMETOCCEN, Pearl Harbor, Hawaii issues warnings on tropical cyclones in the South Pacific, which are east of 180° longitude. In accordance with CINCPACINST 3140.1W, Southern Hemisphere tropical cyclones are numbered sequentially from 1 July through 30 June. This convention is established to encompass the Southern Hemisphere tropical cyclone season, which primarily occurs from January through April. There are two Southern Hemisphere ocean basins for warning purposes - the South Indian Ocean (west of 135° East longitude) and the South Pacific (east of 135° East longitude) - which are identified by appending the suffixes "S" and "P," respectively, to the tropical cyclone number.

Intensity estimates for Southern Hemisphere tropical cyclones are derived from the interpretation of satellite imagery using the Dvorak (1984) technique and, when available, from surface observations and radar data. The Dvorak technique relates specific cloud signatures to maximum sustained one-minute average surface wind speeds. The conversion from maximum sustained winds to minimum sea-level pressure is obtained from Atkinson and Holliday (1977) (Table 4-1).

4.2 SOUTH PACIFIC AND SOUTH INDIAN OCEAN TROPICAL CYCLONES

The total number of significant tropical cyclones during the 1997 season (1 July 1996 - 30 June 1997; Table 4-2) was 38 which was approximately, more than the overall climatological mean for the previous 16 years as shown in Table 4-3. Looking at the annual variation of Southern Hemisphere Tropical Cyclones by ocean basins (Table 4-4), it becomes apparent that tropical cyclone activity was enhanced in the southern Indian Ocean and Australian regions, and remained slightly reduced in the South Pacific.

The JTWC warned on Southern Hemisphere tropical cyclones for 266 days of the 1997 season. This equates to roughly to 3 out of every 4 days of the 1997 Southern Hemisphere season having a tropical cyclone in active warning status. During 63 of the 266 days there were two or more Southern Hemisphere tropical cyclones in warning status at the same time.

A chronology of 1997 Southern Hemisphere tropical activity is provided in Figure 4-1. Composites of the tropical cyclone best tracks for the Southern Indian Ocean, the Australian Region, and the South Pacific Ocean, appear in Figures 4-2, 4-3, 4-4, 4-5, and 4-6 respectively.

Table 4-1 MAXIMUM SUSTAINED 1-MINUTE MEAN SURFACE WINDS AND EQUIVALENT MINIMUM SEA-LEVEL PRESSURE RELATIONSHIP (ATKINSON AND HOLLIDAY, 1977)

WIND-KT	(M/SEC)	PRESSURE (MB)
30	(15)	1000
35	(18)	997
40	(21)	994
45	(23)	991
50	(26)	987
55	(28)	984
60	(31)	980
65	(33)	976
70	(36)	972
75	(39)	967
80	(41)	963
85	(44)	958
90	(46)	954
95	(49)	948
100	(51)	943
105	(54)	938
110	(57)	933
115	(59)	927
120	(62)	922
125	(64)	916
130	(67)	910
135	(69)	906
140	(72)	898
145	(75)	892
150	(77)	885
155	(80)	879
160	(82)	872
165	(85)	965
170	(87)	858
175	(90)	851
180	(93)	844

TABLE 4-2 SOUTHERN HEMISPHERE TROPICAL CYCLONES FOR 1997 (01 JULY 1996 - 30 JUNE 1997)

TROPICAL CYCLONE	PERIOD OF WARNING	NUMBERS OF WARNINGS ISSUED	ESTIMATED MAXIMUM INTENSITY KT	(M/SEC)	ESTIMATED MSLP (MB)
01S LINDSAY	10 JUL - 11 JUL	2	35	(18)	997
02S -	17 AUG - 20 AUG	7	45	(23)	991
03S -	07 SEP - 09 SEP	9	40	(21)	994
04S ANTOINETTE	17 OCT - 21 OCT	10	65	(33)	976
05S MELANIE/BELLAMINE	29 OCT - 11 NOV	27	125	(64)	916
06P CYRIL	23 NOV - 26 NOV	7	50	(26)	987
07S CHANTELLE	24 NOV - 29 NOV	16	65	(33)	976
08S DANIELLA	02 DEC - 10 DEC	17	120	(62)	922
09S ELVINA	09 DEC - 14 DEC	12	55	(28)	984
10P NICHOLAS	13 DEC - 15 DEC	5	45	(23)	991
11S OPHELIA	14 DEC - 20 DEC	16	55	(28)	984
12P PHIL*	23 DEC-02 JAN/09-12 JAN	36	85	(44)	958
13P FERGUS	24 DEC - 30 DEC	14	90	(46)	954
14S FABRIOLA	02 JAN - 08 JAN	13	60	(31)	980
15S RACHEL	02 JAN - 08 JAN	16	80	(41)	963
16P DRENA	03 JAN - 10 JAN	16	120	(62)	922
17P EVAN♦	10 JAN - 16 JAN	0 (13)	70	(36)	972
18S -	11 JAN - 13 JAN	6	45	(23)	991
19S PANCO-HELINDA	19 JAN - 06 FEB	36	125	(64)	916
20S GRETELLE	20 JAN - 31 JAN	26	115	(59)	927
21S ILETTA	23 JAN - 28 JAN	11	75	(39)	968
22P FREDA*	26-30 JAN/31-02 FEB	18	65	(33)	976
23S JOSIE	08 FEB - 16 FEB	17	90	(46)	954
24P GILLIAN	10 FEB - 12 FEB	11	45	(23)	991
25S KARLETTE	16 FEB - 26 FEB	21	65	(33)	976
26P HAROLD	16 FEB - 21 FEB	15	55	(38)	984
27S -	19 FEB - 25 FEB	21	45	(23)	991
28P ITA♦	24 FEB - 24 FEB	0 (3)	35	(18)	997
29P -	26 FEB - 27 FEB	3	45	(23)	991
30S LIZETTE	27 FEB - 02 MAR	8	75	(39)	968
31P GAVIN	03 MAR - 12 MAR	23	115	(59)	927
32P JUSTIN	06 MAR - 25 MAR	77	90	(46)	954
33P HINA	13 MAR - 18 MAR	12	75	(39)	968
34P IAN♦	17 APR - 19 APR	0 (7)	55	(28)	984
35P JUNE	02 MAY - 05 MAY	12	65	(33)	976
36S RHONDA	10 MAY - 16 MAY	16	100	(51)	944
37P -	28 MAY - 30 MAY	5	35	(18)	997
38P KELI	10 JUN - 15 JUN	5 (6)	115	(59)	927
JTWC TOTAL		566			
♦ NPMOC TOTAL		(29)			
GRAND TOTAL		595			

* REGENERATED

♦ WARNINGS ISSUED BY NPMOC

Table 4-3 MONTHLY DISTRIBUTION OF SOUTH PACIFIC AND SOUTH INDIAN OCEAN TROPICAL CYCLONES

YEAR	JUL	AUG	SEP	OCT	NOV	DEC	JAN	FEB	MAR	APR	MAY	JUN	TOTAL
(1958-1977) AVERAGE *	-	-	-	0.4	1.5	3.6	6.1	5.8	4.7	2.1	0.5	-	24.7
1981	0	0	0	1	3	2	6	5	3	3	1	0	24
1982	1	0	0	1	1	3	9	4	2	3	1	0	25
1983	1	0	0	1	1	3	5	6	3	5	0	0	25
1984	1	0	0	1	2	5	5	10	4	2	0	0	30
1985	0	0	0	0	1	7	9	9	6	3	0	0	35
1986	0	0	1	0	1	1	9	9	6	4	2	0	33
1987	0	1	0	0	1	3	6	8	3	4	1	1	28
1988	0	0	0	0	2	3	5	5	3	1	2	0	21
1989	0	0	0	0	2	1	5	8	6	4	2	0	28
1990	2	0	1	1	2	2	4	4	10	2	1	0	29
1991	0	0	1	1	1	3	2	5	5	2	1	1	22
1992	0	0	1	1	2	5	4	11	3	2	1	0	30
1993	0	0	1	1	0	5	7	7	2	2	2	0	27
1994	0	0	0	0	2	4	8	4	9	3	0	0	30
1995	0	0	0	0	2	2	5	4	5	4	0	0	22
1996	0	0	0	0	1	3	7	6	6	4	1	0	28
1997	1	1	1	2	2	6	9	8	3	1	3	1	38
TOTAL	6	2	6	10	26	58	105	113	79	49	18	3	475
AVERAGE (1981-1997)	0.4	0.1	0.4	0.6	1.5	3.4	6.2	6.6	4.6	2.9	1.1	0.2	28

* (Gray, 1978)

Table 4-4 ANNUAL VARIATION OF SOUTHERN HEMISPHERE TROPICAL CYCLONES BY OCEAN BASINS

YEAR (1958-1977)	SOUTH INDIAN (WEST OF 105°E)	AUSTRALIAN (105°E - 165°E)	SOUTH PACIFIC (EAST OF 165°E)	TOTAL
AVERAGE*	8.4	10.3	5.9	24.6
1981	13	8	3	24
1982	12	11	2	25
1983	7	6	12	25
1984	14	14	2	30
1985	14	15	6	35
1986	14	16	3	33
1987	9	8	11	28
1988	14	2	5	21
1989	12	9	7	28
1990	18	8	3	29
1991	11	10	1	22
1992	11	6	13	30
1993	10	16	1	27
1994	16	10	4	30
1995	11	7	4	22
1996	13	11	4	28
1997	17	5	16	38
TOTAL	216	162	97	475
AVERAGE (1981-1996)	12.7	9.5	5.7	27.9

* (Gray,1978)

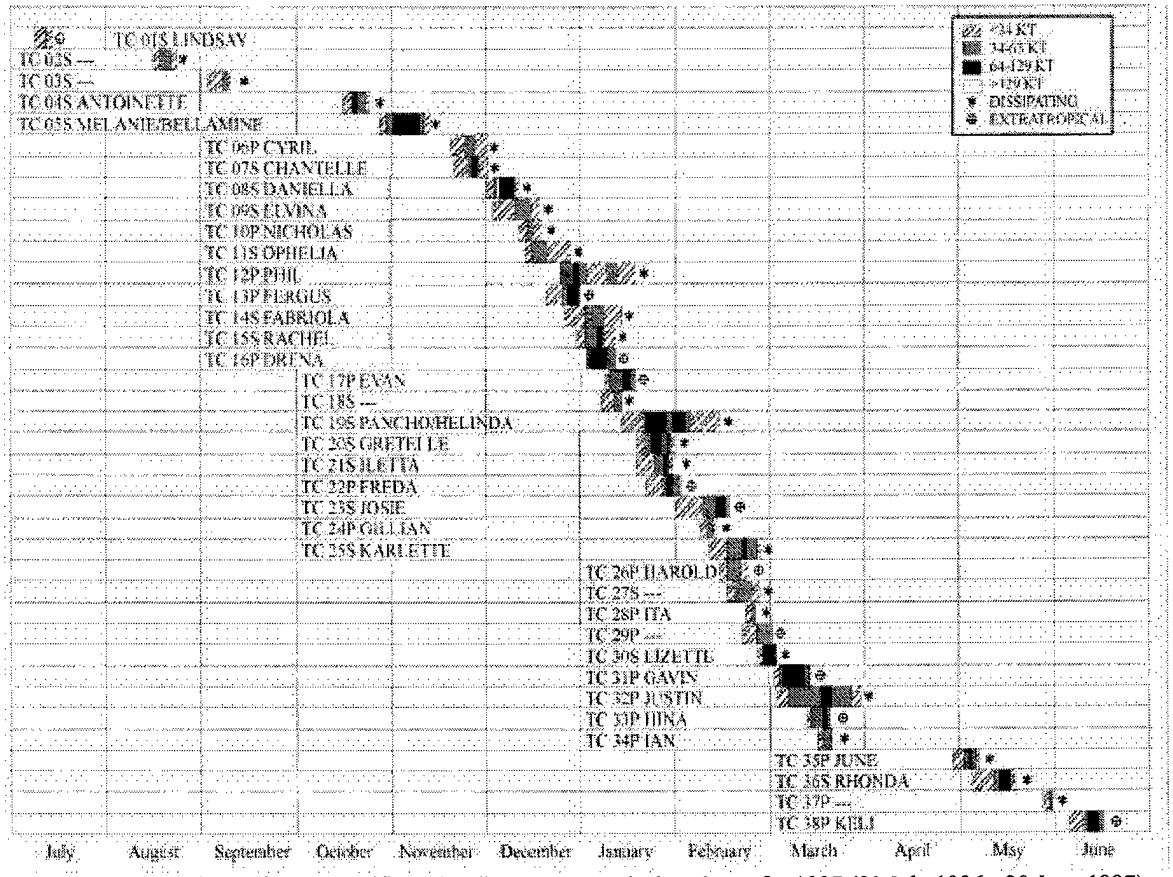

Figure 4-1 Chronology of South Pacific and Indian Ocean tropical cyclones for 1997 (01 July 1996 - 30 June 1997)

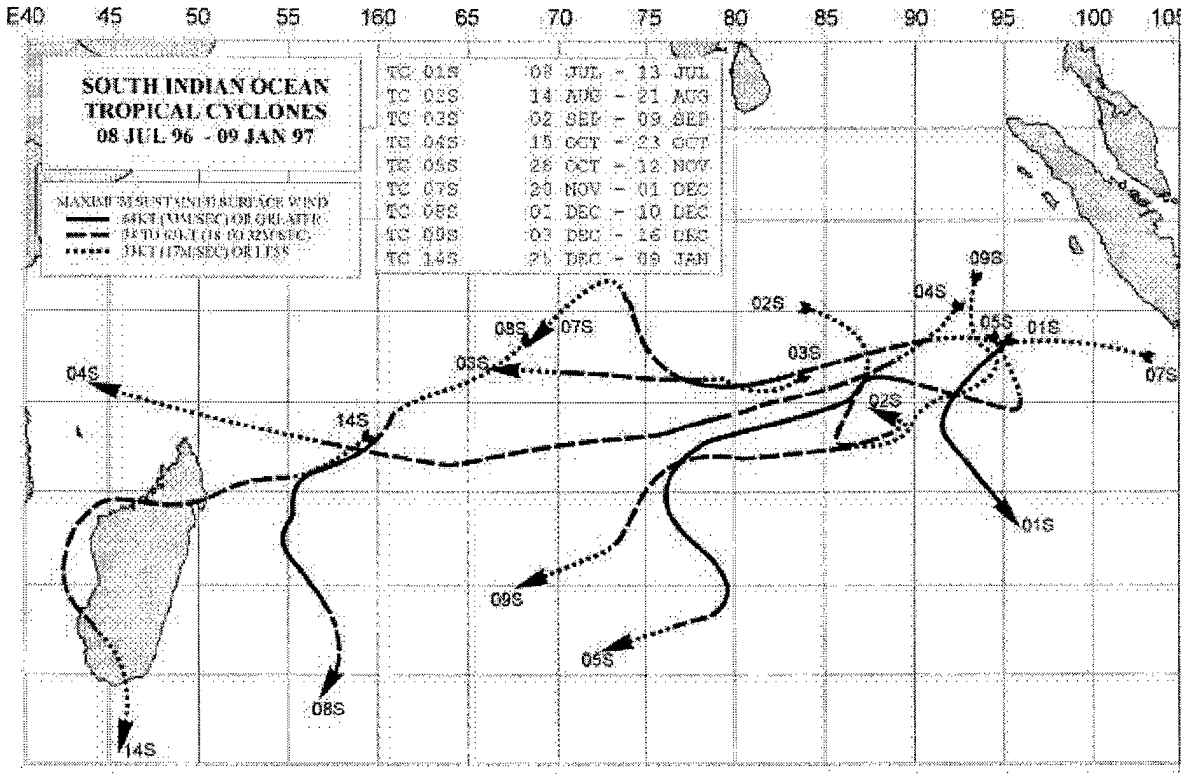

Figure 4-2 Tropical Cyclone best tracks for the South Indian Ocean

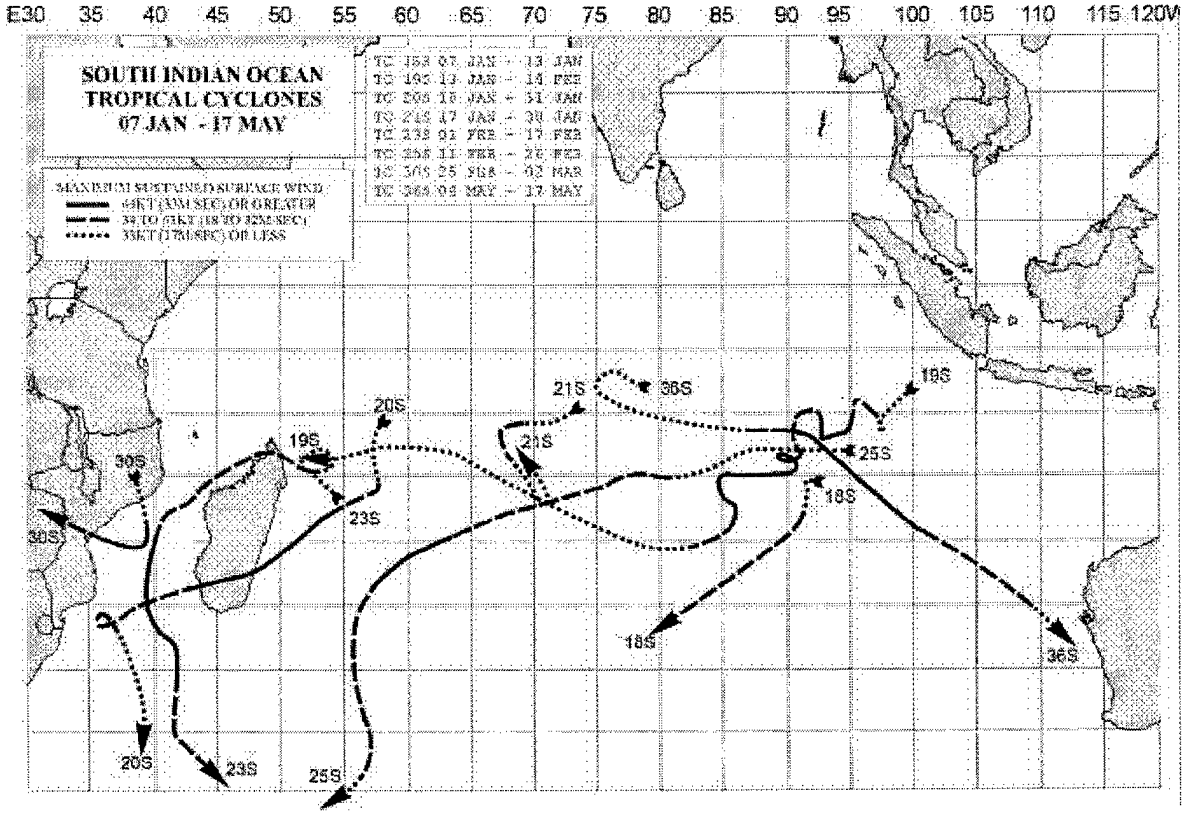

Figure 4-3 Tropical Cyclone best tracks for the South Indian Ocean

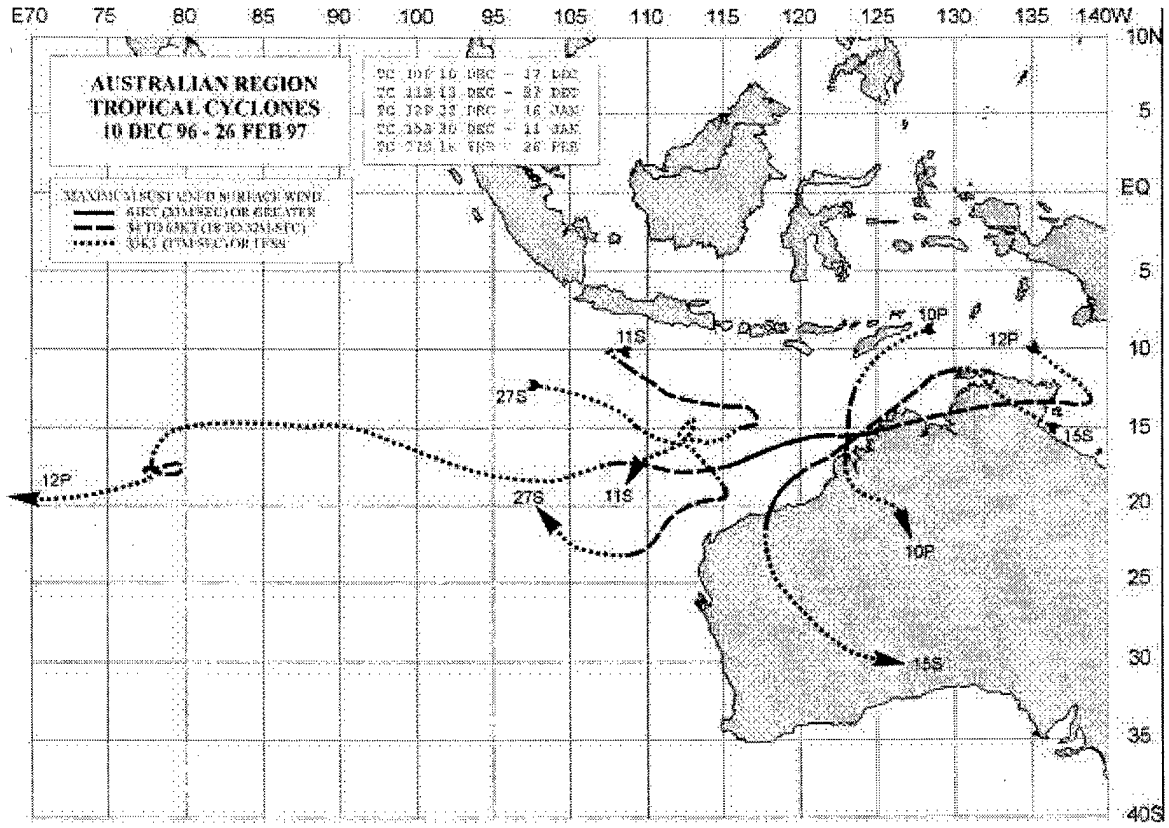

Figure 4-4 Tropical Cyclone best tracks for the Australian Region

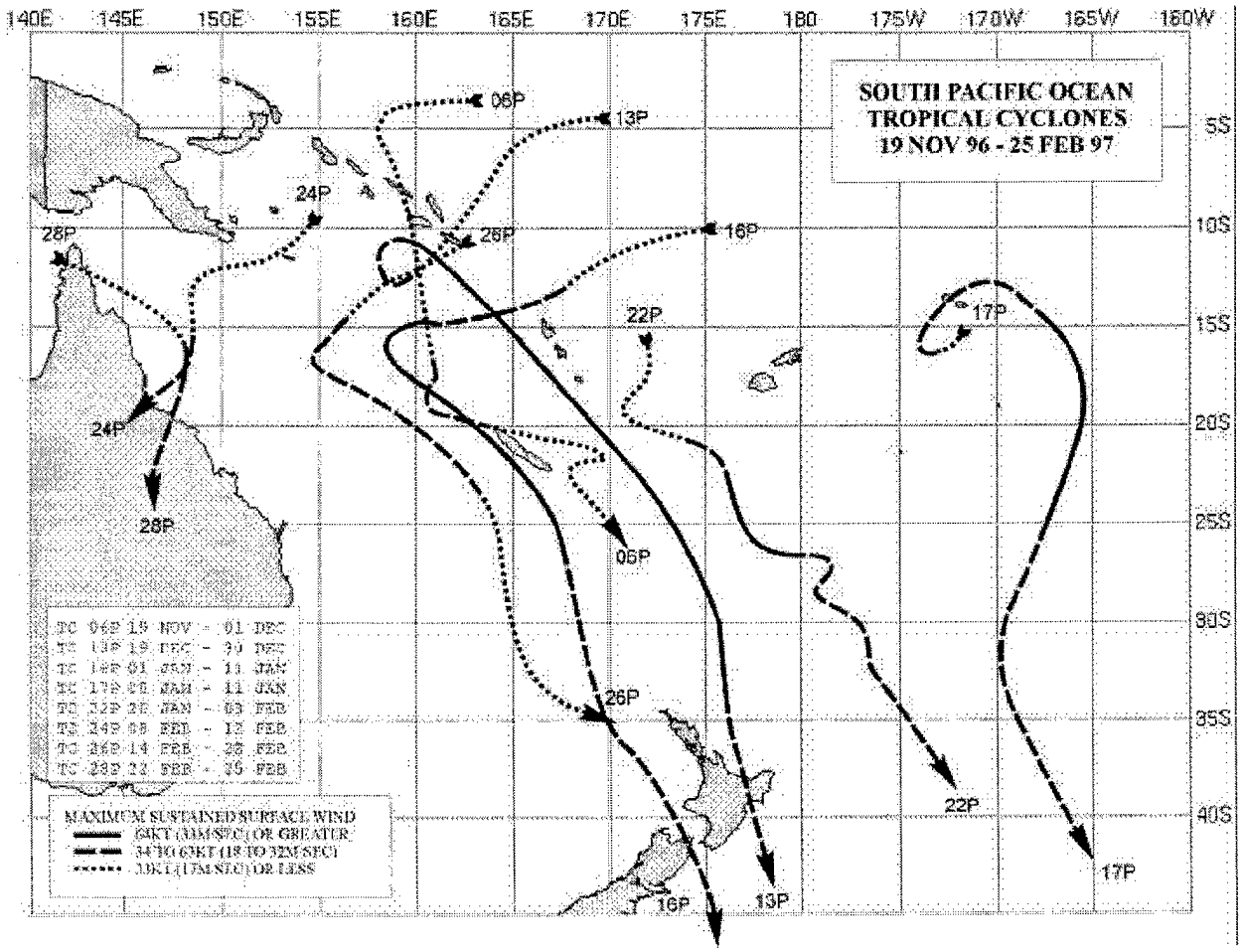

Figure 4-5 Tropical Cyclone best tracks for the South Pacific Ocean

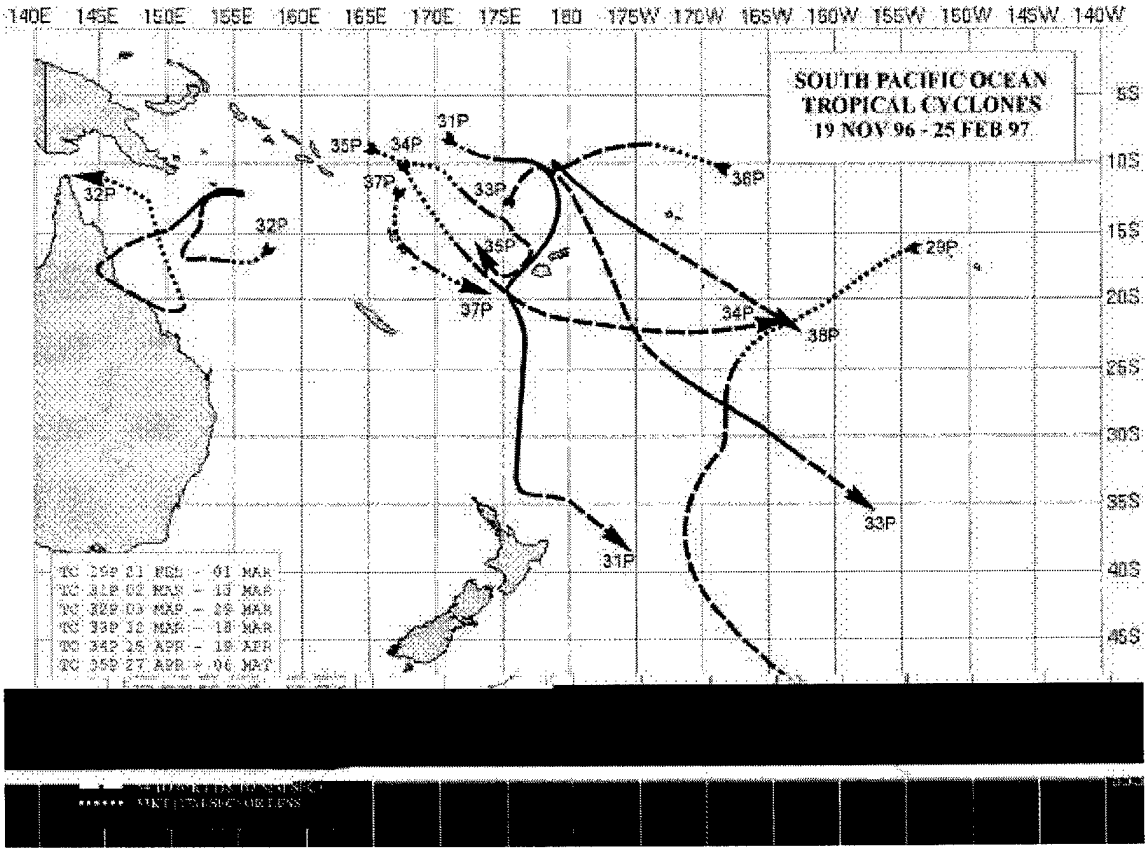

Figure 4-6 Tropical Cyclone best tracks for the South Pacific Ocean

5. SUMMARY OR FORECAST VERIFICATION

5.1 ANNUAL FORECAST VERIFICATION

Verification of warning positions and intensities at initial, 12-, 24-, 48- and 72-hour forecast periods was made against the final best track. The (scalar) track forecast, along-track and cross-track errors (illustrated in Figure 5-1) were calculated for each verifying JTWC forecast. These data, in addition to a detailed summary for each tropical cyclone, are included as Chapter 6. This section summarizes verification data for 1997 and contrasts it with annual verification statistics from previous years.

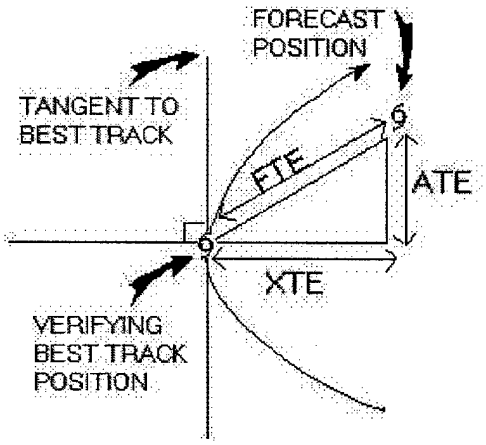

Figure 5-1 Definition of cross-track error (XTE), along-track error (ATE) and forecast track error (FTE). In this example, the forecast position is ahead of and to the right of the verifying best track position. Therefore, the XTE is positive (to the right of the best track) and the ATE is positive (ahead or faster than the best track). Adapted from Tsui and Miller, 1988.

5.1.1 NORTHWEST PACIFIC OCEAN The frequency distributions of errors for initial warning positions and 12-, 24-, 36-, 48- and 72-hour forecasts are presented in Figures 5-2a through 5-2f. Table 5-1 includes mean track, along-track and cross-track errors for 1983-1997. Figure 5-3 shows mean track errors and a 5-year running mean of track errors at 24-, 48- and 72-hours for the past 20 years. Table 5-2 lists annual mean track errors from 1959, when the JTWC was founded, until the present.

5.1.2 NORTH INDIAN OCEAN The frequency distributions of errors for warning positions and 12-, 24-, 36-, 48- and 72-hour forecasts are presented in Figures 5-4a through 5-4f, respectively. Table 5-3 includes mean track, along-track and cross-track errors for 1983-1997. Figure 5-5 shows mean track errors and a 5-year running mean of track errors at 24-, 48- and 72-hours for the past 20 years.

5.1.3 SOUTH PACIFIC AND SOUTH INDIAN OCEANS The frequency distributions of errors for warning positions and 12-, 24-, 36-, 48- and 72-hour forecasts are presented in Figures 5-6a through 5-6f, respectively. Table 5-4 includes mean track, along-track and cross-track errors for 1983-1997. Figure 5-7 shows mean track errors and a 5-year running mean of track errors at 24-, 48- and 72-hours for the 17 years that the JTWC has issued warnings in the region.

5.2 COMPARISON OF OBJECTIVE TECHNIQUES

JTWC uses a variety of objective techniques for guidance in the warning preparation process. Multiple techniques are required, because each technique has

particular strengths and weaknesses which vary by basin, numerical model initialization, time of year, synoptic situation and forecast period. The accuracy of objective aid forecasts depends on both the specified position and the past motion of the tropical cyclone as determined by the working best track. JTWC initializes its objective techniques using an extrapolated working best track position so that the output of the techniques will start at the valid time of the next warning initial position.

Unless stated otherwise, all of the objective techniques discussed below run in all basins covered by JTWC's AOR and provide forecast positions at 12-, 24-, 36-, 48-, and 72-hours unless the technique aborts prematurely during computations. The techniques can be divided into six general categories: extrapolation, climatology and analogs, statistical, dynamic, hybrids, and empirical or analytical.

5.2.1 EXTRAPOLATION (XTRP) Past speed and direction are computed using the rhumb line distance between the current and 12 hour old positions of the tropical cyclone. Extrapolation from the current warning position is used to compute forecast positions.

5.2.2 CLIMATOLOGY and ANALOGS

5.2.2.1 CLIMATOLOGY (CLIM) Employs time and location windows relative to the current position of the tropical cyclone to determine which historical storms will be used to compute the forecast. The historical database is 1945-1981 for the Northwest Pacific, and 1900 to 1990 for the rest of JTWC's AOR. Objective intensity forecasts are available from these databases. Scatter diagrams of expected tropical cyclone motion at bifurcation points are also available from these databases.

5.2.2.2 ANALOG A revised Typhoon Analog 1993 (TYAN93) picks the top matches with the basin climatology of historical tropical cyclone best tracks. Matches are based upon the differences between the direction and speed of the superimposed historical best track positions and the past direction and speed of the cyclone. Specifically, the directions and speeds are calculated from the 12-hour old position to the current "fix" position and the 24-hr old position to the "fix" position. Separate comparisons are made for climatology cyclone tracks classified as "straight," "recurver" and "other". There is also a "total" group, that includes the top matches without regard to classification of tracks.

TYAN93 works in the same manner for all basins. The time-window is +/- 35 days from the "fix." The space-window is +/- 2.5 degrees latitude and +/- 5 degrees longitude from the "fix" position on the first pass of each forecast. The maximum-wind-speed window is as follows (for basins with climatology wind speeds): a. If "fix" wind speed is < 25 kt, (13 m/s) climatology cyclone wind speed must be < 30 kt. (15 m/s) b. If "fix" wind speed is 30 kt, (15 m/s) climatology cyclone wind speed must be in range from 25 to 35 kt. (13 to 17 m/s) c. If "fix" wind speed is > 35 kt (17 m/s), climatology cyclone wind speed must be at least 35 kt. (17 m/s). Matching is based upon weighted direction and speed errors. Forecasting is based upon "straight" and "recurver" type climatology tropical cyclones, where the 12-hour and 24-hour best "straight" ("recurver") matches are combined into one set of best matches for "straight" ("recurver").

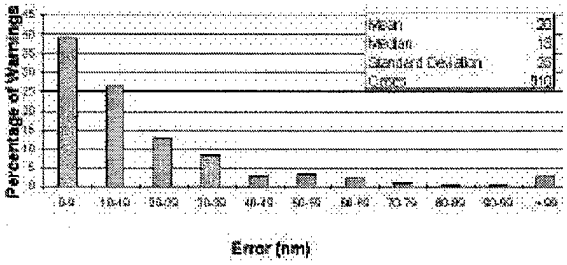

Figure 5-2a Frequency distribution of initial warning position errors (10-nm increments) for western North Pacific Ocean tropical cyclones in 1997. The largest error, 168 nm, occurred on Super Typhoon Keith (29W).

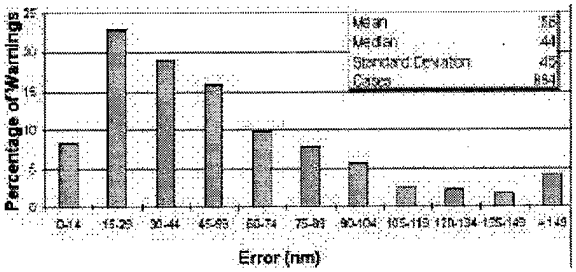

Figure 5-2b Frequency distribution of 12-hour track forecast errors (15-nm increments) for western North Pacific Ocean tropical cyclones in 1997. The largest error, 334 nm, occurred on Super Typhoon Keith (29W).

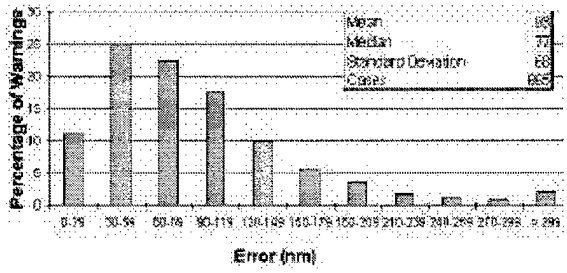

Figure 5-2c Frequency distribution of 24-hour track forecast errors for western North Pacific Ocean tropical cyclones in 1997. The largest error, 499 nm, occurred on Tropical Storm Levi (05W).

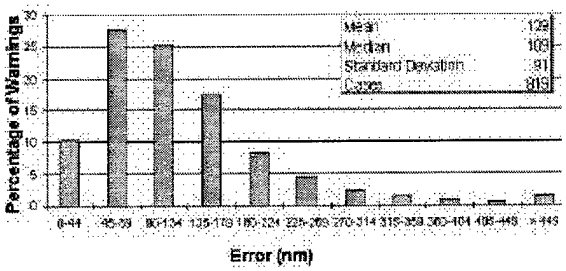

Figure 5-2d Frequency distribution of 36-hour track forecast errors for western North Pacific Ocean tropical cyclones in 1997. The largest error, 706 nm, occurred on Typhoon Linda (30W).

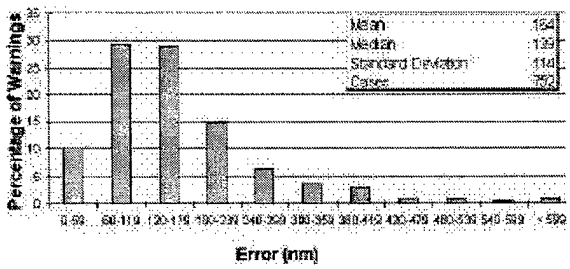

Figure 5-2e Frequency distribution of 48-hour track errors for western North Pacific Ocean tropical cyclones in 1997. The largest error, 891 nm, occurred on Tropical Storm Levi (05W).

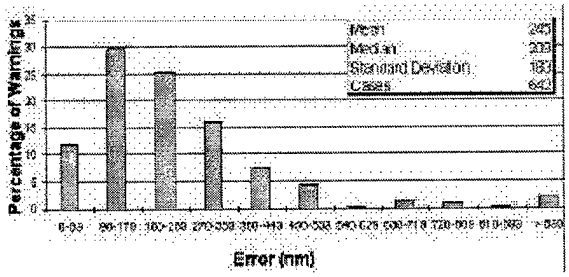

Figure 5-2f Frequency distribution of 72-hour track forecast errors for western North Pacific Ocean tropical cyclones in 1997. The largest error, 1382 nm, occurred on Super Typhoon Oliwa (02C).

5.2.3 STATISTICAL

5.2.3.1 CLIMATOLOGY AND PERSISTENCE (CLIPER or CLIP) A statistical regression technique that is based on climatology, current position and 12-hour and 24-hour past movement. This technique is used as a crude baseline against which to measure the forecast skill of other, more sophisticated techniques. CLIP in the western North Pacific uses third-order regression equations, and is based on the work of Xu and Neumann (1985). CLIPER has been available outside this basin since mid-1990, with regression coefficients recently recomputed by FNMOC based on the updated 1900-1989 database.

5.2.3.2 COLORADO STATE UNIVERSITY MODEL (CSUM) A statistical-dynamical technique based on the work of Matsumoto (1984). Predictor parameters include the current and 24-hr old position of the storm, heights from the current and 24-hr old NOGAPS 500-mb analyses, and heights from the 24-hr and 48-hr NOGAPS 500-mb prognoses. Height values from 200-mb fields are substituted for storms that have an intensity exceeding 90 kt (45 m/s) and are located north of the subtropical ridge. Three distinct sets of regression equations are used depending on whether the storm's direction of motion falls into "below," "on" or "above" the subtropical ridge categories. During the development of the regression equation coefficients for CSUM, the so-called "perfect prog" approach was used, in which verifying analyses were substituted for the numerical prognoses that are used when CSUM is run operationally. Thus, CSUM was not "tuned" to any particular version of NOGAPS, and in fact, the performance of CSUM should presumably improve as new versions of NOGAPS improve. CSUM runs only in the western North Pacific, South China Sea, and North Indian Ocean basins.

5.2.3.3 JTWC92 or JT92 JTWC92 is a statistical-dynamical model for the western North Pacific Ocean basin which forecasts tropical cyclone positions at 12-hour intervals to 72 hours. The model uses the deep-layer mean height field derived from the NOGAPS forecast fields. These deep-layer mean height fields are spectrally truncated to wave numbers 0 through 18 prior to use in JTWC92. Separate forecasts are made for each position. That is, the forecast 24-hour position is not a 12-hour forecast from the forecasted 12-hour position.

JTWC92 uses five internal sub-models which are blended and iterated to produce the final forecasts. The first sub-model is a statistical blend of climatology and persistence, known as CLIPER. The second sub-model is an analysis mode predictor, which only uses the "analysis" field. The third sub-model is the forecast mode predictor, which uses only the forecast fields. The fourth sub-model is a combination of 1 and 2 to produce a "first guess" of the 12-hourly forecast positions. The fifth sub-model uses the output of the "first guess" combined with 1, 2, and 3 to produce the forecasts. The iteration is accomplished by using the output of sub-model 5 as though it were the output from sub-model 4. The optimum number of iterations has been determined to be three.

When JTWC92 is used in the operational mode, all the NOGAPS fields are forecast fields. The 00Z and 12Z tropical forecasts are based upon the previous 12-hour old synoptic time NOGAPS forecasts. The 06Z and 18Z tropical forecasts are based on the previous 00Z and 12Z NOGAPS forecasts, respectively. Therefore, operationally, the second sub-model uses

forecast fields and not analysis fields.

5.2.4 DYNAMIC

5.2.4.1 NOGAPS VORTEX TRACKING ROUTINE (NGPS/X) Tropical cyclone vortices are tracked at FNMOC by converting the 1000-mb u and v wind component fields into isogons. The intersection of isogons are either the center of a cyclonic or anticyclonic circulation, or a col. The tracking program starts at the last known location of the cyclone - a warning position. Based on this position and the last known speed and direction of movement, the program hunts for the next cyclonic center representing the tropical cyclone. Confidence factors are generated within the program and are modified, as required, by a quality control program that formats the data for transmission.

5.2.4.2 GEOPHYSICAL FLUID DYNAMICS MODEL - NAVY (GFDN) This model uses a triple nested movable mesh with 18 sigma levels. The outer mesh domain covers a 75°x75° area with a horizontal resolution of 1° and is fixed for the duration of the model run based on the initial location and movement of the tropical cyclone (TC). The 10°x10° middle and a 5°x5° inner (resolution 1/6°) nested meshes move with the cyclone. Based on the global analysis and an initialization message, the TC is removed from the global analysis, and replaced by a synthetic vortex which has an asymmetric (beta-advection) component added. Boundary conditions are updated periodically from forecast fields generated by a global forecast model. In addition to standard output fields, the model outputs TC track forecasts and maximum isotach swaths indicating the location of maximum winds in relation to the TC track.

5.2.4.3 ONE-WAY (INTERACTIVE) TROPICAL CYCLONE MODEL (OTCM) This technique is a coarse resolution (205-km grid), three layer, primitive equation model with a horizontal domain of 6400 x 4700 km. OTCM is initialized using 6-hour or 12-hour prognostic fields from the latest NOGAPS run, and the initial fields are smoothed and adjusted in the vicinity of the storm to induce a persistence bias into OTCM's forecast. A symmetric bogus vortex is then inserted, and the boundaries updated every 12 hours by NOGAPS fields as the integration proceeds. The bogus vortex is maintained against frictional dissipation by an analytical heating function. The forecast positions are based on the movement of the vortex in the lowest layer of the model (effectively 850-mb).

5.2.4.4 FNMOC BETA AND ADVECTION MODEL (FBAM) This model is an adaptation of the Beta and Advection model used by the National Center for Environmental Prediction (NCEP). The forecast motion results from a calculation of environmental steering and an empirical correction for the observed vector difference between that steering and the 12-hour old storm motion. The steering is computed from the NOGAPS Deep Layer Mean (DLM) wind fields which are a weighted average of the wind fields computed for the 1000-mb to 100-mb levels. The difference between past storm motion and the DLM steering is treated as if the storm were a Rossby wave with an "effective radius" propagating in response to the horizontal gradient of the coriolis parameter, beta. The forecast proceeds in one-hour steps, recomputing the effective radius as beta changes with storm latitude, and blending in a persistence bias for the first 12 hours.

5.2.5 HYBRIDS

5.2.5.1 HALF PERSISTENCE AND CLIM-ATOLOGY (HPAC) Forecast positions generated by equally weighting the forecasts given by XTRP and CLIM.

5.2.5.2 BLENDED (BLND) A simple average of JTWC's six primary forecast aids: OTCM, CSUM, FBAM, JT92, CLIP, and HPAC.

5.2.5.3 WEIGHTED (WGTD) A weighted average of the forecast guidance used to compute BLND: OTCM (29%), CSUM (22%), FBAM (14%), JT92 (14%), HPAC (14%), and CLIP (7%).

5.2.5.4 DYNAMIC AVERAGE (DAVE) A simple average of all dynamic forecast aids: NOGAPS (NGPS), Bracknell (EGRR), Japanese Typhoon Model (JTYM), JT92, FBAM, OTCM, and CSUM.

5.2.6 EMPIRICAL OR ANALYTICAL

5.2.6.1 DVORAK An estimation of a tropical cyclone's current and 24-hour forecast intensity is made from the interpretation of satellite imagery (Dvorak, 1984). These intensity estimates are used with other intensity related data and trends to forecast short-term tropical cyclone intensity.

5.2.6.2 MARTIN/HOLLAND The technique adapts an earlier work (Holland, 1980) and specifically addresses the need for realistic 35-, 50- and 100-kt (18-, 26- and 51-m/sec) wind radii around tropical cyclones. It solves equations for basic gradient wind relations within the tropical cyclone area, using input parameters obtained from enhanced infrared satellite imagery. The diagnosis also includes an asymmetric area of winds caused by tropical cyclone movement. Satellite-derived size and intensity parameters are also used to diagnose internal steering components of tropical cyclone motion known collectively as "beta-drift."

5.2.6.3 TYPHOON ACCELERATION PREDICTION TECHNIQUE (TAPT) — This technique (Weir, 1982) utilizes upper-tropospheric and surface wind fields to estimate acceleration associated with the tropical cyclone's interaction with the mid-latitude westerlies. It includes guidelines for the duration of acceleration, upper limits and probable path of the cyclone.

5.3 TESTING AND RESULTS

A comparison of selected techniques is included in Table 5-5 for all western North Pacific tropical cyclones, Table 5-6 for all North Indian Ocean tropical cyclones and Table 5-7 for the Southern Hemisphere. For example, in Table 5-5 for the 12-hour mean forecast error, 734 cases available for a homogeneous comparison, the average forecast error at 12 hours was 72 nm (133 km) for NGPS and 53 nm (98 km) for JTWC. The difference of 19 nm (35 km) is shown in the lower right. Differences are not always exact, due to computational round-off which occurs for each of the cases available for comparison.

Table 5-1 INITIAL POSITION AND FORECAST ERRORS (NM) FOR THE WESTERN NORTH PACIFIC FOR 1983-1997

	Initial Position		24-Hour				48-Hour				72-Hour			
	Num	Error	Num	Track	Along	Cross	Num	Track	Along	Cross	Num	Track	Along	Cross
1983	445	16	342	117	76	73	253	260	169	164	184	407	259	263
1984	611	22	492	117	84	64	378	232	163	131	286	363	238	216
1985	592	18	477	117	80	68	336	231	153	138	241	367	230	227
1986	743	21	645	126	85	70	535	261	183	151	412	394	276	227
1987	657	18	563	107	71	64	465	204	134	127	389	303	198	186
1988	465	23	373	114	85	58	262	216	170	103	183	315	244	159
1989	710	20	625	120	83	69	481	231	162	127	363	350	265	177
1990	794	21	658	103	72	60	525	203	148	110	432	310	225	168
1991	835	22	733	96	69	53	599	185	137	97	484	287	229	146
1992	941	25	841	107	77	59	687	205	143	116	568	305	210	172
1993	853	26	725	112	79	63	570	212	151	117	437	321	226	173
1994	1058	24	938	105	76	56	776	186	131	105	631	258	176	152
1995	599	29	539	123	89	67	421	215	159	117	319	325	240	167
1996	922	25	880	105	76	56	711	178	134	89	607	272	203	137
1997	910	20	865	93	76	55	752	164	134	87	642	245	202	120
15-Year Average 1983-1997	742	22	646	111	79	62	517	212	151	119	412	321	228	179

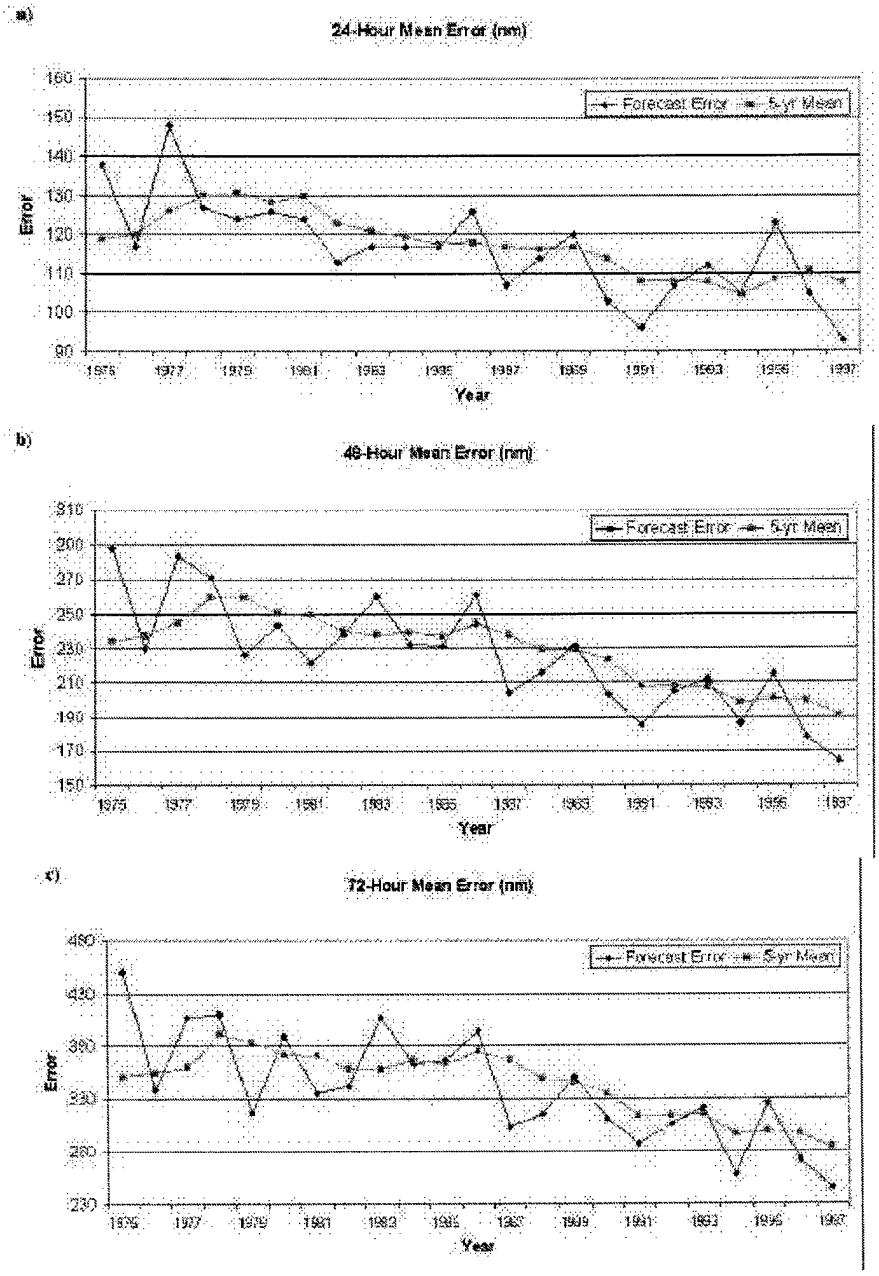

Figure 5-3 Mean track forecast error (nm) and 5-year running mean for a) 24 hours b) 48 hours and c) 72 hours for the western North Pacific Ocean tropical cyclones for the period 1975 to 1997.

Table 5-2 MEAN FORECAST TRACK ERRORS (NM) FOR WESTERN NORTH PACIFIC TROPICAL CYCLONES FOR 1959-1997

	24-HOUR				48-HOUR				72-HOUR			
YEAR	TY (1)	TC	CROSS TRACK (2)	ALONG TRACK (2)	TY (1)	TC	CROSS TRACK (2)	ALONG TRACK (2)	TY (1)	TC	CROSS TRACK (2)	ALONG TRACK (2)
1959	117*				267*							
1960	177*				354*							
1961	136				274							
1962	144				287				476			
1963	127				246				374			
1964	133				284				429			
1965	151				303				418			
1966	136				280				432			
1967	125				276				414			
1968	105				229				337			
1969	111				237				349			
1970	98	104			181	190			272	279		
1971	99	111	64		203	212	118		308	317	177	
1972	116	117	72		245	245	146		382	381	210	
1973	102	108	74		193	197	134		245	253	162	
1974	114	120	78		218	226	157		357	348	245	
1975	129	138	84		279	288	181		442	450	290	
1976	117	117	71		232	230	132		336	338	202	
1977	140	148	83		266	283	157		390	407	228	
1978	120	127	71	87	241	271	151	194	459	410	218	296
1979	113	124	76	81	219	226	138	146	319	316	182	214
1980	116	126	76	86	221	243	147	165	362	389	230	266
1981	117	124	77	80	215	221	131	146	342	334	219	206
1982	114	113	70	74	229	238	142	162	337	342	211	223
1983	110	117	73	76	247	260	164	169	384	407	263	259
1984	110	117	64	84	228	232	131	163	361	363	216	238
1985	112	117	68	80	228	231	138	153	355	367	227	230
1986	117	126	70	85	261	261	151	183	403	394	227	276
1987	101	107	64	71	211	204	127	134	318	303	186	198
1988	107	114	58	85	222	216	103	170	327	315	159	244
1989	107	120	69	83	214	231	127	162	325	350	177	265
1990	98	103	60	72	191	203	110	148	299	310	168	225
1991	93	96	53	69	187	185	97	137	298	287	146	229
1992	97	107	59	77	194	205	116	143	295	305	172	210
1993	102	112	63	79	205	212	117	151	320	321	173	226
1994**	96	105	56	76	172	186	105	131	244	258	152	176
1995	105	123	67	89	200	215	117	159	311	325	167	240
1996	85	105	56	76	157	178	89	134	252	272	137	203
1997	86	93	55	76	159	164	87	134	251	245	120	202

1. Forecasts were verified for typhoons when intensities were at least 35kt (18 m/sec).

2. Cross-track and along-track errors were adopted by the JTWC in 1986. Right angle errors (used prior to 1986) were recomputed as cross-track errors after-the fact to extend thedata base. See Figure 5-1 for the definitions of cross-track and along-track.

*Forecast positions north of 35 degrees north latitude were not verified.

**Statistics were recalculated to resolve earlier ALONG- and CROSS-Track discrepancies.

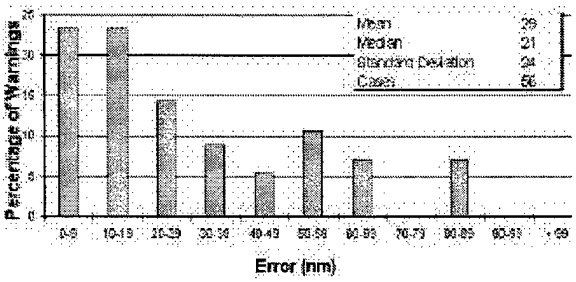

Figure 5-4a Frequency distribution of initial warning position errors (10-nm increments) for North Indian Ocean tropical cyclones in 1997. The largest error, 87 nm, occurred on Tropical Cyclone 02B.

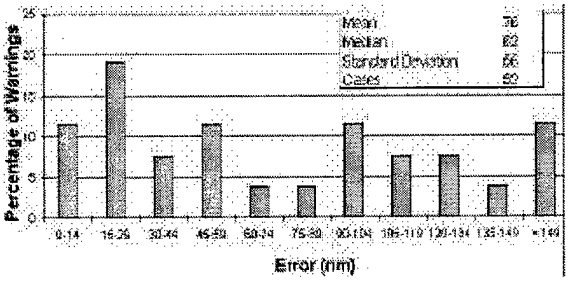

Figure 5-4b Frequency distribution of 12-hour track forecast errors (15-nm increments) for North Indian Ocean tropical cyclones in 1997. The largest error, 232 nm, occurred on Tropical Cyclone 01B.

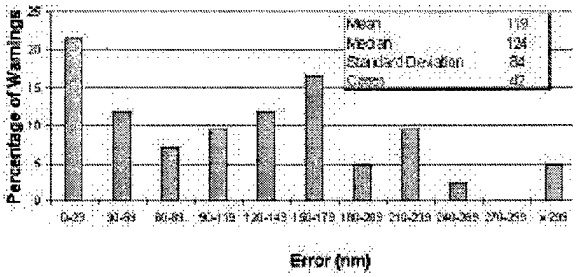

Figure 5-4c Frequency distribution of 24-hour track forecast errors for North Indian Ocean tropical cyclones in 1997. The largest error, 316 nm, occurred on Tropical Cyclone 01B.

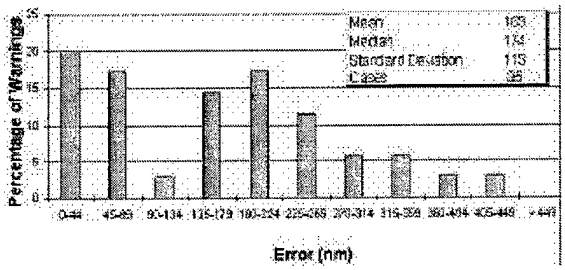

Figure 5-4d Frequency distribution of 36-hour track forecast errors for North Indian Ocean tropical cyclones in 1997. The largest error, 406 nm, occurred on Tropical Cyclone 02B.

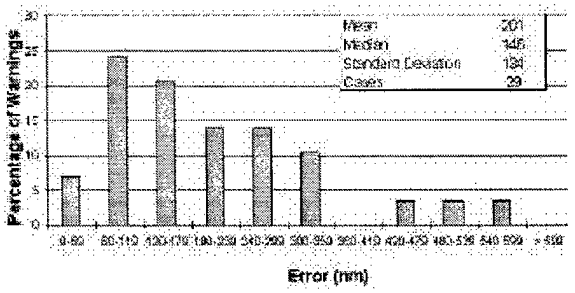

Figure 5-4e Frequency distribution of 48-hour track errors for North Indian Ocean tropical cyclones in 1997. The largest error, 541 nm, occurred on Typhoon Cyclone 02B.

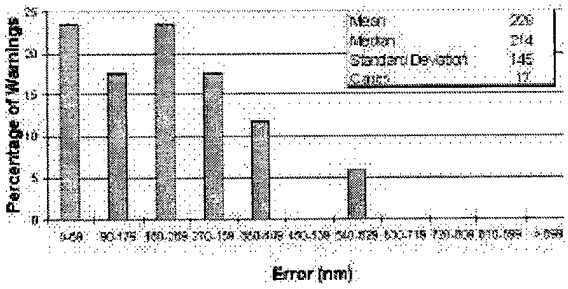

Figure 5-4f Frequency distribution of 72-hour track forecast errors for North Indian Ocean tropical cyclones in 1997. The largest error, 545 nm, occurred on Tropical Cyclone 02B.

Table 5-3 INITIAL POSITION AND FORECAST POSITION ERRORS (NM) FOR THE NORTH INDIAN OCEAN FOR 1983 - 1997

	Initial Position		24-Hour				48-Hour				72-Hour			
	Num	Error	Num	Track	Along	Cross	Num	Track	Along	Cross	Num	Track	Along	Cross
1983	18	38	7	117	90	50	18	153	137	53	0			
1984	67	33	42	154	124	67	20	274	217	139	16	338	339	121
1985	53	31	30	122	102	53	8	242	119	194	0			
1986	28	52	16	134	118	53	7	168	131	80	5	269	189	180
1987	83	42	54	144	97	100	25	205	125	140	21	305	219	188
1988	44	34	30	120	89	63	18	219	112	176	12	409	227	303
1989	44	19	33	88	62	50	17	146	94	86	12	216	164	111
1990	46	31	36	101	85	43	24	146	117	67	17	185	130	104
1991	56	38	43	129	107	54	27	235	200	89	14	450	356	178
1992	191	35	149	128	73	86	100	244	141	166	62	398	276	218
1993	36	27	28	125	87	79	20	198	171	74	12	231	176	116
1994	60	25	44	97	80	44	28	153	124	63	13	213	177	92
1995	54	30	47	138	119	58	32	262	247	77	20	342	304	109
1996	135	33	123	134	94	80	85	238	181	127	58	311	172	237
1997	56	29	42	119	87	49	29	201	168	92	17	228	195	110
15-YEAR AVERAGE														
1983-1997	65	33	48	123	94	62	31	206	152	108	19	300	225	159

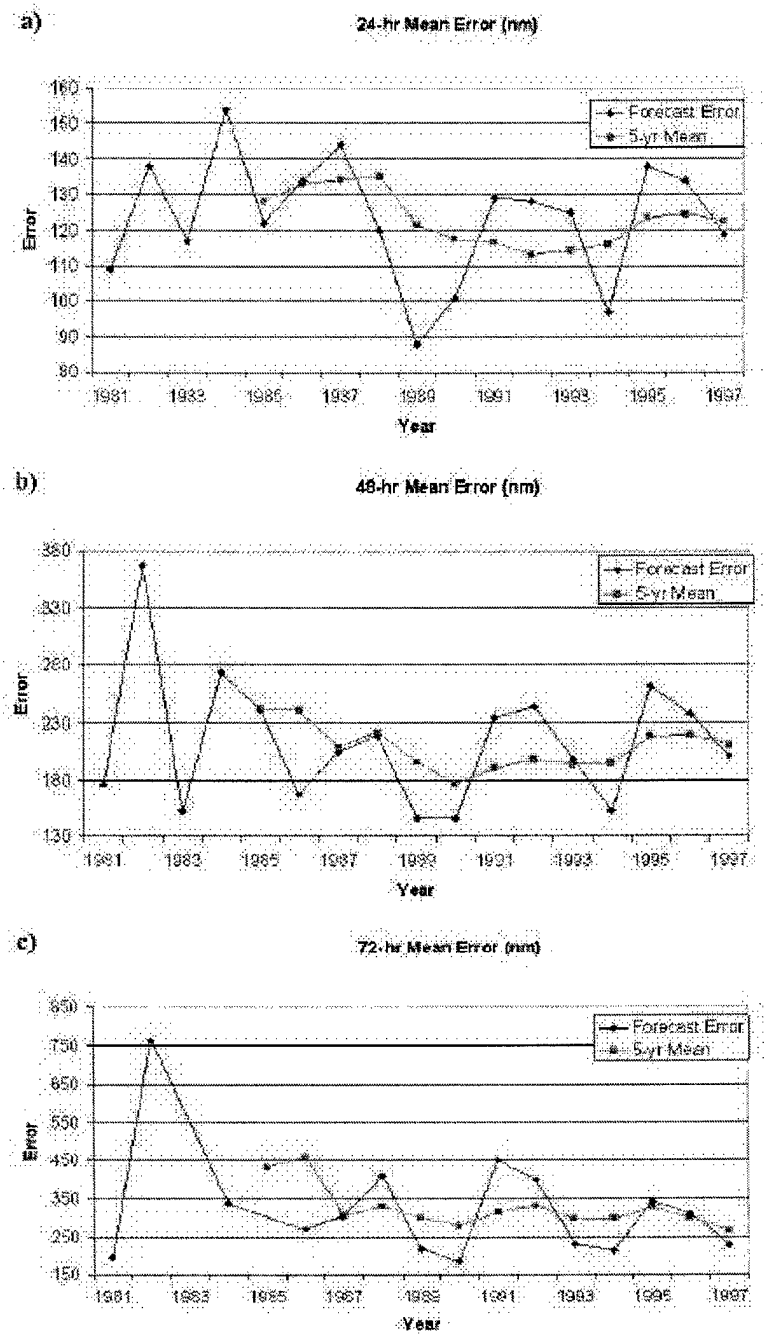

Figure 5-5 Mean track forecast error (nm) and 5-year running mean for a) 24 hours b) 48 hours and c) 72 hours for the western North Indian Ocean tropical cyclones for the period 1981 to 1997.

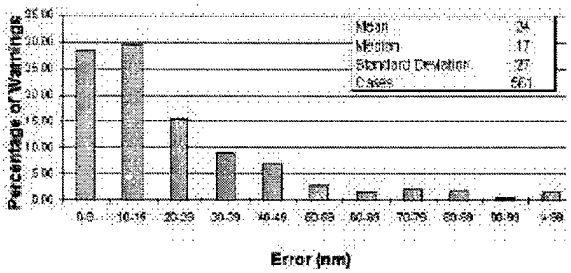

Figure 5-6a Frequency distribution of initial warning position errors for South Pacific and South Indian Ocean tropical cyclones in 1997. The largest error, 251 nm, occurred on Tropical Cyclone 21S (Iletta).

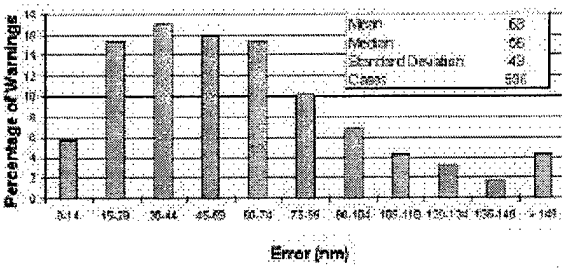

Figure 5-6b Frequency distribution of 12-hour track forecast errors for South Pacific and South Indian Ocean tropical cyclones in 1997. The largest error , 373 nm, occurred on Tropical Cyclone 25S (Karlette).

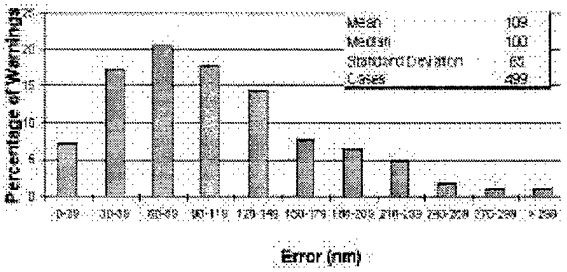

Figure 5-6c Frequency distribution of 24-hour track forecast errors for South Pacific and South Indian Ocean tropical cyclones in 1997. The largest error, 412 nm, occurred on Tropical Cyclone 25S (Karlette)

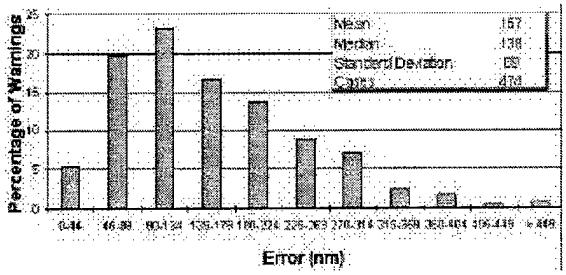

Figure 5-6d Frequency distribution of 36-hour track forecast errors for South Pacific and South Indian Ocean tropical cyclones in 1997. The largest error, 545 nm, occurred on Tropical Cyclone 05S (Melanie).

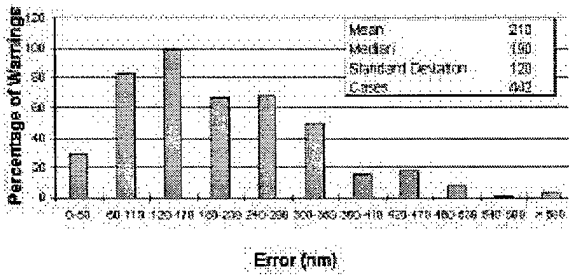

Figure 5-6e Frequency distribution of 48-hour track forecast errors for South Pacific and South Indian Ocean tropical cyclones in 1997. The largest error, 732 nm, occurred on Tropical Cyclone 05S (Melanie).

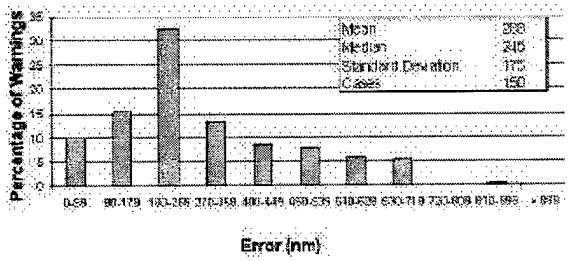

Figure 5-6f Frequency distribution of 72-hour track forecast errors for South Pacific and South Indian Ocean tropical cyclones in 1997. The largest error, 854 nm, occurred on Tropical Cyclone 26S (Harold).

TABLE 5-4 INITIAL POSITION AND FORECAST POSITION ERRORS (NM) FOR THE SOUTHERN HEMISPHERE FOR 1983-1997

	Initial Position		24-Hour				48-Hour				72-Hour			
	Warnings	Error	Num	Track	Along	Cross	Num	Track	Along	Cross	Num	Track	Along	Cross
1983	191	35	163	130	88	77	126	241	158	145				
1984	301	36	252	133	90	79	191	231	159	134				
1985	306	36	257	134	92	79	193	236	169	132				
1986	279	40	227	129	86	77	171	262	169	164				
1987	189	46	138	145	94	90	101	280	153	138				
1988	204	34	99	146	98	83	48	290	246	144				
1989	287	31	242	124	84	73	186	240	166	136				
1990	272	27	228	143	105	74	177	263	178	152				
1991	264	24	231	115	75	69	185	220	152	129				
1992	267	28	230	124	91	64	208	240	177	129				
1993	257	21	225	102	74	57	176	199	142	114				
1994	386	28	345	115	77	68	282	224	147	134				
1995	245	24	222	108	82	55	175	198	144	108	53	291	169	190
1996	343	24	298	125	90	67	237	240	174	129	46	277	221	133
1997	561	24	499	109	82	72	442	210	163	135	150	288	248	175
15-YEAR AVERAGE														
1983-1997	290	31	244	125	87	72	193	87	166	135	83	285	213	166

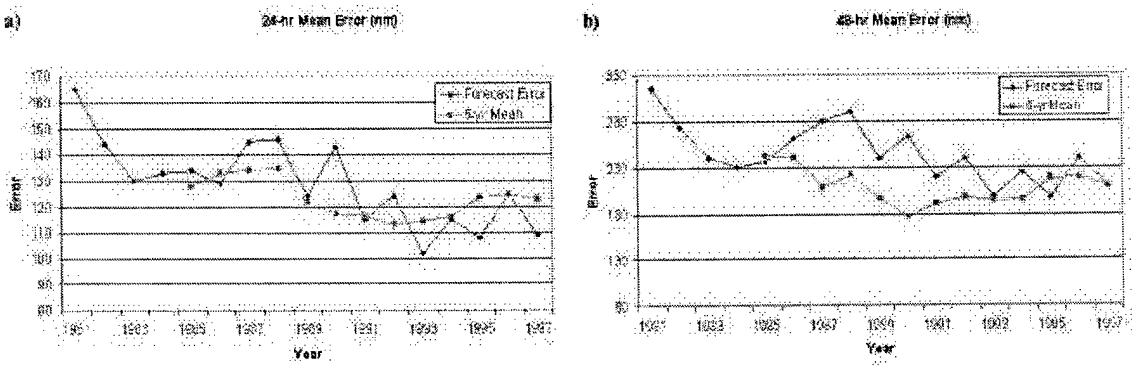

Figure 5-5 Mean track forecast error (nm) and 5-year running mean for a) 24 hours b) 48 hours for the South Indian Ocean tropical cyclones for the period 1981 to 1997.

Table 5-5 1997 ERROR STATISTICS FOR SELECTED OBJECTIVE TECHNIQUES THE NORTHWEST PACIFIC
(1 JAN 1997 - 31 DEC 1997)

12-HOUR MEAN FORECAST ERROR(NM)

	JTWC		NGPS		GFDN		FBAM		CSUM		JGSM		JTYM		CLIP		DAVE	
JTWC	849	55																
	55	0																
NGPS	734	53	758	73														
	72	19	73	0														
GFDN	700	51	647	70	712	67												
	67	16	65	-5	67	0												
FBAM	814	55	717	72	677	66	868	60										
	56	1	55	-17	51	-15	60	0										
CSUM	743	55	652	72	618	66	787	59	793	63								
	59	4	57	-15	54	-12	63	4	63	0								
JGSM	315	47	312	60	262	64	310	49	291	51	321	53						
	53	6	52	-8	52	-12	53	4	53	2	53	0						
JTYM	313	47	267	72	299	55	302	47	282	51	6	92	319	56				
	56	9	56	-16	55	0	55	8	55	4	83	-9	56	0				
CLIP	840	55	739	72	698	66	865	60	792	63	319	53	310	56	897	64		
	61	6	59	-13	56	-10	64	4	64	1	52	-1	52	-4	64	0		
DAVE	757	56	673	73	640	67	770	59	723	62	284	54	276	57	792	63	793	58
	56	0	54	-19	51	-16	57	-2	57	-5	47	-7	49	-8	58	-5	58	0

Number of Cases	X-Axis Technique Error
Y-Axis Technique Error	Error Difference (Y-X)

KEY FOR ERROR STATISTICS TABLES

24- HOUR MEAN FORECAST ERROR (NM)

	JTWC		NGPS		GFDN		FBAM		CSUM		EGRR		JGSM		JTYM		CLIP		DAVE	
JTWC	816	92																		
	92	0																		
NGPS	718	90	739	112																
	111	21	112	0																
GFDN	678	87	635	109	686	99														
	98	11	99	-10	99	0														
FBAM	786	93	703	111	658	98	841	104												
	99	6	99	-12	91	-7	104	0												
CSUM	716	93	639	111	601	98	762	102	767	114										
	110	17	108	-3	105	7	114	12	114	0										
EGRR	336	87	329	102	269	99	340	100	317	107	376	105								
	99	12	97	-5	97	-2	100	0	97	-10	105	0								
JGSM	312	81	312	97	262	98	307	93	288	100	279	89	319	81						
	81	0	81	-16	82	-16	82	-11	82	-18	79	-10	81	0						
JTYM	306	81	265	110	295	87	296	84	276	100	6	129	6	133	312	89				
	88	7	88	-22	87	0	88	4	88	-12	134	5	109	-24	89	0				
CLIP	809	93	723	111	677	98	838	104	766	114	352	100	317	81	304	88	867	116		
	112	19	110	-1	106	8	115	11	116	2	113	13	100	19	100	12	116	0		
DAVE	728	93	657	111	619	97	744	101	698	113	316	95	282	82	271	89	763	114	764	91
	88	-5	87	-24	83	-14	90	-11	90	-23	84	-11	80	-2	80	-9	91	-23	91	0

Table 5-5 (Continued) 36-HOUR MEAN FORECAST ERROR (NM)

	JTWC		NGPS		GFDN		FBAM		CSUM		JGSM		JTYM		CLIP		DAVE	
JTWC	770	129																
	129	0																
NGPS	666	125	682	149														
	148	23	149	0														
GFDN	643	124	590	146	648	135												
	135	11	131	-15	135	0												
FBAM	742	129	654	150	625	135	801	159										
	153	24	148	-2	145	10	159	0										
CSUM	674	129	595	150	570	135	724	156	729	170								
	165	36	162	12	159	24	170	14	170	0								
JGSM	293	117	288	135	249	134	289	149	270	152	300	109						
	110	-7	109	-26	109	-25	110	-39	111	-41	109	0						
JTYM	293	116	249	147	283	124	284	132	264	155	6	179	299	116				
	111	-5	109	-38	110	-14	114	-18	114	-41	142	-37	116	0				
CLIP	763	129	671	149	643	135	798	159	728	170	298	110	292	115	825	176		
	170	41	167	18	164	29	175	16	176	6	158	48	161	46	176	0		
DAVE	684	129	610	148	585	131	708	157	664	168	265	112	259	116	724	174	725	128
	123	-6	121	-27	117	-14	128	-29	127	-41	118	6	115	-1	128	-46	128	0

48-HOUR MEAN FORECAST ERROR (NM)

	JTWC		NGPS		GFDN		FBAM		CSUM		EGRR		JGSM		JTYM		CLIP		DAVE	
JTWC	707	163																		
	163	0																		
NGPS	596	159	615	189																
	189	30	189	0																
GFDN	594	159	529	186	602	176														
	176	17	173	-13	176	0														
FBAM	682	164	591	190	582	177	756	220												
	211	47	208	18	203	26	220	0												
CSUM	617	161	538	193	528	175	683	215	686	227										
	219	58	216	23	211	36	227	12	227	0										
EGRR	296	157	274	175	238	177	304	214	281	218	334	168								
	163	6	153	-22	155	-22	162	-52	153	-65	168	0								
JGSM	283	157	269	178	238	183	278	211	259	215	252	156	288	139						
	139	-18	139	-39	135	-48	138	-73	139	-76	133	-23	139	0						
JTYM	276	155	231	197	269	170	271	196	251	213	6	188	6	212	284	151				
	146	-9	141	-56	143	-27	148	-48	150	-63	158	-30	176	-36	151	0				
CLIP	701	163	607	188	598	176	755	220	685	227	314	163	287	139	278	149	779	244		
	231	68	228	40	224	48	242	22	242	15	241	78	228	89	229	80	244	0		
DAVE	625	164	551	189	543	170	664	217	623	225	277	156	254	141	246	151	681	241	681	166
	159	-5	157	-32	154	-16	166	-51	166	-59	158	2	161	20	158	7	166	-75	166	0

Table 5-5 (Continued) 72-HOUR MEAN FORECAST ERROR(NM)

	JTWC		NGPS		GFDN		FBAM		CSUM		EGRR		JGSM		JTYM		CLIP		DAVE	
JTWC	598	245																		
	245	0																		
NGPS	491	229	515	279																
	284	55	279	0																
GFDN	484	232	431	278	500	284														
	282	50	270	-8	284	0														
FBAM	578	245	497	282	485	285	662	351												
	328	83	332	50	320	35	351	0												
CSUM	523	243	448	285	440	283	594	341	597	338										
	319	76	311	26	310	27	337	-4	338	0										
EGRR	239	239	222	264	189	284	255	339	232	336	280	233								
	232	-7	216	-48	218	-66	227	-112	213	-123	233	0								
JGSM	239	240	225	277	197	296	241	341	222	336	210	223	249	214						
	215	-25	211	-66	197	-99	213	-128	215	-121	204	-19	214	0						
JTYM	232	240	194	297	222	277	232	322	211	329	3	155	5	277	242	238				
	232	-8	211	-86	219	-58	235	-87	239	-90	248	93	200	-77	238	0				
CLIP	592	245	508	280	496	284	661	351	596	338	261	227	248	213	236	236	680	389		
	354	109	353	73	344	60	387	36	382	44	396	169	378	165	367	131	389	0		
DAVE	525	246	460	280	447	274	579	351	542	342	229	216	218	213	206	236	591	385	591	264
	251	5	248	-32	249	-25	263	-88	262	-80	259	43	276	63	259	23	264	-121	264	0

Table 5-6 1997 ERROR STATISTICS FOR SELECTED OBJECTIVE TECHNIQUES IN THE NORTH INDIAN OCEAN
(1 JAN 1997 - 31 DEC 1997)

12 HOUR MEAN FORECAST ERRORS(NM)

	JTWC		NGPS		OTCM		GFDN		CLIP		HPAC	
JTWC	52	76										
	76	0										
NGPS	47	72	48	75								
	74	2	75	0								
OTCM	40	77	38	70	40	96						
	96	19	92	22	96	0						
GFDN	43	79	41	78	35	98	44	110				
	108	29	105	27	106	8	110	0				
CLIP	50	78	47	71	40	96	42	106	56	83		
	86	8	79	8	83	-13	89	-17	83	0		
HPAC	51	77	47	71	40	96	42	106	56	83	57	86
	86	9	80	9	84	-12	90	-16	87	4	86	0

24 HOUR MEAN FORECAST ERRORS(NM)

	JTWC		NGPS		OTCM		GFDN		CLIP		HPAC	
JTWC	42	119										
	119	0										
NGPS	39	122	43	112								
	113	-9	112	0								
OTCM	25	111	27	94	27	123						
	123	12	123	29	123	0						
GFDN	33	128	36	121	23	125	36	209				
	216	88	209	88	205	80	209	0				
CLIP	41	121	43	112	27	123	36	209	50	133		
	135	14	139	27	134	11	144	-65	133	0		
HPAC	42	119	43	112	27	123	36	209	50	133	51	138
	135	16	141	29	122	-1	148	-61	140	7	138	0

Table 5-6 (Continued) 36 HOUR MEAN FORECAST ERRORS(NM)

	JTWC		NGPS		OTCM		GFDN		CLIP		HPAC	
JTWC	35	164										
	164	0										
NGPS	32	167	35	136								
	133	-34	136	0								
OTCM	15	159	17	120	17	167						
	176	17	167	47	167	0						
GFDN	27	172	27	145	13	178	27	314				
	314	142	314	169	281	103	314	0				
CLIP	34	168	35	136	17	167	27	314	42	195		
	198	30	206	70	217	50	208	-106	195	0		
HPAC	35	164	35	136	17	167	27	314	42	195	43	200
	195	31	205	69	196	29	209	-105	203	8	200	0

48 HOUR MEAN FORECAST ERRORS(NM)

	JTWC		NGPS		OTCM		GFDN		CLIP		HPAC	
JTWC	29	201										
	201	0										
NGPS	26	200	27	157								
	154	-46	157	0								
OTCM	8	231	8	171	8	224						
	224	-7	224	53	224	0						
GFDN	21	206	21	170	8	224	21	352				
	352	146	352	182	375	151	352	0				
CLIP	28	206	27	157	8	224	21	352	34	248		
	258	52	260	103	326	102	264	-88	248	0		
HPAC	29	201	27	157	8	224	21	352	34	248	35	243
	239	38	240	83	292	68	245	-107	247	-1	243	0

72 HOUR MEAN FORECAST ERRORS(NM)

	JTWC		NGPS		OTCM		GFDN		CLIP		HPAC	
JTWC	17	228										
	228	0										
NGPS	13	203	13	125								
	125	-78	125	0								
OTCM	2	108	1	136	2	413						
	413	305	464	328	413	0						
GFDN	11	200	9	149	2	413	11	441				
	441	241	376	227	538	125	441	0				
CLIP	17	228	13	125	2	413	11	441	22	343		
	358	130	289	164	420	7	382	-59	343	0		
HPAC	17	228	13	125	2	413	11	441	22	343	22	300
	285	57	226	101	172	-241	261	-180	300	-43		

Table 5-7 1997 ERROR STATISTICS FOR SELECTED OBJECTIVE TECHNIQUES IN THE SOUTHERN HEMISPHERE (1 JUL 1996 - 30 JUN 1997)

12-HOUR MEAN FORECAST ERROR (NM)

	JTWC		NGPS		OTCM		GFDN		CLIP		HPAC	
JTWC	540	64										
	64	0										
NGPS	434	60	721	85								
	83	23	85	0								
OTCM	416	60	636	83	700	110						
	108	48	109	26	110	0						
GFDN	209	58	284	76	274	111	314	84				
	83	25	82	6	84	-27	84	0				
CLIP	536	64	505	84	488	109	242	83	704	124		
	108	44	104	20	100	-9	123	40	124	0		
HPAC	529	63	499	83	485	109	238	82	693	122	696	76
	70	7	70	-13	69	-40	66	-16	76	-46	76	0

24-HOUR MEAN FORECAST ERROR (NM)

	JTWC		NGPS		OTCM		GFDN		EGRR		CLIP		HPAC	
JTWC	503	110												
	110	0												
NGPS	412	107	705	127										
	125	18	127	0										
OTCM	385	104	606	123	662	171								
	171	67	170	47	171	0								
GFDN	196	99	275	121	258	184	299	122						
	117	18	119	-2	120	-64	122	0						
EGRR	186	101	276	116	235	163	104	123	342	134				
	111	10	114	-2	112	-51	116	-7	134	0				
CLIP	501	109	497	127	463	171	231	118	225	115	684	178		
	158	49	156	29	149	-22	182	64	164	49	178	0		
HPAC	496	109	492	126	461	171	228	118	223	115	675	175	678	132
	122	13	124	-2	123	-48	116	-2	124	9	132	-43	132	0

36-HOUR MEAN FORECAST ERROR (NM)

	JTWC		NGPS		OTCM		GFDN		CLIP		HPAC	
JTWC	478	158										
	158	0										
NGPS	393	156	667	174								
	165	9	174	0								
OTCM	358	150	564	171	615	235						
	230	80	234	63	235	0						
GFDN	188	143	263	167	237	255	283	165				
	156	13	160	-7	158	-97	165	0				
CLIP	476	157	473	168	431	235	222	160	656	237		
	213	56	215	47	205	-30	239	79	237	0		
HPAC	466	156	459	163	428	235	214	158	638	231	641	188
	175	19	179	16	179	-56	169	11	187	-44	188	0

Table 5-7 (continued) 48-HOUR MEAN FORECAST ERROR (NM)

	JTWC		NGPS		OTCM		GFDN		EGRR		CLIP		HPAC	
JTWC	446	211												
	211	0												
NGPS	367	210	630	211										
	212	2	211	0										
OTCM	318	201	518	203	563	302								
	300	99	301	98	302	0								
GFDN	175	192	248	216	219	319	271	221						
	213	21	217	1	209	-110	221	0						
EGRR	156	200	234	192	194	286	89	229	298	190				
	191	-9	183	-9	177	-109	186	-43	190	0				
CLIP	444	210	449	212	399	306	214	216	194	187	627	301		
	277	67	277	65	269	-37	300	84	292	105	301	0		
HPAC	433	208	436	207	397	306	206	212	189	183	609	296	611	247
	231	23	241	34	238	-68	226	14	241	58	248	-48	247	0

72-HOUR MEAN FORECAST ERROR (NM)

	JTWC		NGPS		OTCM		GFDN		EGRR		CLIP		HPAC	
JTWC	147	295												
	295	0												
NGPS	137	303	541	286										
	319	16	286	0										
OTCM	114	297	415	274	461	426								
	435	138	419	145	426	0								
GFDN	90	265	213	313	184	438	238	343						
	329	64	332	19	331	-107	343	0						
EGRR	54	280	190	255	153	406	72	370	244	258				
	273	-7	246	-9	247	-159	263	-107	258	0				
CLIP	146	295	390	295	328	428	194	351	156	265	551	417		
	387	92	399	104	394	-34	406	55	409	144	417	0		
HPAC	147	295	379	290	325	426	188	342	151	259	536	411	538	635
	299	4	348	58	343	-83	352	10	347	88	366	-45	365	0

6. TROPICAL CYCLONE WARNING VERIFICATION STATISTICS

6.1 GENERAL

Since 1959, JTWC has compiled data on tropical cyclones (TC) within its Area of Responsibility (AOR). In this 39-year period, over 32,000 warnings were verified on over 1,800 TCs. The verification data include best tracks (6-hourly positions and associated intensities), JTWC forecasts (12-, 24-, 36-, 48- and 72-hour position, intensity and wind radii), and fixes made from satellite, aircraft, radar, and synoptic data. These data are archived and available upon request.

Efforts are underway to make this information available via anonymous File Transfer Protocol (FTP) over the Internet; however, until this project is complete JTWC will provide the data by FTP upon request. To request data by Internet, send e-mail to: jtops@npmoc.navy.mil. If the Internet is not an option, data can be copied to 3.5" computer diskettes (that you provide) upon request. Plan for one diskette for each year and ocean basin. Mail them with your request to: NAVPACMETOCCEN/JTWC, Box 113, Pearl Harbor, HI, 96860-5050.

6.2 WARNING VERIFICATION STATISTICS

6.2.1 WESTERN NORTH PACIFIC

This section includes verification statistics for each significant TC in the western North Pacific during 1997.

JTWC BEST TRACK, FORECAST TRACK AND INTENSITY ERRORS BY WARNING

TROPICAL STORM HANNAH (01W)

	WRN	BEST TRACK			POSITION ERRORS						WIND ERRORS					
DTG	NO.	LAT	LONG	WIND	00	12	24	36	48	72	00	12	24	36	48	72
97011100		4.0N	176.0E	15												
97011106		4.0N	175.4E	15												
97011112		4.0N	174.7E	15												
97011118		4.0N	173.9E	15												
97011200		4.0N	173.2E	15												
97011206		4.0N	172.2E	15												
97011212		4.0N	171.0E	15												
97011218		3.9N	169.5E	15												
97011300		3.9N	167.8E	15												
97011306		4.0N	166.4E	15												
97011312		4.2N	164.8E	15												
97011318		4.4N	163.2E	15												
97011400		4.6N	161.3E	15												
97011406		4.8N	159.7E	15												
97011412		5.0N	158.2E	15												
97011418		5.0N	156.5E	15												
97011500		5.0N	155.0E	15												
97011506		5.0N	153.5E	15												
97011512		5.1N	151.9E	15												
97011518		5.2N	150.6E	15												
97011600		5.4N	149.3E	15												
97011606		5.6N	148.3E	15												
97011612		5.8N	147.4E	15												
97011618		6.0N	146.4E	15												
97011700		6.2N	145.4E	15												
97011706		6.4N	144.5E	20												
97011712		6.5N	143.6E	20												

TROPICAL STORM HANNAH (01W) (CONTINUED)

DTG	WRN NO.	BEST TRACK LAT	LONG	WIND	POSITION ERRORS 00	12	24	36	48	72	WIND ERRORS 00	12	24	36	48	72
97011718		6.5N	142.4E	20												
97011800		6.6N	141.9E	20												
97011806		6.6N	141.3E	20												
97011812		6.5N	140.8E	20												
97011818		6.3N	140.2E	25												
97011900		6.0N	139.7E	30												
97011906	1	6.0N	139.7E	30	23	48	72	88			-5	-15	-25	-20		
97011912		6.4N	138.5E	40												
97011918	2	6.4N	138.5E	40	24	38	43	72	174	157	-5	-5	5	10	5	15
97012000	3	6.7N	138.0E	45	33	42	41	56	102	77	5	10	15	15	20	30
97012006	4	7.0N	137.4E	50	21	36	36	96	110	77	-5	0	5	10	15	20
97012012	5	7.1N	136.9E	45	26	26	104	180	147	155	0	0	5	0	5	15
97012018	6	7.3N	136.4E	45	32	36	139	173	108	72	0	0	5	5	10	15
97012100	7	7.7N	135.7E	45	125	47	79	59	130	182	0	0	5	10	15	15
97012106	8	8.3N	134.7E	45	106	65	70	130	222	277	0	0	10	25	25	35
97012112	9	9.3N	133.8E	45	109	130	193	277	350	333	-10	0	15	20	20	20
97012118	10	10.2N	133.5E	45	117	152	241	323	374	366	0	5	15	10	10	5
97012200	11	10.8N	133.4E	45	13	58	116	178	186	149	-5	5	5	10	5	0
97012206	12	11.0N	133.0E	40	24	83	113	150			-10	0	-5	-5		
97012212		10.0N	132.9E	30												
97012218	13	10.0N	132.9E	30	116	175	190	163			0	0	0	-5		
97012300		9.3N	133.1E	30												
97012306	14	9.3N	133.1E	30	0	53	83	93			-5	0	0	-5		
97012312		8.6N	132.5E	25												
97012318	15	8.6N	132.5E	25	46	99	166	261			0	0	0	-5		
97012400		9.0N	131.8E	25												
97012406	16	9.0N	131.8E	25	18	17	43	100			0	0	0	-5		
97012412		9.6N	131.3E	25												
97012418	17	9.6N	131.3E	25	21	63	108				0	0	-5			
97012500		10.5N	131.1E	25												
97012506		11.1N	131.2E	25												
97012512		11.3N	130.9E	25												
97012518		11.2N	130.5E	25												
97012600		10.9N	130.0E	25												
97012606		10.3N	129.5E	25												
97012612		9.8N	128.9E	25												
97012618		9.5N	128.2E	25												
97012700		9.1N	127.7E	25												
97012706		8.8N	127.6E	25												
97012712		8.4N	127.6E	25												
		AVERAGE			51	69	109	150	191	185	3	2	7	10	13	17
		# CASES			17	17	17	16	10	10	17	17	17	16	10	10

SUPER TYPHOON ISA (02W)

DTG	WRN NO.	BEST TRACK LAT	LONG	WIND	POSITION ERRORS 00	12	24	36	48	72	WIND ERRORS 00	12	24	36	48	72
97082806		11.8N	166.7W	15												
97082812		11.8N	167.1W	25												
97082818		11.8N	167.6W	25												
97082900		11.8N	168.1W	25												
97082906		11.8N	168.6W	25												
97082912		11.8N	169.0W	25												
97082918		11.9N	169.3W	25												
97083000		12.1N	169.5W	25												
97083006		12.3N	170.0W	25												
97083012		12.4N	170.6W	25												
97083018		12.4N	171.3W	25												
97083100		12.5N	172.0W	25												
97083106		12.6N	172.6W	25												
97083112		12.7N	173.1W	25												
97083118		12.7N	173.6W	25												
97090100		12.7N	174.1W	25												
97090106		12.7N	174.6W	25												
97090112		12.7N	175.2W	25												
97090118		12.7N	175.8W	30												
97090200		12.8N	176.4W	30												
97090206		13.0N	176.9W	30												

SUPER TYPHOON ISA (02W) (CONTINUED)

DTG	WRN NO.	BEST TRACK LAT	LONG	WIND	POSITION ERRORS 00	12	24	36	48	72	WIND ERRORS 00	12	24	36	48	72
97090212		13.1N	177.3W	30												
97090218	1	13.2N	177.7W	30	11						5					
97090300	2	13.3N	178.2W	35	37						0					
97090306	3	13.3N	178.7W	35	102						0					
97090312	4	13.2N	179.2W	35	117						5					
97090318	5	13.1N	179.8W	35	0						0					
97090400	6	13.1N	179.4E	35	26						-5					
97090406	7	13.1N	178.3E	35	42	96	140	133	173	260	0	5	10	15	20	5
97090412	8	13.1N	177.0E	35	107	204	217	213	265	304	0	5	10	15	20	10
97090418	9	13.3N	175.5E	35	166	250	257	268	307	295	5	10	15	20	15	5
97090500	10	13.7N	174.0E	35	83	154	228	270	276	272	0	0	5	5	0	-10
97090506	11	14.2N	172.9E	35	42	87	118	136	160	217	-5	-5	-5	-5	-10	-20
97090512	12	14.6N	172.1E	35	34	86	88	93	114	171	0	0	0	-5	-15	-20
97090518	13	15.0N	171.3E	35	53	58	55	69	100	147	0	5	0	-5	-10	-15
97090600	14	15.5N	170.4E	35	39	99	132	91	30	36	0	0	-5	-15	-20	-50
97090606	15	16.0N	169.1E	35	36	188	195	170	146	126	0	-5	-15	-20	-15	-50
97090612	16	16.4N	167.8E	35	31	40	13	56	86	70	0	-5	-15	-20	-25	-80
97090618	17	16.7N	166.5E	40	25	16	33	81	86	86	-5	-10	-20	-25	-30	-90
97090700	18	17.0N	165.3E	45	18	64	121	145	142	96	0	0	0	0	-25	-70
97090706	19	17.3N	164.3E	50	11	29	58	64	57	29	0	-5	-5	-10	-40	-70
97090712	20	17.5N	163.4E	55	6	33	56	58	51	30	0	0	0	-20	-50	-60
97090718	21	17.7N	162.6E	60	21	51	67	86	88	108	0	0	-5	-30	-60	-55
97090800	22	17.9N	161.8E	60	13	29	59	92	97	115	0	5	-15	-45	-55	-50
97090806	23	18.0N	161.0E	65	22	62	91	120	111	139	0	-5	-30	-60	-55	-50
97090812	24	18.1N	159.9E	65	20	154	162	172	183	218	0	-25	-55	-65	-60	-50
97090818	25	18.1N	158.7E	75	21	42	66	82	116	157	-5	-30	-60	-55	-50	-30
97090900	26	18.1N	157.5E	90	8	18	32	63	112	171	-10	-40	-50	-45	-40	-15
97090906	27	18.1N	156.2E	105	6	17	40	74	104	139	-10	-40	-35	-30	-25	-10
97090912	28	18.2N	154.9E	125	11	47	87	102	109	143	15	0	-10	-25	-20	-15
97090918	29	18.4N	153.5E	140	23	56	79	97	105	148	0	-5	-15	-25	-15	-10
97091000	30	18.6N	152.1E	140	12	29	54	78	110	186	0	-5	-15	-20	-10	0
97091006	31	18.9N	150.8E	140	6	16	21	16	0	65	0	-5	-15	-15	-10	0
97091012	32	19.1N	149.4E	140	5	20	17	8	18	60	-5	-5	-10	-10	-5	5
97091018	33	19.3N	148.0E	140	5	13	8	12	32	71	0	-5	-5	-10	0	5
97091100	34	19.5N	146.6E	140	0	13	32	54	79	145	0	5	10	10	20	20
97091106	35	19.9N	145.3E	140	5	245	251	257	260	272	0	5	0	0	10	15
97091112	36	20.3N	144.0E	135	23	53	67	62	79	124	0	5	5	15	15	10
97091118	37	20.8N	142.7E	130	0	5	16	56	84	107	0	0	5	10	5	10
97091200	38	21.3N	141.4E	125	13	30	54	84	110	106	0	0	10	5	0	-5
97091206	39	21.9N	140.1E	125	12	11	26	69	144	130	0	10	15	15	10	-5
97091212	40	22.5N	138.7E	120	0	32	68	115	119	187	0	10	10	10	10	0
97091218	41	23.2N	137.4E	115	8	30	63	89	84	209	0	5	5	10	10	0
97091300	42	24.0N	136.1E	105	17	24	42	51	106	101	0	0	0	-5	-15	-15
97091306	43	24.9N	134.9E	105	8	30	44	93	141	57	0	0	5	0	-15	-10
97091312	44	25.7N	133.8E	100	13	53	77	114	139	82	0	0	-5	-10	-25	-10
97091318	45	26.5N	132.6E	100	20	226	158	74	16	221	-5	10	30	20	10	10
97091400	46	27.3N	131.5E	95	8	56	122	189	221	168	-10	-10	-10	-15	-15	10
97091406	47	27.9N	130.6E	90	16	55	111	171	190	245	-10	-10	-15	-10	-20	10
97091412	48	28.3N	130.0E	90	7	41	87	109	84		-20	-20	-20	-15	-15	
97091418	49	28.6N	129.7E	85	7	24	50	24	72		-20	-20	-15	-10	0	
97091500	50	28.9N	129.5E	85	0	27	31	66	90		-20	-20	-15	-20	0	
97091506	51	29.3N	129.5E	85	0	5	36	110	180		-20	-15	-15	-5	10	
97091512	52	29.9N	129.7E	80	6	49	83	120			-15	-10	-10	5		
97091518	53	30.6N	130.1E	75	20	42	132	169			-10	-10	0	15		
97091600	54	31.6N	130.7E	70	11	78	181				-5	-15	5			
97091606	55	33.0N	131.7E	65	20	126	219				-10	0	10			
97091612	56	34.1N	133.1E	60	19	33					-15	0				
97091618	57	35.1N	134.6E	45	15	18					-10	5				
97091700	58	36.2N	136.2E	35	7						-5					
97091706	59	37.7N	138.4E	25	15						0					
		AVERAGE			25	64	91	105	120	147	4	8	13	17	20	24
		# CASES			59	51	49	47	45	41	59	51	49	47	45	41

TROPICAL STORM JIMMY (03W)

DTG	WRN NO.	BEST TRACK LAT	LONG	WIND	POSITION ERRORS 00	12	24	36	48	72	WIND ERRORS 00	12	24	36	48	72
97041800		5.1N	168.0E	15												

TROPICAL STORM JIMMY (03W) (CONTINUED)

DTG	WRN NO.	BEST TRACK LAT	LONG	WIND	POSITION ERRORS 00	12	24	36	48	72	WIND ERRORS 00	12	24	36	48	72
97041806		5.2N	167.3E	15												
97041812		5.4N	166.5E	15												
97041818		5.6N	165.7E	15												
97041900		5.8N	164.8E	15												
97041906		6.2N	164.1E	15												
97041912		6.6N	163.4E	15												
97041918		6.9N	162.6E	15												
97042000		7.2N	161.9E	15												
97042006		7.4N	161.2E	15												
97042012		7.5N	160.7E	20												
97042018		7.6N	160.2E	20												
97042100		7.8N	159.7E	20												
97042106		8.1N	159.3E	25												
97042112		8.6N	158.8E	25												
97042118		9.4N	158.2E	30												
97042200		10.3N	157.6E	30												
97042206	1	11.3N	157.1E	35	21	35	58	33	134	291	-5	0	-5	-10	-10	10
97042212	2	12.3N	156.5E	35	18	83	86	68	120	283	0	-5	-5	-15	-10	15
97042218	3	13.2N	155.5E	35	47	86	87	84	104	244	0	-10	-10	-15	-10	20
97042300	4	14.1N	154.7E	40	16	23	98	181	255	341	0	0	0	5	5	20
97042306	5	15.0N	154.2E	45	5	47	125	161	194		-10	-15	-15	-10	-10	
97042312	6	15.8N	153.8E	45	5	23	39	122	224		0	-5	-10	-10	0	
97042318	7	16.7N	153.6E	50	12	30	49	127	230		-5	-5	-10	-5	5	
97042400	8	17.6N	153.8E	55	13	36	103	169	247		-5	-5	-5	0	0	
97042406	9	18.5N	154.1E	55	22	61	123	185			-5	-5	0	5		
97042412	10	19.1N	154.5E	55	66	196	333	487			-5	-5	5	10		
97042418	11	19.5N	154.8E	55	111	253	403				-5	0	10			
97042500	12	19.9N	155.2E	50	32	62	111				0	10	15			
97042506	13	20.3N	155.8E	45	11	61					-5	5				
97042512	14	20.6N	156.5E	35	24	55					5	10				
97042518	15	20.9N	157.2E	30	8						0					
97042600		21.4N	157.7E	25												
		AVERAGE			28	76	135	162	189	290	3	6	8	9	6	16
		# CASES			15	14	12	10	8	4	15	14	12	10	8	4

TROPICAL STORM KELLY (04W)

DTG	WRN NO.	BEST TRACK LAT	LONG	WIND	POSITION ERRORS 00	12	24	36	48	72	WIND ERRORS 00	12	24	36	48	72
97050406		2.7N	171.4E	15												
97050412		3.2N	171.1E	15												
97050418		4.0N	170.8E	15												
97050500		5.0N	170.4E	15												
97050506		5.9N	170.0E	15												
97050512		6.5N	169.8E	15												
97050518		6.8N	169.4E	15												
97050600		6.9N	168.9E	15												
97050606		7.4N	168.3E	20												
97050612		8.1N	167.8E	25												
97050618		8.9N	167.4E	25												
97050700	1	9.5N	167.2E	25	6	54	124	242	353	478	0	0	0	0	10	25
97050706	2	9.9N	167.1E	25	18	85	180	299	371	448	0	5	5	5	15	25
97050712	3	10.3N	167.0E	30	37	105	195	295	370	419	0	0	0	15	25	45
97050718	4	10.6N	166.9E	30	18	82	182	243	312	331	0	-5	0	20	30	50
97050800	5	10.9N	166.9E	35	0	61	135	200	247	230	0	-5	5	20	30	55
97050806	6	11.1N	167.0E	40	36	48	30	21	17	55	-5	-10	5	15	20	40
97050812	7	11.3N	167.1E	45	61	66	50	73	133	248	0	10	20	30	40	60
97050818	8	11.5N	167.1E	45	56	60	102	160	229		0	15	25	25	35	
97050900	9	11.9N	166.9E	40	13	50	79	140	211		0	0	0	0	10	
97050906	10	12.4N	166.4E	35	5	0	46	127	226		0	5	0	5	10	
97050912	11	12.9N	165.8E	35	11	16	44	111	197		0	5	5	10	10	
97050918	12	13.3N	165.1E	30	5	16	86	176			0	0	5	5		
97051000		13.7N	164.2E	30												
97051006	13	14.1N	163.0E	30	29	75	122				0	5	5			
97051012		14.5N	161.7E	25												
97051018	14	14.9N	160.3E	20	29	76					5	0				
97051100		15.2N	158.8E	15												
97051106		15.5N	157.2E	15												
97051112		15.8N	155.6E	15												

TROPICAL STORM KELLY (04W) (CONTINUED)

AVERAGE	24	57	106	174	243	316	1	5	6	13	21	43
# CASES	14	14	13	12	11	7	14	14	13	12	11	7

TROPICAL STORM LEVI (05W)

	WRN	BEST TRACK			POSITION ERRORS						WIND ERRORS					
DTG	NO.	LAT	LONG	WIND	00	12	24	36	48	72	00	12	24	36	48	72
97052300		16.8N	111.0E	15												
97052306		16.8N	111.7E	15												
97052312		16.8N	112.5E	15												
97052318		16.8N	113.3E	15												
97052400		16.8N	114.1E	15												
97052406		16.8N	114.9E	15												
97052412		16.8N	115.7E	15												
97052418		16.8N	116.5E	15												
97052500		16.8N	117.2E	20												
97052506		16.8N	117.9E	20												
97052512		16.8N	118.6E	20												
97052518	1	16.6N	119.3E	25	39	23	104	136			0	5	0	-5		
97052600	2	16.5N	120.0E	25	17	73	158	183	196	305	0	0	0	-10	0	5
97052606	3	16.4N	120.9E	25	0	67	120	134	143	247	0	0	-5	-5	5	10
97052612	4	16.5N	122.2E	25	18	117	132	135	142	306	0	0	-5	0	0	0
97052618	5	17.0N	123.6E	25	50	99	103	124	153	395	0	-5	-5	-5	-5	-10
97052700	6	17.6N	124.7E	25	38	23	25	42	108	456	0	-10	-5	-10	-5	-5
97052706	7	18.2N	125.4E	30	17	24	40	52	84	436	0	0	0	0	-5	-5
97052712	8	18.7N	125.8E	35	21	116	186	195	114	131	0	10	-10	-15	-20	-10
97052718	9	19.4N	126.0E	35	21	71	124	131	151	250	0	5	-10	-15	-20	-5
97052800	10	20.2N	126.1E	35	28	86	125	89	129	103	0	-5	-10	-15	-10	0
97052806	11	21.1N	126.2E	40	22	33	20	76	186	139	0	0	0	-5	-5	5
97052812	12	22.0N	126.3E	45	62	74	49	96	137	284	0	0	0	0	0	5
97052818	13	23.1N	126.6E	45	69	54	144	252	211	220	0	0	0	0	5	5
97052900	14	24.1N	127.3E	45	16	94	204	234	143		0	-5	0	0	10	
97052906	15	25.2N	128.6E	45	12	81	155	143			0	-5	-5	5		
97052912	16	26.2N	130.4E	45	0	42	64	231			0	0	0	10		
97052918	17	27.3N	132.6E	45	8	38	136				0	0	5			
97053000	18	28.4N	135.2E	40	6	121	362	630	891		0	5	10	10	5	
97053006	19	29.4N	137.6E	40	38	231	499				0	5	10			
97053012		30.1N	139.6E	35												
97053018		30.6N	141.0E	30												
97053100		30.9N	142.2E	25												
97053106		31.3N	143.8E	25												
97053112		31.6N	145.4E	25												
97053118		32.0N	147.3E	25												
97060100		32.5N	149.5E	25												
97060106		32.9N	151.8E	25												
97060112		33.1N	154.5E	30												
97060118		33.2N	157.6E	30												
97060200		33.3N	161.1E	30												
97060206		33.5N	164.8E	35												
97060212		34.1N	168.8E	35												
97060218		34.8N	173.1E	45												
97060300		35.7N	177.7E	40												
97060306		36.7N	177.2W	40												
97060312		37.8N	171.8W	40												
97060318		38.9N	166.1W	35												
97060400		40.0N	160.2W	35												
AVERAGE	26	78	145	170	200	273	0	3	4	6	7	5
# CASES	19	19	19	17	14	12	19	19	19	17	14	12

TYPHOON MARIE (06W)

DTG	WRN NO.	BEST TRACK LAT	LONG	WIND	POSITION ERRORS 00	12	24	36	48	72	WIND ERRORS 00	12	24	36	48	72
97052512		9.1N	161.4E	20												
97052518		9.3N	161.2E	20												
97052600		9.5N	161.0E	20												
97052606		9.7N	160.8E	25												
97052612		9.8N	160.5E	25												
97052618	1	10.1N	159.9E	25	25	62	102	158	192	267	0	-5	0	5	10	-20
97052700	2	10.7N	159.3E	30	51	103	136	201	260	372	-5	-5	0	5	0	-25
97052706	3	11.4N	158.7E	30	68	114	161	232	323	440	-5	-5	0	0	-10	-25
97052712	4	12.1N	158.1E	30	84	126	197	263	320	348	-5	-5	0	-10	-20	-25
97052718	5	12.6N	157.8E	30	102	142	212	306	379	466	-5	-5	-5	-20	-30	-30
97052800	6	13.0N	157.8E	30	102	151	223	310	367	434	-5	0	-10	-25	-30	-30
97052806	7	13.3N	157.9E	30	109	154	245	324	373	469	-5	-5	-20	-35	-30	-30
97052812	8	13.6N	158.0E	30	11	58	127	176	204	296	-5	-15	-30	-40	-30	-50
97052818	9	13.9N	158.2E	35	37	54	59	83	84	196	-5	-25	-40	-40	-50	-55
97052900	10	14.4N	158.5E	45	26	84	160	211	242	367	-5	-25	-40	-40	-55	-45
97052906	11	15.0N	158.9E	55	13	50	136	218	283	526	-5	-20	-20	-15	-15	5
97052912	12	15.8N	159.3E	65	0	13	41	115	212	558	-15	-25	-20	-20	-20	0
97052918	13	16.7N	159.6E	75	12	23	73	143	235	604	-25	-25	-25	-20	-15	5
97053000	14	17.6N	159.9E	80	8	13	86	178	294	705	-15	-5	-5	-15	-10	0
97053006	15	18.5N	160.0E	80	12	72	110	171	275	698	-10	-10	-5	-10	-5	5
97053012	16	19.6N	160.1E	80	6	17	61	131	238	586	-10	-25	-25	-20	-20	-5
97053018	17	20.8N	160.2E	85	0	23	36	49	80	354	-15	-25	-20	-15	-15	-5
97053100	18	22.0N	160.3E	90	0	13	64	148	233		0	-15	-10	-10	-10	
97053106	19	23.1N	160.7E	90	0	27	106	212	344		0	-10	-5	-5	-5	
97053112	20	24.2N	161.6E	90	8	60	98	156	217		0	0	0	0	-5	
97053118	21	25.3N	162.6E	85	16	5	49	135	256		-10	-5	-5	-5	-10	
97060100	22	26.4N	164.0E	75	17	79	201	332			0	-5	-5	-5		
97060106	23	27.8N	166.0E	70	22	64	149	224			-5	-5	0	-5		
97060112	24	29.0N	168.3E	65	0	34	136				0	-5	0			
97060118	25	30.6N	171.3E	60	31	133	281				0	0	0			
97060200	26	32.3N	174.6E	55	46	139					0	-5				
97060206	27	34.3N	178.4E	50	77	152					-5	-5				
97060212		36.5N	177.4W	50												
97060218		38.4N	172.4W	50												
		AVERAGE			33	73	131	195	258	453	6	11	12	16	19	21
		# CASES			27	27	25	23	21	17	27	27	25	23	21	17

SUPER TYPHOON NESTOR (07W)

DTG	WRN NO.	BEST TRACK LAT	LONG	WIND	POSITION ERRORS 00	12	24	36	48	72	WIND ERRORS 00	12	24	36	48	72
97060106		6.0N	171.0E	15												
97060112		5.9N	170.3E	15												
97060118		5.8N	169.6E	15												
97060200		5.7N	168.9E	15												
97060206		5.6N	168.2E	15												
97060212		5.5N	167.5E	15												
97060218		5.5N	166.8E	15												
97060300		5.4N	166.1E	15												
97060306		5.3N	165.6E	15												
97060312		5.3N	165.2E	15												
97060318		5.4N	164.8E	15												
97060400		5.7N	164.3E	20												
97060406		6.1N	163.8E	20												
97060412		6.6N	163.3E	20												
97060418		7.3N	162.5E	20												
97060500		7.9N	161.6E	20												
97060506		8.3N	160.6E	20												
97060512		8.7N	159.5E	25												
97060518		9.0N	158.2E	30												
97060600	1	9.3N	156.8E	35	18	67	114	157	171	230	-10	-5	0	0	-5	-40
97060606	2	9.7N	155.4E	35	38	75	129	168	178	248	-5	0	5	10	-5	-35
97060612	3	10.1N	154.3E	35	8	54	106	132	162	243	-5	0	5	0	-15	-50
97060618	4	10.5N	153.4E	35	24	79	133	157	205	265	-5	0	0	-15	-30	-65
97060700	5	11.0N	152.5E	35	43	104	133	159	197	287	-5	0	-10	-25	-45	-70
97060706	6	11.7N	151.8E	35	30	48	72	116	158	266	0	5	-10	-25	-45	-75
97060712	7	12.4N	151.2E	35	8	39	125	220	303	444	0	-5	-20	-35	-50	-50

SUPER TYPHOON NESTOR (07W) (CONTINUED)

97060718	8	12.9N	150.5E	35	26	99	195	236	271	243	0	-15	-30	-45	-60	-40
97060800	9	13.3N	150.2E	45	29	65	100	133	154	131	0	-20	-40	-60	-65	-40
97060806	10	13.7N	149.9E	55	24	60	103	139	149	211	-10	-30	-50	-70	-70	-35
97060812	11	14.3N	149.8E	65	16	23	52	63	51	143	-10	-25	-40	-40	-40	-25
97060818	12	14.8N	149.7E	75	0	18	26	18	56	142	0	-10	-25	-20	-10	0
97060900	13	15.2N	149.5E	90	0	16	34	59	74	138	0	-15	-15	-15	-5	0
97060906	14	15.6N	149.2E	100	5	6	24	49	86	100	0	-20	-20	-5	0	0
97060912	15	16.1N	149.0E	115	18	20	22	48	58	32	0	-10	-15	0	25	10
97060918	16	16.6N	148.8E	125	12	46	61	71	65	22	-10	-15	-5	5	25	15
97061000	17	17.2N	148.4E	130	12	12	16	17	17	96	-5	-10	5	25	15	20
97061006	18	17.8N	148.0E	135	5	16	32	53	39	107	0	10	20	25	20	20
97061012	19	18.4N	147.4E	140	11	28	33	33	60	87	0	10	30	25	20	45
97061018	20	18.9N	146.8E	130	17	45	46	52	69	100	0	15	15	5	-5	15
97061100	21	19.4N	146.0E	130	0	24	37	47	60	228	0	15	5	0	0	25
97061106	22	20.1N	145.2E	125	5	25	32	53	71	236	0	5	0	0	0	30
97061112	23	20.7N	144.4E	115	8	24	21	16	48	285	0	-5	-10	-10	5	20
97061118	24	21.5N	143.6E	115	0	36	43	66	72	145	0	-5	-10	-15	5	15
97061200	25	22.1N	142.8E	115	0	6	17	16	20	95	0	-5	-5	10	15	15
97061206	26	22.9N	142.1E	115	0	12	24	58	73	198	0	0	-5	15	20	15
97061212	27	24.0N	141.7E	115	12	12	11	30	98	302	0	5	20	25	25	20
97061218	28	25.3N	141.6E	110	0	30	28	24	105		0	-5	15	15	10	
97061300	29	26.6N	141.7E	105	12	44	75	117	216		0	10	15	10	5	
97061306	30	28.0N	142.0E	105	18	33	73	109	187		0	15	20	10	5	
97061312	31	29.6N	142.8E	80	31	33	74	192	252		0	0	0	-10	-15	
97061318	32	31.2N	143.9E	75	15	46	106	177			0	5	0	-10		
97061400	33	33.1N	145.6E	65	25	58	23	44			0	10	0	-5		
97061406	34	34.9N	147.8E	60	11	24	47				5	10	0			
97061412	35	36.2N	150.8E	55	0	68	69				5	0	0			
97061418	36	37.5N	154.6E	55	0	54					0	0				
97061500	37	38.4N	159.0E	55	11	11					0	5				
97061506		39.2N	162.7E	55												
97061512		40.0N	166.7E	50												
		AVERAGE			14	40	64	92	121	187	2	9	13	18	21	29
		# CASES			37	37	35	33	31	27	37	37	35	33	31	27

TYPHOON OPAL (08W)

	WRN	BEST TRACK			POSITION ERRORS						WIND ERRORS					
DTG	NO.	LAT	LONG	WIND	00	12	24	36	48	72	00	12	24	36	48	72
97061312		12.1N	138.8E	15												
97061318		12.1N	138.0E	15												
97061400		12.2N	137.2E	15												
97061406		12.4N	136.4E	15												
97061412		12.7N	135.6E	15												
97061418		13.1N	134.9E	20												
97061500	1	13.6N	134.2E	25	67	100	166	220	248	259	0	5	0	0	-10	-15
97061506	2	14.1N	133.6E	25	13	8	45	79	103	219	0	0	-5	-10	-20	-15
97061512	3	14.5N	133.2E	25	8	50	74	99	120	210	0	0	0	-10	-25	-15
97061518	4	14.8N	133.0E	30	55	105	141	149	152	214	0	0	-5	-15	-20	-10
97061600	5	15.0N	132.8E	35	8	39	72	95	152	262	0	-5	-15	-30	-20	-10
97061606	6	15.3N	132.6E	40	5	24	51	96	151	236	0	-5	-20	-25	-15	10
97061612	7	15.6N	132.5E	45	8	5	26	95	149	271	0	-10	-25	-15	-5	5
97061618	8	16.0N	132.4E	55	29	47	90	134	179	293	-10	-20	-25	-15	-5	10
97061700	9	16.5N	132.4E	65	0	18	88	143	223	369	-10	-20	-10	10	10	25
97061706	10	17.3N	132.6E	75	12	41	89	147	222	394	0	-5	10	25	20	35
97061712	11	18.2N	132.8E	90	0	46	74	115	147	383	0	10	25	25	35	30
97061718	12	19.5N	133.2E	90	13	42	90	125	136	436	0	10	25	30	40	30
97061800	13	20.9N	133.6E	90	11	36	60	93	156	398	0	10	25	35	45	30
97061806	14	22.4N	133.6E	90	13	20	31	8	99	61	0	10	20	30	35	25
97061812	15	24.0N	133.6E	90	8	22	15	27	126		0	10	25	40	30	
97061818	16	25.7N	133.6E	90	13	15	24	87	171		0	5	15	25	10	
97061900	17	27.4N	133.6E	90	0	28	35	141	159		0	10	20	10	15	
97061906	18	29.1N	133.7E	85	5	23	90	204	167		0	5	15	5	20	
97061912	19	30.6N	134.2E	80	0	30	143	171			0	5	5	5		
97061918	20	32.1N	135.0E	75	15	97	194	123			0	5	-5	5		
97062000	21	33.9N	136.5E	65	15	130	132				0	0	5			
97062006	22	35.9N	138.8E	55	9	95	180				0	-10	5			

TYPHOON OPAL (08W) (CONTINUED)

97062012	23	38.6N	141.1E	55	11	135					-5	0					
97062018	24	40.5N	143.2E	55	43	218					-10	5					
97062100	25	41.2N	145.5E	45	36						0						
97062106	26	41.4N	148.0E	40	73						5						
			AVERAGE		18	58	87	118	159	287	2	7	14	18	21	19	
			# CASES		26	24	22	20	18	14	26	24	22	20	18	14	

TYPHOON PETER (09W)

	WRN	BEST TRACK			POSITION ERRORS						WIND ERRORS					
DTG	NO.	LAT	LONG	WIND	00	12	24	36	48	72	00	12	24	36	48	72
97061512		5.5N	162.4E	15												
97061518		5.7N	161.4E	15												
97061600		5.9N	160.4E	15												
97061606		6.1N	159.4E	15												
97061612		6.4N	158.4E	15												
97061618		6.7N	157.4E	15												
97061700		7.0N	156.4E	15												
97061706		7.4N	155.5E	15												
97061712		7.8N	154.6E	15												
97061718		8.1N	153.6E	15												
97061800		8.5N	152.7E	15												
97061806		8.9N	151.6E	15												
97061812		9.3N	150.2E	15												
97061818		9.7N	148.6E	15												
97061900		10.0N	146.7E	15												
97061906		10.2N	144.7E	15												
97061912		10.4N	143.0E	15												
97061918		10.6N	141.7E	15												
97062000		11.0N	140.9E	15												
97062006		11.6N	140.6E	15												
97062012		11.9N	140.4E	15												
97062018		12.1N	140.0E	15												
97062100		12.2N	139.5E	25												
97062106		12.3N	138.7E	25												
97062112		12.5N	137.7E	20												
97062118		12.8N	136.4E	20												
97062200		13.0N	135.0E	20												
97062206		13.2N	133.8E	25												
97062212		13.3N	132.8E	30												
97062218		13.4N	131.9E	30												
97062300		13.5N	131.1E	30												
97062306	1	13.6N	130.4E	30	31	129	161	190	248	314	-5	-10	-5	-5	-10	-20
97062312	2	13.8N	129.7E	35	34	34	105	200	258	332	-10	-5	0	10	10	0
97062318	3	14.0N	129.0E	35	11	45	108	143	169	243	0	5	10	5	5	0
97062400	4	14.2N	128.2E	35	37	104	174	164	160	262	0	0	5	0	-5	-5
97062406	5	14.8N	127.7E	35	50	119	148	152	174	343	0	0	-5	-5	-15	-5
97062412	6	15.7N	127.3E	35	84	159	188	219	289	528	0	0	-5	-10	-15	-5
97062418	7	16.7N	127.0E	35	96	126	135	162	205	362	0	-10	-10	-20	-15	0
97062500	8	17.6N	127.0E	35	96	69	62	92	145	329	0	-5	-10	-15	-10	5
97062506	9	18.4N	127.0E	45	30	76	94	94	128	139	0	0	-10	-5	-5	5
97062512	10	19.1N	126.9E	45	13	24	16	81	160	368	0	-5	-10	-5	-5	10
97062518	11	20.0N	126.8E	50	6	23	78	157	222	373	0	-10	-5	0	10	25
97062600	12	20.9N	126.7E	55	5	30	72	102	70	294	0	0	5	10	5	0
97062606	13	22.1N	126.6E	65	12	49	103	121	104	457	0	10	20	35	20	-5
97062612	14	23.5N	126.5E	65	0	21	52	66	133	518	0	10	20	40	25	-10
97062618	15	24.9N	126.3E	65	13	60	109	144	336	633	0	10	25	30	25	-15
97062700	16	26.5N	126.3E	65	17	72	83	253	492	708	0	0	5	0	-5	-35
97062706	17	28.3N	126.4E	65	6	37	34	160	400	376	-5	0	-5	0	-15	-35
97062712	18	30.0N	127.0E	65	26	19	127	333	512	270	-5	5	0	-5	-20	-35
97062718	19	31.6N	128.0E	60	7	30	184	399	414	138	0	0	0	-15	-25	-30
97062800	20	32.8N	129.7E	55	0	119	305	468	374	213	0	0	-10	-20	-35	-25
97062806	21	33.9N	132.5E	50	11	153	346	359	246		0	5	-15	-25	-35	
97062812	22	35.6N	136.4E	45	0	77	181	206	296	311	0	-5	-20	-35	-35	-5
97062818	23	37.6N	140.3E	40	0	125	96	13			0	-10	-25	-35		
97062900	24	39.9N	144.0E	45	9	60	129	325			-5	-20	-35	-35		
97062906		42.5N	148.3E	50												

TYPHOON PETER (09W) (CONTINUED)

97062912	44.2N	151.8E	55
97062918	44.9N	154.2E	60
97063000	45.2N	155.9E	70
97063006	45.4N	157.2E	70
97063012	45.6N	158.5E	70
97063018	45.8N	159.7E	65
97070100	46.0N	160.8E	60
97070106	46.2N	161.7E	55
97070112	46.5N	162.6E	50
97070118	46.8N	163.6E	45
97070200	47.1N	164.5E	40
97070206	47.3N	165.5E	40
97070212	47.6N	166.7E	35
97070218	47.9N	167.9E	35
97070300	48.3N	169.9E	30
97070306	48.6N	172.6E	30
97070312	48.9N	176.0E	30
97070318	49.2N	179.8E	30
97070400	49.3N	176.0W	30

AVERAGE	25	74	129	192	252	358	1	5	11	15	16	13
# CASES	24	24	24	24	22	21	24	24	24	24	22	21

SUPER TYPHOON ROSIE (10W)

	WRN	BEST TRACK			POSITION ERRORS						WIND ERRORS					
DTG	NO.	LAT	LONG	WIND	00	12	24	36	48	72	00	12	24	36	48	72
97071500		7.9N	142.4E	15												
97071506		8.0N	142.1E	15												
97071512		8.1N	141.8E	15												
97071518		8.2N	141.5E	15												
97071600		8.2N	141.2E	15												
97071606		8.2N	140.9E	15												
97071612		8.2N	140.6E	15												
97071618		8.2N	140.3E	15												
97071700		8.2N	140.0E	15												
97071706		8.3N	139.7E	15												
97071712		8.5N	139.4E	15												
97071718		8.8N	139.0E	15												
97071800		9.1N	138.5E	15												
97071806		9.7N	138.1E	20												
97071812		10.3N	137.8E	25												
97071818	1	10.9N	137.8E	25	67	144	187	192	225	317	0	0	0	-5	-15	-40
97071900	2	11.5N	138.0E	30	42	72	96	133	166	276	0	0	-5	-10	-25	-50
97071906	3	12.1N	138.3E	30	8	53	123	159	176	225	0	0	-5	-15	-30	-60
97071912	4	12.8N	138.3E	30	29	111	191	227	250	220	0	-5	-10	-20	-30	-75
97071918	5	13.4N	137.8E	35	37	90	123	135	144	111	0	-5	-15	-30	-35	-75
97072000	6	13.7N	137.0E	40	52	98	121	139	143	91	-5	-10	-15	-20	-25	-35
97072006	7	14.1N	136.3E	45	33	91	141	186	236	250	0	-10	-15	-15	-25	-20
97072012	8	14.5N	135.6E	55	5	30	45	66	68	91	0	-5	-10	-10	-40	-20
97072018	9	15.0N	135.1E	60	18	56	71	104	125	139	0	-15	-15	-25	-40	-15
97072100	10	15.5N	134.6E	70	25	44	91	128	158	171	5	5	0	-25	-15	10
97072106	11	16.0N	134.1E	80	8	0	45	86	112	90	0	0	-15	-25	-10	20
97072112	12	16.5N	133.6E	85	8	25	57	99	130	116	-5	-10	-40	-20	-10	30
97072118	13	17.0N	133.1E	90	13	58	117	169	185	176	0	-15	-35	-15	-5	30
97072200	14	17.4N	132.6E	100	12	55	90	126	158	200	0	-30	-15	0	15	30
97072206	15	17.7N	132.2E	115	8	21	54	86	120	189	0	-10	0	0	15	30
97072212	16	18.2N	132.0E	140	0	13	34	73	114	215	0	0	-5	5	20	30
97072218	17	18.7N	131.9E	140	12	32	54	82	125	227	0	0	-5	10	20	20
97072300	18	19.3N	131.8E	135	12	6	16	37	78	166	0	0	5	20	20	15
97072306	19	19.9N	131.9E	130	0	16	28	57	101	139	0	-5	5	10	10	0
97072312	20	20.7N	132.1E	130	11	24	36	67	127	116	0	5	15	10	10	-5
97072318	21	21.5N	132.3E	125	8	16	37	82	118	38	0	10	15	10	10	0
97072400	22	22.4N	132.5E	115	11	5	39	96	129	60	0	10	5	5	0	-5
97072406	23	23.4N	132.8E	105	0	8	28	57	95	274	0	5	0	0	-5	0
97072412	24	24.6N	133.2E	95	8	12	5	28	74	307	0	-5	-5	-10	-15	-5
97072418	25	25.9N	133.6E	90	0	18	31	51	141	248	0	0	0	-5	-10	0
97072500	26	27.1N	134.0E	90	18	15	39	68	192	285	0	5	0	0	0	5

SUPER TYPHOON ROSIE (10W) (CONTINUED)

97072506	27	28.3N	134.5E	85	16	5	4	86	146	285	0	5	5	0	5	5
97072512	28	29.5N	134.8E	80	5	16	64	118	109	246	0	0	0	5	0	10
97072518	29	30.7N	135.0E	75	7	31	86	116	161	486	0	0	5	10	5	10
97072600	30	31.9N	135.0E	75	6	64	116	155	271	660	0	0	5	5	5	10
97072606	31	33.3N	134.7E	70	7	99	125	222	367	829	0	0	5	5	5	10
97072612	32	34.8N	134.2E	65	20	101	220	285	412		0	10	5	10	10	
97072618	33	35.7N	133.0E	55	18	91	102	174	283		0	10	10	10	10	
97072700	34	36.0N	132.3E	45	26	117	164	248	318		0	0	10	10	10	
97072706	35	35.8N	132.5E	40	5	53	151	249	306		0	0	5	10	5	
97072712	36	35.9N	132.9E	40	15	51	110	187			0	5	10	10		
97072718	37	36.2N	133.7E	35	5	75	179	294			0	0	0	-5		
97072800	38	36.3N	134.6E	30	34	125	214				0	0	0			
97072806		35.9N	135.5E	30												
97072812		35.5N	136.4E	25												
97072818		35.0N	137.2E	25												
97072900		34.4N	137.5E	25												
97072906		33.8N	137.6E	25												
			AVERAGE		16	51	91	132	174	234	0	5	8	11	15	22
			# CASES		38	38	38	37	35	31	38	38	38	37	35	31

TROPICAL STORM SCOTT (11W)

	WRN	BEST TRACK			POSITION ERRORS						WIND ERRORS					
DTG	NO.	LAT	LONG	WIND	00	12	24	36	48	72	00	12	24	36	48	72
97072012		23.5N	149.9E	20												
97072018		23.7N	149.4E	20												
97072100		24.0N	149.1E	20												
97072106		24.2N	148.8E	20												
97072112		24.4N	148.6E	20												
97072118		24.7N	148.3E	20												
97072200		25.2N	148.0E	20												
97072206		25.8N	147.8E	20												
97072212		26.3N	148.1E	20												
97072218		26.8N	148.6E	20												
97072300		27.5N	149.3E	20												
97072306		28.4N	149.9E	20												
97072312		29.3N	150.4E	20												
97072318		30.2N	150.9E	20												
97072400		30.9N	151.3E	25												
97072406	1	31.5N	151.3E	30	10	42	78	204			0	0	0	-5		
97072412		31.7N	151.1E	30												
97072418	2	31.9N	150.8E	30	10	94	214	442			0	0	-5	-5		
97072500		31.7N	151.4E	30												
97072506	3	31.3N	151.6E	30	41	28	170				0	-5	-10			
97072512		30.7N	151.6E	30												
97072518		29.9N	152.0E	30												
97072600		28.5N	152.6E	30												
97072606		26.9N	153.3E	30												
97072612		25.3N	153.8E	30												
97072618		23.6N	154.3E	30												
97072700	4	22.7N	154.9E	30	26	126	180	168	150	152	-5	0	10	20	20	30
97072706	5	22.0N	155.7E	35	26	71	73	69	75	136	0	20	35	40	30	45
97072712	6	23.0N	156.6E	35	16	154	233	192	209	164	0	5	15	15	15	25
97072718	7	23.8N	156.1E	35	21	101	111	86	123	308	0	10	15	5	15	25
97072800	8	24.0N	155.1E	35	22	92	102	152	191	405	0	5	0	-5	5	5
97072806	9	24.0N	154.7E	35	10	106	270	388	524	964	0	0	-10	-10	0	5
97072812	10	23.9N	154.2E	35	8	97	168	272	423	827	0	-5	-10	0	0	5
97072818	11	24.3N	154.5E	40	21	124	185	306	503	957	0	-10	-10	0	0	0
97072900	12	24.9N	155.5E	45	8	89	198	360	578	1024	0	-5	10	15	20	15
97072906	13	25.4N	155.8E	55	24	60	168	355	562	970	0	10	20	20	25	15
97072912	14	25.6N	156.0E	55	13	46	184	394	592	1039	0	20	20	20	25	15
97072918	15	26.2N	156.2E	55	11	40	190	369	538	928	0	20	25	25	25	20
97073000	16	26.7N	156.4E	45	0	55	165	237	302	439	0	-5	0	0	-5	-5
97073006	17	27.4N	156.9E	45	31	39	30	36	110	174	0	0	5	0	-5	-5
97073012	18	28.4N	157.7E	45	15	31	61	120	151	264	0	0	5	-5	-5	-5
97073018	19	29.4N	159.0E	40	59	79	122	211	206	333	0	0	0	-10	-10	-15
97073100	20	30.2N	160.3E	40	33	84	188	261	203		0	0	-5	-10	-5	
97073106	21	30.8N	161.7E	35	31	88	190	194	121		0	0	-10	-5	-5	

TROPICAL STORM SCOTT (11W) (CONTINUED)

97073112	22	31.1N	163.1E	35	11	96	150	123	116		0	-5	-10	-5	-5	
97073118	23	31.2N	164.5E	35	20	70	73	46	226		-5	-10	-5	-5	-5	
97080100	24	31.3N	166.1E	40	20	96	157	226			-10	-10	-5	-5		
97080106	25	31.6N	168.1E	40	21	36	114	241			0	5	5	5		
97080112	26	32.3N	169.9E	40	0	15	52				0	5	0			
97080118	27	33.4N	170.9E	35	0	54	194				0	0	0			
97080200	28	35.1N	172.1E	35	0	91					0	0				
97080206	29	36.7N	172.8E	35	0	106					0	0				
97080212	30	38.1N	174.6E	35	0						0					
97080218		40.4N	177.7E	35												
		AVERAGE			17	77	149	228	296	568	1	5	9	10	11	15
		# CASES			30	29	27	24	20	16	30	29	27	24	20	16

TYPHOON TINA (12W)

	WRN	BEST TRACK			POSITION ERRORS						WIND ERRORS					
DTG	NO.	LAT	LONG	WIND	00	12	24	36	48	72	00	12	24	36	48	72
97072100		4.3N	152.3E	15												
97072106		4.9N	151.5E	15												
97072112		5.4N	150.8E	15												
97072118		5.9N	150.0E	15												
97072200		6.4N	149.2E	15												
97072206		6.7N	148.8E	15												
97072212		6.9N	148.4E	15												
97072218		7.0N	148.0E	15												
97072300		7.0N	147.6E	20												
97072306		7.0N	147.1E	20												
97072312		7.2N	146.4E	20												
97072318		7.5N	145.6E	20												
97072400		8.0N	144.9E	20												
97072406		8.5N	144.1E	20												
97072412		9.0N	143.5E	20												
97072418		9.4N	143.0E	20												
97072500		10.1N	142.8E	20												
97072506		10.8N	142.7E	20												
97072512		11.5N	142.7E	20												
97072518		12.2N	142.8E	20												
97072600		12.8N	142.6E	15												
97072606		12.9N	142.4E	15												
97072612		12.9N	141.9E	15												
97072618		12.8N	141.3E	15												
97072700		12.6N	140.7E	15												
97072706		12.5N	140.0E	15												
97072712		12.4N	139.0E	15												
97072718		12.4N	137.9E	15												
97072800		12.6N	136.8E	15												
97072806		13.2N	136.0E	15												
97072812		14.0N	135.7E	25												
97072818		14.8N	135.6E	25												
97072900		15.4N	135.4E	25												
97072906		15.6N	135.2E	25												
97072912		15.5N	134.8E	25												
97072918	1	15.4N	134.2E	25	8	71	204	292	371	437	0	-5	-5	0	-5	-10
97073000	2	15.2N	133.9E	25	42	125	226	278	314	309	0	-5	-5	0	-10	-10
97073006	3	14.8N	133.9E	30	68	167	236	294	330	401	0	0	5	10	10	10
97073012	4	14.3N	134.3E	30	35	36	51	76	113	233	0	0	5	5	5	10
97073018	5	13.9N	134.7E	35	34	56	85	126	178	315	0	5	5	5	0	10
97073100	6	13.6N	135.0E	35	8	6	42	113	187	331	0	0	-5	-5	-10	-10
97073106	7	13.5N	135.1E	35	18	55	111	158	201	265	0	0	0	-5	-5	-5
97073112	8	13.4N	135.2E	35	8	63	119	147	159	193	0	-5	-5	-5	-5	-10
97073118	9	13.2N	135.2E	40	11	76	138	164	193	235	0	0	-5	0	0	-20
97080100	10	13.1N	135.0E	45	17	76	116	154	183	208	0	5	5	10	5	-5
97080106	11	13.2N	134.7E	45	13	37	60	94	110	198	0	5	10	10	10	0
97080112	12	13.3N	134.3E	50	41	80	96	91	67	58	-5	0	10	10	15	10
97080118	13	13.4N	134.0E	55	67	75	79	62	35	73	0	5	10	10	10	0
97080200	14	13.6N	133.6E	55	5	16	44	63	103	138	0	5	5	5	5	-5
97080206	15	13.8N	133.2E	55	0	29	35	42	80	196	0	5	5	-5	-5	-15
97080212	16	14.0N	132.7E	55	13	16	26	67	114	189	0	0	0	-10	-5	-15

TYPHOON TINA (12W) (CONTINUED)

97080218	17	14.2N	132.1E	55	29	84	128	171	199	227	0	-5	-10	-10	-10	-15
97080300	18	14.6N	131.5E	60	8	32	48	41	45	67	0	5	5	15	5	0
97080306	19	15.1N	130.9E	60	0	12	12	46	76	89	0	0	5	10	0	0
97080312	20	15.8N	130.3E	65	13	18	21	28	55	60	0	0	15	15	20	25
97080318	21	16.5N	129.7E	70	25	64	66	61	78	93	-5	0	10	10	20	25
97080400	22	17.3N	129.0E	75	33	56	73	95	100	91	0	5	10	15	20	30
97080406	23	18.0N	128.4E	75	21	56	84	119	125	182	0	0	5	15	20	30
97080412	24	18.7N	127.8E	75	21	41	16	42	96	213	0	-10	-10	0	5	5
97080418	25	19.4N	127.3E	80	8	12	45	68	125	258	-5	-15	-10	0	5	10
97080500	26	20.1N	127.0E	85	11	11	17	17	31	71	-5	0	0	10	15	25
97080506	27	20.9N	126.7E	90	12	49	60	84	99	122	0	10	20	25	20	30
97080512	28	21.6N	126.5E	90	8	25	20	18	21	23	5	10	25	30	25	35
97080518	29	22.3N	126.4E	90	20	52	50	72	91	246	0	-5	0	0	5	25
97080600	30	23.2N	126.4E	90	11	12	5	5	7	235	0	0	5	5	10	30
97080606	31	24.1N	126.4E	90	0	11	6	5	44	398	0	0	5	10	15	30
97080612	32	24.9N	126.4E	85	0	16	19	23	69	463	0	0	5	10	15	20
97080618	33	25.7N	126.5E	85	5	0	18	11	57	264	0	0	10	15	20	5
97080700	34	26.8N	126.5E	80	0	37	72	93	66	179	0	0	5	10	10	0
97080706	35	27.5N	126.4E	80	0	18	43	38	43		0	5	10	20	10	
97080712	36	28.5N	126.2E	75	0	35	65	24	126		0	5	10	10	0	
97080718	37	29.2N	126.2E	70	0	39	63	50	108		0	5	20	0	-5	
97080800	38	30.4N	125.9E	65	0	27	39	185	368		0	0	5	-5	-15	
97080806	39	31.5N	126.0E	60	20	41	108	143			0	5	5	-5		
97080812	40	32.6N	126.4E	55	20	38	150	185			0	5	0	-10		
97080818	41	34.0N	127.4E	45	23	112	110				0	-5	-10			
97080900	42	35.6N	128.8E	40	15	88	162				0	-5	-10			
97080906	43	37.5N	131.3E	40	0	23					-5	-5				
97080912	44	39.1N	134.4E	40	0	29					-5	-10				
97080918		40.9N	137.5E	40												
97081000		42.5N	141.6E	45												
		AVERAGE			16	46	76	97	126	208	1	4	7	9	10	14
		# CASES			44	44	42	40	38	34	44	44	42	40	38	34

TYPHOON VICTOR (13W)

	WRN	BEST TRACK			POSITION ERRORS						WIND ERRORS					
DTG	NO.	LAT	LONG	WIND	00	12	24	36	48	72	00	12	24	36	48	72
97072812		15.0N	119.6E	15												
97072818		15.0N	119.0E	15												
97072900		15.1N	118.4E	15												
97072906		15.2N	117.8E	15												
97072912		15.3N	117.2E	15												
97072918		15.4N	116.6E	15												
97073000		15.5N	116.0E	15												
97073006		15.8N	115.5E	20												
97073012		16.1N	115.1E	20												
97073018	1	16.4N	114.7E	25	17	28	57	62	82	112	0	-5	-10	-15	-15	-5
97073100	2	16.6N	114.2E	30	18	17	26	50	47	197	0	0	-5	0	-5	20
97073106	3	16.8N	113.8E	30	8	12	58	66	84	282	0	-5	-5	-5	-10	25
97073112	4	17.1N	113.5E	35	13	18	26	16	57	178	-5	-5	0	-5	-5	25
97073118	5	17.7N	113.5E	40	45	82	58	55	138	318	-5	-5	-5	-10	10	30
97080100	6	18.3N	113.7E	45	8	23	36	17	98	259	0	5	0	-10	5	10
97080106	7	18.9N	113.9E	45	21	49	41	36	126		0	0	-5	0	5	
97080112	8	19.4N	114.0E	45	12	36	16	90	174		0	-5	-10	10	5	
97080118	9	19.8N	114.0E	50	0	11	66	132	186		-5	-10	5	10	10	
97080200	10	20.3N	114.0E	55	0	42	114	186	199		-10	-15	15	10	15	
97080206	11	21.1N	114.0E	60	0	50	112	150			-5	5	15	15		
97080212	12	22.3N	114.1E	65	0	52	109	158			-10	10	10	15		
97080218	13	23.6N	113.8E	50	0	53	115				0	10	10			
97080300	14	24.9N	113.8E	35	0	5	70				0	5	10			
97080306	15	26.3N	113.7E	30	13	50					0	5				
97080312		27.6N	113.9E	25												
97080318		28.8N	114.3E	20												

TYPHOON VICTOR (13W) (CONTINUED)

97080400		30.0N	114.8E	15													
			AVERAGE		11	36	65	85	120	225	3	6	8	9	9	19	
			# CASES		15	15	14	12	10	6	15	15	14	12	10	6	

SUPER TYPHOON WINNIE (14W)

	WRN	BEST TRACK			POSITION ERRORS						WIND ERRORS					
DTG	NO.	LAT	LONG	WIND	00	12	24	36	48	72	00	12	24	36	48	72
97080500		5.6N	168.0E	15												
97080506		5.7N	167.7E	15												
97080512		5.8N	167.4E	15												
97080518		5.9N	167.1E	15												
97080600		6.1N	166.7E	20												
97080606		6.3N	166.2E	20												
97080612		6.5N	165.4E	20												
97080618		6.8N	164.4E	20												
97080700		7.2N	163.0E	20												
97080706		7.8N	161.7E	20												
97080712		8.7N	160.6E	20												
97080718		9.5N	159.7E	20												
97080800		10.3N	158.8E	25												
97080806	1	11.3N	158.1E	25	29	67	106	122	142	138	0	0	0	-10	-20	-30
97080812	2	12.2N	157.3E	30	37	61	94	151	173	273	0	5	0	-10	-20	-25
97080818	3	13.0N	156.5E	30	36	54	87	137	167	305	0	0	-10	-20	-30	-35
97080900	4	13.7N	155.8E	30	49	77	130	140	183	302	0	-10	-20	-30	-35	-50
97080906	5	14.4N	155.2E	35	0	26	72	136	180	236	0	-20	-30	-40	-40	-50
97080912	6	14.8N	154.6E	45	18	60	96	151	198	233	-5	-20	-30	-35	-40	-40
97080918	7	15.1N	154.1E	55	18	42	95	132	163	139	-5	-20	-35	-35	-40	-35
97081000	8	15.4N	153.6E	65	5	29	59	82	106	99	-5	-15	-20	-30	-40	-30
97081006	9	15.8N	152.8E	75	5	30	78	114	109	70	-5	-20	-20	-35	-40	-25
97081012	10	16.0N	151.8E	85	8	48	72	84	79	12	-5	-15	-25	-45	-35	-15
97081018	11	16.1N	150.8E	95	0	25	49	37	24	54	-10	-15	-30	-40	-30	-5
97081100	12	16.2N	150.1E	100	5	57	110	125	162	244	-5	-10	-25	-15	-10	25
97081106	13	16.4N	149.4E	105	13	44	77	101	154	201	-10	-20	-25	-15	-5	15
97081112	14	16.6N	148.7E	115	12	30	48	80	123	152	-15	-35	-25	-15	-5	20
97081118	15	16.8N	148.0E	125	0	41	57	72	86	99	-15	-25	-20	-10	0	25
97081200	16	17.2N	147.1E	140	16	49	72	101	102	77	-10	0	0	5	25	25
97081206	17	17.6N	146.0E	140	0	5	41	56	85	120	0	0	0	0	10	25
97081212	18	18.0N	144.9E	140	0	18	41	55	73	88	0	0	0	15	15	30
97081218	19	18.4N	143.9E	140	8	45	57	83	96	109	0	0	0	10	15	25
97081300	20	18.9N	143.1E	140	8	37	46	65	66	123	0	-5	10	10	10	25
97081306	21	19.5N	142.2E	135	8	29	61	77	118	225	0	0	10	15	20	25
97081312	22	20.1N	141.3E	135	5	21	40	63	102	198	0	15	15	15	25	30
97081318	23	20.5N	140.3E	130	0	17	12	34	71	168	0	10	15	20	20	25
97081400	24	21.0N	139.5E	115	8	30	53	50	65	124	0	0	-5	5	5	10
97081406	25	21.5N	138.7E	115	6	36	51	66	100	153	0	5	5	5	5	10
97081412	26	22.0N	137.7E	110	11	28	45	77	121	214	0	0	5	10	10	10
97081418	27	22.5N	136.7E	105	12	42	65	105	147	207	0	5	5	5	5	0
97081500	28	22.8N	135.7E	105	0	13	28	69	100	171	0	15	15	20	20	15
97081506	29	23.0N	134.8E	95	0	0	28	60	94	151	0	0	0	0	5	5
97081512	30	23.3N	134.0E	90	5	17	29	50	82	175	0	5	5	5	5	-5
97081518	31	23.6N	133.1E	90	0	16	40	60	97	239	0	0	5	5	5	5
97081600	32	23.8N	132.1E	85	0	29	42	66	91	218	0	5	10	5	5	15
97081606	33	24.0N	131.1E	85	0	24	52	75	117	254	0	5	10	5	5	25
97081612	34	24.1N	130.2E	80	5	6	8	30	73	206	0	5	0	-5	-10	15
97081618	35	24.3N	129.2E	80	0	28	36	73	112	290	0	0	0	-5	0	20
97081700	36	24.7N	128.2E	75	8	6	30	78	132	379	0	-5	-10	-15	-5	5
97081706	37	25.1N	127.0E	75	11	34	22	36	98	312	0	0	-5	-10	-10	0
97081712	38	25.4N	126.0E	75	0	20	55	111	161	533	0	0	-5	0	0	0
97081718	39	25.9N	124.9E	75	0	30	67	114	197	552	0	0	5	10	5	0
97081800	40	26.6N	124.0E	75	0	24	55	72	166	417	0	0	0	0	0	-5
97081806	41	27.4N	122.7E	75	16	30	38	89	124		0	0	0	0	-10	
97081812	42	28.2N	121.4E	75	15	36	31	104	198		0	5	10	0	-10	
97081818	43	29.1N	120.2E	65	24	42	13	95	193		0	15	15	0	-5	
97081900	44	30.1N	119.0E	55	16	65	195	318			0	0	-5	-10		
97081906		31.2N	118.3E	45												
97081912		32.1N	117.8E	35												

SUPER TYPHOON WINNIE (14W) (CONTINUED)

97081918		33.7N	117.8E	30										
97082000		35.4N	117.8E	30										
97082006		37.0N	118.4E	30										
97082012		38.4N	119.4E	30										
97082018		39.5N	120.9E	30										
97082100		40.7N	122.5E	30										
97082106		41.8N	124.6E	30										
97082112		42.9N	126.7E	30										
97082118		44.1N	128.8E	30										
97082200		45.1N	130.7E	25										
97082206		45.7N	131.8E	25										
97082212		46.2N	133.1E	25										
97082218		46.7N	134.3E	25										
97082300		47.2N	135.5E	20										
			AVERAGE		10	34	59	91	122	207	2	8	11	14	15	20
			# CASES		44	44	44	44	43	40	44	44	44	44	43	40

TYPHOON YULE (15W)

	WRN	BEST TRACK			POSITION ERRORS						WIND ERRORS					
DTG	NO.	LAT	LONG	WIND	00	12	24	36	48	72	00	12	24	36	48	72
97080906		3.1N	179.0E	20												
97080912		3.1N	178.0E	20												
97080918		3.4N	177.1E	20												
97081000		4.0N	176.0E	20												
97081006		4.9N	175.2E	20												
97081012		5.2N	174.1E	20												
97081018		5.9N	173.0E	20												
97081100		6.8N	172.0E	20												
97081106		7.5N	171.1E	20												
97081112		7.4N	170.7E	20												
97081118		7.2N	170.4E	20												
97081200		7.0N	170.0E	20												
97081206		8.1N	169.5E	20												
97081212		8.7N	169.7E	20												
97081218		8.3N	170.4E	20												
97081300		7.9N	170.9E	20												
97081306		7.6N	171.4E	20												
97081312		7.0N	171.1E	20												
97081318		6.7N	170.4E	20												
97081400		6.6N	169.0E	20												
97081406		7.4N	168.0E	20												
97081412		7.5N	166.9E	20												
97081418		7.2N	165.7E	20												
97081500		6.8N	164.1E	25												
97081506		7.1N	163.3E	25												
97081512		7.7N	163.3E	25												
97081518		8.0N	163.6E	25												
97081600		8.3N	163.9E	25												
97081606		8.5N	164.0E	25												
97081612		8.8N	164.1E	25												
97081618	1	9.7N	164.6E	30	46	176	304	442	540	659	0	-5	0	5	10	5
97081700	2	10.6N	165.1E	30	11	41	124	209	191	291	0	-5	0	10	10	0
97081706	3	11.2N	165.8E	35	26	101	175	223	213	396	0	5	10	15	15	5
97081712	4	11.8N	166.3E	35	56	113	177	137	159	367	0	5	15	15	10	5
97081718	5	12.3N	167.0E	35	23	76	109	92	159	298	0	5	10	10	5	5
97081800	6	13.0N	167.6E	35	48	125	192	234	213	296	0	5	0	-10	-15	-10
97081806	7	13.8N	168.0E	35	30	23	46	54	127	373	0	0	-5	-5	0	10
97081812	8	14.5N	168.6E	30	53	143	210	207	133	290	5	0	-10	-10	0	10
97081818	9	15.7N	168.1E	35	54	137	136	116	103	306	0	-5	-15	-10	0	10
97081900	10	16.3N	167.3E	35	63	95	77	66	116	398	0	-10	-15	-10	0	10
97081906	11	17.1N	166.9E	40	47	26	37	80	140	476	0	-5	-5	0	5	15

TYPHOON YULE (15W) (CONTINUED)

97081912	12	17.9N	166.8E	45	29	33	87	123	177	507	-5	-10	-5	0	5	15
97081918	13	18.5N	167.2E	50	13	71	134	153	189	457	-5	-5	0	5	10	20
97082000	14	19.1N	167.2E	55	12	34	58	97	181	499	-5	0	5	10	15	15
97082006	15	19.7N	167.5E	55	16	63	77	120	238	534	0	5	10	15	15	5
97082012	16	20.2N	167.7E	55	30	61	97	188	361	675	0	5	10	15	15	0
97082018	17	20.8N	168.0E	55	39	73	110	283	471	704	0	5	10	15	15	0
97082100	18	21.9N	168.0E	55	20	95	116	128	134	324	0	5	5	0	-10	-30
97082106	19	23.0N	168.2E	55	11	64	132	223	364	326	0	0	0	-5	-15	-30
97082112	20	24.0N	168.6E	55	6	32	118	222	349		0	0	0	-5	-25	
97082118	21	25.0N	169.0E	55	0	73	114	236	320		0	0	0	-10	-25	
97082200	22	27.3N	169.9E	55	0	35	136	297	377		0	0	0	-15	-25	
97082206	23	29.5N	170.9E	55	12	73	143	139			-10	-15	-25	-30		
97082212	24	32.1N	171.8E	55	36	159	343				-10	-15	-30			
97082218	25	35.2N	171.8E	55	58	270	464				-5	-20	-30			
97082300	26	38.7N	171.1E	55	68	304					-5	-30				
97082306	27	41.9N	169.0E	60	50	105	251	475			0	10	15	10		
97082312		44.3N	167.1E	65												
97082318		45.7N	166.0E	65												
97082400		47.0N	165.0E	65												
97082406		48.3N	163.9E	65												
97082412		48.7N	163.4E	65												
97082418		49.2N	163.0E	65												
97082500		49.6N	163.1E	65												
97082506		49.7N	163.6E	65												
97082512		49.6N	164.8E	65												
97082518		50.4N	166.2E	65												
97082600		51.1N	167.3E	60												
97082606		51.2N	168.8E	50												
97082612		51.3N	170.5E	45												
97082618		51.3N	172.4E	40												
97082700		52.0N	174.1E	35												
		AVERAGE			32	97	153	190	239	431	2	6	9	10	11	11
		# CASES			27	27	26	24	22	19	27	27	26	24	22	19

TROPICAL DEPRESSION (16W)

	WRN	BEST TRACK			POSITION ERRORS						WIND ERRORS					
DTG	NO.	LAT	LONG	WIND	00	12	24	36	48	72	00	12	24	36	48	72
97081300		9.3N	174.3W	15												
97081306		9.6N	174.8W	15												
97081312		9.9N	175.3W	15												
97081318		10.1N	175.7W	15												
97081400		10.2N	176.2W	15												
97081406		10.4N	176.7W	15												
97081412		10.7N	177.4W	15												
97081418		11.0N	178.1W	15												
97081500		11.3N	178.8W	15												
97081506		11.6N	179.3W	15												
97081512		12.0N	180.0W	15												
97081518		12.4N	179.3E	15												
97081600		12.7N	178.8E	15												
97081606		13.1N	178.3E	15												
97081612		13.6N	177.6E	15												
97081618		14.3N	176.8E	15												
97081700		14.8N	175.7E	20												
97081706		15.4N	174.3E	20												
97081712		16.1N	172.9E	25												
97081718		16.7N	171.7E	30												
97081800	1	17.2N	170.4E	30	71	46	45				-5	-5	0			
97081806	2	17.3N	169.2E	30	56	103					-5	0				
97081812	3	17.2N	168.3E	30	62	118					-5	0				
97081818	4	16.8N	167.6E	25	24						0					
97081900	5	16.3N	167.3E	25	0						0					

TROPICAL DEPRESSION (16W) (CONTINUED)

AVERAGE	43	90	45							3	2	0			
# CASES	5	3	1							5	3	1			

TYPHOON ZITA (17W)

	WRN	BEST TRACK			POSITION ERRORS						WIND ERRORS					
DTG	NO.	LAT	LONG	WIND	00	12	24	36	48	72	00	12	24	36	48	72
97081912		16.9N	115.0E	25												
97081918		17.5N	115.5E	25												
97082000		18.1N	116.4E	30	0						-10					
97082006		18.7N	117.3E	30	18						-5					
97082012		19.1N	117.2E	35	49						-10					
97082018		19.6N	116.7E	35	17						-15					
97082100	1	20.0N	115.5E	40	34	100	137	213	274		-5	-10	-20	-20	-35	
97082106	2	20.1N	114.3E	45	0	17	16	27	53		-5	0	-10	0	10	
97082112	3	20.1N	113.2E	50	13	33	30	53	96		-5	-10	-10	0	35	
97082118	4	20.1N	112.3E	55	0	63	111	153	246		0	-10	-10	15	55	
97082200	5	20.5N	111.4E	65	12	49	50	101			0	-10	0	25		
97082206	6	21.0N	110.1E	75	16	62	105	116			0	0	10	25		
97082212	7	21.3N	108.8E	75	6	68	49				0	-15	15			
97082218	8	21.3N	107.8E	75	11	38	107				-15	-10	5			
97082300	9	21.2N	106.8E	75	8	63					-20	10				
97082306	10	21.2N	105.6E	55	12	121					-15					
97082312		22.0N	104.4E	30												
97082318		22.8N	102.9E	25												
AVERAGE					14	62	76	111	168		8	8	10	14	34	
# CASES					14	10	8	6	4		14	10	8	6	4	

TYPHOON AMBER (18W)

	WRN	BEST TRACK			POSITION ERRORS						WIND ERRORS					
DTG	NO.	LAT	LONG	WIND	00	12	24	36	48	72	00	12	24	36	48	72
97081912		14.0N	136.0E	25												
97081918		14.0N	135.5E	25												
97082000		14.0N	135.0E	25												
97082006		14.0N	134.5E	25												
97082012		14.1N	134.0E	25												
97082018		14.2N	133.6E	25												
97082100		14.3N	133.2E	25												
97082106	1	14.5N	133.0E	30	118	100	96	124	151	175	-5	-15	-30	-35	-35	-40
97082112	2	14.6N	132.7E	35	18	39	46	55	66	72	-5	-20	-30	-30	-35	-45
97082118	3	14.6N	132.4E	40	17	23	29	39	37	53	-5	-25	-30	-30	-30	-45
97082200	4	14.7N	132.0E	50	18	48	84	104	117	147	5	0	10	10	15	5
97082206	5	15.0N	131.7E	60	13	48	78	84	92	53	-5	0	5	10	15	10
97082212	6	15.3N	131.5E	65	18	49	54	45	37	51	0	5	0	5	10	0
97082218	7	15.7N	131.3E	65	25	45	45	31	31	54	0	0	0	0	5	10
97082300	8	16.0N	131.1E	65	31	40	41	54	67	84	0	-5	-5	-5	0	25
97082306	9	16.3N	130.8E	70	17	26	49	78	96	138	0	0	-5	-10	-5	25
97082312	10	16.5N	130.6E	75	16	23	58	93	117	157	0	0	-5	-10	-5	20
97082318	11	16.7N	130.4E	75	8	21	56	87	121	150	0	-5	-10	-10	5	15
97082400	12	16.9N	130.1E	80	11	12	24	39	66	114	0	-5	-10	-5	15	20
97082406	13	17.1N	129.7E	85	8	33	47	66	84	72	0	-5	-5	10	20	15
97082412	14	17.2N	129.3E	90	0	6	24	58	77	102	0	-5	0	20	20	15
97082418	15	17.3N	128.9E	95	8	21	62	90	95	88	0	0	15	25	20	15
97082500	16	17.4N	128.5E	100	0	8	33	53	61	29	0	5	25	25	20	15
97082506	17	17.6N	128.2E	100	8	23	51	54	56	29	0	15	25	15	10	10
97082512	18	17.7N	127.9E	100	5	29	49	43	25	50	0	20	20	10	5	15
97082518	19	17.8N	127.7E	90	17	47	57	51	33	91	10	20	15	5	-5	10
97082600	20	17.9N	127.5E	85	0	18	41	41	42	162	15	10	0	-15	-10	0
97082606	21	18.1N	127.3E	85	5	18	28	17	39	172	15	5	-5	-15	-5	10
97082612	22	18.4N	127.0E	90	11	18	18	50	85	210	10	15	15	5	15	15
97082618	23	18.8N	126.6E	95	13	17	34	64	121	217	5	10	15	10	15	30
97082700	24	19.1N	126.2E	100	0	13	8	37	94	183	0	0	5	10	0	35
97082706	25	19.4N	125.7E	105	11	17	38	79	118	168	-5	0	10	10	5	25
97082712	26	19.7N	125.1E	110	0	17	48	102	135	174	0	15	25	15	20	15

TYPHOON AMBER (18W) (CONTINUED)

97082718	27	20.2N	124.4E	110	6	23	77	114	144	210	0	20	15	15	20	5
97082800	28	20.8N	123.7E	105	0	29	63	105	133		0	10	-10	10	25	
97082806	29	21.5N	123.1E	100	5	37	69	94	119		0	0	-5	20	20	
97082812	30	22.4N	122.5E	95	6	36	58	88	114		0	0	5	20	10	
97082818	31	23.4N	121.7E	95	16	18	20	72	167		0	-10	10	15	5	
97082900	32	24.4N	121.0E	90	21	12	33	87			0	-5	20	10		
97082906	33	25.3N	120.3E	80	12	23	73	153			0	0	10	5		
97082912	34	26.2N	119.7E	65	22	49	133				0	20	5			
97082918	35	27.0N	119.1E	50	42	86	172				10	15	5			
97083000	36	28.0N	118.4E	30	59	93					0	5				
97083006		29.0N	117.4E	30												
97083012		30.1N	116.2E	25												
97083018		31.4N	115.2E	25												
		AVERAGE			17	33	55	72	89	119	3	8	12	13	14	18
		# CASES			36	36	35	33	31	27	36	36	35	33	31	27

SUPER TYPHOON BING (19W)

	WRN	BEST TRACK			POSITION ERRORS						WIND ERRORS					
DTG	NO.	LAT	LONG	WIND	00	12	24	36	48	72	00	12	24	36	48	72
97082400		9.5N	172.0E	15												
97082406		10.0N	171.8E	15												
97082412		10.3N	171.0E	15												
97082418		10.4N	170.2E	15												
97082500		10.5N	169.1E	15												
97082506		10.6N	167.7E	15												
97082512		10.7N	166.2E	15												
97082518		10.8N	164.6E	15												
97082600		10.9N	163.1E	15												
97082606		11.0N	161.5E	15												
97082612		11.2N	160.0E	20												
97082618		11.4N	158.5E	20												
97082700		11.5N	156.9E	20												
97082706	1	11.6N	155.3E	20	93	44	23	63	110	231	5	5	0	-5	-15	-25
97082712	2	11.7N	153.8E	20	76	25	29	81	139	237	5	5	0	-10	-15	-20
97082718	3	11.9N	152.4E	20	71	30	72	128	187	202	5	5	-5	-15	-15	-25
97082800	4	12.1N	150.9E	25	82	55	34	46	89	120	0	-5	-10	-15	-15	-35
97082806	5	12.5N	149.5E	25	59	61	68	88	118	151	0	-10	-15	-15	-20	-45
97082812	6	13.0N	148.1E	30	43	51	70	97	98	177	0	-5	-10	-10	-15	-45
97082818	7	13.4N	146.8E	35	30	23	39	66	75	358	0	-5	-5	-10	-15	-50
97082900	8	13.8N	145.5E	40	29	59	94	98	47	241	0	-5	-5	-10	-20	-55
97082906	9	14.2N	144.2E	45	8	47	75	20	82	194	-5	-5	-10	-15	-30	-65
97082912	10	14.4N	142.8E	50	13	26	79	130	174	278	0	0	-5	-15	-30	-65
97082918	11	14.8N	141.5E	50	18	61	107	170	236	343	0	-5	-10	-25	-40	-60
97083000	12	15.4N	140.3E	55	12	13	51	84	107	152	0	0	-5	-15	-35	-35
97083006	13	16.0N	139.1E	60	13	64	107	87	52	104	0	-5	-15	-25	-45	-30
97083012	14	16.6N	138.5E	65	0	29	85	137	138	191	0	-10	-25	-45	-50	-30
97083018	15	17.2N	138.4E	70	13	69	127	173	174	165	0	-15	-30	-50	-40	-20
97083100	16	18.0N	138.4E	80	8	34	79	121	122	143	-5	-25	-45	-50	-40	-15
97083106	17	18.9N	138.5E	90	11	60	114	151	151	200	-15	-35	-55	-45	-35	-10
97083112	18	20.0N	138.6E	100	6	55	108	131	121	249	-15	-40	-45	-30	-25	-5
97083118	19	21.3N	138.8E	110	11	53	92	107	88	274	-20	-40	-30	-20	-15	-5
97090100	20	22.6N	139.0E	125	5	34	64	64	31	254	-25	-35	-30	-20	-10	0
97090106	21	23.9N	139.0E	135	6	28	50	40	7	318	-10	-5	0	5	15	30
97090112	22	25.2N	138.9E	135	8	46	62	39	23	258	-10	0	10	10	15	25
97090118	23	26.3N	138.6E	130	17	60	54	18	51	83	-10	-5	5	5	5	10
97090200	24	27.2N	138.3E	125	17	79	89	114	157	205	-5	5	15	10	10	15
97090206	25	28.1N	138.3E	120	0	51	85	136	164	162	0	10	20	15	15	15
97090212	26	28.9N	138.8E	110	0	28	87	98	44	145	5	15	20	15	15	10
97090218	27	30.0N	139.5E	105	0	31	99	91	179	374	0	5	10	10	10	5
97090300	28	31.2N	140.5E	95	0	57	117	174	183	40	0	5	10	10	10	5
97090306	29	32.4N	141.9E	90	0	68	112	132	95		0	5	10	10	5	
97090312	30	33.5N	144.1E	85	0	33	47	47	84		5	5	5	5	-5	
97090318	31	34.8N	146.8E	80	0	26	55	123	195		5	5	5	0	0	
97090400	32	36.8N	150.0E	75	11	47	87	150	156		-10	0	5	0	5	

SUPER TYPHOON BING (19W) (CONTINUED)

DTG	WRN NO.	BEST TRACK LAT	LONG	WIND	POSITION ERRORS 00	12	24	36	48	72	WIND ERRORS 00	12	24	36	48	72
97090406	33	38.8N	153.3E	70	15	21	75	121			-5	5	5	0		
97090412	34	40.7N	156.8E	65	12	27	82	93			0	5	5	5		
97090418	35	42.6N	160.4E	60	50	144	242				0	0	0			
97090500	36	44.7N	164.3E	55	154	293	313				0	-10	-10			
97090506		46.6N	168.4E	55												
97090512		48.5N	172.8E	55												
97090518		49.8N	177.5E	55												
97090600		50.5N	178.3W	50												
		AVERAGE			25	54	89	101	115	209	5	10	14	16	20	27
		# CASES			36	36	36	34	32	28	36	36	36	34	32	28

TROPICAL STORM CASS (20W)

DTG	WRN NO.	BEST TRACK LAT	LONG	WIND	POSITION ERRORS 00	12	24	36	48	72	WIND ERRORS 00	12	24	36	48	72
97082600		19.1N	112.3E	15												
97082606		19.1N	112.6E	25												
97082612		19.1N	112.9E	25												
97082618		19.0N	113.2E	25												
97082700		18.8N	113.6E	25												
97082706		18.5N	114.1E	25												
97082712		18.2N	114.5E	25												
97082718		17.9N	114.8E	25												
97082800	1	17.6N	114.9E	30	23	36	8	106	250	392	0	10	10	10	30	50
97082806	2	17.3N	115.1E	30	13	24	82	209	327	452	0	5	0	10	25	50
97082812	3	17.1N	115.5E	30	29	103	219	352	426		0	-5	-15	0	5	
97082818	4	17.1N	116.0E	30	37	76	179	282	314		0	-10	-10	0	10	
97082900	5	17.6N	117.0E	35	80	148	248	306	332		0	-10	0	10	20	
97082906	6	18.3N	117.9E	40	69	181	294	334	391		0	5	10	25	35	
97082912	7	19.9N	118.3E	45	60	169	250	306			0	10	15	25		
97082918	8	21.6N	118.6E	40	121	226	270	332			5	10	20	30		
97083000	9	23.1N	118.7E	35	114	128	132				10	20	15			
97083006	10	24.6N	118.2E	35	0	32	88				0	5	5			
97083012	11	25.5N	117.6E	30	16	72					0	0				
97083018		26.2N	117.0E	25												
97083100		26.9N	116.4E	25												
97083106		27.8N	115.5E	20												
		AVERAGE			51	109	177	279	340	422	1	8	10	14	21	50
		# CASES			11	11	10	8	6	2	11	11	10	8	6	2

TYPHOON DAVID (21W)

DTG	WRN NO.	BEST TRACK LAT	LONG	WIND	POSITION ERRORS 00	12	24	36	48	72	WIND ERRORS 00	12	24	36	48	72
97090900		9.9N	171.1E	15												
97090906		10.0N	170.5E	15												
97090912		10.1N	169.9E	20												
97090918		10.1N	169.3E	20												
97091000		10.1N	168.7E	20												
97091006		10.4N	168.4E	25												
97091012		10.5N	168.8E	25												
97091018		10.4N	169.3E	25												
97091100		10.8N	169.8E	25												
97091106		11.2N	170.2E	25												
97091112		11.8N	170.4E	25												
97091118	1	12.3N	170.1E	25	50	88	133	144	154	313	0	-10	-20	-25	-30	-50
97091200	2	12.9N	169.7E	30	77	147	175	183	225	370	-5	-5	-10	-15	-25	-45
97091206	3	13.4N	168.9E	35	30	64	51	72	111	256	-5	-10	-15	-20	-30	-45
97091212	4	14.0N	168.0E	40	13	29	34	38	94	197	-10	-15	-20	-25	-35	-35
97091218	5	14.5N	167.2E	45	13	30	33	51	101	152	-5	-5	-10	-10	-20	-10
97091300	6	14.7N	166.4E	50	35	122	176	214	216	207	-5	-5	-5	-5	-5	20
97091306	7	15.0N	165.6E	55	11	64	114	157	164	105	0	0	5	-5	15	25
97091312	8	15.5N	164.9E	60	16	74	141	196	203	175	0	-5	-5	-5	15	30
97091318	9	16.1N	164.2E	65	24	84	170	241	260	278	-5	-10	-15	-5	15	35
97091400	10	17.0N	163.3E	70	37	108	209	247	269	355	-5	-10	-10	0	10	40
97091406	11	17.9N	162.5E	75	13	71	138	177	223	389	0	-10	-5	0	10	40

TYPHOON DAVID (21W) (CONTINUED)

97091412	12	19.0N	161.5E	85	17	69	124	158	219	356	-5	-10	-5	0	15	40
97091418	13	20.1N	160.3E	95	30	78	95	105	141	207	-10	0	5	10	25	50
97091500	14	21.1N	158.9E	95	0	21	24	65	135	301	-5	5	10	20	35	60
97091506	15	21.9N	157.5E	95	5	8	0	38	81	114	-5	5	10	25	35	60
97091512	16	22.4N	156.3E	95	6	30	60	110	135	157	0	5	15	30	30	45
97091518	17	23.0N	155.2E	95	12	29	70	117	144	210	0	5	20	25	35	35
97091600	18	23.5N	154.0E	95	11	55	93	112	115	245	0	10	25	25	35	30
97091606	19	24.0N	152.6E	95	0	27	55	68	77	189	0	15	25	35	35	30
97091612	20	24.4N	151.0E	90	20	57	65	91	73	322	0	15	20	35	30	30
97091618	21	24.8N	149.4E	85	24	44	68	109	142	141	0	10	20	20	15	20
97091700	22	25.3N	147.8E	80	8	20	70	109	243	198	0	0	15	10	5	5
97091706	23	25.8N	146.2E	80	0	18	85	190	295	292	0	10	10	5	0	0
97091712	24	26.5N	144.9E	80	5	53	10	26	76	262	0	15	10	5	5	0
97091718	25	27.2N	143.6E	70	0	31	60	98	174	213	0	0	0	-5	-5	-10
97091800	26	27.9N	142.4E	65	30	25	84	192	276		0	-5	-10	-15	-25	
97091806	27	29.1N	141.9E	65	5	25	68	126	84		0	-5	-10	-15	-20	
97091812	28	30.5N	141.6E	65	6	61	146	104	12		0	-5	-5	-15	-20	
97091818	29	32.2N	141.5E	65	0	33	68	17	41		0	-5	-5	-10	-20	
97091900	30	34.0N	142.5E	65	15	77	91	58			-10	-15	-25	-20		
97091906	31	36.5N	144.4E	65	38	149	141	147			-15	-15	-20	-20		
97091912	32	39.1N	147.4E	60	17	84	96	109	136		0	0	5	0	5	
97091918	33	41.8N	151.0E	60	37	77	90	98	118		0	5	0	0	0	
97092000	34	44.7N	154.8E	60	65	100	54	96	195		0	5	0	5	0	
97092006	35	47.3N	158.9E	55	17	77	79	128			0	0	0	5		
97092012		49.5N	163.7E	55												
97092018		51.2N	169.1E	55												
97092100		51.2N	174.9E	55												
97092106		50.8N	179.6W	55												
97092112		50.4N	174.4W	50												
97092118		49.9N	169.5W	50												
97092200		49.3N	165.3W	50												
		AVERAGE			20	61	91	120	155	241	3	7	11	13	19	32
		# CASES			35	35	35	35	32	25	35	35	35	35	32	25

TYPHOON FRITZ (22W)

	WRN	BEST TRACK			POSITION ERRORS						WIND ERRORS					
DTG	NO.	LAT	LONG	WIND	00	12	24	36	48	72	00	12	24	36	48	72
97091712		13.0N	114.0E	15												
97091718		13.3N	114.3E	15												
97091800		13.6N	114.0E	15												
97091806		13.7N	113.6E	20												
97091812		13.6N	113.2E	20												
97091818		13.4N	112.8E	20												
97091900		13.2N	112.5E	20												
97091906		13.0N	112.2E	20												
97091912		12.8N	111.9E	20												
97091918		12.5N	111.6E	20												
97092000		12.4N	111.3E	20												
97092006		12.3N	111.0E	20												
97092012		12.5N	110.7E	20												
97092018	1	12.7N	110.4E	25	17	51	98	114	127	159	0	0	5	5	5	-10
97092100	2	13.1N	110.2E	25	37	94	120	120	120	150	0	10	15	15	5	-10
97092106	3	13.6N	109.9E	25	58	102	102	102	105	144	0	0	0	0	-5	-30
97092112	4	14.3N	109.8E	25	78	87	88	93	121	265	0	0	0	-10	-5	-30
97092118	5	14.8N	110.1E	25	64	36	41	78	125	282	0	-5	-5	-10	-15	-30
97092200	6	15.2N	110.6E	25	31	43	68	101	139	270	0	-5	-15	-10	-25	-30
97092206	7	15.4N	110.9E	30	37	80	101	127	152	285	0	0	-5	-10	-25	-15
97092212	8	15.6N	111.1E	30	59	75	75	74	72	209	0	-10	-5	-20	-25	-5
97092218	9	15.8N	111.3E	35	55	58	75	84	119	304	0	-10	-20	-35	-30	15
97092300	10	15.9N	111.3E	45	6	26	55	112	190	424	0	0	-15	-25	-20	25
97092306	11	16.0N	111.2E	45	13	34	84	142	179	291	0	-10	-20	-20	-20	20
97092312	12	16.0N	111.1E	45	26	49	80	112	149		0	-10	-20	-25	-20	
97092318	13	16.0N	111.0E	55	13	50	91	146	191		0	-10	-10	-5	0	
97092400	14	16.0N	110.8E	65	6	36	88	144	187		0	-10	-10	10	20	
97092406	15	16.0N	110.4E	75	11	46	110	174	224		0	0	10	35	45	
97092412	16	16.0N	109.9E	75	18	26	47	47			-5	-10	-20	-10		

TYPHOON FRITZ (22W) (CONTINUED)

97092418	17	16.0N	109.4E	75	23	52	92	136			0	-10	-5	0		
97092500	18	16.0N	108.7E	75	30	53	95				0	-5	0			
97092506	19	15.8N	107.9E	65	33	75	120				0	5	10			
97092512	20	15.5N	107.1E	55	28	75					0	10				
97092518	21	15.1N	106.3E	40	47	104					0	10				
97092600		14.7N	105.6E	30												
97092606		14.3N	104.9E	20												
			AVERAGE		33	60	86	113	147	254	0	6	10	14	18	20
			# CASES		21	21	19	17	15	11	21	21	19	17	15	11

TROPICAL STORM ELLA (23W)

	WRN	BEST TRACK			POSITION ERRORS						WIND ERRORS					
DTG	NO.	LAT	LONG	WIND	00	12	24	36	48	72	00	12	24	36	48	72
97091818		22.0N	175.6W	15												
97091900		22.1N	176.5W	15												
97091906		22.2N	177.7W	15												
97091912		22.4N	178.9W	15												
97091918		22.5N	179.9E	20												
97092000		22.7N	178.7E	25												
97092006		22.9N	177.3E	30												
97092012		23.2N	175.9E	35												
97092018		23.6N	174.0E	35												
97092100	1	24.2N	171.9E	35	16	99	165	228	223	458	-10	0	-5	5	10	15
97092106	2	24.9N	169.4E	30	16	76	129	140	95	435	-5	-5	-5	5	15	15
97092112	3	25.6N	166.8E	30	34	99	144	128	46	415	0	-5	5	10	20	15
97092118	4	26.1N	164.5E	35	37	97	140	88	44	72	-5	-5	5	10	20	15
97092200	5	26.5N	162.3E	40	41	120	137	101	35	189	-5	5	10	15	10	10
97092206	6	26.8N	160.2E	40	10	39	83	134	110		0	5	10	10	5	
97092212	7	27.1N	158.3E	35	13	95	234	271	242		5	0	0	-5	-5	
97092218	8	27.6N	157.2E	35	5	123	342	497	344		0	0	0	-5	-5	
97092300	9	28.6N	156.2E	35	31	208	464	606	449		0	5	0	-5	0	
97092306	10	30.5N	156.2E	35	90	267	424	415			0	5	0	-5		
97092312	11	32.2N	157.4E	30	121	287	368	342			0	0	-5	-5		
97092318		34.2N	158.9E	30												
97092400	12	36.3N	160.8E	30	0	7	25				0	-5	-5			
97092406		37.7N	163.3E	30												
97092412	13	38.6N	165.7E	30	34	172					0	0				
97092418		39.3N	167.9E	30												
97092500	14	39.8N	169.7E	25	0						0					
			AVERAGE		32	130	222	269	177	314	2	3	4	7	10	14
			# CASES		14	13	12	11	9	5	14	13	12	11	9	5

TYPHOON GINGER (24W)

	WRN	BEST TRACK			POSITION ERRORS						WIND ERRORS					
DTG	NO.	LAT	LONG	WIND	00	12	24	36	48	72	00	12	24	36	48	72
97092112		10.3N	174.7E	15												
97092118		10.3N	174.4E	15												
97092200		10.2N	173.7E	15												
97092206		10.2N	173.0E	20												
97092212		10.2N	171.8E	20												
97092218	1	10.2N	170.3E	25	41	108	159	196	216	336	0	5	5	10	5	5
97092300	2	10.6N	168.8E	25	26	97	164	231	308	472	0	0	5	0	0	-5
97092306	3	11.2N	167.4E	25	29	83	163	242	326	514	0	0	0	-5	0	-15
97092312	4	12.1N	166.3E	30	24	85	138	192	256	255	0	5	0	0	15	-25
97092318	5	12.9N	165.3E	30	25	67	113	179	257	314	0	0	-5	0	10	-35
97092400	6	13.7N	164.5E	35	26	49	90	152	193	250	0	-10	-10	-5	0	-50
97092406	7	14.6N	163.8E	40	12	40	90	136	186	257	0	-5	0	0	-10	-45
97092412	8	15.3N	163.2E	45	50	108	165	202	245	315	0	0	5	0	-25	-35

TYPHOON GINGER (24W) (CONTINUED)

97092418	9	16.0N	162.6E	50	21	85	158	167	209	299	0	5	5	-5	-30	-25
97092500	10	16.9N	162.1E	55	18	74	111	170	218	307	0	5	0	-30	-40	-5
97092506	11	17.9N	161.6E	60	12	11	61	117	155	237	0	0	-10	-40	-45	0
97092512	12	18.9N	161.1E	65	13	38	92	117	133	199	0	-10	-45	-60	-50	-20
97092518	13	19.8N	160.7E	70	18	100	138	155	163	174	0	-15	-45	-60	-45	-15
97092600	14	20.1N	160.5E	75	33	82	113	138	139	238	0	-30	-50	-45	-15	-5
97092606	15	20.4N	160.3E	85	0	11	13	48	121	413	0	-30	-45	-30	-5	5
97092612	16	20.8N	160.1E	115	13	50	50	84	150	514	0	-10	-5	25	30	45
97092618	17	21.4N	159.7E	125	42	49	23	26	112	568	0	-15	0	30	30	50
97092700	18	21.9N	159.2E	145	21	50	60	87	101	36	0	0	0	-10	-20	-10
97092706	19	22.4N	158.7E	145	12	36	49	87	67	104	0	5	5	-10	-15	-10
97092712	20	22.9N	158.2E	140	8	32	92	172	121	215	0	25	5	0	-10	-5
97092718	21	23.7N	157.8E	135	8	50	115	125	156	179	0	15	5	5	0	0
97092800	22	24.6N	157.4E	115	22	44	65	87	175	212	0	-10	-10	-15	-20	-10
97092806	23	25.6N	157.3E	110	21	12	43	45	83		0	-10	-5	-5	-20	
97092812	24	26.8N	157.3E	110	10	20	77	156	189		0	0	0	0	-10	
97092818	25	28.2N	157.6E	110	0	36	71	190	194		0	5	10	0	-5	
97092900	26	29.8N	158.5E	100	18	73	154	189	182		0	5	5	-5	-5	
97092906	27	31.6N	159.8E	95	12	30	116	146			0	10	5	0		
97092912	28	33.8N	161.9E	90	35	138	156	203			0	5	5	5		
97092918	29	36.4N	164.1E	80	38	62	120				0	0	5			
97093000	30	39.5N	166.9E	75	69	149	263				0	0	0			
97093006	31	42.1N	170.3E	75	106	249					0	5				
97093012		43.8N	173.5E	65												
97093018		45.5N	176.8E	60												
97100100		47.1N	179.5W	55												
		AVERAGE			26	69	108	145	180	292	0	8	10	14	18	19
		# CASES			31	31	30	28	26	22	31	31	30	28	26	22

TROPICAL STORM HANK (25W)

	WRN	BEST TRACK			POSITION ERRORS						WIND ERRORS					
DTG	NO.	LAT	LONG	WIND	00	12	24	36	48	72	00	12	24	36	48	72
97092700		18.2N	111.2E	15												
97092706		18.2N	111.6E	15												
97092712		18.2N	112.0E	15												
97092718		18.4N	112.5E	15												
97092800		18.5N	113.0E	15												
97092806		18.6N	113.5E	15												
97092812		18.6N	113.8E	20												
97092818		18.6N	114.1E	20												
97092900		18.6N	114.3E	20												
97092906		18.6N	114.5E	20												
97092912		18.5N	114.7E	20												
97092918		18.4N	114.8E	20												
97093000		18.2N	114.9E	20												
97093006		18.0N	114.9E	20												
97093012		17.8N	114.8E	20												
97093018		17.6N	114.6E	20												
97100100		17.4N	114.4E	20												
97100106		17.2N	114.0E	20												
97100112		16.9N	113.6E	25												
97100118		16.6N	113.3E	25												
97100200		16.2N	113.0E	25												
97100206		15.7N	112.7E	25												
97100212		15.3N	112.5E	30												
97100218		14.9N	112.2E	35												
97100300	1	14.8N	111.7E	40	18	32	110	196	294		-5	10	15	0	-10	
97100306	2	14.8N	111.2E	40	30	66	155	255			0	15	0	-5		
97100312	3	14.9N	110.7E	35	13	62	119	192			0	0	-5	-5		
97100318	4	15.3N	110.0E	30	24	84	144				0	-5	-5			
97100400	5	16.0N	109.2E	30	16	74	149				0	5	5			

TROPICAL STORM HANK (25W) (CONTINUED)

97100406	6	16.6N	108.3E	30	18	29	59			0	5	10			
97100412	7	17.3N	107.3E	25	39	53				5	0				
97100418		18.0N	106.3E	25											
97100500		18.9N	105.4E	25											
97100506		19.6N	104.7E	20											
			AVERAGE		23	57	123	215	295	1	6	7	3	10	
			# CASES		7	7	6	3	1	7	7	6	3	1	

TROPICAL DEPRESSION (26W)

	WRN	BEST TRACK			POSITION ERRORS						WIND ERRORS					
DTG	NO.	LAT	LONG	WIND	00	12	24	36	48	72	00	12	24	36	48	72
97092912		13.0N	151.0E	15												
97092918		13.4N	150.9E	15												
97093000		13.8N	150.8E	15												
97093006		14.4N	150.8E	15												
97093012		14.8N	150.7E	15												
97093018		15.2N	150.6E	15												
97100100		15.7N	150.5E	15												
97100106		16.2N	150.3E	15												
97100112		16.4N	149.5E	15												
97100118		16.2N	148.1E	15												
97100200		15.7N	146.4E	15												
97100206		15.6N	145.0E	15												
97100212		16.1N	143.5E	20												
97100218		16.7N	141.8E	25												
97100300		17.1N	140.9E	30												
97100306		17.4N	140.1E	30												
97100312		17.6N	139.5E	30												
97100318		17.7N	139.2E	30												
97100400	1	17.8N	138.9E	30	8	30	76	119	152	159	-5	-5	0	0	5	20
97100406	2	17.8N	138.7E	30	34	82	139	173	176	130	-5	-5	0	0	5	15
97100412	3	17.8N	138.5E	30	30	47	61	69	74	34	-5	-5	0	5	10	20
97100418	4	17.8N	138.4E	30	24	54	66	73	72	18	-5	-5	0	5	10	20
97100500	5	17.8N	138.3E	30	24	54	106	130	114		-5	-5	0	5	10	
97100506	6	17.9N	138.1E	30	29	80	127	145	132		-5	-5	0	0	10	
97100512	7	18.1N	137.9E	30	36	97	151	193			-5	-5	-5	5		
97100518		18.5N	137.6E	30												
97100600	8	18.9N	137.2E	30	72	132	187	249			0	0	5	5		
97100606		19.2N	136.6E	30												
97100612	9	19.5N	136.0E	30	6	28	73				0	5	0			
97100618		19.6N	135.2E	30												
97100700	10	19.6N	134.2E	25	0	18					0	-5				
97100706		19.5N	133.1E	25												
97100712		19.3N	132.2E	25												
97100718		19.1N	131.3E	25												
			AVERAGE		27	63	110	144	120	85	4	5	1	3	8	19
			# CASES		10	10	9	8	6	4	10	10	9	8	6	4

SUPER TYPHOON IVAN (27W)

	WRN	BEST TRACK			POSITION ERRORS						WIND ERRORS					
DTG	NO.	LAT	LONG	WIND	00	12	24	36	48	72	00	12	24	36	48	72
97100912		7.0N	177.0E	15												
97100918		7.0N	175.0E	15												
97101000		7.0N	173.0E	15												
97101006		6.9N	171.0E	15												
97101012		6.7N	169.2E	15												
97101018		6.6N	167.6E	15												

SUPER TYPHOON IVAN (27W) (CONTINUED)

97101100		6.6N	166.2E	20													
97101106		6.7N	164.9E	20													
97101112		7.0N	163.2E	20													
97101118		7.6N	161.6E	20													
97101200		8.3N	160.0E	20													
97101206		9.0N	158.3E	20													
97101212		9.5N	156.8E	20													
97101218		9.9N	155.3E	20													
97101300		10.1N	154.1E	20													
97101306	1	10.4N	152.8E	25	29	54	96	152	161	214	0	-10	-15	-20	-25	-35	
97101312	2	10.8N	151.5E	35	11	47	109	159	193	232	-5	-5	-5	0	0	-5	
97101318	3	11.2N	150.1E	40	13	42	106	128	146	286	0	5	5	10	5	-20	
97101400	4	11.6N	148.6E	40	13	66	99	134	158	278	0	0	5	5	0	-40	
97101406	5	12.0N	147.0E	45	6	26	30	29	60	180	0	0	0	-5	5	-40	
97101412	6	12.4N	145.4E	50	5	13	16	13	53	125	0	5	0	-5	-5	-50	
97101418	7	12.7N	143.8E	55	8	8	34	5	46	117	0	-5	-10	-5	-30	-50	
97101500	8	13.0N	142.6E	60	6	32	55	67	89	120	0	-5	-10	-10	-45	-40	
97101506	9	13.3N	141.4E	65	8	16	13	64	114	140	0	-5	5	-20	-35	-25	
97101512	10	13.7N	140.0E	70	11	13	69	125	158	203	0	-5	-5	-40	-45	-25	
97101518	11	14.0N	138.8E	80	29	63	134	184	211	243	0	10	-15	-35	-45	-15	
97101600	12	14.3N	137.6E	85	29	55	104	141	188	225	0	0	-35	-45	-35	-15	
97101606	13	14.4N	136.1E	95	12	60	118	151	182	221	0	-25	-40	-50	-30	-10	
97101612	14	14.5N	134.6E	105	11	44	90	125	150	213	-5	-40	-45	-40	-40	-35	
97101618	15	14.6N	133.1E	120	0	37	60	93	116	173	-5	-20	-35	-30	-35	-25	
97101700	16	14.5N	131.7E	140	13	16	13	52	93	146	0	-30	-25	-30	-35	-15	
97101706	17	14.5N	130.5E	145	13	18	60	94	129	133	-5	-35	-20	-25	-30	-5	
97101712	18	14.6N	129.3E	155	21	75	131	175	216	238	0	-10	-15	-25	-25	15	
97101718	19	14.6N	128.3E	160	0	63	108	145	179	199	0	-5	-20	-20	-15	10	
97101800	20	14.8N	127.2E	150	8	49	97	145	172	130	0	-10	-15	-15	-5	25	
97101806	21	15.2N	126.3E	145	0	21	75	144	163	100	0	-5	-10	-5	5	30	
97101812	22	15.6N	125.4E	145	5	18	46	96	142	168	0	-5	-5	5	20	35	
97101818	23	16.0N	124.7E	140	5	16	80	122	171	209	0	0	5	15	30	35	
97101900	24	16.5N	124.0E	140	12	40	62	92	103	126	0	0	5	20	35	30	
97101906	25	17.1N	123.4E	135	6	49	119	178	196	204	0	0	5	15	25	25	
97101912	26	17.6N	122.7E	130	0	23	86	123	141	158	0	0	10	25	30	15	
97101918	27	18.1N	122.2E	120	12	16	42	60	75	42	0	10	20	30	30	15	
97102000	28	18.4N	122.0E	110	6	26	90	135	161	114	0	5	25	30	20	10	
97102006	29	18.7N	121.9E	100	5	41	117	168	172	188	0	10	20	20	10	0	
97102012	30	19.0N	121.9E	90	6	62	147	198	194	231	0	15	20	15	5	5	
97102018	31	19.3N	122.3E	80	16	86	155	175	171	275	0	15	20	15	5	5	
97102100	32	19.5N	123.0E	70	16	33	49	90	134	185	0	5	-5	-10	-15	-25	
97102106	33	19.8N	123.7E	65	17	6	21	61	94	95	0	5	-5	-10	-15	-25	
97102112	34	20.1N	124.6E	60	5	28	48	72	126	120	0	0	-10	-10	-15	-20	
97102118	35	20.4N	125.5E	60	8	49	98	110	137	115	-5	-5	-15	-15	-20	-15	
97102200	36	20.8N	126.4E	60	13	71	108	121	140	284	-5	-10	-10	-15	-20	-10	
97102206	37	21.4N	127.1E	60	12	55	82	103	182	282	-5	-15	-10	-15	-20	-10	
97102212	38	22.0N	127.7E	65	24	21	50	81	138	147	-10	-10	-10	-15	-15	-10	
97102218	39	22.6N	128.4E	65	11	54	99	161	203	218	-10	-10	-15	-20	-15	-10	
97102300	40	23.2N	129.2E	60	0	21	12	56	82	94	-10	-15	-20	-20	-15	-20	
97102306	41	24.0N	130.3E	60	0	6	43	95	132		-10	-15	-20	-15	-10		
97102312	42	24.9N	131.5E	60	20	76	174	234	334		-10	-15	-15	-10	-10		
97102318	43	25.6N	132.7E	60	8	17	37	94	209		-10	-15	-10	-10	-10		
97102400	44	26.2N	134.0E	60	8	36	45	62	132		-10	-10	-5	-10	-10		
97102406	45	26.8N	135.0E	60	12	10	30	84			-15	-5	-5	-10			
97102412	46	27.5N	136.3E	55	12	37	55	150			-5	0	-5	-10			
97102418		28.3N	137.7E	50													
97102500		28.7N	139.5E	45													
97102506		29.0N	141.3E	45													
97102512		29.2N	143.0E	45													
97102518		29.2N	144.9E	45													
97102600		29.2N	146.9E	45													
		AVERAGE			11	38	77	115	149	180	3	9	14	18	20	21	
		# CASES			46	46	46	46	44	40	46	46	46	46	44	40	

SUPER TYPHOON JOAN (28W)

	WRN	BEST TRACK			POSITION ERRORS						WIND ERRORS					
DTG	NO.	LAT	LONG	WIND	00	12	24	36	48	72	00	12	24	36	48	72
97101100		3.8N	178.6E	15												
97101106		4.3N	177.0E	15												
97101112		5.2N	175.3E	15												
97101118		6.1N	173.6E	20												
97101200		6.9N	171.9E	20												
97101206		7.9N	170.5E	20												
97101212		9.1N	169.3E	25												
97101218		10.2N	168.4E	25												
97101300		10.9N	168.0E	25												
97101306	1	11.4N	167.4E	25	21	121	139	156	181	192	0	0	0	0	5	-40
97101312	2	11.7N	167.0E	30	34	46	47	65	118	225	0	5	5	5	5	-35
97101318	3	11.9N	166.5E	30	23	0	6	51	107	170	0	5	5	10	0	-30
97101400	4	12.3N	165.5E	30	25	65	74	47	72	138	0	0	0	5	-15	-45
97101406	5	12.7N	164.4E	35	37	60	47	59	90	152	0	0	5	-5	-30	-65
97101412	6	13.0N	163.4E	40	13	34	41	42	46	110	-5	-5	-5	-25	-50	-65
97101418	7	13.2N	162.4E	45	5	29	37	29	24	115	0	-5	-20	-45	-55	-50
97101500	8	13.4N	161.5E	50	18	47	66	89	145	236	-5	-5	-25	-50	-50	-20
97101506	9	13.4N	160.5E	50	8	29	51	75	105	127	0	-10	-35	-45	-65	-20
97101512	10	13.4N	159.4E	60	0	6	8	60	102	155	0	-20	-45	-50	-60	-30
97101518	11	13.4N	158.3E	70	5	18	32	68	120	197	0	-30	-40	-65	-35	-20
97101600	12	13.5N	157.1E	90	8	25	73	122	177	232	-5	-25	-35	-50	-15	-20
97101606	13	13.6N	155.9E	105	0	35	96	156	229	294	-15	-25	-55	-30	-20	-15
97101612	14	13.7N	154.7E	125	6	49	105	166	215	265	0	0	-20	-10	-25	-25
97101618	15	13.9N	153.2E	125	13	57	109	164	203	176	0	-20	-5	-15	-30	-35
97101700	16	14.2N	151.6E	140	5	18	76	91	135	154	-15	-20	0	-25	-30	-35
97101706	17	14.4N	150.1E	160	5	13	70	122	144	127	-5	10	5	-10	-15	-25
97101712	18	14.8N	148.6E	160	11	60	92	109	100	98	0	25	-5	-10	-15	-25
97101718	19	15.3N	147.1E	140	0	24	21	6	24	101	0	-10	-30	-35	-50	-65
97101800	20	15.9N	145.6E	135	8	18	42	68	156	465	0	-25	-35	-40	-55	-65
97101806	21	16.5N	144.3E	140	0	13	58	119	277	595	0	-20	-30	-40	-50	-60
97101812	22	17.0N	143.1E	150	6	24	85	177	337	740	0	-5	-10	-15	-25	-45
97101818	23	17.6N	141.8E	145	6	48	106	214	368	739	0	0	-10	-15	-40	-40
97101900	24	18.1N	140.7E	145	0	32	103	268	475	802	0	0	-15	-20	-40	-40
97101906	25	18.5N	139.7E	140	5	13	102	299	510	845	0	-10	-15	-30	-40	-40
97101912	26	19.0N	138.8E	140	0	49	126	234	382	667	0	-10	-15	-25	-40	-40
97101918	27	19.5N	138.0E	140	0	28	54	101	173	417	0	0	-15	-15	-25	-30
97102000	28	20.1N	137.4E	140	5	17	66	142	255	439	0	-5	-15	-20	-25	-25
97102006	29	20.8N	137.0E	135	5	39	105	186	257	452	0	-15	-15	-15	-25	-25
97102012	30	21.5N	136.7E	135	5	24	34	12	0	230	0	-5	-10	-10	-20	-25
97102018	31	22.3N	136.6E	140	0	21	53	88	94	210	0	0	0	-5	-15	-20
97102100	32	23.2N	136.9E	135	12	27	70	122	138	244	0	0	0	-5	-5	-15
97102106	33	24.1N	137.4E	130	5	37	89	112	160	303	0	0	5	0	0	-10
97102112	34	25.0N	138.3E	130	0	16	55	66	102	352	0	10	5	10	0	-10
97102118	35	26.0N	139.5E	120	0	27	58	87	147	338	0	0	-5	0	-10	-15
97102200	36	27.1N	141.1E	115	12	31	97	164	263	346	0	-5	-5	-15	-15	-5
97102206	37	28.1N	143.1E	110	8	66	141	173	269	186	0	-10	-5	-15	-10	-5
97102212	38	28.9N	145.3E	110	12	90	114	198	306	138	0	0	-5	-15	-10	-5
97102218	39	29.2N	147.7E	105	13	57	99	180	269		0	5	0	-10	0	
97102300	40	29.5N	150.1E	95	10	62	136	233	362		0	-5	-5	-10	0	
97102306	41	29.6N	152.5E	90	37	54	125	161	59		0	-5	-5	-5	-5	
97102312	42	29.9N	155.1E	90	31	109	199	300	365		0	0	-5	0	-5	
97102318	43	29.9N	158.0E	85	55	98	210	343	517		5	10	10	5	-5	
97102400	44	29.9N	161.0E	80	60	109	249	468			0	0	5	0		
97102406		30.0N	164.2E	75												
97102412		30.1N	167.6E	75												
97102418		31.1N	171.7E	65												
97102500		33.2N	175.8E	60												
97102506		36.4N	178.5E	60												
97102512		39.9N	179.7W	60												
97102518		43.4N	178.1W	60												
		AVERAGE			12	43	86	141	200	310	1	8	13	19	24	31
		# CASES			44	44	44	44	43	38	44	44	44	44	43	38

SUPER TYPHOON KEITH (29W)

	WRN	BEST TRACK			POSITION ERRORS						WIND ERRORS					
DTG	NO.	LAT	LONG	WIND	00	12	24	36	48	72	00	12	24	36	48	72
97102212		6.5N	175.5E	15												
97102218		6.5N	175.2E	15												
97102300		6.6N	175.0E	15												
97102306		6.7N	174.7E	15												
97102312		6.8N	174.5E	15												
97102318		6.9N	174.2E	15												
97102400		7.0N	174.0E	15												
97102406		7.0N	173.7E	15												
97102412		7.1N	173.5E	20												
97102418		7.2N	173.2E	20												
97102500		7.3N	173.0E	20												
97102506		7.5N	172.8E	20												
97102512		7.6N	172.5E	20												
97102518		7.7N	172.3E	20												
97102600		7.7N	172.1E	20												
97102606		7.7N	171.8E	20												
97102612		7.6N	171.4E	20												
97102618		7.2N	170.8E	25												
97102700		6.8N	170.2E	25												
97102706		6.4N	169.7E	25												
97102712		6.0N	169.3E	30												
97102718	1	5.9N	169.1E	30	101	136	139	132	118	93	-5	0	10	10	15	-5
97102800	2	5.9N	168.8E	35	122	137	131	119	86	72	0	10	15	20	15	-10
97102806	3	6.0N	168.4E	35	149	189	221	242	239	275	0	5	5	10	10	-15
97102812	4	6.2N	167.9E	35	168	149	147	144	141	166	5	10	15	20	10	-25
97102818	5	6.4N	167.1E	35	114	80	80	72	83	75	5	5	10	10	-5	-35
97102900	6	6.5N	166.1E	40	118	86	47	21	8	33	0	0	0	-5	-25	-45
97102906	7	6.6N	165.1E	45	67	42	34	29	47	100	-5	-5	-10	-20	-35	-50
97102912	8	6.8N	164.1E	45	42	35	58	72	45	50	0	-10	-20	-35	-45	-55
97102918	9	7.2N	163.1E	50	17	72	103	88	71	102	-5	-15	-30	-40	-50	-50
97103000	10	7.6N	162.0E	55	29	24	29	48	60	74	0	-10	-25	-35	-40	-25
97103006	11	7.9N	160.8E	65	24	30	71	89	76	53	0	-10	-25	-30	-30	-10
97103012	12	8.3N	159.7E	75	11	8	38	53	65	45	0	-15	-20	-30	-30	-5
97103018	13	8.6N	158.5E	90	17	47	74	79	72	32	0	-10	-15	-20	-5	-15
97103100	14	8.9N	157.5E	105	5	30	51	85	101	88	0	-10	-20	-15	5	0
97103106	15	9.4N	156.6E	115	17	61	105	146	151	125	-10	-20	-25	-10	10	10
97103112	16	10.1N	155.6E	125	21	54	98	122	127	99	-5	-10	-10	10	5	15
97103118	17	10.7N	154.4E	135	8	26	62	87	109	81	-5	-15	-5	15	-5	15
97110100	18	11.4N	153.1E	145	0	37	71	87	91	63	-5	-10	5	10	10	10
97110106	19	12.1N	151.7E	150	5	44	63	84	75	53	-5	0	15	0	20	5
97110112	20	12.7N	150.1E	155	5	31	42	51	37	87	0	15	10	10	20	15
97110118	21	13.3N	148.6E	150	0	18	43	51	54	58	10	15	-5	15	15	15
97110200	22	13.9N	147.2E	145	0	21	21	23	54	68	15	10	10	20	10	20
97110206	23	14.4N	145.8E	140	6	23	41	79	106	79	15	0	20	20	5	25
97110212	24	14.8N	144.3E	145	0	8	32	72	121	174	5	5	15	5	5	25
97110218	25	15.2N	142.9E	155	0	21	32	91	143	204	-5	15	15	0	10	30
97110300	26	15.5N	141.7E	140	0	24	56	94	123	150	10	20	10	10	15	35
97110306	27	15.7N	140.5E	130	0	31	42	45	41	116	15	15	0	10	15	25
97110312	28	15.9N	139.2E	125	5	23	42	75	96	155	15	5	5	10	15	20
97110318	29	16.1N	138.0E	125	0	23	16	36	78	142	15	0	10	15	20	20
97110400	30	16.2N	137.1E	130	5	36	61	92	127	244	0	0	5	10	15	15
97110406	31	16.5N	136.2E	135	0	37	64	96	128	232	-10	0	5	10	10	5
97110412	32	17.0N	135.6E	125	8	0	45	84	123	274	-5	0	5	5	-5	0
97110418	33	17.4N	135.1E	120	8	40	85	113	128	306	-5	5	10	5	-15	-5
97110500	34	18.0N	134.9E	115	8	41	73	107	118	301	-5	0	5	0	-5	0
97110506	35	18.6N	135.0E	110	8	50	89	107	157	473	-10	-10	-10	-20	-20	-10
97110512	36	19.1N	135.4E	105	6	23	104	147	220	671	-5	-5	-10	-15	-15	-10
97110518	37	19.6N	135.8E	100	17	53	65	49	41	485	-5	0	-10	-20	-20	-20
97110600	38	20.3N	136.3E	95	16	61	90	146	216	745	0	0	-5	-15	-15	-15
97110606	39	21.3N	137.0E	90	6	82	145	152	82	488	0	-10	-10	-10	-10	-10
97110612	40	22.3N	137.7E	90	8	17	29	82	250	700	-5	-10	-10	-10	-15	-5
97110618	41	23.3N	138.5E	90	8	46	91	212	441	778	-10	-10	-10	-10	-15	-5
97110700	42	24.4N	139.6E	85	12	56	81	221	400	432	-10	-5	-5	-10	-10	-5
97110706	43	25.5N	141.3E	80	13	39	106	290	482		-5	0	0	-10	-5	
97110712	44	26.5N	143.1E	75	12	74	281	528	725		-10	-5	-5	-5	0	
97110718	45	27.8N	145.4E	70	27	162	429	704	826		-10	-10	-15	-10	-5	
97110800	46	28.6N	148.3E	65	24	143	363	562	602		-5	-5	-5	-5	-5	
97110806	47	30.2N	152.4E	60	66	237	392	389			-5	-10	-5	-5		
97110812	48	31.7N	157.3E	60	124	334	453	407			-5	0	5	0		

SUPER TYPHOON KEITH (29W) (CONTINUED)

97110818	33.5N	162.7E	60
97110900	35.7N	168.1E	55
97110906	37.0N	174.0E	50
97110912	37.7N	179.2E	45
97110918	38.0N	176.5W	45
97111000	38.0N	172.9W	45

AVERAGE	30	64	105	144	167	216	6	7	11	13	15	18
# CASES	48	48	48	48	46	42	48	48	48	48	46	42

TYPHOON LINDA (30W)

	WRN	BEST TRACK			POSITION ERRORS						WIND ERRORS					
DTG	NO.	LAT	LONG	WIND	00	12	24	36	48	72	00	12	24	36	48	72
97102500		6.0N	140.0E	15												
97102506		6.3N	139.1E	15												
97102512		6.9N	137.8E	15												
97102518		7.7N	136.6E	15												
97102600		8.4N	135.5E	15												
97102606		9.2N	134.7E	15												
97102612		10.0N	133.7E	15												
97102618		10.7N	133.1E	15												
97102700		11.0N	132.7E	15												
97102706		11.1N	132.0E	15												
97102712		11.5N	131.3E	15												
97102718		11.6N	130.7E	15												
97102800		11.8N	129.9E	15												
97102806		11.8N	129.2E	15												
97102812		11.8N	128.4E	15												
97102818		11.8N	127.6E	15												
97102900		11.6N	126.9E	15												
97102906		11.0N	126.3E	15												
97102912		10.5N	125.5E	15												
97102918		9.9N	124.5E	15												
97103000		9.8N	123.3E	15												
97103006		9.5N	122.0E	15												
97103012		9.3N	120.6E	15												
97103118	1	8.2N	114.7E	35	34	36	37	88	111	168	-5	-5	-5	5	0	20
97110100	2	8.2N	113.5E	40	51	56	80	97	124	219	-5	-10	-5	0	0	30
97110106	3	8.2N	112.2E	45	24	77	133	162	192	300	-10	-15	-5	-10	0	30
97110112	4	8.2N	110.5E	50	21	86	120	131	153	231	-5	0	10	-10	0	30
97110118	5	8.4N	108.8E	55	13	36	47	52	88	143	0	10	-5	5	30	35
97110200	6	8.7N	107.2E	55	21	45	34	48	94	138	0	10	0	10	25	30
97110206	7	8.9N	105.9E	55	8	34	83	103	133	114	0	0	0	25	25	30
97110212	8	9.2N	104.6E	55	0	25	51	84	116	96	0	-5	5	10	25	30
97110218	9	9.5N	103.6E	65	6	36	74	120	125	114	0	10	35	15	25	30
97110300	10	10.0N	102.6E	65	18	48	91	123	116	151	0	10	30	35	30	30
97110306	11	10.5N	101.6E	65	0	46	96	101	85	104	0	25	20	30	30	30
97110312	12	11.0N	100.5E	65	6	40	72	67	76	221	0	10	20	25	30	20
97110318	13	11.6N	99.3E	50	31	70	53	33	58	208	0	-5	10	15	20	15
97110400	14	12.1N	98.0E	45	54	50	45	68	87	208	0	0	0	10	15	10
97110406	15	12.7N	96.8E	45	67	85	114	132	151	308	0	0	0	10	15	5
97110412	16	13.1N	95.9E	45	21	53	106	172	256		0	-5	-10	-20	-40	
97110418	17	13.4N	95.1E	45	21	59	125	195	290		0	-5	-10	-20	-40	
97110500	18	13.6N	94.3E	50	41	96	150	203	246		0	0	-10	-35	-40	
97110506	19	13.8N	93.6E	50	23	30	42	95	151	292	0	0	0	-20	-25	-25
97110512	20	14.0N	93.1E	50	32	79	137	187	251	380	0	0	-20	-25	-20	-20
97110518	21	14.2N	92.8E	50	41	88	143	176	242	372	0	0	-20	-20	-20	-15
97110600	22	14.6N	92.5E	50	36	70	96	151	219	334	0	-15	-20	-15	-20	-10
97110606	23	14.8N	92.2E	50	29	46	64	138	216		0	-20	-20	-20	-20	
97110612	24	14.9N	92.0E	65	8	37	130	257	409		0	5	5	-5	-15	
97110618	25	15.0N	91.8E	65	18	58	139	249	380		0	10	5	0	-10	
97110700	26	15.0N	91.4E	65	35	91	157	257	388		0	15	5	5	-5	
97110706	27	14.9N	90.9E	60	18	78	150	253	359		-5	-5	-5	0	5	
97110712	28	14.8N	90.7E	55	36	90	158	240	343		0	-5	0	5	10	
97110718	29	14.7N	90.5E	55	13	49	68	90			-5	0	5	10		
97110800	30	14.7N	90.4E	55	16	36	73	116			5	10	10	15		
97110806	31	14.7N	90.4E	50	26	39	84				5	10	15			

TYPHOON LINDA (30W) (CONTINUED)

97110812	32	14.7N	90.2E	45	55	90	137				0	10	20			
97110818	33	14.9N	90.1E	40	63	99					-5	5				
97110900	34	15.1N	90.2E	35	47	77					0	10				
97110906	35	15.3N	90.3E	30	0						0					
97110912		15.5N	90.5E	25												
			AVERAGE		27	60	97	140	195	216	1	7	10	14	19	23
			# CASES		35	34	32	30	28	19	35	34	32	30	28	19

TYPHOON MORT (31W)

	WRN	BEST TRACK			POSITION ERRORS						WIND ERRORS					
DTG	NO.	LAT	LONG	WIND	00	12	24	36	48	72	00	12	24	36	48	72
97110700		10.1N	150.8E	15												
97110706		10.2N	149.8E	15												
97110712		10.3N	148.8E	15												
97110718		10.5N	147.8E	20												
97110800		10.7N	146.9E	20												
97110806		10.8N	146.0E	20												
97110812		10.9N	145.1E	20												
97110818		11.0N	144.2E	20												
97110900		11.1N	143.3E	20												
97110906		11.1N	142.6E	20												
97110912		11.1N	142.2E	20												
97110918		11.1N	141.9E	20												
97111000		11.1N	141.5E	20												
97111006		11.1N	141.1E	20												
97111012		11.1N	140.4E	20												
97111018	1	11.2N	139.6E	25	23	34	62	76	62	72	0	-5	-15	-15	-10	20
97111100	2	11.4N	138.9E	30	24	18	21	35	36	93	0	-10	-15	-15	-10	35
97111106	3	11.7N	138.3E	35	16	47	65	82	76	151	0	0	5	10	25	65
97111112	4	12.1N	137.5E	45	23	59	85	99	116	210	-5	-5	5	10	35	65
97111118	5	12.4N	136.6E	50	0	13	29	48	83	187	-5	-10	0	10	45	55
97111200	6	12.7N	135.7E	55	5	11	25	48	48	105	0	5	10	30	60	55
97111206	7	13.0N	134.9E	60	5	12	32	60	72	88	0	0	10	40	60	50
97111212	8	13.3N	134.1E	60	5	26	47	66	91	99	0	0	20	50	60	50
97111218	9	13.4N	133.3E	65	16	54	69	78	82	133	0	0	30	50	50	60
97111300	10	13.5N	132.6E	65	18	36	62	102	139	171	0	15	45	50	50	65
97111306	11	13.6N	131.9E	65	5	17	52	98	115	146	0	25	40	40	35	65
97111312	12	13.6N	131.1E	55	5	24	58	92	95	129	10	35	40	35	35	70
97111318	13	13.7N	130.2E	45	33	57	81	92	96	171	20	35	30	30	45	65
97111400	14	13.8N	129.2E	35	11	5	34	28	50		0	0	-15	-25	-10	
97111406	15	13.9N	128.2E	35	8	24	24	21	36		0	-10	-20	-15	0	
97111412	16	14.1N	127.1E	35	44	50	58	71			0	-15	-25	-10		
97111418	17	14.4N	126.1E	45	18	39	64	59			0	-15	-10	5		
97111500	18	14.7N	125.1E	50	0	34	54	67			0	0	10	10		
97111506	19	14.9N	124.4E	55	18	55	66				0	10	10			
97111512	20	15.0N	123.8E	55	26	62	72				0	10	15			
97111518	21	15.1N	123.2E	45	26	50	84				0	15	15			
97111600	22	15.3N	122.5E	35	13	23					0	10				
97111606	23	15.6N	121.8E	25	0	6					0	0				
97111612		15.9N	121.1E	20												
97111618		16.0N	120.5E	15												
			AVERAGE		15	33	55	68	80	136	2	10	18	25	35	55
			# CASES		23	23	21	18	15	13	23	23	21	18	15	13

SUPER TYPHOON OLIWA (02C)

	WRN	BEST TRACK			POSITION ERRORS						WIND ERRORS					
DTG	NO.	LAT	LONG	WIND	00	12	24	36	48	72	00	12	24	36	48	72
97082806		11.8N	166.7W	15												
97082812		11.8N	167.1W	25												
97082818		11.8N	167.6W	25												
97082900		11.8N	168.1W	25												
97082906		11.8N	168.6W	25												
97082912		11.8N	169.0W	25												
97082918		11.9N	169.3W	25												
97083000		12.1N	169.5W	25												
97083006		12.3N	170.0W	25												
97083012		12.4N	170.6W	25												
97083018		12.4N	171.3W	25												
97083100		12.5N	172.0W	25												
97083106		12.6N	172.6W	25												
97083112		12.7N	173.1W	25												
97083118		12.7N	173.6W	25												
97090100		12.7N	174.1W	25												
97090106		12.7N	174.6W	25												
97090112		12.7N	175.2W	25												
97090118		12.7N	175.8W	30												
97090200		12.8N	176.4W	30												
97090206		13.0N	176.9W	30												
97090212		13.1N	177.3W	30												
97090218	1	13.2N	177.7W	30	11	5	30	146	363	738	5	0	5	10	15	25
97090300	2	13.3N	178.2W	35	37	66	145	363	615	988	0	5	10	15	20	30
97090306	3	13.3N	178.7W	35	102	204	285	453	689	1150	0	5	10	15	20	30
97090312	4	13.2N	179.2W	35	117	174	329	592	831	1380	5	10	10	15	20	30
97090318	5	13.1N	179.8W	35	0	170	295	525	718	1210	0	10	10	15	20	25
97090400	6	13.1N	179.4E	35	26	235	367	593	829	1382	-5	10	10	15	20	20
97090406	7	13.1N	178.3E	35	42	96	140	133	173	260	0	5	10	15	20	5
97090412	8	13.1N	177.0E	35	107	204	217	213	265	304	0	5	10	15	20	10
97090418	9	13.3N	175.5E	35	166	250	257	268	307	295	5	10	15	20	15	5
97090500	10	13.7N	174.0E	35	83	154	228	270	276	272	0	0	5	5	0	-10
97090506	11	14.2N	172.9E	35	42	87	118	136	160	217	-5	-5	-5	-5	-10	-20
97090512	12	14.6N	172.1E	35	34	86	88	93	114	171	0	0	0	-5	-15	-20
97090518	13	15.0N	171.3E	35	53	58	55	69	100	147	0	5	0	-5	-10	-15
97090600	14	15.5N	170.4E	35	39	99	132	91	30	36	0	0	-5	-15	-20	-50
97090606	15	16.0N	169.1E	35	36	188	195	170	146	126	0	-5	-15	-20	-15	-50
97090612	16	16.4N	167.8E	35	31	40	13	56	86	70	0	-5	-15	-20	-25	-80
97090618	17	16.7N	166.5E	40	25	16	33	81	86	86	-5	-10	-20	-25	-30	-90
97090700	18	17.0N	165.3E	45	18	64	121	145	142	96	0	0	0	0	-25	-70
97090706	19	17.3N	164.3E	50	11	29	58	64	57	29	0	-5	-5	-10	-40	-70
97090712	20	17.5N	163.4E	55	6	33	56	58	51	30	0	0	0	-20	-50	-60
97090718	21	17.7N	162.6E	60	21	51	67	86	88	108	0	0	-5	-30	-60	-55
97090800	22	17.9N	161.8E	60	13	29	59	92	97	115	0	5	-15	-45	-55	-50
97090806	23	18.0N	161.0E	65	22	62	91	120	111	139	0	-5	-30	-60	-55	-50
97090812	24	18.1N	159.9E	65	20	154	162	172	183	218	0	-25	-55	-65	-60	-50
97090818	25	18.1N	158.7E	75	21	42	66	82	116	157	-5	-30	-60	-55	-50	-30
97090900	26	18.1N	157.5E	90	8	18	32	63	112	171	-10	-40	-50	-45	-40	-15
97090906	27	18.1N	156.2E	105	6	17	40	74	104	139	-10	-40	-35	-30	-25	-10
97090912	28	18.2N	154.9E	125	11	47	87	102	109	143	15	0	-10	-25	-20	-15
97090918	29	18.4N	153.5E	140	23	56	79	97	105	148	0	-5	-15	-25	-15	-10
97091000	30	18.6N	152.1E	140	12	29	54	78	110	186	0	-5	-15	-20	-10	0
97091006	31	18.9N	150.8E	140	6	16	21	16	0	65	0	-5	-15	-15	-10	0
97091012	32	19.1N	149.4E	140	5	20	17	8	18	60	-5	-5	-10	-10	-5	5
97091018	33	19.3N	148.0E	140	5	13	8	12	32	71	0	-5	-5	-10	0	5
97091100	34	19.5N	146.6E	140	0	13	32	54	79	145	0	5	10	10	20	20
97091106	35	19.9N	145.3E	140	5	245	251	257	260	272	0	5	0	0	10	15
97091112	36	20.3N	144.0E	135	23	53	67	62	79	124	0	5	5	15	15	10
97091118	37	20.8N	142.7E	130	0	5	16	56	84	107	0	0	5	10	5	10
97091200	38	21.3N	141.4E	125	13	30	54	84	110	106	0	0	10	5	0	-5
97091206	39	21.9N	140.1E	125	12	11	26	69	144	130	0	10	15	15	10	-5
97091212	40	22.5N	138.7E	120	0	32	68	115	119	187	0	10	10	10	10	0
97091218	41	23.2N	137.4E	115	8	30	63	89	84	209	0	5	5	10	10	0
97091300	42	24.0N	136.1E	105	17	24	42	51	106	101	0	0	0	-5	-15	-15
97091306	43	24.9N	134.9E	105	8	30	44	93	141	57	0	0	5	0	-15	-10
97091312	44	25.7N	133.8E	100	13	53	77	114	139	82	0	0	-5	-10	-25	-10

SUPER TYPHOON OLIWA (02C) (CONTINUED)

97091318	45	26.5N	132.6E	100	20	226	158	74	16	221	-5	10	30	20	10	10
97091400	46	27.3N	131.5E	95	8	56	122	189	221	168	-10	-10	-10	-15	-15	10
97091406	47	27.9N	130.6E	90	16	55	111	171	190	245	-10	-10	-15	-10	-20	10
97091412	48	28.3N	130.0E	90	7	41	87	109	84		-20	-20	-20	-15	-15	
97091418	49	28.6N	129.7E	85	7	24	50	24	72		-20	-20	-15	-10	0	
97091500	50	28.9N	129.5E	85	0	27	31	66	90		-20	-20	-15	-20	0	
97091506	51	29.3N	129.5E	85	0	5	36	110	180		-20	-15	-15	-5	10	
97091512	52	29.9N	129.7E	80	6	49	83	120			-15	-10	-10	5		
97091518	53	30.6N	130.1E	75	20	42	132	169			-10	-10	0	15		
97091600	54	31.6N	130.7E	70	11	78	181				-5	-15	5			
97091606	55	33.0N	131.7E	65	20	126	219				-10	0	10			
97091612	56	34.1N	133.1E	60	19	33					-15	0				
97091618	57	35.1N	134.6E	45	15	18					-10	5				
97091700	58	36.2N	136.2E	35	7						-5					
97091706	59	37.7N	138.4E	25	15						0					
		AVERAGE			25	73	108	144	185	274	4	8	13	17	20	24
		# CASES			59	57	55	53	51	47	59	57	55	53	51	47

SUPER TYPHOON PAKA (05C)

	WRN	BEST TRACK			POSITION ERRORS						WIND ERRORS					
DTG	NO.	LAT	LONG	WIND	00	12	24	36	48	72	00	12	24	36	48	72
97112818		5.6N	166.3W	20												
97112900		5.9N	166.1W	25												
97112906		6.1N	166.0W	25												
97112912		6.4N	165.8W	25												
97112918		6.7N	165.5W	25												
97113000		7.1N	165.3W	25												
97113006		7.4N	165.2W	25												
97113012		7.7N	165.2W	25												
97113018		7.8N	165.3W	25												
97120100		7.9N	165.4W	25												
97120106		8.0N	165.6W	30												
97120112		8.0N	165.9W	30												
97120118		8.0N	166.3W	30												
97120200		8.0N	166.7W	30												
97120206		8.0N	167.1W	35												
97120212	1*	8.0N	167.2W	40	NOTE: * = ADVISORY ISSUED BY CENTRAL PACIFIC											
97120218	2*	8.1N	167.3W	45	HURRICANE CENTER											
97120300	3*	8.1N	167.4W	45												
97120306	4*	8.1N	167.5W	50												
97120312	5*	8.1N	167.6W	55												
97120318	6*	8.2N	167.8W	55												
97120400	7*	8.3N	168.2W	55												
97120406	8*	8.4N	168.7W	55												
97120412	9*	8.4N	169.3W	50												
97120418	10*	8.4N	170.1W	50												
97120500	11*	8.3N	171.3W	50												
97120506	12*	8.2N	172.3W	50												
97120512	13*	8.1N	173.5W	45												
97120518	14*	7.9N	175.0W	45												
97120600	15*	7.7N	176.7W	40												
97120606	16*	7.6N	177.7W	35												
97120612	17*	7.5N	178.4W	35												
97120618	18	7.4N	179.1W	40	93	119	165	203	253	356	-5	-15	-25	-20	-10	-15
97120700	19	7.4N	179.7W	45	62	84	110	148	182	336	-5	-15	-20	-10	-15	-25
97120706	20	7.4N	179.9E	50	55	82	124	182	253	424	-10	-20	-20	-10	-15	-30
97120712	21	7.4N	179.4E	55	76	110	164	219	312	467	-10	-15	-5	-10	-10	-40
97120718	22	7.4N	178.8E	60	107	147	197	250	291	427	-5	5	15	0	-10	-50
97120800	23	7.3N	178.1E	60	93	120	150	179	232	418	-10	5	0	-5	-15	-60
97120806	24	7.1N	177.2E	55	18	42	84	149	237	402	-10	0	-5	-5	-25	-70
97120812	25	6.9N	176.5E	45	30	48	63	122	224	386	0	0	-5	-10	-35	-75
97120818	26	6.7N	175.5E	45	42	59	106	186	275	473	0	0	-5	-20	-45	-80
97120900	27	6.6N	174.6E	45	0	42	72	113	155	280	0	0	-5	-25	-55	-85

SUPER TYPHOON PAKA (05C) (CONTINUED)

97120906	28	6.6N	174.1E	45	0	21	26	5	48	149	0	0	-15	-35	-65	-85
97120912	29	6.7N	173.5E	45	24	42	47	53	62	78	0	-5	-25	-45	-65	-75
97120918	30	6.8N	172.7E	45	0	17	36	45	45	50	0	-15	-35	-55	-70	-70
97121000	31	6.8N	171.9E	50	5	25	38	53	96	119	0	-20	-45	-60	-75	-65
97121006	32	6.8N	171.2E	60	8	29	48	71	101	162	-5	-20	-35	-50	-60	-45
97121012	33	6.7N	170.5E	70	21	29	18	37	75	102	-15	-30	-40	-55	-55	-55
97121018	34	6.7N	169.8E	80	13	21	59	75	87	127	-15	-30	-40	-50	-45	-55
97121100	35	6.7N	169.1E	90	11	33	84	136	167	207	-10	-15	-15	-5	10	-15
97121106	36	6.8N	168.5E	100	6	40	73	98	134	204	-10	-5	5	20	30	-5
97121112	37	7.1N	167.7E	105	16	30	36	68	115	193	-5	0	15	30	20	-10
97121118	38	7.3N	167.3E	110	24	30	42	72	109	228	-5	0	20	35	10	-15
97121200	39	7.6N	166.5E	115	0	8	40	97	171	357	-10	0	15	15	5	-15
97121206	40	7.8N	165.8E	115	0	26	67	118	162	210	0	15	30	15	5	-10
97121212	41	8.0N	165.1E	110	0	39	80	128	178	188	5	20	20	10	5	0
97121218	42	8.3N	164.1E	105	5	21	50	90	129	159	10	25	10	5	0	0
97121300	43	8.7N	163.0E	100	13	25	40	88	123	110	5	5	5	0	-5	5
97121306	44	9.1N	161.8E	95	12	54	105	158	190	122	0	-25	-20	-20	-20	-5
97121312	45	9.6N	160.5E	105	6	47	108	159	165	100	0	-10	-15	-20	-15	-5
97121318	46	10.0N	159.0E	115	13	65	105	146	157	122	0	-10	-15	-20	-10	-10
97121400	47	10.4N	157.4E	120	0	55	104	106	94	31	-5	-15	-20	-20	-5	-15
97121406	48	10.9N	155.7E	125	13	46	72	82	63	16	-10	-20	-20	-15	0	-20
97121412	49	11.4N	154.0E	130	0	18	35	50	39	58	-10	-20	-15	-5	-5	-30
97121418	50	12.0N	152.5E	135	0	16	8	13	21	37	5	0	-5	-5	-30	-65
97121500	51	12.4N	150.8E	140	0	6	13	31	21	71	0	0	0	-10	-35	-70
97121506	52	12.7N	149.5E	140	5	18	26	29	25	85	0	5	5	-15	-40	-55
97121512	53	13.0N	148.3E	140	0	8	16	13	13	69	0	10	5	-15	-40	-50
97121518	54	13.3N	147.1E	135	6	16	35	34	55	100	5	5	-20	-40	-60	-50
97121600	55	13.5N	146.2E	130	0	18	23	35	58	112	-10	15	-5	-25	-50	-40
97121606	56	13.7N	145.3E	125	0	24	26	40	63	123	0	-15	-30	-45	-45	-35
97121612	57	13.7N	144.7E	130	5	0	13	40	69	108	-5	-20	-35	-50	-40	-30
97121618	58	13.7N	143.9E	135	0	5	21	58	75	139	-10	-30	-50	-45	-40	-25
97121700	59	13.7N	143.0E	140	0	13	46	80	85	151	-15	-35	-55	-40	-35	-20
97121706	60	13.7N	142.1E	145	0	29	67	88	117	210	-25	-35	-25	-20	-15	5
97121712	61	13.8N	141.4E	150	6	32	61	79	120	220	-5	-15	0	5	10	35
97121718	62	14.0N	140.6E	155	5	16	16	45	78	141	0	5	5	10	10	55
97121800	63	14.3N	139.7E	160	0	11	46	67	78	153	0	-5	-5	5	15	75
97121806	64	14.6N	139.0E	145	5	18	42	49	79	215	-10	-10	0	10	30	80
97121812	65	14.9N	138.2E	140	0	11	30	72	132	233	-5	0	5	15	40	85
97121818	66	15.0N	137.3E	135	13	16	59	104	164	248	-5	-5	-5	15	45	75
97121900	67	15.3N	136.3E	130	0	37	80	105	151	277	-15	-10	-20	-5	20	20
97121906	68	15.7N	135.6E	125	16	50	78	103	162	302	-10	-5	-5	15	25	25
97121912	69	16.1N	135.0E	120	5	5	57	126	166	281	-5	0	5	25	15	20
97121918	70	16.5N	134.3E	115	5	22	91	143	191		0	15	25	30	20	
97122000	71	16.8N	133.8E	110	12	47	103	144	206		0	10	30	25	20	
97122006	72	17.1N	133.4E	95	0	31	58	98	137		0	15	30	30	25	
97122012	73	17.3N	133.2E	85	34	106	163	186	202		0	25	25	25	20	
97122018	74	17.4N	133.1E	65	62	124	162	168			5	20	20	20		
97122100	75	17.5N	132.9E	45	58	88	95	72			15	15	10	10		
97122106	76	17.5N	132.6E	40	30	26	8				10	10	15			
97122112	77	17.5N	132.3E	35	8	32	83				0	5	5			
97122118	78	17.6N	132.0E	30	6	26					0	5				
97122200		17.7N	131.8E	25												
97122206		17.9N	131.6E	20												
97122212		18.4N	131.4E	20												
			AVERAGE		17	40	68	99	132	199	5	12	17	22	28	40
			# CASES		61	61	60	58	56	52	61	61	60	58	56	52

6.2.2 NORTH INDIAN OCEAN— This section includes verification statistics for each warning in the North Indian Ocean during 1997.

JTWC BEST TRACK, FORECAST TRACK AND INTENSITY ERRORS BY WARNING

TROPICAL CYCLONE 01B

	WRN	BEST TRACK			POSITION ERRORS						WIND ERRORS					
DTG	NO.	LAT	LONG	WIND	00	12	24	36	48	72	00	12	24	36	48	72
97051300		3.2N	91.9E	15												
97051306		3.3N	91.9E	15												
97051312		3.5N	91.8E	15												
97051318		3.7N	91.7E	15												
97051400		4.0N	91.6E	20												
97051406		4.4N	91.6E	25												
97051412		5.1N	91.4E	30												
97051418	1	6.2N	90.8E	35	66	120	118	179	269	305	-10	-15	-15	-5	-5	-5
97051500	2	7.2N	90.4E	40	81	91	135	255	354	397	5	5	15	20	25	15
97051506	3	8.0N	90.2E	45	53	96	178	267	296	264	0	5	15	15	20	10
97051512	4	8.3N	90.3E	50	54	135	185	190	124	32	0	5	10	10	15	5
97051518	5	8.6N	90.4E	50	53	102	157	174	146	169	0	5	5	5	10	0
97051600	6	9.0N	90.6E	50	13	85	171	228	276	420	5	0	-5	-5	-5	-10
97051606	7	9.7N	91.0E	50	21	87	150	189	235	319	0	-5	-10	-10	-15	-15
97051612	8	10.6N	91.3E	55	13	69	134	180	199	209	-5	-10	-15	-20	-20	-15
97051618	9	11.6N	91.5E	60	31	106	172	149	133	132	0	0	0	-5	-5	20
97051700	10	12.6N	91.5E	65	41	108	145	136	139	82	0	-5	-15	-10	-25	-25
97051706	11	13.6N	91.2E	70	11	44	47	52	62	299	-5	-10	-20	-15	-20	-10
97051712	12	14.4N	90.7E	75	18	34	23	39	44		-10	-15	-20	-15	-45	
97051718	13	15.2N	90.4E	80	11	43	74	86	122		-5	-10	-10	-10	5	
97051800	14	16.2N	90.2E	90	6	50	74	84	232		0	0	-5	0	30	
97051806	15	17.2N	90.3E	95	5	21	18	39	329		-5	-5	-10	15	20	
97051812	16	18.3N	90.4E	100	5	8	18	186			-10	-15	-15	5		
97051818	17	19.3N	90.5E	105	6	11	45	345			0	0	15	15		
97051900	18	20.2N	90.8E	110	23	55	231				0	0	35			
97051906	19	21.1N	91.1E	115	0	21	316				0	10	15			
97051912	20	22.1N	91.6E	115	8	173					0	10				
97051918	21	23.2N	92.3E	90	0	232					0	5				
97052000	22	25.5N	94.7E	65	32						0					
97052006		27.8N	97.5E	50												
			AVERAGE		25	81	126	164	198	239	3	6	13	11	18	12
			# CASES		22	21	19	17	15	11	22	21	19	17	15	11

TROPICAL CYCLONE 02B

	WRN	BEST TRACK			POSITION ERRORS						WIND ERRORS					
DTG	NO.	LAT	LONG	WIND	00	12	24	36	48	72	00	12	24	36	48	72
97092000		13.1N	83.8E	15												
97092006		13.2N	83.7E	15												
97092012		13.3N	83.6E	15												
97092018		13.4N	83.5E	15												
97092100		13.5N	83.5E	20												
97092106		13.7N	83.4E	20												
97092112		13.9N	83.4E	20												
97092118		14.1N	83.3E	25												
97092200		14.3N	83.2E	25												
97092206		14.5N	83.1E	25												

TROPICAL CYCLONE 02B (CONTINUED)

DTG	WRN NO.	BEST TRACK LAT	LONG	WIND	POSITION ERRORS 00	12	24	36	48	72	WIND ERRORS 00	12	24	36	48	72
97092212		14.7N	83.1E	25												
97092218		15.0N	83.0E	25												
97092300		15.2N	82.9E	25												
97092306		15.3N	82.7E	25												
97092312		15.4N	82.4E	25												
97092318		15.7N	82.3E	25												
97092400		16.1N	82.3E	30												
97092406		16.5N	82.5E	30												
97092412		16.9N	82.7E	30												
97092418	1	17.2N	83.2E	35	12	54	92	194	302	545	0	5	0	-10	-35	0
97092500		17.3N	83.8E	35												
97092506	2	17.6N	84.4E	35	81	151	261	385	485		0	-10	-15	-25	-30	
97092512	3	18.1N	84.9E	35	87	174	309	406	541		0	-15	-20	-25	5	
97092518	4	18.8N	85.7E	45	12	111	220	313	428		0	-5	-15	-10	30	
97092600	5	19.4N	86.7E	55	16	107	170	288			0	0	0	35		
97092606	6	20.0N	88.0E	55	38	131	211	329			0	0	5	50		
97092612	7	21.0N	89.4E	60	6	29	95				0	5	20			
97092618	8	21.8N	90.4E	65	24	28	133				0	-5	10			
97092700	9	22.6N	91.2E	65	85	125					0	15				
97092706	10	23.7N	92.3E	65	0	54					0	25				
97092712		24.8N	93.4E	35												
97092718		26.0N	94.4E	25												
		AVERAGE			37	97	187	320	440	545	0	9	11	26	25	0
		# CASES			10	10	8	6	4	1	10	10	8	6	4	1

TROPICAL CYCLONE 03A

DTG	WRN NO.	BEST TRACK LAT	LONG	WIND	POSITION ERRORS 00	12	24	36	48	72	WIND ERRORS 00	12	24	36	48	72
97110400		7.8N	68.7E	15												
97110406		7.8N	68.3E	15												
97110412		7.9N	67.9E	15												
97110418		8.0N	67.6E	15												
97110500		8.0N	67.3E	15												
97110506		8.1N	66.8E	15												
97110512		8.3N	66.0E	15												
97110518		8.5N	65.2E	15												
97110600		8.9N	64.5E	15												
97110606		9.1N	63.6E	15												
97110612		9.2N	62.6E	15												
97110618		9.4N	61.3E	15												
97110700		9.5N	60.3E	20												
97110706		9.5N	59.3E	25												
97110712		9.8N	58.2E	25												
97110718		10.1N	56.6E	30												
97110800		10.2N	55.5E	35												
97110806	1	10.3N	54.6E	35	50	8	42	24	63		0	5	5	15	15	
97110812	2	10.5N	53.6E	35	60	54	64				0	-5	-20			
97110818	3	10.6N	52.7E	30	60	18					5	-10				
97110900	4	10.9N	51.7E	30	59	32					0	-10				
97110906	5	11.2N	51.1E	35	104	164					-5	10				
97110912	6	11.4N	50.9E	35	120	186					0	5				
97110918	7	11.7N	50.8E	20	43						10					
97111000		11.9N	50.7E	20												
97111006		12.3N	50.5E	20												
		AVERAGE			71	77	54	24	64		3	8	13	15	15	
		# CASES			7	6	2	1	1		7	6	2	1	1	

TROPICAL CYCLONE 04A

DTG	WRN NO.	BEST TRACK LAT	LONG	WIND	POSITION ERRORS 00	12	24	36	48	72	WIND ERRORS 00	12	24	36	48	72
97110212		7.9N	81.6E	15												

TROPICAL CYCLONE 04A (CONTINUED)

97110218		7.7N	81.5E	15												
97110300		7.5N	81.4E	15												
97110306		7.4N	81.3E	15												
97110312		7.3N	81.2E	15												
97110318		7.2N	81.1E	15												
97110400		7.2N	81.0E	15												
97110406		7.2N	80.8E	15												
97110412		7.3N	80.7E	15												
97110418		7.4N	80.6E	15												
97110500		7.6N	80.5E	15												
97110506		7.8N	80.4E	20												
97110512		8.0N	80.3E	20												
97110518		8.2N	80.2E	20												
97110600		8.5N	80.1E	20												
97110606		9.1N	80.1E	20												
97110612		9.7N	80.2E	20												
97110618		10.0N	80.2E	20												
97110700		10.2N	80.1E	20												
97110706		10.2N	79.9E	20												
97110712		10.2N	79.5E	20												
97110718		10.3N	79.0E	20												
97110800		10.3N	78.1E	20												
97110806		10.3N	77.1E	20												
97110812		10.3N	76.0E	25												
97110818		10.3N	74.9E	25												
97110900		10.3N	73.7E	25												
97110906		10.7N	72.6E	25												
97110912		11.0N	71.6E	25												
97110918		11.3N	70.6E	30												
97111000	1	11.5N	69.8E	30	69	132	174	216	258	265	0	0	-10	-10	-5	10
97111006	2	11.7N	69.0E	35	41	68	91	114	128	108	0	-5	-10	-10	-10	10
97111012	3	11.9N	68.2E	35	21	29	48	66	96	58	0	-10	-10	-10	-10	10
97111018	4	12.2N	67.4E	45	13	8	26	55	70	51	0	-5	0	5	15	35
97111100	5	12.5N	66.7E	50	13	11	11	21	40	214	0	0	5	5	25	40
97111106	6	12.8N	66.1E	55	21	21	13	23	79		0	5	10	20	35	
97111112	7	13.2N	65.5E	55	31	13	13	13	85		0	5	10	30	35	
97111118	8	13.5N	65.1E	55	5	18	24	30	112		0	5	15	35	40	
97111200	9	13.8N	64.8E	55	18	24	17	75	181		5	5	25	35	40	
97111206	10	14.1N	64.5E	55	11	16	56	141			0	10	25	30		
97111212	11	14.4N	64.2E	55	12	56	130	248			0	20	20	20		
97111218	12	14.6N	63.7E	50	21	92	183				0	10	15			
97111300	13	14.6N	63.2E	40	33	104	212				5	5	5			
97111306	14	14.6N	62.6E	35	55	147					0	0				
97111312	15	14.5N	61.9E	35	29	101					0	0				
97111318	16	14.2N	61.2E	30	6						0					
97111400	17	13.7N	60.4E	30	6						0					
			AVERAGE		24	56	77	92	117	140	0	5	12	20	24	21
			# CASES		17	15	13	11	9	5	17	15	13	11	9	5

7. TROPICAL CYCLONE (TC) SUPPORT SUMMARY

7.1 SOUTHERN HEMISPHERE APPLICATION OF THE SYSTEMATIC APPROACH TO TROPICAL CYCLONE TRACK FORECASTING

Author: Russell L. Elsberry
Naval Postgraduate School
Monterey, CA 93943

The environment structure conceptual models of the Systematic Approach to Tropical Cyclone Track Forecasting technique of Carr and Elsberry have been applied to all Southern Hemisphere tropical cyclones during January 1994 - June 1997. Whereas three of the four synoptic patterns from the western North Pacific could be applied with relatively small modifications, a new High (H) amplitude synoptic pattern was defined to classify the situations with large meridional penetrations of mid-latitude troughs deep into the Southern Hemisphere tropics. Some changes in terminology were required to describe the synoptic regions that have characteristic track directions. All 1592 cases during the period could be described as existing within one or more of these four synoptic patterns and 11 synoptic regions. Important track changes were found to be associated with transitions between these synoptic patterns and regions. Three binary tropical cyclone interactions defined for the western North Pacific were adapted for use in the Southern Hemisphere with considerable success. A preliminary climatology of occurrences for the synoptic pattern/region combinations, transitions between combinations, and binary tropical cyclone interactions are calculated. Sequences of synoptic analyses related to the transitions are described to aid in the application.

7.2 STATISTICAL POST-PROCESSING OF NOGAPS TRACK FORECASTS

Author: Russell L. Elsberry
Naval Postgraduate School
Monterey, CA 93943

A statistical post-processing technique has been developed and tested to reduce the Navy global model (NOGAPS) track forecast errors for a sample of western North Pacific tropical cyclones during 1992-96. In addition to the basic storm characteristics, the set of 24 predictors includes various segments in the 00-36 hour NOGAPS forecast track as well as a 00-36 hour backward extrapolation that is compared with the known recent track positions. Another key piece of information is the offset of the initial NOGAPS position relative to an updated (here best-track) position that will be known by about 6 hours after the corresponding synoptic times, which is when the NOGAPS forecast is actually available for use by the forecaster. For the development sample, the adjusted NOGAPS track errors are reduced by about 50 nm (93 km) at 12 hours, 33 nm (61 km) at 36 hours, and 24 nm (44 km) at 72 hours. Independent tests with a 1997 western North Pacific sample, 1995-97 Atlantic sample, and 1996-97 eastern and central North Pacific sample of NOGAPS forecasts have similar improvements from the post-processing technique. Thus, the technique appears to have a general applicability to Northern Hemisphere tropical cyclones.

7.3 AUTOMATED TROPICAL CYCLONE FORECASTING SYSTEM

Authors: C.R. Sampson and A.J. Schrader, Naval Research Laboratory, Monterey CA 93943

The Automated Tropical Cyclone Forecasting System (ATCF) version 3.2 was installed at JTWC, NPMOC, and NLMOC. This version features the following capabilities: an improved conventional meteorological database - TEDS 3.52; electronic logs for forecast operations; web pages for use in ATCF system support and communications; ECMWF and NCEP NWP model data display; scatterometer and cloud track wind display; NOAA compliant four-quadrant wind radii capability; geographic labels, and Tropical Cyclone Formation Alert (TCFA) graphic overlay generation for use on Joint Maritime Command Information System (JMCIS) workstations. Current work is focused on ATCF 3.3, to be installed in the spring of 1999. This version should include the capability to forecast beyond 72 hours and be year 2000 compliant. These capabilities involve a redesign of the tropical cyclone database format and a significant number of code changes. The new database will have capability to store a number of tropical cyclone parameters such as: minimum sea level pressure; radius of outermost closed isobar; radius of maximum winds; maximum wind gusts and eye diameter. It should also be easy to incorporate more forecast periods and tropical cyclone parameters with this new format.

7.4 SSM/I TROPICAL CYCLONE STRUCTURE

Authors: Jeff Hawkins, Naval Research Laboratory, Monterey, CA 93943
Co-authors: Richard Bankert, Paul Tag, Naval Research Laboratory, Monterey, CA 93943,
Juanita Chase, Doug May, Ron Holyer, Naval Research Laboratory, Stennis Space Center, MS 93943, and
Marla Helveston, Analysis & Technology, Bay St. Louis, MS 39520

The Special Sensor Microwave/Imager (SSM/I) has a suite of passive microwave channels that enable it to penetrate non-raining clouds and map out tropical cyclone (TC) associated rain and moisture structure. This ability to detect rainbands, eyewall(s) and eye/center locations can significantly assist the analyst and typhoon duty officer (TDO) when upper-level clouds obscure geostationary and/or polar orbiter visible (vis) and infrared (IR) imagery. TC structure is valuable for positioning and understanding storm intensity. This information, as well as any intensity trend, can then be used to upgrade the confidence and accuracy of storm warnings/advisories.

The Naval Research Laboratory's Marine Meteorology Division in Monterey, CA (NRL-MRY) has been exploring new methods to extract additional information from the wealth already contained in TC SSM/I imagery. Initial focus has been aimed at the high resolution (12-15 km) 85 GHz channels that nicely map TC structure and readily depict storm rainbands, eyewall(s) and center locations. This has been done by processing over 1500 SSM/I passes

coincident with TCs ranging in strength from tropical disturbances to super typhoons and, east of the dateline, CAT 5 hurricanes.

Results to date indicate the SSM/I can greatly assist the analyst locate the storm center when intensities are in excess of 30-40 kt. This threshold can change for given systems, but is used here as a generic number. The user should note that the cloud (and thus rain) organization for weak systems is poor at best and vis/IR data can be just as good and/or better than SSM/I data for trying to determine the center in the beginning stages of tropical systems. However, there is no upper bound for SSM/I capabilities, and it is useful with systems in the range of 150 kt-sustained winds. Particular note should be made that these SSM/I views are not constrained by central dense overcasts, shear or embedded centers that can cause problems with vis/IR imagery.

Two methods have been explored to extract TC intensities from automated analyses of SSM/I digital data. The first effort involves a neural network method which:

1) Uses 85 GHz, H-polarization brightness temperatures.

2) Represents the TC pattern in 85 GHz images via its Empirical Orthogonal Functions (EOF).

3) Trains the neural net with the EOFs most highly correlated with intensity.

4) Trains the net with a dependent storm data base using JTWC/NHC best track intensities.

The data base now contains over 750 TCs in the dependent data set and verification using "independent" cases has now shown skill ramping up storm intensity and weakening the storm as seen in real cases. The RMS error is still greater than our goal of 15 kts, but significant progress indicates this may become a viable technique within the next year.

The second effort utilizes computer vision capabilities to analyze both 85 GHz and rainrate products from the SSM/I. The same set of storms used to train the neural network is also used here. Spatial and textural measures, as well as those using various frequencies within the spectrum, were developed to extract features that are most highly correlated with TC intensity. Some of these features are analogous to those used within the Dvorak method, such as banding of particular temperature ranges, minimum brightness temperature, rainrates above a certain threshold, etc. Results to date indicate an RMS error less than 20 m/s and getting close to 15 m/s. Some large outliers exit, but many of them appear to be related to poor best track values. Note that no time averaging has yet been applied in either the neural network or computer vision methods.

Additional work, with well over 1,000 high quality storm hits, is underway. The Tropical Rainfall Mapping Mission (TRMM) Microwave Imager (TMI) and radar data will be added in the next update to this effort. TMI channels are basically identical to the SSM/I, with the addition of a low frequency 10 GHz channel that can assist with the determination of sea surface temperature and wind speed retrieval. TMI is mounted on a platform with an orbital altitude approximately one-half that utilized by the SSM/I platforms. This results in twice the

spatial resolution (5 km) but half of the footprint (approximately 750 km). Also of note, the 35 degree orbit inclination will permit more frequent TC coverage compared to more typical polar orbiters such as the DMSP/NOAA suite of satellites.

7.5 TROPICAL CYCLONE SCATTEROMETER STUDIES

Authors: Jeff Hawkins, Naval Research Laboratory, Monterey, CA 93943, and Roger Edson, Analysis & Technology, Guam

The ERS series of scatterometers have provided the bulk of the active microwave surface derived wind measurements from space since the launch of ERS-1 in 1991. ERS-2 continued to produce a 500-km swath of surface wind vectors throughout JTWC's Area Of Responsibility (AOR) during 1997, using a frequency that permits wind retrievals even under rainy conditions prevalent with tropical cyclones (TCs). The 50-km spatial resolution is coarse, but can often be sufficient to specify the radii of gale force winds as well as help position storm centers. Storm positioning is especially important for the weaker developing systems, when cloud/rain patterns are poorly defined and knowledge of the surface wind field is critical is assisting the analysts to achieve their goal.

ERS-2's 500-km swath presents often clustered but infrequent TC overflights. TCs can often move for days before the next pass clips or passes sufficiently over the storm to provide useful data. This major limitation was partially mitigated with the availability of the NASA SCATterometer (NSCAT) in the summer of 1996. Although the satellite platform suffered a terminal power failure in the Spring of 1997, the instrument produced a wealth of surface wind vectors in two 600-km swaths, one on each side of the spacecraft. The percentage of swaths detecting TCs rose significantly when compared with ERS-2 and the "revisit time" between overflights for a given storm was reduced dramatically.

NSCAT surface winds proved very useful for specifying the radius of gale force winds and assisting in finding storm centers. Some problems were encountered in early versions of the wind retrieval algorithm and these improved with time. The spectral window utilized by NSCAT was not as impervious to TC rainbands and thus rain attenuation in heavy rain was troublesome. Although heavy rain should boost the backscattered return and create higher winds, cases were often found where the wind speeds were significantly reduced. Efforts are underway to utilize SSM/I and/or combined SSM/I-IR methods to map out rain areas that can then be used to incorporate attenuation corrections for enhanced wind vector retrievals.

NSCAT's premature termination has led to a new NASA program called QUIKSCAT. This new scatterometer will have frequencies similar to NSCAT, but will employ a rotating dish antenna instead of the multiple stick antennas for ERS and NSCAT. QUIKSCAT will have a major advantage in providing a contiguous 1800-km swath and thus remove the NSCAT problem of dealing with the 350-km gap that existed in the middle of the two 600-km swaths. Validation will occur during the winter

of 98-99 and JTWC should have operational access to the data set by Spring of 1999.

7.6 UPPER TROPOSPHERIC OUTFLOW PATTERNS OVER SEVERAL VERY INTENSE TROPICAL CYCLONES OF THE WESTERN NORTH PACIFIC AS REVEALED BY SOUNDINGS, DOPPLER RADAR, AND WATER-VAPOR WINDS

Authors: Bill Ward National Weather Service, Tiyan, Guam and
Mark A. Lander, ONR-sponsored research at the University of Guam, Mangilao, Guam

As a warm-core vortex, the cyclonic circulation of a tropical cyclone (TC) weakens with height. In a mature TC, the peak winds occur within the lowest kilometer of the atmosphere. The intensity and areal extent of the cyclonic wind field decreases with altitude. In most text-book illustrations (e.g., Chen and Gray 1986), the cyclonic-flow region of the tropical cyclone is shown to decrease in size as one ascends to the upper troposphere, and in the outflow layer (above 200 hPa) the flow is depicted as predominantly anticyclonic.

Soundings from islands of the western North Pacific, vertical wind profiles of tropical cyclones obtained from Doppler radars located on Guam and Kwajalein, and water-vapor winds from the University of Wisconsin, have been collected during the lifetimes of several very intense tropical cyclones that have occurred in the western North Pacific. These data reveal that the extent of cyclonic circulation at upper levels is far more extensive than is commonly depicted, and that the signature bands and plumes of anticyclonically curved cirrus surrounding these tropical cyclones (which are unusually interpreted as evidence of antcyclonic outflow aloft) are not indicative of anticyclonic flow; but rather, they exist in cyclonically curved flow for several hundred km outward from the TC core, propagating outward and deriving their curvature from horizontal shear.

Outflow jets -- often referred to as outflow channels -- (another feature commonly thought to exist in the upper tropospheric flow surrounding TCs) are not found in our data set. Instead, broad areas of flow with an outward directed radial component (with respect to the cyclone center) nearly encircle the TC. Specific areas may contain somewhat enhanced flow, but these tend to be regions that are no smaller than a full quadrant of azimuth (in earth-relative coordinates). In storm-relative coordinates, the radially directed outward flow is even more symmetrical, and exhibits a decreased azimuthal concentration of outflow.

High-speed jet streaks existing at the periphery of tropical cyclones (usually marked by long cirrus plumes) have no concentrated links to the TC's core. Indeed, all airflow directed outward at upper levels from the tropical cyclone core appears to flow across a velocity minimum before it accelerates and enters these peripheral jets.

Some common tropical cyclone outflow patterns emerge from our data. They show that common operational estimation of tropical cyclone outflow from satellite imagery -- specifically, determination of the regions of good or poor outflow, and the assumption of the existence of outflow jets (or channels)

based on the pattern of the cirrus cloud plumes -- is flawed.

7.7 SOME CHARACTERISTICS OF TROPICAL CYCLONE INTENSIFICATION AS REVEALED BY HOURLY DIGITAL DVORAK ANALYSIS

Author: Mark A. Lander, ONR-sponsored research at the University of Guam, Mangilao, Guam

One of the utilities installed on the satellite image processing equipment at the Joint Typhoon Warning Center (JTWC), Guam, is an automated routine for computing Dvorak "T" numbers for TCs that possess eyes. The routine adapts the rules of the Dvorak technique as subjectively applied to enhanced infrared imagery in order to arrive at an objective T number, or "Digital Dvorak" T number (referred to as DD numbers). In the western North Pacific, infrared imagery is available hourly from the GMS satellite. When applicable, hourly DD numbers were calculated for all typhoons of 1996 and some of the more intense typhoons of 1995 and 1997.

The evolution of the DD numbers for several of the more intense typhoons that occurred during 1995, 1996 and 1997, has revealed some characteristic changes that occur during the lifetimes of many of these TCs. In many cases, large fluctuations in the time series of the DD numbers can be correlated with changes in the structure of the eye -- the formation of concentric wall clouds being the most common type of change. Also, when compared with the TC's best-track data, other common features of the DD numbers emerge: during the intensifying phase of the TC, the DD numbers tend to rise more rapidly and peak earlier than the operationally determined T numbers from conventional subjective Dvorak analysis.

The characteristics of the time series of the DD numbers imply short-term fluctuations in the convective behavior of TCs. These fluctuations suggest that there may be corresponding rapid and large fluctuations in the TC's intensity. If real, this behavior has major ramifications for operational warning accuracy and for intensity research (which depends largely on best-track data for its intensity input and for its source of validation data). This also questions our knowledge of the rates of TC spin-up and spin-down in relation to the convective fluctuations. An exploration of the behavior of the DD numbers may lay the groundwork for future modifications to current methods of estimating tropical cyclone intensity from satellite imagery.

7.8 EVALUATION OF A SIMPLE TECHNIQUE FOR PREDICTING THE PEAK INTENSITY AND THE TIMING OF PEAK INTENSITY FOR TROPICAL CYCLONES OF THE WESTERN NORTH PACIFIC

Authors: G. McCulloch, S. Cocks, and P. Hildebrand, Joint Typhoon Warning Center, Guam, and Mark A. Lander, ONR-sponsored research at the University of Guam, Mangilao, Guam

In recent years, operational regional numerical models designed for tropical cyclone applications (e.g., the Japanese Typhoon Model (JTYM), and the model developed by the Geophysical Fluid Dynamics Laboratory (GFDL), Princeton) have become capable of simulating realistic tropical cyclone

structure, as well as the capacity for large magnitude intensity change that approach those which can occur in nature. Intensity predictions from real-time model runs are now routinely distributed to tropical cyclone warning centers. The level of skill of these intensity predictions (and of those made by the warning agencies) is difficult to evaluate since there are few simple baselines against which to compare them.

Many specific problems reside under the umbrella of tropical cyclone intensity forecasting. Presently, at JTWC, the forecaster is required to produce intensity forecasts in short (e.g., 12 hour) increments for periods of up to 72 hours. Additional forecast challenges remain largely unexplored such as the determination of the peak intensity and the timing of the peak intensity from a given stage in the development of the tropical cyclone. Contained in the widely used Dvorak techniques is a basic rule that an intensifying tropical cyclone intensifies at an average rate of one "T" number per day (up to a particular point). This corresponds to an increase of wind speed of approximately 20 kt per day. Dvorak also found that westward moving tropical cyclones are allowed a longer time in which to develop than are those that move northwestward. These, in turn, develop for a longer period of time than those tropical cyclones moving northward.

A simple technique (unpublished), developed by Mundell (a former typhoon forecaster at Joint Typhoon Warning Center, Guam), provides guidance in determining the tropical cyclone peak intensity and the timing of this intensity. He found that the time to peak intensity as measured from specific intensity thresholds, such as minimal tropical storm intensity (35 kt) and minimum typhoon intensity (65 kt), was a strong function of the latitude at which these thresholds were reached. Further, the magnitude of the peak intensity was also a function of the latitude of occurrence of the benchmark intensities (e.g., the lower the latitude of achieving minimal typhoon intensity, the higher the peak and the longer the time delay until peak).

The Mundell techniques also encourage the forecaster to consider parameters that are often not given as much thought as the track forecast, diagnostic intensity estimate, and short-range intensity predictions. These include issues such as the number of days will it take a particular TC to reach peak intensity; and the eventual peak intensity. Such statistics are not even routinely compiled in post-analysis. As efforts are made to provide better intensity forecasts, and to consider questions such as the peak and time to peak of individual TCs, the Mundell techniques offer a simple starting point for producing and evaluating forecast of these parameters, and for understanding the problem of TC intensity change.

7.9 A LOOK AT GLOBAL TROPICAL CYCLONE ACTIVITY: BASIN INTERCOMPARISONS AND RELATIONSHIPS WITH ENSO, QBO, AND OTHER LARGE-SCALE CLIMATE FEATURES

Authors: Mark A. Lander, and Charles P. Guard, ONR-sponsored researach at the University of Guam, Mangilao, Guam

The time series representing the annual tabulation of tropical cyclone (TC) numbers (from the annual global total, as well as the annual totals within individual ocean basins) appears highly erratic (i.e., there is no persistence and the values seem to jump substantially from one year to the next). Time-lag autocorrelations of these time series confirm this - all have small negative values at a one-year time lag. Also, most of the time series have prominent spikes of both exceptionally low and high values. The high years are referred to as 'prolific' years, and the low years as 'meager' years. The 'prolific' years and 'meager' years are identified within the global and basin distributions. The range in the annual TC numbers within any givin basin is large. The global annual average is 85 with a range of 66 to 105; the western North Pacific annual average is 27 with a range of 19 to 36; the North Atlantic annual average is 10 with a range of 4 to 19; the eastern North Pacific annual average is 16 with a range of 8 to 24; the North Indian Ocean annual average is 5 with a range of 2 to 13; and the Southern Hemisphere annual average is 27 with a range of 19 to 38. The difference of 39 between the maximum and minimum annual global number of TCs is more than twice that of any individual basin.

Given the relative rarity of TC formation (as a global atmospheric phenomenon) coupled with the aforementioned phenomenon of basin "prolific" and "meager" years, a natural question arises. Are there compensations among the annual individual basin TC numbers that act in a manner as to stabilize the global TC number (i.e., negative correlations among some or all of the TC basins); or is the annual global TC number destabilized by positive correlations among some or all of the TC basins? The latter appears to be true. Cross-correlations between the basins reveal weak positive correlations amongst the western North Pacific, eastern North Pacific, and the Southern Hemisphere. During the 27-year period 1969 to 1997 there were 16 years with at least one basin experiencing a "prolific" or a "meager" year. Five of these years had two, or more, "prolific" and/or "meager" years. Only two of the years (1969 and 1995) had different basins simultaneously qualified for both "prolific" and "meager" labels; the "prolific" years during these two years were those of the North Atlantic.

There are strong relationships of the annual number of tropical cyclones in the North Atlantic with El Niño Southern Oscillation (ENSO) and with the Quasi Biennial Oscillation (QBO). In other basins these relationships are weaker, and, at least with ENSO, the effects are primarily upon the locations of the TCs and not the annual numbers. Ongoing reasearch includes further exploration of the spatial and temporal properties of the global TC distribution and examination of the effects of ENSO, QBO, and other climatic features on the

global and basin tropical-cyclone time series. The effects of the strong ENSO event of 1997-98 on the global TC distribution are receiving emphasis.

7.10 TECHNIQUES INCORPORATING SSM/I IMAGERY INTO DVORAK TROPICAL CYCLONE INTENSITY ESTIMATES

Authors: S.B. Cocks, and I. Johnson, Joint Typhoon Warning Center, Guam
Co-authors: Mark A. Lander and Charles P. Guard, ONR-sponsored research at the Univeristy of Guam, Guam

The Dvorak tropical cyclone intensity estimation technique for use on visible satellite data was introduced in 1975, with an additional technique for infrared satellite data introduced in 1984. The techniques have performed well throughout ocean basins across the world for nearly two decades of operational use. There are, however, cases where determination of the intensity of a tropical cyclone using the Dvorak methods has been inaccurate - particularly with the infrared techniques. This often occurs when the exact location and/or structure of the low-level circulation center is not known. Instances include the central dense overcast feature, the central cold cover, or the embedded center pattern (infrared imagery only). The Special Sensor Microwave/Imager (SSM/I) has the advantage of sensing through thick cloud cover, which can show the structure of a tropical cyclone that would otherwise be unseen in infrared or visible satellite imagery. SSM/I imagery can indicate the presence and location of low-level circulation centers and banding features; and can detect whether or not an eye is developing or already exists. These particular structural features of the TC are often not discernible in conventional satellite imagery. This study endeavors to develop similar rules for estimating the intensity of TCs using SSM/I imagery, and to explore ways to incorporate the SSM/I into Dvorak's conventional techniques- producing more versatile and accurate intensity estimates.

Using time matched visible, infrared, and SSM/I imagery in cases where the intensity estimate, given by Dvorak infrared or visible satellite methods, is clear-cut, features in the SSM/I imagery are found that are indicative of tropical cyclone intensity. There is clearly a relationship between TC intensity and specific properties as seen on microwave imagery. The SSM/I technique for estimating intensity was applied upon an independent set of tropical cyclones and the results were compared to those produced by established methods.

Results of the study so far indicate that subjective estimation of SSM/I imagery is possible; however, the accuracy of such estimates, on average, are not as good as those provided by the use of Dvorak's techniques on conventional visible and infrared satellite imagery. While it is possible that further research may uncover additional properties of microwave imagery that may allow a more accurate estimate of TC intensity, we feel that the biggest pay-off of the SSM/I imagery will come from providing a discipline to conventional Dvorak estimates of TC intensity. When the Dvorak intensity estimate for a given TC is not clear-cut, SSM/I imagery can provide valuable information that will allow one to arrive at a more representative estimate.

BIBLIOGRAPHY

Arnold, C.P., and C.C. Olsen, 1974: Tropical cyclone position and intensity analysis using satellite data. First Weather Wing Pamphlet 105-10, 97 pp.

Atkinson, G.D., 1974: Investigation of gust factors in tropical cyclones. Fleet Weather Center Technical Note: JTWC 74-1, 9pp.

_____, **and C.R. Holliday, 1977:** Tropical cyclone minimum sea-level pressure and maximum sustained wind relationship for the western North Pacific. *Mon. Wea. Rev.*, **105**, No. 4, pp 421-427 (also Fleet Weather Central/JTWC Technical Note 75-1).

Black, and F.D. Marks, 1991: the structure of an eye wall meso-vortex in Hurricane Hugo (1989). Preprints, 19th Conf. on Hurricanes and Tropical Meteor., AMS, Miami, FL, pp 357-358.

Brand, S., 1970: Interaction of binary tropical cyclones in the western North Pacific Ocean. J. Meteor. Soc. Japan, 50, pp 332-341.

Businger, S., and Baik, J-J., 1991: An arctic hurricane over the Bering Sea. *Mon. Wea. Rev.*, **119**, pp 2293-2322.

Carr, L.E., and R.L. Elsberry, 1994: Monsoonal interactions leading to sudden tropical cyclone track changes. *Mon. Wea. Rev.*, **123**, pp 265-289.

_____, **and** _____, **1994:** Systematic and integrated approach to tropical cyclone track forecasting, Part 1: Description of basic approach. Naval Postgraduate School publication NPS-MR-002. Naval Postgraduate School, Monterey, CA 93943. 65 pp. plus figs. and append.

_____, _____, **and Boothe, 1997:** Systematic approach to tropical cyclone forecasting: scenario-specific model and objective guidance traits. Preprints, 22nd Conference on Hurricanes and Tropical Meteorology. American Meteorlogical Society, Boston, MA.

_____, _____,**and** _____, **1997b:** Condensed and updated version of the systematic approach meteorological knowledge base – Western North Pacific. Tech. Rep. Naval Postgraduate School (in press).

Chen, L., and W.M. Gray, 1986: Global view of the upper level outflow patterns associated with tropical cyclone intensity change during FGGE. Dept. of Atmos. Science Paper No. 392, Colorado State University, Fort Collins, CO, 80523, 126 pp.

Climate Prediction Center (CPC), 1997: Graphical illustrations of global wind, pressure, and temperature patterns and their anomalies (also ENSO advisories and discussions). *Climate Diagnostics Bulletin*. No. **97**(1-12) Approximately 80 pp per monthly issue. [Available from U.S. Dept. of Commerce, Washington, DC, 20233.]

Diercks, J.M., R.C. Weir and M.K. Kopper, 1982: Forecast verification and reconnaissance data for Southern Hemisphere tropical cyclones (July 1980 through June 1982). NOCC/JTWC Technical Note 82-1, 77 pp.

Dong, K., 1988: El Niño and tropical cyclone frequency in the Australian region and the northwest pacific. *Aust. Meteor. Mag.*, **36**, 219-255.

_____, **and C.J. Neumann, 1983:** On the relative motion of binary tropical cyclones. *Mon. Wea. Rev.*, **111**, pp 945-953

Dunnavan, G.M., 1981: Forecasting intense tropical cyclones using 700-mb equivalent potential temperature and central sea-level pressure. NOCC/JTWC Technical Note 81-1, 12 pp.

Dvorak, V.F., 1975: Tropical Cyclone intensity analysis and forecasting from satellite imagery. *Mon. Wea. Rev.*, **103**, pp 420-430.

_____, **1984:** Tropical Cyclone intensity analysis using satellite data. NOAA Tech. Rep. NESDIS 11. US Dept. of Commerce, 46 pp.

Gray, W.M., 1978: Hurricanes: their formation, structure and likely role in the tropical circulation. Meteorology over the tropical oceans, Roy. *Meteor. Soc.*, pp 155-218.

Guard, C. P., 1997: *Preprints of the 22nd AMS Conference on Hurricanes and Tropical Meteorology, Ft. Collins, CO, May 19-23, 1997.* American Meteorological Society, Boston MA, pp. 476-477.

Guard, C.P., 1983: A study of western North Pacific tropical storms and typhoons that intensify after recurvature. First Weather Wing Technical Note-83/002, 28 pp.

_____, and M.A. Lander, 1995: Scale relating tropical cyclone wind speed to potential damage for the tropical Western Pacific Ocean.

Hebert, P.H., and K.O. Poteat, 1975: A satellite classification technique for subtropical cyclones. NOAA Technical Memorandum NWS SR-83, 25 pp.

Holland, G.J., 1980: An analytical model of wind and pressure profiles in hurricanes. *Mon. Wea. Rev.*, **108**, No. 8, pp 1212-1218.

Holliday, C.R., and A.H. Thompson, 1979: Climatological characteristics of rapidly intensifying typhoons. *Mon. Wea. Rev.*, **107**, No 8, pp 1022-1034.

Jorgensen, D.P., 1984: Mesoscale and convective scale characteristics of mature hurricanes. Part II: core structure of Hurricane Allen (1980). J. Atmos. Sci., 41, 1287-1311.

JTWC, 1960: Typhoon Carmen. 1960 Annual Tropical Typhoon Report, JTWC, 103-108. [NTIS AD 786147.]

_____, 1979: Super Typhoon Tip. 1979 Annual Tropical Typhoon Report, JTWC, 72-77. [NTIS AD A082071.]

_____, 1993: Illustration of the cloud distribution in a monsoon depression. 1993 Annual Tropical Cyclone Report, JTWC, p 130. [NTIS AD A285097].

_____, 1994: Timing of peak intensity with respect to the time of recurvature. 1994 Annual Tropical Cyclone Report, JTWC, Figure 3-03-3, p 51. [NTIS AD A301618]

Lander, 1994a: Description of a monsoon gyre and its effects on the tropical cyclones in the western North Pacific during August 1991. *Weather and Forecasting*, **9**, pp 640-654.

_____, 1994b: An exploration of the relationships between tropical storm formation in the Western North Pacific and ENSO, *Mon. Wea. Rev.*, **122**, No. 4, pp 636-651.

_____, and G.J. Holland, 1993: On the interaction of tropical-cyclone scale vortices. I: Observations. *Quart. J. Roy. Meteor. Soc.*, **119**, pp 1347-1361.

Marks, F.D. Jr., and R.A. Houze Jr., 1984: Airborne Doppler radar observations in Hurricane Debby. *Bull. Amer. Meteor. Soc.*, **44**, pp 1296-1317.

Matsumoto, C.R., 1984: A statistical method for one- to three-day tropical cyclone track prediction. Department of Atmospheric Science Paper No. 379, Colorado State University, Fort Collins, CO 80523, 201 pp.

Miller, D.W., and M.A. Lander, 1997a: Intensity estimation of tropical cyclones during extratropical transition. JTWC/SATOPS Technical Note 97-002.

Mundell, D.B., 1990: Prediction of tropical cyclone rapid intensification events. Thesis for fulfillment of Master's degree submitted to Colorado State University, Fort Collins, CO 80523, 186 pp.

Ramage, C.S., 1971: Monsoon Meteorology. Academic Press, 296 pp.

Stewart, S.R., and D. Wolff, 1997: Convectively induced mesocyclonic vortices in the eyewall of tropical cyclones as seen by WSR-88D doppler radars. Preprints 22nd Conf. On Hurricanes and Tropical Meteor., Ft. Collins, CO.

_____, and S.W. Lyons, 1996: A WSR-88D radar view of Tropical Cyclone Ed. *Weather and Forecasting*, **11**, pp 115-135.

Wakimoto, R.M., and P.G. Black, 1993: Damage survey of Hurricane Andrew and its relationship to the radar-detected eyewall. Proc. 20th Conf. Hurr. and Trop. Meteor., San Antonio, Texas, Amer. Meteor. Soc., pp 54-57.

Weatherford, C.L., 1984: Typhoon structural variability. Colorado State University Atmospheric Science Paper No. 391, 77 pp. [Available from Department of Atmospheric

Science, Colorado State University, Fort Collins, CO 80523.]

Weir, R.C., 1982: Predicting the acceleration of northward-moving tropical cyclones using upper-tropospheric winds. NOCC/JTWC Technical Note 82-2, 40 pp.

Willoughby, H.E., 1990: Temporal changes in the primary circulation in tropical cyclones . *J. Atmos. Sci.*, **47**, pp 242-264.

_____, J.A. Clos, and M.G. Shoreibah, 1982: Concentric eye walls, secondary wind maxima, and the evolution of the hurricane vortex. J. Atmos. Sci., 39, pp 395-411.

Wirfel, W.P. and S.A. Sandgathe, 1986: Forecast verification and reconnaissance data for Southern Hemisphere tropical cyclones (July 1982 through June 1984). NOCC/JTWC Technical Note 86-1, 102 pp.

Xu, Y., and C.J. Neumann, 1985: A statistical model for the prediction of western North Pacific tropical cyclone motion. NOAA Technical Memorandum NWS NHC 28, 30 pp.

Zehr, R.M., 1992: Tropical cyclogenesis in the western North Pacific. NOAA Technical Report, NESDIS 61, U.S. Dept. of Commerce, Washington DC, 181 pp.

APPENDIX A
DEFINITIONS

BEST TRACK - A subjectively smoothed path, versus a precise and very erratic fix-to-fix path, used to represent tropical cyclone movement, and based on an assessment of all available data.

BINARY INTERACTION - Binary interaction is a mutual cyclonic orbit of two tropical cyclones around their centroid. Lander and Holland (1993) showed that the behavior of most binary tropical cyclones consists of an approach, sudden capture, then a period of steady cyclonic orbit followed by a sudden escape or (less frequently) a merger.

CENTER - The vertical axis or core of a tropical cyclone. Usually determined by cloud vorticity patterns, wind and/or pressure distribution.

EPHEMERIS - Position of a body (satellite) in space as a function of time; used for gridding satellite imagery. Since ephemeris gridding is based solely on the predicted position of the satellite, it is susceptible to errors from vehicle wobble, orbital eccentricity, the oblateness of the Earth, and variation in vehicle speed.

EXPLOSIVE DEEPENING - A decrease in the minimum sea-level pressure of a tropical cyclone of 2.5 mb/hr for at least 12 hours or 5 mb/hr for at least six hours (Dunnavan 1981).

EXTRATROPICAL - A term used to indicate that a cyclone has lost its "tropical" characteristics. The term implies both poleward displacement from the tropics and the conversion of the cyclone's primary energy source from the release of latent heat of condensation to baroclinic processes. In the XT technique (Miller and Lander 1997a) a tropical cyclone is defined as having completed extratropical transition when the circulation center has moved poleward of the polar jet maximum or when water vapor imagery clearly indicates the system has become entirely cold-core. It is important to note that cyclones can become extratropical and still maintain winds of typhoon or storm force.

EYE - The central area of a tropical cyclone when it is more than half surrounded by wall cloud.

INTENSITY - The maximum sustained 1-minute mean surface wind speed, typically within one degree of the center of a tropical cyclone.

MAXIMUM SUSTAINED WIND - The highest surface wind speed averaged over a 1-minute period of time. (Peak gusts over water average 20 to 25 percent higher than sustained winds).

MEI-YU FRONT - The Term " mei-yu" is the Chinese expression for "plum rains". The mei-yu front is a persistant east-west zone of disturbed weather during spring which is quasi -stationary and stretches from the east China coast, across Taiwan, and eastward into the Pacific south of Japan.

MONSOON DEPRESSION - A tropical cyclonic vortex characterized by: 1) its large size, the outer-most closed isobar may have a diameter on

the order of 600 nm (1000 km); 2) a loosely organized cluster of deep convective elements; 3) a low-level wind distribution which features a 100-nm (200-km) diameter light-wind core which may be partially surrounded by a band of gales; and, 4) a lack of a distinct cloud system center. Note: most monsoon depressions which form in the western North Pacific eventually acquire persistent central convection and accelerated core winds marking its transition into a conventional tropical cyclone.

MONSOON GYRE - A mode of the summer monsoon circulation of the western North Pacific characterized by: 1) a very large nearly circular low-level cyclonic vortex that has an outer-most closed isobar with diameter on the order of 1200 nm (2500 km); 2) a cloud band rimming the southern through eastern periphery of the vortex/surface low; 3) a relatively long (two week) life span - initially, a subsident regime exists in its core and western and northwestern quadrants with light winds and scattered low cumulus clouds; later, the area within the outer closed isobar may fill with deep convective cloud and become a monsoon depression or tropical cyclone; and, 4) the large vortex cannot be the result of the expanding wind field of a preexisting monsoon depression or tropical cyclone. Note: a series of small or very small tropical cyclones may emerge from the "head" or leading edge of the peripheral cloud band of a monsoon gyre (JTWC 1993; Lander 1994a).

RAPID DEEPENING - A decrease in the minimum sea-level pressure of a tropical cyclone of 1.75 mb/hr or 42 mb for 24-hours (Holliday and Thompson 1979).

RECURVATURE - The turning of a tropical cyclone from an initial path toward the west and poleward to east and poleward, after moving poleward of the mid-tropospheric subtropical ridge axis.

REVERSE-ORIENTED MONSOON TROUGH - The distinguishing characteristics of a reverse-oriented monsoon trough in the western North Pacific are a SW-NE (i.e., reverse) orientation of the trough axis with respect to the normal NW-SE orientation of the trough axis, and the penetration of the trough axis into subtropical areas normally the province of easterly flow.

SIGNIFICANT TROPICAL CYCLONE - A tropical cyclone becomes "significant" with the issuance of the first numbered warning by the responsible warning agency.

SIZE - The areal extent of a tropical cyclone, usually measured radially outward from the center to the outer-most closed isobar. Based on an average radius of the outer-most closed isobar, size categories in degrees of latitude follow: $< 2°$ = very small, $2°$ to $3°$ = small, $3°$ to $6°$ = medium (average), $6°$ to $8°$ = large, and $8°$ or greater = very large (Brand 1972 and a modification of Merrill 1982).

STRENGTH - The average wind speed of the surrounding low-level wind flow, usually measured within a one to three degree annulus of the center of a tropical cyclone (Weatherford and Gray 1985).

SUBTROPICAL CYCLONE - A low pressure system that forms over the

ocean in the subtropics and has some characteristics of a tropical circulation, but not a central dense overcast. Although of upper cold low or low-level baroclinic origins, the system can transition to a tropical cyclone.

SUPER TYPHOON - A typhoon with maximum sustained 1-minute mean surface winds of 130 kt (67 m/sec) or greater.

TROPICAL CYCLONE - A non-frontal, migratory low-pressure system, usually of synoptic scale, originating over tropical or subtropical waters and having a definite organized circulation.

TROPICAL DEPRESSION - A tropical cyclone with maximum sustained 1-minute mean surface winds of 33 kt (17 m/sec) or less.

TROPICAL DISTURBANCE - A discrete system of apparently organized convection, generally 100 to 300 nm (185 to 555 km) in diameter, originating in the tropics or subtropics, having a non-frontal, migratory character and having maintained its identity for 12- to 24-hours. The system may or may not be associated with a detectable perturbation of the low-level wind or pressure field. It is the basic generic designation which, in successive stages of development, may be classified as a tropical depression, tropical storm, typhoon or super typhoon.

TROPICAL STORM - A tropical cyclone with maximum 1-minute mean sustained surface winds in the range of 34 to 63 kt (18 to 32 m/sec), inclusive.

TROPICAL UPPER-TROPOSPHERIC TROUGH (TUTT) - A dominant climatological system and a daily upper-level synoptic feature of the summer season, over the tropical North Atlantic, North Pacific and South Pacific Oceans (Sadler 1979). Cold core lows in the TUTT are referred to as cells, or TUTT cells.

TYPHOON (HURRICANE) - A tropical cyclone with maximum sustained 1-minute mean surface winds of 64 to 129 kt (33 to 66 m/sec). West of 180° E longitude they are called typhoons and east of 180° E longitude hurricanes.

WALL CLOUD - An organized band of deep cumuliform clouds that immediately surrounds the central area of a tropical cyclone. The wall cloud may entirely enclose or partially surround the center.

WESTERLY WIND BURST - A short-duration low-level westerly wind event along and near the equator in the western Pacific Ocean (and sometimes in the Indian Ocean) (Luther et al. 1983). Typically, a westerly wind burst (WWB) lasts several days and has westerly winds of at least 10 kt (5 m/sec) (Keen 1988). Most WWBs occur during the monsoon transition months of April-May, and November-December. They show some relationship to the ENSO phenomenon (Luther et al. 1983; Ramage 1986). Some WWBs are even more energetic, with wind speeds of 30 kt (15 m/sec) observed during well-developed systems. These intense WWBs are associated with a large cluster of deep-convective cloud along the equator. An intense WWB is a necessary precursor to the formation of tropical cyclone twins symmetrical with respect to the equator (Keen 1982; Lander 1990

APPENDIX B
NAMES FOR TROPICAL CYCLONES IN THE WESTERN NORTH PACIFIC OCEAN AND SOUTH CHINA SEA

Column 1		Column 2		Column 3		Column 4	
ANN	*AN*	**ABEL**	*A-bel*	**AMBER**	*AM-ber*	**ALEX**	*AL-x*
BART	*BART*	**BETH**	*BETH*	**BING**	*BING*	**BABS**	*BABS*
CAM	*KAM*	**CARLO**	*KAR-lo*	**CASS**	*KASS*	**CHIP**	*CHIP*
DAN	*DAN*	**DALE**	*DAY-l*	**DAVID**	*DAY-vid*	**DAWN**	*DAWN*
EVE	*EEV*	**ERNIE**	*ER-nee*	**ELLA**	*EL-la*	**ELVIS**	*EL-vis*
FRANKIE	*FRANK-ee*	**FERN**	*FERN*	**FRITZ**	*FRITZ*	**FAITH**	*FAITH*
GLORIA	*GLOR-ee-uh*	**GREG**	*GREG*	**GINGER**	*JIN-jer*	**GIL**	*GIL*
HERB	*HERB*	**HANNAH**	*HAN-nah*	**HANK**	*HANGK*	**HILDA**	*HIL-dah*
IAN	*EE-an*	**ISA**	*EE-sah*	**IVAN**	*I-van*	**IRIS**	*I-ris*
JOY	*JOY*	**JIMMY**	*JIM-ee*	**JOAN**	*JONE*	**JACOB**	*JAY-kob*
KIRK	*KIRK*	**KELLY**	*KEL-lee*	**KEITH**	*KEETH*	**KATE**	*KATE*
LISA	*LEE-sah*	**LEVI**	*LEEV-eye*	**LINDA**	*LIN-dah*	**LEO**	*LEE-o*
MARTY	*MAR-tee*	**MARIE**	*mah-REE*	**MORT**	*MORT*	**MAGGIE**	*MAG-gee*
NIKI	*NI-kee*	**NESTOR**	*NES-tor*	**NICHOLE**	*nik-KOL*	**NEIL**	*NEEL*
ORSON	*OR-son*	**OPAL**	*O-pel*	**OTTO**	*OT-tow*	**OLGA**	*OL-gah*
PIPER	*PI-per*	**PETER**	*PEE-ter*	**PENNY**	*PEN-nee*	**PAUL**	*PAUL*
RICK	*RICK*	**ROSIE**	*RO-zee*	**REX**	*REX*	**RACHEL**	*RAY-chel*
SALLY	*SAL-lee*	**SCOTT**	*SKOT*	**STELLA**	*STEL-lah*	**SAM**	*SAM*
TOM	*TOM*	**TINA**	*TEE-nah*	**TODD**	*TOD*	**TANYA**	*TAHN-yah*
VIOLET	*VI-uh-let*	**VICTOR**	*vik-TOR*	**VICKI**	*VIK-kee*	**VIRGIL**	*VER-jil*
WILLIE	*WIL-lee*	**WINNIE**	*WIN-nee*	**WALDO**	*WAL-do*	**WENDY**	*WEN-dee*
YATES	*YATES*	**YULE**	*YOU-l*	**YANNI**	*YAN-ni*	**YORK**	*YORK*
ZANE	*ZANE*	**ZITA**	*ZEE-tah*	**ZEB**	*ZEB*	**ZIA**	*ZEE-uh*

NOTE 1: Assign names in rotation, alphabetically, starting with (ANN) for first tropical cyclone of 1996. When the last name in Column 4 (ZIA) has been used, the sequence will begin again with the first name in Column 1 (ANN).

NOTE 2: Pronunciation guide for names is italicized.

SOURCE: CINCPACINST 3140.1W

APPENDIX C
CONTRACTIONS

AB Air Base

ABW Air Base Wing

ABIO Significant Tropical Weather Advisory for the Indian Ocean

ABPW Significant Tropical Weather Advisory for the Western Pacific Ocean

ACCS Air Control Center Squadron

ACFT Aircraft

ADEOS Japanese Advanced Earth Observing Satellite

ADP Automated Data Processing

AFB Air Force Base

AFDIS Air Force Dial-In System

AFWA Air Force Weather Agency

AIREP Aircraft (Weather) Report

AJTWC Alternate Joint Typhoon Warning Center

AMOS Automatic Meteorological Observing Station

AOR Area of Responsibility

ARC Automated Remote Collection (system)

ARGOS (International Service for Drifting Buoys)

ARQ Automated Response to Query

ATCF Automated Tropical Cyclone Forecast (system)

ATCR Annual Tropical Cyclone Report

AUTODIN Automated Digital Network

AVHRR Advanced Very High Resolution Radiometer

AWDS Automated Weather Distribution System

AWN Automated Weather Network

BLND Blended (Hybrid Aid)

BRAC Base Realignment and Closure

CDO Central Dense Overcast

CI Current Intensity

CIMSS Cooperative Institute for Meterological Satellite Studies

CIV Civilian

CLD Cloud

CLIM Climatology

CLIP or **CLIPER** Climatology and Persistence Technique

CM Centimeter(s)

C-MAN Coastal-Marine Automated Network

CMOD Compact meteorological and Oceanographic Drifter (buoy)

COMNAVMETOCCOM or **CNMOC** Commander Naval Meteorology and Oceanography Command

CPA Closest Point of Approach

CPHC Central Pacific Hurricane Center

CSC Cloud System Center

CSUM Colorado State University Model

CW Continuous Wave

DAVE Name of a Hybrid Aid

DD Digital Dvorak

DDN Defense Data Network

DEG Degree(s)

DFS Digital Facsimile System

DISN Defense Information Systems Network

DMS Defense Messaging System

DMSP Defense Meteorological Satellite Program

DOD Department of Defense

DSN Defense Switched Network

DTG Date Time Group

EGRR Bracknell Model

ENSO El Niño-Southern Oscillation

ERS European Remote Sensing Satellite

FBAM FNOC Beta and Advection Model

FI Forecast Intensity (Dvorak)

FLENUMETOCCEN Fleet Numerical Meteorology and Oceanography Center

FT Foot/Feet

FTP File Transfer Protocol

GFDN Geophysical Fluid Dynamics-Navy Model

GCA Great Circle Arc

GFDN Geophysical Fluid Dynamics - Navy

GMS Japan Geostationary Meteorological Satellite

GMT Greenwich Mean Time

GOES Geostationary Operational Environmental Satellite

GSRS Geostationary Satellite Receiving System

GTS Global Telecommunications System

HIRS High Resolution Infrared Sounder

hPa Hectopascal

HPAC Mean of XTRP and CLIM Techniques (Half Persistence and Climatology)

HF High Frequency

HR Hour(s)

HRPT High Resolution Picture Transmission

ICAO International Civil Aviation Organization

INIT Initial

INST Instruction

IP Internet Protocol

IR Infrared

JGSM Japanese Global Spectral model

JTWC Joint Typhoon Warning Center

JTWC92 Statistical-Dynamical or JT92 Objective Technique

JTYM Japanese Typhoon Model

KM Kilometer(s)

KT Knot(s)

LAN Local Area Network

LAT Latitude

LLCC Low-Level Circulation Center

LONG Longitude

LUT Local User Terminal

LVL Level

M Meter(s)

MAX Maximum

MB Millibar(s)

MBAM Medium Beta and Advection Model

MCAS Marine Corps Air Station

MCS Mesoscale Convective System

MET Meteorological

METEOSAT European Meteorological Satellite

MIDDAS Meteorological Imagery, Data Display, and Analysis System

MIN Minimum

MINI-MET Mini-Meteorological (buoy)

MISTIC Mission Sensor Tactical Imaging Computer

MM Millimeter(s)

MOVG Moving

MSLP Minimum Sea-level Pressure

MSU Microwave Sounding Unit

NARDAC Naval Regional Data Automation Center

NAS Naval Air Station

NASA National Aeronautics and Space Administration

NAVPACMETOCCEN Naval Pacific Meteorology and Oceanography Center (Hawaii)

NAVPACMETOCCEN WEST Naval Pacific Meteorology and Oceanography Center West (Guam)

NCEP National Centers for Environmental Prediction

NEDN Naval Environmental Data Network

NESDIS National Environmental Satellite, Data, and Information Service

NESN Naval Environmental Satellite Network

NEXRAD Next Generation (Doppler Weather) Radar (WSR-88D)

NGDC National Geophysical Data Center

NHC National Hurricane Center

NIPRNET Non-secure Internet Protocol Router Network

NM Nautical Mile(s)

NMC National Meteorological Center

NOAA National Oceanic and Atmospheric Administration

NODDES Naval Environmental Data Network Oceanographic Data Distribution and Expansion System

NOGAPS Navy Operational or **NGPS** Global Atmospheric Prediction System

NODDS Naval Oceanography Data Distribution Systems

NPS Naval Postgraduate School

NR Number

NRL Naval Research Laboratory

NRL-MRY Naval Research Laboratory at Monterey, CA

NRPS or Navy Operational

NORAPS Regional Atmospheric Prediction System

NSCAT NASA Scatterometer

NSDS-G Naval Satellite Display System - Geostationary

NTWP Naval Telecommunications Area Master Station, Western Pacific

SIPRNET Secret Internet Protocol Router Network

NWP Northwest Pacific

NWS National Weather Service

OBS Observations

OLS Operational Linescan System

ONR Office of Naval Research

OSS Operations Support Squadron

OSB Ocean Sciences Branch

OTCM One-Way (Interactive) Tropical Cyclone Model

PACAF Pacific Air Force

PACMEDS Pacific Meteorological Data System

PACOM Pacific Command

PAGASA Philippine Atmospheric Geophysical, and Astronomical Services Administation

PC Personal Computer

PCN Position Code Number

PDN Public Data Network

PIREP Pilot Weather Report(s)

QBO Quasi-Biennial Oscillation

RADOB Radar Observation

RECON Reconnaissance

RECR Recurve (Forecast Aid)

RMSE Root mean square error

ROCI Radius of outer-most closed isobar

SAT Satellite

SCS South China Sea

SDHS Satellite Data Handling System

SEC Second(s)

SFC Surface

SGDB Satellite Global Data Base

SIPRNET Secret Internet Protocol Router Network

SLP Sea-Level Pressure

SPAWRSYSCOM Space and Naval Warfare Systems Command

SPIDR Space Physics Interactive Data Resource

SSM/I Special Sensor Microwave/Imager

SST Sea Surface Temperature

SSU Stratosphere Sounding Unit

ST Subtropical

STNRY Stationary

STR Subtropical Ridge

STRT Straight (Forecast Aid)

STY Super Typhoon

SWDIS Satellite Weather Data Imaging System

TAPT Typhoon Acceleration Prediction Technique

TC Tropical Cyclone

TCFA Tropical Cyclone Formation Alert

TD Tropical Depression

TDA Typhoon Duty Assistant

TDO Typhoon Duty Officer

TELEFAX Telephone Facsimile

TESS Tactical Environmental Support System

TIFF Tagged Image File Format

TIROS-N Television Infrared Observational Satellite-Next Generation

TOGA Tropical Ocean Global Atmosphere

TOVS TIROS Operational Vertical Sounder

TS Tropical Storm

TUTT Tropical Upper-Tropospheric Trough

TY Typhoon

TYAN Typhoon Analog (Forecast Aid)

ULCC Upper-Level Circulation Center

US United States

USAF United States Air Force

USCINCPAC Commander-in-Chief Pacific (AF - Air Force, FLT - Fleet)

USN United States Navy

VIS Visual

WAN Wide Area Network

WESTPAC Western (North) Pacific

WGTD Weighted (Hybrid Aid)

WMO World Meteorological Organization

WNP Western North Pacific

WRN or **WRNG** Warning(s)

WSD Wind Speed and Direction

WSR-88D Weather Surveillance Radar - 1988 Doppler

WVTW Water Vapor Tracked Winds

WWB Westerly Wind Burst

WWW World Wide Web

XT Extratropical

XTRP Extrapolation

Z Zulu time (Greenwich Mean Time/Universal Coordinated Time)

APPENDIX D

PAST ANNUAL TROPICAL CYCLONE REPORTS

Copies of the past Annual Tropical Cyclone Reports for DOD agencies or contractors can be obtained through:

Defense Technical Information Center (DTIC)
DTIC-BR (Reference & Retrieval Division)
8725 John J. Kingman Road
Suite 0940
Ft. Belvoir, VA 22060-6218

Phone: comm (703) 767-8274
DSN 427-9070
Fax: comm (703) 767-9070
DSN 427-9070

Copies for non-DOD agencies or users can be obtained from:

National Technical Information Service
5285 Port Royal Road
Springfield, VA 22161

Phone: (703) 487-4650
Fax: (703) 321-8547

Refer to the following numbers when ordering:

Year	Acquisition Number	Year	Acquisition Number	Year	Acquisition Number
1959	AD 786147	1972	AD 768334	1985	AD A168284
1960	AD 786148	1973	AD 777093	1986	AD A184082
1961	AD 786149	1974	AD 010271	1987	AD A191883
1962	AD 786128	1975	AD A023601	1988	AD A207206
1963	AD 786208	1976	AD A038484	1989	AD A232469
1964	AD 786209	1977	AD A055512	1990	AD A239910
1965	AD 786210	1978	AD A070904	1991	AD A251952
1966	AD 785891	1979	AD A082071	1992	AD A274464
1967	AD 785344	1980	AD A094668	1993	AD A285097
1968	AD 785251	1981	AD A112002	1994	AD A301618
1969	AD 785178	1982	AD A124860	1995	AD A321611
1970	AD 785252	1983	AD A137836	1996	AD A332916
1971	AD 768333	1984	AD A153395		

INTERNET DOCUMENT INFORMATION FORM

A. Report Title: 1997 Annual Tropical Cyclone Report

B. DATE Report Downloaded From the Internet: September 14, 2000

C. Report's Point of Contact: (Name, Organization, Address, Office Symbol, & Ph #): U. S. Naval Pacific Meteorology and Oceanography Center/ Joint Typhoon Warning Center
Pearl Harbor, Hawaii

D. Currently Applicable Classification Level: Unclassified

E. Distribution Statement A: Approved for Public Release

F. The foregoing information was compiled and provided by:
DTIC-OCA Initials: __pm__ **Preparation Date September 14, 2000**

The foregoing information should exactly correspond to the Title, Report Number, and the Date on the accompanying report document. If there are mismatches, or other questions, contact the above OCA Representative for resolution.